Advances in Astronomy

Recent Trends in Celestial Mechanics

Lead Guest Editor: Elbaz I. Abouelmagd
Guest Editors: Abdullah A. Ansari, Euaggelos E. Zotos, Gang Zhang, and Juan L. G. Guirao

Recent Trends in Celestial Mechanics

Advances in Astronomy

Recent Trends in Celestial Mechanics

Lead Guest Editor: Elbaz I. Abouelmagd
Guest Editors: Abdullah A. Ansari, Euaggelos E. Zotos, Gang Zhang, and Juan L. G. Guirao

Contents

Hindawi
Advances in Astronomy
Volume 2021, Article ID 6665238, 11 pages
https://doi.org/10.1155/2021/6665238

Research Article

Fractal Basins of Convergence of a Seventh-Order Generalized Hénon–Heiles Potential

Euaggelos E. Zotos,[1] **Fredy L. Dubeibe**,[2] **and A. Riaño-Doncel**[2]

[1]*Department of Physics, School of Science, Aristotle University of Thessaloniki, Thessaloniki GR-541 24, Greece*
[2]*Facultad de Ciencias Humanas y de la Educación, Universidad de los Llanos, Villavicencio, Colombia*

Correspondence should be addressed to Euaggelos E. Zotos; evzotos@physics.auth.gr

Received 26 November 2020; Accepted 5 July 2021; Published 14 July 2021

Academic Editor: Michael Küppers

This article aims to investigate the points of equilibrium and the associated convergence basins in a seventh-order generalized Hénon–Heiles potential. Using the well-known Newton–Raphson iterator, we numerically locate the positions of the points of equilibrium, while we also obtain their linear stability. Furthermore, we demonstrate how the two variable parameters, entering the generalized Hénon–Heiles potential, affect the convergence dynamics of the system as well as the fractal degree of the basin diagrams. The fractal degree is derived by computing the (boundary) basin entropy as well as the uncertainty dimension.

1. Introduction

It is well known that every differentiable symmetry of the action of a physical system has a corresponding conservation law. Therefore, by Noether's theorem in every stationary axisymmetric system, the energy and the angular momentum along the symmetry axis are conserved. However, at the end of the XIX 19th century, it was shown that in some cases there existed an additional hidden conserved quantity (see, e.g., [1, 2]), the so-called third integral of motion. This discovery increased the interest of researchers who initiated systematic studies in this topic, among whom Contopoulos stands out by his studies on the existence of the third integral of motion in galactic dynamics [3–7].

An important landmark on the existence of the third integral of motion in axisymmetric potentials is provided by the work of Hénon and Heiles [8], who performed a systematic and complete numerical investigation on this topic and found that the third integral exists for only a limited range of initial conditions. The potential selected for the study in [8] can be considered a particular case of the general Hamiltonian found by Contopoulos in [3]:

$$H = \frac{1}{2}\left(\dot{x} + \dot{y} + \omega_1^2 x^2 + \omega_2^2 y^2 + \varepsilon x y^2 + \varepsilon' x^3\right). \tag{1}$$

Set $\omega_1 = \omega_2 = \varepsilon = 1$ and $\varepsilon' = -1/3$, and swap variables $(x, y) \longrightarrow (y, x)$.

The Hamiltonian presented above (1) (and consequently the Hénon–Heiles potential) can be derived as a series expansion up to the third order of the effective potential for stationary axisymmetric systems with reflection symmetry $V(r, z) = V(r, -z)$ (see [9]).

$$V(r, z) = U(r, z) + \frac{L^2}{2r^2}. \tag{2}$$

Since then, some efforts have been made to generalize the Hénon–Heiles potential. Around 1980, Verhulst [10] expanded the potential (2) up to the fourth order seeking to study resonances 1 : 1, 1 : 2, 1 : 3, and 2 : 1. Some years ago, a generalized Hénon–Heiles potential was derived by expanding the effective potential up to the fifth order, aiming to study the equilibrium points and basins of convergence of the new potential [11] and to analyze the dynamical effect on bounded and unbounded orbits of including higher-order terms in the series expansion [12]. More recently, a seventh-order version of the stationary axisymmetric potential was presented [13], and it was found that when higher-order

contributions of the potential are taken into account, the chaoticity of the system is reduced in comparison with the lower-order version of the Hénon–Heiles system.

The practical importance of the Hénon–Heiles-like potentials lies in its applications to the stellar kinematics and velocity ellipsoid in our galaxy, where the observed distribution of star's velocities near the Sun can be explained if a third integral exists [14]. Also, these potentials have been used to investigate quantum manifestations of chaos and level repulsion in classical chaotic Hamiltonians [15] and to calculate the lifetimes and energies for metastable states exploiting the property that the dynamics of this potential change from quasiperiodic to chaotic for higher energies [16]. In the context of general relativity, these potentials have been used to analyze the emission of gravitational waves and to show the differences among wave emissions from regular and chaotic motion [17], to study the geodesic motion of test particles in vacuum gravitational pp-wave spacetimes [18], or to perform numerical investigations related to the integrability of orbits of test particles moving around a black hole representing the galactic center [19], just to name some examples.

In this paper, we rewrite the general form of the seventh-order potential [13] in terms of two arbitrary parameters α and δ denoting the contributions of the fifth-order and seventh-order terms, in which the constants are set in such a form that the new potential exhibits an increasing number of fixed points for some values of the free parameters (note that in [13] the number of fixed points is always four). Aiming to perform a full numerical analysis of the new potential, we shall investigate the existence of equilibrium points using the standard Newton–Raphson iterative scheme. In particular, we will use the so-called basins of convergence [20] to explore the optimal initial conditions for which the numerical method is faster and accurate (see, e.g., [21–24]). Moreover, using the probability density function, we shall analyze the influence of the free parameters on the convergence of the Newton–Raphson scheme. The fractal degree of the basin diagram will be investigated through the basin entropy and the boundary basin entropy introduced recently by Daza et al. [25–27].

The remainder of this paper is organized as follows. In Section 2, the derivation of the generalized potential along with the new approximate potential is presented. Applying the standard linear stability analysis, in Section 3, the existence and stability of the libration points of the system are calculated as a function of two parameters α and δ related to the contribution of higher-order terms. In Section 4, the Newton–Raphson basins of convergence are presented using color code diagrams. Also, we show the biparametric evolution of the basin entropy, the boundary basin entropy, and the uncertainty dimension as a function of α and δ. Finally, in Section 5, we present the main conclusions of our numerical study.

2. The Model Potential

As already pointed out in the Introduction, in a previous paper [13], we derived a generalization of the Hénon–Heiles potential through a Taylor series expansion up to the seventh order of a generic potential with axial and reflection symmetries. The effective potential is of the form $V(r,z) = U(r,z) + L^2/2r^2$, where r and z denote the radial distance and height of the usual cylindrical coordinates, with $V(r,z) = V(r,-z)$. The seventh-order approximate potential can be written as

$$\begin{aligned} V(\xi,z) \approx{}& a_1\xi^4 + z^4\left(a_2 + b_2\xi + c_3\xi^2 + d_4\xi^3\right) + z^2 \\ &\times \left(a_3\xi^2 + b_3\xi^3 + c_4\xi^4 + d_3\xi^5 + \omega_2^2 + \xi\varepsilon\right) \\ &+ \beta\xi^3 + b_1\xi^5 + c_1\xi^6 + z^6\left(c_2 + d_2\xi\right) \\ &+ d_1\xi^7 + \xi^2\omega_1^2, \end{aligned} \tag{3}$$

with

$$\xi = r - r_0,$$

$$\omega_1^2 = \frac{3L_z^2}{2r_0^4} + \frac{1}{2}\frac{\partial^2 V_{\text{eff}}}{\partial r^2}\Big|_*,$$

$$\omega_2^2 = \frac{1}{2}\frac{\partial^2 V_{\text{eff}}}{\partial z^2}\Big|_*,$$

$$\varepsilon = -\frac{1}{2}\frac{\partial^3 V_{\text{eff}}}{\partial r\partial z^2}\Big|_*,$$

$$\beta = -\frac{2L_z^2}{r_0^5} + \frac{1}{6}\frac{\partial^3 V_{\text{eff}}}{\partial r^3}\Big|_*,$$

$$a_1 = \frac{5L_z^2}{2r_0^6} + \frac{1}{24}\frac{\partial^4 V_{\text{eff}}}{\partial r^4}\Big|_*,$$

$$a_2 = \frac{1}{24}\frac{\partial^4 V_{\text{eff}}}{\partial z^4}\Big|_*,$$

$$a_3 = \frac{1}{4}\frac{\partial^4 V_{\text{eff}}}{\partial r^2\partial z^2}\Big|_*,$$

$$b_1 = -\frac{3L_z^2}{r_0^7} + \frac{1}{120}\frac{\partial^5 V_{\text{eff}}}{\partial r^5}\Big|_*,$$

$$b_2 = \frac{1}{24}\frac{\partial^5 V_{\text{eff}}}{\partial r\partial z^4}\Big|_*,$$

$$b_3 = \frac{1}{12}\frac{\partial^5 V_{\text{eff}}}{\partial r^3\partial z^2}\Big|_*.$$

$$c_1 = \frac{7L_z^2}{12r_0^8} + \frac{1}{720}\frac{\partial^6 V_{\text{eff}}}{\partial r^6}\Big|_*,$$

$$c_2 = \frac{1}{720}\frac{\partial^6 V_{\text{eff}}}{\partial z^6}\Big|_*,$$

$$c_3 = \frac{1}{48}\frac{\partial^6 V_{\text{eff}}}{\partial r^2\partial z^4}\Big|_*,$$

$$
\begin{aligned}
c_4 &= \frac{1}{48}\frac{\partial^6 V_{\text{eff}}}{\partial r^4 \partial z^2}\Big|_*, \\
d_1 &= -\frac{4L_z^2}{r_0^9} + \frac{1}{5040}\frac{\partial^7 V_{\text{eff}}}{\partial r^7}\Big|_*, \\
d_2 &= \frac{1}{720}\frac{\partial^7 V_{\text{eff}}}{\partial r \partial z^6}\Big|_*, \\
d_3 &= \frac{1}{240}\frac{\partial^7 V_{\text{eff}}}{\partial r^5 \partial z^2}\Big|_*, \\
d_4 &= \frac{1}{144}\frac{\partial^7 V_{\text{eff}}}{\partial r^3 \partial z^4}\Big|_*,
\end{aligned}
\tag{4}
$$

where $|_*$ denotes evaluation at $(r_0, 0)$.

It should be pointed out that, unlike our previous study, in the present paper, we redefine the constant factors of the polynomial with two main objectives: first, we introduce two arbitrary parameters α and β, such that, setting $\alpha = \delta = 0$, the new potential reduces to the well-known classical Hénon–Heiles potential, and, second, we aim to obtain a large spectrum of fixed points. This last process was carried out numerically by varying each coefficient and observing the total number of fixed points until obtaining the combination that exhibits the richest dynamics for the system. The specific replacements are as follows: $z \longrightarrow x$, $\xi \longrightarrow y$, $a_1 = a_2 = b_1 = -b_2 = -b_3 = -\delta$, $a_3 = -2\delta$, $c_1 = c_2 = d_1 = d_2 = d_3 = d_4 = 2\alpha$, $c_3 = c_4 = \alpha$, $\omega_1 = \omega_2 = 1/\sqrt{2}$, $\beta = -1/3$, and $\varepsilon = 1$.

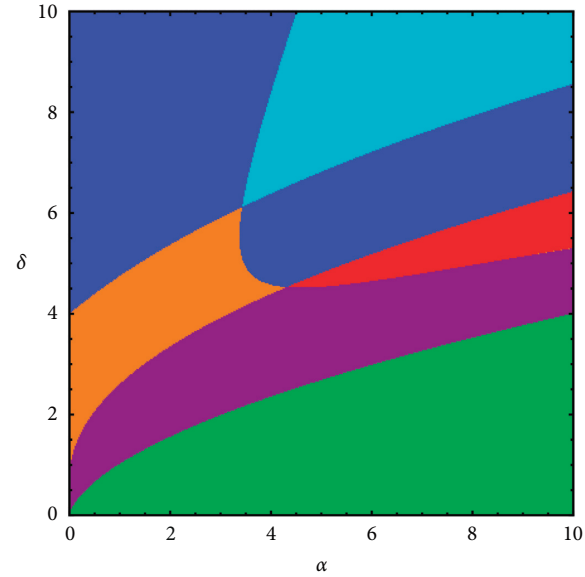

Figure 1: Color basins on the (α, δ)-plane, corresponding to different number of equilibrium points. 4 points (green); 6 points (purple); 8 points (red); 10 points (orange); 12 points (blue); 14 points (cyan).

Therefore, after applying the previous replacements into equation (3), the final potential reads

$$
\begin{aligned}
V(x, y) = {} & \frac{1}{6}\left(3x^2 + 3y^2 + 6x^2 y - 2y^3\right) \\
& + \alpha\left[2x^6(y+1) + x^4 y^2 (2y+1) + x^2 y^4 \times (2y+1) + 2y^6 (y+1)\right] \\
& + \delta\left[x^4(y-1) + x^2(y-2)y^2 - y^4(y+1)\right].
\end{aligned}
\tag{5}
$$

In the next sections, the main properties and characteristics of the new seventh-order potential are analyzed.

3. Equilibrium Points

The number of points of equilibrium is a function of the values of the parameters α and δ. Our analysis suggests that when $\alpha \in [0, 10]$ and $\delta \in [0, 10]$, we have six cases, depending on the total number of libration points. In Figure 1, we present the color basins on the (α, δ)-plane which correspond to a different number of points of equilibrium. It is interesting to note that in all cases the system has always an even number of libration points. Moreover, it is observed that the number of equilibria becomes mainly affected by the two parameters (α, δ) since the basins do not form vertical or horizontal bands.

Figure 2 shows the equilibrium positions, for eight cases, with values of α and δ, corresponding to all possible combinations of libration points. The coordinates of the libration points are presented as the intersection points of the curves $V_x = 0$ (green lines) and $V_y = 0$ (blue lines). We should note that in Figure 1 we have seen that there exist two basins corresponding to 12 points of equilibrium. It turns out that the geometry of the curves $V_x = 0$ and $V_y = 0$, as well as the locations of the equilibrium points, is different in each case. Therefore, we have eight different cases (counting also the classical HH system with $\alpha = \delta = 0$), regarding the total number of libration points.

Once the coordinates of the equilibrium conditions (x_0, y_0) are determined, one can also study their linear stability. The linear stability or instability of a libration point is obtained through the following characteristic equation:

$$
\lambda^4 + \left(V_{xx} + V_{yy}\right)\lambda^2 + V_{xx}V_{yy} - V_{xy}^2 = 0, \tag{6}
$$

where V_{xx}, V_{yy}, and V_{xy} denote the second-order partial differentials of the potential $V(x, y)$ with respect to the subindex variable.

When the quartic equation (6) has four pure imaginary roots, the respective point of equilibrium is linearly stable. The existence of four pure imaginary roots is secured by the three following conditions:

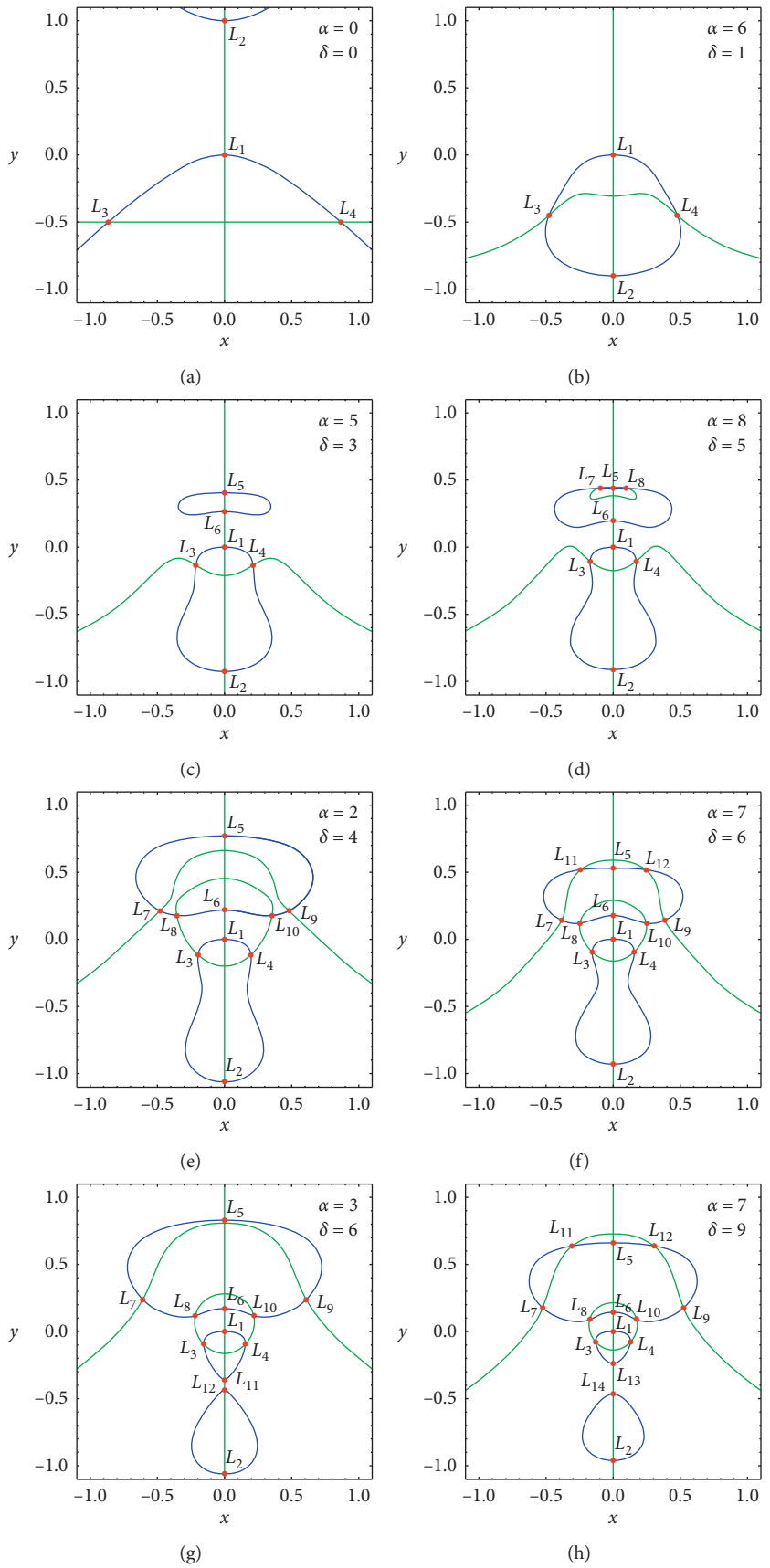

FIGURE 2: Contours of the equations $V_x = 0$ (green) and $V_y = 0$ (blue). The intersection points (red dots) designate the positions of the equilibrium points $(L_i, i = 1, \ldots, 14)$, for different values of α and δ, corresponding to the eight different cases.

$$V_{xx} + V_{yy} > 0,$$
$$V_{xx}V_{yy} - V_{xy}^2 > 0, \quad (7)$$
$$\left(V_{xx} + V_{yy}\right)^2 - 4\left(V_{xx}V_{yy} - V_{xy}^2\right) \geq 0,$$

which must simultaneously be fulfilled.

Our computations indicate the following:

(i) When 4 equilibria exist, only L_1 is linearly stable, while the rest of them are linearly unstable

(ii) When 6 equilibria exist, only L_1 and L_5 are linearly stable, while the rest of them are linearly unstable

(iii) When 8 equilibria exist, only L_1, L_7, and L_8 are linearly stable, while the rest of them are linearly unstable

(iv) When 10 equilibria exist, only L_1 and L_5 are linearly stable, while the rest of them are linearly unstable

(v) When 12 equilibria exist (the case with the middle blue basin in Figure 1), only L_1, L_{11}, and L_{12} are linearly stable, while the rest of them are linearly unstable

(vi) When 12 equilibria exist (the case with the upper blue basin in Figure 1), only L_1 and L_5 are linearly stable, while the rest of them are linearly unstable

(vii) When 14 equilibria exist, only L_1, L_{11}, and L_{12} are linearly stable, while the rest of them are linearly unstable

The general conclusion is that the point equilibrium located at the origin with $x = y = 0$ is always linearly stable, regardless of the particular values of the parameters α and δ.

4. The Newton–Raphson Basins of Convergence

Knowing the equilibrium positions of a dynamical system is very important. However, in many cases (including our modified HH system), the coordinates of the libration points cannot be derived analytically. Then, the equilibrium solutions can be derived only by employing numerical methods. One of the easiest ways of solving numerically a system of equations (in our case the coupled system $V_x = V_y = 0$) is by using the Newton–Raphson (NR) iterative scheme.

$$x_{n+1} = x_n - \left(\frac{V_x V_{yy} - V_y V_{xy}}{V_{yy}V_{xx} - V_{xy}^2}\right)_{(x_n, y_n)},$$
$$y_{n+1} = y_n + \left(\frac{V_x V_{yx} - V_y V_{xx}}{V_{yy}V_{xx} - V_{xy}^2}\right)_{(x_n, y_n)}. \quad (8)$$

It is a well-known fact that the outcomes of any numerical method are influenced by the choice of the starting conditions. In particular, both the speed and the accuracy of any numerical scheme fully depend on the chosen initial conditions. There exist starting conditions for which the iterator diverges, while there also exist starting conditions leading to one of the roots of the system. The ideal initial conditions (regarding fast convergence and accuracy) form the so-called NR basins of convergence (NR-BoC). This is exactly the importance of identifying the location of the NR-BoC of a dynamical system.

In Figures 3(a)–3(h), we present the structure of the NR-BoC on the configuration (x, y)-plane, for the eight different cases, classified in terms of the number of equilibrium points. In all cases, the values of the parameters α and δ are the same as those of the panels of Figure 2. For our computations, the NR scheme was allowed to perform up to 500 iterations, while the desired accuracy, regarding the (x, y) equilibrium positions, was set to 10^{-16}.

From the basin diagrams of Figure 3, it is observed that many structures on the configuration (x, y)-plane are very complicated. Moreover, some of the NR-BoC have a finite domain, while others extend to infinity. Nevertheless, in all cases, there exist well-defined structures containing ideal starting conditions for the numerical scheme. In Figure 4, we display color maps showing how the required number of iterations N is distributed on the (x, y)-plane. Furthermore, in Figure 5, we provide the probability distributions.

The histograms displayed in Figure 5 with the probability distributions may provide additional information about the properties of the modified NR method. For example, the right-hand side of the histograms can be fitted by using the well-known Laplace distribution or double exponential distribution, which is the simplest and most suitable choice [28–30].

The probability density function (PDF) for the double exponential distribution reads

$$P(N|l, d) = \frac{1}{2d} \begin{cases} \exp\left(-\dfrac{l - N}{d}\right), & \text{if } N < l, \\ \exp\left(-\dfrac{N - l}{d}\right), & \text{if } N \geq l, \end{cases} \quad (9)$$

where the quantities $d > 0$ and l are known as the diversity and the location parameter, respectively. Since we are interested only in the probability tails for the histograms, we need only the $N \geq l$ part of the PDF.

We aim to understand how the parameters α and δ influence the convergence properties of the NR scheme. To this end, we defined a 1024×1024 grid of (α, δ) values and, for each pair, we used the NR scheme for classifying a set of 300×300 (x_0, y_0) initial conditions, on the configuration plane and in particular inside the squared region $-5 \leq x, y \leq +5$.

In Figure 6(a), we present the evolution of the average number of iterations $\langle N \rangle$, needed by the NR method for providing the coordinates of the equilibria with the desired accuracy. Figures 6(b) and 6(c) depict the distributions of the location parameter (l) and the diversity (d) of the Laplace PDF. Our results strongly indicate that the Laplace PDF is an excellent candidate for fitting the probability histograms, if we take into account the fact that the numerical values of $\langle N \rangle$ and l are very close: $|l - \langle N \rangle| \leq 2$). Additionally, from the distribution of the diversity d, shown in Figure 6(d), we

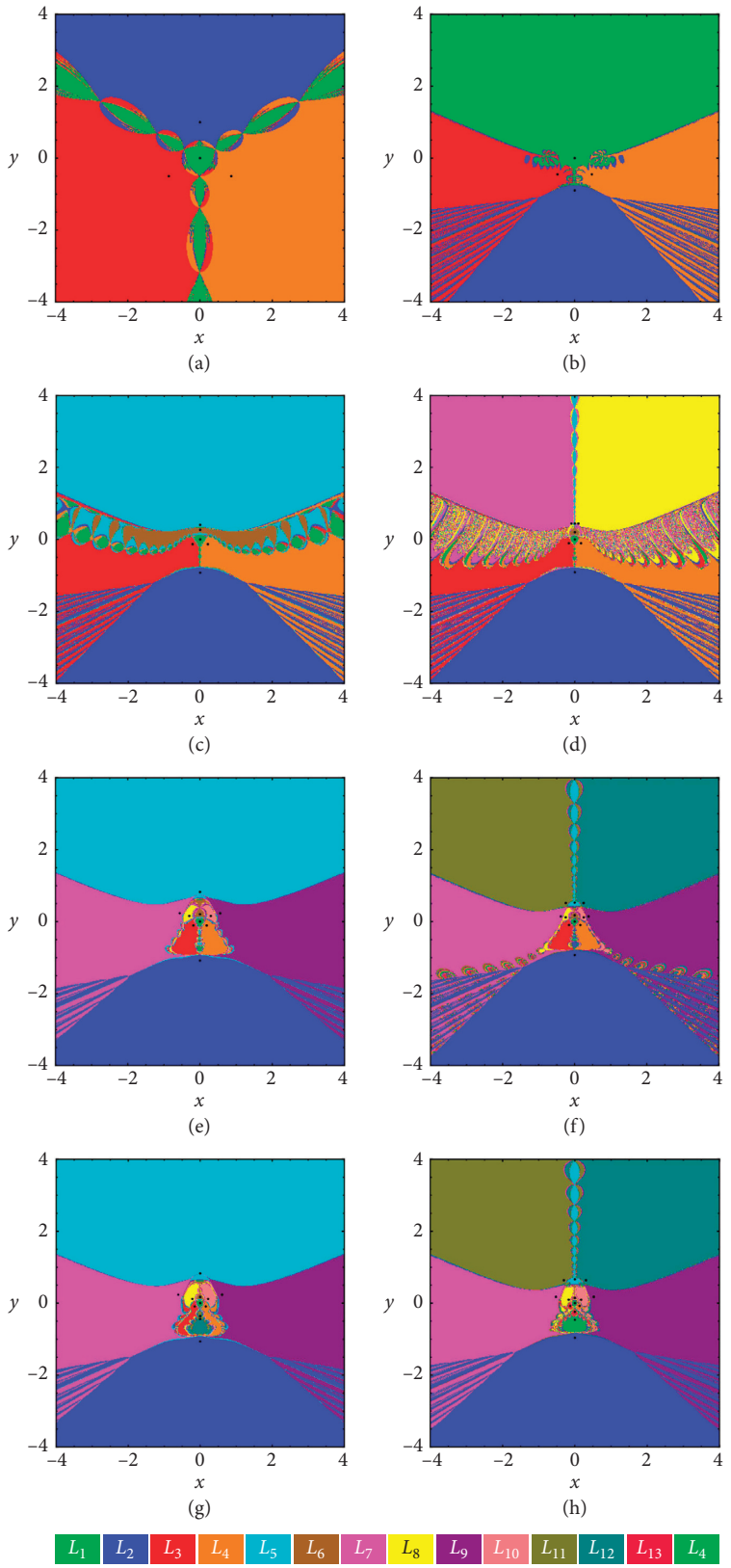

FIGURE 3: Basin color diagrams of the NR-BoC on the configuration (x, y)-plane. The values of the parameters α and δ are as in the respective panels of Figure 2. The positions of the libration points are marked, using black dots.

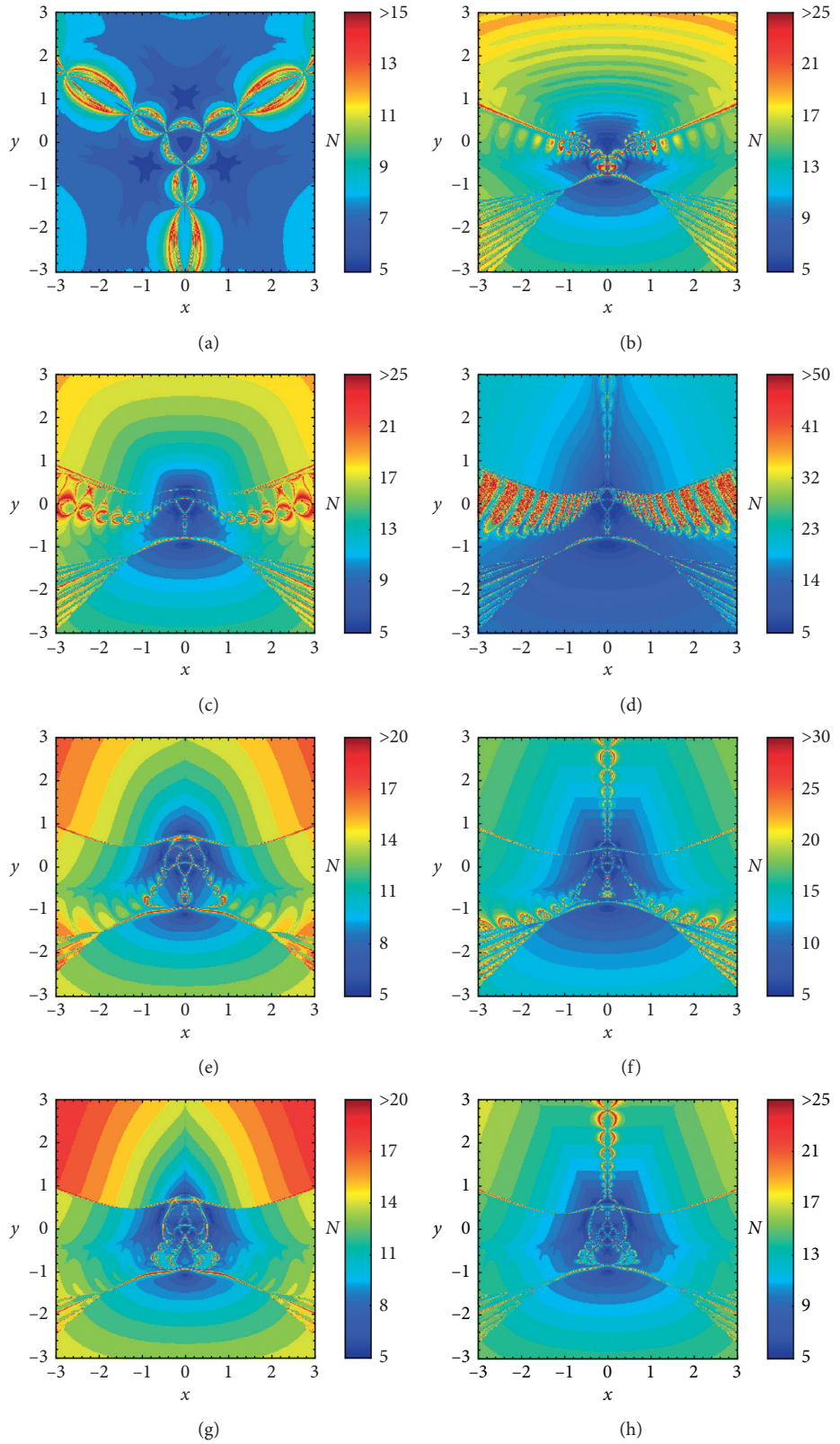

FIGURE 4: Color maps showing the distribution of the required number of iterations N, on the configuration (x, y)-plane. The values of the parameters α and δ are as in the respective panels of Figure 2.

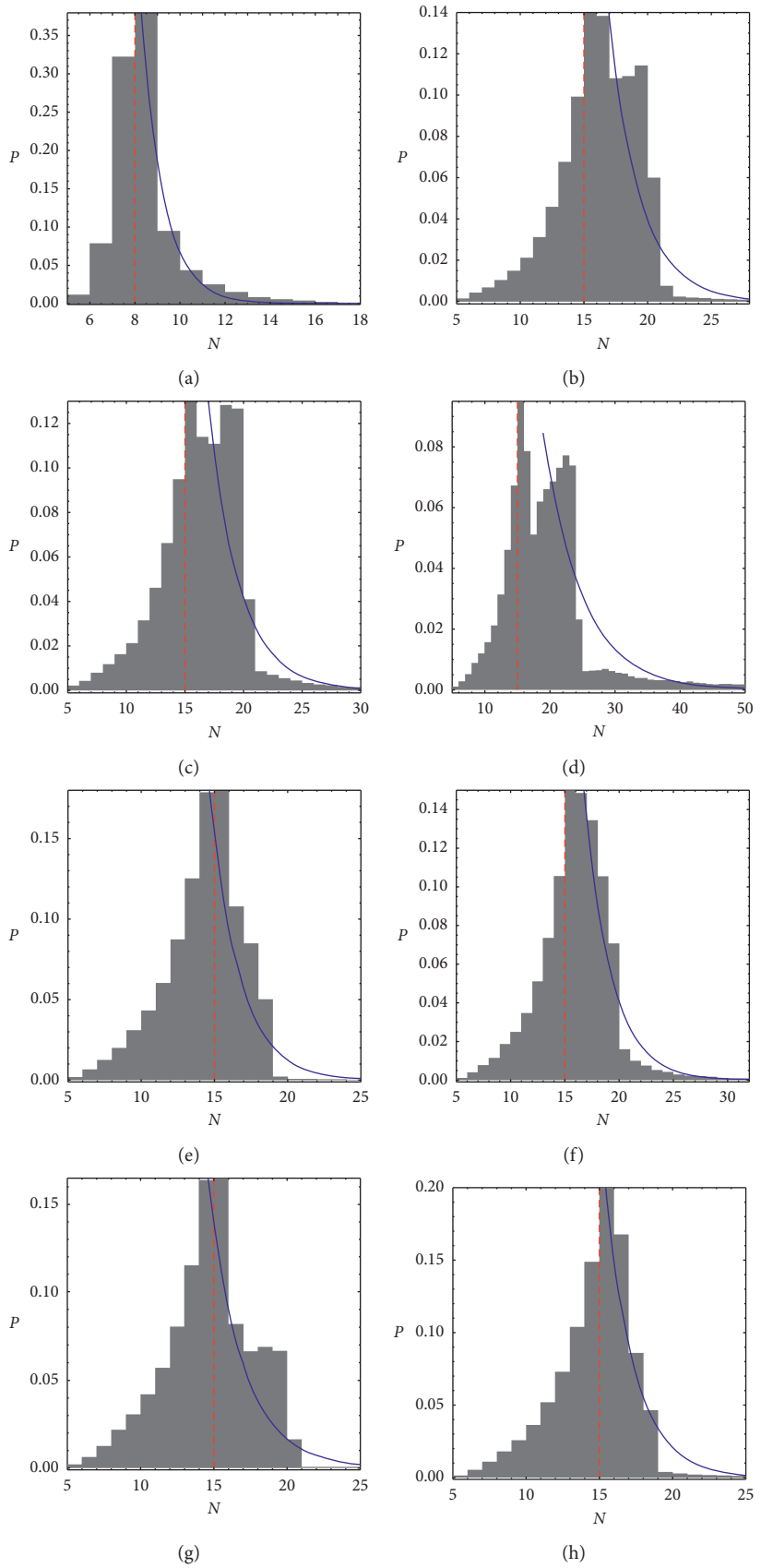

Figure 5: Probability histograms for the eight cases of Figure 3. The most probable number of iterations is indicated by dashed, vertical, red lines, while the blue lines correspond to the best fitting curves.

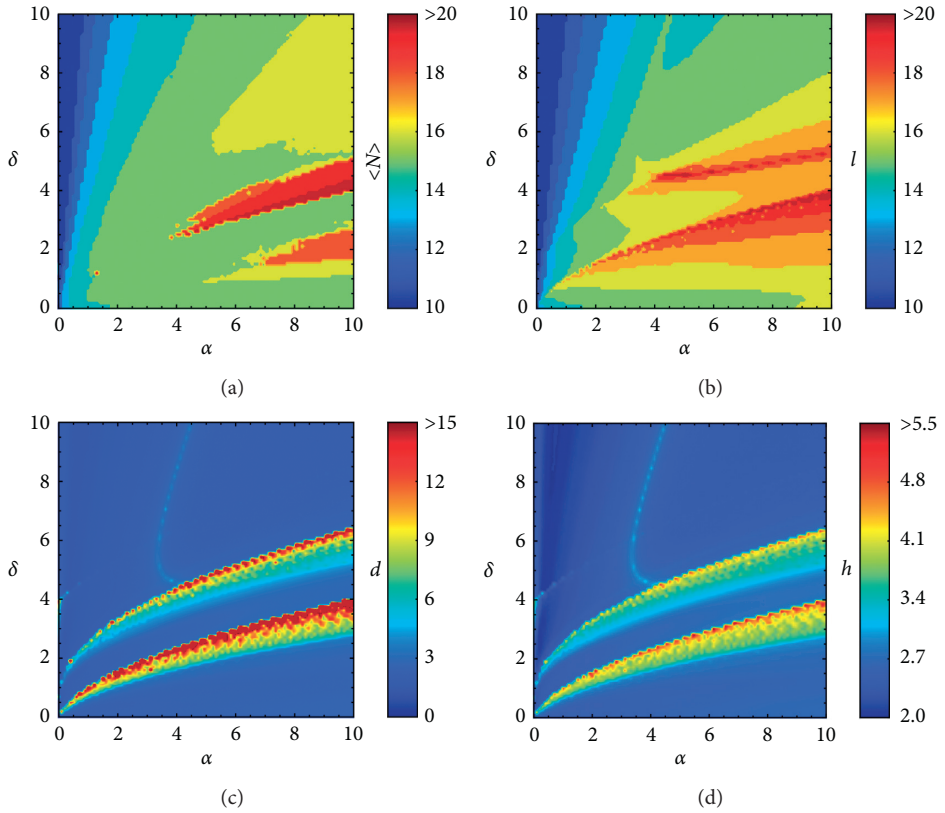

Figure 6: Biparametric evolution of (a) $\langle N \rangle$, (b) l, (c) d, (d) and h, as a function of (α, δ).

can conclude that the probability histograms are very well organized around the average value $\langle N \rangle$, since in most of the cases the numerical value of the diversity is relatively low ($d < 5$). Finally, Figure 6(d), we show how the differential entropy, defined as $h = 1 + \ln(2d)$, evolves as a function of the values (α, δ). It is seen that both quantities d and h have very similar parametric evolutions. If we take into consideration the combined information from all four panels of Figure 6, we can argue that the NR method works faster when the system has either 4, 10, 12, or 14 points of equilibrium, while when 6 or 8 libration points exist, the convergence of the NR scheme is considerably slower.

Previously, in Figure 3, we have seen that there are certain regions on the (x, y)-plane, where using the corresponding starting conditions it is very difficult to know beforehand to which point of equilibrium they are going to converge. These regions are composed of a fractal mixture of final states (equilibria), and they are of course the exact opposite of the basins of convergence. In order to obtain quantitative information about the fractal degree of the BCs on the (x, y)-plane, we shall compute the basin entropy S_b [25, 27]. This modern tool indicates the fractal degree of a basin diagram by examining its topological properties. In Figure 7(a), we show the distribution of the numerical values of S_b, as a function of (α, δ). Now we can conclude, without any doubt, that when the system has eight points of equilibrium, we encounter the most fractal NR-BoC, while the fractal degree is considerably lower for a higher number of libration points.

Unfortunately, the transition between smooth and fractal boundaries cannot be determined by the basin entropy S_b. The main reason for this drawback is that the basin entropy addresses the uncertainty to link a set of initial conditions to their corresponding final states. Therefore, if we are interested in detecting small variations in the basin boundary, we must use another indicator, the boundary basin entropy S_{bb}, which was introduced for the first time in 2016 by Daza et al. [25]. For obtaining the boundary basin entropy, all we have to do is to divide the total entropy between the number of cells that fall in the boundaries of the convergence basins. This tool gives us the possibility to safely conclude that if the basin boundary is fractal or not, by using the so-called "log 2 criterion," with the sufficient condition, if $S_{bb} > \ln 2$, then the boundary is certainly fractal. The distribution of the values of S_{bb}, as a function of (α, δ), is given in Figure 7(b). We see that when eight points of equilibrium exist, the basin boundaries on the (x, y)-plane are always fractal, while on the other hand when the system has only 4 libration points, the basin boundary entropy exhibits the smaller values when compared to the other cases.

Finally, another standard way to measure the level of fractality of a basin diagram is by computing the fractal dimension [31]. At this point, it is important to emphasize that the results obtained with the basin boundary entropy S_{bb} and the fractal dimension D_0 are related but they do not necessarily have to be the same because the first numerical tool allows us to assess easily that some boundaries are

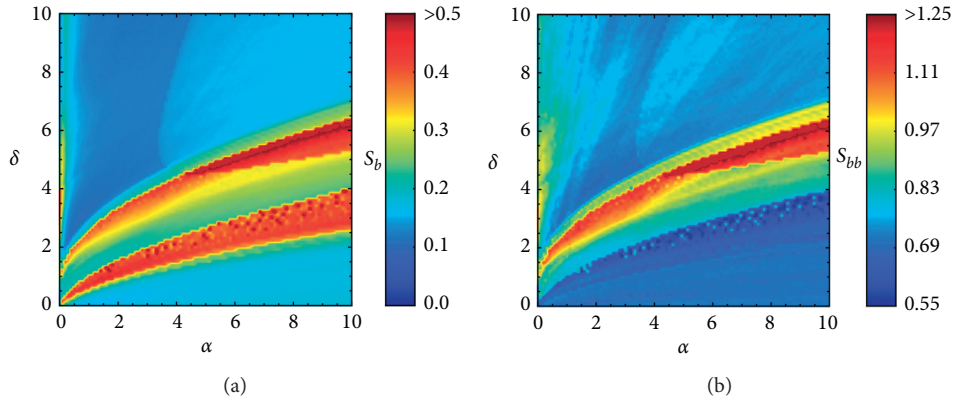

Figure 7: Biparametric evolution of the (a) basin entropy S_b and (b) boundary basin entropy S_{bb}, as a function of (α, δ).

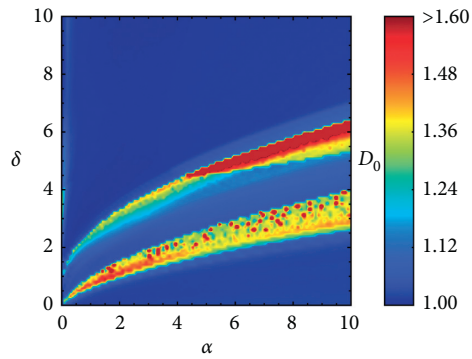

Figure 8: Biparametric evolution of the uncertainty dimension D_0, as a function of (α, δ).

fractal, while the second one provides information about the whole basin, since the fractal dimension is an intrinsic property of the system [32, 33]. In Figure 8, we present the dependence of the uncertainty dimension D_0 with the parameters α and δ. As usual, when the fractal dimension equals one, the fractality is zero, while if its value tends to 2, it suggests complete fractality of the respective basin diagram. It is seen that D_0 displays the highest values when eight points of equilibrium exist, while the lowest values are observed for the cases with 10, 12, and 14 libration points. One should certainly note the large similarity on the parametric evolutionary pattern of D_0 with respect to that of the basin entropy S_b. This similarity can be explained by considering that these two computer-based analysis techniques are grounded on box-counting methodologies.

5. Discussion

In this work, we explored, using numerical techniques, the equilibrium points and the convergence properties of the associated basins of convergence of a seventh-order generalized Hénon–Heiles potential. The Newton–Raphson root method was used for locating the (x, y) coordinates of the points of equilibrium, while their linear stability was also revealed as a function of both parameters α and δ. Modern color-coded plots were deployed for illustrating the convergence basins on the (x, y)-plane. Finally, we managed to determine how the parameters α and δ affect both the accuracy and speed of the NR method, while the fractal degree of the respective basin diagrams was estimated by computing the (boundary) basin entropy and the uncertainty dimension.

The routine of the bivariate NR scheme was coded in FORTRAN 77 (see, e.g., [34]). For the taxonomy of the starting points on the (x, y)-plane, we needed, per grid, roughly 3 minutes using a Quad-Core i7 4.0 GHz CPU. All the plots of the paper have been developed using the software Mathematica ® [35].

Data Availability

The data underlying this article will be shared by the corresponding author upon reasonable request.

Conflicts of Interest

The authors declare that they have no conflicts of interest.

Acknowledgments

This work was partially supported by COLCIENCIAS (Colombia) (Grant 8863) and by Universidad de los Llanos.

References

[1] P. Stäckel, "Eine charackteristische eigenschaft der flächen, deren linienelement gegeben wird," *Mathematische Annalen*, vol. 35, pp. 91–103, 1890.

[2] P. Stäckel, "Uber die bewegung eines punktes in einer *n*-fachen mannigfaltigkeit," *Mathematische Annalen*, vol. 42, pp. 537–563, 1893.

[3] G. Contopoulos, "On the relative motions of stars in a galaxy," *Stockholm Observatoriums Annalen*, vol. 19, p. 10, 1957.

[4] G. Contopoulos, "A third integral of motion in a galaxy:," *Zeitschrift für Astrophysik*, vol. 49, p. 273, 1960.

[5] G. Contopoulos, "An application of a third integral of motion," *Observatory*, vol. 82, p. 80, 1962.

[6] G. Contopoulos, "On the existence of a third integral of motion," *The Astronomical Journal*, vol. 68, p. 1, 1963.

[7] G. Contopoulos, "Some applications of a third integral of motion," *The Astronomical Journal*, vol. 68, p. 70, 1963.

[8] M. Hénon and C. Heiles, "The applicability of the third integral of motion: some numerical experiments," *The Astronomical Journal*, vol. 69, pp. 73–79, 1964.
[9] G. Contopoulos, *Order and Chaos in Dynamical Astronomy*, p. 435, Springer, Berlin, Germany, 2002.
[10] F. Verhulst, "Discrete symmetric dynamical systems at the main resonances with application to axi-symmetric galaxies," *Philosophical Transactions of the Royal Society of London. Series A, Mathematical and Physical Sciences*, vol. 290, no. 1375, pp. 435–465, 1979.
[11] E. E. Zotos, A. Riaño-Doncel, and F. L. Dubeibe, "Basins of convergence of equilibrium points in the generalized Hénon-Heiles system," *International Journal of Non-linear Mechanics*, vol. 99, pp. 218–228, 2018.
[12] F. L. Dubeibe, A. Riaño-Doncel, and E. E. Zotos, "Dynamical analysis of bounded and unbounded orbits in a generalized Hénon-Heiles system," *Physics Letters A*, vol. 382, no. 13, pp. 904–910, 2018.
[13] F. L. Dubeibe, E. E. Zotos, and W. Chen, "On the dynamics of a seventh-order generalized Hénon-Heiles potential," *Results in Physics*, vol. 18, Article ID 103278, 2020.
[14] G. Contopoulos, "A review of the "third" integral," *Mathematics in Engineering*, vol. 2, no. 3, pp. 472–511, 2020.
[15] E. Caurier and B. Grammaticos, "Extreme level repulsion for chaotic quantum Hamiltonians," *Physics Letters A*, vol. 136, no. 7-8, pp. 387–390, 1989.
[16] B. A. Waite and W. H. Miller, "Mode specificity in unimolecular reaction dynamics: the Henon-Heiles potential energy surface," *The Journal of Chemical Physics*, vol. 74, no. 7, pp. 3910–3915, 1981.
[17] F. Kokubun, "Gravitational waves from the Hénon-Heiles system," *Physical Review D*, vol. 57, no. 4, pp. 2610–2612, 1998.
[18] K. Veselý and J. Podolský, "Chaos in a modified Hénon-Heiles system describing geodesics in gravitational waves," *Physics Letters A*, vol. 271, no. 5-6, pp. 368–376, 2000.
[19] W. M. Vieira and P. S. Letelier, "Chaos around a hénon-heiles-inspired exact perturbation of a black hole," *Physical Review Letters*, vol. 76, no. 9, pp. 1409–1412, 1996.
[20] H. E. Nusse and J. A. Yorke, "Basins of attraction," *Science*, vol. 271, no. 5254, pp. 1376–1380, 1996.
[21] C. N. Douskos, "Collinear equilibrium points of Hill's problem with radiation and oblateness and their fractal basins of attraction," *Astrophysics and Space Science*, vol. 326, no. 2, pp. 263–271, 2010.
[22] T. J. Kalvouridis and M. C. Gousidou-Koutita, "Basins of attraction in the copenhagen problem where the primaries are magnetic dipoles," *Applied Mathematics*, vol. 3, no. 6, pp. 541–548, 2012.
[23] E. E. Zotos, "Fractal basins of attraction in the planar circular restricted three-body problem with oblateness and radiation pressure," *Astrophysics and Space Science*, vol. 361, no. 6, p. 181, 2016.
[24] E. E. Zotos, "Basins of convergence of equilibrium points in the pseudo-Newtonian planar circular restricted three-body problem," *Astrophysics and Space Science*, vol. 362, no. 10, p. 195, 2017.
[25] A. Daza, A. Wagemakers, B. Georgeot, D. Guéry-Odelin, and M. A. F. Sanjuán, "Basin entropy: a new tool to analyze uncertainty in dynamical systems," *Scientific Reports*, vol. 6, no. 1, Article ID 31416, 2016.
[26] A. Daza, B. Georgeot, D. Guéry-Odelin, A. Wagemakers, and M. A. F. Sanjuán, "Chaotic dynamics and fractal structures in experiments with cold atoms," *Physical Review A*, vol. 95, Article ID 13629, 2017.
[27] A. Daza, A. Wagemakers, B. Georgeot, D. Guéry-Odelin, and M. A. F. Sanjuán, "Basin entropy, a measure of final state unpredictability and its application to the chaotic scattering of cold atoms," in *Chaotic, Fractional, and Complex Dynamics: New Insights and Perspectives, Understanding Complex Systems*, M. Edelman, Ed., Springer International Publishing AG, Berlin, Germany, 2018.
[28] A. E. Motter and Y. C. Lai, "Dissipative chaotic scattering," *Physical Review E*, vol. 65, Article ID 15205, 2001.
[29] J. M. Seoane, J. Aguirre, M. A. F. Sanjuán, and Y.-C. Lai, "Basin topology in dissipative chaotic scattering," *Chaos: An Interdisciplinary Journal of Nonlinear Science*, vol. 16, no. 2, Article ID 23101, 2006.
[30] J. M. Seoane and M. A. F. Sanjuán, "Exponential decay and scaling laws in noisy chaotic scattering," *Physics Letters A*, vol. 372, no. 2, pp. 110–116, 2008.
[31] E. Ott, *Chaos in Dynamical Systems*, Cambridge University Press, Cambridge, UK, 1993.
[32] J. Aguirre, J. C. Vallejo, and M. A. F. Sanjuán, "Wada basins and chaotic invariant sets in the Hénon-Heiles system," *Physical Review E*, vol. 64, Article ID 66208, 2001.
[33] J. Aguirre, R. L. Viana, and M. A. F. Sanjuán, "Fractal Structures in nonlinear dynamics," *Reviews of Modern Physics*, vol. 81, no. 1, pp. 333–386, 2009.
[34] H. P. Press, S. A. Teukolsky, W. T. Vetterling, and B. P. Flannery, *Numerical Recipes in FORTRAN 77*, Cambridge University Press, Cambridge, UK, 2nd edition, 1992.
[35] S. Wolfram, *The Mathematica Book*, Wolfram Media, Champaign, IL, USA, Fifth edition, 2003.

Hindawi
Advances in Astronomy
Volume 2021, Article ID 6660028, 11 pages
https://doi.org/10.1155/2021/6660028

Research Article

The Stability of Certain Motion of a Charged Gyrostat in Newtonian Force Field

A. A. Elmandouh [1,2] **and Fatimah H. Alsaad** [1]

[1] *Department of Mathematics and Statistics, College of Science, King Faisal University, P.O. Box 400, Al-Ahsaa 31982, Saudi Arabia*
[2] *Department of Mathematics, Faculty of Science, Mansoura University, Mansoura 35516, Egypt*

Correspondence should be addressed to A. A. Elmandouh; aelmandouh@kfu.edu.sa

Received 7 November 2020; Revised 1 December 2020; Accepted 4 February 2021; Published 22 February 2021

Academic Editor: Elbaz Abouelmagd

This work aims to study the stability of certain motions of a rigid body rotating about its fixed point and carrying a rotor that rotates with constant angular velocity about an axis parallel to one of the principal axes. This motion is presumed to take place due to the combined influence of the magnetic field and the Newtonian force field. The equations of motion are deduced, and moreover, they are expressed as a Lie–Poisson Hamilton system. The permanent rotations are calculated and interpreted mechanically. The sufficient conditions for instability are presented employing the linear approximation method. The energy-Casimir method is applied to gain sufficient conditions for stability. The regions of linear stability and Lyapunov stability are illustrated graphically for certain values of the parameters.

1. Introduction

A gyrostat is a simple multibody which consists of a rigid body and other bodies which are usually called rotors moving in such a way that their motion does not change the distribution of mass for the gyrostat [1]. The gyrostat is also well known in the literature as a *dual-spin* body due to the motion of the two bodies which compose the gyrostat. Volterra [2] had first introduced the notions of gyrostat when he strived to study the motion of the Earth's polar axis and interpret variations in the Earth's latitude by means of the internal motion which keeps the mass distribution of the planet fixed. This model is used in a variety of numerous applications in different branches of physics besides their classical applications in astronomy and mechanics. For example, the gyrostat was utilized as a model of the Earth that takes into account some stationary transport processes on it [2], as a model of the atmosphere and of rotating fluid (e.g., [3]) and as a controlling device in satellite dynamics (e.g., [4]).

Most of the works related to the rigid body and its extension to gyrostat can be assorted into three categories. The first is the *integrability problem* and the searching for the complete set of the first integrals of the motions. Borisov and Mamaev [5] contain most of those integrable problems up to 2001, and some cases were presented by several authors (see, e.g., [6–10]). The second category regards the problem of study *periodic solutions, bifurcation, and chaos* in some problems of rigid body-gyrostat (see, e.g., [11–14]). The third one is the *stability problem* of the equilibria in the dynamics of a rigid body-gyrostat moving in an orbit or about its fixed point (see, e.g., [15–23]).

The current work is interested in studying the stability of permanent rotations for the motion of a charged gyrostat moving due to the combined influence of the magnetic field and Newtonian force field. This work is regarded as an extension of some previous works. In [17], Iñarrea et al. examined the stability of permanent rotations of a heavy rigid body carrying a rotor that rotates about one of the principal axes by a constant angular velocity. This study was

followed by Elmandouh who studied this problem in the case of a charged heavy gyrostat [20]. Vera studied the stability of relative equilibrium for a gyrostat in Newtonian force field [19].

This work is organized as follows: in Section 2, we deduce equations of the motion and rewrite them as a Lie–Poisson Hamilton system. Section 3 contains the permanent rotations and their interpretation mechanically. In Section 4, we study the stability of those permanent rotations by applying both methods linear approximation method and energy-Casimir method. Section 5 involves the results found.

2. Equations of Motion

We consider the rotation of a charged rigid body about its fixed point and assume this body carries an axisymmetric rotor aligning along one of the principal axes of the body and rotating with a constant angular velocity. This motion is assumed to happen due to the combined influence of a homogeneous magnetic field $\vec{\mathcal{H}}$ and Newtonian forces field. For motion description, we choose two frames $O\xi_1\zeta_1\eta_1$ and $O\xi_2\zeta_2\eta_2$ fixed in the space and in the body, respectively (see Figure 1). Furthermore, the body frame $O\xi_2\zeta_2\eta_2$ is assumed to be the principal axes of the inertia at the fixed point O, and consequently, the principal inertia matrix of the gyrostat is $\mathbb{I} = \mathrm{diag}(A, B, C)$. Let $\vec{\gamma} = (\gamma_1, \gamma_2, \gamma_3)$ and $\vec{\omega} = (\omega_1, \omega_2, \omega_3)$ are the unit vector along $O\eta_1$-axis and the angular velocity of the gyrostat, respectively. The two vectors $\vec{\omega}$ and $\vec{\gamma}$ are referred to the body frame.

The vector $\vec{\gamma}$ is written in terms of Eulerian angle as illustrated in [1]:

$$\vec{\gamma} = (\gamma_1, \gamma_2, \gamma_3) = (\sin\theta\sin\varphi,\ \sin\theta\cos\varphi,\ \cos\theta), \tag{1}$$

where θ, ψ, and φ indicate the angle of nutation between the two axes $O\eta_2$ and $O\eta_1$, the precession angle about the $O\eta_2$ axis, and the angle of proper rotation, respectively. The homogeneous magnetic field $\vec{\mathcal{N}}$ is presumed to be a constant and influences in the direction of the $O\eta_1$-axis, and therefore, it can be written as

$$\vec{\mathcal{N}} = \beta\vec{\gamma}, \tag{2}$$

where β denotes the magnitude of the magnetic field. Now, we are going to introduce the equations of the motion. The whole angular momentum of the gyrostat is

$$\vec{\mathcal{G}} = \vec{\pi} + \vec{\mathcal{K}}, \tag{3}$$

where $\vec{\pi} = \mathbb{I}\vec{\omega}$ is the angular momentum of the gyrostat when the rotor is relatively at rest and $\vec{\mathcal{K}} = (0, 0, k)$ is the gyrostatic momentum, that is, the relative angular momentum of the rotor with respect to the body. Following the theorem of angular momentum about the point O, fixed point, we obtain

$$\frac{\mathrm{d}\vec{\mathcal{G}}}{\mathrm{d}t} = \vec{\mathcal{M}}_0, \tag{4}$$

where $\vec{\mathcal{M}}_0$ indicates the total torque of the external forces about the fixed point O.

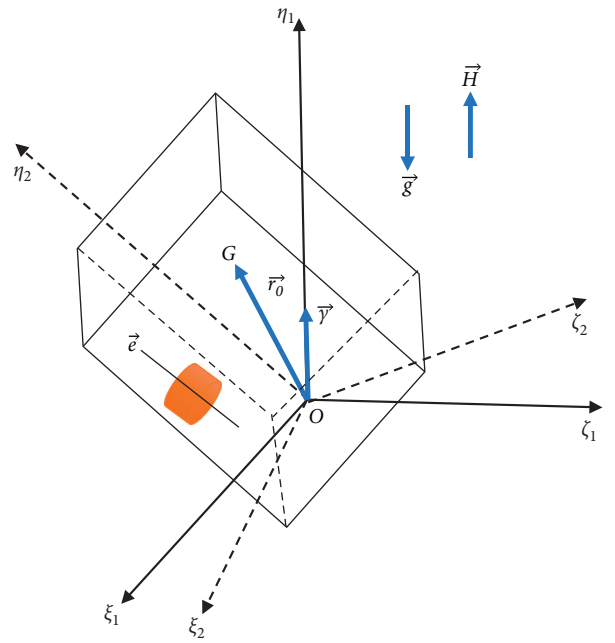

Figure 1: References frames and gyrostat.

According to [1], the potential function for the Newtonian forces field takes the following form:

$$U(\gamma_1, \gamma_2, \gamma_3) = mg\vec{r}_0 \cdot \vec{\gamma} + \frac{n}{2}\vec{\gamma} \cdot \mathbb{I}\vec{\gamma}, \tag{5}$$

where $\vec{r}_0 = (x_0, y_0, z_0)$ is the center of mass vector, and for simplicity, we assume the center of mass lies on $O\eta_2$ and $n = (3g/R)$, where R is the distance between the center of the attraction and the fixed point O (R is assumed very large compared with the dimensions of the body). The torque due to the potential forces derived from the potential function (5) is given as follows [24]:

$$\vec{\mathcal{M}}_0^1 = \vec{\gamma} \times \frac{\partial U}{\partial \vec{\gamma}} = mg\vec{\gamma} \times \vec{r}_0 + n\vec{\gamma} \times \mathbb{I}\vec{\gamma}. \tag{6}$$

Now, we calculate the torque appearing due to the magnetic field about the fixed point O. Let p be any point from the body which moves with velocity $\vec{u}(p)$, carry a charge $\mathrm{d}q$, and its position vector $\vec{r}$ with respect to the fixed point O. This point is influenced by Lorentz forces $\mathrm{d}\vec{F} = \mathrm{d}q(\vec{u} \times \vec{\mathcal{H}}) = \beta\rho\mathrm{d}V[(\vec{\omega} \times \vec{r}) \times \vec{\gamma}] = \beta\rho\mathrm{d}V\ [(\vec{\omega} \cdot \vec{\gamma})\vec{r} - (\vec{r} \cdot \vec{\gamma})\vec{\omega}]$, where ρ is the charge density and $\mathrm{d}V$ is the element's volume from the body. Hence, the torque arising due to the magnetic field takes the following form:

$$\vec{\mathcal{M}}_0^2 = \int_V \vec{r} \times \mathrm{d}\vec{F} = \vec{\omega} \times \beta\rho\int_V \vec{r}\,(\vec{r} \cdot \vec{\gamma})\mathrm{d}V = \vec{\omega} \times A\vec{\gamma}, \tag{7}$$

where A is the 3×3 constant matrix which is assumed to be $A = \mathrm{diag}(a, b, d)$ for simplicity. Thus, the total torque about the fixed point O is

$$\begin{aligned}\vec{\mathscr{M}}_0 &= \vec{\mathscr{M}}_0^1 + \vec{\mathscr{M}}_0^2 \\ &= mg\vec{\gamma} \times \vec{r}_0 + n\vec{\gamma} \times \mathbb{I}\vec{\gamma} + \vec{\omega} \times A\vec{\gamma}.\end{aligned} \tag{8}$$

Taking into account the two equations (4) and (8), the equations of motion in the body frame take the following form:

$$\dot{\vec{\pi}} = -\vec{\omega} \times (\vec{\pi} + \vec{\mu}) + mg\vec{\gamma} \times \vec{r}_0 + n\vec{\gamma} \times \mathbb{I}\vec{\gamma}, \tag{9}$$

where

$$\vec{\mu} = \vec{\mathscr{K}} + A\vec{\gamma}. \tag{10}$$

Notably, the expression (10) represents the torque of the gyroscopic forces (forces rely on the velocity). Because $\vec{\gamma}$ is a unit vector fixed in the space, we obtain

$$\dot{\vec{\gamma}} = \vec{\gamma} \times \vec{\omega}. \tag{11}$$

Despite the variables utilized in two equations (9) and (11) are not canonical, we can describe this motion by means of a Hamiltonian function in the framework of Lie–Poisson systems. The Hamiltonian function takes the following form:

$$H = \frac{1}{2}\left(\frac{\pi_1^2}{A} + \frac{\pi_2^2}{B} + \frac{\pi_3^2}{C}\right) + mgz_0\gamma_3 + \frac{n}{2}\left(A\gamma_1^2 + B\gamma_2^2 + C\gamma_3^2\right). \tag{12}$$

According to [25], we write the equations of the motion (9) and (11) as a Hamiltonian–Poisson system that is spanned by the matrix $\Pi_{\vec{\mu}}$:

$$\Pi_{\vec{\mu}} = \begin{pmatrix} 0 & -\pi_3 - \mu_3 & \pi_2 + \mu_2 & 0 & -\gamma_3 & \gamma_2 \\ \pi_3 + \mu_3 & 0 & -\pi_1 - \mu_1 & \gamma_3 & 0 & -\gamma_1 \\ -\pi_2 - \mu_2 & \pi_1 + \mu_1 & 0 & -\gamma_2 & \gamma_1 & 0 \\ 0 & -\gamma_3 & \gamma_2 & 0 & 0 & 0 \\ \gamma_3 & 0 & -\gamma_1 & 0 & 0 & 0 \\ -\gamma_2 & \gamma_1 & 0 & 0 & 0 & 0 \end{pmatrix}, \tag{13}$$

as long as the Jacobi identity is verified, i.e.,

$$\Pi_{\vec{\mu}}^{li}\partial_l\Pi_{\vec{\mu}}^{jk} + \Pi_{\vec{\mu}}^{lj}\partial_l\Pi_{\vec{\mu}}^{ki} + \Pi_{\vec{\mu}}^{lk}\partial_l\Pi_{\vec{\mu}}^{ij} = 0, \quad i, j, k = 1, 2, \ldots, 6. \tag{14}$$

Alternatively, the condition (14) is equivalently verified if the equation

$$\vec{\gamma} \cdot \nabla_{\vec{\gamma}} \times \vec{\mu} = 0, \tag{15}$$

is satisfied. By direct calculations, we can prove that vector $\vec{\mu}$, shown in (10), satisfied the condition (15), and consequently, the equations of motion (9) and (11) are rewritten as

$$\dot{\vec{Y}} = \Pi_{\vec{\mu}}\vec{\nabla}H, \tag{16}$$

where $Y = (\pi_1, \pi_2, \pi_3, \gamma_1, \gamma_2, \gamma_3)$ and $\vec{\nabla}H$ is the naive gradient of H. In addition to the Hamilton (12), this system admits two Casimirs:

$$\begin{aligned} C_1 &\coloneqq \gamma_1^2 + \gamma_2^2 + \gamma_3^2 = 1, \quad \text{geometric integral,} \\ C_2 &\coloneqq \pi_1\gamma_1 + \pi_2\gamma_2 + \pi_3\gamma_3 + \frac{1}{2}\left(a\gamma_1^2 + b\gamma_2^2 + d\gamma_3^2\right) + k\gamma_3 = \alpha_0, \quad \text{area integral,} \end{aligned} \tag{17}$$

where α_0 is a constant.

3. Permanent Rotations

To find the permanent rotations, we place $\dot{\vec{\pi}} = \dot{\vec{\gamma}} = \vec{0}$ into the two equations of motion (9) and (11); we obtain

$$\vec{\omega} \times (\vec{\pi} + \vec{\mathscr{K}} + A\vec{\gamma}) - mg\vec{\gamma} \times \vec{r}_0 - n\vec{\gamma} \times \mathbb{I}\vec{\gamma} = 0, \tag{18}$$

$$\vec{\gamma} \times \vec{\omega} = 0. \tag{19}$$

Equation (19) implies the two vectors $\vec{\omega}$ and $\vec{\gamma}$ are parallel, and consequently, $\vec{\omega} = \omega\vec{\gamma}$, where ω is the magnitude of angular velocity of the gyrostat in the body frame. Thus, equation (18) becomes

$$\vec{\gamma} \times \left[\left(\omega^2 - n\right)\mathbb{I}\vec{\gamma} + \omega(\vec{\mathscr{K}} + A\vec{\gamma}) - mg\vec{r}_0\right] = 0. \tag{20}$$

The scalar form for equation (20) is

$$\gamma_1\left[\gamma_3(C - A)\left(\omega^2 - n\right) + \omega\left(k + \gamma_3(d - a)\right) - mgz_0\right] = 0, \tag{21}$$

$$\gamma_2\left[\gamma_3(C - B)\left(\omega^2 - n\right) + \omega\left(k + \gamma_3(d - b)\right) - mgz_0\right] = 0, \tag{22}$$

$$\gamma_1\gamma_2\left[(B - A)\left(\omega^2 - n\right) + \omega(b - a)\right] = 0. \tag{23}$$

From equation (23), we have three possibilities $\gamma_1 = \gamma_2 = 0$, $\gamma_1 = 0, \gamma_2 \neq 0$, and $\gamma_1 \neq 0, \gamma_2 = 0$. We study these cases one by one. Hereinafter, the permanent rotation is written in the form $\mathscr{E} = (A\omega\gamma_{10}, B\omega\gamma_{20}, C\omega\gamma_{30}, \gamma_{10}, \gamma_{20}, \gamma_{30})$.

(i) When $\gamma_1 = \gamma_2 = 0$, equations (21)–(23) are satisfied, identically. Using the geometric integral (2), we get $\gamma_3 = \pm 1$. The permanent rotation is $\mathscr{E}_1^{\pm} = (0, 0, \pm C\omega, 0, 0, \pm 1)$. $\mathscr{E}_1^{+}$ characterizes the rotation of the gyrostat about the vertical axis in the upward direction. This means the angle θ between the two axes $O\eta_1$ and $O\eta_2$ is zero; i.e., the fixed point

O lies down the center of the mass of the gyrostat. In a similitude way, the permanent rotation $\mathscr{E}_1^-$ is explained as the rotation of the gyrostat in the down direction; i.e., the fixed point O lies above the center of mass of the gyrostat.

(ii) When $\gamma_1 = 0$ and $\gamma_2 \neq 0$, the geometric integral (2) reduces to $\gamma_2^2 + \gamma_3^2 = 1$, which has a parametric solution $\gamma_2 = \sin\theta$ and $\gamma_3 = \cos\theta$. Taking into account the obtained results, equations (21)–(23) become

$$\left[(B-C)\left(n-\omega^2\right) + (d-b)\omega + Cn\right]\cos\theta + k\omega - mgz_0 = 0, \tag{24}$$

which represents the existence condition for a family of the permanent rotations taking the form $\mathscr{E}_2 = (0, B\omega\sin\theta, C\omega\cos\theta, 0, \sin\theta, \cos\theta)$. It represents a rotation of a gyrostat with a constant angular velocity about an axis having a direction cosine $(0, \sin\theta, \cos\theta)$.

(iii) When $\gamma_1 \neq 0$ and $\gamma_2 = 0$, the geometric integral becomes $\gamma_1^2 + \gamma_3^2 = 1$, which admits the parametric solution $\gamma_1 = \sin\theta$ and $\gamma_3 = \cos\theta$. Regarding the obtained results, equations (21)–(23) reduce to

$$\left[(A-C)\left(n-\omega^2\right) + \omega(d-a)\right]\cos\theta + k\omega - mgz_0 = 0, \tag{25}$$

that is, the condition for the existence of the family of the permanent rotations $\mathscr{E}_3 = (A\omega\sin\theta, 0, C\omega\cos\theta, \sin\theta, 0, \cos\theta)$. $\mathscr{E}_3$ is explained as the rotation of a gyrostat with a constant angular velocity about an axis with direction cosines $(\sin\theta, 0, \cos\theta)$.

Collecting the obtained results, we introduce down the following.

Theorem 1. *The mechanical system (9) and (11) characterizing the rotations of a charged gyrostat in Newtonian field has four permanent rotations. They are as follows:*

(i) $\mathscr{E}_1^{\pm} = (0, 0, \pm C\omega, 0, 0, \pm 1)$.

(ii) $\mathscr{E}_2 = (0, B\omega\sin\theta, C\omega\cos\theta, 0, \sin\theta, \cos\theta)$ *provided that* $[(B-C)(n-\omega^2) + (d-b)\omega + Cn]\cos\theta + k\omega - mgz_0 = 0$ *is satisfied.*

(iii) $\mathscr{E}_3 = (A\omega\sin\theta, 0, C\omega\cos\theta, \sin\theta, 0, \cos\theta)$ *if the condition* $[(A-C)(n-\omega^2) + \omega(d-a)]\cos\theta + k\omega - mgz_0 = 0$ *is verified.*

4. Stability Analysis

This section aims to examine the stability of the permanent rotations introduced in Theorem 1. We apply a linear approximation method to determine the sufficient conditions for instability that are also necessary conditions for the stability. We evaluate the tangent flow for the equations of the motion at the permanent rotation $\mathscr{E}$, and we get

$$\frac{d\mathbf{y}}{dt} = \mathfrak{J}(\mathrm{E})\mathbf{y}, \tag{26}$$

where $\mathfrak{J}(\mathscr{E})$ is the Jacobi matrix calculated at the permanent rotation $\mathscr{E}$. To examine the linear stability, we find the eigenvalues of the Jacobi matrix and those eigenvalues are the roots of the characteristic equation

$$\det\left[\mathfrak{J}(\mathscr{E}) - \lambda I_6\right] = 0, \tag{27}$$

where I_6 refers the 6×6 identity matrix.

The energy-Casimir method is utilized to find sufficient conditions for stability. This method was employed in several works such as [15–23]. The energy-Casimir method is briefly presented in the following.

Theorem 2. *Assuming* $(\mathscr{M}, \{\cdot,\cdot\}, \mathscr{N})$ *is a Poisson system and* $\mathscr{E} \in \mathscr{M}$ *is an equilibrium point for the Hamiltonian vector* $X_{\mathscr{N}}$. *If there is a set of Casimirs* $C_i \in C^{\infty}, i = 1, 2, \ldots, n$ *satisfies*

$$\begin{aligned} &\mathbf{d}\left(\mathscr{N} + \sum_{i=1}^{n} C_i\right)(\in) = 0, \\ &\mathbf{d}^2\left(\mathscr{N} + \sum_{i=1}^{n} C_i\right)(\in)|_{\mathscr{W}\times\mathscr{W}}, \end{aligned} \tag{28}$$

is definite for $\mathscr{W}$ *that is defined by*

$$\mathscr{W} = \bigcap_{i=1}^{n} \ker \mathbf{d}C_i(\mathscr{E}). \tag{29}$$

Then, $\mathscr{E}$ is stable and $\mathscr{E}$ is usually stable if $\mathscr{W} = \{0\}$.

4.1. Stability of $\mathscr{E}_1^{\pm}$. This section aims to examine the stability of the permanent rotation $\mathscr{E}_1^{\pm}$ which describes the rotation about the vertical axis with a constant angular velocity in two cases characterized by whether the fixed point O is above or down the gyrostat center of mass.

To obtain the necessary conditions for the stability, we compute the tangent flow of the equations of the motion (9) and (11) in the permanent rotation $\mathscr{E}_1^{\pm}$, and we obtain an equation in the form (26) and its characteristic equation (27) admits the following form:

$$\lambda^2\left(\lambda^4 + P_1\lambda^2 + Q_1\right) = 0, \tag{30}$$

where

$$P_1 = \frac{1}{AB}\left[(A(A-C)+B(B-C))n+(C(C-A)+B(2A-C))\omega^2 - mgz_0(A+B)+(d+k)^2\right.$$
$$\left.\mp\omega[Aa+Bb+(d+k)(A+B-2C)]\right], \tag{31}$$
$$Q_1 = \frac{1}{AB}\left[\pm(B-C)\left(\omega^2-n\right)+(b-d-k)\omega \pm mgz_0\right]\left[\pm(A-C)\left(\omega^2-n\right)+(a-d-k)\omega \pm mgz_0\right].$$

Thus, we can formulate the following.

Theorem 3. *Let a charged gyrostat move about its fixed point O due to the Newtonian force field, then the necessary condition for its rotation about the vertical axis up or down is linearly stable if* $P_1 \geq 0$, $Q_1 \geq 0$, *and* $P_1^2 - 4Q_1 \geq 0$. *Or, equivalently, this motion is Lyapunov unstable if at least one of these conditions is not satisfied.*

Now, we are going to determine the sufficient conditions for the stability by employing the energy-Casimir method that is presented in Theorem 2. We introduce the augmented Hamilton in the following form:

$$\mathcal{N} = \frac{1}{2}\left(\frac{\pi_1^2}{A}+\frac{\pi_2^2}{B}+\frac{\pi_3^2}{C}\right)+mgz_0\gamma_3+\frac{n}{2}\left(A\gamma_1^2+B\gamma_2^2+C\gamma_3^2\right)+\nu_1\left[\gamma_1^2+\gamma_2^2+\gamma_3^2\right]$$
$$+\ \nu_2\left[\pi_1\gamma_1+\pi_2\gamma_2+\pi_3\gamma_3+\frac{1}{2}\left(a\gamma_1^2+b\gamma_2^2+d\gamma_3^2\right)+k\gamma_3\right], \tag{32}$$

where ν_1 and ν_2 are arbitrary constants which are determined by taking into account and $\mathscr{E}_1^{\pm}$ is a critical point for the augmented Hamilton $\mathcal{N}$, i.e.,

$$\frac{\partial \mathcal{N}}{\partial \pi_i}\Big|_{\mathscr{E}_1^{\pm}} = 0,$$
$$\frac{\partial \mathcal{N}}{\partial \gamma_i}\Big|_{\mathscr{E}_1^{\pm}} = 0, \tag{33}$$
$$i = 1,2,3.$$

Equation (33) implies

$$\nu_1 = \frac{C}{2}\left(\omega^2-n\right) \pm \frac{1}{2}\left[\omega(k\pm d)-mgz_0\right], \quad \nu_2 = -\omega. \tag{34}$$

The subspace $\mathscr{W}$ is determined by

$$\mathscr{W} = \ker \mathbf{d}C_1\left(\mathscr{E}_1^{\pm}\right) \cap \ker \mathbf{d}C_2\left(\mathscr{E}_1^{\pm}\right), \tag{35}$$

where

$$\mathbf{d}C_1\left(\mathrm{E}_1^{\pm}\right) = \pm 2\mathrm{d}\gamma_3,$$
$$\mathbf{d}C_2\left(\mathrm{E}_1^{\pm}\right) = \pm \mathrm{d}\pi_3 + (k\pm d\pm C\omega)\mathrm{d}\gamma_3. \tag{36}$$

After some calculation, the basis of the subspace $\mathscr{W}$ is

$$\mathfrak{B}_{\mathscr{W}} = \left\{\vec{e}_1, \vec{e}_2, \vec{e}_4, \vec{e}_5\right\}, \tag{37}$$

where $\vec{e}_i$ are the canonical basis of $\mathbb{R}^6$. The Hessian matrix for the augmented Hamilton (32) in the reduced subspace $\mathscr{W}$ is

$$\mathrm{Hess}|_{\mathscr{W}\times\mathscr{W}} = \begin{pmatrix} \frac{1}{A} & 0 & 0 & -\omega \\ 0 & \frac{1}{B} & -\omega & 0 \\ 0 & -\omega & x & 0 \\ -\omega & 0 & 0 & y \end{pmatrix}, \tag{38}$$

where

$$x = C\omega^2 + n(B-C) \mp mgz_0 + \omega(d\pm k-b),$$
$$y = C\omega^2 + n(A-C) \mp mgz_0 + \omega(d\pm k-a). \tag{39}$$

We investigate the definiteness of the Hessian matrix (38) by applying the Sylvester criterion and so we evaluate its principal minors:

$$\Delta_1 = \frac{1}{A},$$
$$\Delta_2 = \frac{1}{AB},$$
$$\Delta_3 = \frac{1}{AB}\left[(C-B)\left(\omega^2-n\right)+\omega(d\pm k-b)\mp mgz_0\right], \tag{40}$$
$$\Delta_4 = \Delta_3\left[(C-A)\left(\omega^2-n\right)+\omega(d\pm k-a)\mp mgz_0\right].$$

It is obvious that $\Delta_1 > 0$ and $\Delta_2 > 0$ while $\Delta_3 > 0$ if

$$\pm mgz_0 < (C-B)\left(\omega^2 - n\right) + \omega(k+d-b) = \chi_1, \tag{41}$$

and $\Delta_4 > 0$ if

$$\pm mgz_0 < (C-A)\left(\omega^2 - n\right) + \omega(k+d-a) = \chi_2. \tag{42}$$

The two inequalities (41) and (42) verify together if

$$\pm mgz_0 < \min(\chi_1, \chi_2). \tag{43}$$

Thus, we can formulate the theorem.

Theorem 4. *The sufficient condition of the stability for the permanent rotation $\mathscr{E}_1^{\pm}$ to be Lyapunov stable is (43).*

Figure 2 determines the regions of linear stability and Lyapunov stability for $\mathscr{E}_1^{\pm}$. In Figure 2(a), the regions in pink determine the linear stability, while the white zones represent the instability. Notably, the solid lines in Figure 2 are determined by $P_1 0, Q_1 = 0, P_1^2 - 4Q_1 = 0$. Figure 2(b) specifies the regions of Lyapunov stability in yellow, and the dash lines are specified by $mgz_0 = \min(\chi_1, \chi_2)$. Figure 3(c) clarifies the regions of Lyapunov stability appears as a portion from the regions of linear stability.

Similar figures can be used to describe the zones of the stability and instability for the permanent rotation $\mathscr{E}_1^{-}$.

4.2. Stability of $\mathscr{E}_2$. We endeavor to find the necessary and sufficient conditions for a family of the permanent rotation $\mathscr{E}_2$ by utilizing the linear approximation and energy-Casimir method, respectively.

Calculating the tangent flow of the equations of the motion (9) and (11) in the equilibrium position $\mathscr{E}_2$, we get an equation in the form (26) and its characteristic equation (27) takes the following form:

$$\lambda^2\left(\lambda^4 + P_2\lambda^2 + Q_2\right) = 0, \tag{44}$$

where

$$\begin{aligned}
P_2 = {} & \frac{\omega(2bB - Aa)\sin^2\theta}{AC} + \frac{(A+C)}{AC}\left\{\left[(B-A)n + (B-C)\omega^2 + b\omega\right]\cos^2\theta - B\left(\omega^2 + n\right) - b\omega\right\} \\
& + \frac{2k\cos\theta}{AB} \times [d - (A+B-C)\omega] \\
& - \frac{\cos^2\theta}{ABC}\left\{(B-C)\left(B^2 + C^2 - 2AC\right)\omega^2 + C\omega[\mathrm{d}B - 2(C-A)d + A(d-a)] - Cd^2 + Bb^2 - nC\left(A^2 - BC\right)\right\} \\
& + \frac{k^2}{AB} + \frac{1}{AC}\left[\omega^2\left(B^2 + 2AC\right) + b^2 + n\left(A^2 + C^2\right)\right] - \frac{\mathrm{d}\omega}{A},
\end{aligned} \tag{45}$$

$$\begin{aligned}
Q_2 = {} & \frac{\sin^2\theta}{ABC}\left[(B-A)\left(\omega^2 - n\right) - \omega(a-b)\right]\left[\left((B-C)\left(\left(n + 3\omega^2\right)(B-C) + 3\omega(b-d)\right) + (b-d)^2\right)\cos^2\theta\right. \\
& \left. + 2(2k(B-C)\omega + b - d)\cos\theta + \left(\left(n - \omega^2\right)(C-B) - \omega(d-b)\right)B + k^2\right].
\end{aligned}$$

Notice that we use the existence condition (24) to eliminate the weight of the gyrostat mg. Now, we can write down the following.

Theorem 5. *The family of permanent rotation $\mathscr{E}_2$ is linearly stable if the conditions $P_2 \geq 0$, $Q_2 \geq 0$, and $P_2^2 - 4Q_2 \geq 0$ are met. Or, equivalently, it is Lyapunov instable if at least one of these conditions is not satisfied.*

To complete our study about the stability of $\mathscr{E}_2$, we apply the energy-Casimir method to find the stability's sufficient conditions. We utilize the same augmented Hamilton (34) and determine the values the two constants ν_1 and ν_2 leading to $\mathscr{E}_2$ becomes a critical point for this augmented Hamilton, i.e.,

$$\begin{aligned}
\left.\frac{\partial \mathscr{N}}{\partial \pi_i}\right|_{\mathscr{E}_2} &= 0, \\
\left.\frac{\partial \mathscr{L}}{\partial \gamma_i}\right|_{\mathscr{E}_2} &= 0, \\
i &= 1, 2, 3.
\end{aligned} \tag{46}$$

Equation (46) leads to

$$\begin{aligned}
\nu_1 &= \frac{1}{2}\left[B\left(\omega^2 - n\right) + b\omega\right], \\
\nu_2 &= -\omega.
\end{aligned} \tag{47}$$

Following Theorem 2, the subspace $\mathscr{W}$ is specified by

$$\mathscr{W} = \ker \mathbf{d}C_1(\mathscr{E}_2) \cap \ker \mathbf{d}C_2(\mathscr{E}_2), \tag{48}$$

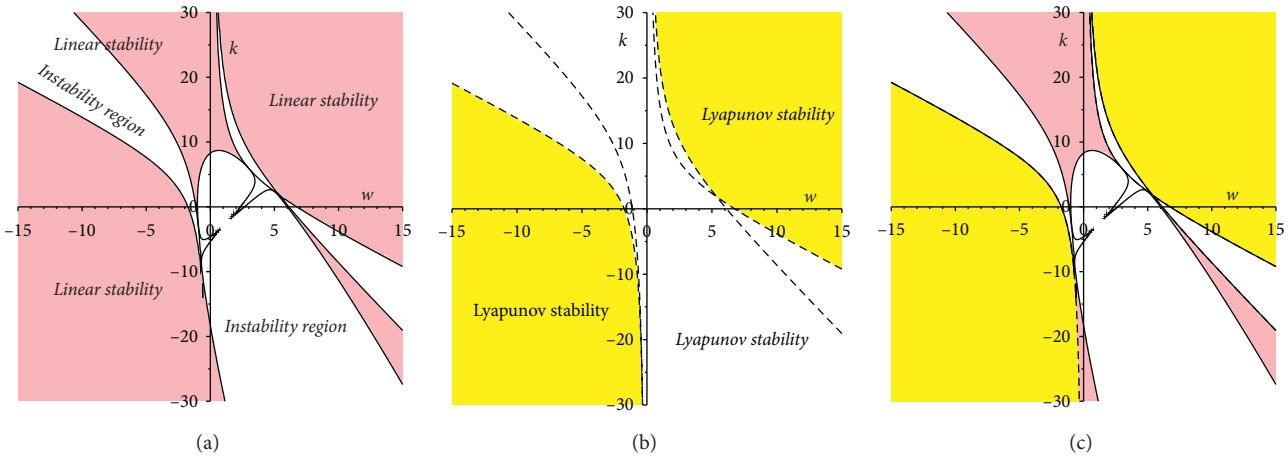

FIGURE 2: Regions of stability and instability for the permanent rotation $\mathscr{E}_1^+$ in the plane of the two parameters k and ω and $A = 3, B = 4, C = 5, d = 5, b = 10, a = 15, g = 9.8, m = 1, z0 = 1$.

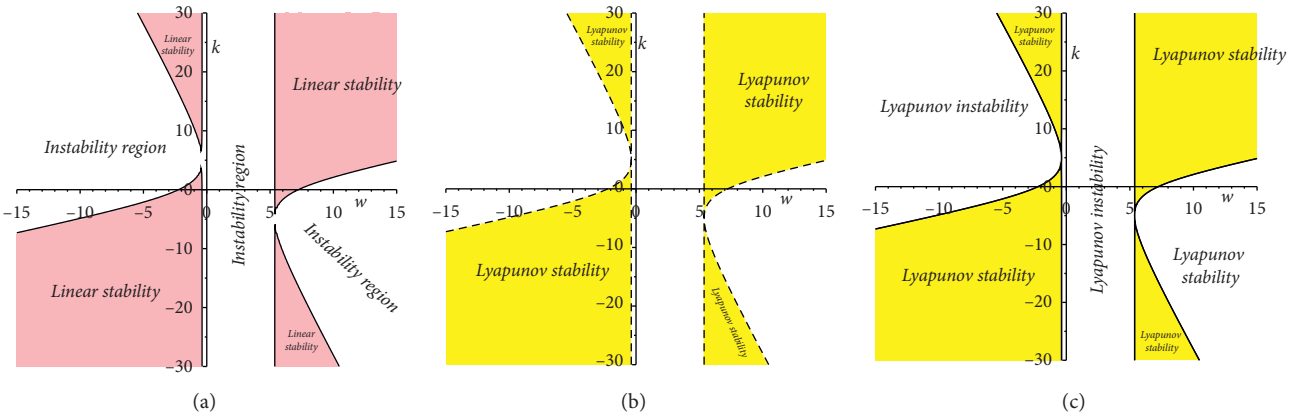

FIGURE 3: Regions of stability and instability for the permanent rotation $\mathscr{E}_2$ in the plane of the two parameters k and ω and $A = 3, B = 4, C = 5, d = 5, b = 10, a = 15, g = 9.8, m = 1, z0 = 1$.

where

$$\begin{aligned} \mathbf{d}C_1(\mathscr{E}_2) &= \mathrm{d}\gamma_3 + \frac{\sin\theta}{\cos\theta}\mathrm{d}\gamma_2, \\ \mathbf{d}C_2(\mathscr{E}_2) &= \frac{\sin\theta}{\cos\theta}\mathrm{d}\pi_2 + \mathrm{d}\pi_3 + \frac{\sin\theta}{\cos^2\theta}[((B-C)\omega + b - d)\cos\theta - k]\mathrm{d}\gamma_2. \end{aligned} \tag{49}$$

After some manipulations, we show that the subspace $\mathscr{W}$ is spanned by the vectors

$$\vec{e}_1,\ \cos\theta\vec{e}_2 - \sin\theta\vec{e}_3,\ \vec{e}_4,\ \sin\theta[\cos(\theta)((B-C)\omega + b - d) - k]\vec{e}_3 - \cos^2\theta\vec{e}_5 + \sin\theta\cos\theta\vec{e}_6, \tag{50}$$

where $\overrightarrow{e}_i$ are the canonical basis of $\mathbb{R}^6$. The Hessian matrix corresponding to the Hamiltonian (32) with (47) takes the following form:

$$\mathrm{Hess}|_{\mathscr{W}\times\mathscr{W}} = \begin{pmatrix} \frac{1}{A} & 0 & 0 & -\omega \\ 0 & \frac{\cos^2\theta}{B} + \frac{\sin^2\theta}{C} & \delta_1 & 0 \\ 0 & \delta_1 & \delta_2 & 0 \\ -\omega & 0 & 0 & B\omega^2 + (b-a)\omega + n(A-B) \end{pmatrix}, \tag{51}$$

where

$$\begin{aligned} \delta_1 &= \frac{1}{C}\left[((B-C)\omega + b - d)\cos^3\theta - k\cos^2\theta + ((2C-B)\omega - b + d)\cos\theta + k\right], \\ \delta_2 &= B\omega^2\cos^4\theta + \frac{\sin^2\theta\cos^2\theta}{C}\left[\omega^2\left(B^2 - 3BC + 3C^2\right) + (b-d)(2B-3C)\omega + Cn(C-B) + (b-d)^2\right] \\ &\quad - \frac{2k\sin^2\theta\cos\theta}{C}\left[(B-2C)\omega + b - d\right] + k^2\sin^2\theta. \end{aligned} \tag{52}$$

To investigate the definiteness of Hessian matrix (51), we utilize the Sylvester criterion and so we compute the principal minors. They take the following form:

$$\begin{aligned} \Delta_1 &= \frac{1}{A}, \\ \Delta_2 &= \frac{1}{A}\left[\frac{\cos^2\theta}{B} + \frac{\sin^2\theta}{C}\right], \\ \Delta_3 &= \frac{\sin^2\theta\cos^2\theta}{ABC}\left\{\left[(B-C)^2\left(3\omega^2 + n\right) + 3\omega(b-d)(B-C) - (b-d)^2\right]\cos^2\theta - 2k[2\omega(B-C) + b - d]\cos\theta\right. \\ &\quad \left. + B(B-C)\left(\omega^2 - n\right) + B\omega(b-d) - k^2\right\}, \\ \Delta_4 &= \left[(B-A)\left(\omega^2 - n\right) + (b-a)\omega\right]\Delta_3. \end{aligned} \tag{53}$$

It is clear that Δ_1 and Δ_2 are always positive, whereas Δ_3 and Δ_4 are positive if

$$\begin{aligned} &\frac{\sin^2\theta\cos^2\theta}{ABC}\left\{\left[(B-C)^2\left(3\omega^2 + n\right) + 3\omega(b-d)(B-C) - (b-d)^2\right]\cos^2\theta\right. \\ &\left. -2k[2\omega(B-C) + b - d]\cos\theta + B(B-C)\left(\omega^2 - n\right) + B\omega(b-d) - k^2\right\} > 0, \end{aligned} \tag{54}$$

$$\Phi(\omega) \coloneqq (B-A)\left(\omega^2 - n\right) + (b-a)\omega > 0. \tag{55}$$

$\Phi(\omega)$ is a quadratic polynomial in ω, and its discriminant is always positive and so it has two real roots (say) ω_1, ω_2. Thus, we have two cases: (1) when $B > A$, the condition (55) is satisfied if $\omega \in]-\infty, \omega_1[\bigcup]\omega_2, \infty[$; (2) if $B < A$, the condition (55) is verified if $\omega \in]\omega_1, \omega_2[$. Notice that if $A = B$ and $b = a$, the energy-Casimir does not furnish any information about the sufficient conditions of the stability.

Theorem 6. *The sufficient condition for the stability of the equilibrium position $\mathscr{E}_2$ is*

$$\begin{aligned}&\left[(B-C)^2\left(3\omega^2+n\right)+3\omega(b-d)(B-C)-(b-d)^2\right]\cos^2\theta\\&\quad-2k[2\omega(B-C)+b-d]\cos\theta+B(B-C)\left(\omega^2-n\right)+B\omega(b-d)-k^2>0,\end{aligned}\tag{56}$$

with one of the two conditions $B > A$, $\omega \in]-\infty, \omega_1[\bigcup]\omega_2, \infty[$ or $B < A$, $\omega \in]\omega_1, \omega_2[$ is verified.

The regions of linear and nonlinear (Lyapunov) stability are clarified by Figure 3. Figure 3(a) delimits the regions of linear stability in pink color, while as the white regions display the sufficient conditions for the instability of the permanent rotation $\mathscr{E}_2$. Notably, the solid lines which are the boundary of those regions are characterized by the equations $P_2 = 0, Q_2 = 0, P_2^2 - 4Q_2 = 0$. The regions in yellow appear in Figure 3(b) represent the regions of Lyapunov stability for $\mathscr{E}_2$. Figure 3(c) illustrates that the regions of Lyapunov stability appear as a part of the regions of linear stability. Notably, on the boundary of linear stability regions (solid lines in Figure 3(a) and also in Figure 3(c)), the permanent rotation $\mathscr{E}_2$ is unstable.

4.3. Stability of $\mathscr{E}_3$. The stability analysis for the family of the permanent rotations $\mathscr{E}_3$ is done by applying similar procedures to $\mathscr{E}_2$ stability study. The necessary and sufficient conditions for the stability of $\mathscr{E}_3$ can be obtained by replacing $A \leftrightarrow B$ and $a \leftrightarrow b$ in the Theorems 5 and 6, respectively. Thus, we can formulate the following two theorems.

Theorem 7. *The family of permanent rotations $\mathscr{E}_3$ is linearly stable if*

$$\begin{aligned}P_3&=\frac{\omega(2aA-Bb)\sin^2\theta}{BC}+\frac{(B+C)}{BC}\left\{\left[(A-B)n+(A-C)\omega^2+a\omega\right]\cos^2\theta-A\left(\omega^2+n\right)-a\omega\right\}+\frac{2k\cos\theta}{AB}\\&\quad\times[d-(A+B-C)\omega]-\frac{\cos^2\theta}{ABC}\left\{(A-C)\left(A^2+C^2-2BC\right)\omega^2+C\omega[\mathrm{d}A-2(C-B)d+B(d-b)]\right.\\&\quad\left.-Cd^2+Aa^2-nC\left(B^2-AC\right)\right\}+\frac{k^2}{AB}+\frac{1}{BC}\left[\omega^2\left(A^2+2BC\right)+a^2+n\left(B^2+C^2\right)\right]-\frac{\mathrm{d}\omega}{B}\geq 0,\\Q_3&=\frac{\sin^2\theta}{ABC}\left[(A-B)\left(\omega^2-n\right)-\omega(b-a)\right]\left[\left((A-C)\left(\left(n+3\omega^2\right)(A-C)+3\omega(a-d)\right)+(a-d)^2\right)\cos^2\theta\right.\\&\quad\left.+2(2(A-C)\omega+a-d)k\cos\theta+\left(\left(n-\omega^2\right)(C-A)-\omega(d-a)\right)A+k^2\right]\geq 0,\\P_3^2-4Q_3^2&\geq 0.\end{aligned}\tag{57}$$

Or, equivalently, it is unstable if at least one of the conditions (57) is verified.

Theorem 8. *The sufficient condition for the stability of the equilibrium position $\mathscr{E}_3$ is*

$$\begin{aligned}&\left[(A-C)^2\left(3\omega^2+n\right)+3\omega(a-d)(A-C)-(a-d)^2\right]\cos^2\theta\\&\quad-2k[2\omega(A-C)+a-d]\cos\theta+A(A-C)\left(\omega^2-n\right)+A\omega(a-d)-k^2>0,\end{aligned}\tag{58}$$

where one of the two conditions $B > A$, $\omega \in]-\infty, \omega_1[\bigcup]\omega_1, \infty[$ or $A < B$, $\omega \in]\omega_1, \omega_2[$ is verified.

Figure 4 displays the regions of sufficient and necessary conditions for the family of permanent rotations $\mathscr{E}_3$. Figure 4(a) illustrates the regions on linear stability in pink, while the zones of Lyapunov instability delimit in white and the solid lines which separate these zones are determined by $P_3 = 0, Q_3 = 0, P_3^2 - 4Q_3 = 0$. Figure 4(b) determines the region of Lyapunov stability in yellow. Figure 4(c) clarifies

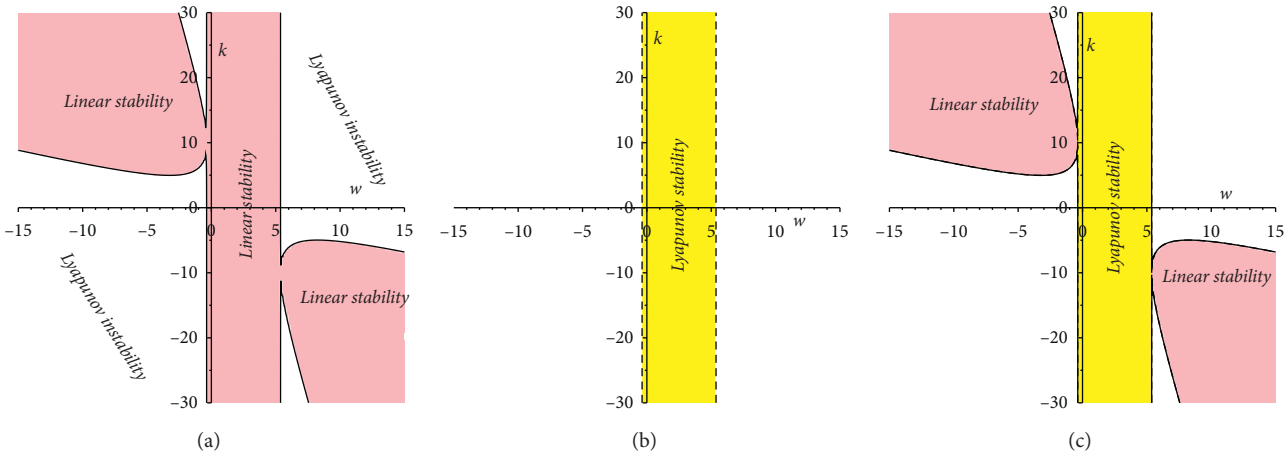

FIGURE 4: Regions of stability and instability for the permanent rotation $\mathscr{E}_4$ in the plane of the two parameters k and ω and $A = 3, B = 4, C = 5, d = 5, b = 10, a = 15, g = 9.8, m = 1, z0 = 1$.

the zones of Lyapunov stability appear as a portion of linear stability.

5. Conclusions

In this work, we have considered the motion of a charged rigid body carrying a rotor rotating about an axis which is parallel to one of the principal axes with a constant velocity. We have assumed the motion happens due to the combination influence of a uniform constant magnetic field and Newtonian force field. The equations of the motion have been constructed and rewritten as a Lie–Poisson Hamilton system. The permanent rotations $\mathscr{E}_1$ have been obtained and collected in Theorem 1. The first two permanent rotations $\mathscr{E}_1^{\pm}$ are mechanically interpreted as the rotation of the gyrostat about the vertical up or down with a constant angular velocity. The permanent rotation $\mathscr{E}_2$ is explained as the rotation of a gyrostat with a constant angular velocity about an axis having a direction cosine $(0, \sin\theta, \cos\theta)$. The permanent rotation $\mathscr{E}_3$ is interpreted as the rotation of the gyrostat with a constant angular velocity about an axis having a direction cosine $(\sin\theta, 0, \cos\theta)$. The linear stability of those equilibrium positions has been studied by applying the linear approximation method, and the obtained results have been collected in Theorems 3, 5, and 7. However, the Lyapunov stability of those permanent rotations have been examined by utilizing the energy-Casimir method, and the finding results have been presented in Theorems 4, 6, and 8. In the plane of the two variables k and ω, the regions of linear stability have been clarified in pink (see Figures 2(a), 3(a), and 4(a)), while the regions of Lyapunov stability have been illustrated in yellow (see Figures 2(b), 3(b), and 4(b)). Moreover, we illustrate the regions of Lyapunov stability appear as a part of the regions of linear stability.

Data Availability

No data were used to support the study.

Conflicts of Interest

The authors declare that they have no conflicts of interest.

References

[1] E. Leimanis, *The General Problem of the Motion of Coupled Rigid Bodies about a Fixed Point*, Springer, Berlin, Germany, 1965.
[2] V. Volterra, "Sur la théorie des variations des latitudes," *Acta Mathematica*, vol. 22, pp. 201–357, 1899.
[3] A. Gluhovsky and C. Tong, "The structure of energy conserving low-order models," *Physics of Fluids*, vol. 11, no. 2, pp. 334–343, 1999.
[4] P. C. Hughes, *Spacecraft Attitude Dynamics*, Wiley, New York, NY, USA, 1986.
[5] A. V. Borisov and I. S. Mamaev, *Rigid Body Dynamics-Hamiltonian Methods*, Integrability. Chaos. Institute of Computer Science, Izhevsk, Russia, 2001.
[6] H. M. Yehia and A. A. Elmandouh, "New conditional integrable cases of motion of a rigid body with Kovalevskaya's configuration," *Journal of Physics A: Mathematical and Theoretical*, vol. 44, Article ID 012001, 2011.
[7] H. M. Yehia and A. A. Elmandouh, "A new integrable problem with a quartic integral in the dynamics of a rigid body," *Journal of Physics A: Mathematical and Theoretical*, vol. 46, no. 14, Article ID 142001, 2013.
[8] A. A. Elmandouh, "New integrable problems in rigid body dynamics with quartic integrals," *Acta Mechanica*, vol. 226, no. 8, pp. 2461–2472, 2015.
[9] A. A. Elmandouh, "New integrable problems in the dynamics of particle and rigid body," *Acta Mechanica*, vol. 226, no. 11, pp. 3749–3762, 2015.
[10] H. M. Yehia and A. M. Hussein, "New families of integrable two-dimensional systems with quartic second integrals," *Nelineinaya Dinamika*, vol. 16, no. 2, pp. 211–242, 2020.
[11] V. Tsogas, T. J. Kalvouridis, and A. G. Mavraganis, "Equilibrium states of a gyrostat satellite in an annular configuration of N big bodies," *Acta Mechanica*, vol. 175, no. 1–4, pp. 181–195, 2005.
[12] A. Elipe and V. Lanchares, "Two equivalent problems: gyrostats in free motion and parametric quadratic

Hamiltonians," *Mechanics Research Communications*, vol. 24, no. 6, pp. 583–590, 1997.

[13] T. Kalvouridis and V. Tsogas, "Rigid body dynamics in the restricted ring problem of $n+1$ bodies," *Astrophysics and Space Science*, vol. 282, no. 4, pp. 749–763, 2002.

[14] T. S. Amer, A. A. Galal, I. M. Abady, and H. F. Elkafly, "The dynamical motion of a gyrostat for the irrational frequency case," *Applied Mathematical Modelling*, vol. 89, pp. 1235–1267, 2020.

[15] T. S. Amer, "On the rotational motion of a gyrostat about a fixed point with mass distribution," *Nonlinear Dynamics*, vol. 54, no. 3, pp. 189–198, 2008.

[16] J. A. Vera and A. Vigueras, "Hamiltonian dynamics of a gyrostat in the n-body problem: relative equilibria," *Celestial Mechanics and Dynamical Astronomy*, vol. 94, no. 3, pp. 289–315, 2006.

[17] M. Iñarrea, V. Lanchares, A. I. Pascual, and A. Elipe, "Stability of the permanent rotations of an asymmetric gyrostat in a uniform Newtonian field," *Applied Mathematics and Computation*, vol. 293, pp. 404–415, 2017.

[18] J. L. G. Guirao and J. A. Vera, "Equilibria, stability and Hamiltonian Hopf bifurcation of a gyrostat in an incompressible ideal fluid," *Physica D: Nonlinear Phenomena*, vol. 241, no. 19, pp. 1648–1654, 2012.

[19] J. A. Vera, "The gyrostat with a fixed point in a Newtonian force field: relative equilibria and stability," *Journal of Mathematical Analysis and Applications*, vol. 401, no. 2, pp. 836–849, 2013.

[20] A. A. Elmandouh, "On the stability of the permanent rotations of a charged rigid body-gyrostat," *Acta Mechanica*, vol. 228, no. 11, pp. 3947–3959, 2017.

[21] A. A. Elmandouh, "On the stability of certain motions of a rigid body-gyrostat in an incompressible ideal fluid," *International Journal of Non-linear Mechanics*, vol. 120, Article ID 103419, 2020.

[22] A. A. Elmandouh and A. G. Ibrahim, "Hamiltonian structure, equilibria, and stability for an axisymmetric gyrostat motion in the presence of gravity and magnetic fields," *Acta Mechanica*, vol. 230, no. 7, pp. 2539–2548, 2019.

[23] M. Iñarrea, V. Lanchares, A. I. Pascual, and A. Elipe, "On the stability of a class of permanent rotations of a heavy asymmetric gyrostat," *Regular and Chaotic Dynamics*, vol. 22, no. 7, pp. 824–839, 2017.

[24] H. M. Yehia, "On the motion of a rigid body acted upon by potential and gyroscopic forces: I. The equations of motion and their transformations," *Journal of Mechanical Theory and Applications*, vol. 5, pp. 747–754, 1986.

[25] P. Birtea, I. Caşu, and D. Comănescu, "Hamilton-Poisson formulation for the rotational motion of a rigid body in the presence of an axisymmetric force field and a gyroscopic torque," *Physics Letters A*, vol. 375, no. 45, pp. 3941–3945, 2011.

Hindawi
Advances in Astronomy
Volume 2021, Article ID 6657500, 11 pages
https://doi.org/10.1155/2021/6657500

Research Article

Impacts of Poynting–Robertson Drag and Dynamical Flattening Parameters on Motion around the Triangular Equilibrium Points of the Photogravitational ER3BP

Aishetu Umar[1] and Aminu Abubakar Hussain[2]

[1]*Department of Mathematics, Faculty of Physical Sciences, Ahmadu Bello University, Zaria, Nigeria*
[2]*Department of Mathematics, Faculty of Natural and Applied Sciences, Nasarawa State University, Keffi, Nigeria*

Correspondence should be addressed to Aminu Abubakar Hussain; dadinduniya@gmail.com

Received 10 December 2020; Revised 2 January 2021; Accepted 27 January 2021; Published 11 February 2021

Academic Editor: Elbaz Abouelmagd

Using an analytical and numerical study, this paper investigates the equilibrium state of the triangular equilibrium points $L_{4,5}$ of the Sun-Earth system in the frame of the elliptic restricted problem of three bodies subject to the radial component of Poynting–Robertson (P–R) drag and radiation pressure factor of the bigger primary as well as dynamical flattening parameters of both primary bodies (i.e., Sun and Earth). The equations of motion are presented in a dimensionless-pulsating coordinate system $(\xi - \eta)$, and the positions of the triangular equilibrium points are found to depend on the mass ratio (μ) and the perturbing forces involved in the equations of motion. A numerical analysis of the positions and stability of the triangular equilibrium points of the Sun-Earth system shows that the perturbing forces have no significant effect on the positions of the triangular equilibrium points and their stability. Hence, this research work concludes that the motion of an infinitesimal mass near the triangular equilibrium points of the Sun-Earth system remains linearly stable in the presence of the perturbing forces.

1. Introduction

The study of the equilibrium state of an infinitesimal mass (a test particle) with regard to the dynamical system of the restricted three-body problem (R3BP) remains one of the most important and interesting aspects in the study of celestial mechanics and dynamical astronomy. The elliptic restricted three-body problem (ER3BP) deals with the description-study of the motion of an infinitesimal mass (m_3), in the vicinity of the gravitational fields of two dominant bodies m_1 and m_2 which are called the primaries (bigger primary and smaller primary, respectively), where $m_1 \geq m_2 \gg m_3$. These primary bodies revolve about their common centre of mass in elliptic orbits, under the influence of their mutual gravitational attraction. The ER3BP admits five equilibrium points at which the test particle (infinitesimal mass) would remain fixed if placed there. Three of such points lie on the line joining the two dominant bodies m_1 and m_2, called the collinear equilibrium points L_i $(i = 1, 2, 3)$, and are unstable, while the other two points form equilateral triangles with the two dominant bodies, called the triangular equilibrium points L_4 and L_5, and are stable for $0 < \mu < \mu_c$, where μ is the mass ratio defined by $\mu = (m_2/(m_1 + m_2))$ and μ_c is the critical mass parameter [1].

In an attempt to have a much more realistic description of the motion of an infinitesimal mass over the decades, the classical R3BP has been modified in the sense that additional dynamical potentials of the system were considered in different approaches [2–8] and others.

Abouelmagd [9] in his study of the R3BP found out that the locations of the triangular points and their linear stability are affected by the oblateness of the more massive primary, up to the second zonal harmonic J_4. In his numerical study, he concluded that the existence of J_4 sometimes does not affect the stability of the equilibrium points as in the Earth-Moon, Saturn-Phoebe, and Uranus-Caliban systems. Also, Abouelmagd et al. [10] examined the effects of oblateness of the three participating bodies together with small perturbations in Coriolis and centrifugal forces. Afterwards, Abouelmagd et al. [11] studied the effect of the first two even zonal harmonic

coefficients of both the primaries as well as the periodic orbits around the equilibrium points. They found out that the triangular equilibrium points are linearly stable for $0 < \mu < \mu_C$ and unstable for $\mu_C \le \mu \le 0.5$, while the collinear equilibrium points remain linearly unstable.

Singh and Tyokyaa [12] examined the stability of the triangular points in the ER3BP with oblateness up to the second zonal harmonic J_4 of both primaries. They concluded that the location and linear stability of the triangular points are affected by the oblateness of the primary bodies, eccentricity of the orbits of the primaries, and the semi-major axis of the system and both destabilized the system. In the same year, Singh et al. [13] investigated the influence of the zonal harmonics (J_2 and J_4) of the primary and the radiation pressure of the secondary on the locations and linear stability of the triangular points. They however claimed that the parameters involved in the system affect the positions of the equilibrium points and destabilize the system as well.

The Doppler shift and absorptions and subsequent reemission of incident radiation, that is, the so-called Poynting–Robertson's (P–R) drag, are often neglected by many researchers in the estimation of light radiation force. Poynting [14] while studying radiation in the Solar System stated that radiation affects temperature and small bodies. He asserted that particles such as cosmic dust grain or small meteors are affected considerably by gravitational and light radiation force as they approach luminous celestial bodies. Furthermore, infinitesimal bodies in solar orbits suffer a gradual loss of angular momentum and ultimately spiral into the Sun. Later, Robertson [15] in a modified theory of Poynting considered only terms of the first order in the ratio of velocity of the particles to that of light. He investigated the dynamical effects of drag in the Solar System and derived the expression for the times of fall from circular orbits. Thus at a cosmically rapid rate, the P–R effect sweeps small particles of the Solar System into the sun.

Researchers like Burns et al. [16], Murray [17], Singh and Simeon [18], Alhussain [19], Chakraborty and Narayan [20], Amuda et al. [21], and others studied the R3BP by taking into account the P–R drag in different views. Mishra et al. [22] examined the stability of triangular points under the assumption that the bigger primary is a source of radiation with the incident P–R drag while the smaller is an oblate spheroid in the frame of the ER3BP. They concluded that the triangular points are unstable. In a recent study, Singh and Amuda [23] investigated the linear stability around $L_{4,5}$ of a test particle in the field of post-AGB binary system with the effective P–R drag force. They asserted that P–R drag and the mass parameter μ contribute in shifting the locations of the triangular points and the triangular points are unstable in the linear sense due to the presence of complex conjugate roots.

The aim of the present paper is to further investigate the effects of radiation pressure and P–R drag of the bigger primary on $L_{4,5}$ in the ER3BP, taking into account the effects of dynamical flattening parameters of the primary bodies.

2. Equations of Motion

Let m_1, m_2, and m_3 be the three masses, m_1 and m_2 being the dominant bodies having an elliptic orbit about their common centre of mass, while m_3 being the infinitesimal mass which moves in the same plane with the dominant bodies under the influence of their force-field without influencing their motion. Let (x_1, y_1, z_1), (x_2, y_2, z_2), and (x_3, y_3, z_3) denote the coordinates of m_1, m_2, and m_3, respectively, in the sidereal coordinates. Using Newton's law, the equations of motion of an infinitesimal mass m_3 in the sidereal coordinates system can be represented as

$$m_3\ddot{x}_3 = \frac{\partial V}{\partial x_3},$$

$$m_3\ddot{y}_3 = \frac{\partial V}{\partial y_3}, \tag{1}$$

$$m_3\ddot{z}_3 = \frac{\partial V}{\partial z_3},$$

where $V = m_3k^2((m_1/R_1) + (m_2/R_2))$; R_1 and R_2 are the distances of an infinitesimal mass from m_1 and m_2, respectively, and are defined as $R_i^2 = (x - x_i)^2 + (y - y_i)^2 + (z - z_i)^2$; k^2 is the Gaussian constant of gravitation and the dot indicates differentiation with respect to time t.

Equations (1) can be rewritten as [3]

$$\ddot{x}_3 = \frac{\partial W}{\partial x_3},$$

$$\ddot{y}_3 = \frac{\partial W}{\partial y_3}, \tag{2}$$

$$\ddot{z}_3 = \frac{\partial W}{\partial z_3},$$

where $W = (V/m_3)$.

Now, we choose and rotate the synodic coordinates uniformly with a positive unit rate, which has the same origin at the centre of mass of the two dominant bodies with the sidereal coordinates. The direction of the $x-$axis is chosen such that the two dominant bodies always lie on it. Therefore, the equations of motion in sidereal coordinates are related to the equations of motion in synodic coordinates with respect to the true anomaly. By transforming the equations of motion from true anomaly to eccentric anomaly in a dimensionless-pulsating (rotating) coordinate system (ξ, η, ζ), we have

$$\xi'' + \frac{e\xi' \sin E}{\rho} - \frac{2\left(1 - e^2\right)^{(1/2)}\eta'}{\rho} = \frac{\partial \Omega}{\partial \xi},$$

$$\eta'' + \frac{e\eta' \sin E}{\rho} + \frac{2\left(1 - e^2\right)^{(1/2)}\xi'}{\rho} = \frac{\partial \Omega}{\partial \eta}, \tag{3}$$

$$\zeta'' + \frac{e\zeta' \sin E}{\rho} = \frac{\partial \Omega}{\partial \zeta},$$

where the prime $(\prime)$ represents differentiation with respect to eccentric anomaly (E) and $\Omega(\xi, \eta, \zeta) = (1/(n^2\rho))[(n^2/2)(\xi^2 + \eta^2) - ((en^2)/(2\rho))(\cos E - e)\zeta^2 + \overline{W}]$, $\rho = (1 - e \cos E)$, e and n are the eccentricity of the orbits and mean motion

of the dominant bodies, while $\overline{W} = -(\overline{V}/m_3), \overline{V} = -k^2 m_3((m_1/r_1) + (m_2/r_2))$, $r_i (i = 1, 2)$ are the distances of an infinitesimal mass from the bigger primary and smaller primary, respectively, and are defined as $r_i^2 = (\xi - \xi_i)^2 + \eta^2 + \zeta^2$, $(i = 1, 2).$, $\xi_1 = -((m_2 a)/(m_1 + m_2))$, $\xi_2 = ((m_1 a)/(m_1 + m_2))$, and a is the semi-major axis of m_2 around m_1. See [3, 24, 25].

Now, integrating equations (3) with respect to the eccentric anomaly (E) and averaging, we get

$$\begin{aligned} \xi'' - 2\eta' &= \frac{\partial \overline{\Omega}}{\partial \xi}, \\ \eta'' + 2\xi' &= \frac{\partial \overline{\Omega}}{\partial \eta}, \\ \zeta'' &= \frac{\partial \overline{\Omega}}{\partial \zeta}, \end{aligned} \tag{4}$$

where $\overline{\Omega}$ is the potential-like function defined by $\overline{\Omega}(\xi, \eta, \zeta) = (1 - e^2)^{-(1/2)}[(1/2)(\xi^2 + \eta^2) + (\overline{W}/n^2)]$.

Thus, the defined dynamical system in equations (4) is the required equations of motion for the ER3BP.

Let q be the radiation pressure factor of the bigger primary which is given by

$$F_{g1} - F_{p1} = F_{g1}\left(1 - \frac{F_{p1}}{F_{g1}}\right) = qF_{g1}. \tag{5}$$

This implies that $q = 1 - (F_{p1}/F_{g1})$ such that $0 < 1 - q = \alpha \ll 1$ [26], where F_{g1} is the gravitational force of m_1 and F_{p1} is the radiation pressure of m_1.

Considering the potential theory, the external gravitational potential due to a body that has axial symmetry can be written in terms of Legendre polynomials as $\overline{V}_0 = -((k^2 m_0)/r_0)[1 - \sum_{n=2}^{\infty} J_n P_n(\cos\theta)(\overline{R}_0/r_0)^n]$ (see de Pater and Lissauer [27] for more details), where m_0 denotes the mass of the body; r_0 denotes the radial distance from the centre of the particle to the centre of any other body; θ denotes the angle between the body's symmetry axis and vector to the particle; $\overline{R}_0$ denotes the mean radius of the body; J_n denotes the dimensionless coefficient that characterizes the degree of nonspherical components of the potential, J_n is zero for odd n, and when n is even, J_n is called a zonal harmonic coefficient; and the term $P_n(\cos\theta)$ denotes the Legendre polynomials of degree n and is defined by $P_n(x) = (1/(2^n n!))(d^n/dx^n)(x^2 - 1)^n$. We assume that the infinitesimal mass moves in the same plane of motion as the dominant bodies and this plane coincides with the equatorial plane (*i.e.* $\theta = 90^0$). Therefore, the potential energy of the infinitesimal mass under the effects of the dynamical flattening parameters of both dominant bodies can be written as

$$\overline{V} = -k^2 m_3\left[m_1\left(\frac{1}{r_1} + \frac{A_1}{2r_1^3} - \frac{3A_2}{8r_1^5}\right) + m_2\left(\frac{1}{r_2} + \frac{B_1}{2r_2^3} - \frac{3B_2}{8r_2^5}\right)\right], \tag{6}$$

where $A_i = J_{2i}^A \overline{R}_1^{2i}$ and $B_i = J_{2i}^B \overline{R}_2^{2i}$ $(i = 1, 2)$ represent the dynamical flattening parameters of the bigger and smaller primaries, respectively, J_{2i}^A and $J_{2i}^B (i = 1, 2)$ are the zonal harmonics coefficients; $r_i (i = 1, 2)$ is defined as in equation (3); and $\overline{R}_1$ and $\overline{R}_2$ are the mean radii of the dominant masses m_1 and m_2, respectively.

The distance between the dominant bodies is $r = a(1 - e\cos E)$ in the elliptic orbit, where a, e, and E are semi-major axis between the dominant bodies, common eccentricity of the dominant bodies, and eccentric anomaly, respectively.

And the mean distance between them is as follows:

$$\frac{1}{2\pi}\int_0^{2\pi} r\,\mathrm{d}E = a. \tag{7}$$

Assuming that the dominant bodies are in elliptical motion with constant angular velocity n(mean motion), then the orbits of m_1 and m_2 with respect to the centre of mass, with semi-major axes, would be $a_1 = (m_2/(m_1 + m_2))a$ and $a_2 = (m_1/(m_1 + m_2))a$, respectively, having the same eccentricity; thus, the motion of the bigger and smaller primary can be written as [1, 28]

$$\begin{aligned} m_1 n^2 a_1 &= \frac{k^2 m_1 m_2}{r^2}\left[1 + \frac{3A_1}{2r^2} + \frac{3B_1}{2r^2} - \frac{15A_2}{8r^4} - \frac{15B_2}{8r^4}\right], \\ m_2 n^2 a_2 &= \frac{k^2 m_1 m_2}{r^2}\left[1 + \frac{3A_1}{2r^2} + \frac{3B_1}{2r^2} - \frac{15A_2}{8r^4} - \frac{15B_2}{8r^4}\right], \end{aligned} \tag{8}$$

where n, r, and k are the mean motion, distance between the dominant bodies, and Gaussian constant of gravitation, respectively. The distance between the dominant bodies r is defined to be the semi-major axis a of the orbit (i.e., $r = a$), since the dominant bodies are in elliptic orbits.

Hence, adding equations (8) together, we obtain

$$n^2(a_1 + a_2) = \frac{k^2(m_1 + m_2)}{a^2}\left[1 + \frac{3A_1}{2a^2} + \frac{3B_1}{2a^2} - \frac{15A_2}{8a^4} - \frac{15B_2}{8a^4}\right]. \tag{9}$$

Assume that the sum of the masses of the dominant bodies and the semi-major axis between them are the units of mass and length, respectively; i.e., $m_1 + m_2 = 1$, and $a_1 + a_2 = a = 1$. Also, the unit of time is chosen so as to make the Gaussian constant, $k^2 = 1$. Hence, equation (9) becomes

$$n^2 = 1 + \frac{3A_1}{2} + \frac{3B_1}{2} - \frac{15A_2}{8} - \frac{15B_2}{8}. \tag{10}$$

Using equations (4), (5), (6), and (10), the equations of motion of an infinitesimal mass in the frame of the ER3BP can be modified, taking into account the dynamical flattening parameters of both dominant bodies together with the radiation pressure as well as P–R drag due to the bigger primary in a dimensionless-pulsating (rotating) coordinate system (ξ, η) as

$$\begin{aligned} \xi'' - 2\eta' &= U_\xi, \\ \eta'' + 2\xi' &= U_\eta, \end{aligned} \tag{11}$$

where

$$
\begin{aligned}
U_\xi &= \frac{\partial \overline{\Omega}}{\partial \xi} - \frac{\left(1-e^2\right)^{-(1/2)} W_1 N_1}{n^2 r_1^2},\\
U_\eta &= \frac{\partial \overline{\Omega}}{\partial \eta} - \frac{\left(1-e^2\right)^{-(1/2)} W_1 N_2}{n^2 r_1^2},\\
\overline{\Omega} &= \left(1-e^2\right)^{(-1/2)} \left[\frac{\xi^2+\eta^2}{2} + \frac{1}{n^2}\left\{\frac{(1-\mu)q}{r_1} + \frac{(1-\mu)A_1 q}{2r_1^3} - \frac{3(1-\mu)A_2 q}{8r_1^5} + \frac{\mu}{r_2} + \frac{\mu B_1}{2r_2^3} - \frac{3\mu B_2}{8r_2^5}\right\}\right],\\
N_1 &= \frac{(\xi+\mu)\left[(\xi+\mu)\xi' + \eta\eta'\right]}{r_1^2} + \xi' - n\eta,\\
N_2 &= \frac{\eta\left[(\xi+\mu)\xi' + \eta\eta'\right]}{r_1^2} + \eta' + n(\xi+\mu),\\
W_1 &= \frac{(1-\mu)(1-q)}{c_d},
\end{aligned}
\tag{12}
$$

and c_d is the dimensionless speed of light [18, 22, 29].

3. Locations of the Triangular Equilibrium Points $L_{4,\,5}$

To obtain the equilibrium positions of an infinitesimal mass, the equations $\xi' = \eta' = \xi'' = \eta'' = 0$ must be satisfied in the equations of motion (11); i.e., they are the solutions of the equations $U_\xi = U_\eta = 0$, and thus resulting in

$$
\begin{aligned}
&\xi n^2 - \frac{(1-\mu)(\xi+\mu)q}{r_1^3} - \frac{3(1-\mu)(\xi+\mu)qA_1}{2r_1^5} + \frac{15(1-\mu)(\xi+\mu)qA_2}{8r_1^7} - \frac{\mu(\xi+\mu-1)}{r_2^3}\\
&\quad - \frac{3\mu(\xi+\mu-1)B_1}{2r_2^5} + \frac{15\mu(\xi+\mu-1)B_2}{8r_2^7} + \frac{Wn\eta}{r_1^2} = 0,
\end{aligned}
\tag{13}
$$

$$
\begin{aligned}
&n^2\eta - \frac{(1-\mu)q\eta}{r_1^3} - \frac{3(1-\mu)q\eta A_1}{2r_1^5} + \frac{15(1-\mu)q\eta A_2}{8r_1^7} - \frac{\mu\eta}{r_2^3} - \frac{3\mu\eta B_1}{2r_2^5}\\
&\quad + \frac{15\mu\eta B_2}{8r_2^7} - \frac{Wn(\xi+\mu)}{r_1^2} = 0,
\end{aligned}
\tag{14}
$$

which can be rewritten as

$$
\left[n^2 - \frac{(1-\mu)q}{r_1^3} - \frac{3(1-\mu)qA_1}{2r_1^5} + \frac{15(1-\mu)qA_2}{8r_1^7} - \frac{\mu}{r_2^3} - \frac{3\mu B_1}{2r_2^5} + \frac{15\mu B_2}{8r_2^7}\right]\eta = \frac{Wn(\xi+\mu)}{r_1^2}.
\tag{15}
$$

Multiplying equations (13) and (14) by η and $(\xi+\mu)$, respectively, we obtain

$$\xi\eta n^2 - \frac{(1-\mu)(\xi+\mu)\eta q}{r_1^3} - \frac{3(1-\mu)(\xi+\mu)\eta q A_1}{2r_1^5} + \frac{15(1-\mu)(\xi+\mu)\eta q A_2}{8r_1^7} - \frac{\mu(\xi+\mu-1)\eta}{r_2^3} - \frac{3\mu(\xi+\mu-1)\eta B_1}{2r_2^5} + \frac{15\mu(\xi+\mu-1)\eta B_2}{8r_2^7} + \frac{Wn\eta^2}{r_1^2} = 0, \tag{16}$$

$$n^2(\xi+\mu)\eta - \frac{(1-\mu)(\xi+\mu)q\eta}{r_1^3} - \frac{3(1-\mu)(\xi+\mu)q\eta A_1}{2r_1^5} + \frac{15(1-\mu)(\xi+\mu)q\eta A_2}{8r_1^7} - \frac{\mu(\xi+\mu)\eta}{r_2^3} - \frac{3\mu(\xi+\mu)\eta B_1}{2r_2^5} + \frac{15\mu(\xi+\mu)\eta B_2}{8r_2^7} - \frac{Wn(\xi+\mu)^2}{r_1^2} = 0. \tag{17}$$

Subtracting equation (17) from equation (16), we obtain

$$n^2 = \frac{Wn}{\mu\eta} + \frac{1}{r_2^3} + \frac{3B_1}{2r_2^5} - \frac{15B_2}{8r_2^7} = 0. \tag{18}$$

Using equation (18) in equation (15), we have

$$n^2 = \frac{q}{r_1^3} + \frac{3qA_1}{2r_1^5} - \frac{15qA_2}{8r_1^7} + \frac{Wn(\xi+\mu)}{r_1^2\eta(1-\mu)} - \frac{Wn}{\eta(1-\mu)}. \tag{19}$$

In the absence of the dynamical flattening parameters $(A_i = B_i = 0, i = 1, 2)$ and P–R drag (i.e., $W = 0$), the solutions of equations (18) and (19) are $r_1 = r_2 = 1$. Then, considering the above parameters, the solutions of equations (18) and (19) would change slightly by

$$r_1 = 1 + \varepsilon_1, \quad r_2 = 1 + \varepsilon_2, \tag{20}$$

where $\varepsilon_i\,(i = 1, 2) \ll 1$.

Substituting equations (20) in equations (18) and (19) together with help of equation (10), we obtain the series equations in terms of $\varepsilon_i\,(i = 1, 2) \ll 1$. Solving these equations by holding the expressions which contain A_i, B_i, A_1^2, B_1^2, $A_1B_1\,(i = 1, 2)$ (since $A_i = J_{2i}^A \overline{R}_1^{2i}$ and $B_i = J_{2i}^B \overline{R}_2^{2i} i = 1, 2$, then A_1^2, B_1^2, A_1B_1, A_2, and B_2 have the same powers of mean radii of the dominant bodies), α (where $\alpha = 1 - q$) and W also by restricting ourselves only to the quadratic terms in $\varepsilon_i\,(i = 1, 2) \ll 1$, we have

$$\varepsilon_1 = -\frac{\alpha}{3} - \frac{B_1}{2} + \frac{5B_2}{8} + \frac{5A_1B_1}{4} + \frac{B_1^2}{2} - \frac{W}{3\sqrt{3}(1-\mu)}, \quad \varepsilon_2 = -\frac{A_1}{2} + \frac{5A_2}{8} + \frac{5A_1B_1}{4} + \frac{A_1^2}{2} + \frac{2W}{3\sqrt{3}\mu}. \tag{21}$$

Substituting equations (21) in equations (20), we have

$$r_1 = 1 - \frac{\alpha}{3} - \frac{B_1}{2} + \frac{5B_2}{8} + \frac{5A_1B_1}{4} + \frac{B_1^2}{2} - \frac{W}{3\sqrt{3}(1-\mu)}, \quad r_2 = 1 - \frac{A_1}{2} + \frac{5A_2}{8} + \frac{5A_1B_1}{4} + \frac{A_1^2}{2} + \frac{2W}{3\sqrt{3}\mu}. \tag{22}$$

Using $r_1^2 = (\xi+\mu)^2 + \eta^2$ & $r_2^2 = (\xi+\mu-1)^2 + \eta^2$ defined in equations (3), then the exact solutions of the triangular points $L_{4,5}$ are

$$\xi = \frac{1}{2} - \mu + \frac{1}{2}\left(r_1^2 - r_2^2\right), \quad \eta = \pm\sqrt{\frac{r_1^2 + r_2^2}{2} - \left(\frac{r_2^2 - r_1^2}{2}\right)^2 - \frac{1}{4}}. \tag{23}$$

Substituting equation (22) in (23), we obtain

$$\xi = \frac{1}{2} - \mu - \frac{\alpha}{3} + \frac{1}{2}(A_1 - B_1) - \frac{5}{8}(A_2 - B_2) - \frac{5}{8}\left(A_1^2 - B_1^2\right) - \frac{W(2-\mu)}{3\sqrt{3}\mu(1-\mu)},$$

$$\eta = \pm\frac{\sqrt{3}}{2}\left[1 - \frac{2\alpha}{9} - \frac{1}{3}(A_1 + B_1) + \frac{5}{12}(A_2 + B_2) + \frac{7}{36}\left(A_1^2 + B_1^2\right) + \frac{17A_1B_1}{9} + \frac{2W(2-3\mu)}{9\sqrt{3}\,\mu(1-\mu)}\right]. \tag{24}$$

Hence, equations (24) are the required locations of the triangular equilibrium points $L_{4,5}$ denoted by $(\xi, \pm\eta)$.

4. Stability of the Triangular Equilibrium Points

To examine the stability of the triangular equilibrium points, we place the infinitesimal mass at one of the equilibrium points and give it a small velocity. The point is stable for the oscillatory solutions with small amplitude and unstable for exponentially diverging solutions.

Assume that (ξ_0, η_0) are the coordinates of the equilibrium points under consideration and let (x, y) be the small displacements from these coordinates of the equilibrium points.

These can be written as

$$\begin{aligned}\xi &= \xi_0 + x,\\ \eta &= \eta_0 + y.\end{aligned} \tag{25}$$

Now, using equations (25) and holding only the linear terms of Taylor's theorem as the second and higher power of x and y being very small, equation (11) become

$$\begin{aligned}x'' - 2y' &= U^0_\xi + xU^0_{\xi\xi} + yU^0_{\xi\eta} + x'U^0_{\xi\xi'} + y'U^0_{\xi\eta'},\\ y'' + 2x' &= U^0_\eta + xU^0_{\eta\xi} + yU^0_{\eta\eta} + x'U^0_{\eta\xi'} + y'U^0_{\eta\eta'},\end{aligned} \tag{26}$$

where the superscript 0 of equations (26) indicates that the partial derivatives are evaluated at the equilibrium points (ξ_0, η_0). At equilibrium points, $U^0_\xi = U^0_\eta = 0$. Hence, equations (26) become

$$\begin{aligned}x'' - 2y' &= xU^0_{\xi\xi} + yU^0_{\xi\eta} + x'U^0_{\xi\xi'} + y'U^0_{\xi\eta'},\\ y'' + 2x' &= xU^0_{\eta\xi} + yU^0_{\eta\eta} + x'U^0_{\eta\xi'} + y'U^0_{\eta\eta'}.\end{aligned} \tag{27}$$

Suppose $x = Ae^{\lambda t}$ and $y = Be^{\lambda t}$ are the trial solution of equations (27) (variational equations). Then, by using these values of the trial solutions in equations (27), we get

$$\begin{aligned}\left(\lambda^2 - U^0_{\xi\xi} - \lambda U^0_{\xi\xi'}\right)A + \left(-2\lambda - U^0_{\xi\eta} - \lambda U^0_{\xi\eta'}\right)B = 0,\\ \left(\lambda^2 - U^0_{\eta\eta} - \lambda U^0_{\eta\eta'}\right)B + \left(2\lambda - U^0_{\eta\xi} - \lambda U^0_{\eta\xi'}\right)A = 0.\end{aligned} \tag{28}$$

Equations (28) have a nontrivial solution if

$$\begin{vmatrix}\lambda^2 - U^0_{\xi\xi} - \lambda U^0_{\xi\xi'} & -2\lambda - U^0_{\xi\eta} - \lambda U^0_{\xi\eta'}\\ 2\lambda - U^0_{\eta\xi} - \lambda U^0_{\eta\xi'} & \lambda^2 - U^0_{\eta\eta} - \lambda U^0_{\eta\eta'}\end{vmatrix} = 0. \tag{29}$$

Hence, the required characteristic equation of this dynamical system is given by [3, 22]

$$\lambda^4 + a_0\lambda^3 + a_1\lambda^2 + a_2\lambda + a_3 = 0, \tag{30}$$

where

$$\begin{aligned}a_0 &= -\left(U^0_{\xi\xi'} + U^0_{\eta\eta'}\right),\\ a_1 &= 4 - \left(U^0_{\xi\xi} + U^0_{\eta\eta}\right) + 2\left(U^0_{\xi\eta'} + U^0_{\eta\xi'}\right) + U^0_{\xi\xi'}U^0_{\eta\eta'} - U^0_{\xi\eta'}U^0_{\eta\xi'},\\ a_2 &= U^0_{\xi\xi}U^0_{\eta\eta'} + U^0_{\xi\xi'}U^0_{\eta\eta} + 2\left(U^0_{\xi\eta} - U^0_{\eta\xi}\right) - U^0_{\xi\eta'}U^0_{\eta\xi} - U^0_{\xi\eta}U^0_{\eta\xi'},\\ a_3 &= U^0_{\xi\xi}U^0_{\eta\eta} - U^0_{\xi\eta}U^0_{\eta\xi}.\end{aligned} \tag{31}$$

Now, the second partial derivatives of the modified potential-like function U at triangular equilibrium points are

$$\begin{aligned}U^0_{\xi\xi} &= \frac{3}{4} + \frac{3e^2}{8} - \left(\frac{1}{2} - \frac{3\mu}{2}\right)\alpha + \left(\frac{9}{4} - 3\mu\right)A_1 - \left(\frac{15}{4} - \frac{75\mu}{16}\right)A_2 - \left(\frac{3}{4} - 3\mu\right)B_1 + \left(\frac{15}{16} - \frac{75\mu}{16}\right)B_2\\ &\quad - \left(\frac{3}{4} - \frac{27\mu}{16}\right)A_1^2 + \left(\frac{45}{16} - \frac{27\mu}{16}\right)B_1^2 - \frac{15A_1B_1}{8} - \frac{W\left(\mu^2 - 13\mu + 8\right)}{4\sqrt{3}\mu(1-\mu)},\\ U^0_{\eta\eta} &= \frac{9}{4} + \frac{9e^2}{8} + \left(\frac{1}{2} - \frac{3\mu}{2}\right)\alpha + \frac{3A_1}{4} - \left(\frac{15}{4} - \frac{45\mu}{16}\right)A_2 + \frac{3B_1}{4} - \left(\frac{15}{16} + \frac{45\mu}{16}\right)B_2\\ &\quad - \left(\frac{15}{4} - \frac{45\mu}{16}\right)A_1^2 - \left(\frac{15}{16} + \frac{45\mu}{16}\right)B_1^2 + \frac{39A_1B_1}{8} + \frac{W\left(5\mu^2 - 17\mu + 8\right)}{\sqrt{3}\mu(1-\mu)},\\ U^0_{\xi\eta} &= \frac{3\sqrt{3}}{2}\left[\left(\frac{1}{2} - \mu\right) + \left(\frac{1}{2} - \mu\right)\frac{e^2}{2} - \left(\frac{1}{9} + \frac{\mu}{9}\right)\alpha + \left(\frac{5(1-\mu)}{6} + \frac{\mu}{6}\right)A_1 - \left(\frac{5(1-\mu)}{3} + \frac{5\mu}{24}\right)A_2\right.\\ &\quad - \left(\frac{(1-\mu)}{6} + \frac{5\mu}{6}\right)B_1 + \left(\frac{5(1-\mu)}{24} + \frac{5\mu}{3}\right)B_2 - \left(\frac{10}{9} - \frac{73\mu}{72}\right)A_1^2 + \left(\frac{7}{72} + \frac{73\mu}{72}\right)B_1^2\\ &\quad \left. + \left(\frac{13(1-\mu)}{36} - \frac{13\mu}{36}\right)A_1B_1 - \frac{W\left(27\mu^2 - 31\mu + 8\right)}{18\sqrt{3}\mu(1-\mu)}\right],\end{aligned} \tag{32}$$

$$\Omega^0_{\eta\xi} = \Omega^0_{\xi\eta}, U^0_{\xi\xi'} = -\frac{5W}{4}, U^0_{\eta\eta'} = -\frac{7W}{4} U^0_{\xi\eta'} = U^0_{\eta\xi'} = -\frac{\sqrt{3}W}{4}, \left(U^0_{\xi\eta'}\right)^2 = 0.$$

Hence, the general expressions for the roots of the characteristic equation (30) are

$$\begin{aligned}
\lambda_1 &\longrightarrow -\frac{1}{2}\sqrt{\frac{a_0^2}{2}-\frac{4a_1}{3}-\frac{M}{4\sqrt{R}}-P-Q}-\frac{a_0}{4}-\frac{\sqrt{R}}{2},\\
\lambda_2 &\longrightarrow \frac{1}{2}\sqrt{\frac{a_0^2}{2}-\frac{4a_1}{3}-\frac{M}{4\sqrt{R}}-P-Q}-\frac{a_0}{4}-\frac{\sqrt{R}}{2},\\
\lambda_3 &\longrightarrow -\frac{1}{2}\sqrt{\frac{a_0^2}{2}-\frac{4a_1}{3}+\frac{M}{4\sqrt{R}}-P-Q}-\frac{a_0}{4}+\frac{\sqrt{R}}{2},\\
\lambda_4 &\longrightarrow \frac{1}{2}\sqrt{\frac{a_0^2}{2}-\frac{4a_1}{3}+\frac{M}{4\sqrt{R}}-P-Q}-\frac{a_0}{4}+\frac{\sqrt{R}}{2},
\end{aligned} \tag{33}$$

where

$$\begin{aligned}
K &= a_1^2 - 3a_0a_2 + 12a_3,\\
L &= 2a_1^3 - 9a_0a_1a_2 + 27a_2^2 + 27a_0^2a_3 - 72a_1a_3,\\
M &= -a_0^3 + 4a_0a_1 - 8a_2,\\
p &= \frac{\left(L+\sqrt{L^2-4K^3}\right)^{(1/3)}}{3\times 2^{(1/3)}},\\
Q &= \frac{2^{(1/3)}K}{3\left(L+\sqrt{L^2-4K^3}\right)^{(1/3)}},\\
R &= P+\frac{a_0^2}{4}-\frac{2a_1}{3}-Q.
\end{aligned} \tag{34}$$

5. Numerical Application

In this section, we study numerically the locations and stability of the triangular equilibrium points $L_{4,5}$ of the Sun-Earth system, by taking into account the dynamical flattening parameters of both the Sun (m_1) and Earth (m_2), the radiation pressure factor, and P–R drag of the Sun.

For the purpose of computation in this paper, the astrophysical data of the Sun-Earth system are borrowed from NASA ADS, Ragos et al. [29], Mecheri et al. [30], and Singh and Umar [31].

The first two even zonal harmonics of the Sun are $J_2^A \sim 2.2\times10^{-7}$ & $J_4^A \sim -4.5\times10^{-9}$ and those of the Earth are $J_2^B \sim 1.0\times10^{-3}$ & $J_4^B \sim -1.6\times10^{-6}$. Also, the orbital eccentricity of the Earth is $e \sim 0.0167$. Now, the dynamical flattening parameters of the primary bodies are given by $A_1 \sim 5.0\times10^{-12}$, $A_2 \sim -2.0\times10^{-18}$, $B_1 \sim 2.0\times10^{-12}$, and $B_2 \sim -5.2\times10^{-24}$.

The radiation pressure factor of the Sun q is defined as $q = 1-\alpha$ such that α can be expressed as $\alpha = (L_\odot/(2\pi G m_1 c\overline{\kappa}))$ [28], where $L_\odot$ is the luminosity of the Sun, G is the gravitational constant, c is the speed of light, and $\overline{\kappa}$ is the mass per unit area. By using Stefan–Boltzmann's law, the luminosity of the primary can be expressed as $L_\odot = 4\pi\overline{R}_\odot^2\sigma T_\odot^4$, where σ is the Stefan–Boltzmann's constant (see [28]). Also, the dimensionless velocity of light and the mass ratio of the Sun-Earth system are given by $c_d \sim 10064.84$ and $\mu \sim 3.0035\times10^{-6}$, respectively [29].

6. Discussion

The modified equations of motion of an infinitesimal mass in the framework of the elliptic restricted three-body problem under the effects of dynamical flattening parameters of both primaries, radiation pressure factor, and P–R drag of the bigger primary (i.e., the Sun) are given in equations (11), while the locations and characteristic equation of the triangular points $L_{4,5}$ are given in equations (24) and (34), respectively.

Figure 1 shows the effects of the perturbing forces involved in the problem under consideration for the three different cases and classical case as well on the locations of triangular equilibrium points $L_{4,5}$. Graph (a) is the classical case, graph (b) shows the effects of radiation pressure factor together with P–R drag, and graph (c) shows the effects of dynamical flattening parameters while graph (d) shows the combine effects of radiation pressure factor, P–R drag, and dynamical flattening parameters. This clearly shows that the perturbing forces under consideration have no significant effect on the locations of the triangular equilibrium points $L_{4,5}$ in the vicinity of the Sun-Earth system. These effects can only be seen in the table (see Table 1).

Table 2 shows numerical roots of the characteristic equation (30) for the classical case, as well as three other cases. In all cases, the characteristic roots reveal that all the roots are purely imaginary. This shows that the perturbing forces under consideration have no significant effect on the stability of the triangular equilibrium points $L_{4,5}$. Hence, the motion of an infinitesimal mass near the triangular equilibrium points $L_{4,5}$ of the Sun-Earth system is stable in the linear sense under the influence of these perturbations.

For $A_1^2 = B_1^2 = A_1B_1 = 0$ and $W = 0$, the present results of the triangular points in the circular case are in conformity with Singh and Taura [5] for $p_2 = M_b = 0$ in their results and for $\alpha = W = 0$, which also agrees with those of Abouelmagd et al. [11]; the difference in configuration of the primary bodies is responsible for the difference in sign.

Their results are [5, 11]

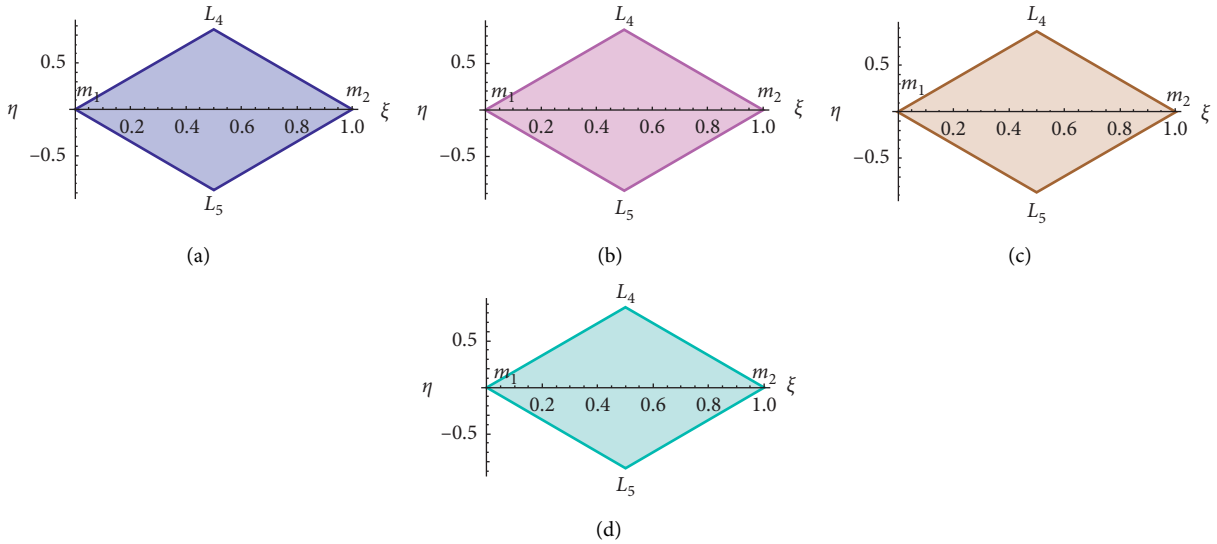

Figure 1: Effects of radiation pressure factor, P–R drag, and dynamical flattening parameters on the locations of triangular equilibrium points $L_{4,5}$ of the Sun-Earth system. (a) Blue triangle is for the classical case. (b) Purple triangle is for $A_i = B_i = 0,\ W \neq 0,\ \alpha \neq 0$ case. (c) Brown triangle is for $A_i \neq 0,\ B_i \neq 0,\ W = \alpha = 0$ case. (d) Turquoise triangle is for $A_i \neq 0,\ B_i \neq 0,\ W \neq 0,\ \alpha \neq 0$ case.

Table 1: Effects of radiation pressure factor, P–R drag, and dynamical flattening parameters on the locations of triangular equilibrium points $L_{4,5}$ of the Sun-Earth system.

	Case $(i = 1, 2)$	ξ	$\pm\eta$
1	Classical	0.4999969965000000	0.866025403784439
2	$A_i = B_i = 0, W \neq 0, \alpha \neq 0$	0.4999969964999347	0.866025403784474
3	$A_i \neq 0, B_i \neq 0, W = \alpha = 0$	0.4999969965015000	0.866025403782418
4	$A_i \neq 0, B_i \neq 0, W \neq 0, \alpha \neq 0$	0.4999969965014348	0.866025403782454

Table 2: Effects of radiation pressure factor, P–R drag, and dynamical flattening parameters on the stability of triangular equilibrium points $L_{4,5}$ of the Sun-Earth system.

	Case $(i = 1, 2)$	$\lambda_{1,2}$	$\lambda_{3,4}$	Remark
1	Classical	$\pm 0.004504233279349719i$	$\pm 0.999780664387228i$	Stable
2	$A_i = B_i = 0, W \neq 0, \alpha \neq 0$	$\pm 0.004504233327067630i$	$\pm 0.999780664386725i$	Stable
3	$A_i \neq 0, B_i \neq 0, W = \alpha = 0$	$\pm 0.004504233279348517i$	$\pm 0.999780664379725i$	Stable
4	$A_i \neq 0, B_i \neq 0, W \neq 0, \alpha \neq 0$	$\pm 0.004504233327101427i$	$\pm 0.999780664379223i$	Stable

$$
\begin{aligned}
r_1^2 &= (x+\mu)^2 + y^2,\\
r_2^2 &= (x+\mu-1)^2 + y^2,\\
\xi &= \frac{1}{2}\left[1 - 2\mu - \frac{2p_1}{3} + \frac{2p_2}{3} + A_1 - \frac{5}{4}A_2 - B_1 + \frac{5}{4}B_2\right],\\
\eta &= \pm\frac{\sqrt{3}}{2}\left[1 - \frac{2(p_1+p_2)}{9} - \frac{A_1}{3} + \frac{5A_2}{12} - \frac{B_1}{3} + \frac{5B_2}{12} - \frac{4M_b(2r_C-1)}{9\left(r_C^2+T^2\right)^{(2/3)}}\right],
\end{aligned}
\tag{35}
$$

$$
\begin{aligned}
r_1^2 &= (x-\mu)^2 + y^2,\\
r_2^2 &= (x-\mu+1)^2 + y^2,\\
x_{4,5} &= \mu - \frac{1}{2} - \frac{1}{2}(A_1 - B_1) + \frac{5}{8}(A_2 - B_2) + \frac{5}{8}\left(A_1^2 - B_1^2\right),\\
y_{4,5} &= \pm\frac{\sqrt{3}}{2}\left\{1 - \frac{1}{3}(A_1 - B_1) + \frac{5}{12}(A_2 + B_2) + \frac{1}{36}\left[7\left(A_1^2 + B_1^2\right) + 68A_1B_1\right]\right\}.
\end{aligned}
\tag{36}
$$

In the case $A_i = B_i = 0\,(i = 1, 2)$ in the present work, the obtained results of the triangular points in the circular case are in agreement with those of Singh and Simeon [18] by taking $\sigma_i = \sigma_i' = \delta_2 = W_2 = 0\,(i = 1, 2)$, and $W_1 \longrightarrow W$ in their results.

Their results are

$$x = \frac{1}{2} - \mu - \frac{\delta_1}{3} + \frac{\delta_2}{3} - \frac{W_1(2-\mu)}{3\mu(1-\mu)\sqrt{3}} - \frac{W_2(1+\mu)}{3\mu(1-\mu)\sqrt{3}} - \frac{(4+\mu)\sigma_1}{8\mu} + \frac{(4+3\mu)\sigma_1'}{8(1-\mu)} + \frac{(-7+3\mu)\sigma_2'}{8(1-\mu)}$$

$$y = \pm\frac{\sqrt{3}}{2}\left\{1 - \frac{2\delta_1}{9} - \frac{2\delta_2}{9} - \frac{1}{3}\left(\frac{23}{4} - \frac{1}{1-\mu}\right)\sigma_1' + \frac{1}{3}\left(\frac{19}{4} - \frac{1}{1-\mu}\right)\sigma_2' + \frac{1}{3}\left(\frac{-23}{4} + \frac{1}{\mu}\right)\sigma_1 + \frac{1}{3}\left(\frac{19}{4} - \frac{1}{\mu}\right)\right. \tag{37}$$

$$\left.\sigma_2 + \frac{W_1(2-3\mu)}{9\mu(1-\mu)} + \frac{W_2(1-3\mu)}{9\mu(1-\mu)}\right.$$

Our results for the second partial derivatives and the characteristic equation differ from those of Singh and Taura [5], Abouelmagd et al. [11], and Singh and Simeon [18] due to the elliptic nature of our potential-like function. However, the P–R drag parts of the partial derivatives coincide with those of Singh and Simeon [18], that is, for $\delta_2 = W_2 = 0, W \longrightarrow W_1$, and $\alpha \longrightarrow \delta_1$. Their results for the second partial derivatives are

$$\Omega_{xx}^0 = \frac{3}{4} + \delta_1\left(\frac{3\mu}{2} - \frac{1}{2}\right) + \delta_2\left(\frac{1}{2} - \frac{3\mu}{2}\right) + \left(\frac{57}{16} + \frac{45\mu}{16} - \frac{3}{2\mu}\right)\sigma_1 + \left(\frac{3}{16} - \frac{93\mu}{16} + \frac{3}{2\mu}\right)\sigma_2$$

$$+\left(\frac{39}{8} - \frac{69\mu}{16} - \frac{3\mu^2}{2(1-\mu)}\right)\sigma_1' + \left(\frac{-9}{2} + \frac{117\mu}{16} + \frac{3\mu^2}{2(1-\mu)}\right)\sigma_2' - \frac{W_1\left(\mu^2 - 13\mu + 8\right)}{4\mu(1-\mu)\sqrt{3}} + \frac{W_2\left(\mu^2 + 11\mu - 4\right)}{4\mu(1-\mu)\sqrt{3}},$$

$$\Omega_{yy}^0 = \frac{9}{4} + \delta_1\left(\frac{1}{2} - \frac{3\mu}{2}\right) + \delta_2\left(-1 + \frac{3\mu}{2}\right) + \left(\frac{87}{16} - \frac{45\mu}{16} + \frac{3}{2\mu}\right)\sigma_1 + \left(\frac{-21}{6} + \frac{45\mu}{16} - \frac{3}{2\mu}\right)\sigma_2$$

$$+\left(\frac{33}{8} + \frac{135\mu}{16} - \frac{33\mu}{8(1-\mu)} + \frac{45\mu^2}{8(1-\mu)}\right)\sigma_1' + \left(-\frac{135\mu}{16} + \frac{33\mu}{8(1-\mu)} - \frac{45\mu^2}{8(1-\mu)}\right)\sigma_2'$$

$$+\frac{W_1\left(5\mu^2 - 17\mu + 8\right)}{4\mu(1-\mu)\sqrt{3}} - \frac{W_2\left(5\mu^2 + 7\mu - 4\right)}{4\mu(1-\mu)\sqrt{3}},$$

$$\Omega_{xy} = \frac{3\sqrt{3}}{2}\left\{\frac{1}{2} - \mu - \frac{\delta_1(1+\mu)}{9} + \frac{\delta_2(2-\mu)}{9} + \left(\frac{47}{24} - \frac{89\mu}{24} - \frac{1}{3\mu}\right)\sigma_1 + \left(\frac{9}{24} - \frac{37\mu}{24} + \frac{1}{3\mu}\right)\sigma_2 + \left(\frac{25}{12} - \frac{85\mu}{24} + \frac{\mu}{6(1-\mu)} + \frac{\mu^2}{6(1-\mu)}\right)\sigma_1'\right.$$

$$\left.+\left(\frac{-3}{2} + \frac{11\mu}{8} - \frac{\mu}{6(1-\mu)} - \frac{\mu^2}{6(1-\mu)}\right)\sigma_2' - \frac{W_1\left(27\mu^2 - 31\mu + 8\right)}{18\mu(1-\mu)\sqrt{3}} - \frac{W_2\left(27\mu^2 - 23\mu + 4\right)}{18\mu(1-\mu)\sqrt{3}}\right.,$$

$$\Omega_{xy}^0 = \Omega_{yx}^0, \Omega_{x\dot{x}}^0 = \frac{-5W_1 - 5W_2}{4}, \Omega_{y\dot{y}}^0 = \frac{-7W_1 - 7W_2}{4}, \Omega_{x\dot{y}}^0 = -\frac{\sqrt{3}W_1}{4} + \frac{\sqrt{3}W_2}{4}, \left(\Omega_{x\dot{y}}^0\right)^2 = 0. \tag{38}$$

Thus, for $A_2 = B_2 = W = 0$ in the elliptic case of the triangular points, the obtained results coincide with those of Narayan and Shrivastava [6]; that is, for $\alpha \longrightarrow \epsilon^{(1)}$, $A_1 \longrightarrow A_1, B_1 \longrightarrow A_2, A_1\epsilon^{(1)} = 0\ \&\ \epsilon^{(2)} = 0$. Their results are

$$x_0 = \frac{1}{2} - \mu + \frac{A_1}{2} - \frac{A_2}{2} + \frac{\epsilon^{(2)}}{3} - \frac{\epsilon^{(1)}}{3} - \frac{A_1\epsilon^{(1)}}{2} + \frac{A_2\epsilon^{(2)}}{2}$$

$$y_0 = \pm\frac{\sqrt{3}}{2}\left[1 - \frac{A_1}{3} - \frac{A_2}{3} - \frac{2\epsilon^{(1)}}{9} - \frac{2\epsilon^{(2)}}{9} - \frac{A_1\epsilon^{(1)}}{3} - \frac{A_2\epsilon^{(2)}}{3}\right]. \tag{39}$$

In the elliptic case, the obtained results do not agree with those of Singh and Umar [4] and Singh and Tyokyaa [12]. This is because we have used the modified mean motion (n)(equation (10)) which does not contain the eccentricity (e) and semi-major axis (a). However, by substituting $e = 0$ and $a = 1$, their results in the triangular case coincide fully with ours upon relaxing some parameters in our problem. The same applies to the second partial derivatives.

Their results are [12, 14]

$$
\begin{aligned}
n^2 &= \frac{1}{a}\left[1 + \frac{3A_1}{2} + \frac{3B_1}{2} - \frac{15A_2}{8} - \frac{15B_2}{8} + \frac{3e^2}{2}\right],\\
\xi &= \frac{1}{2} - \mu + \frac{1}{2}\left(A_1 - B_1 - \frac{5}{4}A_2 a^{-(2/3)} + \frac{5}{4}B_2 a^{-(2/3)}\right),\\
\eta^2 &= a^{(2/3)} - \frac{1}{4} - a^{(2/3)}\left(e^2 + A_1 + B_1 - \frac{5}{4}A_2 - \frac{5}{4}B_2\right) + \left(\frac{A_1}{2} + \frac{B_1}{2} - \frac{5}{8}A_2 a^{-(2/3)} + \frac{5}{8}B_2 a^{-(2/3)}\right),
\end{aligned}
\tag{40}
$$

$$
\begin{aligned}
n^2 &= \frac{1}{a}\left[1 + \frac{3A_1}{2} + \frac{3A_2}{2} + \frac{3e^2}{2}\right],\\
\xi &= \frac{1}{2} - \mu + \frac{1}{2}\left[\left((aq_1)^{(2/3)}\right)\left(1 - e^2 - A_1 - A_2 + A_1(aq_1)^{(2/3)}\right) - (aq_2)^{(2/3)}\left(1 - e^2 - A_1 - A_2 + A_2(aq_2)^{(2/3)}\right)\right],\\
\eta &= \pm\left\{\left((aq_1)^{(2/3)}\right)\left(1 - e^2 - A_1 - A_2 + A_1(aq_1)^{(2/3)}\right) - \frac{1}{4}\left(1 + 2(aq_1)^{(2/3)}\right)\left(1 - e^2 - A_1 - A_2 + A_1(aq_1)^{(2/3)}\right)\right.\\
&\quad \left. -2\left((aq_2)^{(2/3)}\right)\left(1 - e^2 - A_1 - A_2 + A_2(aq_2)^{(2/3)}\right)\right\}^{(1/2)}.
\end{aligned}
\tag{41}
$$

The P–R drag finds importance in the investigation of the stability of zodiacal cloud, orbital evolution of cometary meteor steams, asteroidal particles, and dust rings around planets. This model is applicable not only to the Sun-Earth system but also to other systems in both the solar and stellar systems as well.

Data Availability

The data used to support the findings of this study are available from the corresponding author upon request.

Disclosure

It is part of work/research for the partial fulfilment of Ph.D. in Mathematics by the authors, respectively.

Conflicts of Interest

The authors declare that they have no conflicts of interest.

References

[1] V. Szebehely, *Theory of Orbits. The Restricted Problem of Three-Bodies*, Academic Press, New York, NY, USA, 1967.

[2] J. F. L. Simmons, A. J. C. McDonald, and J. C. Brown, "The restricted three-body problem with radiation pressure," *Celestial Mechanics*, vol. 35, p. 145, 1985.

[3] J. Singh and A. Umar, "Motion in the Photogravitational elliptic restricted three-body problem under an oblate primary," *The Astronomical Journal*, vol. 143, pp. 109–131, 2012a.

[4] J. Singh and A. Umar, "On the stability of triangular equilibrium points in the elliptic R3BP under radiating and oblate primaries," *Astrophysics and Space Science*, vol. 341, pp. 349–358, 2012b.

[5] J. Singh and J. J. Taura, "Combined effect of oblateness, radiation and a circular cluster of material points on the stability of triangular liberation points in the R3BP," *Astrophysics and Space Science*, vol. 351, no. 2, pp. 499–506, 2014.

[6] A. Narayan and A. Shrivastava, "Existence of resonance stability of triangular equilibrium points in circular case of the planar elliptical restricted three-body problem under the oblate and radiating primaries around the binary system," *Advances in Astronomy*, vol. 2014, Article ID 287174, 17 pages, 2014.

[7] M. Jain and R. Aggarwal, "A study of non-collinear libration points in restricted three body problem with Stokes drag effect when smaller primary is an oblate spheroid," *Astrophysics and Space Science*, vol. 358, p. 51, 2015.

[8] A. Umar and A. A. Hussain, "Motion in the ER3BP with an oblate primary and triaxial stellar companion," *Astrophysics and Space Science*, vol. 361, p. 344, 2016.

[9] E. I. Abouelmagd, "Existence and stability of triangular points in the restricted three-body problem with numerical applications," *Astrophysics and Space Science*, vol. 342, no. 1, pp. 45–53, 2012.

[10] E. I. Abouelmagd, H. M. Asiri, and M. A. Sharaf, "The effect of oblateness in the perturbed restricted three-body problem," *Meccanica*, vol. 48, pp. 2479–2490, 2013.

[11] E. I. Abouelmagd, M. S. Alhothuali, J. L. G. Guirao, and H. M. Malaikah, "The effect of zonal harmonic coefficients in the framework of the restricted three-body problem," *Advances in Space Research*, vol. 55, pp. 1660–1672, 2015.

[12] J. Singh and R. K. Tyokyaa, "Stability of triangular points in the elliptic restricted three-body problem with oblateness up to zonal harmonic J_4 of both primaries," *European Physical Journal Plus*, vol. 131, pp. 365–375, 2016.

[13] J. Singh, B. Ashagwu, and A. Umar, "Influence of the zonal harmonic of the primary on $L_{4,5}$in the photogravitational ER3BP," *International Frontier Science Letters*, vol. 10, pp. 23–36, 2016.
[14] J. H. Poynting, "Radiation in the solar system: its effect on temperature and its pressure on small bodies," *MNRAS*, vol. 64, pp. 525–552, 1903.
[15] H. P. Robertson, "Dynamical effects of radiation in the solar system," *MNRAS*, vol. 97, pp. 423–438, 1937.
[16] J. A. Burns, P. L. Lamy, and S. Soter, "Radiation forces on the small particles in the solar system," *ICARUS*, vol. 40, pp. 1–48, 1979.
[17] C. D. Murray, "Dynamical effects of drag in the circular restricted three body problem: location and stability of the Lagrangian equilibrium points," *ICARUS*, vol. 112, pp. 465–484, 1994.
[18] J. Singh and A. M. Simeon, "Motion around the triangular equilibrium points in the circular restricted three-body problem under triaxial luminous primaries with Poynting-Robertson drag," *International Frontier Science Letters*, vol. 12, pp. 1–21, 2017.
[19] Z. A. Alhussain, "Effects of Poynting–Robertson drag on the circular restricted three-body problem with variable masses," *Journal of Taibah University for Science*, vol. 12, no. 4, pp. 455–463, 2018.
[20] A. Chakraborty and A. Narayan, "Effect of stellar wind and Poynting–Robertson drag on photogravitational elliptic restricted three-body problem," *Solar System Research*, vol. 52, no. 2, pp. 168–179, 2018.
[21] T. O. Amuda, J. Singh, and L. Oni, "Motion around equilibrium points of an oblate body in the PR3BP with disc," *Indian Journal of Physics*, 2020.
[22] K. Mishra, J. P. Sharma, and B. Ishwar, "Stability of triangular equilibrium points in the Photogravitational elliptic restricted three body problem with Poynting-Robertson drag," *International Journal of Advanced Astronomy*, vol. 4, no. 1, pp. 33–38, 2016.
[23] J. Singh and T. O. Amuda, "Stability analysis of triangular equilibrium points in restricted three-body problem under effects of circumbinary disc, radiation and drag forces," *Journal of Astrophysics and Astronomy*, vol. 40, no. 1, pp. 1–14, 2019.
[24] J. M. A. Danby, *Fundamentals of Celestial Mechanics*, Willmann-Bell, Inc., Richmond, VA, USA, 2nd ed. edition, 1988.
[25] C. D. Murray and S. F. Dermott, *Solar System Dynamics*, Cambridge University Press, Cambridge, UK, 1999.
[26] V. V. Radzievskii, "The restricted problem of three bodies taking account of light pressure," *Astronomical Zhurnal*, vol. 27, pp. 250–256, 1950.
[27] I. D. Pater and J. J. Lissauer, *Planetary Sciences*, Cambridge University Press, New York, NY, USA, 2001.
[28] S. Yousuf and R. Kishor, "Effects of the albedo and disc on the zero velocity curves and linear stability of equilibrium points in the generalized restricted three-body problem," *Monthly Notices of the Royal Astronomical Society*, vol. 488, no. 2, pp. 1894–1907, 2019.
[29] O. Ragos, E. A. Perdios, V. S. Kalantonis, and M. N. Vrahatis, "On the equilibrium points of the relativistic restricted three-body problem," *Nonlinear Analysis: Theory, Methods & Applications*, vol. 47, no. 5, pp. 3413–3418, 2001.
[30] R. Mecheri, T. Abdelatif, A. Irbah, J. Provost, and G. Berthomieu, "New values of gravitational moments J2and J4deduced from helioseismology," *Solar Physics*, vol. 222, no. 2, pp. 191–197, 2004.
[31] J. Singh and A. Umar, "Effect of oblateness of an artificial satellite on the orbits around the triangular points of the earth-moon system in the axisymmetric ER3BP," *Differential Equations and Dynamical Systems*, vol. 25, no. 1, pp. 11–27, 2015.

Hindawi
Advances in Astronomy
Volume 2021, Article ID 6658051, 12 pages
https://doi.org/10.1155/2021/6658051

Research Article

Chaotic Oscillation of Satellite due to Aerodynamic Torque

Rashmi Bhardwaj [1] **and Mohammad Sajid** [2]

[1]*University School of Basic and Applied Sciences, Non-Linear Dynamics Research Lab, Guru Gobind Singh Indraprastha University, Dwarka, New Delhi, India*
[2]*Department of Mechanical Engineering, College of Engineering, Qassim University, Buraidah-51452, Al Qassim, Saudi Arabia*

Correspondence should be addressed to Rashmi Bhardwaj; rashmib22@gmail.com

Received 7 December 2020; Revised 11 January 2021; Accepted 28 January 2021; Published 10 February 2021

Academic Editor: Elbaz Abouelmagd

This study presents the chaotic oscillation of the satellite around the Earth due to aerodynamic torque. The orbital plane of the satellite concurs is same as the tropical plane of Earth. The half-width of riotous separatrix is assessed utilizing Chirikov's measure. Variety of boundary techniques shows that streamlined force boundary (ε), unpredictability of circle (e), and mass-proportion (ω_0) convert normal wavering to the disorganized one. We studied the behavior of trajectories due to change in parameters with Lyapunov exponents and time series plots. The theory is applied to Resourcesat-1, an artificial satellite of the Earth.

1. Introduction

Artificial satellites are widely used in telecommunication, mass media and weather forecast, agriculture, and navigation. Satellites are widely used in agriculture and forestry for crop inventory, yield prediction, and soil/crop condition monitoring. Resourcesat-1 (also known as IRS-P6) is an advanced remote sensing satellite built by the Indian Space Research Organization (ISRO). The tenth satellite of ISRO in IRS series, Resourcesat-1, is intended to not only continue the remote sensing data services provided by IRS-1C and IRS-1D, both of which have far outlived their designed mission lives, but also vastly enhance the data quality. The major objectives of Resourcesat-1 are to provide continued remote sensing data services on operational basis for integrated land and water resources management with enhanced multispectral/spatial coverage and stereo imaging and also to develop new areas of applications to take full advantages of increased spatial and spectral resolutions. For a country like India, with populations separated by rough terrain and different languages, communications satellites provide remote populations access to education and to medical expertise that would otherwise not reach them [1].

Satellite exhibits chaotic motion under the influence of different torques and, for the low-thrust tug-debris tethered system in a Keplerian orbit, experiences chaotic attitude motion. Aslanov et al. [2] introduced steady and insecure fixed answers for the in-plane movement of the framework in a roundabout circle, which rely upon the estimation of the pull's pushed. Bhardwaj and Kaur [3] studied the satellite motion under the effect of aerodynamic torque and explained in detail about the nonresonance oscillation. Also, they discussed that under the influence of magnetic torque for different mass parameters, tumbling of satellite experiences shows the chaotic signal [4]. Bhardwaj and Sethi [5] discussed that air drag exhibits resonance criteria for nonlinear motion. Rotational nonlinear oscillation of the satellite under the influence of combined aerodynamic and magnetic torque was discussed by Bhardwaj et al. [6], and they concluded that with the change in mass parameter, the dynamics of the satellite altered. Bhardwaj and Tuli [7] discussed the nonlinear planar oscillation of a satellite under the influence of third-body torque, and it is concluded that Hyperion tumbled more chaotically with the change in the third body torque parameter. Planar oscillation of a satellite in an elliptic orbit for magnetic torque was studied by

Bhardwaj and Kaur [8], and they observed that as eccentricity changed, the oscillation of satellite exhibits chaotic motion which increases with the increase in eccentricity. Bhardwaj and Bhatnagar [9–12] studied the nonlinear planar rotational oscillation of the satellite in circular orbit for magnetic torque and for third-body torque in elliptic orbit, and it is concluded that the mass parameter and torque parameter play an important role in changing the motion from regular to the chaotic one.

Chegini et al. [13, 14] explored mathematically turmoil in demeanor elements of an adaptable satellite made out of an inflexible body and two indistinguishable unbending boards connected to the fundamental body with springs using analytical and numerical methods. Clemson and Stefanovska [15] discussed the analysis of nonautonomous dynamics for extracting properties of interactions and the direction of couplings for chaotic, stochastic, and nonautonomous behaviour. For the chaotic class, the Lorenz system; for the stochastic class, the noise forced Duffing system; and for the nonautonomous class, the Poincare oscillator with quasiperiodic forcing discussed and gave a good review to distinguish nonautonomous dynamics from chaos or stochasticity. Doroshin [16] got altered numerical models and dynamical frameworks to give an idea of heteroclinic chaos and its local suppression in attitude dynamics for dual spin spacecraft and gyrostat satellites. Gutnik and Sarychev [17] mathematically simulated the motion of the satellite under aerodynamic torque for the control system influenced by the active dumping torques. Inarrea and Lanchares [18] examined the pitch movement elements of an awry rocket in round circle affected by a gravity inclination force and accepted that shuttle is irritated by a little streamlined drag force corresponding to the precise speed of the body about its mass community. Koupriano and Shevchenko [19] considered the issue of recognizability of clamorous systems in turn of planetary satellites utilizing Jacobian assessment approach. Kuptsov and Kuznets [20] discussed the Lyapunov analysis of strange pseudohyperbolic attractors and briefly analyzed about the angles between tangent subspaces, local volume expansion, and contraction.

The phenomenon of chaos is generally related to the field of dynamical systems, and it can be characterized in the dynamics by sensitive dependence on the initial conditions. Chaos is a fascinating mathematical and physical phenomenon. The study of chaos shows that simple systems can exhibit a complex and unpredictable behaviour. The chaos in the dynamics can be identified and quantified by several techniques. A positive value of the Lyapunov exponent provides chaos in the dynamics which is discussed by Letellier [21]. Liu and Cui [22] analyzed the nonlinear model which should be adopted for the sailcraft in long duration missions, and the restricted position of the sliding mass could be selected elaborately to utilize the resultant torque by the gravitational and center-of-mass or center-of-pressure torques. Melnikov and Shevchenko [23] considered the issue of figuring the Lyapunov season of the disorganized movement region for resonances in satellite movement. Pritykin et al. [24] discussed the long-term evolution of attitude motion for defunct satellites in nearly polar orbits. Rosengren et al. [25] indicated that the sporadic and random characters of the Global Navigation Satellite Systems' circles mirror a comparative inconsistency in the circles of numerous divine bodies in our solar framework. Rawashdeh [26] studied the attitude analysis of small satellites using model-based simulation. Efimov et al. [27] discussed about long-term attitude dynamics of space debris for sun-synchronous orbits and studied about Cassini cycles and chaotic stabilization. Chang [28] gave an idea of stability, chaos detection, and quenching chaos for the swing equation system. Wang et al. [29] developed the six-dimensional hyperchaotic system and applied for secure communication circuit implementation. Wolf et al. [30] introduced the main calculations that permit the assessment of nonnegative Lyapunov types from an exploratory time arrangement.

Apparently, none of the creators have contemplated the bedlam affected by the streamlined force in an elliptic circle. In the current examination, we contemplated the tumultuous movement of a satellite affected by a streamlined force in an elliptic circle. In this study, the condition of movement for the framework is inferred. Utilizing variety of boundaries techniques, the unrest, libration, and endless period separatrix are examined. The mathematical recreation of tumultuous movement affected by the streamlined force is examined for Earth-Resourcesat-1 satellite.

2. Mathematical Model

Let an inflexible satellite S revolve in elliptic circle around Earth E with the end goal that orbital plane concurs with central plane of Earth. S is thought a trihub body with head snapshots of inactivity $A < B < C$ at its focal point of mass, and C is the snapshot of idleness about turn hub which is opposite to the orbital plane. Let $\overrightarrow{r}$ be the sweep vector of focal point of mass of S, ν be the true anomaly, θ be the point that the long hub of S makes with fixed line EF lying in the orbital plane, and $(\eta/2)$ be the point between the span vector and long pivot as shown in Figure 1.

Equation of motion for the system, see details as given in [3], is obtained as

$$\begin{aligned}\frac{d^2\eta}{d\nu^2} + n^2\eta = {} & -e\cos\nu\frac{d^2\eta}{d\nu^2} + 2e\sin\nu\frac{d\eta}{d\nu} \\ & + 4e\sin\nu + n^2(\eta - \sin\eta) \\ & + \varepsilon\left(A_*\nu^2\sin\nu + B_*\nu\sin\nu + C_*\sin\nu + D_*\nu + E_*\right),\end{aligned} \tag{1}$$

where $n^2 = ((3(B-A))/C) =$ mass parameter; $\varepsilon = ((\rho SC_d l^2)/(C\Omega^2)) =$ aerodynamic torque parameter; $A_* = ((a^2(1-e))/\Omega^2 l) =$ constant; $B_* = (((\omega a(2e-1))/\Omega)\cos i + ((2V_1 a(1-2e))/\Omega l)) =$ constant; $C_* = (\omega V_1(2e-1)\cos i + ((V_1^2(1-2e))/l) + ((\omega ae)/2\Omega)\sin i) =$ constant; $D_* = (((\omega a(2e-1))/\Omega)\sin i) =$ constant; $E_* = \omega V_1(2e-1)\sin i =$ constant; and

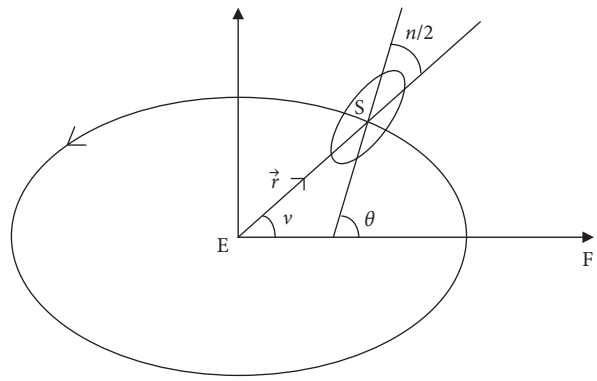

Figure 1: S revolving around Earth E.

$$\frac{d^2\theta}{dt^2} = \frac{\mu}{r^3}\left(-2e\sin\nu - e\sin\nu\frac{d\eta}{d\nu} + \frac{1}{2}(1+e\cos\nu)\frac{d^2\eta}{d\nu^2}\right). \tag{2}$$

From equations (1) and (2), we get

$$\frac{d^2\theta}{dt^2} = -\frac{\mu}{2r^3}\left(n^2\sin\delta - \varepsilon_1 \cdot \left(A_*\nu^2\sin\nu + B_*\nu\sin\nu + C_*\sin\nu + D_*\nu + E_*\right)\right). \tag{3}$$

Taking $n^2 = \omega_0^2 = ((3(B-A))/C)$; $\theta = \nu + (\delta/2) \Rightarrow \delta = 2(\theta - \nu)$, equation (3) becomes

$$\frac{d^2\theta}{dt^2} = -\frac{\mu}{2r^3}\left(\omega_0^2\sin(2(\theta-\nu)) - \varepsilon_1 \cdot \left(A_*\sin\nu^3 + B_*\sin\nu^2 + C_*\sin\nu + D_*\nu + E_*\right)\right). \tag{4}$$

In condition (4), if units are picked to the point that orbital time of S is 2π and its semisignificant pivot is 1, at that point dimensionless, time is equivalent to mean longitude or genuine inconsistency which is 2π intermittent and $\mu = 1$. As r and ν are 2π occasional as expected, utilizing Fourier-like Poisson series (Wisdom et al. [31]), equation (4) becomes

$$\frac{d^2\theta}{dt^2} + \frac{\omega_0^2}{2}\sum H\left(\frac{m}{2}, e\right)\sin(2\theta - mt) - \frac{\varepsilon}{2}\left(A_*\sin\nu^3 + B_*\sin\nu^2 + C_*\sin\nu + D_*\nu + E_*\right) = 0, \tag{5}$$

$H((m/2), e)$ corresponds to $e^{2|(m/2)-1|}$ and is given by Cayley [32] and Goldreich and Peale [33]. At the point, if e is little, $H((m/2), e) \cong -(e/2)$. The half whole number $(m/2)$ is signified by the image p. Resonances happen at whatever point one of the contentions of the sine or cosine capacities is almost fixed, for example, at whatever point $|(d\theta/dt) - p| \ll (1/2)$. In such cases, it is to rework the condition of movement as far as the gradually changing reverberation variable $\nu_p = \theta - pt \Rightarrow ((d^2\nu_p)/dt^2) = ((d^2\theta)/dt^2) \Longrightarrow 2\nu_p = 2\theta - mt$. Equation (5) can be written as

$$\frac{d^2\nu_p}{dt^2} + \frac{\omega_0^2}{2}H(p,e)\sin 2\nu_p - \frac{\varepsilon}{2}\left(A_*\sin\nu^3 + B_*\sin\nu^2 + C_*\sin\nu + D_*\nu + E_*\right) = 0. \tag{6}$$

This is pendulum perturbed by $(\varepsilon/2)(A_*\sin\nu^3 + B_*\sin\nu^2 + C_*\sin\nu + D_*\nu + E_*)$. When $\varepsilon \neq 0$, condition (6) speaks to the condition of movement of upset pendulum given by

$$\left(d^2x_p/dt^2\right) + f'\left(x_p\right) = m_p g\prime\left(x_p, t\right), \tag{7}$$

where $x_p = 2\nu_p$; $f'(x_p) = k_{1p}^2\sin x_p$; $k_{1p}^2 = \omega_0^2 H(p,e)$; $m_p = \varepsilon$; and $g'(x_p, t) = A_*\sin t^3 + B_*\sin t^2 + C_*\sin t + D_*t + E_*$. The unperturbed piece of condition (7) is $((d^2x_p)/dt^2) + f'(x_p) = 0 \Rightarrow (dx_p/dt)^2 = 2k_{1p}^2\cos x_p + c_{1p}$. The integration constant is defined as c_{1p}. If $c_{1p} + 2k_{1p}^2 \geq 0$, then motion is said to be real. Three kinds of motions are defined based on the conditions $c_{1p} > 2k_{1p}^2$, $c_{1p} < 2k_{1p}^2$, and $c_{1p} = 2k_{1p}^2$.

2.1. Category-I. We consider $c_{1p} > 2k_{1p}^2$. For $c_{1p} > 2k_{1p}^2$, the value of (dx_p/dt) never vanishes; it is either certain or negative, and the pendulum is seeming well and good or the other. For this situation, the unperturbed arrangement is

$$x_p = l_p + c_{1p}\sin l_p + o\left(c_{1p}^2\right),$$
$$l_p = n_p t + \varepsilon_1,$$
$$c_{1p} = \frac{k_{1p}^2}{n_p^2};$$
$$\frac{1}{n_p} = \frac{1}{2\pi}\int_0^{2\pi}\frac{dx_p}{\left(c_{1p} + 2k_{1p}^2\cos x_p\right)^{(1/2)}}, \tag{8}$$

Table 1: Earth-Resourcesat-1 system for fixed values of $A_* = 3.36E + 09, B_* = 1596.387, C_* = -103631, D_* = -4E + 08, E_* = 200.1022, e = 0.001, \varepsilon$, and variation in n.

Figure no.	n	ε	Graphical behaviour of Poincare map	Graphical behaviour of Lyapunov exponent
2	0.0001	0.000000000000000001	Regular curves disintegrate as ε increases	Chaotic
3		0.00000000000001		Chaotic
4	0.9	0.000000000000000001		Periodic
5		0.00000000000001		Periodic and chaotic

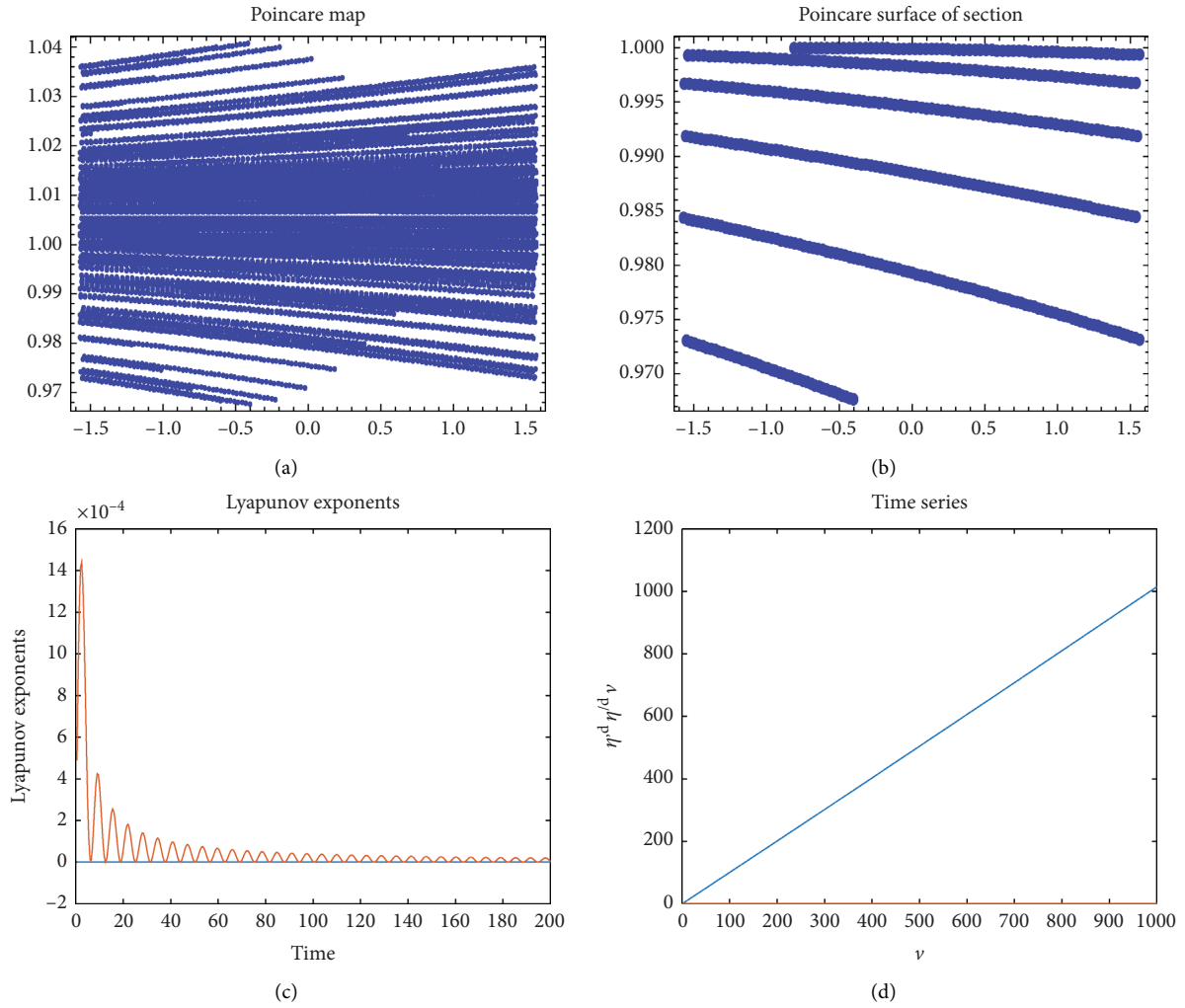

Figure 2: For $n = 0.0001, \varepsilon = 0.000000000000000001, A_* = 3.36E + 09, D_* = -4E + 08, B_* = 1596.387, C_* = -103631, E_* = 200.1022$, and $e = 0.001$. (a) Poincare map, (b) Poincare surface of section, (c) Lyapunov exponent, and (d) time series.

where c_{1p} and ε_1 are the discretionary constants, and l_p is a contention. Intermittent segment of this arrangement can be viewed as swaying about the mean condition of movement which is unrest with a period $(2\pi/n_p)$. Half plentifulness of wavering is clearly not exactly π, and it diminishes as n_p increments. Here, we may see that $(\mathrm{d}x_p/\mathrm{d}t) \neq 0$, and the movement is supposed to be of type I, for example, upheaval. Brown and Shook [34] proposed the theory of variation of parameters for the perturbed pendulum which gives

$$\frac{\mathrm{d}c_{1p}}{\mathrm{d}t} = \frac{m}{k_p}\frac{\partial x}{\partial l}g',$$

$$\frac{\mathrm{d}l_p}{\mathrm{d}t} = n - \frac{m}{k_p}\frac{\partial x}{\partial c_1}g', \tag{9}$$

$$k_p = \frac{\partial}{\partial c_{1p}}\left(n_p\frac{\partial x}{\partial l}\right)\frac{\partial x}{\partial l} - n_p\frac{\partial^2 x}{\partial l^2}\frac{\partial x}{\partial c_{1p}},$$

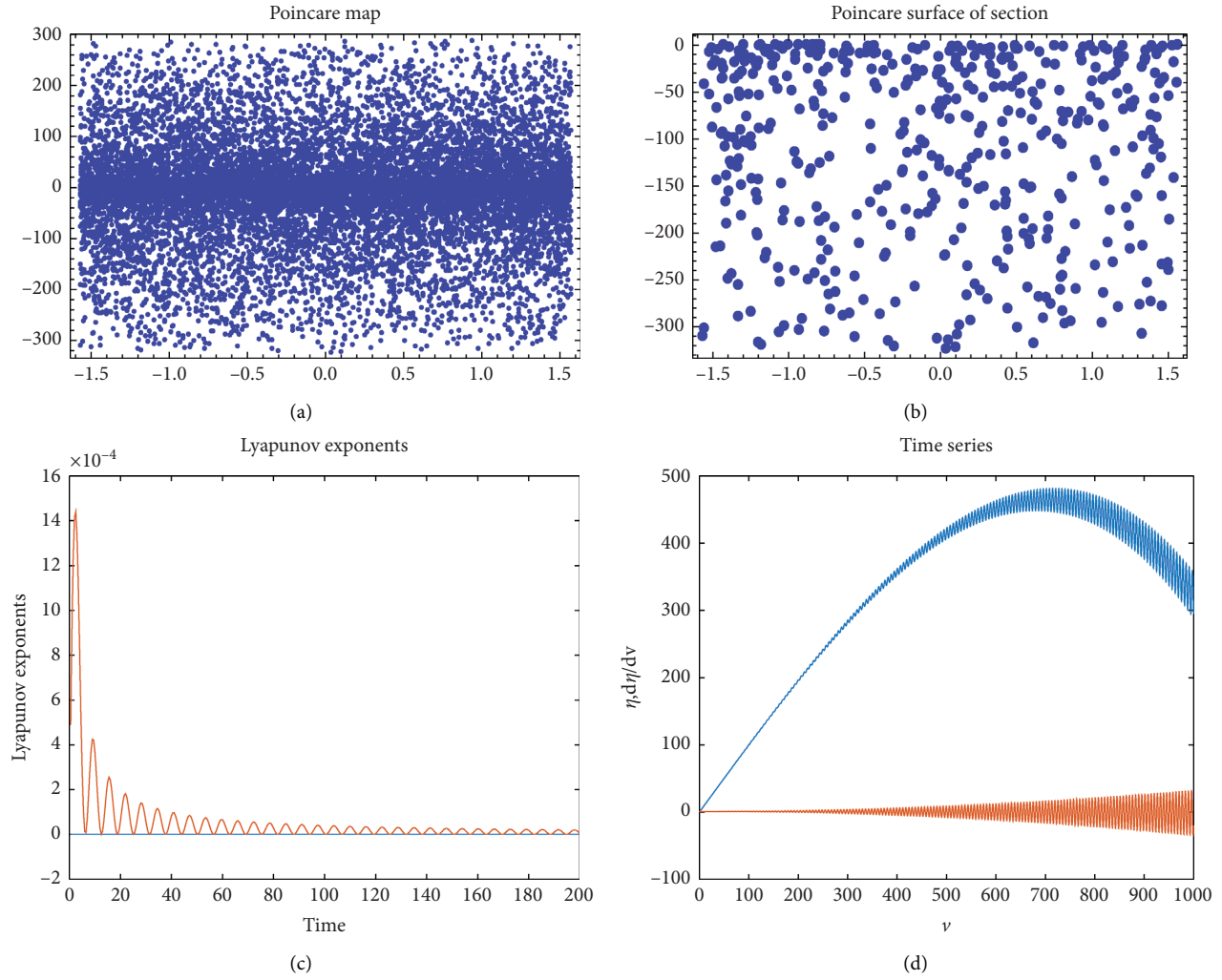

FIGURE 3: For $n = 0.0001, \varepsilon = 0.00000000000001, A_* = 3.36E+09, D_* = -4E+08, \quad B_* = 1596.387, C_* = -103631, E_* = 200.1022,$ and $e = 0.001$. (a) Poincare map, (b) Poincare surface of section, (c) Lyapunov exponent, and (d) time series.

since $c_{1p} = (k_{1p}^2/n_p^2)$. Therefore,

$$\begin{aligned}
\frac{\partial n_p}{\partial c_{1p}} &= -\frac{n_p}{2c_{1p}}, \\
\frac{\partial x_p}{\partial l_p} &= 1 + c_{1p}\cos l_p, \\
\frac{\partial^2 x_p}{\partial {l_p}^2} &= -c_{1p}\sin l_p, \\
\frac{\partial x_p}{\partial c_{1p}} &= \sin l_p, \\
\frac{\partial^2 x_p}{\partial c_{1p}\partial l_p} &= \cos l_p.
\end{aligned} \tag{10}$$

Putting the above values and writing $k_p = k_{1p}$, equation (9) can be written as

$$\begin{aligned}
k_{1p} = &-\frac{n_p}{2c_{1p}} - \frac{n_p c_{1p}\cos^2 l_p}{2} \\
&+ n_p c_{1p} \cong -\frac{n_p}{2c_{1p}}.
\end{aligned} \tag{11}$$

Hence, $(\mathrm{d}c_{1p}/\mathrm{d}t) \cong 0$; so, c_{1p} is the second order approximation constant. Second equation of (9) gives

$$\begin{aligned}
\frac{\mathrm{d}l_p}{\mathrm{d}t} = &\, n_p + \frac{2m_p c_{1p}}{n_p}\sin l_p \\
&\cdot \left(A_* \sin t^3 + B_* \sin t^2 + C_* \sin t + D_* t + E_*\right).
\end{aligned} \tag{12}$$

Rejecting second or higher order terms, we get

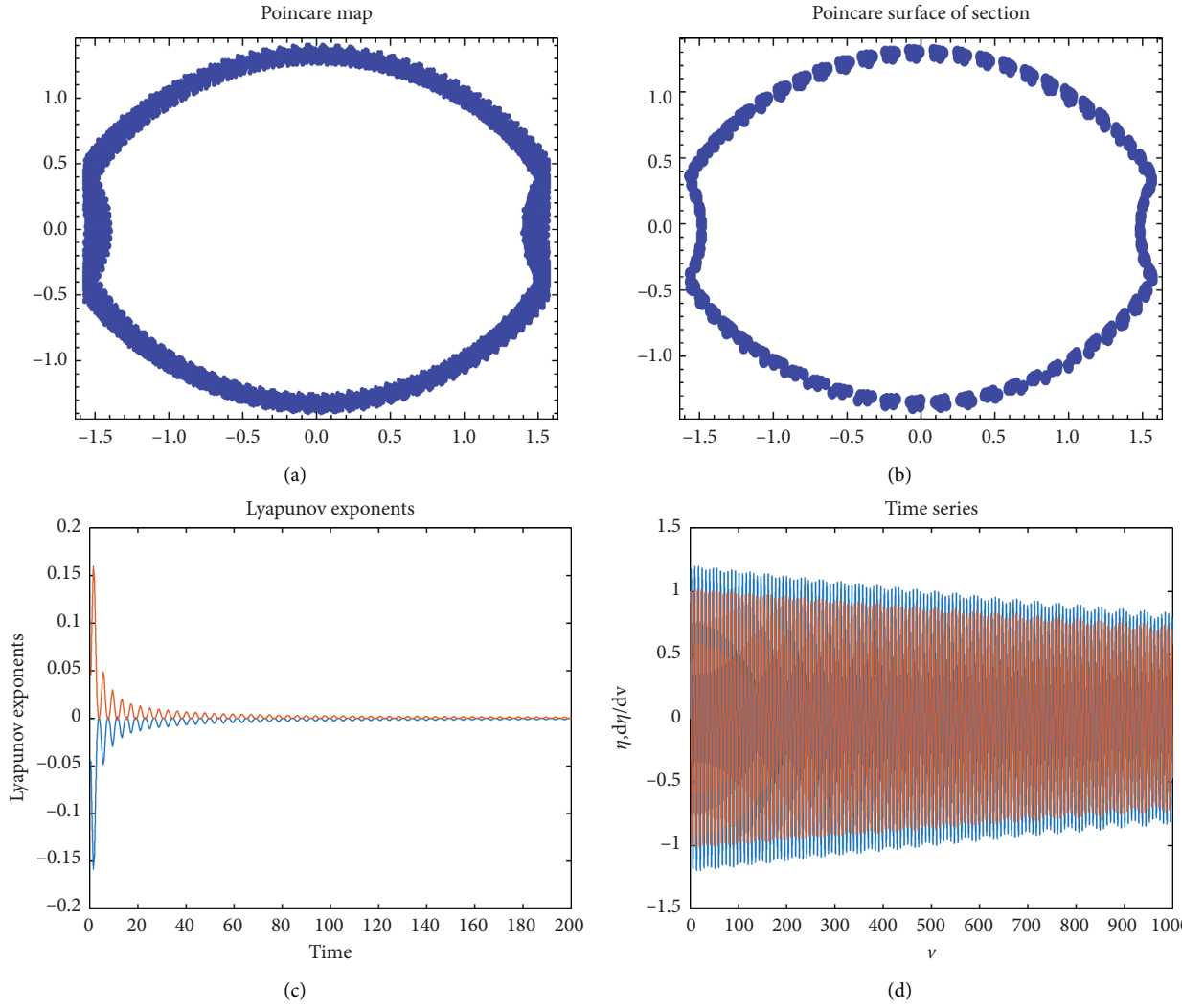

FIGURE 4: For $n = 0.9, \varepsilon = 0.000000000000000001, A_* = 3.36E + 09, D_* = -4E + 08, \quad B_* = 1596.387, C_* = -103631, E_* = 200.1022,$ and $e = 0.001$. (a) Poincare map, (b) Poincare surface of section, (c) Lyapunov exponent, and (d) time series.

$$\frac{d^2 l_p}{dt^2} = \left(\frac{2C_* m_p c_{1p}}{n_p} + \frac{2D_* m_p c_{1p}}{n_p} - \frac{6E_*^2 m_p^2 c_{1p}}{n_p^2} + \frac{4E_*^2 m_p^2 c_{1p}^2}{n_p}\right) \cdot \sin l_p + \left(1 + 2c_{1p}\right)\left(C_* m_p \sin t + D_* m_p t + E_* m_p\right),$$

$$\frac{d^2 l_p}{dt^2} + k_{2p}^2 \sin l_p = m_p\left(1 + 2c_{1p}\right)\left(C_* \sin t + D_* t + E_*\right). \tag{13}$$

Let $l_p = x_p$, $(d^2 x_p/dt^2) + k_{2p}^2 \sin x_p = m_p g\prime\prime(x_p, t)$, where $g\prime\prime(x_p, t) = (1 + 2c_{1p})(C_* \sin t + D_* t + E_*)$, and $k_{2p}^2 = -(((2C_* m_p c_{1p})/n_p) + ((2D_* m_p c_{1p})/n_p) - ((6E_*^2 m_p^2 c_{1p})/n_p) + ((4E_*^2 m_p^2 c_{1p}^2)/n_p))$. The unperturbed part of the above equation is $(d^2 x_p/dt^2) + k_{2p}^2 \sin x_p = 0 \Rightarrow (dx_p/dt)^2 = 2k_{2p}^2 \cos x_p + c_{2p}$, where c_{2p} is a constant of integration. Three types of motions are obtained for the motion of pendulum.

(1) If $(dx_p/dt) \neq 0$, then motion of type 1 exists. For type 1, the solution is $x_p = N_p t + \varepsilon_{2p} + (k_{2p}^2/N_p^2) \sin(N_p t + \varepsilon_{2p}) + \cdots$; $(1/N_p) = (1/2\pi)\int_0^{2\pi} (dx_p/(c_{2p} + 2k_{2p}^2 \cos x_p)^{(1/2)})$, where c_{2p} and ε_{2p} are the arbitrary constants. For first approximation, $N_p = N_{0p}$; so, $x_p = x_{0p} + (k_{2p}^2/N_{0p}^2)\sin(x_{0p})$, where $x_{0p} = N_{0p} t + \varepsilon_{2p}$. This is situation of unrest.

(2) If $(dx_p/dt) = 0$ at 0 or π, then motion of type 2 exists. For type 2, solution is $x_p = \lambda_p \sin(p\prime t + \lambda_0)$, where $p\prime = \sqrt{((2m_p \omega_0^2 H(p,e))/n_p^3)(C_* + D_* + ((E_*^2 m_p)/n_p)(-3 + 2((2\omega_0^2 H(p,e))/n_p^2)))}$, λ_p, λ_0 are defined as the constants of integration. This is situation of libration.

(3) Type 3 when $c_{2p} = 2k_{2p}^2 = -((4\omega_0^2 m_p H(p,e))/n_p^3)(C_* + D_* + ((E_*^2 m_p)/n_p)(2((\omega_0^2 H(p,e))/n_p^2) - 3))$. Solution is $x_p + \pi = 4\tan^{-1} \exp(k_{2p} t + \alpha_0)$. The arbitrary constant is defined as α_0. It is observed that

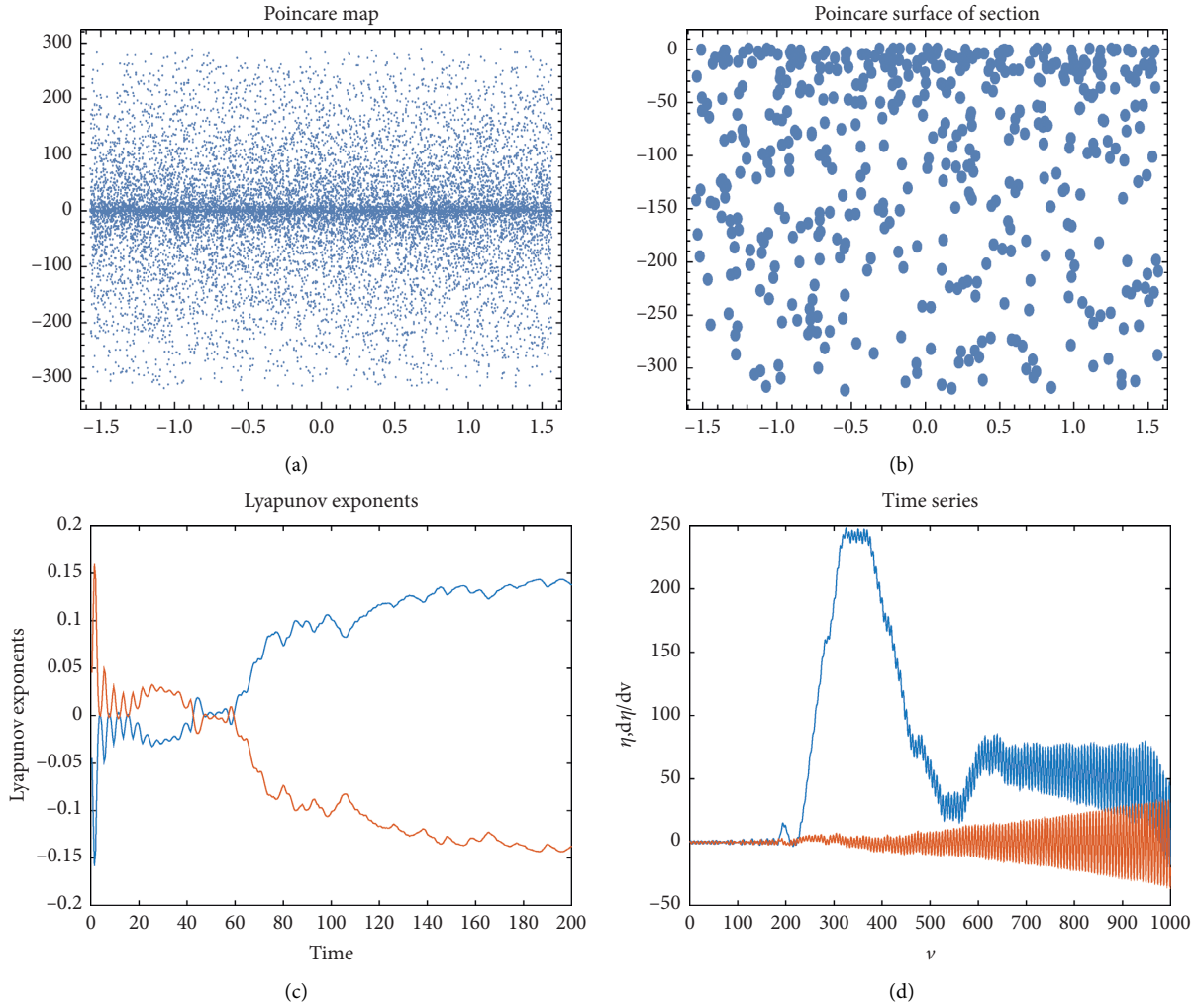

Figure 5: For $n = 0.9, \varepsilon = 0.00000000000001, A_* = 3.36E + 09, D_* = -4E + 08$, $B_* = 1596.387, C_* = -103631, E_* = 200.1022$, and $e = 0.001$. (a) Poincare map, (b) Poincare surface of section, (c) Lyapunov exponent, and (d) time series.

Table 2: Earth-Resourcesat-1 system for fixed values of $A_* = 3.36E + 09, B_* = 1596.387, C_* = -103631, D_* = -4E + 08, E_* = 200.1022, e = 0.001, n$, and variation in ε.

Figure no.	ε	n	Graphical behaviour of Poincare map	Graphical behaviour of Lyapunov exponent
6	0.00000000000000000000000005	0.00001	Curves behave chaotically but remains almost same	Chaotic
7		0.005		Chaotic
8	0.000000000000000000005	0.4		Periodic and chaotic
9		0.8		Periodic

as $t \longrightarrow \pm\infty$, $(dx_p/dt) = 0$ as $x_p \longrightarrow \pm\pi$ are consequently higher subsidiaries of x_p way to deal with zero. As x_p ways to deal with $\pm\pi$, t watches out for uncertain capacity of x_p. This is case of boundless period separatrix.

We presumed that because of the aftereffects of type 1, type 2, and type 3, the streamlined force assumes a huge part in changing the movement of upset to libration or to boundless period separatrix.

2.2. Category-II: $c_{1p} < 2k_{1p}^2$. For this situation, unperturbed arrangement is $x_p = c_{1p} \sin l_p + o(c_{1p}^3)$, $l_p = n_p t + \varepsilon_1$, and $n_p = k_{1p}(1 - (1/16)c_{1p}^2 + \cdots)$, where c_{1p} and ε_1 are the discretionary constants, and l_p is a contention. If there should arise an occurrence of bothered pendulum by utilizing the hypothesis of variety of boundaries, we get $k_p = (\partial/\partial c_{1p})(n_p(\partial x/\partial l))(\partial x/\partial l) - n_p(\partial^2 x/\partial l^2)(\partial x/\partial c_{1p})$, $k_p \cong k_{1p} c_{1p}$,

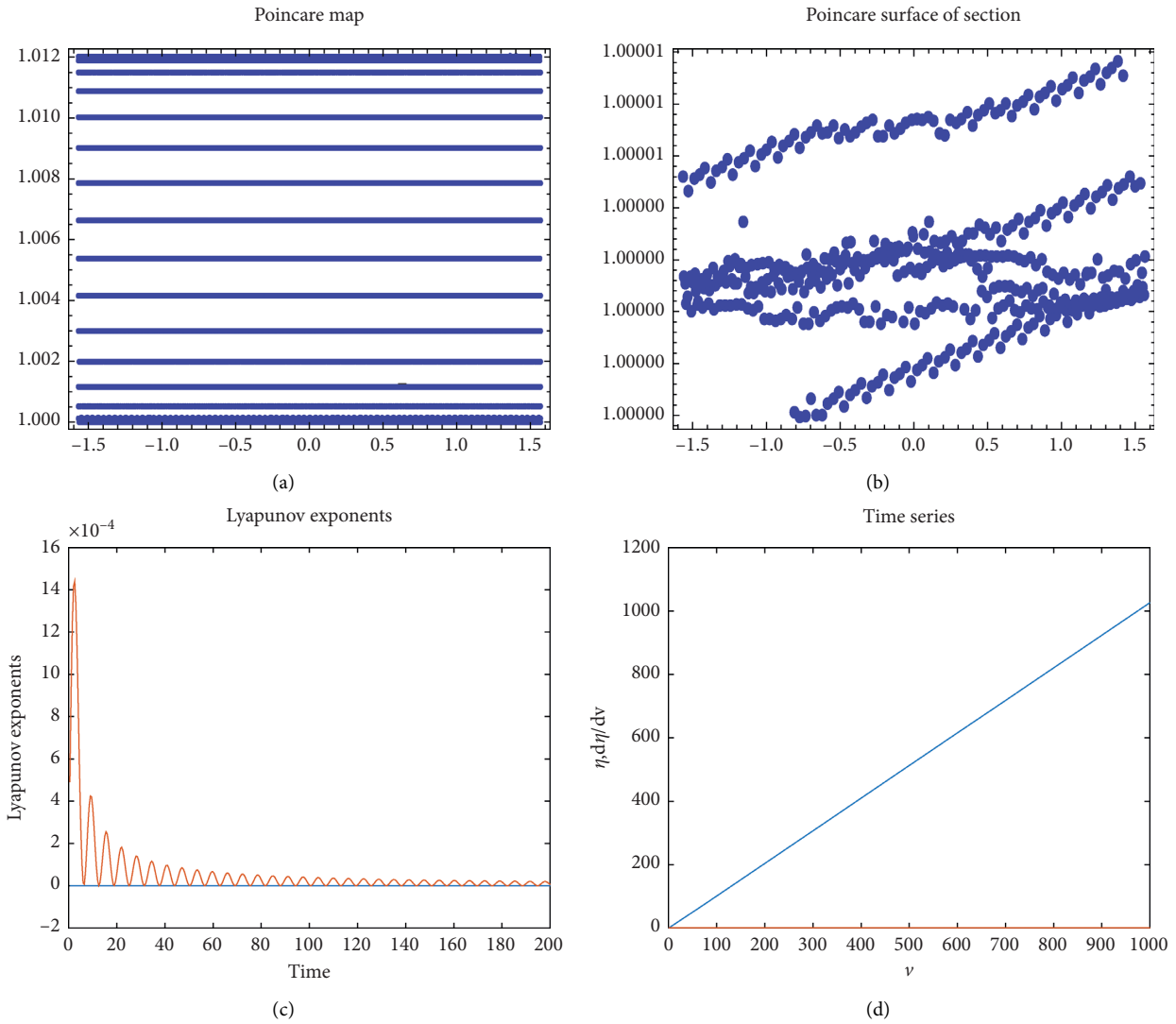

FIGURE 6: For $n = 0.00001, \varepsilon = 0.00000000000000000000000005, A_* = 3.36E + 09, \quad D_* = -4E + 08, B_* = 1596.387, C_* = -103631, E_* = 200.1022$, and $e = 0.001$. (a) Poincare map, (b) Poincare surface of section, (c) Lyapunov exponent, and (d) time series.

$$\begin{aligned}
\frac{d^2 l_p}{dt^2} &= \frac{m_p}{k_{1p}c_{1p}}\left(-C_* - D_* + \frac{m_p E_*^2}{k_{1p}c_{1p}^2}\right)\sin l_p \\
&\quad - \frac{m_p}{c_{1p}}\left(C_* \sin t + D_* t + E_*\right) \\
&\quad + \frac{m_p^2}{k_{1p}^2 c_{1p}^2}\left(C_* E_* \sin t + D_* E_* t + E_*^2\right), \\
\Rightarrow \frac{d^2 l_p}{dt^2} + k_{3p}^2 \sin l_p &= -\frac{m_p}{c_{1p}}\left(C_* \sin t + D_* t + E_*\right) \\
&\quad + \frac{m_p^2}{k_{1p}^2 c_{1p}^2}\left(C_* E_* \sin t + D_* E_* t + E_*^2\right),
\end{aligned} \tag{14}$$

where $k_{3p}^2 = -(m_p/k_{1p}c_{1p})(-C_* - D_* + (m_p E_*^2/k_{1p}c_{1p}^2))$. The unperturbed part of the equation is $((d^2 l_p)/dt^2) + k_{3p}^2 \sin l_p = 0$, where l_p is little, and the arrangement of above condition is $l_p = e^{k_{3p}t} + e^{-k_{3p}t}$. It is again a condition of a pendulum, and as in a prior case, the movement is alluded as upset, libration, and boundless period separatrix.

2.3. Category-III: $c_{1p} = 2k_{1p}^2$. The unperturbed arrangement is

$$x_p + \pi = 4 \tan^{-1} \exp\left(k_{1p}t + \alpha_0\right), \tag{15}$$

where α_0 is a discretionary steady. This is the situation of endless period separatrix as asymptotic forward and in reverse so as to insecure harmony. In this class, the idea of unperturbed arrangement does not change by considering the streamlined force. Close to the endless period, separatrix

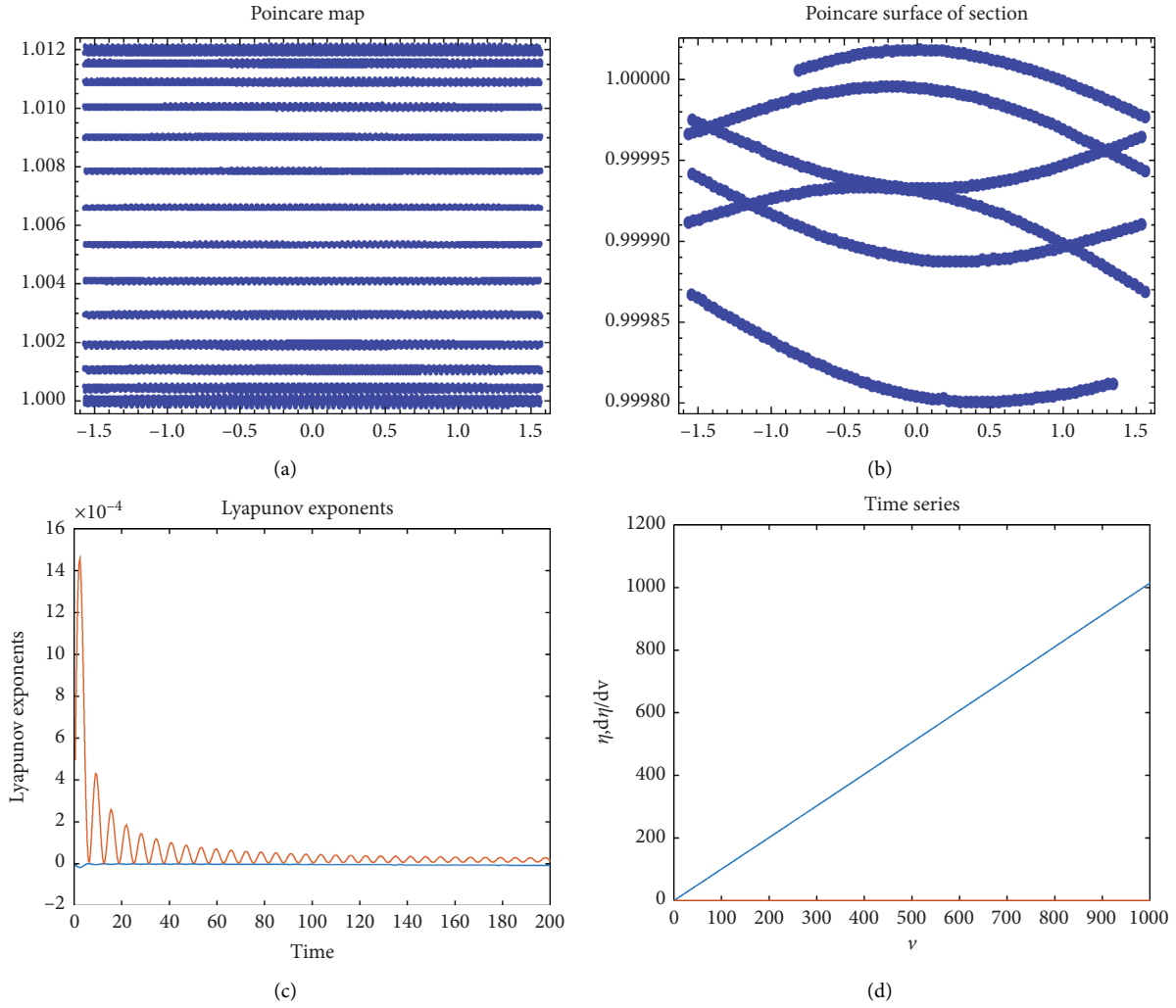

FIGURE 7: For $n = 0.005, \varepsilon = 0.00000000000000000005, A_* = 3.36E + 09, \quad D_* = -4E + 08, B_* = 1596.387, C_* = -103631, E_* = 200.1022$, and $e = 0.001$. (a) Poincare map, (b) Poincare surface of section, (c) Lyapunov exponent, and (d) time series.

widened by high recurrence term into tight clamorous band for little n, and half width of disordered separatrix is given by

$$\omega_p = \frac{I_p - I_p^s}{I_p^s} = 4\pi\varepsilon_1\lambda^3 e^{-(\pi\lambda/2)}, \tag{16}$$

where ε_1 is the proportion of coefficient of closest annoying high-recurrence term to coefficient of perturbed term, and $\lambda = \Omega/\omega$ is the proportion of recurrence distinction between full term and closest nonfull term (Ω) to recurrence of little sufficiency freedoms (ω).

3. Spin-Orbit Phase Space

Utilizing Poincare surface of the segment by taking a gander at directions stroboscopically with period 2π, the segment is drawn with $(d\eta/dv)$ versus v at each periapse section. On account of semi-intermittent direction, focuses are contained in smooth bends, while for clamorous directions, they seem to the top off region in the stage space in an arbitrary way. Since direction indicated by η is identical to the direction signified by $\pi + \eta$, we have, consequently, confined the span from 0 to π.

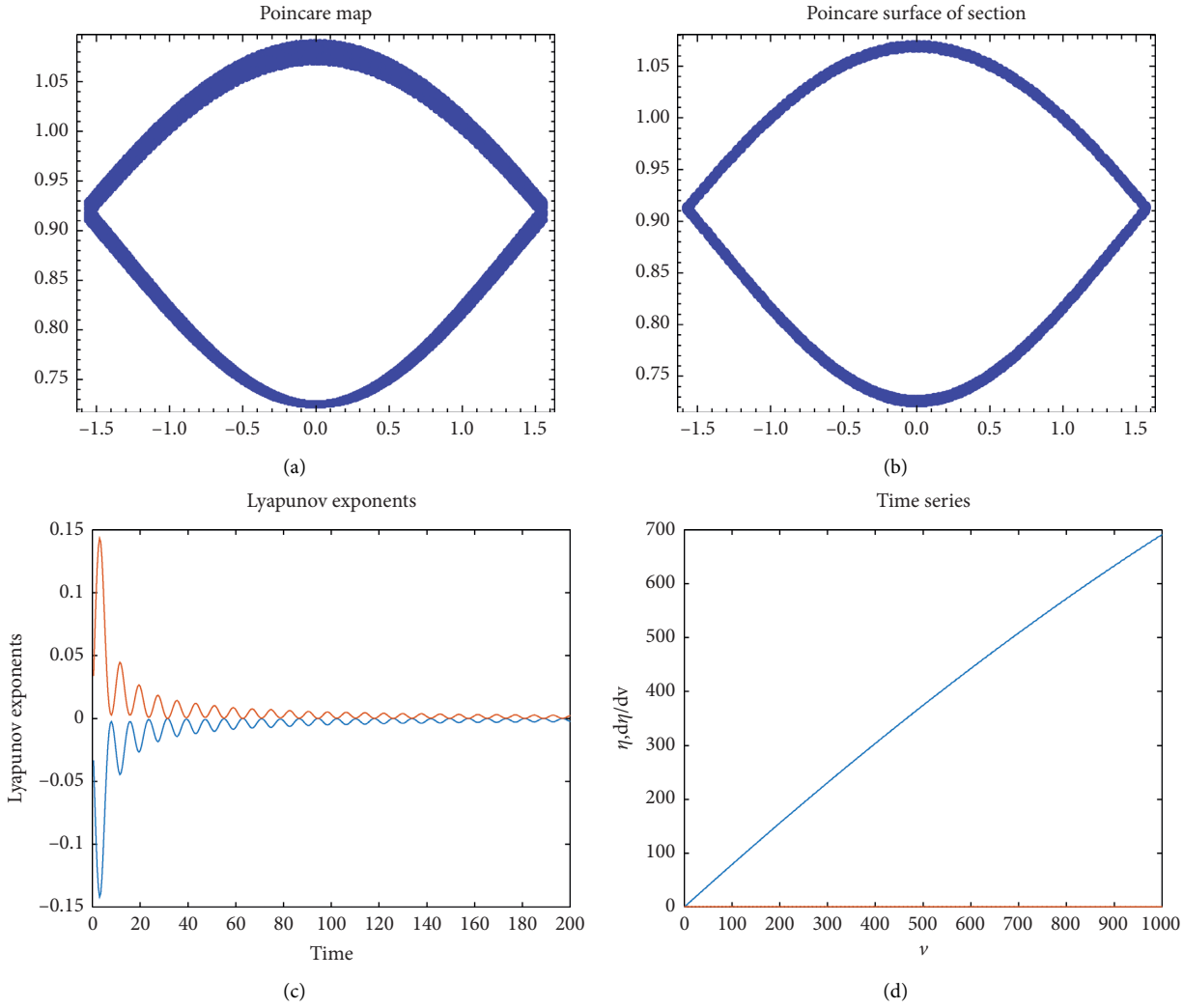

FIGURE 8: For $n = 0.4, \varepsilon = 0.00000000000000000005, A_* = 3.36E + 09, D_* = -4E + 08, B_* = 1596.387, C_* = -103631, E_* = 200.1022$, and $e = 0.001$. (a) Poincare map, (b) Poincare surface of section, (c) Lyapunov exponent, and (d) time series.

4. Results and Discussion

Poincare map, surface of section, and Lyapunov exponents have been plotted for Earth's artificial satellite Resourcesat-1. For the satellite, it is assumed that semimajor axis = $a = 7.195^*10^3$ km, flightiness = $e = 0.001$, tendency = $i = 98.69^\circ$, and angular velocity = $\Omega = 1.034^*10^{-3}$ rad/sec. The effect of mass parameter (n) and aerodynamic torque parameter (ε) is studied on the nonstraight wavering of a satellite in an elliptic circle. Poincare maps, surface of section, Lyapunov exponents, and time series for different values of mass parameter and aerodynamic toque parameter are plotted as described in tables and figures. Table 1 gives the details of figures for Earth − Resourcesat − 1 for fixed values of A_*, $B_*, C_*, D_*, E_*, \varepsilon$, and e, and the variation of values of n from $0 \le n \le 1$ is shown in Figures 2–5. Table 2 gives description of figures for the Earth-Resourcesat-1 system at fixed values of parameters, n, and e, and the variation of values of ε from

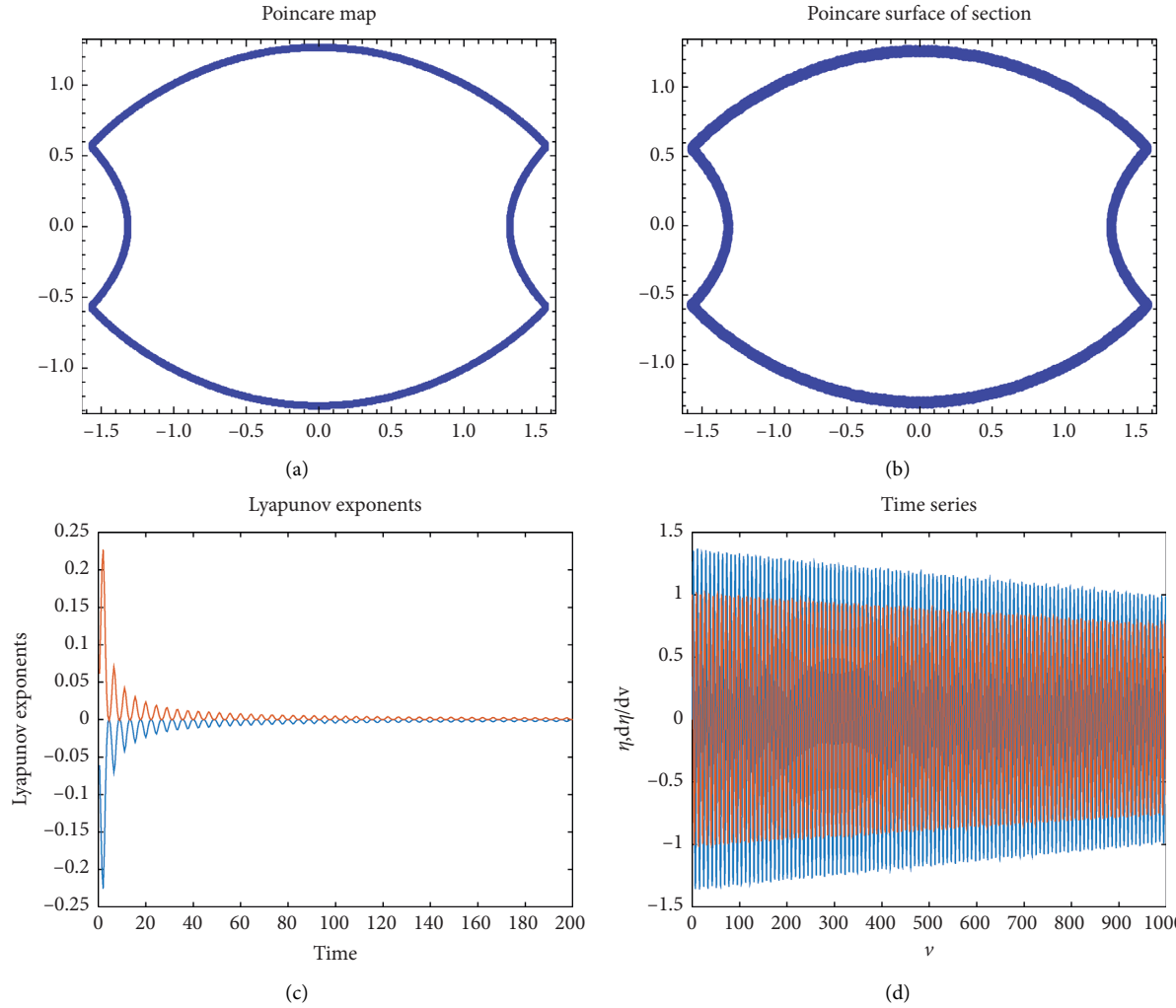

Figure 9: For $n = 0.8, \varepsilon = 0.000000000000000000005, A_* = 3.36E + 09, D_* = -4E + 08, B_* = 1596.387, C_* = -103631, E_* = 200.1022$, and $e = 0.001$. (a) Poincare map, (b) Poincare surface of section, (c) Lyapunov exponent, and (d) time series.

$0 \leq \varepsilon \leq 0.5$ which are plotted is shown in Figures 6–9. From the plots, it is observed that regular curves disintegrate, and this disintegration increases as ε increases and curves behaves chaotically but remains almost same.

5. Conclusion

From these investigations, we conclude that the streamlined force assumes an extremely huge function in changing the movement of insurgency into movement of libration or endless period separatrix. Likewise, we see that standard movement changes into a turbulent one for certain estimations of the streamlined force boundary and mass boundary n. Half width of disordered separatrices assessed by Chirikov's basis is not influenced by the streamlined force. It was seen that counterfeit satellite's turn circle stage space is overwhelmed by a chaotic zone which increments further because of the streamlined force. It is additionally seen that normal bends begin breaking down because of the streamlined force and mass boundary, and this deterioration increments as the streamlined force and mass boundary increments. It is concluded that aerodynamic torque and n change regular movement to the chaotic motion.

Data Availability

No data were used to support this study.

Conflicts of Interest

The authors declare that they have no conflicts of interest.

References

[1] https://www.isro.gov.in/Spacecraft/irs-p6-resourcesat-1 - 14 May 2020.

[2] V. S. Aslanov, A. K. Misra, and V. V. Yudintsev, "Chaotic attitude motion of a low-thrust tug-debris tethered system in a Keplerian orbit," *Acta Astronautica*, vol. 139, pp. 419–427, 2017.

[3] R. Bhardwaj and M. Kaur, "Aerodynamic Torque exhibits non-resonance oscillation in satellite motion," *Mathematica*

Applicanda (Applied Mathematics), vol. 44, no. 2, pp. 247–262, 2016.

[4] R. Bhardwaj and P. Kaur, "Chaotic attitude tumbling of satellite in magnetic field," *American Journal of Applied Sciences*, vol. 3, no. 10, pp. 2037–2041, 2006.

[5] R. Bhardwaj and M. Sethi, "Resonance in satelliteâ€s motion under air drag," *American Journal of Applied Sciences*, vol. 3, no. 12, pp. 2184–2189, 2006.

[6] R. Bhardwaj, M. Sethi, and P. Kaur, "Rotational motion of a satellite under the influence of aerodynamic or magnetic torque," in *Modern Mathematical Methods and Algorithms for Real World Systems*, A. H. Siddiqi, I. S. Duff, and O. Christensen, Eds., pp. 174–184, Anamaya Publishers, Lado Sarai - Mehrauli, Delhi, 2006.

[7] R. Bhardwaj and R. Tuli, "Non-linear planar oscillation of a satellite leading to chaos under the influence of third-body torque," in *Mathematical models and Methods for Real World Systems*, K. M. Furati and A. H. Siddiqi, Eds., Chapman & Hall/ CRC, Boca Raton, Florida, pp. 301–336, 2005.

[8] R. Bhardwaj and P. Kaur, "Chaos in non-linear oscillation of a satellite in elliptic orbit under magnetic torque," in *International Workshop on Applications of Wavelets to Real World Problems*, A. Siddiqui, Ed., pp. 240–258, Istanbul Commerce University Publication, Istanbul, Turkey, 2005.

[9] R. Bhardwaj and K. B. Bhatnagar, "Nonlinear planar oscillation of a satellite in a circular orbit under the influence of magnetic torque (II)," *Indian Journal of Pure & Applied Mathematics*, vol. 29, no. 2, pp. 139–150, 1998.

[10] R. Bhardwaj and K. B. Bhatnagar, "Chaos in nonlinear planar oscillation of a satellite in an elliptical orbit under the influence of third body torque," *Indian Journal of Pure & Applied Mathematics*, vol. 28, no. 3, pp. 391–422, 1997.

[11] R. Bhardwaj and K. B. Bhatnagar, "Nonlinear planar oscillation of a satellite in a circular orbit under the influence of magnetic torque (I)," *Indian Journal of Pure & Applied Mathematics.*vol. 26, no. 12, pp. 1225–1240, 1995.

[12] K. B. Bhatnagar and R. Bhardwaj, "Rotational motion of a satellite on an elliptical orbit under the influence of third body torque (I)," *Bulletin of Astronomical Society of India*, vol. 22, pp. 359–367, 1994.

[13] M. Chegini, H. Sadati, and H. Salarieh, "Chaos analysis in attitude dynamics of a flexible satellite," *Nonlinear Dynamics*, vol. 93, no. 3, pp. 1421–1438, 2018.

[14] M. Chegini, H. Sadati, and H. Salarieh, "Analytical and numerical study of chaos in spatial attitude dynamics of a satellite in an elliptic orbit," in *Proceedings of the Institution of Mechanical Engineers, Part C: Journal of Mechanical Engineering Science*vol. 233, no. 2, pp. 561–577, 2019.

[15] P. T. Clemson and A. Stefanovska, "Discerning non-autonomous dynamics," *Physics Reports*, vol. 542, no. 4, pp. 297–368, 2014.

[16] A. V. Doroshin, "Heteroclinic chaos and its local suppression in attitude dynamics of an asymmetrical dual-spin spacecraft and gyrostat-satellites. The part I-main models and solutions," *Communications in Nonlinear Science and Numerical Simulation*, vol. 31, no. 1-3, pp. 151–170, 2016.

[17] S. A. Gutnik and V. A. Sarychev, "Mathematical simulation of satellite motion with an aerodynamic attitude control system influenced by active damping torques," *Computational Mathematics and Mathematical Physics*, vol. 60, no. 10, pp. 1721–1729, 2020.

[18] M. Iñarrea and V. Lanchares, "Chaotic pitch motion of an asymmetric non-rigid spacecraft with viscous drag in circular orbit," *International Journal of Non-linear Mechanics*, vol. 41, no. 1, pp. 86–100, 2006.

[19] V. Kouprianov and I. Shevchenko, "Rotational dynamics of planetary satellites: a survey of regular and chaotic behavior," *Icarus*, vol. 176, no. 1, pp. 224–234, 2005.

[20] P. V. Kuptsov and S. P. Kuznetsov, "Lyapunov analysis of strange pseudohyperbolic attractors: angles between tangent subspaces, local volume expansion and contraction," *Regular and Chaotic Dynamics*, vol. 23, no. 7-8, pp. 908–932, 2018.

[21] C. Letellier, *Chaos in Nature World Scientific Series on Nonlinear Science Series A*, Vol. 94, World Scientific Publishing, Singapore, 2nd edition, 2019.

[22] J. Liu and N. Cui, "Rigid-flexible coupled dynamics analysis for solar sails," in *Proceedings of the Institution of Mechanical Engineers, Part G: Journal of Aerospace Engineering*vol. 233, no. 1, pp. 324–340, 2019.

[23] A. V. Melnikov and I. I. Shevchenko, "Chaotic dynamics of satellite systems," *Solar System Research*, vol. 39, no. 4, pp. 322–332, 2005.

[24] D. Pritykin, S. Efimov, and V. Sidorenko, "Defunct satellites in nearly polar orbits: long-term evolution of attitude motion," *Open Astronomy*, vol. 27, no. 1, pp. 264–277, 2018.

[25] A. J. Rosengren, E. M. Alessi, A. Rossi, and G. B. Valsecchi, "Chaos in navigation satellite orbits caused by the perturbed motion of the Moon," *Monthly Notices of the Royal Astronomical Society*, vol. 449, no. 4, pp. 3522–3526, 2015.

[26] S. A. Rawashdeh, "Attitude analysis of small satellites using model-based simulation," *International Journal of Aerospace Engineering*, vol. 2019, Article ID 3020581, 2019.

[27] S. Efimov, D. Pritykin, and V. Sidorenko, "Long-term attitude dynamics of space debris in Sun-synchronous orbits: Cassini cycles and chaotic stabilization," *Celestial Mechanics and Dynamical Astronomy*, vol. 130, no. 10, p. 62, 2018.

[28] S.-C. Chang, "Stability, chaos detection, and quenching chaos in the swing equation system," *Mathematical Problems in Engineering*, vol. 2020, Article ID 6677084, 2020.

[29] J. Wang, W. Yu, J. Wang, Y. Zhao, J. Zhang, and D. Jiang, "A new six-dimensional hyperchaotic system and its secure communication circuit implementation," *International Journal of Circuit Theory and Applications*, vol. 47, no. 5, pp. 702–717, 2019.

[30] A. Wolf, J. B. Swift, H. L. Swinney, and J. A. Vastano, "Determining lyapunov exponents from a time series," *Physica D: Nonlinear Phenomena*, vol. 16, no. 3, pp. 285–317, 1985.

[31] J. Wisdom, S. J. Peale, and F. Mignard, "The chaotic rotation of Hyperion," *Icarus*, vol. 58, no. 2, pp. 137–152, 1984.

[32] A. Cayley, "Tables of the developments of functions in the theory of elliptic motion," *Memoirs of the Royal Astronomical Society*, vol. 29, p. 191, 1859.

[33] P. Goldreich and S. Peale, "Spin-orbit coupling in the solar system," *The Astronomical Journal*, vol. 71, p. 425, 1966.

[34] E. W. Brown and C. A. Shook, *Planetary Theory*, Dover Publication. Inc., New York, USA, 1964.

Hindawi
Advances in Astronomy
Volume 2020, Article ID 1348319, 17 pages
https://doi.org/10.1155/2020/1348319

Research Article

Evolution of Periodic Orbits within the Frame of Formation Satellites

Elbaz I. Abouelmagd,[1] **Mitali J. Doshi**,[2] **and Niraj M. Pathak**[2]

[1]*Celestial Mechanics and Space Dynamics Research Group (CMSDRG), Astronomy Department, National Research Institute of Astronomy and Geophysics (NRIAG), Helwan 11421, Cairo, Egypt*
[2]*Department of Mathematics, Faculty of Technology, Dharmsinh Desai University, Nadiad, Gujarat 3870001, India*

Correspondence should be addressed to Elbaz I. Abouelmagd; elbaz.abouelmagd@nriag.sci.eg

Received 20 July 2020; Revised 20 November 2020; Accepted 30 November 2020; Published 21 December 2020

Academic Editor: Juan L. G. Guirao

In the framework of formation satellites, the periodic orbits of deputy satellite are analyzed when the chief satellite is moving in an elliptical orbit. This analysis is developed on 1- to 10-loop periodic orbits of the deputy satellite. These orbits along with their associated loops are discussed under some specific initial position sets. The effects of different initial velocities, initial true anomalies, and eccentricities on the initial position and orbital period of periodic orbits of deputy satellite are investigated.

1. Introduction

The periodic orbits have substantial and leading role in exploring and understanding the behavior of dynamical systems. At most, they define strange attractors, which lead to chaotic dynamical systems. The special solution of a dynamical system, which repeats and generates itself in time, is called *periodic orbit*. From the mathematical point of view, the orbit is a set of points associated by the evolution function of the proposed dynamical system. These points are considered as a subset from the phase space, which are covered by the dynamical system trajectory within frame of a particular set from the initial conditions. Some recent works, analyzing the periodic orbits, are addressed in [1–4].

The sufficient condition for the existence of periodic orbits is given when the Hamilton system is a function in the action-angle variables; further, these obtained results are applied to Hamiltonian of the perturbed Kepler problem in [5]. Also, a geometric approach to asymptotically stabilize with a phase of fixed periodic orbits for global Hamiltonian dynamical system is established in [6]. While in [7], the new families of periodic orbits analytically for the Hamilton system are found, which characterize the local motion in the region around the galaxy center. Furthermore, in [8], the theory of averaging is applied to prove the existence of twelve families of periodic orbits in a 3-dimension for a galactic Hamiltonian dynamical system. Since we are interested to evaluate the periodic orbits within frame of formation satellites, we will give also an overview about the literatures and importance of formation satellites in the following paragraphs.

The formation flying of small multiple satellites as a replacement of using single large satellite has shown great interest for different defense- and science-based space missions. Formation flying consists of a set of satellites, which have the same dynamic state and governed by one control law. Abundance and precision of the proposed system in terms of formation satellites are more effective tools, which give a job more accuracy than using a conventional large single satellite. It also reduces the maintenance and launching costs, extremely expands the surveillance area, and gives more resilience into the design of space mission. For example, a sensor of ground observation can be loaded on bunch of satellites flying in a specified formation for increasing aperture size instead of constructing a large single satellite with more expense. There are chances of aborting the whole mission in the event of satellite failure. Proper management of satellites cluster with special planning and scheduling reduces the chances of failure.

Using formation satellite in space-based missions has many advantages, but at the expense of increased complexity and different challenges like high-precision relative navigation [9], distributed communication [10], stable formation design [11], trajectory optimization and control [12], and attitude synchronization [13]. In formation satellite, trajectory optimization and control problem are two important tasks to achieve a successful launching of satellites set in the space. These tasks comprise maintaining the small satellites in a stable formation within frame of enough accuracy against different perturbations of orbit and maneuvering of formation for guiding and performing control command for reconfiguring from perturbed satellite formation to one stable formation.

The precise model of relative motion in order to analyze satellites formation flying is a basic need which covers accurate linear and nonlinear satellites models of relative motion taking into account J_2 perturbations. Different relative dynamic models are proposed in the literature using different assumptions with many methodologies. It is necessary to make a comparative study to choose appropriate models for specified missions with perturbation that should be considered for definite applications.

A considerable work is accomplished into satellite formation flying for libration point mission with different models that characterize the relative motion satellites between two or more in low Earth orbit (LEO). The major fundamental of this work is carried out by Hill in [14]. While the relative motion within frame of Clohessy–Wiltshire equations is written in terms of a Cartesian or curvilinear coordinates tracing a circular reference orbit around the Earth and models by using orbit elements differences to characterize relative orbits [15]. The extended version of the Hill equations was given in [16] that involves the influent of the zonal harmonic parameter J_2 using a force gradient method to time-varying form. It was verified and applied to linear quadratic regulator design and evaluated for the station-keeping task in [17].

In [18], the force gradient modelling approach for satellite formation flying around the libration point L_2 using periodic halo motion as a reference is investigated. The optimal maneuver problem can be characterized as a state transition problem based on Hill's system and maximum principle of Pontryagin. The optimal solution can be obtained by solving the state transition equations and performing the simulation study [19]. In a formation satellite, a magnetic field approach helps a large number of closely located satellites in tracking each other in six degrees of freedom without disturbing their positions and orientation relative to each other (see [20, 21] for details).

The relative motion control is an important task required in the formation of the flying missions. Different control methods without fuel consumption are of a specific interest. A number of these methods based on atmosphere drag effects, electrostatic magnetic field, and the Lorentz force have been proposed, but exchanging mass between satellites is a novel technique for formation flying relative motion control [22].

This paper is organized into four sections. The importance and applications of formation satellites are discussed in Section 1 as a part of literature review. Model description and derived governing equations of motion are covered in Section 2. Analysis of the given sets of initial positions for deputy satellite, which generate periodic orbits, is investigated in Section 3. While in Section 4, we compare the effect of variation in eccentricity of chief satellite's orbit on periodic orbits of deputy satellite with number of loops. Finally, conclusion is drawn from the analysis becomes the part of Section 5.

2. Model Description

Consider two spacecrafts orbiting a common primary and its mass is m. Mainly, the motion of these two spacecrafts is governed by the Kepler model or the dynamical system of two bodies [23–26]. One of the spacecraft is termed as a chief satellite, and the second is referred as a deputy satellite, where their masses are m_0 and m_1, respectively. Then, the equations of relative motion of deputy satellite with respect to chief satellite under the setup of the Keplerian two-body problem are obtained as follows: we consider a chief-fixed, local vertical local horizontal (LVLH) rotating frame, also known as EulerHill frame. Here, the origin is located at the position of chief satellite, as shown in Figure 1.

From two-body problem, the motion of the chief and deputy satellites around the primary (Earth or any planet) in inertial frame of reference are given by

$$\ddot{\mathbf{r}}_0 = -\mu_0 \frac{\mathbf{r}_0}{r_0^3},$$
$$\ddot{\mathbf{r}}_1 = -\mu_1 \frac{\mathbf{r}_1}{r_1^3}, \tag{1}$$

where $\mu_0 = m + m_0$ and $\mu_1 = m + m_1$, but $m_0, m_1 \ll m$; then, we can approximate $\mu_0 \approx \mu_1 = \mu$. Thereby, the solutions of equation (1) are controlled by

$$r_0 = \frac{a_0\left(1 - e_0^2\right)}{\left(1 + e_0 \cos f_0\right)},$$
$$r_1 = \frac{a_1\left(1 - e_1^2\right)}{\left(1 + e_1 \cos f_1\right)}, \tag{2}$$

where $a_0\,(a_1), e_0\,(e_1)$, and $f_0\,(f_1)$ are the semimajor axis, eccentricity, and true anomaly of chief (deputy) satellite's orbit, respectively.

Now, we assume that ρ is the position vector of deputy satellite relative to chief satellite; hence, $\boldsymbol{\rho} = \mathbf{r}_1 - \mathbf{r}_0$, and the relative motion of deputy satellite is

$$\ddot{\boldsymbol{\rho}} = -\mu \frac{\mathbf{r}_0 + \boldsymbol{\rho}}{\left|\mathbf{r}_0 + \boldsymbol{\rho}\right|^3} + \mu \frac{\mathbf{r}_0}{r_0^3}, \tag{3}$$

where $\mathbf{r}_0 = [r_0, 0, 0]^T$, $\boldsymbol{\rho} = [x, y, z]^T$, $f_0 = \theta_0 - \omega$, and ω is the argument of periapsis. But ω is a constant. Thereby, we can define the angular velocity vector $\boldsymbol{\Omega} = [0, 0, \dot{\theta}_0\,]^T$.

The general relation between the velocity and acceleration in the inertial frame and the rotating by the angular velocity Ω is controlled by

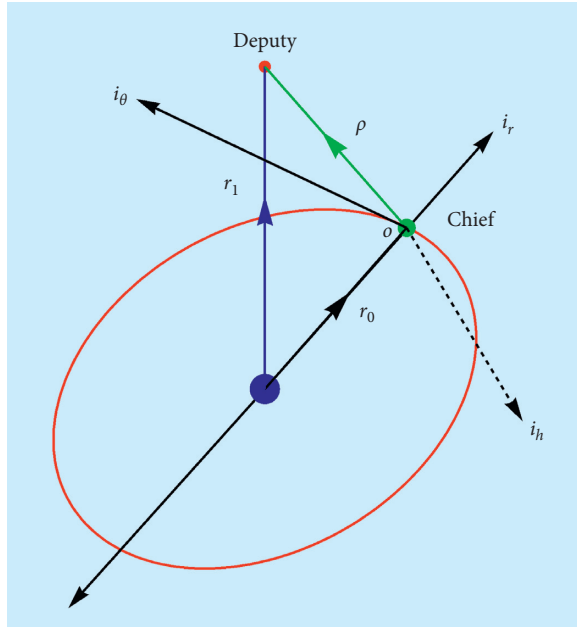

Figure 1: Configuration of the LVLH frame.

$$\dot{\boldsymbol{\rho}}^{\mathcal{J}} = \dot{\boldsymbol{\rho}}^{\mathcal{R}} + \boldsymbol{\Omega} \wedge \boldsymbol{\rho},$$
$$\ddot{\boldsymbol{\rho}}^{\mathcal{J}} = \ddot{\boldsymbol{\rho}}^{\mathcal{R}} + 2\,\boldsymbol{\Omega} \wedge \dot{\boldsymbol{\rho}}^{\mathcal{R}} + \boldsymbol{\Omega} \wedge (\boldsymbol{\Omega} \wedge \boldsymbol{\rho}) + \dot{\boldsymbol{\Omega}} \wedge \boldsymbol{\rho}, \tag{4}$$

where

$$\dot{\boldsymbol{\rho}}^{\mathcal{R}} = \dot{x}i_r + \dot{y}i_\theta + \dot{z}i_h,$$
$$\ddot{\boldsymbol{\rho}}^{\mathcal{R}} = \ddot{x}i_r + \ddot{y}i_\theta + \ddot{z}i_h. \tag{5}$$

Utilizing equations (3)–(5) componentwise equations of relative motion are given by

$$\ddot{x} - 2\dot{\theta}_0\dot{y} - \ddot{\theta}_0 y - \dot{\theta}_0^2 x = -(r_0 + x)F(x, y, z, r_0) + G(r_0),$$
$$\ddot{y} + 2\dot{\theta}_0\dot{x} + \ddot{\theta}_0 x - \dot{\theta}_0^2 y = -yF(x, y, z, r_0), \ddot{z}, = -zF(x, y, z, r_0), \tag{6}$$

where

$$F(x, y, z, r_0) = \frac{\mu}{\left[(r_0 + x)^2 + y^2 + z^2\right]^{3/2}},$$
$$G(r_0) = \frac{\mu}{r_0^2}. \tag{7}$$

The system of equation (6) represents the general relative motion with respect to independent time variable. In order to have docile analysis for these equations, we will change the independent time variable by the true anomaly and scale the relative positions by the chief satellite radius. Thereby, we take $\overline{x} = x/r_0, \overline{y} = y/r_0, \overline{z} = z/r_0$; since $v = \sqrt{\dot{\mathbf{r}}.\dot{\mathbf{r}}}$ is the velocity, $h = r_0^2\dot{\theta}_0 = r_0^2 f_0$ and $P = h^2/\mu$ is the semilatus rectum; then with help of equation (2), the velocity and accelerations components are controlled by

$$\dot{x} = \frac{h_0}{P_0}\left[(1 + e_0\cos f_0)\frac{\mathrm{d}\overline{x}}{\mathrm{d}f_0} + \overline{x}(e_0 \sin f_0)\right],$$
$$\dot{y} = \frac{h_0}{P_0}\left[(1 + e_0\cos f_0)\frac{\mathrm{d}\overline{y}}{\mathrm{d}f_0} + \overline{y}(e_0 \sin f_0)\right], \tag{8}$$
$$\dot{z} = \frac{h_0}{P_0}\left[(1 + e_0\cos f_0)\frac{\mathrm{d}\overline{z}}{\mathrm{d}f_0} + \overline{z}(e_0 \sin f_0)\right],$$

$$\ddot{x} = \frac{h_0^2}{P_0^3}\Upsilon^2(f_0)\left[\Upsilon(f_0)\frac{\mathrm{d}^2\overline{x}}{\mathrm{d}f_0^2} + \overline{x}(e_0\cos f_0)\right], \ddot{y}$$
$$= \frac{h_0^2}{P_0^3}\Upsilon^2(f_0)\left[\Upsilon(f_0)\frac{\mathrm{d}^2\overline{y}}{\mathrm{d}f_0^2} + \overline{y}(e_0\cos f_0)\right], \ddot{z}$$
$$= \frac{h_0^2}{P_0^3}\Upsilon^2(f_0)\left[\Upsilon(f_0)\frac{\mathrm{d}^2\overline{z}}{\mathrm{d}f_0^2} + \overline{z}(e_0\cos f_0)\right], \tag{9}$$

where

$$\Upsilon(f_0) = (1 + e_0\cos f_0). \tag{10}$$

Substituting equations (8) and (9) into equation (6), we get

$$\frac{\mathrm{d}^2\overline{x}}{\mathrm{d}f_0^2} - 2\frac{\mathrm{d}\overline{y}}{\mathrm{d}f_0} = \frac{1 + \overline{x}}{(1 + e_0\cos f_0)}[1 - \Gamma(\overline{x}$$

$$\frac{\mathrm{d}^2\overline{y}}{\mathrm{d}f_0^2} + 2\frac{\mathrm{d}\overline{x}}{\mathrm{d}f_0} = \frac{\overline{y}}{(1 + e_0\cos f_0)}[1 - \Gamma(\overline{x}$$

$$\frac{\mathrm{d}^2\overline{z}}{\mathrm{d}f_0^2} = \frac{-\overline{z}}{(1 + e_0\cos f_0)}[e_0\cos f_0 + \Gamma(\overline{x}, t\overline{y}n, q\overline{z})], \tag{11}$$

where

$$\Gamma(\overline{x}, t\overline{y}n, q\overline{z}) = \frac{1}{\left[(1+\overline{x})^2 + \overline{y}^2 + \overline{z}^2\right]^{3/2}}. \quad (12)$$

We will drop the subscript zero and bar for simplicity, thereby equation (11) can be rewritten with a simple form as

$$\frac{d^2x}{df^2} - 2\frac{dy}{df} = \frac{\partial W}{\partial x},$$

$$\frac{d^2y}{df^2} + 2\frac{dx}{df} = \frac{\partial W}{\partial y}, \quad (13)$$

$$\frac{d^2z}{df^2} = \frac{\partial W}{\partial z},$$

where

$$W = \frac{1}{1+e\cos f}\left[\frac{1}{2}\left(x^2 + y^2 - ez^2\cos f\right) - U\right],$$

$$U = 1 - x - \frac{1}{\left[(1+x)^2 + y^2 + z^2\right]^{3/2}}. \quad (14)$$

Equations (13) and (14) are the governing equations of motion of deputy satellite with respect to chief satellite in the LVLH frame.

3. Analysis of Periodic Orbits

Since the trajectory of phase space is defined uniquely for any provided set of specified conditions, we will analyze the initial position of deputy satellite, which provides periodic orbits under different values for initial true anomalies and eccentricities of chief satellite. In this context, System (11) can be used to accomplish our goal. This system consists of second-order nonlinear differential equations, which can be converted into system of first-order differential equations and then integrated with the Runge–Kutta fourth-order method.

The numerical integration will be developed with a step size of 0.001 during each iteration. It is important that, during simulation, true anomaly f is considered as a variable. Notation f^0 stands for initial value of true anomaly. During each iteration of simulation, true anomaly f varies between f^0 and $f^0 + 4\pi$. Software MATLAB is used to perform the simulation. In this study, the periodic orbits up to ten loops are obtained for different values of f^0 and e, where f^0 is referred as the initial true anomaly while e is the eccentricity of the orbit of chief satellite. The initial position of the deputy satellite is given as $(x^0, 0, z^0)$ and initial velocity is taken as $(0, y^0, 0)$. The orbital period and number of loops are denoted as T and NL, respectively.

3.1. Periodic Orbits When $e = 0.1$. In this section, we analyze periodic orbits of deputy satellite with 1–10 loops when eccentricity e of chief satellite's orbit is taken in to account as 0.1. During this analysis, the effect of initial velocity of deputy satellite in the y direction and initial true anomaly of deputy satellite are considered. Thus, two different sets of initial velocities of deputy satellite $(0, 0.002, 0)$ and $(0, 0.005, 0)$ are taken into account. Also, three different values of initial true anomaly f^0 of deputy satellites are taken as $\pi/6$, $\pi/3$, and $\pi/2$. This analysis will be investigated numerically and graphically through Figures 2–6 and Table 1. The initial position of deputy satellite and orbital period of the periodic orbits is obtained for each set of orbits with 1–10 loops. It is observed that the orbital period decreases as velocity increases for given number of loops, eccentricity, and initial true anomaly.

Figures 2(a)–2(f) show the two-dimensional view of the periodic orbits with the number of loops 1 to 6 with a given value of x^0. These orbits are obtained when the initial true anomaly and initial velocities are $\pi/6$ and (0, 0.002, 0), respectively.

Figures 3(a)–3(f) cover the three-dimensional view of the periodic orbits with the number of loops from 1 to 6 with a given value of x^0. These orbits are obtained when the initial true anomaly and initial velocity are $\pi/3$ and (0, 0.002, 0), respectively.

Figures 4(a)–4(f) show the three-dimensional view of periodic orbits with the number of loops from 5 to 10 with given value of x^0. These orbits are obtained when initial true anomaly and initial velocity are $\pi/3$ and (0, 0.005, 0), respectively. All the orbits are plotted in the same dimensions so that the comparative study can be possible. The comparative study of periodic orbits for different initial values of velocities depicts that shape and geometric parameters of orbits are same though the values of initial velocities are different.

Figures 5(a)–5(f) show the periodic orbits with the number of loops 3 to 8 with a given value of x^0. These orbits are obtained when the initial true anomaly and initial velocity are $\pi/2$ and (0, 0.002, 0), respectively.

The analysis of the periodic orbits for three different initial true anomalies $\pi/6$, $\pi/3$, and $\pi/2$ are observed in Table 1. Two different sets of initial velocities (0, 0.002, 0) and (0, 0.005, 0) are considered for the study when $e = 0.1$. The initial position of deputy satellite and orbital period of the periodic orbits are obtained for each set of orbits with 1–10 loops. The orbital period is conserved as the velocity increases for given number of loops, eccentricity, and initial true anomaly.

The variation in initial position and period of the periodic orbits is given in Figures 6(a) and 6(b) for initial velocities (0, 0.002, 0) and (0, 0.005, 0), respectively. From these graphs, it can be observed that, as the number of loops in the given orbit increases, the initial position of the periodic orbit moves towards the origin (the initial position of chief satellite) irrespective of the initial value of the true anomaly. From these graphs, it can also be observed that, as number of loops in the given orbit increases, the period of the periodic orbit increases irrespective of the initial true anomaly.

3.2. Periodic Orbits When $e = 0.2$. Now, we have considered the eccentricity of chief satellite's orbit as 0.2 to analyze the effect of eccentricity of chief satellite's orbit, on periodic

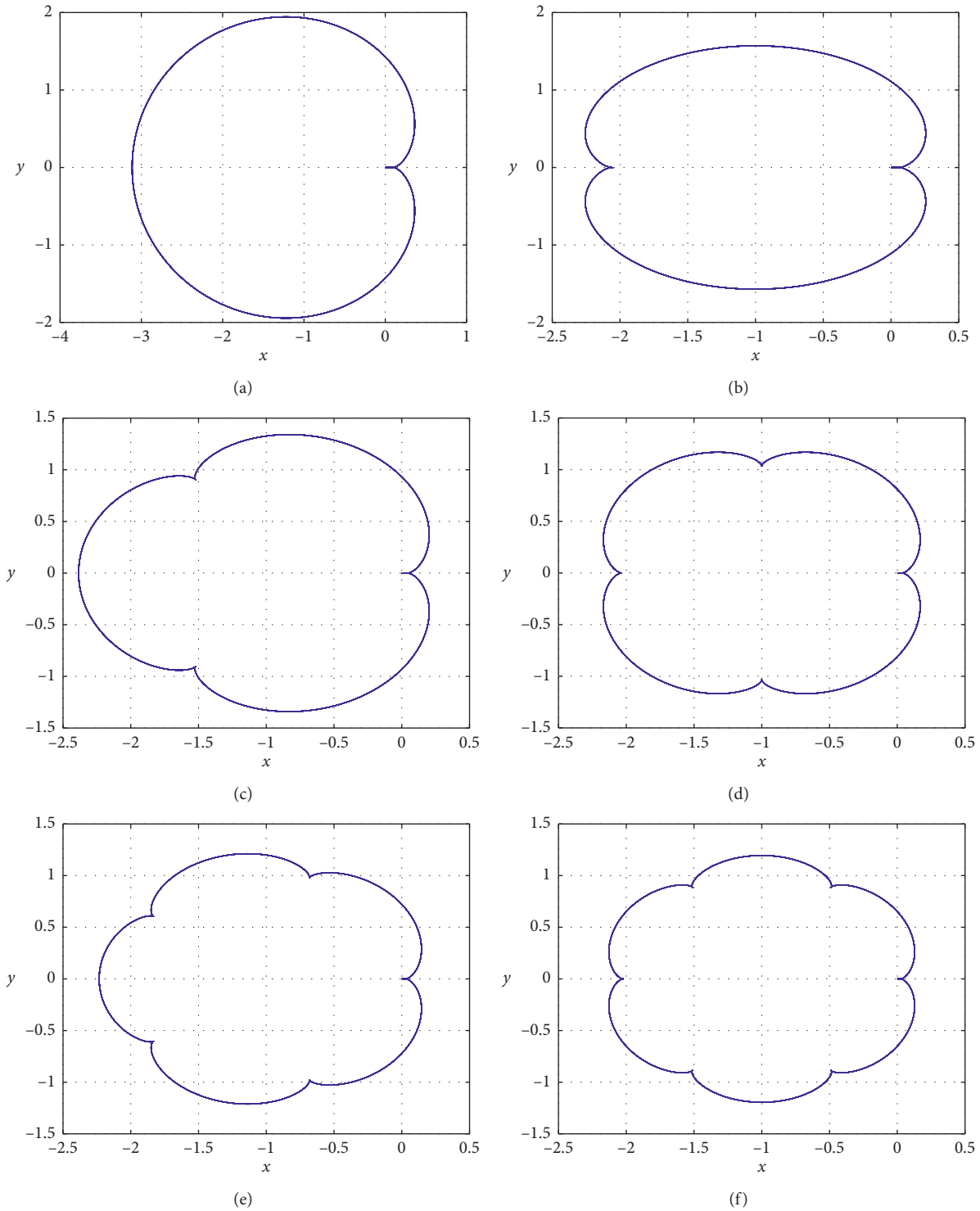

FIGURE 2: Periodic orbits when $e = 0.1$, $f^0 = \pi/6$, and velocity $\dot{y}^0 = 0.002$. (a) Single-loop orbit, when $x^0 = 0.097990643050$. (b) Two-loop orbit, when $x^0 = 0.060941913025$. (c) Three-loop orbit, when $x^0 = 0.0442639955$. (d) Four-loop orbit, when $x^0 = 0.03469385$. (e) Five-loop orbit, when $x^0 = 0.02847325$. (f) Six-loop orbit, when $x^0 = 0.02410242$.

orbits of deputy satellite with 1–10 loops. Here, we have considered the proposed values of initial velocity of deputy satellite and initial true anomaly of deputy satellite with $e = 0.1$. So that the comparative study is possible and effect of individual parameter and combination of more than one parameter can be investigated. This analysis will be

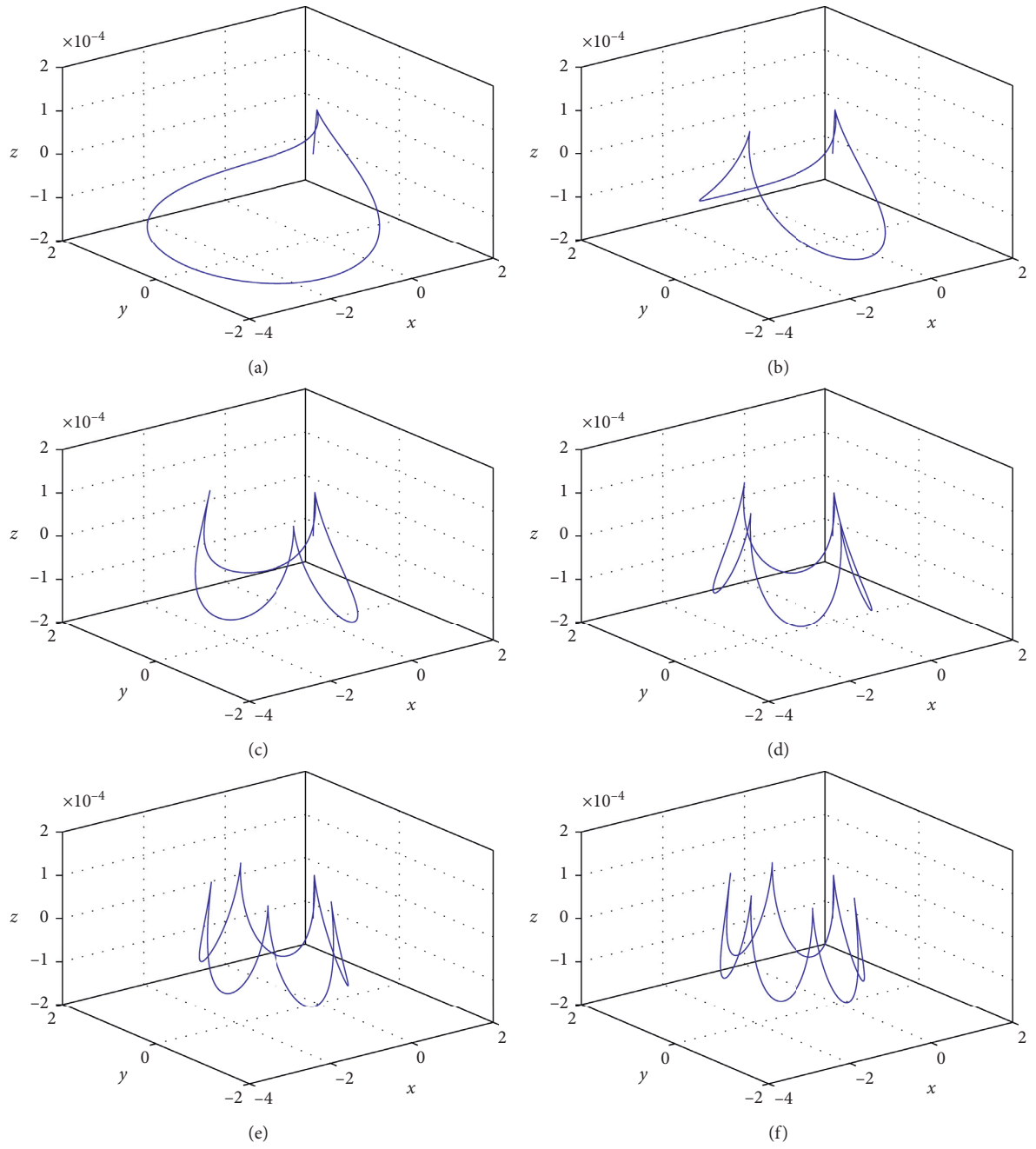

FIGURE 3: Periodic orbits when $e = 0.1$, $f^0 = \pi/3$, and velocity $\dot{y}^0 = 0.002$. (a) Single-loop orbit, when $x^0 = 0.093525298500$. (b) Two-loop orbit, when $x^0 = 0.059057635000$. (c) Three-loop orbit, when $x^0 = 0.043092145000$. (d) Four-loop orbit, when $x^0 = 0.033847995000$. (e) Five-loop orbit, when $x^0 = 0.027812858705$. (f) Six-loop orbit, when $x^0 = 0.0235613$.

investigated numerically and graphically through Figures 7–10 and Table 2.

Figures 7(a)–7(f) show the periodic orbits with 1 to 6 number of loops with initial true anomaly and velocity of $\pi/6$ and (0, 0.002, 0), w/ respectively.

Figures 8(a)–8(f) show the periodic orbits with 3 to 8 number of loops with an initial true anomaly and velocity of $\pi/3$ with (0, 0.002, 0), respectively.

Figures 9(a)–9(f) show the periodic orbits with the number of loops 5 to 10 with a given value of x^0. These orbits are obtained when the initial true anomaly and initial velocities are $\pi/2$ and (0, 0.002, 0), respectively.

The analysis of periodic orbits for three initial values of true anomalies $\pi/6$, $\pi/3$, and $\pi/2$ with eccentricity $e = 0.2$ is given in Table 2. The entire study has been performed by considering two different sets of initial velocities as (0, 0.002, 0)

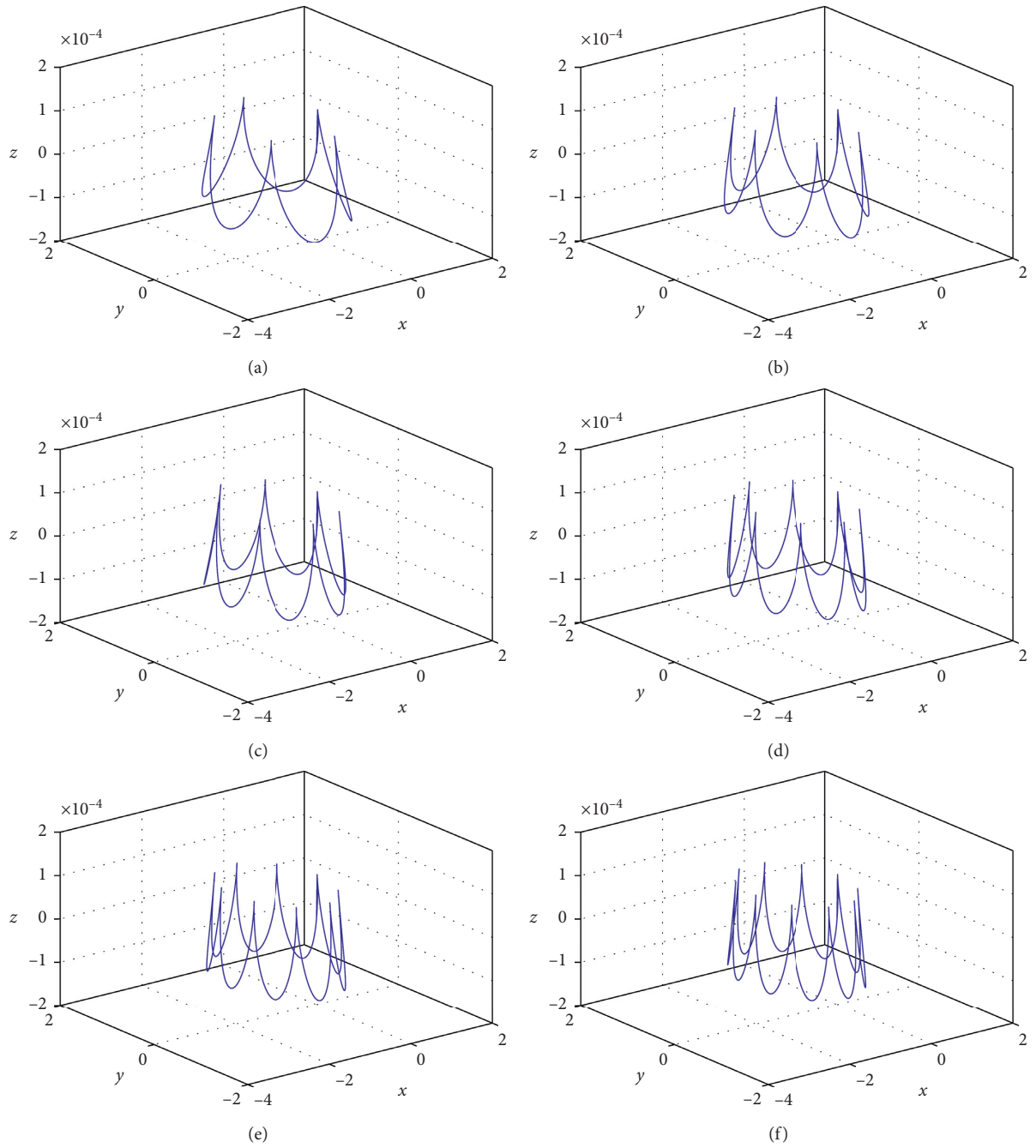

Figure 4: Periodic orbits when $e = 0.1$ and $f^0 = \pi/3$ and velocity $\dot{y}^0 = 0.005$. (a) Five-loop orbit, when $x^0 = 0.026250375000$. (b) Six-loop orbit, when $x^0 = 0.022008125000$. (c) Seven-loop orbit, when $x^0 = 0.018857650000$. (d) Eight-loop orbit, when $x^0 = 0.016425375000$. (e) Nine-loop orbit, when $x^0 = 0.01449068105$. (f) Ten-loop orbit, when $x^0 = 0.012915$.

and (0, 0.005, 0). The initial position and period of the periodic orbits are obtained for each set of orbits with 1–10 loops.

Figures 10(a) and 10(b) indicates the variation in the initial position and period of the periodic orbits for initial velocities (0, 0.002, 0) and (0, 0.005, 0), respectively. Here, eccentricity of chief satellite's orbit is considered 0.2. From these graphs, it can be observed that, as number of loops in the given orbit increases, the initial position of the periodic orbit moves towards the origin (the initial position of chief satellite) irrespective of the initial value of true anomaly. From these graphs, it can also be observed that, as number of loops in the given orbit increases, the period of the periodic orbit increases irrespective of the initial true anomaly.

4. Effect of Eccentricity of Chief Satellite's Orbit

In the previous section, we have considered that the eccentricity e of chief satellite's orbit is 0.1 and 0.2, respectively. But, in the current section, we compare the effect of variation in eccentricity of chief satellite's orbit on periodic orbits of

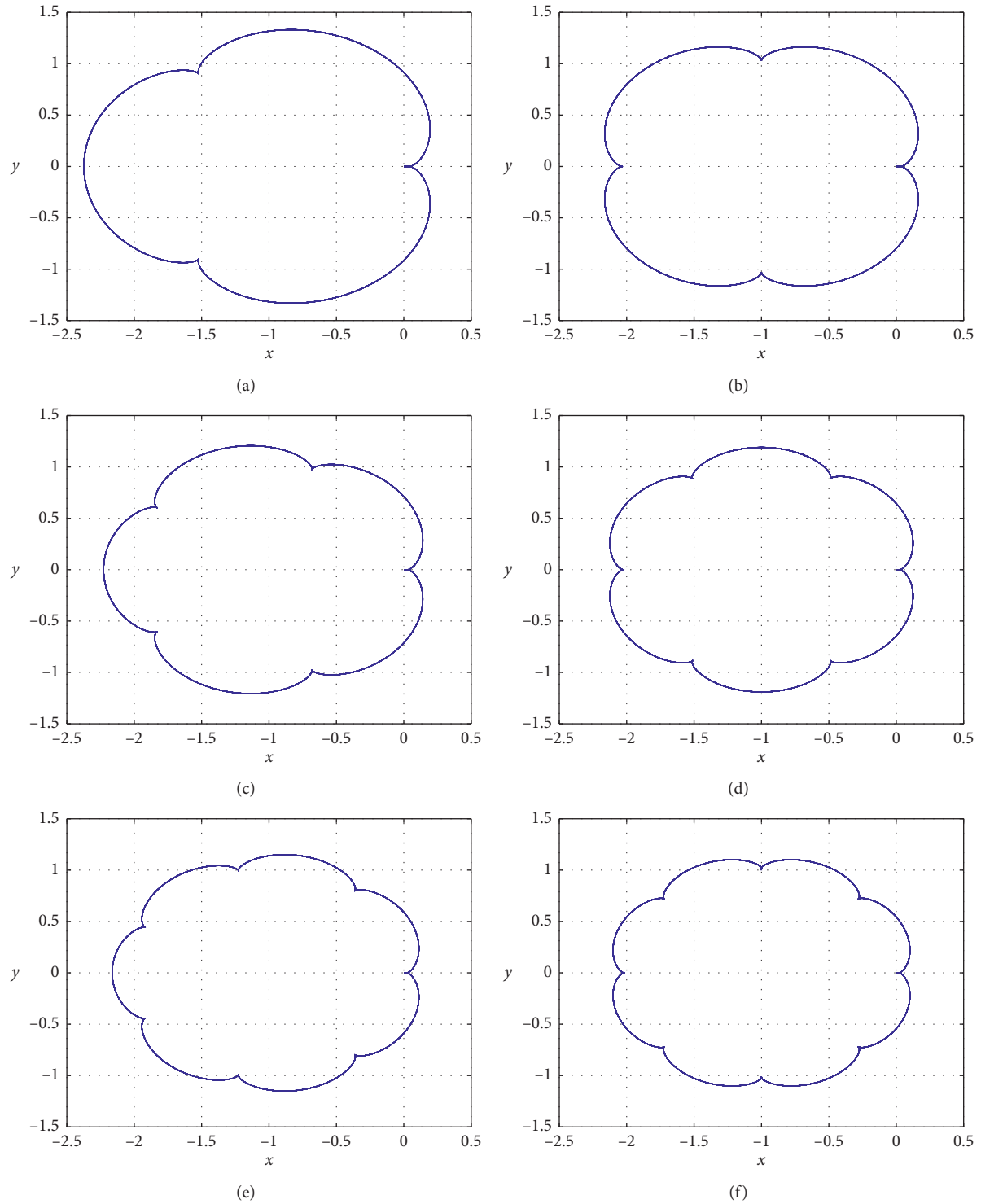

FIGURE 5: Periodic orbits when $e = 0.1$, $f^0 = \pi/2$, and velocity $\dot{y}^0 = 0.002$. (a) Three-loop orbit, when $x^0 = 0.041398075500$. (b) Four-loop orbit, when $x^0 = 0.032620475000$. (c) Five-loop orbit, when $x^0 = 0.0268523875$. (d) Six-loop orbit, when $x^0 = 0.0227732155$. (e) Seven-loop orbit, when $x^0 = 0.0197361$. (f) Eight-loop orbit, when $x^0 = 0.017387015$.

deputy satellite with the number of loops 1–10. This effect on initial position and orbital period of periodic orbits of deputy satellite with 1–10 number of loops will be shown in Figures 11–13.

Figures 11(a) and 11(b) give the relation between the initial position and orbital period and number of loops with consideration of three different values of true anomaly as $\pi/6$, $\pi/3$, and $\pi/2$. The velocity is taken in magnitude as (0,

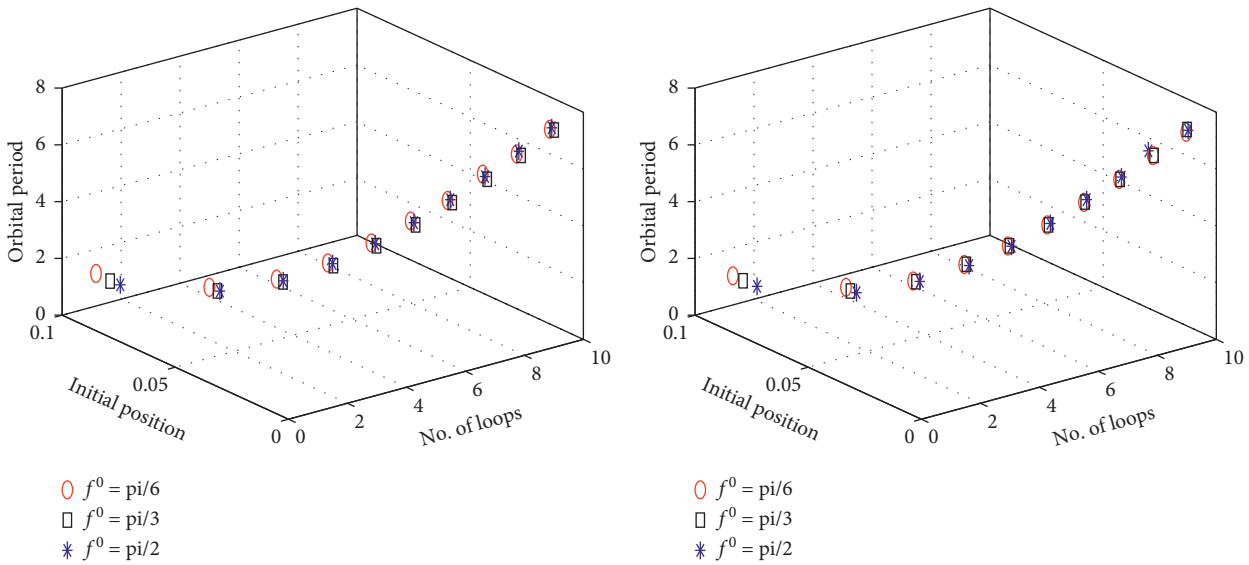

Figure 6: Variation in the initial position of deputy satellite and orbital period when $e = 0.1$. (a) Velocity $\dot{y}^0 = 0.002$. (b) Velocity $\dot{y}^0 = 0.005$.

Table 1: Analysis of periodic orbits with $e = 0.1$.

f^0	$\dot{y}^0$	z^0	x^0	T	NL
$\pi/6$	0.002	0.0001	0.097990643050	1.250	01
			0.060941913025	1.885	02
			0.044263995500	2.520	03
			0.034693850000	3.140	04
			0.028473250000	3.765	05
			0.024102420000	4.400	06
			0.020861979500	5.020	07
			0.018363295500	5.650	08
			0.016377575000	6.275	09
			0.014761465000	6.900	10
$\pi/6$	0.005	0.0001	0.096286152500	1.250	01
			0.059311045000	1.885	02
			0.042667625000	2.520	03
			0.033117650000	3.140	04
			0.026910306500	3.765	05
			0.022548855000	4.400	06
			0.019315450000	5.020	07
			0.016822145000	5.650	08
			0.014840725000	6.275	09
			0.013228150000	6.900	10
$\pi/3$	0.002	0.0001	0.093525298500	1.260	01
			0.059057635000	1.885	02
			0.043092145000	2.520	03
			0.033847995000	3.140	04
			0.027812858705	3.770	05
			0.023561300000	4.400	06
			0.020403925000	5.030	07
			0.017966250000	5.655	08
			0.016027250000	6.285	09
			0.014448085000	6.950	10

Table 1: Continued.

f^0	$\dot{y}^0$	z^0	x^0	T	NL
$\pi/3$	0.005	0.0001	0.091825025000	1.260	01
			0.057428285000	1.885	02
			0.041496687050	2.520	03
			0.032272425000	3.140	04
			0.026250375000	3.770	05
			0.022008125000	4.400	06
			0.018857650000	5.030	07
			0.016425375000	5.655	08
			0.014490681050	6.285	09
			0.012915000000	6.950	10
$\pi/2$	0.002	0.0001	0.087338089500	1.276	01
			0.056357275000	1.907	02
			0.041398075500	2.540	03
			0.032620475000	3.170	04
			0.026852387500	3.803	05
			0.022773215500	4.450	06
			0.019736100000	5.070	07
			0.017387015000	5.700	08
			0.015515950000	6.334	09
			0.013990535000	6.960	10
$\pi/2$	0.005	0.0001	0.085643905000	1.276	01
			0.054730207500	1.907	02
			0.039803926500	2.540	03
			0.031045825000	3.170	04
			0.025290650000	3.803	05
			0.021220605000	4.450	06
			0.018190250000	5.070	07
			0.015846495000	5.700	08
			0.013979735000	6.334	09
			0.012457750000	6.960	10

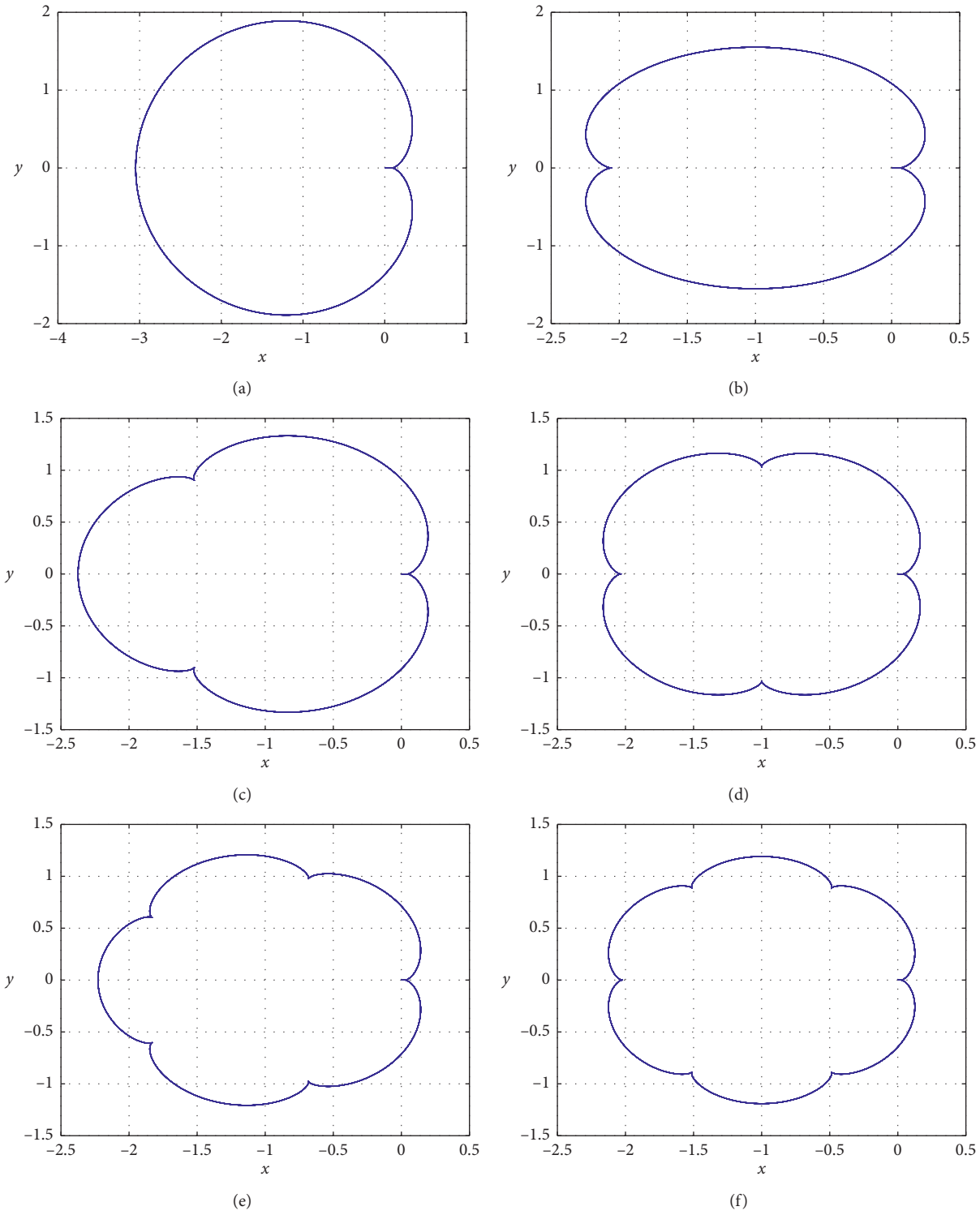

Figure 7: Periodic orbits when $e = 0.2$, $f^0 = \pi/6$, and velocity $\dot{y}^0 = 0.002$. (a) One-loop orbit, when $x^0 = 0.088265415$. (b) Two-loop orbit, when $x^0 = 0.0567688625$. (c) Three-loop orbit, when $x^0 = 0.041657425$. (d) Four-loop orbit, when $x^0 = 0.032808755$. (e) Five-loop orbit, when $x^0 = 0.026999870500$. (f) Six-loop orbit, when $x^0 = 0.022894322500$.

0.002, 0). It has been observed from the Figure 11(a) for single-loop orbit that, as the true anomaly increases, the initial position of the periodic orbit moves towards zero. Thus, it has been observed from the comparative study that, in both the cases of initial velocities and eccentricities, as true anomaly increases, the initial position of periodic orbit moves towards zero. Also, it can be seen that, as we shift towards 1- to 10-loop periodic orbit, the difference in the initial position due to the true anomaly decreases. Thus, initial locations of periodic orbits for three different values of

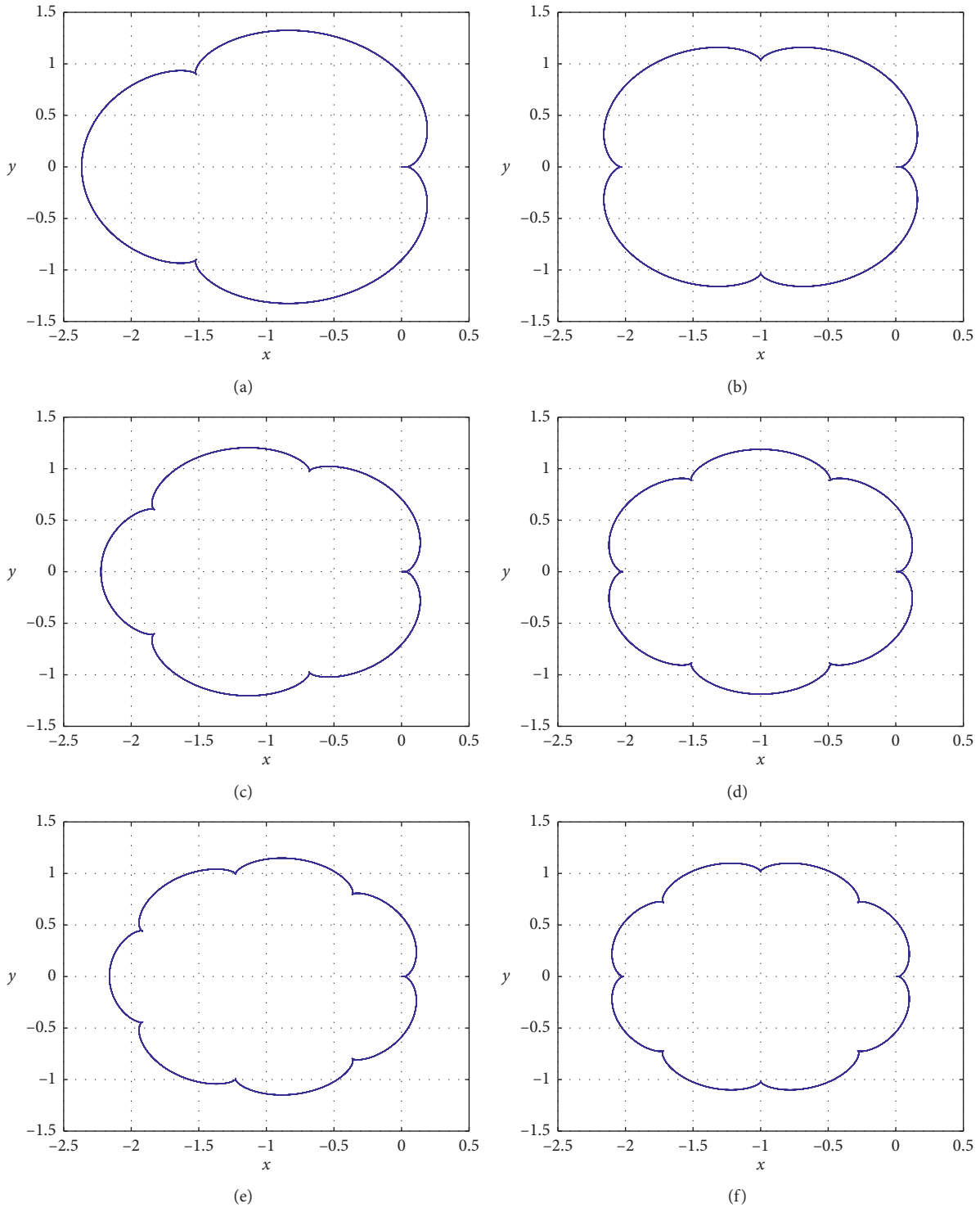

FIGURE 8: Periodic orbits when $e = 0.2$, $f^0 = \pi/3$ and velocity $\dot{y}^0 = 0.002$. (a) Three loops orbit, when $x^0 = 0.0396983975$. (b) Four loops orbit, when $x^0 = 0.031383115$. (c) Five loops orbit, when $x^0 = 0.0258816925$. (d) Six loops orbit, when $x^0 = 0.02197541025$. (e) Seven loops orbit, when $x^0 = 0.019059245000$. (f) Eight loops orbit, when $x^0 = 0.016799437500$.

true anomaly come closer to each other as the number of loops increases from 1 to 10. Variation in periods of periodic orbits with respect to the number of loops for three different values of true anomaly as $\pi/6$, $\pi/3$, and $\pi/2$ is shown in Figure 11(b) with a velocity (0, 0.002, 0). It has been seen in both cases of initial velocities and eccentricities that orbital period increases with the increasing number of loops.

Figures 12(a) and 12(b) give the relation between the initial position and orbital period and number of loops with consideration of three different values of true anomaly as

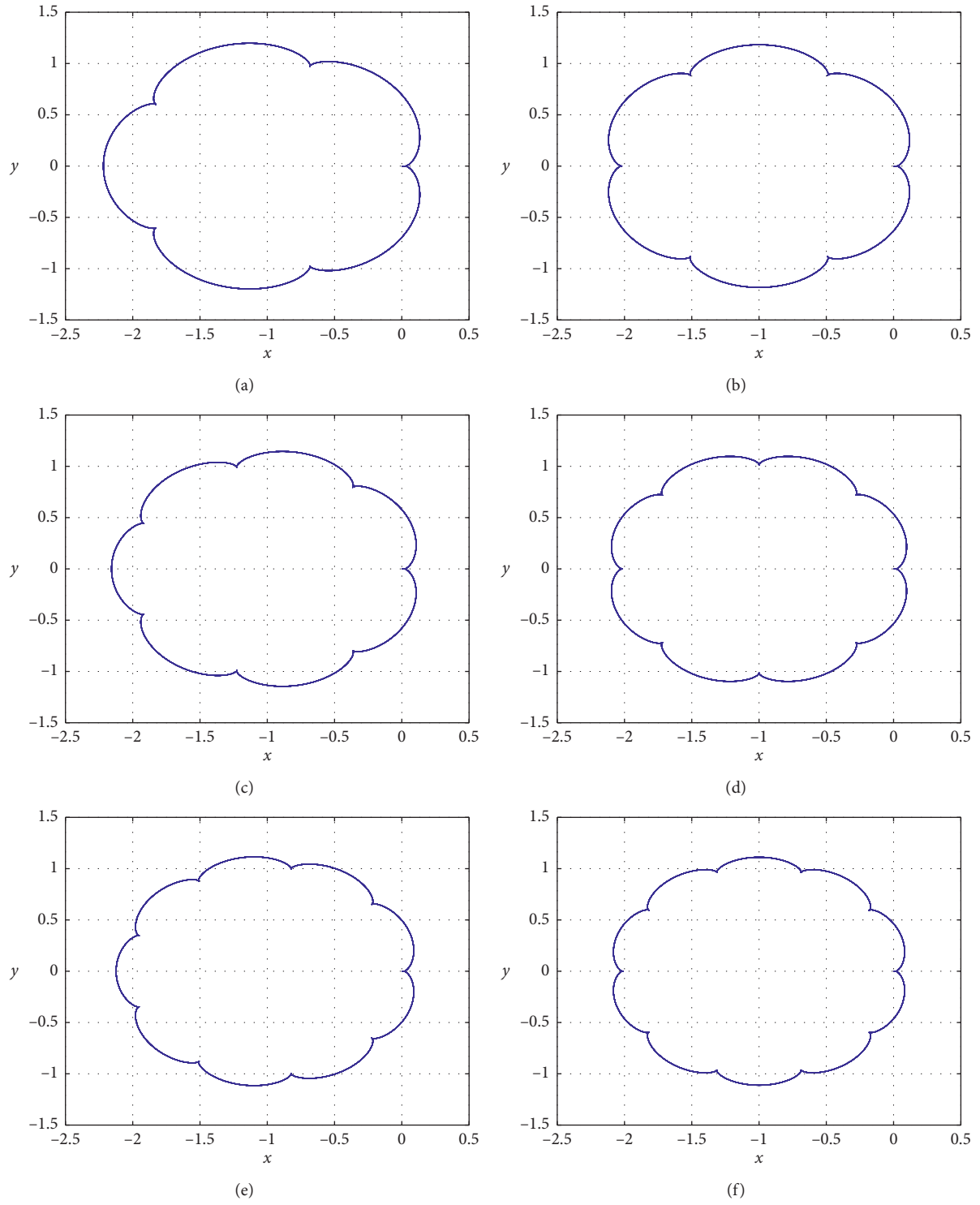

Figure 9: Periodic orbits when $e = 0.2$, $f^0 = \pi/2$, and velocity $\dot{y}^0 = 0.002$. (a) Five-loop orbit, when $x^0 = 0.024156265$. (b) Six-loop orbit, when $x^0 = 0.020553885$. (c) Seven-loop orbit, when $x^0 = 0.01785125$. (d) Eight-loop orbit, when $x^0 = 0.0157495245$. (e) Nine-loop orbit, when $x^0 = 0.029191930500$. (f) Ten-loop orbit, when $x^0 = 0.027620026500$.

$\pi/6$, $\pi/3$, and $\pi/2$. The velocity is taken in magnitude as (0, 0.005, 0). It has been observed from the Figure 12(a) for single-loop orbit that, as the true anomaly increases, the initial position of periodic orbit moves towards zero. Thus, it has been observed from the comparative study that, in both the cases of initial velocities and eccentricities, as true anomaly increases, the initial position of periodic orbit moves towards zero. Also, it can be seen that, as we shift towards 1- to 10-loop periodic orbit, the difference in the initial position due to the true anomaly decreases. Thus, the

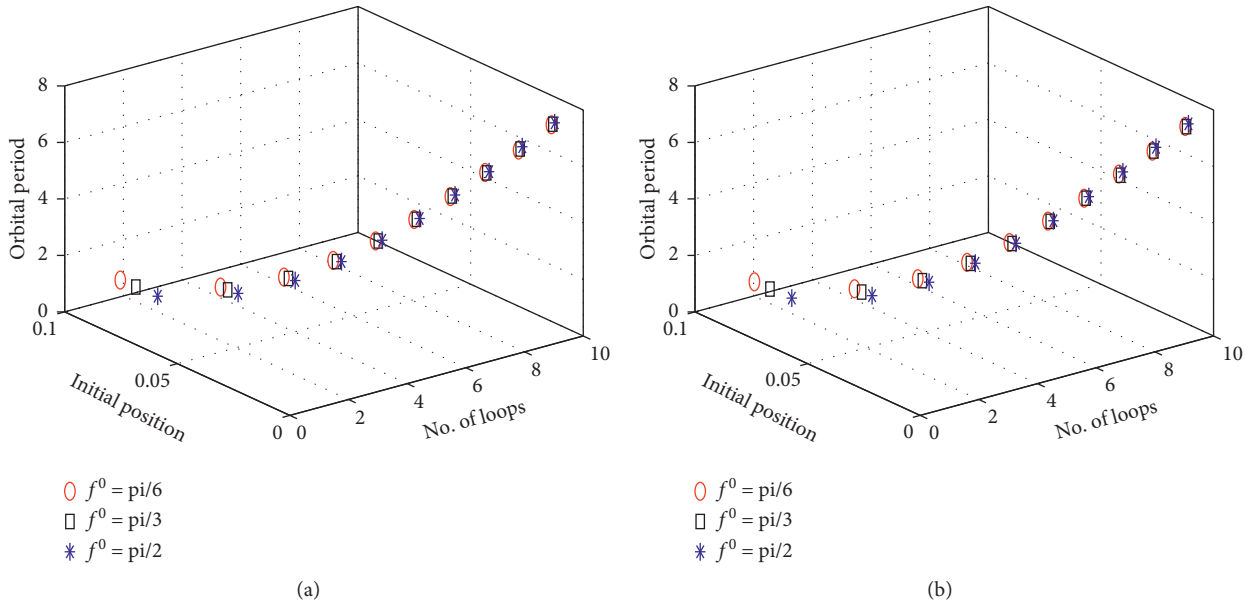

Figure 10: Variation in the initial position of deputy satellite and orbital period when $e = 0.2$. (a) Velocity $\dot{y}^0 = 0.002$. (b) Velocity $\dot{y}^0 = 0.005$.

Table 2: Analysis of periodic orbits with $e = 0.2$.

f^0	$\dot{y}^0$	z^0	x^0	T	NL
$\pi/6$	0.002	0.0001	0.088265415000	1.272	01
			0.056768862500	1.910	02
			0.041657425000	2.533	03
			0.032808755000	3.165	04
			0.026999870500	3.797	05
			0.022894322500	4.450	06
			0.019838765000	5.062	07
			0.017476085000	5.700	08
			0.015594612750	6.325	09
			0.014060927500	6.956	10
$\pi/6$	0.005	0.0001	0.086570301500	1.272	01
			0.055141436550	1.910	02
			0.040063075000	2.533	03
			0.031233975000	3.165	04
			0.025437996500	3.797	05
			0.021341635000	4.450	06
			0.018292920100	5.062	07
			0.015935540000	5.700	08
			0.014058295500	6.325	09
			0.012528082500	6.956	10
$\pi/3$	0.002	0.0001	0.081430725000	1.293	01
			0.053676025000	1.926	02
			0.039698397500	2.600	03
			0.031383115000	3.200	04
			0.025881692500	3.837	05
			0.021975410250	4.474	06
			0.019059245000	5.115	07
			0.016799437500	5.748	08
			0.014996967500	6.386	09
			0.013525826550	7.025	10

Table 2: Continued.

f^0	$\dot{y}^0$	z^0	x^0	T	NL
$\pi/3$	0.005	0.0001	0.079742645000	1.293	01
			0.052051320000	1.926	02
			0.038105645000	2.600	03
			0.029809435000	3.200	04
			0.024320665000	3.837	05
			0.020423376500	4.474	06
			0.017513965000	5.115	07
			0.015259385000	5.748	08
			0.013461085000	6.386	09
			0.011993350000	7.025	10
$\pi/2$	0.002	0.0001	0.071713530000	1.328	01
			0.049027550000	1.968	02
			0.036708365000	2.612	03
			0.029191930500	3.257	04
			0.024156265000	3.903	05
			0.020553885000	4.550	06
			0.017851250000	5.195	07
			0.015749524500	5.843	08
			0.014068710500	6.488	09
			0.012694067500	7.135	10
$\pi/2$	0.005	0.0001	0.070036225000	1.328	01
			0.047407175000	1.968	02
			0.035118165000	2.612	03
			0.027620026500	3.257	04
			0.022596595500	3.903	05
			0.019002955000	4.550	06
			0.016306865000	5.195	07
			0.014210250000	5.843	08
			0.012533505000	6.488	09
			0.011162205000	7.135	10

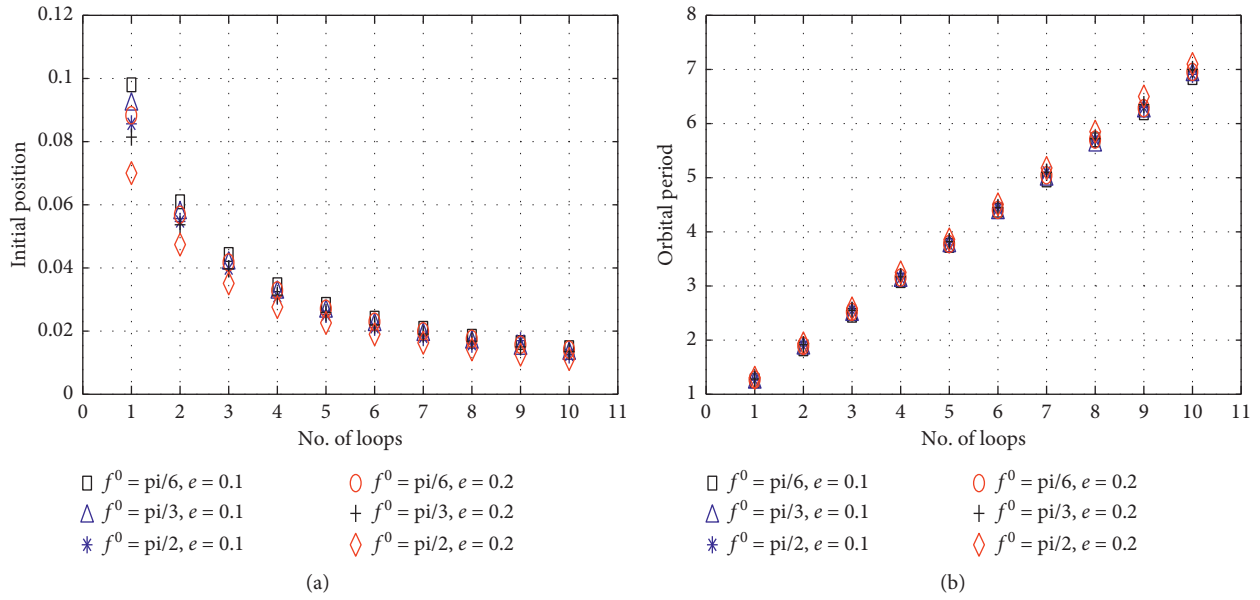

Figure 11: Variation in (a) the initial position of periodic orbits and (b) orbital period when $\dot{y}^0 = 0.002$.

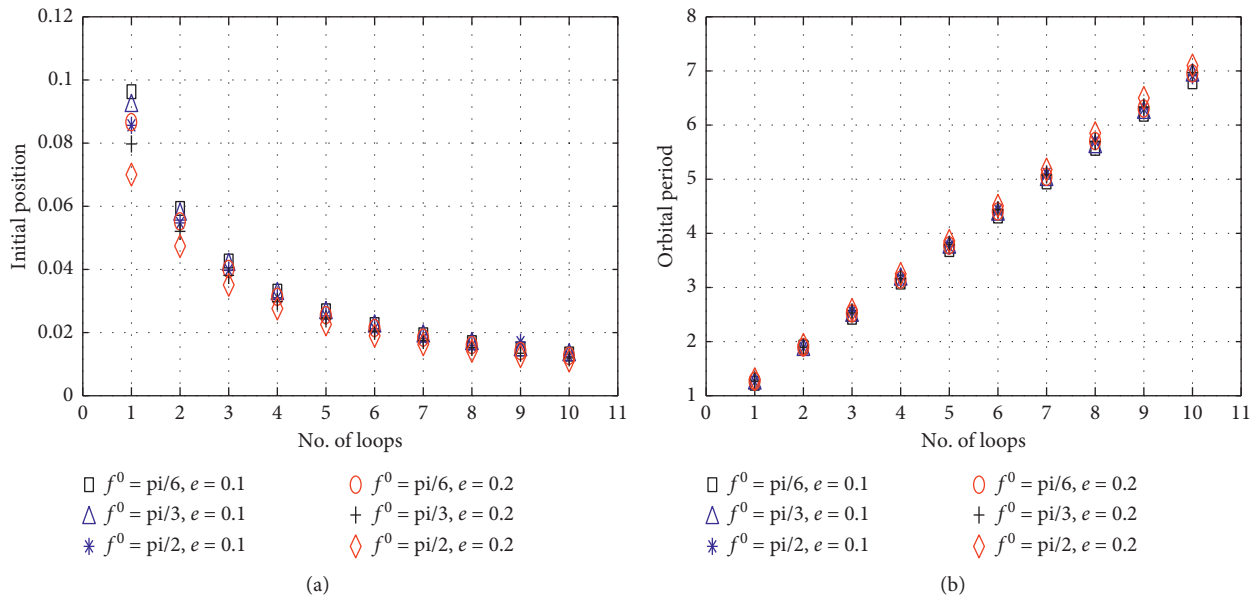

Figure 12: Variation in the (a) initial position of periodic orbits and (b) orbital period when $\dot{y}^0 = 0.005$.

initial locations of periodic orbits for three different values of true anomaly come closer to each other as the number of loops increases from 1 to 10. The variation in periods of periodic orbits with respect to the number of loops for three different values of true anomaly as $\pi/6$, $\pi/3$, and $\pi/2$ is shown in Figure 12(b) with a velocity (0, 0.005, 0). It has been seen in both cases of initial velocities and eccentricities that orbital period increases with increasing number of loops.

Figures 13(a)–13(c) show the variation in the initial position and period with respect to number of loops for two different eccentricities 0.1 and 0.2 with given initial true anomalies $\pi/6$, $\pi/3$, and $\pi/2$, respectively. In these three figures, the velocity is considered as (0, 0.002, 0). This gives information about the variation in the initial position and orbital period when the values of eccentricity are changed as shown in all figures. The sharp observation for the single-loop orbit depicts that, for the given value of true anomaly, as the eccentricity goes on increasing and the initial position of periodic orbit shifts towards $x^0 = 0$. It has also been observed that, moving in the direction from 1- to 10-loop orbit, differences in the initial position for a given value of true anomaly decreases with increasing eccentricity. The orbital period is conserved as the velocity increases for a given number of loops, eccentricity, and initial true anomaly.

It is observed that, with the ascending number of loops, the initial position of periodic orbits approaches to the origin

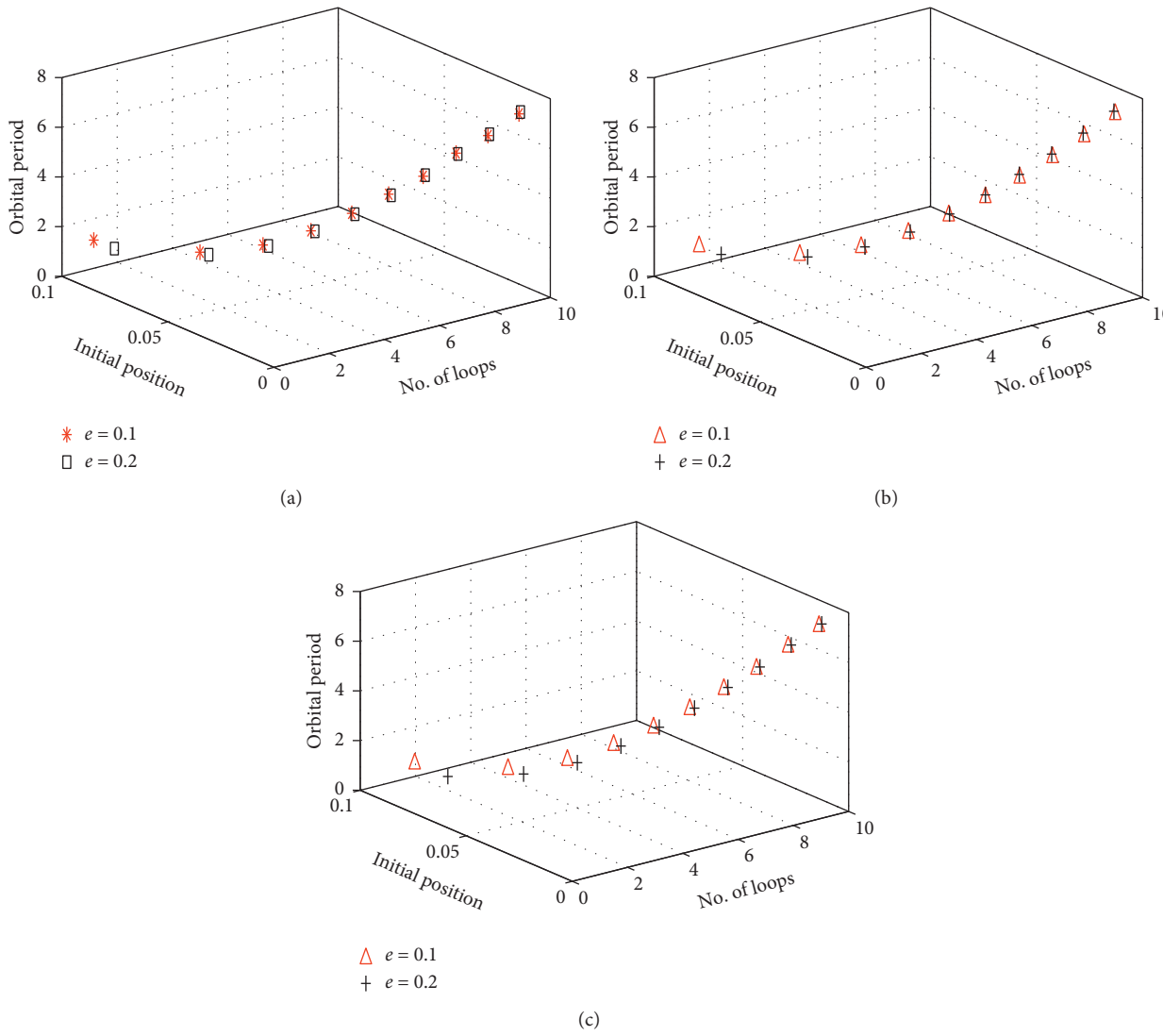

Figure 13: Variation in the initial position and orbital period, when velocity is (0, 0.002, 0). (a) $f^0 = \pi/6$. (b) $f^0 = \pi/3$. (c) $f^0 = \pi/2$.

with an increasing value of orbital periods. When the eccentricity is 0.1, for all the true anomalies, we get two-dimensional periodic orbits, but especially when true anomaly approaches to $\pi/3$, the orbits becomes three-dimensional periodic and then again, as true anomaly approaches $\pi/2$, the three-dimensional orbits becomes quasi in nature. Whereas when the eccentricity is 0.2, we get two-dimensional periodic orbits for all the true anomalies. The nature of three dimensional orbits becomes highly quasi with an increasing value of the true anomaly. Thus, as the eccentricity increases, the nature of periodic orbits becomes more chaotic with an increasing value of true anomaly.

The periodic solution plays a vital role in the field of celestial mechanics. However, a solution feature in the form of mathematical expression for the behavior of the trajectory does not directly appear, but these features can be clearly shown when the solution is graphically represented. It also identifies the orbit whether it is loop or without loop. In case an orbit is having loops, the number of loops with internal position or external position can be determined easily with the same solution too. An orbital period of the orbit is the most important parameter that gives information about the time required to complete one revolution by the deputy satellite. The value of this parameter is determined easily by the periodic solution. It is evident from this study that, as the number of loops increases, the period of the periodic orbit increases. Periodic orbits with a lower number of orbital periods have been more emphasized in celestial mechanics. In this regard, the main focus of this study is 1- to 10-loop periodic orbit with a value of period less than 7. In formation satellites, the initial true anomaly and initial velocity of deputy satellite play an important role which affects the initial position of periodic orbits of deputy satellite. Also, in the LVLH frame, the origin is located at the position of chief satellite, so the eccentricity of the orbit of chief satellite also affects the initial position and orbital period of deputy

satellite. Thus, it is important to study the effect of these parameters on periodic orbit of deputy satellite.

5. Conclusion

The main focus of this work is on periodic orbit of deputy satellite in the elliptical case of formation satellites. The analysis of 1- to 10-loop periodic orbits with different values of initial true anomaly f^0 and eccentricity e of the orbit of chief satellite has been performed by considering the initial position (x^0, 0, 0.0001) and initial velocity (0, $\dot{y}^0$, 0). It has been observed that, as the number of loops ascends from 1 to 10, there is an increment in the orbital period, and the initial position of periodic orbits approaches to origin. For a given number of loops, eccentricity, and initial true anomaly, the orbital period is conserved with regard as velocity ascends.

It is noticed that the effect of eccentricity and initial true anomaly on orbital period is negligible. For the given eccentricity e and initial velocity (0, $\dot{y}^0$, 0), as number of loops increases, the initial position (x^0, 0, 0.0001) shifts towards zero. It has also been concluded that, for the given number of loops, the effect of eccentricity and initial true anomaly on orbital period is negligible. Furthermore, with the given value of initial true anomaly f^0 and initial velocity (0, $\dot{y}^0$, 0), the number of loops and increment in eccentricity e and initial position (x^0, 0, 0.0001) approach the origin. Thus, to conclude with that for given value of true anomaly and eccentricity, there is a decrement in the value between the differences in initial position vectors with the ascending number of loops. In other words, for a given value of true anomaly and eccentricity, the difference in the initial position (Δx, 0, 0.0001) decreases as the number of loops increases.

Finally, we summarize and state that, in the frame work of formation satellite, 1–10 loop periodic orbits of deputy satellite are analyzed. In this analysis, there are three parameters, namely, initial true anomaly, initial velocity of deputy satellite, and eccentricity of orbit of chief satellite. The initial position and orbital period are investigated for these orbits.

It is observed that, with the ascending number of loops, the initial position of periodic orbits approaches to origin with an increasing value of orbital periods. When the eccentricity is 0.1, for all the true anomalies, we get two-dimensional periodic orbits, but especially when true anomaly approaches to $\pi/3$, the orbits become three-dimensional periodic and then, again as true anomaly approaches $\pi/2$, the three-dimensional orbits becomes quasi in nature. Whereas when eccentricity is 0.2, we get two-dimensional periodic orbits for all the true anomalies. The nature of three-dimensional orbits becomes highly quasi with an increasing value of true anomaly. Thus, as the eccentricity increases, the nature of periodic orbits becomes more chaotic with an increasing value of true anomaly.

It is remarkable that the orbital period remains unchanged for the given initial true anomaly, eccentricity, and number of loops with ascending velocity. Thus, the orbital period and nature of the periodic orbits are conserved with a negligible displacement in the initial position of the orbits with increasing velocity. It has also been observed that, for a given number of loops, eccentricity, and initial true anomaly with the increment in velocity, there is a decrement in the value of the initial position of the orbit. Thus, to conclude with that for a given value of true anomaly and eccentricity, there is a decrement in the value between the differences in initial position vectors with the ascending number of loops. Also, with the rise in velocity, there is negligible change in the value of differences in the initial position (Δx, 0, 0.0001) corresponding to each loop.

Data Availability

Data sharing is not applicable to this article as no datasets were generated or analyzed during the current study.

Conflicts of Interest

The authors declare that there are no conflicts of interest.

References

[1] F. Alzahrani, E. I. Abouelmagd, J. L. G. Guirao, and A. Hobiny, "On the libration collinear points in the restricted three-body problem," *Open Physics*, vol. 15, no. 1, pp. 58–67, 2017.

[2] E. I. Abouelmagd, J. L. G. Guirao, and J. Llibre, "Periodic orbits for the perturbed planar circular restricted 3–body problem," *Discrete & Continuous Dynamical Systems-B*, vol. 24, no. 3, pp. 1007–1020, 2019.

[3] N. Pathak, V. Thomas, V. O. Thomas, and E. I. Abouelmagd, "The perturbed photogravitational restricted three-body problem: analysis of resonant periodic orbits," *Discrete & Continuous Dynamical Systems - S*, vol. 12, no. 4-5, pp. 849–875, 2019.

[4] N. Pathak, E. I. Abouelmagd, and V. O. Thomas, "On higher order resonant periodic orbits in the photo-gravitational planar restricted three-body problem with oblateness," *The Journal of the Astronautical Sciences*, vol. 66, no. 4, pp. 475–505, 2019.

[5] J. L. G. Guirao, J. Llibre, and J. A. Vera, "Periodic orbits of Hamiltonian systems: applications to perturbed Kepler problems," *Chaos, Solitons & Fractals*, vol. 57, pp. 105–111, 2013.

[6] R. M. Tudoran, "Asymptotic stabilization with phase of periodic orbits of three-dimensional Hamiltonian systems," *Journal of Geometry and Physics*, vol. 121, pp. 33–41, 2017.

[7] M. T. de Bustos, J. L. G. Guirao, J. Llibre, and J. A. Vera, "New families of periodic orbits for a galactic potential," *Chaos, Solitons & Fractals*, vol. 82, pp. 97–102, 2016.

[8] J. Llibre and C. Vidal, "Periodic motion in non-axially symmetric galaxies," *Journal of Geometry and Physics*, vol. 140, pp. 1–9, 2019.

[9] O. Montenbruck, M. Wermuth, and R. Kahle, "GPS based relative navigation for the TanDEM-X mission-first flight results," *Navigation*, vol. 58, no. 4, pp. 293–304, 2011.

[10] R. S. Smith and F. Y. Hadaegh, "Distributed estimation, communication and control for deep space formations," *IET Control Theory & Applications*, vol. 1, no. 2, pp. 445–451, 2007.

[11] C. W. T. Roscoe, S. R. Vadali, K. T. Alfriend, and U. P. Desai, "Satellite formation design in orbits of high eccentricity with performance constraints specified over a region of interest:

mms phase II," *Acta Astronautica*, vol. 82, no. 1, pp. 16–24, 2013.

[12] B. Wu, G. Xu, and X. Cao, "Relative dynamics and control for satellite formation: accommodating j_2 perturbation," *Journal of Aerospace Engineering*, vol. 29, no. 4, Article ID 04016011, 2016.

[13] B. Wu, D. Wang, and E. K. Poh, "Decentralized sliding-mode control for attitude synchronization in spacecraft formation," *International Journal of Robust and Nonlinear Control*, vol. 23, no. 11, pp. 1183–1197, 2013.

[14] G. W. Hill, "Researches in the lunar theory," *American Journal of Mathematics*, vol. 1, no. 1, pp. 5–26, 1878.

[15] J. L. Junkins and H. Schaub, *Analytical Mechanics of Space Systems*, AIAA, Reston, VA, USA, 2003.

[16] S. A. Schweighart and R. J. Sedwick, "High-fidelity linearized J model for satellite formation flight," *Journal of Guidance, Control, and Dynamics*, vol. 25, no. 6, pp. 1073–1080, 2002.

[17] J. A. Roberts and P. C. E. Roberts, "The development of high fidelity linearized J_2 models for satellite formation flying control," in *Proceedings of the 14th AAS/AIAA Space Flight Mechanics Meeting*, Maui, HI, USA, February 2004.

[18] J. A. Roberts, *Development of a Relative Motion Model for Satellite Formation Flying Around L_2*, Cranfield University; School of Engineering, Cranfield, UK, 2004.

[19] Z. Wang and X. Chen, "Optimal maneuver technology for satellite formation flying," in *Informatics in Control, Automation and Robotics*, pp. 287–290, Springer, Berlin, Germany, 2011.

[20] M. A. Nurge, R. C. Youngquist, and S. O. Starr, "A satellite formation flying approach providing both positioning and tracking," *Acta Astronautica*, vol. 122, pp. 1–9, 2016.

[21] R. C. Youngquist, M. A. Nurge, and S. O. Starr, "Alternating magnetic field forces for satellite formation flying," *Acta Astronautica*, vol. 84, pp. 197–205, 2013.

[22] D. Ivanov, M. Ovchinnikov, and S. Shestakov, "Satellite formation flying control by mass exchange," *Acta Astronautica*, vol. 102, pp. 392–401, 2014.

[23] E. I. Abouelmagd, D. Mortari, and H. H. Selim, "Analytical study of periodic solutions on perturbed equatorial two-body problem," *International Journal of Bifurcation and Chaos*, vol. 25, no. 14, Article ID 1540040, 2015.

[24] E. I. Abouelmagd, S. Elshaboury, and H. Selim, "Numerical integration of a relativistic two-body problem via a multiple scales method," *Astrophysics and Space Science*, vol. 361, no. 1, Article ID 38, 2016.

[25] E. I. Abouelmagd, J. Llibre, and J. L. G. Guirao, "Periodic orbits of the planar anisotropic kepler problem," *International Journal of Bifurcation and Chaos*, vol. 27, no. 3, Article ID 1750039, 2017.

[26] E. I. Abouelmagd, "Periodic solution of the two-body problem by KB averaging method within frame of the modified Newtonian potential," *The Journal of the Astronautical Sciences*, vol. 65, no. 3, pp. 291–306, 2018.

Hindawi
Advances in Astronomy
Volume 2020, Article ID 6684728, 10 pages
https://doi.org/10.1155/2020/6684728

Research Article

Motion of the Infinitesimal Variable Mass in the Generalized Circular Restricted Three-Body Problem under the Effect of Asteroids Belt

Ferdaous Bouaziz-Kellil

Department of Mathematics, College of Science and Arts, Qassim University, Buraydah, Saudi Arabia

Correspondence should be addressed to Ferdaous Bouaziz-Kellil; fm.boazuez@qu.edu.sa

Received 6 November 2020; Revised 24 November 2020; Accepted 30 November 2020; Published 18 December 2020

Academic Editor: Elbaz Abouelmagd

The present paper deals with the study of the motion's properties of the infinitesimal variable mass body moving in the same orbital plan as two massive bodies (considered as primaries). It is assumed that the massive bodies have radiating effects, have oblate shapes, and are moving in circular orbits around their common center of mass. Using the procedures established by Singh and Abouelmagd, we determined the equations of motion of the infinitesimal body for which we assumed that under the effects of radiation and oblateness of the primaries, its mass varies following Jean's law. We evaluated analytically and numerically the locations of equilibrium points and examined the stability of these equilibrium points. Finally, we found that all the points are unstable.

1. Introduction

During the last decades, in celestial mechanics and dynamical astronomy, the most studied problem was and remains the restricted three-body problem that we denote in the sequel by R3BP. The problem has been investigated when the orbits of the primaries are either circular or elliptic. One of the reasons that make the problem very attracting is that it represents a general applicable model that can be also endowed with some types of perturbations. By perturbation, we mean the deviations of the body from its normal states due to some outer forces (perturbing effects). Perturbing effects can be in any form, such as Coriolis and centrifugal forces, different shapes of the primaries (as Roche ellipsoid, spherical shell filled with or without fluid, heterogeneous body, homogeneous body, triaxial, oblate, cylindrical, and finite straight segments), zonal harmonic effects, drag forces (P-R drag and strokes drag), resonances (high or low), solar radiation pressure, variable mass, asteroids belt, magnetic dipoles, charged bodies, Yarkovaskii effects, albedo effects, and viscous forces.

Many research studies have been devoted to this problem with different above cited perturbations. Our references are not exhaustive; however, in this introduction, we essentially cite the references that have been used to accomplish this work.

Bhatnagar and Hallan [1] introduced a new type of perturbations in the classical R3BP (i.e., under Coriolis and centrifugal forces), and they have shown that their problem has five libration points out of which three are unstable and two are stable. In their studies, Khanna and Bhatnagar [2] have been concerned by the existence and stability of equilibrium points in the circular R3BP, both with the triaxial shape and with the combination of the triaxial shape and the oblateness of the primaries. More exactly, they assumed that the more massive primary is an oblate spheroid in the first study, and in the second one, they combined the triaxial shape and the oblateness of the primaries. With similar hypothesis of the oblate spheroid shape of the more massive primary, Sharma and Subba Rao [3] investigated the stationary solutions and their characteristic exponents in the classical circular R3BP. Subba Rao and Sharma [4] studied the effect of this type of shape in the classical circular restricted three-body problem and found that the collinear stationary solutions are always unstable, while the nearly

equilateral triangular stationary solutions are stable in some interval depending also on the oblateness factor. In the same topic of shape, Abouelmagd et al. [5] studied the effect of the oblateness associated to small perturbations in the Coriolis and centrifugal forces in R3BP. In particular, they found that the positions of the collinear points and y-coordinate of the triangular points are not affected by the small perturbations in the Coriolis force.

The case where both the primaries are assumed to be triaxial rigid bodies with one of their respective axes assumed to be an axis of symmetry has been investigated by Sharma et al. [6]. The authors supposed that the equatorial plane coincides with the orbital plane of motion. In these conditions, they found three collinear libration points which are always unstable and two triangular libration points which are stable in some intervals like it has been shown by Szebehely [7] for the classical restricted three-body problem. In this study, they also observed that there are long and short periodic elliptical orbits for the triangular libration points within the interval they considered. In the studies by Abouelmagd et al. [8], Ansari et al. [9], Ansari et al. [10], Ansari et al. [11], Ansari et al. [12], Ansari et al. [13], Ansari et al. [14], Ansari [15], and Ansari [16], the authors studied the models of restricted problems both in three-body, four-body, five-body, and six-body by considering various types of perturbations, especially with variable of mass. For Robe's problem, in the study by Ansari [17], the author investigated the motion of the test particle in restricted body problem having heterogeneous irregular primary filled with the viscous fluid, and in the study by Ansari et al. [10], the authors studied Robe's problem in the R3BP subject to viscous force. For the same topic, Abouelmagd et al. [18] studied Robe's problem for which they suppose that the Newton potential is subject to some modification.

On the other hand, Kushvah [19] investigated different mathematical properties due to the asteroids belts for the classical R3BP. The equilibrium points and their stability have been studied numerically. He also showed that the collinear points are unstable and the triangular points are stable in the sense of Lyapunov stability.

For the questions related to the resonance, in the study by Pathak et al. [20], the authors, in both the unperturbed and perturbed cases, investigated the location, the eccentricity, and the period of the first order exterior resonant orbits. They also analyzed the first, third, and fifth order interior resonant periodic orbits. On the other hand, the same team [21] studied resonant orbits in the framework of photogravitational planar restricted three-body problem with oblateness. It is observed that there exist periodic orbits for seventh and ninth order resonance which are passing around the Earth.

In the isotropic radiation case, the mathematical model is governed by the following data:

If F_1 and F_2 are the gravitational forces exerted on m due to m_1 and m_2 and if F_{p_1} and F_{p_2} are the solar radiation pressure exerted on m due to m_1 and m_2, respectively, then the total force exerted on m due to m_i is given by

$$F_i - F_{p_i} = F_i\left(1 - \frac{F_{p_i}}{F_i}\right) = F_i(1 - p_i) = q_i F_i, \quad (i = 1, 2), \tag{1}$$

where $p_i = (\text{radiation pressure due to primary/gravitational force due to primary})$ and $q_i = (1 - p_i)$, $0 < p_i \leq 1$.

Oblate body is a type of triaxial body.

$$\frac{x^2}{a_1^2} + \frac{y^2}{b_1^2} + \frac{z^2}{c_1^2} = 1. \tag{2}$$

When $a_1 = b_1$, it will become an oblate body, and $A_1 = (a_1^2 - c_1^2)/5$ is the oblateness factor, where a_1, b_1, and c_1 are the semiaxes of the triaxial body [22].

Ishwar and Elipe [23] studied the generalized photogravitational R3BP where they assumed that the smaller primary is an oblate body and the massive one is the source of radiation pressure. They found secular solutions at the triangular equilibrium points, and each of these points has either a long or short periodic retrograde elliptical orbits. Singh and Taura [24] devoted their paper to the motion of an infinitesimal body in the generalized R3BP. The authors assumed that both primaries have oblate shapes, radiating and submitted to the effect of gravitational potential from a belt. They determined equations of the motion, located positions of the equilibrium points, and examined their linear stability. To the usual five equilibrium points, they showed that the corresponding problem has additional two new collinear points generated by the potential induced by the belt. They noticed that collinear points are always unstable, while triangular points are stable for certain interval of the mass ratio. Abouelmagd and Ansari [25] studied numerically the bicircular Sun perturbed Earth-Moon-satellite system and illustrated the equilibrium points, Poincaré's surfaces sections, and basins of attracting domain.

In different investigations, it is always supposed that the masses of celestial bodies do not vary with time during the motion, but in reality, many celestial bodies have a variable mass with respect to the time as in the isotropic radiation or the absorption in stars. The isotropic radiation or the absorption in stars generate in general a variation of masses of these celestial bodies and constitute an interesting research topic in the celestial mechanics and dynamical astronomy. These particular last cases have been studied by many researchers in the restricted problem (two-body, three-body, four-body, five-body, and six-body).

Singh and Ishwar [26] and Lukyanov [27] investigated the effect of variable mass in the frame of circular R3BP. For their contribution, Abouelmagd and Mostafa [28] investigated the out-of-plane equilibrium points, the regions of possible motion, and the region of forbidden motion of an infinitesimal body supposed to have a variable mass relatively to Jean's law [29]. Also in R3BP, Zhang et al. [30] investigated the triangular equilibrium points when both the primaries are radiating, and the infinitesimal body has a variable mass according to Jean's law. They used Meshcherskii space-time inverse transformation [31] to test the linear stability of the equilibrium points.

The present study can be applied to study the motion of dust particle, mass of which varies near radiating oblate binary systems surrounded by an asteroids belt.

The asteroid belts having ring shape (Figure 1) can be found in our solar system between the planets. These rings contain many bodies with irregular shapes but are always smaller than the planets themselves. In general, these asteroid belts region lies between the inner boundary (radial distance around 2.06 AU) and outer boundary (the radial distance around 3.27 AU). Systems with asteroid belts were for the first time introduced by Miyamoto and Nagai [32]. This model is known as flattened potential given by the following mathematical formula:

$$V_b(r,z) = \frac{M_b}{\left(r^2 + \left(a + \sqrt{z^2 + b^2}\right)^2\right)^{1/2}}, \tag{3}$$

where M_b is the averaged mass of disc, r is the radial distance of the asteroids belt from the infinitesimal body, and a and b are the flatness and density parameters of the asteroids belt, respectively.

Now, let us describe the organization of our paper. Section 1 presents a nonexhaustive literature review. Section 2 presents the equations of motion, while Sections 3 and 4 contain the investigations of the equilibrium points and of their stability both analytically and numerically. Finally, Section 5 represents our conclusion.

2. Equations of Motion

As it is commonly known, the classical R3BP is a system of three bodies of masses m_1, m_2, and m, where m_1 and m_2 represent the masses of the primaries of the system and that move in circular orbits around their common center of mass representing the origin. In our study, the primaries are assumed to be radiating with the radiation factor q_i $(i = 1, 2)$ and oblate in shape with the oblateness factor A_i $(i = 1, 2)$, respectively. In the synodic coordinate system xyz, the line joining both primaries are taken as the x-axis, while the line perpendicular to this line is known as the y-axis. The mean motion n of the system is considered around z-axis, which is perpendicular to the orbital plane of the primaries. The third

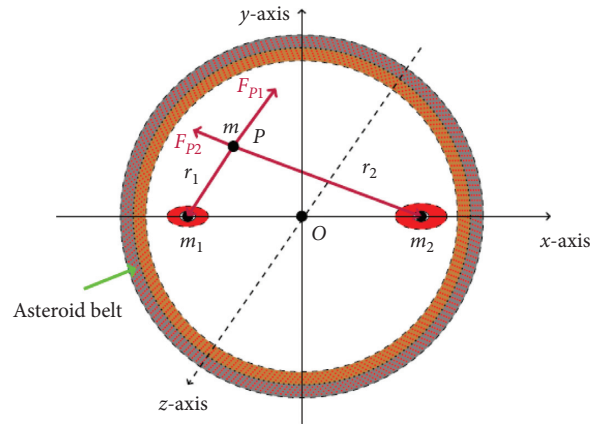

Figure 1: Geometric configuration of the problem with asteroid belt.

body is assumed to have an infinitesimal variable mass $m(t))$ and moves under the influence of the primaries and the asteroids belt of mass M_b. We also assume that this infinitesimal body does not affect the behavior of the primaries as well as the asteroids belt.

Let r_1, r_2, and r be the distances from the infinitesimal body to the primaries m_1, m_2, and the asteroids belt, respectively. The coordinates of the infinitesimal body and the primaries m_1 and m_2 are denoted by (x, y), $(-\mu, 0)$, and $(1-\mu, 0)$, respectively (Figure 1). Following the procedures given by Abouelmagd and Mostafa [28] and by Singh and Taura [24] and by assuming that the variation of mass of the test particle originates from one point having zero momentum, the equations of motion of the third infinitesimal variable mass $m(t)$ body with dimensionless variables in the synodic coordinate system are as follows.

$$\begin{cases} \dfrac{\dot{m}}{m}(\dot{x} - ny) + (\ddot{x} - 2n\dot{y}) = U_x, \\ \dfrac{\dot{m}}{m}(\dot{y} + nx) + (\ddot{y} + 2n\dot{x}) = U_y, \end{cases} \tag{4}$$

where

$$\begin{cases} U = \dfrac{n^2}{2}\left(x^2 + y^2\right) + \dfrac{(1-\mu)q_1}{r_1} + \dfrac{\mu q_2}{r_2} + \dfrac{(1-\mu)A_1 q_1}{2r_1^3} + \dfrac{\mu A_2 q_2}{2r_2^3} + \dfrac{M_b}{\sqrt{r^2 + T^2}}, \\ n^2 = 1 + \dfrac{3}{2}(A_1 + A_2) + \dfrac{2M_b r_c}{\left(r_c^2 + T^2\right)^{3/2}}, \end{cases} \tag{5}$$

with $\begin{cases} r_1^2 = (x+\mu)^2 + y^2, \\ r_2^2 = (x+\mu-1)^2 + y^2, \\ r^2 = x^2 + y^2, \\ r_c^2 = 1 - \mu + \mu^2, \\ T = a + b. \end{cases}$.

In this case, Jean's law reduces to $m = m_0 e^{-\alpha t}$, where α is the constant coefficient; therefore, the mass of the body varies exponentially. Ofcourse, m_0 is the mass of the test particle at the initial time. By using the Meshcherskii space-time transformations to preserve both space dimension and time, we get

$$\begin{cases} x = \beta^{-1/2} x^1, \\ y = \beta^{-1/2} y^1, \end{cases} \tag{6}$$

where $\beta = m/m_0$. Then, the velocity and acceleration components are as follows:

$$\begin{cases} \dot{x} = \beta^{-1/2}\left(\dot{x}^1 + \frac{1}{2}\alpha x^1\right), \\ \dot{y} = \beta^{-1/2}\left(\dot{y}^1 + \frac{1}{2}\alpha y^1\right). \end{cases} \tag{7}$$

$$\begin{cases} \ddot{x} = \beta^{-1/2}\left(\ddot{x}^1 + \alpha\dot{x}^1 + \frac{1}{4}\alpha^2 x^1\right), \\ \ddot{y} = \beta^{-1/2}\left(\ddot{y}^1 + \alpha\dot{y}^1 + \frac{1}{4}\alpha^2 y^1\right). \end{cases} \tag{8}$$

After using equations 6–8, equation (4) becomes

$$\begin{cases} \ddot{x}^1 - 2n\dot{y}^1 = V_{x^1}, \\ \ddot{y}^1 + 2n\dot{x}^1 = V_{y^1}, \end{cases} \tag{9}$$

where

$$V = \left(\frac{n^2}{2} + \frac{\alpha^2}{8}\right)\left(\left(x^1\right)^2 + \left(y^1\right)^2\right) + \beta^{3/2}\left(\frac{(1-\mu)q_1}{\rho_1} + \frac{\mu q_2}{\rho_2} + \frac{(1-\mu)q_1 A_1 \beta}{2\rho_1^3} + \frac{\mu q_2 A_2 \beta}{2\rho_2^3} + \frac{M_b}{\sqrt{\rho^2 + T^2\beta}}\right). \tag{10}$$

ρ_1, ρ_2, and ρ are defined by

$$\begin{cases} \rho_1^2 = \left(x^1 + \sqrt{\beta}\mu\right)^2 + \left(y^1\right)^2, \\ \rho_2^2 = \left(x^1 + \sqrt{\beta}\mu - \sqrt{\beta}\right)^2 + \left(y^1\right)^2, \\ \rho^2 = \left(x^1\right)^2 + \left(y^1\right)^2. \end{cases} \tag{11}$$

3. Analysis of Equilibrium Points

If we replace the derivative with respect to time on the left hand side of system (9) by zero, we get

$$x^1\left(\frac{\alpha^2}{4} + n^2\right) + \beta^{3/2}\left(-\frac{q_1(1-\mu)\left(x^1 + \sqrt{\beta}\mu\right)}{\rho_1^3} - \frac{q_2\left(x^1 + \sqrt{\beta}(-1+\mu)\right)\mu}{\rho_2^3} - \frac{3A_1 q_1 \beta(1-\mu)\left(x^1 + \sqrt{\beta}\mu\right)}{2\rho_1^5} - \frac{3A_2 q_2 \beta\left(x^1 + \sqrt{\beta}(-1+\mu)\right)\mu}{2\rho_2^5} - \frac{M_b x^1}{\left(\rho^2 + T^2\beta\right)^{3/2}}\right) = 0, \tag{12}$$

$$y^1\left(\frac{\alpha^2}{4} + n^2\right) + y^1\beta^{3/2}\left(-\frac{q_1(1-\mu)}{\rho_1^3} - \frac{q_2\mu}{\rho_2^3} - \frac{3A_1 q_1\beta(1-\mu)}{2\rho_1^5} - \frac{3A_2 q_2 \beta\mu}{2\rho_2^5} - \frac{M_b}{\left(\rho^2 + T^2\beta\right)^{3/2}}\right) = 0. \tag{13}$$

3.1. Triangular Equilibrium Points. From equations (12) and (13), we deduce

$$\frac{q_1}{\rho_1^3} + \frac{3A_1 q_1 \beta}{2\rho_1^5} = \frac{q_2}{\rho_2^3} + \frac{3A_2 q_2 \beta}{2\rho_2^5}. \tag{14}$$

Taking in account equation (14), equations (12) and (13) can be written, respectively, as

$$\frac{\alpha^2}{4} + n^2 - \beta^{3/2}\left(\frac{q_1}{\rho_1^3} + \frac{3A_1 q_1 \beta}{2\rho_1^5} + \frac{M_b}{\left(\rho^2 + T^2\beta\right)^{3/2}}\right) = 0, \tag{15}$$

$$\frac{\alpha^2}{4} + n^2 - \beta^{3/2}\left(\frac{q_2}{\rho_2^3} + \frac{3A_2 q_2 \beta}{2\rho_2^5} + \frac{M_b}{\left(\rho^2 + T^2\beta\right)^{3/2}}\right) = 0. \tag{16}$$

In the classical R3BP (i.e., when $\alpha = 0$, $\beta = 1$, $q_i = 0$, and $A_i = 0$), the solution is $(\rho_1 = 1, \rho_2 = 1)$. Therefore, let us consider that the solution in our problem is $(\rho_1 = 1 + \gamma_1,\ \rho_2 = 1 + \gamma_2)$, where $\gamma_1 \ll 1$ and $\gamma_2 \ll 1$. From (15) and (16), we get

$$\gamma_1 = \frac{1}{3} - \frac{p_1}{3}\left(1 + \frac{\alpha^2}{4}\right)\beta^{(-3/2)} + \frac{A_1}{2}\left(1 + \frac{\alpha^2}{4}\right)\beta^{(-1/2)} - \frac{1}{3}\left(n^2 + \frac{\alpha^2}{4}\right)\beta^{(-3/2)} + \frac{M_b}{3\left(\rho^2 + T^2\beta\right)^{3/2}} \tag{17}$$

$$\gamma_2 = \frac{1}{3} - \frac{p_2}{3}\left(1 + \frac{\alpha^2}{4}\right)\beta^{(-3/2)} + \frac{A_2}{2}\left(1 + \frac{\alpha^2}{4}\right)\beta^{(-1/2)} - \frac{1}{3}\left(n^2 + \frac{\alpha^2}{4}\right)\beta^{(-3/2)} + \frac{M_b}{3\left(\rho^2 + T^2\beta\right)^{3/2}}. \tag{18}$$

And from system (11), we get

$$\begin{cases} x^1 = \sqrt{\beta}\left(\frac{1}{2}-\mu\right)+\frac{1}{\sqrt{\beta}}(\gamma_1-\gamma_2), \\ y^1 = \pm\frac{\sqrt{4-\beta}}{2}\left(1+\frac{2}{(4-\beta)}(\gamma_1+\gamma_2)\right). \end{cases} \tag{19}$$

By combining equations (15–19), we obtain

$$\begin{cases} x^1 = \sqrt{\beta}\left(\frac{1}{2}-\mu\right)-\frac{1}{\beta}\left(1+\frac{\alpha^2}{4}\right)\left(\frac{p_1-p_2}{3\beta}-\frac{A_1-A_2}{2}\right), \\ y^1 = \pm\frac{\sqrt{4-\beta}}{2}\left[1+\frac{2}{(4-\beta)}\left(\frac{2}{3}-\frac{p_1+p_2}{3}\left(1+\frac{\alpha^2}{4}\right)\beta^{(-3/2)}+\frac{A_1+A_2}{2}\left(1+\frac{\alpha^2}{4}\right)\beta^{(-1/2)}-\frac{2}{3}\left(n^2+\frac{\alpha^2}{4}\right)\beta^{(-3/2)}+\frac{2M_b}{3\left(\rho^2+T^2\beta\right)^{(3/2)}}\right)\right]. \end{cases} \tag{20}$$

Notice that equation (20) represents the coordinates of triangular equilibrium points.

3.2. Collinear Equilibrium Points. In this subsection and from equation (12), we will determine the collinear equilibrium points. By replacing y^1 by 0 in equation (12), we get

$$f\left(x^1,y^1\right)=x^1\left(\frac{\alpha^2}{4}+n^2\right)+\beta^{3/2}\left(-\frac{q_1(1-\mu)\left(x^1+\sqrt{\beta}\mu\right)}{\rho_1^3}-\frac{q_2\left(x^1+\sqrt{\beta}(-1+\mu)\right)\mu}{\rho_2^3}-\frac{3A_1q_1\beta(1-\mu)\left(x^1+\sqrt{\beta}\mu\right)}{2\rho_1^5}\right. \\ \left.-\frac{3A_2q_2\beta\left(x^1+\sqrt{\beta}(-1+\mu)\right)\mu}{2\rho_2^5}-\frac{M_bx^1}{\left(\rho^2+T^2\beta\right)^{3/2}}\right), \tag{21}$$

and therefore,

$$f\left(x^1,0\right)=s_1\left(x^1\right)+s_2\left(x^1\right), \tag{22}$$

where

$$s_1\left(x^1\right)=x^1\left(\frac{\alpha^2}{4}+n^2\right)+\beta^{3/2}\left(-\frac{q_1(1-\mu)\left(x^1+\sqrt{\beta}\mu\right)}{\left|x^1+\sqrt{\beta}\mu^3\right|}-\frac{q_2\left(x^1+\sqrt{\beta}(-1+\mu)\right)\mu}{\left|x^1+\sqrt{\beta}(-1+\mu)^3\right|}-\frac{3A_1q_1\beta(1-\mu)\left(x^1+\sqrt{\beta}\mu\right)}{2\left|x^1+\sqrt{\beta}\mu\right|^5}\right. \\ \left.-\frac{3A_2q_2\beta\left(x^1+\sqrt{\beta}(-1+\mu)\right)\mu}{2\left|x^1+\sqrt{\beta}(-1+\mu)\right|^5}\right), \tag{23}$$

$$s_2\left(x^1\right)=-\frac{M_bx^1\beta^{3/2}}{\left(\rho^2+T^2\beta\right)^{3/2}}.$$

To determine the locations of collinear equilibrium points, we divide the x-axis in three different subintervals, that is, $x^1\in(-\infty,-\mu\sqrt{\beta})$, $x^1\in(-\mu\sqrt{\beta},(1-\mu)\sqrt{\beta})$, and $x^1\in((1-\mu)\sqrt{\beta},\infty)$, and we will specify our approach in each case separately. Notice that the endpoints of the above intervals correspond to the situations where the infinitesimal body coincides with one of the primaries.

3.2.1. First Case. For the interval $x^1 \in (-\infty, -\mu\sqrt{\beta})$,

$$s_1\left(x^1\right) = x^1\left(\frac{\alpha^2}{4} + n^2\right) + \beta^{3/2}\left(\frac{q_1(1-\mu)}{\left(x^1 + \sqrt{\beta}\,\mu\right)^2} + \frac{q_2\mu}{\left(x^1 + \sqrt{\beta}\,(-1+\mu)\right)^2} + \frac{3A_1q_1\beta(1-\mu)}{2\left(x^1 + \sqrt{\beta}\,\mu\right)^4} + \frac{3A_2q_2\beta\mu}{2\left(x^1 + \sqrt{\beta}\,(-1+\mu)\right)^4}\right),$$

$$s_1'\left(x^1\right) = n^2 + \frac{\alpha^2}{4} + \beta^{(3/2)}\left(-\frac{2q_1(1-\mu)}{\left(x^1 + \sqrt{\beta}\,\mu\right)^3} - \frac{2q_2\mu}{\left(x^1 + \sqrt{\beta}\,(-1+\mu)\right)^3} - \frac{6A_1q_1\beta(1-\mu)}{\left(x^1 + \sqrt{\beta}\,\mu\right)^5} - \frac{6A_2q_2\beta\mu}{\left(x^1 + \sqrt{\beta}\,(-1+\mu)\right)^5}\right) \tag{24}$$

$$= n^2 + \frac{\alpha^2}{4} + \beta^{(3/2)}\left(\frac{2q_1(1-\mu)}{\left|x^1 + \sqrt{\beta}\,\mu\right|^3} + \frac{2q_2\mu}{\left|x^1 + \sqrt{\beta}\,(-1+\mu)\right|^3} + \frac{6A_1q_1\beta(1-\mu)}{\left|x^1 + \sqrt{\beta}\,\mu\right|^5} + \frac{6A_2q_2\beta\mu}{\left|x^1 + \sqrt{\beta}\,(-1+\mu)\right|^5}\right).$$

It is clear that $s_1'(x^1) > 0$ for $x^1 \in (-\infty, -\mu\sqrt{\beta})$, and $s_1(x^1)$ is then a monotonically increasing function and $\lim_{x^1 \longrightarrow -\infty} s_1(x^1) = -\infty$, and $\lim_{x^1 \longrightarrow -\sqrt{\beta}\mu^-} s_1(x^1) = \infty$.

We also have $s_2(x^1) = M_b|x^1|\beta^{3/2}/((x^1)^2 + T^2\beta)^{3/2}$, and $s_2'(x^1) = M_b\beta^{(3/2)}/((x^1)^2 + T^2\beta)^{(3/2)} - 3M_b(x^1)^2\beta^{(3/2)}/((x^1)^2 + T^2\beta)^{(5/2)} < 0$. $\lim_{x^1 \longrightarrow -\infty} s_2(x^1) = 0$, and $\lim_{x^1 \longrightarrow -\sqrt{\beta}\mu^-} s_2(x^1) > 0$, $s_2(x^1)$ is a monotonically increasing function.

As $\lim_{x^1 \longrightarrow -\infty} f(x^1, 0) < 0$ and $\lim_{x^1 \longrightarrow -\sqrt{\beta}\mu^-} f(x^1, 0) > 0$, we can conclude that there exists a unique real in the interval $x^1 \in (-\infty, -\mu\sqrt{\beta})$ for which $f(x^1, 0) = 0$, and the corresponding point will be denoted in the sequel by L_3.

3.2.2. Second Case. For the case where $x^1 \in (-\mu\sqrt{\beta}, (1-\mu)\sqrt{\beta}) = (-\mu\sqrt{\beta}, 0) \cup (0, (1-\mu)\sqrt{\beta})$, we will treat in the first step the subcase when $x^1 \in (-\mu\sqrt{\beta}, 0) = (-\mu\sqrt{\beta}, -T\sqrt{\beta}/\sqrt{2}) \cup ((-T\sqrt{\beta})/\sqrt{2}, 0)$.

Let $x^1 \in (-\mu\sqrt{\beta}, -T\sqrt{\beta}/\sqrt{2})$. Since $\lim_{x^1 \longrightarrow -\sqrt{\beta}\mu^+} s_1(x^1) = -\infty$ and $\lim_{x^1 \longrightarrow -\sqrt{\beta}\mu^+} s_2(x^1) > 0$, we get $\lim_{x^1 \longrightarrow -\sqrt{\beta}\mu^+} f(x^1, 0) < 0$, and $s_1((-T\sqrt{\beta})/\sqrt{2}) + s_2((-T\sqrt{\beta})/\sqrt{2}) > 0$. Consequently, $f((-T\sqrt{\beta})/\sqrt{2}, 0) > 0$, which means there is a unique point for which $f(x^1, 0) = 0$. This point will be denoted in the sequel by L_{b1}.

In the case where $x^1 \in ((-T\sqrt{\beta})/\sqrt{2}, 0)$, we have $s_1((-T\sqrt{\beta})/\sqrt{2}) + s_2((-T\sqrt{\beta})/\sqrt{2}) > 0$, which implies that $f((-T\sqrt{\beta})/\sqrt{2}, 0) > 0$ and $f(0,0) = \beta^{3/2}(-q_1(1-\mu)(\sqrt{\beta}\,\mu)/(\sqrt{\beta}\,\mu)^3 - q_2(\sqrt{\beta}\,(-1+\mu))\mu/(\sqrt{\beta}\,(-1+\mu))^3 - 3A_1q_1\beta(1-\mu)(\sqrt{\beta}\,\mu)/2(\sqrt{\beta}\,\mu)^5 - 3A_2q_2\beta(\sqrt{\beta}\,(-1+\mu))\mu/2(\sqrt{\beta}\,(-1+\mu))^5) < 0$

We can interpret as above that there exists a unique point for which $f(x^1, 0) = 0$. Let us denote this point by L_{b2}.

To complete the study of this second case, let $x^1 \in (0, (1-\mu)\sqrt{\beta})$.

Since $f(0,0) < 0$ and $\lim_{x^1 \longrightarrow \sqrt{\beta}(1-\mu)^-} f(x^1, 0) > 0$, we can conclude that there exists a unique point for which $f(x^1, 0) = 0$. Let L_2 be this point.

3.2.3. Third Case. Let $x^1 \in ((1-\mu)\sqrt{\beta}, \infty)$. Since $\lim_{x^1 \longrightarrow \sqrt{\beta}(1-\mu)^+} s_1(x^1) = -\infty$, $\lim_{x^1 \longrightarrow \infty} s_1(x^1) = \infty$, $s_2(\sqrt{\beta}(1-\mu)) < 0$, and $\lim_{x^1 \longrightarrow \infty} s_2(x^1) = 0$, we can conclude that $\lim_{x^1 \longrightarrow \sqrt{\beta}(1-\mu)^+} f(x^1, 0) < 0$ and $\lim_{x^1 \longrightarrow \infty} f(x^1, 0) > 0$, and then, we conclude that there is a unique real in this interval for which $f(x^1, 0) = 0$. The corresponding point will be denoted by L_1.

The above points L_1, L_2, L_3, L_{b1}, and L_{b2} are called collinear equilibrium points (Figure 2 and 3). These points are similar to points determined in the study by Singh and Taura [24]. Notice that in the classical R3BP, there are only three collinear equilibrium points.

The locations of these equilibrium points are determined numerically and depicted in Figure 4. From analyzing this figure, we can observe that as we increase the value of β, all the equilibrium points are moving away from the origin except L_{b2} (Figure 5).

4. Stability of Equilibrium Points

In this section, let us investigate the stability properties of the small body's motion in its vicinity $(x^{10} + x^{11}, y^{10} + y^{11})$ under the effect of the oblate radiating primaries and the asteroids dust belt, where (x^{11}, y^{11}) are the small displacements from the equilibrium points (x^{10}, y^{10}). To do this, we can write the variational equations for system (9) as

$$\begin{cases} \ddot{x}^{11} - 2n\dot{y}^{11} = V^0_{x^1x^1}x^{11} + V^0_{x^1y^1}y^{11}, \\ \ddot{y}^{11} + 2n\dot{x}^{11} = V^0_{y^1x^1}x^{11} + V^0_{y^1x^1}y^{11}. \end{cases} \tag{25}$$

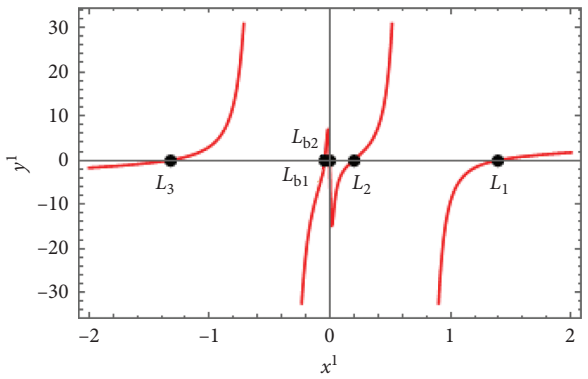

Figure 2: Locations of collinear equilibrium points.

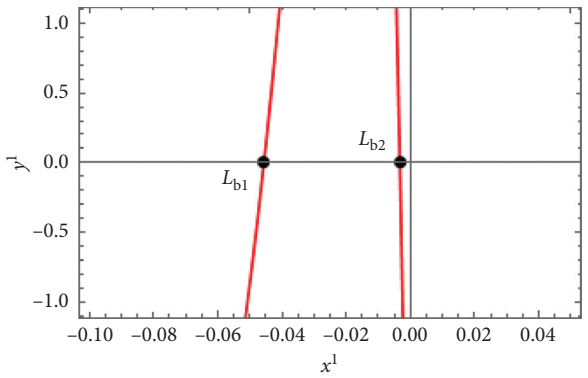

Figure 3: Zoomed part of Figure 2 near L_{b2}.

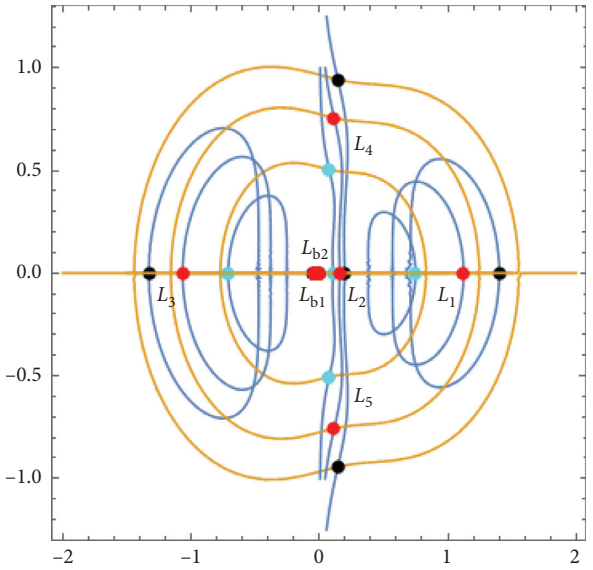

Figure 4: Locations of all equilibrium points for three values of β (0.4 (cyan), 0.9 (red), and 1.4 (black)).

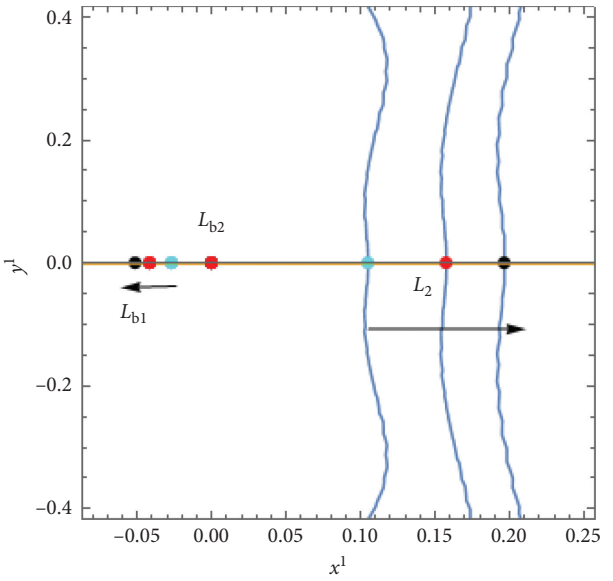

Figure 5: Zoomed part of Figure 4 near L_{b2} and their movement.

The superscript 0 denotes the value at the corresponding equilibrium point.

In the phase space, the above system (25) can be rewritten as

$$\begin{cases} \dot{x} = x^{12}, \\ \dot{y}^{11} = y^{12}, \\ \dot{x}^{12} = 2ny^{12} + V^0_{x^1x^1}x^{11} + V^0_{x^1y^1}y^{11}, \\ \dot{y}^{12} = -2nx^{12} + V^0_{y^1x^1}x^{11} + V^0_{y^1y^1}y^{11}. \end{cases} \tag{26}$$

Due to the variation of the mass and of the distance of the small particle, by using Meshcherskii space-time inverse transformations to examine the stability of the equilibrium points, we then get

$$\begin{cases} x^{13} = \beta^{-1/2}x^{11}, y^{13} = \beta^{-1/2}y^{11}, \\ x^{14} = \beta^{-1/2}x^{12}, y^{14} = \beta^{-1/2}y^{12}. \end{cases} \tag{27}$$

Taking in account equation (26), system (27) can be written as follows:

$$\dot{Y} = B\mathbf{Y}, \tag{28}$$

where

$$Y = \begin{pmatrix} x^{13} \\ y^{13} \\ x^{14} \\ y^{14} \end{pmatrix},$$

Table 1: All the equilibrium points depicted are unstable and determined for $T = 0.02$, $q_1 = 0.90$, $q_2 = 0.85$, $A_1 = 0.03$, $A_2 = 0.02$, $M_b = 0.01$, $\mu = 0.4$, and $\alpha = 0.2$.

Equilibrium points			Roots
β	$x^1 - C_0$	$y^1 - C_0$	
0.40	0.7482467178	0.0000000000	$0.1 \pm 1.46479i$ 1.6105 −1.4105
	0.1051524050	0.0000000000	$0.1 \pm 3.25487i$ −4.46466 4.66466
	−0.7099161991	0.0000000000	$0.1 \pm 1.30658i$ −1.08426 1.28426
	−0.0274388781	0.000000000	$0.1 \pm 10.4769i$ −13.2108 13.4108
	−0.0002097310	0.0000000000	$0.1 \pm 36.3091i$ $0.1 \pm 34.1204i$
	0.0766012649	±0.5044421565	$-0.610786 \pm 0.997642i$ $0.810786 \pm 0.997642i$
0.90	1.1223700767	0.0000000000	$0.1 \pm 1.46479i$ −1.4105 1.6105
	0.1577286075	0.0000000000	$0.1 \pm 3.25487i$ ±4.46466
	−1.0648742987	0.0000000000	$0.1 \pm 1.30658i$ −1.08426 1.28426
	−0.0411583172	0.0000000000	$0.1 \pm 10.4769i$ −13.2108 13.4108
	−0.0003146670	0.0000000000	$0.1 \pm 34.1204i$ $0.1 \pm 36.3091i$
	0.1149018973	±0.7566632347	$-0.610786 \pm 0.997642i$ $0.810786 \pm 0.997642i$
1.40	1.3998414294	0.0000000000	$0.1 \pm 1.46479i$ −1.4105 1.6105
	0.1967221364	0.0000000000	$0.1 \pm 3.25487i$ −4.46466 4.66466
	−1.3281315953	0.0000000000	$0.1 \pm 1.30658i$ −1.08426 1.28426
	−0.0513334406	0.0000000000	$0.1 \pm 10.4769i$ −13.2108 13.4108
	−0.0003923708	0.0000000000	$0.1 \pm 34.1204i$ $0.1 \pm 36.3091i$
	0.1433078443	±0.9437248605	$0.610786 \pm 0.997642i$ $0.810786 \pm 0.997642i$

$$B = \begin{pmatrix} \frac{1}{2}\alpha & 0 & 1 & 0 \\ 0 & \frac{1}{2}\alpha & 0 & 1 \\ V^0_{x^1x^1} & V^0_{x^1y^1} & \frac{1}{2}\alpha & 2n \\ V^0_{y^1x^1} & V^0_{y^1y^1} & -2n & \frac{1}{2}\alpha \end{pmatrix}. \tag{29}$$

The characteristic equation for the matrix B is then

$$\lambda^4 + \alpha_3\lambda^3 + \alpha_2\lambda^2 + \alpha_1\lambda + \alpha_0 = 0, \tag{30}$$

where

$$\begin{cases} \alpha_0 = \frac{1}{16}\alpha^4 + \frac{1}{4}\alpha^2\left(4n^2 - V_{x^1x^1} - V_{y^1y^1}\right) + \left(V_{x^1x^1}V_{y^1y^1} - V^2_{x^1y^1}\right), \\ \alpha_1 = \alpha\left(V_{x^1x^1} + V_{y^1y^1} - 4n^2 - \frac{\alpha^2}{2}\right), \\ \alpha_2 = -\left(V_{x^1x^1} + V_{y^1y^1} - 4n^2 - \frac{3\alpha^2}{2}\right), \\ \alpha_3 = -2\alpha. \end{cases} \tag{31}$$

Table 1 represents the numerical solutions of equation (30), for the values $T = 0.02$, $q_1 = 0.90$, $q_2 = 0.85$, $A_1 = 0.03$, $A_2 = 0.02$, $M_b = 0.01$, $\mu = 0.4$, and $\alpha = 0.2$ (Singh and Taura [24] and Ansari [16]) and three different values of parameter. This table represents also the roots corresponding to each equilibrium points. From a simple interpretation of the results of the table, we can deduce that equilibrium points are unstable because at least one characteristic root is either a positive real number or positive real part of the complex characteristic root. While in the study by Singh and Taura [24], it is shown that some equilibrium points are stable in some intervals; therefore, in our case due to the impact of the variation parameters, all the equilibrium points obtained are unstable.

5. Conclusion

In this paper, we studied the effects of the variation parameters α and β on the behavior of motion of the infinitesimal body in the restricted 3-body problem and also when the mass of this infinitesimal body varies according to Jean's law. We assumed that the primaries have both radiating as well as oblateness effects, and the whole system has an effect of an asteroids belt. Using the Meshcherskii space-time transformation, we have evaluated the equations of motion. From the obtained system of equations of motion, we numerically illustrated the seven equilibrium points where five equilibrium points are collinear and two are noncollinear (i.e., triangular equilibrium points). This conclusion is similar to that made by Singh and Taura [24] but more different from the classical R3BP [7]. Figure 4 shows the location of the seven equilibrium points and their movements for three values of β (0.4, 0.9, and 1.4). Figure 5 is the zoomed part of Figure 4 near the equilibrium point L_{b2}. From these figures, we noticed that as we increase the value of the variation parameter β, all the equilibrium points are moving away from the origin except L_{b2}. Furthermore, we examined the stability of equilibrium points numerically, and Table 1 represents the roots of the characteristic polynomial that shows that at least one of the roots has either positive real part of the complex roots or only a positive real root. These facts confirm that all the equilibrium points are unstable. As a second remark, we deduced that this result is different from the result obtained by Singh and Taura [24] where they have shown that the triangular points are stable for $0 < \mu < \mu_c$, where μ_c is the critical mass ratio influenced by the oblateness and radiation parameters of the primaries and potential from the belt. We can then conclude that the variation of parameters has a great impact on the dynamical behavior of the motion of the infinitesimal body.

Data Availability

The data depicted in the table are used to support the findings of this study are included within the article.

Conflicts of Interest

The author declares that there are no conflicts of interest.

Acknowledgments

The author is thankful to the Deanship of Scientific Research, College of Science at Buraidha, Qassim University, Saudi Arabia, for providing all the research facilities in the completion of this research work. The author wishes to express his sincere thanks to referees who provided precious expertise that greatly helped to improve the paper.

References

[1] K. B. Bhatnagar and P. P. Hallan, "Effect of perturbed potentials on the stability of libration points in the restricted problem," *Celestial Mechanics*, vol. 20, no. 2, pp. 95–103, 1979.

[2] M. Khanna and K. B. Bhatnagar, "Existence and stability of libration points in the restricted three-body problem when the smaller primary is a triaxial rigid body and the bigger one an oblate spheroid," *Indian Journal of Pure and Applied Mathematics (IJPAM)*, vol. 30, no. 7, pp. 721–733, 1999.

[3] R. K. Sharma and P. V. Subba Rao, "Stationary solutions and their characteristic exponents in the restricted three-body problem when the more massive primary is an oblate spheroid," *Celestial Mechanics and Dynamical Astronomy*, vol. 13, no. 2, pp. 137–149, 1976.

[4] P. V. Subba Rao and R. K. Sharma, "A note on the stability of the triangular points of the equilibrium in the restricted three-body problem," *Astronomy and Astrophysics*, vol. 43, no. 3, pp. 381–383, 1975.

[5] E. I. Abouelmagd, H. M. Asiri, and M. A. Sharaf, "The effect of oblateness in the perturbed restricted three-body problem," *Meccanica*, vol. 48, no. 10, pp. 2479–2490, 2013.

[6] R. K. Sharma, Z. A. Taqvi, and K. B. Bhatnagar, "Existence and stability of libration points in the restricted three-body problem when the primaries are triaxial rigid bodies," *Celestial Mechanics and Dynamical Astronomy*, vol. 79, no. 2, pp. 119–133, 2001.

[7] V. Szebehely, *Theory of Orbits*, Academic Press, NY, USA, 1967.

[8] E. I. Abouelmagd, A. A. Ansari, M. S. Ullah, and J. L. García Guirao, "A planar five-body problem in a framework of heterogeneous and mass variation effects," *The Astronomical Journal*, vol. 160, no. 5, p. 216, 2020.

[9] A. A. Ansari, K. R. Meena, and S. N. Prasad, "Perturbed six-body configuration with variable mass," *Romanian Astronomical Journal*, vol. 30, no. 2, pp. 135–152, 2020.

[10] A. A. Ansari, J. Singh, Z. A. Alhussain, and H. Belmabrouk, "Perturbed Robe's CR3BP with viscous force," *Astrophysics and Space Science*, vol. 364, no. 6, p. 95, 2019.

[11] A. A. Ansari, R. Kellil, Z. A. Al-Hussain, and W. Ul-Haq, "Effect of variation of charge in the circular restricted three-body problem with variable masses," *Journal of Taibah University for Science*, vol. 13, no. 1, pp. 670–677, 2019.

[12] A. A. Ansari, R. Kellil, and Z. A. Al-Hussain, "Behavior of an infinitesimal-variable-mass body in CR3BP; the primaries are finite straight segments," *Punjab University Journal of Mathematics*, vol. 51, no. 5, pp. 107–120, 2019.

[13] A. A. Ansari, K. Shalini, and Z. A. Alhussain, "Non-linear stability of L_4in the R3BP when the smaller primary is a heterogeneous triaxial rigid body with N layers," *Italian Journal of Pure and Applied Mathematics*, vol. 41, pp. 297–312, 2019.

[14] A. A. Ansari, A. Ali, M. Alam, and R. Kellil, "Cyclic kite configuration with variable mass of the fifth body in R5BP," *Application and Applied Mathematics: An International Journal (AAM)*, vol. 14, no. 2, pp. 985–1002, 2019.

[15] A. A. Ansari, "The circular restricted four- body problem with triaxial primaries and variable infinitesimal mass," *Applications and Applied Mathematics: An International Journal*, vol. 13, no. 2, pp. 818–838, 2018.

[16] A. A. Ansari, "Effect of Albedo on the motion of the infinitesimal body in circular restricted three-body problem with variable masses," *Italian Journal of Pure and Applied Mathematics*, vol. 38, pp. 581–600, 2017.

[17] A. A. Ansari, "Kind of Robe's restricted problem with heterogeneous irregular primary of N-layers when outer most layer has viscous fluid," *New Astronomy*, vol. 83, p. 101496, 2020.

[18] E. I. Abouelmagd, A. A. Ansari, and M. H. Shehata, "On Robe's restricted problem with a modified Newtonian potential," *International Journal of Geometric Methods in Modern Physics*, 2020.

[19] B. S. Kushvah, "Linear stability of equilibrium points in the generalized photogravitational Chermnykh's problem," *Astrophysics and Space Science*, vol. 318, no. 1-2, pp. 41–50, 2008.

[20] N. Pathak, V. O. Thomas, and E. I. Abouelmagd, "The perturbed photogravitational restricted three-body problem: analysis of resonant periodic orbits," *Discrete and Continuous Dynamical Systems - Series S (DCDS-S)*, vol. 12, no. 4 and 5, pp. 849–875, 2019.

[21] N. Pathak, E. I. Abouelmagd, and V. O. Thomas, "On higher order of resonant periodic orbits in the photogravitational restricted three body problem," *The Journal of the Astronautical Sciences*, vol. 66, no. 4, pp. 475–505, 2019.

[22] A. A. Ansari and E. I. Abouelmagd, "Gravitational potential formulae between two bodies with finite dimensions," *Astronomische Nachrichten*, vol. 341, no. 6-7, pp. 656–668, 2020.

[23] B. Ishwar and A. Elipe, "Secular solutions at triangular equilibrium points in generalized photogravitational restricted three-body problem," *Astrophysics and Space Science volume*, vol. 277, pp. 437–446, 2001.

[24] J. Singh and J. J. Taura, "Motion in the generalized restricted three-body problem," *Astrophysics and Space Science*, vol. 343, no. 1, pp. 95–106, 2013.

[25] E. I. Abouelmagd and A. A. Ansari, "The motion properties of the infinitesimal body in the framework of bicircular Sun perturbed Earth-Moon system," *New Astronomy*, vol. 73, 2019.

[26] J. Singh and B. Ishwar, "Effect of perturbations on the stability of triangular points. In the restricted problem of three bodies with variable mass," *Celestial Mechanics*, vol. 35, no. 3, pp. 201–207, 1985.

[27] L. G. Lukyanov, "On the restricted circular conservative three-body problem with variable masses," *Astronomy Letters*, vol. 35, no. 5, pp. 349–359, 2009.

[28] E. I. Abouelmagd and A. Mostafa, "Out of plane equilibrium points locations and the forbidden movement regions in the restricted three-body problem with variable mass," *Astrophysics and Space Science*, vol. 357, no. 1, 2015.

[29] J. H. Jeans, *Astronomy and Cosmogony*, Cambridge University Press, Cambridge, England, 1928.

[30] M.-J. Zhang, C.-Y. Zhao, and Y.-Q. Xiong, "On the triangular libration points in photogravitational restricted three-body problem with variable mass," *Astrophysics and Space Science*, vol. 337, no. 1, pp. 107–113, 2012.

[31] I. V. Meshcherskii, *Works on the Mechanics of Bodies of Variable Mass*, GITTL, Moscow, Russia, 1949.

[32] M. Miyamoto and R. Nagai, "Three-dimensional models for the distribution of mass in galaxies," *Publications of the Astronomical Society of Japan*, vol. 27, pp. 533–543, 1975.

Hindawi
Advances in Astronomy
Volume 2020, Article ID 6651277, 16 pages
https://doi.org/10.1155/2020/6651277

Research Article

Quartic Integral in Rigid Body-Gyrostat Dynamics

C. Mnasri [1] and A. A. Elmandouh [1,2]

[1]*Department of Mathematics and Statistics, College of Science, King Faisal University, P.O. Box 400, Al-Ahsa 31982, Saudi Arabia*
[2]*Department of Mathematics, Faculty of Science, Mansoura University, Mansoura 35516, Egypt*

Correspondence should be addressed to A. A. Elmandouh; aelmandouh@kfu.edu.sa

Received 8 October 2020; Revised 7 November 2020; Accepted 18 November 2020; Published 11 December 2020

Academic Editor: Elbaz Abouelmagd

In this work, we investigate the problem of constructing new integrable problems in the dynamics of the rigid body rotating about its fixed point as results of the effect of a combination of potential and gyroscopic forces possessing a common symmetry axis. We introduce two new integrable problems in a rigid body dynamics that generalize some integrable problems in this field, known by names of Chaplygin and Yehia–Elmandouh.

1. Introduction

One of the classical problems manifesting in mathematical physics is the issue of determining whether a dynamical system, especially a mechanical one, is integrable or not. Integrability in this context often points out to Liouville integrability. The Liouville integrability concept is defined as the Hamiltonian system with n degrees of freedom that is completely integrable if it has n independent integrals of motion which are in involution, i.e., their Poisson brackets are zero [1]. The integrable systems possess miscellaneous properties such as their behavior that can be globally tested in an infinite interval of time, gratitude to the theories of perturbation, those systems that can be applied to give an appointed inference about the nonintegrable systems nearby them, and in general, the motion equations can be solved by quadratures [2]. The problem of integrability is split into two categories. The first one is finding the sufficient conditions for the integrability, and this requires the construction of a sufficient number of first integrals of motion. Numerous methods can be utilized to construct the first integrals of motion such as the direct method, Darboux method, and Yehia method (see, e.g., [3–13]). The second one deals with obtaining the necessary conditions of the integrability (see, e.g., [14–20]), but we must introduce the required number of the integrals to confirm the integrability.

One of the significant issues in applications in assorted branches of science such as physics and astronomy is the problem of a rigid body and its extension to a gyrostat (see, e.g., [21–23]). So, it is a beneficial model for research from different points of view [24–29]. Consequently, the present work interested in analyzing the general motion of a rigid body about its fixed point that happens under the effect of a combination of potential (velocity-independent) forces and gyroscopic (velocity-dependent) forces. The gyroscopic forces are specified by $\mathrm{l} = (0, 0, l_3)$, while the potential forces are characterized by $V(\gamma)$. As it outlined in [30], this motion can be characterized by the Lagrangian:

$$L = \frac{1}{2}\omega \cdot \omega I + l \cdot \omega - V, \tag{1}$$

where $\omega = (p, q, r)$ is the angular velocity, and $I = \mathrm{diag}(A, B, C)$ is the inertia matrix of the body. The equations of motion corresponding Lagrangian (1) are [30–32]

$$\dot{\omega} I + \omega \times (\omega I + \mu) = \gamma \times \frac{\partial V}{\partial \boldsymbol{\gamma}}, \quad \dot{\gamma} + \omega \times \gamma = 0, \tag{2}$$

where $\gamma = (\gamma_1, \gamma_2, \gamma_3)$ is the unit vector which is fixed upward in space, and μ is expressed as

$$\mu(\gamma_1, \gamma_2, \gamma_3) = \frac{\partial}{\partial \gamma}(l \cdot \gamma) - \left(\frac{\partial}{\partial \gamma} \cdot l\right)\gamma. \tag{3}$$

It is well-known that the Euler-Poisson equation (2) has three classical integrals of motion. They are as follows:

(1) Area integral:

$$I_1 = (\omega I + l) \cdot \gamma = f, \tag{4}$$

where the arbitrary constant f denotes the value of area integral. This integral is sometimes named as a cyclic integral due to it correspondences the cyclic variable ψ, the angle of precession.

(2) Jacobi integral:

$$I_2 = \frac{1}{2}\omega \cdot \omega I + V = h, \tag{5}$$

where the arbitrary constant h identifies the value of the Jacobi integral.

(3) Geometric integral:

$$I_3 = \gamma \cdot \gamma = 1. \tag{6}$$

Taking into account the Jacobi theorem on the last integrating multiplier [33], four integrals of motion are needed to confirm the integrability of the equation of motion (2). Thence, the existence of a fourth integral independent of those (4), (5), and (6) is sufficient to prove the integrability. It is worth noticing that the integrable case either generally integrable or conditionally integrable according to the fourth integral is either valid on an arbitrary level of the cyclic integral I_1 or valid on a single level of cyclic integral I_1 which is usually zero.

The problem of a rigid body which is described by the equation of motion (2) was studied in diverse posterior works from the point of view of the integrability. Those works include three types of problems.

The first problem deals with the problem of the motion of a rigid body about a fixed point under the action of its weight. It is characterized by $V = r_0 \cdot \gamma$, and $\mu = 0$, where r_0 is a constant vector that represents the center of the mass vector. It attracted the attention of the researchers for a long time, nearly two and a half centuries, and thus, it has a great history. It includes three (no more) general integrable problems bearing the names of who discovered them, Euler, Lagrange, and Kowalevski, and one conditional integrable problem of Goriatchev–Chaplygin (see, e.g., [34]).

The second problem concerns the motion of a rigid body about its fixed point under the effect of its weight, and moreover, there is a rotor spinning about its axis of symmetry which is fixed in the body with a constant angular velocity. It is worth mentioning that it is a simple multibody that consists of the main body and the rotor, and it is termed in literatures a gyrostat. The second problem regards as a generalization to the first problem, and it is determined by $V = r_0 \cdot \gamma$ and $\mu = k$, where k is a constant vector characterizing the gyroscopic moment due to the existence of the rotor. It contains three general and one conditional integrable problems generalizing those in the first problem by adding the gyrostatic moment. The general cases are Lagrange, Joukovsky [34], and Yehia [35], while the conditional case is the Sretensky case which generalizes the Goriatchev–Chaplygin case in the first problem. In [36], the author proved that the equations of the motion for the current problem does not own more than the three mentioned cases.

The third problem studies the problem of the motion of a rigid body in an incompressible ideal fluid, infinitely extending and at rest at infinity. The simple connected body is either described by the traditional Kirchoff equations [37] or by their Hamiltonian [38] form, while the body bounded by a multiconnected surface is described either by Lamb equations [39] or by its equivalent Hamiltonian form (see, e.g., [34]). The utilization of the equations of Kirchhoff and Lamb to describe this problem lacks to demonstrate the link between this problem and the other problems of rigid body dynamics. The link between both problems is proved by Yehia who introduced the equations of motion for a rigid body in a liquid by removing the translation motion that appears as cyclic variables (see, [40]), and the reduced problem is described by $V = r_0 \cdot \gamma + (1/2)\gamma J \cdot \gamma$ and $\mu = k - 2\gamma \overline{K}$, where J and $\overline{K}$ are the constant 3×3 matrices. The integrable cases for the third problem have been introduced in [34, 40].

To dodge the ambiguity, we summarize those problems in Table 1. Obviously, each problem is a generalization of the previous one by inserting some of the additional parameters, which represented terms having certain physical interpretations.

According to the methodology used, this work deals only with two-dimensional mechanical systems, as it is outlined down in section two. It is obvious that this problem has three degrees of freedom in which one of them can be ignored due to the presence of a cyclic variable, precession angle, by utilizing the Routh procedure. Thence, the current problem can be characterized by Routhian (see, [41]).

$$R = \frac{1}{2}\left[\frac{\dot{\gamma}^2}{1-\gamma_3^2} + \frac{C\left(1-\gamma_3^2\right)\dot{\varphi}^2}{A-(A-C)\gamma_3^2}\right] + \frac{f\left(C\gamma_3 + Al_3\left(1-\gamma_3^2\right)\right)}{A\left[A-(A-C)\gamma_3^2\right]}\dot{\varphi} - \frac{1}{A}\left(V + \frac{(f-l_3\gamma_3)^2}{2\left[A-(A-C)\gamma_3^2\right]}\right). \tag{7}$$

One can do the transformation,

$$dt = \frac{C\left(1-\gamma_3^2\right)}{A-(A-C)\gamma_3^2}d\tau, \tag{8}$$

Table 1: Different problems in a rigid body dynamics.

No.	Problem	Potential function V	Vector function μ
1	Heavy rigid body	$V = r_0 \cdot \gamma$	$\mu = \mathbf{0}$
2	Heavy gyrostat	$V = \mathbf{r}_0 \cdot \gamma$	$\mu = \mathbf{k}$
3	Rigid body in a liquid	$V = \mathbf{r}_0 \cdot \gamma + (1/2)\gamma\mathbf{J} \cdot \gamma$	$\mu = \mathbf{k} - 2\gamma\overline{\mathbf{K}}$

to Routhian (7), and we get

$$R_0 = \frac{A}{2}\left[\dot{\varphi}^2 + \frac{A-(A-C)\gamma_3^2}{C\left(1-\gamma_3^2\right)^2}\dot{\gamma}_3^2\right] + \frac{fC\gamma_3 + Al_3\left(1-\gamma_3^2\right)}{\left[A-(A-C)\gamma_3^2\right]}\dot{\varphi} - \frac{C\left(1-\gamma_3^2\right)}{\left[A-(A-C)\gamma_3^2\right]}\left[V + \frac{(f-l_3\gamma_3)^2}{2\left[A-(A-C)\gamma_3^2\right]}\right], \tag{9}$$

where τ is the fictitious time, and dash refers to the derivative with respect to τ.

2. Basic Equations

A method for constructing the two-dimensional integrable mechanical systems in which the additional integral is a polynomial in velocities has been presented by Yehia in [42], and it has been developed in [43]. This method has been successfully applied to construct new integrable problems (not necessarily plane) whose complementary integral is a polynomial in velocities up to degree four (e.g., [4–6, 44–49]). This method is restrictively employed for two mechanical systems. There are a wide class of beforementioned systems such as the n-dimensional mechanical systems admitting $(n-2)$ cyclic variables and the particle motion on a smooth surface under the influence of distinct types of forces. A further example is a present problem which describes the rotation of a rigid body about a fixed point under the effect of potential and gyroscopic forces possessing a common axis of symmetry, so the motion has a cyclic variable, and this enables us to apply Routh procedure to lessen the degrees of freedom from three to two [32, 33].

The two-dimensional mechanical systems are described by Lagrangian equation.

$$L = \frac{1}{2}\left(b_{11}\dot{q}_1^{\,2} + 2b_{12}\dot{q}_1\dot{q}_2 + b_{22}\dot{q}_2^{\,2}\right) + b_1\dot{q}_1 + b_2\dot{q}_2 - V, \tag{10}$$

where the functions b_{ij}, b_i, and V rely on the generalized coordinates q_1 and q_2, and dots refer to the derivatives with respect to the time t. Birkhoff theorem [50] guarantees the existence of a certain canonical transformation which is applied to turn Lagrangian (10) into

$$L = \frac{\Lambda}{2}\left(\dot{\xi}^2 + \dot{\eta}^2\right) + l_1\dot{\xi} + l_2\dot{\eta} - V, \tag{11}$$

where Λ, l_1, l_2, and V are the functions in the two variables x and y. The usefulness of this step is to diminish the number of functions from six to four. It is obvious that the Lagrangian (10) has a Jacobi integral in the form

$$I_1 = \frac{\Lambda}{2}\left(\dot{\xi}^2 + \dot{\eta}^2\right) + V = h, \tag{12}$$

where h is an arbitrary constant. According to Liouville theorem for the equivalent Hamiltonian system, system (11) is completely integrable if it has another first integral independent on the Jacobi integral (12).

Executing the time transformation (see Appendix A for more details about time transformation),

$$\mathrm{d}t = \Lambda \mathrm{d}\tau, \tag{13}$$

to Lagrangian (11), we get

$$L_0 = \frac{1}{2}\left(\xi'^2 + \eta'^2\right) + l_1\xi' + l_2\eta' - U, \tag{14}$$

where $U = \Lambda(h - V)$, and $'$ refers to the derivative with respect to τ. The Lagrangian equations corresponding to Lagrangian (14) are

$$\begin{aligned} \xi'' + \Omega\eta' &= \frac{\partial U}{\partial \xi}, \\ \eta'' + \Omega\xi' &= \frac{\partial U}{\partial \eta}, \end{aligned} \tag{15}$$

where $\Omega = \partial l_1/\partial\eta - \partial l_2/\partial\xi$. This system has a Jacobi integral in the form

$$I_1 = \frac{1}{2}\left(\xi'^2 + \eta'^2\right) + U = 0. \tag{16}$$

Now, we are going to find an additional first integral that is independent on the Jacobi integral (16). Based on [42], the complementary integral that is assumed to be quartic in velocities can be expressed as

$$I_2 = \xi'^4 + P_3\xi'^3 + Q_3\xi'^2\eta' + P_2\xi'^2 + Q_2\xi'\eta' + P_1\xi' + Q_1\eta' + R, \tag{17}$$

where the functions P_j, Q_j, and R depend on the two variables ξ and η. Calculating the derivative of (17) with respect to τ and using the Jacobi integral (16) to remove all the even powers of η' as in [42], we get the following nonlinear system of partial differential equations:

$$M.D_\xi X + N.D_\eta X = B, \tag{18}$$

where $X = (P_1 \;\; P_2 \;\; P_3 \;\; Q_1 \;\; Q_2 \;\; Q_3 \;\; R \;\; U \;\; \Omega)^T$ is the vector of the unknown functions. $D_\xi X$ and $D_\eta X$ are partial derivatives according to the variables ξ and η of the vector X. M and N are the matrices and given as follows:

$$M = \begin{pmatrix} 1 & 0 & 0 & 0 & 0 & 0 & 0 & 3P_3 & 0 \\ 1 & 0 & 0 & 0 & 0 & 0 & 0 & 2Q_3 & 0 \\ 0 & 1 & 0 & 0 & 0 & 0 & 0 & 0 & 0 \\ 0 & 1 & 0 & 0 & 0 & 0 & 0 & 0 & 0 \\ 0 & 0 & 1 & 0 & 0 & 0 & 0 & 0 & 0 \\ 0 & 0 & 1 & 0 & 0 & 0 & 0 & 0 & 0 \\ 1 & 0 & 0 & 0 & 0 & 0 & 1 & 2P_1 & 0 \\ 1 & 0 & 0 & 0 & 0 & 0 & 1 & P_1 & 0 \\ 1 & 0 & 0 & 0 & 0 & 0 & 1 & Q_2 & 0 \end{pmatrix}, \tag{19}$$

$$N = \begin{pmatrix} 0 & 0 & 0 & -1 & 0 & 2U & 0 & Q_3 & 0 \\ 0 & 0 & 0 & 1 & 0 & 0 & 0 & 0 & 0 \\ 0 & 0 & 0 & 0 & -1 & 0 & 0 & 0 & 0 \\ 0 & 0 & 0 & 0 & 1 & 0 & 0 & 0 & 0 \\ 0 & 0 & 0 & 0 & 0 & -1 & 0 & 0 & 0 \\ 0 & 0 & 0 & 0 & 0 & 1 & 0 & 0 & 0 \\ 0 & 0 & 0 & 0 & 2U & 0 & 1 & Q_2 & 0 \\ 0 & 0 & 0 & 2U & 0 & 0 & 1 & Q_1 & 0 \\ 0 & 0 & 0 & 0 & 0 & 0 & 1 & 0 & 0 \end{pmatrix}. \tag{20}$$

The right-side vector B is given by $B = (-2\Omega Q_2 \;\; 2\Omega P_2 \;\; -3\Omega Q_3 - 4U \;\; 3\Omega P_3 \;\; 0 \;\; 4\Omega \;\; -\Omega Q_1 + 4\Omega U Q_3 \;\; 2\Omega Q_2 U \;\; \Omega P_1)^T$.

System (18) composed of nine nonlinear partial differential equations with nine unknown functions is not easy to solve exactly. Notice that the solution of this system determines a two-dimensional integrable system with an additional quartic integral in the velocities which is valid on a zero level of Jacobi integral.

The sixth equation in (18), which is $\partial P_3/\partial \xi + \partial Q_3/\partial \eta = 4\Omega$, and the definition of Ω, allow us to write Lagrangian (14) in the form

$$L_0 = \frac{1}{2}\left(\xi'^2 + \eta'^2\right) + \frac{1}{4}\left(P_3\xi' - Q_3\eta'\right) - U. \tag{21}$$

3. Applications to Rigid Body Dynamics

In the present section, we investigate the construction of new integrable systems with a quartic integral in the dynamics of a rigid body movement. Seeing that the metric corresponding to Lagrangian (9) is $ds^2 = d\varphi^2 + g(\gamma_3)d\gamma_3^2$, it is more suitable to use the variable p instead of η through the relation

$$\eta = \int \frac{dp}{f(p)}, \tag{22}$$

where

$$f(p) = \sqrt{(p - p_1)(p - p_2)(p - p_3)(p + p_1 + p_2 + p_3)}, \tag{23}$$

where $p_1, p_2,$ and p_3 are the arbitrary parameters. We consider a certain class of problems in a rigid body dynamics in which the gyroscopic forces are determined by

$$\Omega(\xi, p) = a_1\Omega_1(p)\cos\xi + a_2\Omega_0(p), \tag{24}$$

and the potential forces are characterized by

$$U(\xi, p) = u(p) + a_3\nu(p)\sin\xi - \frac{a_1a_2}{8}f_0(p)\cos\xi + a_1^2 m(p)\cos 2\xi, \tag{25}$$

where $a_1, a_2,$ and a_3 are the arbitrary constants. The motivation for the choice of the two functions (24) and (25) is that they represent a large class of problems in the dynamics of a rigid body. Certain clarifications should be made for two particular cases.

(1) Time-reversible case: this case is characterized by the absence of gyroscopic forces, i.e., $\Omega = 0$. This happens if $a_1 = 0$ and $a_2 = 0$, The potential function (25) reduces to $U = u(p) + a_3\nu(p)\sin\xi$ which is a Kowalevski-type potential. Furthermore, if we change $\xi \longrightarrow 2\xi$, the potential function takes the form $U = u(p) + a_3\nu(p)\sin 2\xi$ which is a Chaplygin-type potential. The previous studies concerning those types of potentials lead to several generalizations for integrable problems in the rigid body dynamics in which the additional integral is a quartic polynomial in the velocities (e.g., [51–53]). This type of problem is referred in literatures as time-reversible systems.

(2) Time-irreversible case: this case involves a gyroscopic forces acting on the motion besides the potential forces. We can split it into two subcases.

   (a) When setting $a_1 = 0$, the gyroscopic forces is characterized by $\Omega = a_2\Omega_0(p)$, and the potential function (25) becomes $U = u(p) + a_3\nu(p)\sin\xi$. The potential function is a type of Kowalevski-gyrostat type potential or Chaplygin-gyrostat type potential (if $\xi \longrightarrow 2\xi$). This problem has been studied in several works such as [51, 52]. These studies lead to a generalization of a Kowalevski case and Chaplygin case by adding a constant gyrostatic moment.

   (b) When $a_1a_2 \neq 0$, the full structure of Ω and U is considered in [49], but the authors solved the basic equations for a special cases leading to the Kowalevski case, and they introduced two integrable problems generalize Kowalevski case and Sokolov case.

Inserting the expressions (22), (24), and (25) into the equations (18)–(21), we have

$$L = \frac{1}{2}\left(\eta'^{2} + \frac{p'^{2}}{f(p)}\right) + (a_1 J_1(p)\cos\xi + a_2 J_0(p))\xi' + u(p) + a_3 v(p)\sin\xi - \frac{a_1 a_2}{8} f_0(p) v(p)\cos\xi + a_1^2 m(p)\cos(2\xi), \tag{26}$$

$$I = \xi'^{4} + P_3\xi'^{3} + \overline{Q}_3\xi'^{2}p\prime + P_2\xi'^{2} + \overline{Q}_2\xi' p\prime + P_1\xi' + \overline{Q}_1 p\prime + R = \varepsilon_0, \tag{27}$$

where $\overline{Q}_j = (Q_j/\sqrt{f(p)})$. In what follows, we inscribe Q instead of $\overline{Q}$ for simplicity. Taking into account the transformation (22) and inserting the two expressions (24) and (25) into the basic equation (18), we get the following nonlinear system of partial differential equations in the following form:

$$Q_3\frac{\mathrm{d}f}{\mathrm{d}p} + 2f\frac{\partial Q_3}{\partial p} - 2\frac{\partial P_3}{\partial \xi} = 0, \tag{28}$$

$$\frac{\partial P_3}{\partial p} + \frac{\partial Q_3}{\partial \xi} - 4a_2\Omega_0 - 4a_1\Omega_1\cos\xi = 0, \tag{29}$$

$$(8a_3 v + 6a_1 f Q_3\Omega_1)\cos\xi - 16a_1^2 m\sin 2\xi - 2f\frac{\partial Q_2}{\partial p} + 2\frac{\partial P_2}{\partial \xi} + a_1 a_2 f_0 v\sin\xi - Q_2\frac{df}{dp} + 6a_2 f Q_3\Omega_0 = 0, \tag{30}$$

$$\frac{\partial Q_2}{\partial \xi} + \frac{\partial P_2}{\partial p} - 3P_3(a_1\Omega_1\cos\xi + a_2\Omega_0) = 0, \tag{31}$$

$$\begin{aligned} &8a_1^2\left\{Q_3 f\frac{\mathrm{d}m}{\mathrm{d}p} + 2fm\frac{\partial Q_3}{\partial p} + Q_3 m\frac{\mathrm{d}f}{\mathrm{d}p}\right\}\cos 2\xi - \left\{a_1 a_2 f_0 v\frac{\mathrm{d}f_0}{\mathrm{d}p}Q_3 - 24a_3 v P_3 + 2a_1 a_2 f f_0 v\frac{\partial Q_3}{\partial p}\right. \\ &\left. + a_1 a_2 f f_0 Q_3\frac{\mathrm{d}v}{\mathrm{d}p} - 16a_1 f Q_2\Omega_1 + a_1 a_2 Q_3 v f\frac{\mathrm{d}f_0}{\mathrm{d}p}\right\} \\ &\cos\xi + \left\{3a_1 a_2 v f_0 Q_3 + 8a_3 v Q_3\frac{\mathrm{d}f}{\mathrm{d}p} + 16a_3 f v\frac{\partial Q_3}{\partial p} + 8a_3 Q_3 f\frac{\mathrm{d}v}{\mathrm{d}p}\right\}\sin\xi + 8Q_3 f \\ &\times\frac{\mathrm{d}u}{\mathrm{d}p} - 48a_1^2 P_3 m\sin 2\xi - 8f\frac{\partial Q_1}{\partial p} - 4Q_1\frac{\mathrm{d}f}{\mathrm{d}p} + 8\frac{\partial P_1}{\partial \xi} \\ &+ 8Q_3 u\frac{\mathrm{d}f}{\mathrm{d}p} + 16fu\frac{\partial Q_3}{\partial p} + 16fa_2 Q_2\Omega_0 = 0, \end{aligned} \tag{32}$$

$$a_1 a_2 f_0 v Q_3\sin\xi + 8(a_3 v Q_3 - a_1\Omega_1 P_2)\cos\xi + 4\frac{\partial Q_1}{\partial \xi} + 4\frac{\partial P_1}{\partial p} - 8a_2 P_2\Omega_0 - 16a_1^2 m Q_3\sin 2\xi = 0, \tag{33}$$

$$\begin{aligned} \frac{\partial R}{\partial \xi} = &\left\{2a_3^3 f Q_3 m\Omega_1 - \frac{a_2^2 a_1}{2} f_0 f v Q_3\Omega_0 - a_1 f Q_1\Omega_1 + 4a_1 Q_3 u\Omega_1 f + \frac{a_1 a_2}{8}Q_2 v f\frac{\mathrm{d}f_0}{\mathrm{d}p} + \frac{a_1 a_2}{4} f f_0 v\frac{\partial Q_2}{\partial p}\right. \\ &\left. - 2a_3 v P_2 + \frac{a_1 a_2}{8}Q_2 f f_0\frac{\mathrm{d}v}{\mathrm{d}p} + \frac{a_1 a_2}{8} f_0 v Q_2\frac{\mathrm{d}f}{\mathrm{d}p}\right\}\cos\xi \\ &+ \left\{-a_1^2 m Q_2\frac{\mathrm{d}f}{\mathrm{d}p} - \frac{a_2 a_1^2}{4} f f_0 v Q_3\Omega_1 - 2a_1^2 m f\frac{\partial Q_2}{\partial p} + 4a_2 a_1^2 f Q_3 m\times\Omega_0 + 2a_1^3 f Q_3 m\Omega_1\right\}\cos 3\xi \\ &- a_1^2 f Q_2\frac{\mathrm{d}m}{\mathrm{d}p}\cos 2\xi + \left\{-2a_3 f v\frac{\partial Q_2}{\partial p} - \frac{a_1 a_2}{4} f_0 v P_2\times Q_2 + 4a_2 a_3 f Q_3\Omega_0 - a_3 f Q_2\frac{\mathrm{d}v}{\mathrm{d}p}\right\}\sin\xi \\ &+ \left\{4a_1^2 P_2 m + 2a_1 a_3 f v Q_3\Omega_1\right\}\sin 2\xi - a_2 f Q_1\Omega_0 - Q_2 f\frac{\mathrm{d}u}{\mathrm{d}p} - Q_2 u\frac{\mathrm{d}f}{\mathrm{d}p} - a_3 v\frac{\mathrm{d}f}{\mathrm{d}p} - Q_2 u\frac{\mathrm{d}f}{\mathrm{d}p} \\ &- \frac{a_1^2 a_2}{4} f f_0 Q_3\Omega_1 + 4a_2 f Q_3 u\Omega_0 - 2fu\frac{\partial Q_2}{\partial p}, \end{aligned} \tag{34}$$

$$\frac{\partial R}{\partial p} = 2a_1^2 mQ_2 \sin 2\xi - \frac{a_1 a_2}{8} Q_2 f_0 \nu \sin \xi + a_1 P_1 \Omega_1 \cos \xi - \frac{a_1 a_2}{8} Q_2 f_0 \nu \sin 3\xi + a_2 P_1 \Omega_0$$
$$a_1^2 \left\{ 16 f m \frac{\partial Q_1}{\partial p} + a_2 f f_0 \nu Q_2 \Omega_1 - 16 a_2 f m Q_2 \Omega_0 + 8 Q_1 m \frac{\mathrm{d}f}{\mathrm{d}p} + 8 Q_1 f \frac{\mathrm{d}m}{\mathrm{d}p} \right\} \cos 2\xi - 8 a_1^3 f Q_2 m \Omega_1 \cos 3\xi$$
$$+ \left\{ -a_1 a_2 f_0 \nu Q_1 \frac{\mathrm{d}f}{\mathrm{d}p} + 2 a_1 a_2^2 f f_0 Q_2 \Omega_0 - a_1 a_2 Q_1 f f_0 \frac{\mathrm{d}\nu}{\mathrm{d}p} - 16 a_1 f u Q_2 \Omega_1 - 8 a_1^3 f m Q_2 \Omega_1 - a_1 a_2 \nu f Q_1 \frac{\mathrm{d}f_0}{\mathrm{d}p} \right.$$
$$\left. + 8 a_1^3 \nu P_1 - 2 a_1 a_2 f_0 f \nu \frac{\partial Q_1}{\partial p} \right\} \cos \xi + \left\{ 16 a_3 f \nu \frac{\partial Q_1}{\partial p} + 8 a_3 \nu Q_1 \frac{\mathrm{d}f}{\mathrm{d}p} - 16 a_2 a_3 f Q_2 \nu \Omega_0 + a_1 a_2 P_1 f_0 \nu + 8 a_3 f Q_1 \frac{\mathrm{d}\nu}{\mathrm{d}p} \right\} \sin \xi$$
$$- 8 a_1 \left(2 a_1 m P_1 + a_3 \nu f Q_2 \Omega_1 \right) \sin 2\xi + 8 Q_1 u \frac{\mathrm{d}f}{\mathrm{d}p} + a_1^2 a_2 f Q_2 f_0 \nu - 16 a_2 f Q_2 u \Omega_0 + 16 f u \frac{\partial Q_1}{\partial p} + 8 Q_1 f \frac{\mathrm{d}u}{\mathrm{d}p} = 0, \tag{35}$$

where

$$\Omega_0 = \frac{\mathrm{d}J_0}{\mathrm{d}p}, \qquad \Omega_1 = \frac{\mathrm{d}J_1}{\mathrm{d}p}. \tag{36}$$

It is obvious that systems (28)–(35) are a nonlinear system of partial differential equations, and so in general, their solution is somewhat difficult. For simplicity, we turn these equations to the system of ordinary differential equations by setting the integral coefficients in a more suitable form. After some trials, the integral coefficients can be expressed as follows:

$$P_3(\xi, p) = a_1 f_0(p) + a_1 f_1(p) \cos \xi,$$
$$Q_3(\xi, p) = 8 a_1 \sin \xi,$$
$$P_2(\xi, p) = P_0(p) + 16 a_3 p \sin \xi + a_1 a_2 G(p) \cos \xi + a_1^2 T(p) \cos 2\xi,$$
$$Q_2(\xi, p) = a_3 q_1(p) \cos \xi + a_1 a_2 q_2(p) \sin \xi + a_1^2 q_3(p) \sin 2\xi,$$
$$P_1(\xi, p) = f_3(p) \cos \xi + a_1^2 a_2 f_4(p) \cos 2\xi + a_1^3 f_5(p) \cos 3\xi + a_1 a_3 f_6(p) \sin 2\xi + a_2 a_3 f_7(p) \sin \xi + f_8(p),$$
$$Q_1(\xi, p) = a_2 a_3 f_9(p) \cos \xi + a_1 a_3 f_{10}(p) (\cos 2\xi + 1) + a_1 f_{11}(p) \sin \xi + a_2 a_1^2 f_{12}(p) \sin 2\xi + a_1^3 f_{13}(p) \sin 3\xi. \tag{37}$$

Inserting the expressions of the integral's coefficients (37) into the equations (28)–(35) and equating the coefficients of trigonometric functions to zero, we obtain the following system of ordinary differential equations:

$$a_1 \left(f_1 + 4 \frac{\mathrm{d}f}{\mathrm{d}p} \right) = 0, \tag{38}$$
$$a_2 f \left(\frac{\mathrm{d}f_0}{\mathrm{d}p} - 4\Omega_0 \right) = 0, \tag{39}$$
$$a_1 \left(4\Omega_1 - \frac{\mathrm{d}f_1}{\mathrm{d}p} - 8 \right) = 0, \tag{40}$$
$$a_3 \left(q_1 \frac{\mathrm{d}f}{\mathrm{d}p} + 2 f \frac{\mathrm{d}q_1}{\mathrm{d}p} - 32 p - 8 \nu \right) = 0, \tag{41}$$

$$a_1 a_2\left(q_2\frac{\mathrm{d}f}{\mathrm{d}p}+2f\frac{\mathrm{d}q_2}{\mathrm{d}p}+2G-f_0\nu-48f\Omega_0\right)=0, \tag{42}$$

$$a_1^2\left(q_3\frac{\mathrm{d}f}{\mathrm{d}p}+2f\frac{\mathrm{d}q_3}{\mathrm{d}p}+4T+16m-24f\Omega_1\right)=0, \tag{43}$$

$$a_1 a_2\left(\frac{\mathrm{d}G}{\mathrm{d}p}-3f_0\Omega_1-3f_1\Omega_0-q_2\right)=0, \tag{44}$$

$$a_1^2\left(2\frac{\mathrm{d}T}{\mathrm{d}p}-3f_1\Omega_1+4q_3\right)=0, \tag{45}$$

$$a_3\left(q_1-16\right)=0, \tag{46}$$

$$\frac{\mathrm{d}P_0}{\mathrm{d}p}-3a_2^2f_0\Omega_0-\frac{3}{2}a_1^2f_1\Omega_1=0, \tag{47}$$

$$a_2 a_3\left(f_9\frac{\mathrm{d}f}{\mathrm{d}p}+2f\frac{\mathrm{d}f_9}{\mathrm{d}p}-2f_7-6f_0\nu-4fq_1\Omega_0\right)=0, \tag{48}$$

$$a_1 a_3\left(f_{10}\frac{\mathrm{d}f}{\mathrm{d}p}+2f\frac{\mathrm{d}f_{10}}{\mathrm{d}p}+8\frac{\mathrm{d}}{\mathrm{d}p}\left(\nu p\right)-4f_6-3f_1\nu-2q_1f\Omega_1\right)=0, \tag{49}$$

$$f_3+a_1\left(f\frac{\mathrm{d}f_{11}}{\mathrm{d}p}+\frac{1}{2}f_{11}\frac{\mathrm{d}f}{\mathrm{d}p}-8f\frac{\mathrm{d}u}{\mathrm{d}p}-8u\frac{\mathrm{d}f}{\mathrm{d}p}\right)+a_1^3\left(4m\frac{\mathrm{d}f}{\mathrm{d}p}+3mf_1\right)+a_1a_2^2\left(\frac{3}{8}f_0\nu-2fq_2\Omega_0\right)=0, \tag{50}$$

$$a_2a_1^2\left(8f_{12}\frac{\mathrm{d}f}{\mathrm{d}p}+16f\frac{\mathrm{d}f_{12}}{\mathrm{d}p}+8\frac{\mathrm{d}}{\mathrm{d}p}\left(f_0\nu f\right)+32f_4+96f_0m-32fq_3\Omega_0-32fq_3\Omega_0-16q_2f\Omega_1\right)=0, \tag{51}$$

$$a_1^3\left(2f\frac{\mathrm{d}f_{13}}{\mathrm{d}p}+f_{13}\frac{\mathrm{d}f}{\mathrm{d}p}+6f_5-8\frac{\mathrm{d}}{\mathrm{d}p}\left(mf\right)-2q_3f\Omega_1+6mf_1\right)=0, \tag{52}$$

$$a_1 a_3\left(f_{10}\frac{\mathrm{d}f}{\mathrm{d}p}+2f\frac{\mathrm{d}f_{10}}{\mathrm{d}p}-8\frac{\mathrm{d}}{\mathrm{d}p}\left(\nu f\right)-2q_1f\Omega_1-3f_1\nu\right)=0, \tag{53}$$

$$a_1\left(2P_0\Omega_1-f_{11}\right)+2a_1a_2^2G\Omega_0+a_1^3\left(16m+T\Omega_1\right)-\frac{\mathrm{d}f_3}{\mathrm{d}p}=0, \tag{54}$$

$$a_1^2a_2\left(2T\Omega_0-2f_{12}+f_0\nu+G\Omega_1-\frac{\mathrm{d}f_4}{\mathrm{d}p}\right)=0, \tag{55}$$

$$a_1^3\left(T\Omega_1-3f_{13}-16m-\frac{\mathrm{d}f_5}{\mathrm{d}p}\right)=0, \tag{56}$$

$$a_2 a_3\left(\frac{\mathrm{d}f_7}{\mathrm{d}p}-f_9-32p\Omega_0\right)=0, \tag{57}$$

$$a_1 a_3\left(\frac{\mathrm{d}f_6}{\mathrm{d}p} - 2f_{10} - 16p\Omega_1 + 8\nu\right) = 0, \tag{58}$$

$$a_1^2 a_2 (G\Omega_1 - f_0\nu) + 2a_2 P_0\Omega_0 - \frac{\mathrm{d}f_8}{\mathrm{d}p} = 0, \tag{59}$$

$$\frac{\partial R}{\partial \xi} = \mathscr{F}_0(p) + \mathscr{F}_1(p)\cos\xi + \mathscr{F}_2(p)\cos 2\xi + \mathscr{F}_3(p)\cos 3\xi + \mathscr{F}_4(p)\sin\xi + \mathscr{F}_5(p)\sin 2\xi + \mathscr{F}_6(p)\sin 3\xi, \tag{60}$$

$$\begin{aligned}\frac{\partial R}{\partial p} = {} & \mathscr{F}_7(p)\cos\xi + \mathscr{F}_8(p)\cos 2\xi + \mathscr{F}_9(p)\cos 3\xi \\ & - a_1^4\left\{q_3 m - \frac{\Omega_1 f_5}{2}\right\}\cos 4\xi + a_3\left\{a_2^2 f_7\Omega_0 + a_1^2\left(\frac{f_6\Omega_1}{2} + mq_1 - \frac{1}{2}\nu q_3\right)\right\} \\ & \sin\xi - \frac{a_1 a_2 a_3}{16}\{\nu(q_1 f_0 + 8q_2) - 8f_7\Omega_1 - 16f_6\Omega_0\}\sin 2\xi + \frac{a_3 a_1^2}{2}\{f_6\Omega_1 + 2mq_1 - \nu q_3\} \\ & \sin 3\xi + \frac{a_1}{2}f_3\Omega_1 - \frac{a_3^2}{2}q_1\nu + a_2 f_8\Omega_0 + a_1^4 q_3 m - \frac{a_1^2 a_2^2}{16}q_2 f_0\nu,\end{aligned} \tag{61}$$

$$\begin{aligned}a_1^4 a_2\Big\{ & f_0 f_5\nu - 8fq_2 m\Omega_1 - \nu f f_{13}\frac{\mathrm{d}f_0}{\mathrm{d}p} - f_0 f_{13}\nu\frac{\mathrm{d}f}{\mathrm{d}p} - 16fq_3 m\Omega_0 - 16f_4 m + fq_3\Omega_1 f_0\nu + \nu f_0 f_5 \\ & - 2ff_0\nu\frac{\mathrm{d}f_{13}}{\mathrm{d}p} + 8ff_{12}\frac{\mathrm{d}m}{\mathrm{d}p} + 8f_{12}m\frac{\mathrm{d}f}{\mathrm{d}p} - f_{13}f_0 f\frac{\mathrm{d}\nu}{\mathrm{d}p} + 16fm\frac{\mathrm{d}f_{12}}{\mathrm{d}p}\Big\} = 0,\end{aligned} \tag{62}$$

$$a_3 a_1^3\left\{\nu f_{13}\frac{\mathrm{d}f}{\mathrm{d}p} + ff_{13}\frac{\mathrm{d}\nu}{\mathrm{d}p} - ff_{10}\frac{\mathrm{d}m}{\mathrm{d}p} - 2fm\frac{\mathrm{d}f_{10}}{\mathrm{d}p} - 2f_6 m - f_{10}m\frac{\mathrm{d}f}{\mathrm{d}p} - \nu f_5 - fq_3\Omega_1\nu + 2f\nu\frac{\mathrm{d}f_{13}}{\mathrm{d}p} + fq_1\Omega_1 m\right\} = 0, \tag{63}$$

$$\begin{aligned}a_1\Big\{ & -16a_1 mf_3 + a_1^2\left(16f_{13}f\frac{\mathrm{d}u}{\mathrm{d}p} + 16fm\frac{\mathrm{d}f_{11}}{\mathrm{d}p} + 8f_{11}f\frac{\mathrm{d}m}{\mathrm{d}p} + 8f_{11}m\frac{\mathrm{d}f}{\mathrm{d}p} - 16fq_3 u\Omega_1 + 16uf_{13}\frac{\mathrm{d}f}{\mathrm{d}p} + 32fu\frac{\mathrm{d}f_{13}}{\mathrm{d}p}\right) \\ & + a_1^2 a_2^2\left(-ff_0 f_{12}\frac{\mathrm{d}\nu}{\mathrm{d}p} + fq_2 f_0\Omega_1\nu + f_4\nu f_0 - 2ff_0\nu\frac{\mathrm{d}f_{12}}{\mathrm{d}p} + 2fq_3 f_0\Omega_0\nu - \nu f f_{12}\frac{\mathrm{d}f_0}{\mathrm{d}p} - 16fq_2\Omega_0 m - f_{12}f_0\nu\frac{\mathrm{d}f}{\mathrm{d}p}\right) \\ & + a_3^2\left(8ff_{10}\frac{\mathrm{d}\nu}{\mathrm{d}p} + 8f_{10}\nu\frac{\mathrm{d}f}{\mathrm{d}p} + 16f\nu\frac{\mathrm{d}f_{10}}{\mathrm{d}p} + 8f_6\nu - 8fq_1\Omega_1\nu\right) - 8a_1^4 q_3 f\Omega_1 m\Big\} = 0,\end{aligned} \tag{64}$$

$$\begin{aligned}a_1^2 a_2 a_3\Big\{ & f_{10}f_0\nu\frac{\mathrm{d}f}{\mathrm{d}p} + 16fq_1 m\Omega_0 - 16mf_7 + f_0 f_6\nu + f_0 f_{10}f\frac{\mathrm{d}\nu}{\mathrm{d}p} - 16fq_3\nu\Omega_0 + 8ff_{12}\frac{\mathrm{d}\nu}{\mathrm{d}p} + 8\nu f_{12}\frac{\mathrm{d}f}{\mathrm{d}p} - 8fq_2\nu\Omega_1 \\ & - 8f_4\nu + ff_{10}\nu\frac{\mathrm{d}f_{10}}{\mathrm{d}p} - 16fm\frac{\mathrm{d}f_9}{\mathrm{d}p} - 8ff_9\frac{\mathrm{d}m}{\mathrm{d}p} + 16f\nu\frac{\mathrm{d}f_{12}}{\mathrm{d}p} - 8f_9 m\frac{\mathrm{d}f}{\mathrm{d}p} - fq_1\Omega_1 f_0\nu + 2ff_0\nu\frac{\mathrm{d}f_{10}}{\mathrm{d}p} = 0,\end{aligned} \tag{65}$$

$$\begin{aligned} & -2a_1^2 f_8 m + \frac{a_1 a_2}{16}f_0 f_3\nu + \frac{a_2 a_1^4}{16}\left\{-ff_{13}\nu\frac{\mathrm{d}\nu}{\mathrm{d}p} - ff_{13}\frac{\mathrm{d}\nu}{\mathrm{d}p} - 2ff_0\nu\frac{\mathrm{d}f_{13}}{\mathrm{d}p} - f_0\nu f_{13}\frac{\mathrm{d}f}{\mathrm{d}p} - f_0 f_5\nu + 2fq_3\Omega_1 f_0\nu\right\} \\ & + a_2 a_1^2\left(ff_{12}\frac{\mathrm{d}u}{\mathrm{d}p} - \frac{1}{16}ff_{11}\nu\frac{\mathrm{d}f}{\mathrm{d}p} + 2fu\frac{\mathrm{d}f_{12}}{\mathrm{d}p} - fq_2 u\Omega_1 + f_{12}u\frac{\mathrm{d}f}{\mathrm{d}p} - \frac{1}{16}ff_{11}f_0\frac{\mathrm{d}\nu}{\mathrm{d}p} - \frac{1}{16}ff_{11}\nu\frac{\mathrm{d}f_0}{\mathrm{d}p} - 2fq_3 u\Omega_0 - \frac{1}{8}ff_0\nu\frac{\mathrm{d}f_{11}}{\mathrm{d}p}\right) \\ & + \frac{a_2 a_3^2}{2}\left\{f_7\nu + 2f\nu\frac{\mathrm{d}f_9}{\mathrm{d}p} - 2fq_1\Omega_0\nu + f_9 f\frac{\mathrm{d}\nu}{\mathrm{d}p} + f_9\nu\frac{\mathrm{d}f}{\mathrm{d}p}\right\} + \frac{a_1^2 a_2^3}{8}fq_2\Omega_0 f_0\nu\Big\} = 0,\end{aligned} \tag{66}$$

$$a_3 8 f_3 v + a_1\left(32 f u\frac{\mathrm{d}f_{10}}{\mathrm{d}p} - 16 f q_1\Omega_1 u - 8 f_{11} v\frac{\mathrm{d}f}{\mathrm{d}p} - 8 f f_{11}\frac{\mathrm{d}v}{\mathrm{d}p} + 16 f_{10} u\frac{\mathrm{d}f}{\mathrm{d}p} + 16 f f_{10}\frac{\mathrm{d}u}{\mathrm{d}p} - 16 v f\frac{\mathrm{d}f_{11}}{\mathrm{d}p}\right) + a_1^3\left(8 f_{13} v\frac{\mathrm{d}f}{\mathrm{d}p} + 16 v f\frac{\mathrm{d}f_{13}}{\mathrm{d}p} + 32 f m\frac{\mathrm{d}f_{10}}{\mathrm{d}p} + 16 m f_{10}\frac{\mathrm{d}f}{\mathrm{d}p} + 8 f_5 v + 16 f f_{10}\frac{\mathrm{d}m}{\mathrm{d}p} - 16 f q_1 m\Omega_1 + 8 f_{13} f\frac{\mathrm{d}v}{\mathrm{d}p}\right) + a_1 a_2^2\left(2 f f_0 q_1\Omega_0 v - f f_0 f_9\frac{\mathrm{d}v}{\mathrm{d}p} - f_0 f_7 v - f_9 f v\frac{\mathrm{d}f_0}{\mathrm{d}p} - 2 f_0 f v\frac{\mathrm{d}f_9}{\mathrm{d}p} + 16 f q_2\Omega_0 v\right)\Bigg\} = 0, \tag{67}$$

$$a_3\Bigg\{16 f_8 v + a_2\left(16 f_9 u\frac{\mathrm{d}f}{\mathrm{d}p} + 16 f_9 f\frac{\mathrm{d}u}{\mathrm{d}p} - 32 f q_1\Omega_0 u + 32 f u\frac{\mathrm{d}f_9}{\mathrm{d}p}\right) + a_2 a_1^2\left(-8 f q_2 v\Omega_1 - 3 f_{10} v f\frac{\mathrm{d}f_0}{\mathrm{d}p} + 8 f_9 f\frac{\mathrm{d}m}{\mathrm{d}p} + 8 f_4 v - 6 f f_0 v\frac{\mathrm{d}f_{10}}{\mathrm{d}p} - 16 f q_1\Omega_0 m - 3 f_0 f_{10} f\frac{\mathrm{d}v}{\mathrm{d}p} + 16 f v\frac{\mathrm{d}f_{12}}{\mathrm{d}p} - 3 f_{10} f_0 v\frac{\mathrm{d}f}{\mathrm{d}p} + 3 f q_1\Omega_1 f_0 v + 8 f_{12} f\frac{\mathrm{d}v}{\mathrm{d}p} + f_6 f_0 v + 8 f_9 m\frac{\mathrm{d}f}{\mathrm{d}p} - 16 f q_3\Omega_0 v + 8 f_{12} v\frac{\mathrm{d}f}{\mathrm{d}p} + 16 f m\frac{\mathrm{d}f_9}{\mathrm{d}p} - 16 f_7 m\right)\Bigg\} = 0, \tag{68}$$

$$a_1\Bigg\{16 f_{11} u\frac{\mathrm{d}f}{\mathrm{d}p} + 16 f_{11} f\frac{\mathrm{d}u}{\mathrm{d}p} + 32 f u\frac{\mathrm{d}f_{11}}{\mathrm{d}p} - 16 a_1 f_3 m + 2 a_2 f_0 f_8 v + a_1^2\left(-8 f_{11} m\frac{\mathrm{d}f}{\mathrm{d}p} - 16 f q_3 u\Omega_1 - 16 f m\frac{\mathrm{d}f_{11}}{\mathrm{d}p} - 8 f_{11} f\frac{\mathrm{d}m}{\mathrm{d}p}\right) + a_1^4\left(8 f f_{13}\frac{\mathrm{d}f}{\mathrm{d}p} + 8 f_{13} m\frac{\mathrm{d}f}{\mathrm{d}p} + 16 f m\frac{\mathrm{d}f_{13}}{\mathrm{d}p}\right) - 32 a_2^2 f q_2\Omega_0 u + a_3^2\left(-8 f q_1\Omega_1 v + 8 f_6 v + 16 f v\frac{\mathrm{d}f_{10}}{\mathrm{d}p} + 8 f_{10} v\frac{\mathrm{d}f}{\mathrm{d}p} + 8 f f_{10}\frac{\mathrm{d}v}{\mathrm{d}p}\right) + a_1^2 a_2^2\left(-f_0 f_{12} f\frac{\mathrm{d}v}{\mathrm{d}p} + f q_2\Omega_1 f_0 v + 16 f q_2\Omega_0 m - f_0 v f_{12}\frac{\mathrm{d}f}{\mathrm{d}p} - f_4 f_0 v - v f f_{12}\frac{\mathrm{d}f_0}{\mathrm{d}p} - 2 f f_0 v\frac{\mathrm{d}f_{12}}{\mathrm{d}p} + 2 f q_3\Omega_0 f_0 v\right)\Bigg\} = 0, \tag{69}$$

$$a_3\Bigg\{a_1^3\left(f_{10} m\frac{\mathrm{d}f}{\mathrm{d}p} + 8 f_{10} f\frac{\mathrm{d}m}{\mathrm{d}p} - 8 f q_1\Omega_1 m + 16 f m\frac{\mathrm{d}f_{10}}{\mathrm{d}p} - 8 f q_3\Omega_1 v - 16 f_6 m\right) + a_1\Bigg\{a_2^2\left(f_7 f_0 v - 2 f f_0 v\frac{\mathrm{d}f_9}{\mathrm{d}p} - f_0 f f_9\frac{\mathrm{d}v}{\mathrm{d}p} + 2 f q_1 f_0 v\Omega_0 - 16 f q_2\Omega_0 v - f_9 f v\frac{\mathrm{d}f_0}{\mathrm{d}p} - f_9 f_0 v\frac{\mathrm{d}f}{\mathrm{d}p}\right) + 32 f u\frac{\mathrm{d}f_{10}}{\mathrm{d}p} + 8 f_{11} v\frac{\mathrm{d}f}{\mathrm{d}p} + 16 f v\frac{\mathrm{d}f_{11}}{\mathrm{d}p} + 16 f_{10}\times u\frac{\mathrm{d}f}{\mathrm{d}p} - 16 f q_1\Omega_1 u + 8 f_{11} f\frac{\mathrm{d}v}{\mathrm{d}p} + 16 f f_{10}\frac{\mathrm{d}u}{\mathrm{d}p}\Bigg\} + 8 v f_3\Bigg\} = 0, \tag{70}$$

where $\mathscr{F}_i(p), i = 0, 1, \ldots, 9$ is given in Appendix B. Systems (38)–(68) consist of thirty-two nonlinear ordinary differential equations in nineteen unknown functions. The solution to this system is somewhat intricate, and we cannot generally solve it as in the reversible case for arbitrary values of the parameters. But we solve it for certain values of the parameters leading to rigid body dynamics.

3.1. Two New Integrable Problems. The metric corresponding to the Lagrangian (9) that describes the metric of a rigid body matches with the Lagrangian (26) if we set

$$\xi = 2(\varphi - \varphi_0), \quad p_1 = p_2 = p_3 = 1, \quad p = 1 + \frac{\gamma_3^4}{1 - \gamma_3^2}. \tag{71}$$

We are going to solve equation (70) taking into account condition (71). As a result of the complexity of those equations, we utilize the Maple program. We consider separately the two cases that are $a_1 a_2 \neq 0$ and $a_2 = 0$. Let us illustrate the causes of choosing those cases. In our works for constructing integrable systems with quartic integrals, it seems that some potentials are appropriate, with the attendance of a constant gyrostatic moment, while others are not. For more elucidation, we admit the Chaplygin case describing the motion of a rigid body in an incompressible ideal fluid and its generalization as an example:

$$V_1 = a\left(\gamma_1^2 - \gamma_2^2\right) + 2 b\gamma_1\gamma_2 + \frac{\lambda}{2\gamma_3^2}, \quad \boldsymbol{\mu} = (0, 0, k), \tag{72}$$

$$V_2 = a\left(\gamma_1^2 - \gamma_2^2\right) + 2 b\gamma_1\gamma_2 + \frac{\lambda}{2\gamma_3^2} + \rho\left(\frac{1}{\gamma_3^4} - \frac{1}{\gamma_3^6}\right), \quad \boldsymbol{\mu} = (0, 0, 0), \tag{73}$$

where $a, b, \lambda,$ andρ are the arbitrary parameters, while k is a constant characterizing the gyrostatic moment. These two cases were previously introduced in [53, 54], respectively. It is worth noticing that the singular term $\rho((1/\gamma_3^4) - (1/\gamma_3^6))$ is not compatible with the existence of the gyrostatic moment as it is outlined in (72), but in the absence of a gyrostatic moment, this term appears. As we see later, this situation appears, and it is followed by the discovery of two new cases. The new cases will be directly announced without any details due to most of the calculations cannot be displayed in a suitable size.

3.1.1. First New Integrable Case. We first consider the case in which $a_2 a_1 \neq 0$; taking into account the condition (71) and using the Maple program, we obtain a new integrable problem in a rigid body dynamic after tedious manipulations which are not writable in a suitable size in the generalized coordinates θ and φ. Therefore, we introduce it in the traditional Euler-Poisson variables for the sake of simplicity and to make the comparison clear with previous results.

Theorem 1. *Let the principal inertia matrix for a rigid body satisfy the condition $A = B = 2C$, and the potential and gyroscopic forces characterized by V andμ, respectively, are given by*

$$V = \kappa\left[c\left(\gamma_2^2 - \gamma_1^2\right) - 2\,d\gamma_1\gamma_2\right] + \frac{\lambda}{\gamma_3^2} + K\left[2c\gamma_1\gamma_2 + d\left(\gamma_2^2 - \gamma_1^2\right)\right]\left(k - \nu\frac{\gamma_1^2 + \gamma_3^2}{\gamma_1^2}\right) - \frac{k\nu\gamma_3^2}{\gamma_1^2} - \frac{\nu^2\gamma_3^2\left(\gamma_3^2 + 2\gamma_2^2\right)}{2\gamma_1^4} + K^2\left[\frac{d^2}{2}\left(\gamma_3^4 + 4\gamma_1^2\gamma_2^2\right) - c^2\left(\gamma_3^2\left(\gamma_1^2 + \gamma_2^2\right) + 2\gamma_1^2\gamma_2^2\right)2 + c\,d\gamma_1\gamma_2\left(\gamma_1^2 - \gamma_2^2\right)\right], \tag{74}$$

$$\boldsymbol{\mu} = \left(2K\gamma_3\left(c\gamma_2 - d\gamma_1\right) - \frac{2\nu\gamma_3\left(1 + \gamma_2^2\right)}{\gamma_1^3}, 2K\gamma_3\left(c\gamma_1 + d\gamma_2\right) + \frac{2\nu\gamma_2\gamma_3}{\gamma_1^2}, k + K\left[2c\gamma_1\gamma_2 + d\left(\gamma_2^2 - \gamma_1^2\right)\right] + \frac{\nu\left(1 + \gamma_2^2\right)}{\gamma_1^2}\right), \tag{75}$$

or, equivalently,

$$\mathbf{l} = \left(0, 0, k + K\left[2c\gamma_1\gamma_2 + d\left(\gamma_2^2 - \gamma_1^2\right)\right] + \frac{\boldsymbol{\nu}\left(1 + \gamma_2^2\right)}{\gamma_1^2}\right), \tag{76}$$

where $k, \kappa, c, d, \lambda, K,$ andν are the arbitrary parameters. Then, the Euler-Poisson equation 2) with (74) and (76) is integrable on a zero level of the area integral:

$$I_1 = 2p\gamma_1 + 2q\gamma_2 + \left(r + k + K\left(2c\gamma_1\gamma_2 + d\left(\gamma_2^2 - \gamma_1^2\right)\right) + \frac{\nu\left(1 + \gamma_2^2\right)}{\gamma_1^2}\right)\gamma_3. \tag{77}$$

The additional integral admits the form

$$I_2 = \left[p^2 - q^2 + c\kappa\gamma_3^2 + cK^2\gamma_3^2\left(c\left(\gamma_1^2 - \gamma_2^2\right) + 2\,d\gamma_1\gamma_2\right) - K\,d\left(2\nu + 2k + \gamma_3^2\left(3k - 3\nu - r\right) - \frac{\lambda\left(\gamma_1^2 - \gamma_2^2\right)}{\gamma_3^2}\right)\right]^2 + \left[2pq + d\kappa\,\gamma_3^2 + dK^2\gamma_3^2\left(\left(\gamma_1^2 - \gamma_2^2\right) + 2\,d\gamma_1\gamma_2\right) + cK\left(\gamma_3^2\left(3k - 3\nu - r\right) - \frac{2\lambda\gamma_1\gamma_2}{\gamma_3^2}\right)\right]^2 + (k - \nu)\left(r - k + \nu\right) - K\left(2c\gamma_1\gamma_2 + d\left(\gamma_2^2 - \gamma_1^2\right)\right)\left[2\left(p^2 + q^2\right)\right] + 2\lambda\left(1 + \frac{1}{\gamma_3^2}\right) + 2\gamma_3^2\left(\left(\gamma_3^2 - 1\right)\left(c^2 + d^2\right)K^2 - 2\,d\left(k - \nu\right)K + c\kappa\right) - 4\gamma_3\left(k - \nu\right)\left(2K\left(k - \nu\right)\left[\left(c\gamma_1 + 2\,d\gamma_2\right) + \kappa\left(d\gamma_1 - 2c\gamma_2\right)\right]q + \gamma_2 p\left(2c\left(k - \nu\right)K + d\kappa\right)\right)$$

$$
\begin{aligned}
&-8(k-\nu)\Big[Kc^2((k-\nu))\times\Big(\gamma_3^4-\gamma_3^2-\frac{1}{4}\Big)K-\kappa\gamma_1\gamma_2\gamma_3^2+c\Big[2(k-\nu)dK^2\gamma_1\gamma_2\gamma_3^2\\
&+K\Big(\frac{d\kappa}{2}\gamma_3^2+d\kappa\gamma_3^2\Big(\gamma_1^2-\frac{1}{2}\Big)-2\lambda\gamma_1\gamma_2\Big)-\frac{\kappa(k-\nu)}{2}\gamma_3^2-\frac{(k-\nu)d^2K^2\big(16\gamma_1^2\gamma_3^2+1\big)}{8}+\Big(d\big((k-\nu)^2+\lambda\big)\gamma_3^2-2d\lambda\Big(\frac{1}{4}-\gamma_1^2\Big)\Big)K\\
&+\frac{K^2\nu\gamma_3^4}{\gamma_1^2}\big(c^2+d^2\big)\Big[\frac{\nu}{\gamma_1^2}\Big]\big(\gamma_3^2\big(2\gamma_1^2+\gamma_3^2\big)\big)-2\big(\gamma_1^2+\gamma_2^2\big)-2K\big(\gamma_1^2+\gamma_2^2\big)\big(2c\gamma_1\gamma_2+d\big(\gamma_2^2-\gamma_1^2\big)+2\big(2\gamma_3^2-1\big)r\big)\\
&+\frac{2\nu^2\big(4\gamma_1^4-\gamma_3^2\big)}{\gamma_1^4}\big(p^2-q^2\big)-\frac{2k\nu\gamma_3^2r^2}{\gamma_1^2}+\frac{2\nu\gamma_3^2\big(p^2+q^2\big)}{\gamma_1^2}\left[2K(c\gamma_2-d\gamma_1)\gamma_1-r\right]\\
&-\frac{4\nu^4\gamma_3^2}{4\gamma_1^8}\Big[\gamma_1^6-\big(1+\gamma_2^2\big)\gamma_4^4+2\big(\gamma_2^2+1\big)^2\gamma_1^2+\gamma_2^2\gamma_3^2\big(\gamma_2^2+2\big)\Big]+\frac{\nu}{\gamma_1^6}r\\
&\times\big[-2\nu^2\big(\gamma_1^2\big(\gamma_1^2+3\gamma_2^2\big)+\gamma_3^2\big(\gamma_1^2+\gamma_2^2\big)\big)-2k\nu\gamma_3^2\gamma_1^2\big(\gamma_1^2-\gamma_2^2+2\big)-\gamma_1^4\big(2\lambda\big(\gamma_3^2-1\big)+4kK\gamma_3^2\big(2c\gamma_1\gamma_2+d\big(\gamma_1^2+\gamma_2^2\big)\big)\big)\\
&-\frac{2\nu^3\gamma_3^2}{\gamma_1^6}\big[k\big(\gamma_1^2\big(5\gamma_1^2+4\gamma_3^2-6\big)+\gamma_3^2\big(2-\gamma_3^2\big)\big)+K\big(\gamma_2\big(2c\gamma_1\big(\gamma_1^2-\gamma_2^2\big)-d\gamma_2^3\big)\big(\gamma_1^2+\gamma_3^2\big)+d\gamma_1^2\big(\gamma_1^2+2\gamma_2^2\big)\big(3\gamma_1^2+\gamma_3^2\big)\big)\\
&+\frac{2\nu\lambda}{\gamma_1^4}\big[\nu\big(\gamma_2^2-\gamma_1^2\big)+\gamma_1^2\big(k+K\big(2c\,d\gamma_1\gamma_2+d\big(\gamma_2^2-\gamma_1^2\big)\big)\big)\big]-\frac{2\nu\gamma_3^2\kappa}{\gamma_1^4}\big[\nu\gamma_2\big(\gamma_2\big(4\gamma_1^4+\gamma_3^2\big)\big)-2\,d\gamma_1\big(2\gamma_1^2+\gamma_3^2\big)+\gamma_1^2(2\gamma_3)\\
&\times(c\gamma_2-d\gamma_1)q-2\gamma_3(c\gamma_1+d\gamma_2)p+k(4\,d\gamma_1\gamma_2-4)\big(\gamma_3^2+4\gamma_2^2\big)+2\nu^2\Big[-5K\,dk\,\gamma_3^6-4\Big(\Big(2cq-\frac{1}{2}dp\Big)\gamma_1+\gamma_2\Big(cp+\frac{3}{2}dq\Big)\Big)\\
&\times K\gamma_3^5+2\big(k\big(\big(5-8\gamma_1^2\big)d+5c\gamma_1\gamma_2\big)K-k^2-2q^2\big)\gamma_3^2-4\Big(5c\gamma_1^3q+\gamma_2(cp+4\,dq)\gamma_1^2+\gamma_1\Big(\frac{dp}{2}-2cq\Big)-\gamma_2\Big(cp+\frac{3\,dq}{2}\Big)\Big)\\
&\times K\gamma_3^3+\gamma_3^2\big(k\big(\big(16\gamma_1^2-8\gamma_1^{-}5\big)d+2\gamma_1\gamma_2\big(6\gamma_1^2-5\big)c\big)K+\gamma_1^2\big(2p^2-6q^2-4k^2\big)+4\gamma_1\gamma_2pq+k^2\big)+8K\big((-cq-dp)\gamma_1^3\big)\\
&\gamma_2(cp-dq)\gamma_1^2+\frac{3}{2}cq\gamma_1+\frac{\gamma_2}{2}(cp+2\,dq)\gamma_3\gamma_1^2+4q\gamma_1^2(2\gamma_1\gamma_2p+q)\big]+\frac{4\nu}{\gamma_1^2}\Big[-\frac{1}{2}kK^2\gamma_3^2\big(c^2+2d^2\big)+\gamma_3^4((2ck\gamma_1))\\
&\times(c\gamma_1+d\gamma_2)+d^2kK^2+\big(\big(3k^2+p^2-2q^2\big)d-3pqc\big)K+2k((3q\gamma_2-p\gamma_1))d+c(2q\gamma_1+\gamma_2q)K\gamma_3^3+\big(2k\big(\big(\gamma_1^4\big)\big)\big)\\
&-c\,d\gamma_1\gamma_2-c^2\gamma_1^2\big(\gamma_2^2+\gamma_3^2\big)K^2+\gamma_3^2\Big(\Big(2k^2\big(\gamma_1^2-2\big)-\frac{1}{2}p^2+\frac{3}{2}q^2\Big)d+2c\big(pq-2k^2\gamma_1^2\gamma_2^2\big)\Big)K+\frac{k^3}{2}\\
&-4Kk\Big(dq\,\gamma_2+c\Big(\gamma_1^2(\gamma_2p-\gamma_1q)+\frac{1}{2}(\gamma_2p+3\gamma_1q)\Big)\gamma_3\Big).
\end{aligned}
\tag{78}
$$

Theorem 1 characterizes a new integrable problem in a rigid body dynamics. The present case generalizes a special version of the case introduced by Yehia and Elmandouh in 2016 by adding a new parameter ν [48]. Also, it includes the case announced by Elmandouh in 2015 ($K=0$) [3]. Moreover, it generalizes the case presented by Yehia and Elmandouh in 2013 by inserting two arbitrary constants ($k=\nu=0$) [6]. It generalizes the integrable case which was introduced by Goriatchev in 1916 by adding four arbitrary parameters ν, k, K, and ρ [55]. It also contains five arbitrary parameters, ν, k, K, λ, and ρ, more than the case introduced by Chaplygin in 1903 [56]. To avoid confusion, we summed up the comparisons between this case and the related earlier cases in Table 2.

Regrettably, the physical interpretation for the whole system with the full set of all associated parameters is unknown. Disregarding the singular terms in both potential and vector functions, the problem describes physically the

Table 2: Comparison the first integrable case with previous results.

No.	Authors	Conditions of the parameters	References
1	Yehia and Elmandouh [48]	$\nu = 0$	[48]
2	Elmandouh [3]	$K = 0$	[3]
3	Yehia and Elmandouh [6]	$k = \nu = 0$	[6]
4	Goriatchev [55]	$\nu = K = \rho = k = 0$	[55]
5	Chaplygin [56]	$\nu = K = \rho = k = \lambda = 0$	[56]

motion of an electrically charged heavy rigid body about a fixed point under the action of potential and gyroscopic forces admitting a common axis of symmetry [6].

3.2. Second New Integrable Problem. In this subsection, we solve the basic equations in the case in which $a_2 = 0$ taking into account the conditions.

Theorem 2. *Let the inertia matrix of a rigid body be $I = diag(2C, 2C, C)$, and assume this body be in motion under the action of a combination of following potential and gyroscopic forces which are characterized by $V and \mu$, respectively,*

$$V = \kappa\left[2\,d\gamma_1\gamma_2 + c\left(\gamma_1^2 - \gamma_2^2\right)\right] + \frac{\lambda}{\gamma_3^2} + \rho\left(\frac{1}{\gamma_3^4} - \frac{1}{\gamma_3^6}\right) - \frac{K\nu\gamma_3^2}{\gamma_1^2}\left[2c\gamma_1\gamma_2 + d\left(\gamma_2^2 - \gamma_1^2\right)\right] + \frac{\nu^2\gamma_3^2\left(\gamma_3^2 - 2\right)}{2\gamma_1^2} + K^2\left[2\,dc\,\gamma_1\gamma_2\left(\gamma_1^2 - \gamma_2^2\right) + \frac{d^2}{2}\left(\gamma_3^2 + 4\gamma_1^2\gamma_2^2\right) - c^2\left(\gamma_3^2\left(\gamma_1^2 + \gamma_2^2\right) + 2\gamma_1^2\gamma_2^2\right)\right], \tag{79}$$

$$\boldsymbol{\mu} = (2\gamma_3)\left(K\left(c\gamma_2 - d\gamma_1\right) - \frac{\nu\left(1 + \gamma_2^2\right)}{g_1^3}\right), 2\gamma_3\left(K\left(c\gamma_1 + d\gamma_2\right) + \frac{\nu\gamma_2^2}{\gamma_1^2}\right), K\left(2c\gamma_1\gamma_2 + d\left(\gamma_2^2 - \gamma_1^2\right) + \nu\frac{\left(2 - \gamma_3^2\right)}{\gamma_1^2}\right), \tag{80}$$

or, equivalently,

$$\mathbf{l} = \left(\mathbf{0}, \mathbf{0}, K\left[2c\gamma_1\gamma_2 + d\left(\gamma_2^2 - \gamma_1^2\right] + \nu\frac{\left(2 - \gamma_3^2\right)}{\gamma_1^2}\right)\right), \tag{81}$$

where $c, d, \kappa, K, \lambda, \rho, and \nu$ are the arbitrary parameters. Then, the Euler-Poisson equation (2) with the two expressions (79) and (80) is completely integrable on a zero level of the cyclic integral:

$$I_1 = 2\left(p\gamma_1 + q\gamma_2\right) + \left(r + K\left[2c\gamma_1\gamma_2 + d\left(\gamma_2^2 - \gamma_1^2\right] + \nu\frac{\left(2 - \gamma_3^2\right)}{\gamma_1^2}\gamma_3\right]. \tag{82}$$

Its additional integral takes the form

$$I_2 = \left[p^2 - q^2 + \gamma_3^2\left(K\,dr + c\kappa\right) + cK^2\gamma_3^2\left(c\left(\gamma_1^2 - \gamma_2^2\right) + 2\,d\gamma_1\gamma_2\right) - \lambda\frac{\left(\gamma_1^2 - \gamma_2^2\right)}{\gamma_3^2}\right]^2 + \left[2pq + d\kappa\gamma_3^2 - \gamma_3^2\left[Kcr - dK^2\left(c\left(\gamma_1^2 - \gamma_2^2\right) + 2\,d\gamma_1\gamma_2\right) - \frac{2\lambda\gamma_1^2\gamma_2^2}{\gamma_3^2} - dK^2\left(c\left(\gamma_1^2 - \gamma_2^2\right) + 2\,d\gamma_1\gamma_2\right) - \frac{2\lambda\gamma_1^2\gamma_2^2}{\gamma_3^2}\right]^2 - \frac{\nu^2\left(\gamma_1^2 + \gamma_2^2\right)^2}{\gamma_1^8\gamma_3^4}\left[2\gamma_1^4\left(\rho + \lambda\gamma_3^4\right) - \nu^2\gamma_3^2\right] + \frac{4\nu\left(p\gamma_1 + q\gamma_2\right)}{\gamma_1^2} \times \left[\frac{\nu^2\gamma_3^3\left(\gamma_1^2 + \gamma_1^2\right)}{\gamma_1^4} + \frac{\left(\gamma_3^2 - 1\right)\left(\gamma_3^4\lambda + \rho\right)}{\gamma_3^5} - 2K^2\left(c^2 + d^2\right)\left(2\gamma_3^2 - 1\right)\gamma_3^3\right] + 2K\left[2c\gamma_1\gamma_2 + d\left(\gamma_2^2 - \gamma_1^2\right)\right]$$

Table 3: Comparison the second new integrable case with previous results.

No.	Authors	Conditions of the parameters	References
1	Yehia and Elmandouh [6]	$\nu = 0$	[6]
2	Goriatchev [55]	$K = \nu = \rho = 0$	[55]
3	Chaplygin [56]	$K = \nu = \lambda = \rho = 0$	[56]

$$\times\left[-\frac{\nu K^2\gamma_3^6\left(c^2+d^2\right)}{\gamma_1^2}-\frac{\rho r}{\gamma_3^4}+\frac{\nu\left(\lambda\gamma_3^4-\rho\right)}{\gamma_1^2\gamma_3^2}+\frac{2\nu^3\gamma_3^4\left(\gamma_1^2+\gamma_2^2\right)}{\gamma_1^6}\right]+2\left(\frac{\rho\kappa}{\gamma_3^4}+\frac{\nu^2\gamma_3^4}{\gamma_1^4}\right)\left[2\,d\gamma_1\gamma_2+c\left(\gamma_1^2-\gamma_2^2\right)\right]$$
$$+2\left(p^2+q^2\right)\left[\frac{\rho\left(\gamma_3^2-1\right)}{\gamma_3^6}+\frac{2\nu\gamma_3\left(p\gamma_1+q\gamma_2\right)}{\gamma_1^2}+\frac{4\nu K\gamma_3^2\left(c\gamma_2-d\gamma_1\right)}{\gamma_1}\right]$$
$$+\rho\left[\frac{\left(\rho-2\lambda\gamma_3^4\right)\left(1-\gamma_3^2\right)^2}{\gamma_3^{12}}+\frac{2K^2}{\gamma_3^4}\left[c^2\left(1-2\gamma_3^2\right)-4\gamma_1\gamma_2\left(c\gamma_2-d\gamma_1\right)\left(c\gamma_1+d\gamma_2\right)\right]\right]$$
$$+\frac{\nu^2\gamma_3^2}{\gamma_1^4}\left[K^2\left(c^2+d^2\right)\gamma_3^2\left(5\gamma_3^2-8\gamma_3^2+2\right)+4K\gamma_3\left(\gamma_1^2+\gamma_2^2\right)\times\left((4cq-dp)\gamma_1+\gamma_2\left(2cp+3\,dq\right)\right)\right.$$
$$\left.-2\gamma_1^2\left[4K\gamma_3\left((c\gamma_1+d\gamma_2)q+(d\gamma_1-c\gamma_2)p\right)+2\left(q^2-p^2\right)-\left(\gamma_1^2+\gamma_2^2\right)\times\left(p^2+3q^2\right)-4pq\gamma_1\gamma_2\right]\right]$$
$$-\frac{2\nu\gamma_3^2}{\gamma_1^4}\left[K\gamma_3^2\left(6cpq+d\left(5q^2-p^2\right)\right)+2\left(cp+dq\right)\left(\kappa\gamma_1\gamma_3+2Kq\right)\left(cp+dq\right)-4\kappa\gamma_2\gamma_3\left(cq-dp\right)\right]. \tag{83}$$

Theorem 2 introduces a new integrable problem in the dynamics of a rigid body. Furthermore, it represents an extension for the related previous results. It adds to the case that was discovered by Yehia and Elmandouh in 2013, one arbitrary parameter ν [6]. It modifies the case introduced by Goriatchev in 1916 by inserting three parameters $K, \nu,$ and ρ [55]. It generalizes the Chaplygin case that was found in 1903 by entering four arbitrary parameters $\nu, \rho, \lambda,$ and K [56]. The comparisons with previous results are summarized in Table 3.

4. Conclusion

In the current work, we had interest in studying the integrability issue of the motion of a rigid body about a fixed point under the action of potential and gyroscopic forces having a common axis of symmetry. We have assumed this problem has a complementary quartic integral in the velocities. We have applied the method by Yehia. The basic equations have been formulated and introduced in a general setting. But as it is outlined in the literature, in the case of the existence of gyroscopic forces, the basic equations have not been solved in a general setting, but it is usually solved for certain values of the parameters leading to the metric of a rigid body dynamics which are valuable and significant problems. We have announced two new integrable problems generalizing the Chaplygin case in a rigid body and its subsequent works by different authors such as Goriatchev, Yehia and Elmandouh, and Elmandouh. The comparison of new results with previous ones is summarized and collected in Tables 2 and 3.

Appendix

A. Time Transformation

Consider Lagrangian in the form

$$L \coloneqq \frac{\Lambda}{2}\left(\dot{x}^2+\dot{y}^2\right)+l_1\dot{x}+l_2\dot{y}-V, \tag{A.1}$$

where $\Lambda, l_1, l_2,$ and V are the functions in x *and* y variables. Lagrangian (A.1) has a Jacobi integral in the form

$$I_1=\frac{\Lambda}{2}\left(\dot{x}^2+\dot{y}^2\right)+V=h, \tag{A.2}$$

where h is the value of the Jacobi integral. Performing the time transformation,

$$\mathrm{d}t=\Lambda\mathrm{d}\tau, \tag{A.3}$$

to the Lagrangian (A.1), we obtain

$$L_0=\frac{1}{2}\left(x'^2+y'^2\right)+l_1x'+l_2y'+\Lambda(h-V), \tag{A.4}$$

where dash refers to the derivative with respect to the fictitious time τ. The Lagrangian (A.4) has a Jacobi integral in the form

$$I_2=\frac{1}{2}\left(x'^2+y'^2\right)-\Lambda(h-V)=h', \tag{A.5}$$

where h' is the value of the Jacobi integral for Lagrangian (A.5). Doing the inverse of the time transformation (A.2) to the Jacobi integral (A.5), we get

$$I_3 = \frac{\Lambda}{2}\left(\dot{x}^2 + \dot{y}^2\right) + V = \frac{h\prime}{V} + h. \tag{A.6}$$

The two integrals of the motion (A.3) and (A.6) are identical if $h\prime = 0$. Thus, the two Lagrangian L and L_0 are equivalent on the zero level of the Jacobi integral for the second one.

B. Coefficients of Equations (60) and (61)

$$\begin{aligned}
\mathscr{F}_0(p) &= -\frac{1}{2}a_1^4\left\{f_{13}f\Omega_1 + q_3 m\frac{\mathrm{d}f}{\mathrm{d}p} + 2fq_3 m - 4Tm + q_3 f\frac{\mathrm{d}m}{\mathrm{d}p} - 16fm\Omega_1\right\}\sin 4\xi \\
&\quad + \frac{a_1a_2a_3}{16}\left\{2ff_0\nu\frac{\mathrm{d}q_1}{\mathrm{d}p} + q_1f_0f\frac{\mathrm{d}\nu}{\mathrm{d}p} - 16ff_{10}\Omega_0 - 16G\nu - 8q_2f\frac{\mathrm{d}\nu}{\mathrm{d}p} + 256f\nu\Omega_0 - 8ff_9\Omega_1 - 16f\nu\frac{\mathrm{d}q_2}{\mathrm{d}p} - 8q_2\nu\frac{\mathrm{d}f}{\mathrm{d}p}\right. \\
&\quad \left. + q_1\nu f\frac{\mathrm{d}f_0}{\mathrm{d}p} - 32pf_0\nu + q_1f_0\nu\frac{\mathrm{d}f}{\mathrm{d}p}\right\}, \\
\mathscr{F}_1(p) &= \frac{1}{2}a_3\left\{-4fu\frac{\mathrm{d}q_1}{\mathrm{d}p} - 2q_1u\frac{\mathrm{d}f}{\mathrm{d}p} - 4\nu P_0 - 2q_1f\frac{\mathrm{d}u}{\mathrm{d}p} + a_1^2\left(16f\nu\Omega_1 + 64pm - 2T\nu - q_1f\frac{\mathrm{d}m}{\mathrm{d}p} - 2fm\frac{\mathrm{d}q_1}{\mathrm{d}p} - 2f\nu\frac{\mathrm{d}q_3}{\mathrm{d}p}\right.\right. \\
&\quad \left.\left. - q_3f\frac{\mathrm{d}\nu}{\mathrm{d}p} - q_1m\frac{\mathrm{d}f}{\mathrm{d}p} - q_3\nu\frac{\mathrm{d}f}{\mathrm{d}p} - 2ff_{10}\Omega_1\right) - 2a_2^2ff_9\Omega_0\right\}, \\
\mathscr{F}_2(p) &= -\frac{a_1a_2a_3}{16}\left\{16\nu G - q_1ff_0\frac{\mathrm{d}\nu}{\mathrm{d}p} - 8q_2f\frac{\mathrm{d}\nu}{\mathrm{d}p} - 2ff_0\nu\frac{\mathrm{d}q_1}{\mathrm{d}p} - q_1\nu f_0\frac{\mathrm{d}f}{\mathrm{d}p} - q_1\nu f\frac{\mathrm{d}f_0}{\mathrm{d}p} - 8q_2\nu\frac{\mathrm{d}f}{\mathrm{d}p} - 32pf_0\nu + 16f_{10}f\Omega_0\right. \\
&\quad \left. + 256\nu\Omega_0 - 16\nu f\frac{\mathrm{d}q_2}{\mathrm{d}p} + 8ff_9\Omega_1\right\}, \\
\mathscr{F}_3(p) &= -\frac{a_1a_2}{16}\left\{-a_1^2q_3f_0\nu\frac{\mathrm{d}f}{\mathrm{d}p} + 2ff_0\nu\frac{\mathrm{d}q_3}{\mathrm{d}p} + 32Gm + q_3ff_0\frac{\mathrm{d}\nu}{\mathrm{d}p} - 16ff_0\nu\Omega_1 + 2T\nu\right\}, \\
\mathscr{F}_4(p) &= -\frac{1}{2}a_1^2a_3\left\{2fm\frac{\mathrm{d}q_1}{\mathrm{d}p} + 64pm - q_3\nu\frac{\mathrm{d}f}{\mathrm{d}p} + q_1f\frac{\mathrm{d}m}{\mathrm{d}p} + ff_{10}\Omega_1 - 2f\nu\frac{\mathrm{d}q_3}{\mathrm{d}p} - q_3f\frac{\mathrm{d}\nu}{\mathrm{d}p} + 16f\nu\Omega_1 + q_1mf\frac{\mathrm{d}f}{\mathrm{d}p}\right. \\
&\quad \left. + 2Tf_0\nu - 16q_2u\frac{\mathrm{d}f}{\mathrm{d}p} - 8ff_{12}\Omega_1 + 8q_2f\frac{\mathrm{d}m}{\mathrm{d}p} - 16fq_2\frac{\mathrm{d}u}{\mathrm{d}p} + 16fm\frac{\mathrm{d}q_2}{\mathrm{d}p} + q_3\nu f\frac{\mathrm{d}f_0}{\mathrm{d}p} + 8q_2m\frac{\mathrm{d}f}{\mathrm{d}p} - 256fm\Omega_0\right\} \\
&\quad + 16q_2f\frac{\mathrm{d}u}{\mathrm{d}p} + 16ff_{11}\Omega_0 - 512fu\Omega_0 + 32fu\frac{\mathrm{d}q_2}{\mathrm{d}p}, \\
\mathscr{F}_5(p) &= -\frac{1}{16}\left\{a_1^2\left(16q_3f\frac{\mathrm{d}u}{\mathrm{d}p} + 8f_{11}f\Omega_1 + 16q_3u\frac{\mathrm{d}f}{\mathrm{d}p} - 64P_0m - 256fu\Omega_1 + 32fu\frac{\mathrm{d}q_3}{\mathrm{d}p}\right)\right. \\
&\quad + a_3^2\left(8q_1\nu\frac{\mathrm{d}f}{\mathrm{d}p} + 16f\nu\frac{\mathrm{d}q_1}{\mathrm{d}p} + 256p\nu + 8q_1f\frac{\mathrm{d}\nu}{\mathrm{d}p}\right) + a_1^2a_2^2\left(16ff_{12}\Omega_0 - q_2f_0f\frac{\mathrm{d}\nu}{\mathrm{d}p} + 2G\nu f_0 - 2ff_0\nu\frac{\mathrm{d}q_2}{\mathrm{d}p}\right. \\
&\quad \left.\left. + 32ff_0\nu\Omega_0 - q_2f_0\nu\frac{\mathrm{d}f}{\mathrm{d}p} - q_2\nu f\frac{\mathrm{d}f_0}{\mathrm{d}p}\right) + 8a_1^4ff_{13}\Omega_1\right\}, \\
\mathscr{F}_6(p) &= -\frac{a_2a_1^3}{16}\left\{-q_3f_0\nu\frac{\mathrm{d}f}{\mathrm{d}p} + 8q_2m\frac{\mathrm{d}f}{\mathrm{d}p} - 256fm\Omega_0 + 16ff_{13}\Omega_0 + 8q_2f\frac{\mathrm{d}m}{\mathrm{d}p} + 16ff_0\nu\Omega_1 + 16fm\frac{\mathrm{d}q_2}{\mathrm{d}p} - 32Gm - q_3f_0f\frac{\mathrm{d}\nu}{\mathrm{d}p}\right. \\
&\quad \left. + 2Tf_0\nu + 8f_{12}f\Omega_1 - q_3\nu f\frac{\mathrm{d}f_0}{\mathrm{d}p} - 2ff_0\nu\frac{\mathrm{d}q_3}{\mathrm{d}p}\right\}, \\
\mathscr{F}_7(p) &= \frac{a_1}{2}\left\{\left(2f_8 + a_1^2a_2f_4\right)\Omega_1 + \left(f_3\Omega_0 + a_2a_1^3\left(q_2m - \frac{1}{16}q_3f_0\nu\right)\right)\right\}, \\
\mathscr{F}_8(p) &= \frac{1}{16}\left\{8a_1^4f_5\Omega_1 + a_1^2a_2^2q_2f_0\nu + 16a_1^2a_2^2f_4\Omega_0 - 8a_3^2q_1\nu + 8a_1f_3\Omega_1\right\}, \\
\mathscr{F}_9(p) &= -a_2a_1^3\left\{q_2m - \frac{1}{2}f_4\Omega_1 - \frac{1}{16}q_3f_0\nu - f_5\Omega_0\right\}.
\end{aligned} \tag{B.1}$$

Data Availability

No data were used to support this study.

Conflicts of Interest

The authors declare that they have no conflicts of interest.

Acknowledgments

The authors acknowledge the Deanship of Scientific Research at King Faisal University for the financial support under the annual research project (Grant No. 180100).

References

[1] O. Babelon, D. Bernard, and M. Talon, *Introduction to Classical Integrable Systems*, Cambridge University Press, Cambridge, UK, 2003.

[2] M. . Tabor, *Chaos and Integrability in Nonlinear Dynamics*, Wiley, NewYork, NY, USA, 1988.

[3] A. A. Elmandouh, "New integrable problems in rigid body dynamics with quartic integrals," *Acta Mechancia*, vol. 226, Article ID 246172, 2015.

[4] A. A. Elmandouh, "New integrable problems in the dynamics of particle and rigid body," *Acta Mechancia*, vol. 226, pp. 2461–2472, Article ID 374962, 2015.

[5] H. M. Yehia, "Atlas of two-dimensional irreversible conservative lagrangian mechanical systems with a second quadratic integral," *Journal of Mathematical Physics*, vol. 48, Article ID 082902, 2007.

[6] H. M. Yehia and A. A. Elmandouh, "A new integrable problem with a quartic integral in the Dynamics of a rigid body," *Journal of Physics A: Mathematical and Theoretical*, vol. 46, no. 14, Article ID 142001, 2013.

[7] M. Karlovini, G. Pucacco, K. Rosquist, and L. Samuelsson, "A unified treatment of quartic invariants at fixed and arbitrary energy," *Journal of Mathematical Physics*, vol. 43, Article ID 404159, 2002.

[8] Z. Hu, M. Aldazharova, T. M. Aldibekov, and V. G. Romanovski, "Integrability of 3-dim polynomial systems with three invariant planes," *Nonlinear Dynamics*, vol. 74, Article ID 107792, 2013.

[9] J. Llibre, R. Ramirez, and N. Sadovskaia, "Integrability of the constrained rigid body," *Nonlinear Dynamics*, vol. 73, Article ID 227390, 2013.

[10] J. Llibre, R. D. Oliveira, and C. Valls, "On the integrability and the zero-hopf bifurcation of a Chen-Wang differential system," *Nonlinear Dynamics*, vol. 80, p. 35361, 2015.

[11] J. Bao and Q. Yang, "Darboux integrability of the stretch-twistfold flow," *Nonlinear Dynamics*, vol. 76, Article ID 797807, 2014.

[12] M. F. Lima, J. Llibre, and C. Valls, "Integrability of the rucklidge system," *Nonlinear Dynamics*, vol. 77, Article ID 144153, 2014.

[13] A. A. Elmandouh, "First integrals of motion for two dimensional weight-homogeneous Hamiltonian systems in curved spaces," *Communications in Nonlinear Science and Numerical Simulation*, vol. 75, pp. 220–235, 2019.

[14] T. Bountis, H. Segur, and F. Vivaldi, "Integrable hamiltonian systems and the painlevé property," *Physical Review A*, vol. 25, no. 3, p. 1257, 1982.

[15] S. L. V. Ziglin, "Branching of solutions and nonexistence of first integrals in hamiltonian mechanics," *Functional Analysis and Its Applications*, vol. 16, p. 1819, 1982.

[16] J. J. Morales-Ruiz, *Differential Galois Theory and Non-integrability of Hamiltonian Systems*, Prog. Math. Birkhauser Verlag, Basel, Switzerland, 1999.

[17] J. J. Morales-Ruiz and J. P. Ramis, "A note on the non-integrability of some hamiltonian systems with a homogeneous potential," *Methods and Applications of Analysis*, vol. 8, p. 11320, 2001.

[18] J. J. Morales-Ruiz and J. P. Ramis, "Galoisian obstructions to integrability of hamiltonian systems," *Methods and Applications of Analysis*, vol. 8, p. 3396, 2001.

[19] A. A. Elmandouh, "On the integrability of 2D hamiltonian systems with variable gaussian curvature," *Nonlinear Dynamics*, vol. 93, p. 93343, 2018.

[20] A. A. Elmandouh, "On the integrability of new examples of two-dimensional hamiltonian systems in curved spaces," *Communications in Nonlinear Science and Numerical Simulation*, vol. 90, Article ID 105368, 2020.

[21] V. Volterra, "Sur la théorie des variations des latitudes," *Acta Mathematica*, vol. 22, pp. 201–357, 1899.

[22] A. Gluhovsky and C. Tong, "The structure of energy conserving low-order models," *Physics of Fluids*, vol. 11, no. 2, pp. 334–343, 1999.

[23] P. C. Hughes, *Spacecraft Attitude Dynamics*, Wiely, New york, NY, USA, 1986.

[24] T. Amer and W. Amer, "Substantial condition for the fourth first integral of the rigid body problem," *Mathematics and Mechanics of Solids*, vol. 23, no. 8, pp. 1237–1246, 2018.

[25] T. S. Amer, A. M. Farag, and W. S. Amer, "The dynamicsamical motion of a rigid body for the case of ellipsoid inertia close to ellipsoid of rotation," *Mechanics Research Communications*, vol. 108, Article ID 103583, 2020.

[26] G. V. Gorr, "Invariant relations and particular solutions of the dynamicsamic equations of a rigid body," *Journal of Applied Mathematics and Mechanics*, vol. 81, no. 4, pp. 286–294, 2017.

[27] A. A. Galal, T. S. Amer, H. El-Kafly, and W. S. Amer, "The asymptotic solutions of the governing system of a charged symmetric body under the influence of external torques," *Results in Physics*, vol. 18, Article ID 103160, 2020.

[28] T. S. Amer, A. A. Galal, I. M. Abady, and H. F. Elkafly, "The Dynamicsamical motion of a gyrostat for the irrational frequency case," *Applied Mathematical Modelling*, vol. 89, pp. 1235–1267, 2021.

[29] A. A. Elmandouh, "On the stability of certain motions of a rigid body-gyrostat in an incompressible ideal fluid," *International Journal of Non-linear Mechanics*, vol. 120, Article ID 103419, 2020.

[30] H. M. Yehia, "On the motion of a rigid body acted upon by potential and gyroscopic forces: I. the equations of motion and their transformations," *Journal of Theoretical and Applied*, vol. 5, pp. 747–754, 1986.

[31] M. P. Kharlamov, "Symmetry in systems with gyroscopic forces," *Mekh Tverd Tela*, vol. 15, pp. 87–93, 1983.

[32] E. Leimanis, *The General Problem of Motion of Coupled Rigid Bodies about a Fixed Point*, Springer, Berlin, Germany, 1965.

[33] E. T. Whittaker, *A Treatise on Analytical Dynamics of Particles and Rigid Bodies*, Dover, New York, NY, USA, 1944.

[34] A. V. Borisov and I. S. Mamaev, *Rigid-BodyDynamics–HamiltonianMethods, Integrability Chaos*, Institute of Computer Science, Moscow, Russia, in Russian, 2005.

[35] H. Yehia, "New integrable cases in the dynamics of rigid bodies," *Mechanics Research Communications*, vol. 13, no. 3, pp. 169–172, 1986.
[36] L. Gavrilov, "Non-integrability of the equations of heavy gyrostat," *Compositio Mathematica*, vol. 82, p. 27591, 1992.
[37] G. R. Kirchhoff, "Über die bewegung eines körpers in einer flüssigkeit," *Journal für die reine und angewandte Mathematik*, vol. 1870, no. 71, 2009.
[38] A. Clebsch, "Über die bewegung eines körpers ineiner flüssigkeit," *Mathematische Annalen*, vol. 238, no. 3, 1871.
[39] H. Lamb, *HydroDynamics*, Dover Publ., New York, NY, USA, 6th edition, 1945.
[40] H. M. Yehia, "On the motion of a rigid body acted upon by potential and gyroscopic forces.II: a new form of the equations of motion of a multiconnected rigid body in an ideal incompressible fluid," *Journal of Mecanical and Theoretical Application*, vol. 5, Article ID 755762, 1986.
[41] H. M. Yehia, "Geometric transformations and new integrable problems of rigid body Dynamics," *Journal of Physics A: Mathematical and General*, vol. 33, no. 23, p. 4393, 2000.
[42] H. M. Yehia, "On the integrability of certain problems in particle and rigid body in an axisymmetric field," *Journal of Mecanical and Theoretical Application*, vol. 5, pp. 55–71, 1986.
[43] H. M. Yehia, "The master integrable two-dimensional system with a quartic second integral," *Journal of Physics A: Mathematical and General*, vol. 39, no. 20, pp. 5807–5824, 2006.
[44] H. M. Yehia, "Generalized natural mechanical systems of two degrees of freedom with quadratic integrals," *Journal of Physics A: Mathematical and General*, vol. 25, Article ID 197221, 1992.
[45] H. M. Yehia, "On certain two dimensional conservative mechanical system with cubic second integral," *Journal of Physics A: Mathematical and General*, vol. 35, Article ID 94699487, 2002.
[46] A. A. Elmandouh, "New integrable problems in a rigid body Dynamics with cubic integral in velocities," *Results in Physics*, vol. 8, pp. 559–568, 2018.
[47] H. M. Yehia and A. A. Elmandouh, "Integrable 2D time-irreversible systems with a cubic second integral," *Advances in Mathematical Physics*, vol. 2016, Article ID 8958747, 10 pages, 2016.
[48] H. M. Yehia and A. A. Elmandouh, "A new conditional integrable case in the dynamics of a rigid body-gyrostat," *Mechanics Research Communications*, vol. 78, pp. 25–27, 2016.
[49] H. M. Yehia and A. A. Elmandouh, "New conditional integrable cases of motion of a rigid body with kovalevskaya's configuration," *Journal of Physics A: Mathematical and Theoretical*, vol. 44, Article ID 012001, 2011.
[50] G. D. Birkhoff, *Dynamicsamical Systems*, American Mathematical Society, New York, NY, USA, 1927.
[51] H. M. Yehia, "Kovalevskaya's integrable case: generalizations and related new results," *Regular and Chaotic Dynamics*, vol. 8, no. 3, pp. 337–348, 2003.
[52] H. M. Yehia and N. Bedwihy, "Certain generalization of kovalevskaya's case," *Mansoura Science Bulletin*, vol. 14, pp. 373–386, 1987.
[53] H. M. Yehia, "Two-dimensional conservative mechanical systems with quartic second integral," *Regular and Chaotic Dynamics*, vol. 11, no. 1, pp. 103–122, 2006.
[54] H. M. Yehia, "New integrable problems in the dynamics of rigid bodies with the kovalevskaya configuration. I - the case of axisymmetric forces," *Mechanics Research Communications*, vol. 23, no. 5, pp. 423–427, 1996.
[55] D. N. Goriatchev, "New case of integrability of the euler dynamicsamical equations," *Varshav University of Izvest*, vol. 3, pp. 1–13, 1916.
[56] S. A. Chaplygin, "A new partial solution of the problem of motion of a rigid body in a liquid," *Trudy Otdel Fiz Nauk Obsh Lyub Estimation*, vol. 11, pp. 7–11, 1903.

Hindawi
Advances in Astronomy
Volume 2020, Article ID 6629183, 12 pages
https://doi.org/10.1155/2020/6629183

Research Article

New Treatment of the Rotary Motion of a Rigid Body with Estimated Natural Frequency

A. I. Ismail [1,2]

[1]*Mechanical Engineering Department, College of Engineering and Islamic Architecture, Umm Al-Qura University, P.O. Box 5555, Makkah, Saudi Arabia*
[2]*Mathematics Department, Faculty of Science, Tanta University, Tanta, P.O. Box 31527, Egypt*

Correspondence should be addressed to A. I. Ismail; aiismail@uqu.edu.sa

Received 6 October 2020; Revised 3 November 2020; Accepted 6 November 2020; Published 7 December 2020

Academic Editor: Juan L. G. Guirao

In this paper, the problem of the motion of a rigid body about a fixed point under the action of a Newtonian force field is studied when the natural frequency $\omega = 0.5$. This case of singularity appears in the previous works and deals with different bodies which are classified according to the moments of inertia. Using the large parameter method, the periodic solutions for the equations of motion of this problem are obtained in terms of a large parameter, which will be defined later. The geometric interpretation of the considered motion will be given in terms of Euler's angles. The numerical solutions for the system of equations of motion are obtained by one of the well-known numerical methods. The comparison between the obtained numerical solutions and analytical ones is carried out to show the errors between them and to prove the accuracy of both used techniques. In the end, we obtain the case of the regular precession type as a special case. The stability of the motion is considered by the phase diagram procedures.

1. Introduction

Consider a rigid body of mass M moves in an asymmetric field around a fixed point O [1]. Let us assume that the surface of its ellipsoid of inertia is optional, as well as the mass center. Let the frame OX, OY, and OZ be a fixed system in space, and the frame Ox, Oy, and Oz is the main axes frame for the surface of the ellipsoid of inertia of the body which moves with the it. Initially, we consider the main axis z for the surface of the ellipsoid of inertia that makes an angle $\xi_0 \neq (k\pi/2)$; $k = 0, 1,$ and 2 with the fixed axis Z in space. Let the body spins with small speed angular velocity r_0 about the axis z. Suppose that $p, q,$ and r represent the components of the angular velocity vector of the body about the main axes of the ellipsoid of the inertia surface; γ, γ', and γ'' are the directional cosines vector of the axis Z; g is the acceleration of gravity; $A, B,$ and C are the principal moments of inertia. The point (x_0, y_0, z_0) is the center of mass in the moving coordinate system; $\underline{R}$ is the position vector of the center of attraction 0_1 on the fixed downward coordinate Z axis, and $\underline{\rho}$ is the position vector of the element dm. Let $\underline{\hat{i}}, \underline{\hat{j}}, \underline{\hat{k}}$, and $\underline{\hat{Z}}$ be the unit vectors in the shown directions (Figure 1). Consider d$\underline{F}$ is the attraction force element due to the attracting center and acted on the element dm at the point $p(x, y, z)$.

2. Formulation of the Problem

Without a loss of generality, we choose the positive direction of both the axis z and the axis x that do not make an obtuse angle ξ_0 with the direction of axis Z. Under the restriction on ξ_0 and the choice of the coordinate system, we get [2]

$$\gamma_0 \geq 0, \quad 0 < \gamma_0'' < 1. \tag{1}$$

The differential equations of motion can be reduced to an autonomous system of two degrees of freedom and one first integral as follows [3]:

$$\begin{aligned} 4\ddot{p}_2 + p_2 &= 4\varepsilon^{-2} F(p_2, \dot{p}_2, \gamma_2, \dot{\gamma}_2, \varepsilon), \\ \ddot{\gamma}_2 + \gamma_2 &= \varepsilon^{-2} \Phi(p_2, \dot{p}_2, \gamma_2, \dot{\gamma}_2, \varepsilon), \end{aligned} \tag{2}$$

$$\gamma_2^2 + \dot{\gamma}_2^2 + 2\varepsilon^{-1}(\nu p_2 \gamma_2 + \nu_2 \dot{p}_2 \dot{\gamma}_2 + s_{21}) + \varepsilon^{-2}(\ldots) = \gamma_0''^{-2} - 1, \tag{3}$$

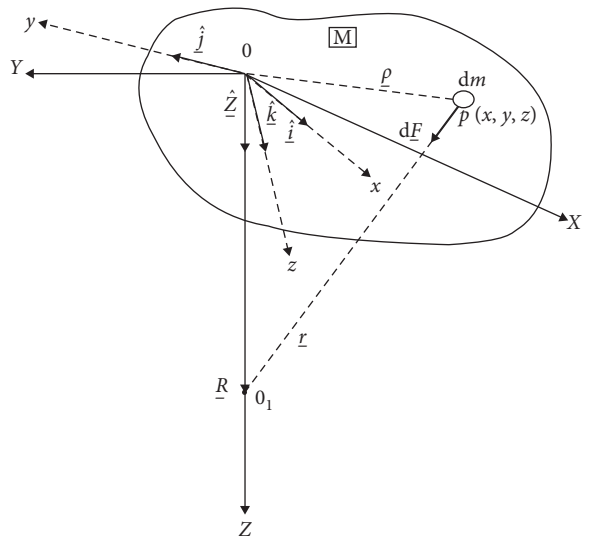

Figure 1: Description of motion in terms of moving and fixed frames.

where

$$\begin{aligned}
F &= C_1 A_1^{-1} p_2 \dot{p}_2^2 + x_0' \dot{p}_2 \dot{\gamma}_2 - y_0' a^{-1} p_2 \dot{\gamma}_2 \\
&\quad - y_0' A_1^{-1} \left(A_1 + a^{-1}\right) \gamma_2 \dot{p}_2 - z_0' a^{-1} p_2 \\
&\quad - 0.75 \nu e_1 p_2 - 0.25 p_2 s_{11} + A_1 b^{-1} x_0' s_{21} + O\left(\varepsilon^{-1}\right) + \cdots, \\
\Phi &= -(1 - C_1) A_1^{-1} p_2 \dot{p}_2 \dot{\gamma}_2 + x_0' \dot{\gamma}_2^2 - y_0' \gamma_2 \dot{\gamma}_2 - z_0' b^{-1} \gamma_2 \\
&\quad + x_0' b^{-1} - A_1^{-2} \gamma_2 \dot{p}_2^2 \\
&\quad + 0.75 \nu \left(e + e_1 \gamma_2\right) - \gamma_2 s_{11} \\
&\quad + \left(1 + B_1\right) p_2 s_{21} + O\left(\varepsilon^{-1}\right) + \cdots,
\end{aligned} \tag{4}$$

$$\begin{aligned}
p_2 &= p_1 - \varepsilon^{-1} \left(e + e_1 \gamma_2\right), \\
\gamma_2 &= \gamma_1 - \varepsilon^{-1} \nu p_2, \\
q_1 &= -A_1^{-1} \dot{p}_2 + \varepsilon^{-1} A_1^{-1} \left(y_0' a^{-1} - e_2 \dot{\gamma}_2\right) + \cdots, \\
r_1 &= 1 + 0.5 \varepsilon^{-2} s_{11} + \cdots, \\
\gamma_1' &= \dot{\gamma}_2 + \varepsilon^{-1} \nu_2 \dot{p}_2 + \cdots, \\
\gamma_1'' &= 1 + \varepsilon^{-1} s_{21} + \varepsilon^{-2} \left(s_{22} - 0.5 s_{11}\right) + \cdots,
\end{aligned} \tag{5}$$

$$\begin{aligned}
p_1 &= \frac{p}{c} \sqrt{\gamma_0''}, \\
&\quad \cdot (pq), \\
r_1 &= \frac{r}{r_0}, \\
\gamma_1 &= \frac{\gamma}{\gamma_0''}, \\
&\quad \cdot (\gamma \gamma' \gamma''), \\
\tau &= r_0^{-1} t, \\
&\quad \cdot \left(\cdot \equiv \frac{\mathrm{d}}{\mathrm{d}\tau} \right);
\end{aligned} \tag{6}$$

$$\begin{aligned}
s_{11} &= \frac{a\left(p_{20}^2 - p_2^2\right) + b\left(\dot{p}_{20}^2 - \dot{p}_2^2\right)}{A_1^2 - 2\left[x_0'\left(\gamma_{20} - \gamma_2\right) + y_0'\left(\dot{\gamma}_{20} - \dot{\gamma}_2\right)\right]}, \\
s_{21} &= a\left(p_{20}\gamma_{20} - p_2\gamma_2\right) - bA_1^{-1}\left(\dot{p}_{20}\dot{\gamma}_{20} - \dot{p}_2\dot{\gamma}_2\right), \\
s_{22} &= a\left[\nu\left(p_{20}^2 - p_2^2\right) + e\left(\gamma_{20} - \gamma_2\right) + e_1\left(\gamma_{20}^2 - \gamma_2^2\right)\right] \\
&\quad + bA_1^{-1}\left[-\nu_2\left(\dot{p}_{20}^2 - \dot{p}_2^2\right) + a^{-1} y_0'\left(\dot{\gamma}_{20} - \dot{\gamma}_2\right) - e_2\left(\dot{\gamma}_{20}^2 - \dot{\gamma}_2^2\right)\right],
\end{aligned} \tag{7}$$

$$\begin{aligned}
A_1 &= \frac{C - B}{A}, \\
&\quad (ABC), \\
a &= \frac{A}{C}, \\
&\quad (ab), \\
c^2 &= \frac{Mgl}{C}, \\
\varepsilon &= \frac{c\sqrt{\gamma_0''}}{r_0}, \\
x_0 &= l x_0', \\
&\quad (xyz), \\
l^2 &= x_0^2 + y_0^2 + z_0^2, \\
4A_1B_1 &= -1, \\
eb &= 4x_0' A_1, \\
3\nu &= 4\left(1 + B_1\right), \\
3e_1 &= 4z_0'\left(A_1 b^{-1} - a^{-1}\right), \\
e_2 &= e_1 + a^{-1} z_0', \\
\nu_2 &= \nu - A_1^{-1}.
\end{aligned} \tag{8}$$

The symbols like ABC are abbreviated equations.

3. Construction of Periodic Solutions with Zeros Basic Amplitudes

In this section, we use the suggested method for constructing the aimed solutions for the autonomous system (2). Consider the condition [4]

$$p_2(0,0) = \dot{p}_2(0,0) = \dot{\gamma}_2(0,\varepsilon) = 0. \tag{9}$$

The generating system for (2) is obtained when $\varepsilon \longrightarrow \infty$ as follows:

$$\begin{aligned}
4\ddot{p}_2^{(0)} + p_2^{(0)} &= 0, \\
\ddot{\gamma}_2^{(0)} + \gamma_2^{(0)} &= 0.
\end{aligned} \tag{10}$$

The solutions for system (10) with a period $T_0 = 4\pi$ are

$$\begin{aligned}
p_2^{(0)} &= a_0^* \cos(0.5\tau), \\
\gamma_2^{(0)} &= b_0^* \cos\tau,
\end{aligned} \tag{11}$$

where a_0^* and b_0^* are constants.

Let system (2) has periodic solutions with a period $T_0 + \alpha$ in the form [5]

$$p_2 = a^* \cos\psi + \sum_{n=1}^{N} \varepsilon^{-n} p_n^*(a^*, \psi) + O\left(\varepsilon^{-N-1}\right),$$
$$\gamma_2 = b^* \cos\phi + \sum_{n=1}^{N} \varepsilon^{-n} \gamma_n^*(a^*, \phi) + O\left(\varepsilon^{-N-1}\right). \tag{12}$$

For these solutions, we let the initial conditions

$$p_2(0,\varepsilon) = a^* = a_0^* + a^*(\varepsilon),$$
$$\gamma_2(0,\varepsilon) = b^* = b_0^* + b^*(\varepsilon), \tag{13}$$
$$\dot{\gamma}_2(0,\varepsilon) = 0.$$

Here, $a^*(\varepsilon), b^*(\varepsilon) \longrightarrow 0$ at $\varepsilon \longrightarrow \infty$. Considering first integral (3) with conditions (13), we get

$$0 < b_0^* = \left(1 - \gamma_0''^2\right)^{1/2} \left(\gamma_0''\right)^{-1} < \infty,$$
$$b^*(\varepsilon) = -\varepsilon^{-1}\nu\left[a_0^* + a^*(\varepsilon)\right] + \cdots. \tag{14}$$

Let a^*, ψ, and ϕ are changed with time according to

$$\dot{a}^* = \sum_{n=1}^{N} \varepsilon^{-n} A_n^*(a^*) + O\left(\varepsilon^{-N-1}\right), \tag{15}$$

$$\dot{\psi} = 0.5 + \sum_{n=1}^{N} \varepsilon^{-n} \psi_n(a^*) + O\left(\varepsilon^{-N-1}\right), \tag{16}$$

$$\dot{\phi} = 1 + \sum_{n=1}^{N} \varepsilon^{-n} \phi_n(a^*) + O\left(\varepsilon^{-N-1}\right). \tag{17}$$

The following derivatives are obtained:

$$\dot{p}_2 = -0.5a^* \sin\psi + O\left(\varepsilon^{-1}\right),$$
$$\dot{\gamma}_2 = -b^* \sin\phi + O\left(\varepsilon^{-1}\right),$$
$$\ddot{p}_2 = -0.25a^* \cos\psi + \varepsilon^{-1}\left[0.25\frac{\partial^2 p_1^*}{\partial\psi^2} - a^*\psi_1 \cos\psi - A_1^* \sin\psi\right]$$
$$+ \varepsilon^{-2}\left[A_1^*\frac{\partial^2 p_1^*}{\partial a^* \partial\psi} - \left(A_2^* + 2A_1^*\psi_1\right)\sin\psi + A_1^*\frac{dA_1^*}{da^*}\cos\psi + 0.25\frac{\partial^2 p_2^*}{\partial\psi^2} + \psi_1\frac{\partial^2 p_1^*}{\partial\psi^2} - a^*\left(\psi_1^2 + 2\psi_2\right)\cos\psi - a^* A_1^* \sin\psi\frac{d\psi_1}{da^*}\right] + O\left(\varepsilon^{-3}\right),$$
$$\ddot{\gamma}_2 = -b^* \cos\phi + \varepsilon^{-1}\left[\frac{\partial^2 \gamma_1^*}{\partial\phi^2} - 2b^*\phi_1 \cos\phi\right]$$
$$+ \varepsilon^{-2}\left[\frac{\partial^2 \gamma_2^*}{\partial\phi^2} + 2\phi_1\frac{\partial^2 \gamma_1^*}{\partial\phi^2} - b^*\left(\phi_1^2 + 2\phi_2\right)\cos\phi + 2A_1^*\frac{\partial^2 \gamma_1^*}{\partial a^* \partial\phi} - b^* A_1^*\frac{d\phi_1}{da^*}\sin\phi\right] + O\left(\varepsilon^{-3}\right). \tag{18}$$

Using equations (7), (12), and (18), we get

$$s_{11}^{(0)} = a a_0^{*2}\left(\cos^2\psi_0 - \cos^2\psi\right) - 0.25bA_1^{-2}a_0^{*2}\sin^2\psi$$
$$- 2b_0^*\left[x_0'\left(\cos\phi_0 - \cos\phi\right) + y_0'\sin\phi\right],$$
$$s_{21}^{(0)} = a_0^* b_0^*\left[a\left(\cos\psi_0\cos\phi_0 - \cos\psi\cos\phi\right) + 0.5bA_1^{-1}\sin\psi\sin\phi\right], \tag{19}$$
$$s_{22}^{(0)} = a\left[\nu a_0^{*2}\left(\cos^2\psi_0 - \cos^2\psi\right) + eb_0^*\left(\cos\phi_0 - \cos\phi\right) + e_1 b_0^{*2}\left(\cos^2\phi_0 - \cos^2\phi\right)\right]$$
$$+ bA_1^{-1}\left[0.25\nu_2 a_0^{*2}\sin^2\psi + a^{-1}y_0' b_0^*\sin\phi + e_2 b_0^{*2}\sin^2\phi\right],$$

Using (4), (12), (18), and (19), we obtain

where ψ_0 and ϕ_0 are the initial values of the corresponding functions.

$$
\begin{aligned}
F^{(0)} &= 0.25C_1A_1^{-1}a_0^{*3}\cos\psi\sin^2\psi + 0.5a_0^*b_0^*x_0'\sin\psi\sin\phi \\
&\quad + a^{-1}a_0^*b_0^*y_0'\cos\psi\sin\phi + 0.5A_1^{-1}\left(A_1 + a^{-1}\right)a_0^*b_0^*y_0'\sin\psi\cos\phi \\
&\quad - z_0'a^{-1}a_0^*\cos\psi - 0.75\nu e_1a_0^*\cos\psi \\
&\quad - 0.25a_0^*\cos\psi\left\{aa_0^{*2}\left(\cos^2\psi_0 - \cos^2\psi\right) - 0.25bA_1^{-2}a_0^{*2}\sin^2\psi - 2b_0^*\left[x_0'\left(\cos\phi_0 - \cos\phi\right) + y_0'\sin\phi\right]\right\} \\
&\quad + A_1b^{-1}x_0'a_0^*b_0^*\left[a\left(\cos\psi_0\cos\phi_0 - \cos\psi\cos\phi\right) + 0.5bA_1^{-1}\sin\psi\sin\phi\right], \\
\Phi^{(0)} &= 0.25\left(C_1 - 1\right)A_1^{-1}a_0^{*2}b_0^*\sin 2\psi\sin\phi + 0.5x_0'b_0^{*2}\left(1 - \cos 2\phi\right) \\
&\quad + 0.5y_0'b_0^{*2}\sin 2\phi - z_0'b^{-1}b_0^*\cos\phi + x_0'b^{-1} \\
&\quad - 0.125A_1^{-2}a_0^{*2}b_0^*\left(1 - \cos 2\psi\right)\cos\phi + 0.75\nu e + 0.75\nu e_1b_0^*\cos\phi \\
&\quad - aa_0^{*2}b_0^*\cos^2\psi_0\cos\phi + 0.5aa_0^{*2}b_0^*\left(1 + \cos 2\psi\right)\cos\phi \\
&\quad + 0.125bA_1^{-2}a_0^{*2}b_0^*\left(1 - \cos 2\psi\right)\cos\phi + 2x_0'b_0^{*2}\cos\phi_0\cos\phi \\
&\quad - x_0'b_0^{*2}\left(1 + \cos 2\phi\right) + y_0'b_0^{*2}\sin 2\phi \\
&\quad + a_0^{*2}b_0^*\left(1 + B_1\right)\left[0.5bA_1^{-1}\sin\psi\sin\phi + a\left(\cos\psi_0\cos\phi_0 - \cos\psi\cos\phi\right)\right]\cos\psi.
\end{aligned}
\tag{20}
$$

Substituting from (12), (18), and (20) into (2) and equating coefficients of ε^{-1} in both sides, we get

$$
\begin{aligned}
&\frac{\partial^2 p_1^*}{\partial\psi^2} + p_1^* = 4a_0^*\psi_1\cos\psi + 4A_1^*\sin\psi, \\
&\frac{\partial^2 \gamma_1^*}{\partial\phi^2} + \gamma_1^* = 2b_0^*\phi_1\cos\phi, \\
&\frac{\partial^2 p_2^*}{\partial\psi^2} + p_2^* = 4A_2^*\sin\psi + a_0^*\left[4\psi_2 + 0.25C_1A_1^{-1}a_0^{*2} - 3.25aa_0^{*2} - 4z_0'a^{-1} - 3\nu e_1 + 0.125bA_1^{-2}a_0^{*2} + 2x_0'b_0^*\cos\phi_0\right]\cos\psi \\
&\qquad + 0.25a_0^{*3}\left(a - C_1A_1^{-1} - 0.25bA_1^{-2}\right)\cos 3\psi + 4aa_0^*x_0'A_1b^{-1}b_0^*\cos\psi_0\cos\phi_0 \\
&\qquad + x_0'a_0^*b_0^*\left(1 - 2aA_1b^{-1}\right)\cos\left(\phi - \psi\right) - x_0'a_0^*b_0^*\left(3 + 2aA_1b^{-1}\right)\cos\left(\phi + \psi\right) \\
&\qquad + y_0'a_0^*b_0^*\left(2a^{-1} - A_1^{-1}a^{-1}\right)\sin\left(\phi - \psi\right) + y_0'a_0^*b_0^*\left(2 + 2a^{-1} + A_1^{-1}a^{-1}\right)\sin\left(\phi + \psi\right), \\
&\frac{\partial^2 \gamma_2^*}{\partial\phi^2} + \gamma_2^* = \left[2\phi_2 - z_0'b^{-1} + 0.125A_1^{-2}a_0^{*2}\left(b - 1\right) + 0.75\nu e_1 - aa_0^{*2}\cos^2\psi_0 - 0.5aB_1a_0^{*2} + 2x_0'b_0^*\cos\phi_0\right]b_0^*\cos\phi \\
&\qquad - 0.5x_0'b_0^{*2} + x_0'b^{-1} + 0.75\nu e + \left(1 + B_1\right)aa_0^{*2}b_0^*\cos\psi_0\cos\phi_0\cos\psi - 0.67x_0'b_0^{*2}\cos 2\phi + 1.5y_0'b_0^{*2}\sin 2\phi \\
&\qquad + 0.5a_0^{*2}\left\{\left[0.25A_1^{-2}\left(1 - b\right) - aB_1 + A_1^{-1}b_0^*\left(b - 1\right)\right]\cos\left(2\psi - \phi\right)\right. \\
&\qquad \left. + \left[0.25A_1^{-2}\left(1 - b\right) - aB_1 - A_1^{-1}b_0^*\left(b - 1\right)\right]\cos\left(2\psi + \phi\right)\right\}.
\end{aligned}
\tag{21}
$$

Canceling singular terms from (21) as in [6], we get

$$\psi_1 = A_1^* = \phi_1 = A_2^* = 0,$$
$$\psi_2 = \left[-0.06C_1A_1^{-1}a_0^{*2} + 0.81aa_0^{*2} + z_0'a^{-1} + 0.75\nu e_1 - 0.02bA_1^{-2}a_0^{*2} - 0.5x_0'b_0^* \cos\phi_0\right], \tag{22}$$
$$\phi_2 = 0.5\left[z_0'b^{-1} - 0.125A_1^{-2}a_0^{*2}(b-1) - 0.75\nu e_1 + aa_0^{*2}\left(0.5B_1 + \cos^2\psi_0\right) - 2x_0'b_0^*\cos\phi_0\right].$$

Substituting from (22) into (15)–(17) and integrating, we obtain

$$a^* = a_0^* \text{ (arbitrary const.)},$$
$$\psi = 0.5\tau + 0.5\varepsilon^{-2}\left[-0.125C_1A_1^{-1}a_0^{*2} - 0.375aa_0^{*2} + 2aa_0^{*2} + 2z_0'a^{-1} + 1.5\nu e_1 - 0.31bA_1^{-2}a_0^{*2} - x_0'b_0^*\cos\phi_0\right]\tau, \tag{23}$$
$$\phi = \tau + 0.5\varepsilon^{-2}\left[z_0'b^{-1} - 0.125A_1^{-2}a_0^{*2}(b-1) - 0.75\nu e_1 + aa_0^{*2}(1 + 0.5B_1) - 2x_0'b_0^*\right]\tau.$$

From the previous results, we get

$$\psi(0) = \psi_0 = 0,$$
$$\phi(0) = \phi_0 = 0. \tag{24}$$

From (13) and (23), we obtain a^* from the order greater than $O(\varepsilon^{-2})$.

The periodic solutions p_2 and γ_2 are obtained by substituting (22) and (23) into (21) and using (12) and (14). Finally, the periodic solutions $p_1, q_1, r_1, \gamma_1, \gamma_1', \text{and } \gamma_1''$ are obtained from (5), (19), (23), and (24).

4. Construction of Periodic Solutions with Nonzeros Basic Amplitudes

We use the large parameter method [7] for constructing the periodic solutions with nonzeros basic amplitudes for system (2) when A<B<C or A>B>C. Consider generating system (10) has periodic solutions with a period $T_0 = 2\pi n$ as follows:

$$p_2^{(0)}(\tau) = E\cos(0.5\tau - \mu),$$
$$\gamma_2^{(0)}(\tau) = M_3\cos\tau, \tag{25}$$

where $E = \sqrt{M_1^2 + M_2^2}$, $\mu = \tan^{-1}(M_2/M_1)$, and M_1, M_2, and M_3 are constants.

Let system (2) has periodic solutions with a period $T_0 + \alpha$ that reduces to generating solutions (21) when $\varepsilon \longrightarrow \infty$, where α is a function of ε such that $\alpha(\infty) = 0$. Consider the following initial conditions:

$$p_2(0,\varepsilon) = \tilde{M}_1,$$
$$\dot{p}_2(0,\varepsilon) = 00.5\tilde{M}_2,$$
$$\gamma_2(0,\varepsilon) = \tilde{M}_3, \tag{26}$$
$$\dot{\gamma}_2(0,\varepsilon) = 0.$$

The notation $\sim$ denotes the following substitution:

$$M_i \longrightarrow \tilde{M}_i = M_i + \beta_i, \quad i = 1, 2, 3, \tag{27}$$

where $\beta_1, 0.5\beta_2$, and β_3 represent the deviations of the initial values of the required solutions from their values of the generating ones M_1, M_2, and M_3, respectively. These deviations are functions of ε and vanish when $\varepsilon \longrightarrow \infty$. Now, we construct the required solutions in the following forms [8]:

$$p_2 = \tilde{E}\cos(\psi - \mu) + \sum_{n=1}^{N}\varepsilon^{-n}p_n^*(\tilde{E}, \psi) + O\left(\varepsilon^{-N-1}\right),$$
$$\gamma_2 = \tilde{M}_3\cos\phi + \sum_{n=1}^{N}\varepsilon^{-n}\gamma_n^*(\tilde{E}, \phi) + O\left(\varepsilon^{-N-1}\right), \tag{28}$$

where p_n^* and γ_n^* are periodic functions in ψ and ϕ, respectively. The quantity $\tilde{M}_3$ is determined from the first integral (3). Let $\tilde{E}, \psi$, and ϕ are changed with time according to

$$\frac{d\tilde{E}}{d\tau} = \sum_{n=1}^{N}\varepsilon^{-n}E_n(\tilde{E}) + O\left(\varepsilon^{-N-1}\right), \tag{29}$$

$$\frac{d\psi}{d\tau} = 0.5 + \sum_{n=1}^{N}\varepsilon^{-n}\psi_n(\tilde{E}) + O\left(\varepsilon^{-N-1}\right), \tag{30}$$

$$\frac{\mathrm{d}\phi}{\mathrm{d}\tau} = 1 + \sum_{n=1}^{N} \varepsilon^{-n}\phi_n(\widetilde{E}) + O\left(\varepsilon^{-N-1}\right). \tag{31}$$

Substituting initial conditions (26) into integral (3), when $\tau = 0$, we deduce that

$$\begin{aligned} 0 < M_3 &= \frac{\sqrt{1-\gamma_0''^2}}{\gamma_0''} < \infty, \\ \beta_3 &= -\varepsilon^{-1}\nu\widetilde{M}_1 + \cdots. \end{aligned} \tag{32}$$

The derivatives become

$$\begin{aligned} \dot{p}_2 &= \frac{\mathrm{d}\widetilde{E}}{\mathrm{d}\tau}\frac{\partial p_2}{\partial \widetilde{E}} + \frac{\mathrm{d}\psi}{\mathrm{d}\tau}\frac{\partial p_2}{\partial \psi}, \\ \dot{\gamma}_2 &= \frac{\mathrm{d}\widetilde{E}}{\mathrm{d}\tau}\frac{\partial \gamma_2}{\partial \widetilde{E}} + \frac{\mathrm{d}\phi}{\mathrm{d}\tau}\frac{\partial \gamma_2}{\partial \phi}, \\ \ddot{p}_2 &= \left(\frac{\mathrm{d}\widetilde{E}}{\mathrm{d}\tau}\right)^2\frac{\partial^2 p_2}{\partial \widetilde{E}^2} + \frac{\mathrm{d}^2\widetilde{E}}{\mathrm{d}\tau^2}\frac{\partial p_2}{\partial \widetilde{E}} + 2\frac{\mathrm{d}\widetilde{E}}{\mathrm{d}\tau}\frac{\mathrm{d}\psi}{\mathrm{d}\tau}\frac{\partial^2 p_2}{\partial \widetilde{E}\partial\psi} + \left(\frac{\mathrm{d}\psi}{\mathrm{d}\tau}\right)^2\frac{\partial^2 p_2}{\partial \psi^2} + \frac{\mathrm{d}^2\psi}{\mathrm{d}\tau^2}\frac{\partial p_2}{\partial \psi}, \\ \ddot{\gamma}_2 &= \left(\frac{\mathrm{d}\widetilde{E}}{\mathrm{d}\tau}\right)^2\frac{\partial^2 \gamma_2}{\partial \widetilde{E}^2} + \frac{\mathrm{d}^2\widetilde{E}}{\mathrm{d}\tau^2}\frac{\partial \gamma_2}{\partial \widetilde{E}} + 2\frac{\mathrm{d}\widetilde{E}}{\mathrm{d}\tau}\frac{\mathrm{d}\phi}{\mathrm{d}\tau}\frac{\partial^2 \gamma_2}{\partial \widetilde{E}\partial\phi} + \left(\frac{\mathrm{d}\phi}{\mathrm{d}\tau}\right)^2\frac{\partial^2 \gamma_2}{\partial \phi^2} + \frac{\mathrm{d}^2\phi}{\mathrm{d}\tau^2}\frac{\partial \gamma_2}{\partial \phi}. \end{aligned} \tag{33}$$

Using equations (7), (28), and (33), we get

$$\begin{aligned} s_{11}^{(0)} &= E^2\left[\left(a\cos^2\mu - 0.5\right) + 0.25bA_1^{-2}\left(\sin^2\mu - 0.5\right) + 0.5\left(0.25bA_1^{-2} - a\right)\cos(\tau - 2\mu)\right] - 2M_3\left[x_0'(1-\cos\tau) + y_0'\sin\tau\right], \\ s_{21}^{(0)} &= M_3E\left[a\cos\mu + 0.5\left(0.5bA_1^{-1} - a\right)\cos(0.5\tau + \mu) - 0.5\left(0.5bA_1^{-1} + a\right)\cos(1.5\tau - \mu)\right], \\ s_{22}^{(0)} &= E^2\left[\nu a\left(\cos^2\mu - 0.5\right) - 0.25bA_1^{-1}\nu_2\left(\sin^2\mu - 0.5\right) - 0.5\left(\nu a + 0.25bA_1^{-1}\nu_2\right)\cos(\tau - 2\mu)\right] \\ &\quad + 0.5M_3^2\left(e_1a + bA_1^{-1}e_2\right)(1-\cos 2\tau) + M_3\left[ae(1-\cos\tau) + by_0'a^{-1}A_1^{-1}\sin\tau\right]. \end{aligned} \tag{34}$$

Using (4), (28), (33), and (34), we obtain

$$\begin{aligned} F^{(0)} &= 0.25C_1A_1^{-1}E^3\cos(0.5\tau - \mu)\sin^2(0.5\tau - \mu) + EM_3\sin\tau\left[0.5x_0'\sin(0.5\tau - \mu) + y_0'a^{-1}\cos(0.5\tau - \mu)\right] \\ &\quad + 0.5y_0'A_1^{-1}\left(A_1 + a^{-1}\right)M_3E\cos\tau\sin(0.5\tau - \mu) - E\left(z_0'a^{-1} + 0.75\nu e_1\right)\cos(0.5\tau - \mu) \\ &\quad - 0.25E\cos(0.5\tau - \mu)\left\{E^2\left[a\cos^2\mu - 0.5 + 0.25bA_1^{-2}\left(\sin^2\mu - 0.5\right) + 0.5\left(0.25bA_1^{-2} - a\right)\cos(\tau - 2\mu)\right]\right. \\ &\quad \left. - 2M_3\left[x_0'(1-\cos\tau) + y_0'\sin\tau\right]\right\} \\ &\quad + A_1b^{-1}x_0'M_3E\left[a\cos\mu + 0.5\left(0.5bA_1^{-1} - a\right)\cos(0.5\tau + \mu) - 0.5\left(0.5bA_1^{-1} + a\right)\cos(1.5\tau - \mu)\right], \\ \Phi^{(0)} &= b^{-1}x_0' - 0.5M_3^2x_0' + 0.75\nu e - \left\{z_0'b^{-1}M_3 + 0.125A_1^{-2}M_3E^2 - 0.75\nu e_1M_3\right. \\ &\quad \left. + M_3E^2\left[a\left(\cos^2\mu - 0.5\right) + 0.25bA_1^{-2}\left(\sin^2\mu - 0.5\right)\right] - 2M_3^2x_0' + 0.5a(1+B_1)M_3E^2\right\}\cos\tau \\ &\quad - 1.5M_3^2\left(x_0'\cos 2\tau - y_0'\sin 2\tau\right) + (1+B_1)M_3E^2a\cos\mu(\cos 0.5\tau\cos\mu + \sin 0.5\tau\sin\mu) \\ &\quad + 0.25E^2M_3\left[0.5(1-C_1)A_1^{-1} + 0.25A_1^{-2}(1-b) + a - (1+B_1)\left(0.5A_1^{-1} + a\right)\right]cos2(\mu - \tau) \\ &\quad + 0.25M_3E^2 \times \left[0.5A_1^{-1}(C_1 - 1) + 0.25A_1^{-2}(1-b) + a + (1+B_1)\left(0.5bA_1^{-1} - a\right)\right]\cos 2\mu. \end{aligned} \tag{35}$$

Substituting from (28), (33), and (35) into initial system (2) and equating coefficients of ε^{-1} and ε^{-2} in both sides, we obtain the following:

Coefficients of ε^{-1}:

$$\frac{\partial^2 p_1^*}{\partial \psi^2} + p_1^* = 4\left(E\psi_1 \cos\mu - E_1 \sin\mu\right)\cos\psi + 4\left(E\psi_1 \sin\mu + E_1 \cos\mu\right)\sin\psi, \tag{36}$$

$$\frac{\partial^2 \gamma_1^*}{\partial \phi^2} + \gamma_1^* = 2\phi_1 M_3 \cos\phi.$$

We neglect the singular terms [4] to get

$$\begin{aligned} E\psi_1 \cos\mu - E_1 \sin\mu &= 0, \\ E\psi_1 \sin\mu + E_1 \cos\mu &= 0, \end{aligned} \tag{37}$$

$$\phi_1 = 0, \tag{38}$$

such that determinant (37) becomes

$$\Delta = E\begin{vmatrix} \cos\mu & -\sin\mu \\ \sin\mu & \cos\mu \end{vmatrix} = E\left(\cos^2\mu + \sin^2\mu\right) = E \neq 0. \tag{39}$$

For this case, the solution of (37) becomes

$$\psi_1 = E_1 = 0. \tag{40}$$

The particular solutions for (36) become

$$p_1^* = \gamma_1^* = 0. \tag{41}$$

Coefficients of ε^{-2}:

$$\begin{aligned} \frac{\mathrm{d}^2 p_2^*}{\mathrm{d}\tau^2} + 0.25p_2^* &= \left[E_2 \cos\mu + E\psi_2 \sin\mu\right]\sin 0.5\tau \\ &- \left\{E_2 \sin\mu - \left[E\psi_2 + 0.06C_1 A_1^{-1} E^3 - z_0' a^{-1} E - 0.75\nu e_1 E - 0.25E^3 a\left(\cos^2\mu - 0.5\right) - 0.06E^3 bA_1^{-2}\left(\sin^2\mu - 0.5\right)\right.\right. \\ &\left.\left. - 0.06E^3\left(0.25bA_1^{-2} - a\right) + 0.5M_3 x_0' E\right]\cos\mu\right\}\cos 0.5\tau \\ &+ A_1 b^{-1} x_0' M_3 Ea\cos\mu - 0.06E^3\left(C_1 A_1^{-1} + 0.25bA_1^{-2} - a\right)\left(\cos 3\mu \cos 1.5\tau + \sin 3\mu \sin 1.5\tau\right) \\ &+ M_3 E\left\{\left[0.5A_1 b^{-1}\left(0.5bA_1^{-1} - a\right)\right]x_0' \cos\mu + 0.5\left[a^{-1} - 0.5A_1^{-1}\left(A_1 + a^{-1}\right) + 0.5\right]y_0' \sin\mu\right\}\cos 0.5\tau \\ &- 0.5M_3 E\left\{\left[A_1 b^{-1}\left(0.5bA_1^{-1} - a\right)\right]x_0' \sin\mu - \left[a^{-1} - \left(1 + A_1^{-1}a^{-1}\right) + 0.5\right]y_0' \cos\mu\right\}\sin 0.5\tau \\ &- 0.5M_3 E\left\{\left[0.25 + \left(0.5 + A_1 b^{-1} a\right)\right]x_0' \cos\mu + \left[a^{-1} + \left(1 + A_1^{-1}a^{-1}\right) + 0.5\right]y_0' \sin\mu\right\}\cos 1.5\tau \\ &- 0.5M_3 E\left\{1.5A_1 b^{-1} a x_0' \sin\mu - \left[a^{-1} + \left(1 + A_1^{-1}a^{-1}\right) + 0.5\right]y_0' \cos\mu\right\}\sin 1.5\tau, \end{aligned} \tag{42}$$

$$\begin{aligned} \frac{\mathrm{d}^2 \gamma_2^*}{\mathrm{d}\tau^2} + \gamma_2^* &= x_0'\left(b^{-1} - 0.5M_3^2\right) + 0.75\nu e \\ &+ M_3\left\{2\phi_2 - z_0' b^{-1} - 0.125A_1^{-2}E^2 + 0.75\nu e_1 - E^2\left[a\left(\cos^2\mu - 0.5\right) + 0.25bA_1^{-2}\left(\sin^2\mu - 0.5\right)\right]\right. \\ &\left. + 2M_3 x_0' - 0.5aE^2\left(1 + B_1\right)\right\}\cos\tau \\ &+ 1.5M_3^2\left(y_0' \sin 2\tau - x_0' \cos 2\tau\right) + \left(1 + B_1\right)M_3 E^2 a\left(\cos\mu \cos 0.5\tau + \sin\mu \sin 0.5\tau\right)\cos\mu \\ &+ 0.125M_3 E^2\left[\left(1 - C_1\right)A_1^{-1} + 0.5A_1^{-2} - \left(0.5bA_1^{-2} - 2a\right) - \left(1 + B_1\right)\left(bA_1^{-1} + 2a\right)\right]\left(\cos 2\mu \cos 2\tau + \sin 2\mu \sin 2\tau\right) \\ &+ 0.125M_3 E^2\left[\left(C_1 - 1\right)A_1^{-1} + 0.5A_1^{-2} - \left(0.5bA_1^{-2} - 2a\right) + \left(1 + B_1\right)\left(bA_1^{-1} - 2a\right)\right]\cos 2\mu. \end{aligned} \tag{43}$$

Neglecting singular terms from (42) and (43) yields [4]

$$\begin{aligned} E_2 &= 0.125E \sin 2\mu\left[0.25C_1 A_1^{-1} E^2 - 4z_0' a^{-1} - 3\nu e_1 - E^2 a\left(\cos^2\mu - 0.5\right) - 0.25E^2 bA_1^{-2}\left(\sin^2\mu - 0.5\right) - 0.25E^2\left(0.25bA_1^{-2} - a\right) + 2M_3 x_0'\right], \\ \psi_2 &= 0.25\cos^2\mu\left[-0.25C_1 A_1^{-1} E^2 + 4z_0' a^{-1} + 3\nu e_1 + E^2 a\left(\cos^2\mu - 0.5\right) + 0.25bE^2 A_1^{-2}\left(\sin^2\mu - 0.5\right) + 0.25E^2\left(0.25bA_1^{-2} - a\right) - 2M_3 x_0'\right], \\ \phi_2 &= 0.5\left\{z_0' b^{-1} + 0.125A_1^{-2}E^2 - 0.75\nu e_1 + E^2\left[a\left(\cos^2\mu - 0.5\right) + 0.25bA_1^{-2}\left(\sin^2\mu - 0.5\right)\right] - 2M_3 x_0' + 0.5a\left(1 + B_1\right)E^2\right\}. \end{aligned} \tag{44}$$

Substituting from (38), (40), and (44) into (29) and (30) and integrating, we get

$$\begin{aligned}
2\widetilde{E} &= 2E - \varepsilon^{-2}E\sin 2\mu\left[-0.25C_1A_1^{-1}E^2 + 4z_0'a^{-1} + 3\nu e_1 + E^2a\left(\cos^2\mu - 0.5\right)\right.\\
&\quad \left. + 0.25bE^2A_1^{-2}\left(\sin^2\mu - 0.5\right) + 0.25E^2\left(0.25bA_1^{-2} - a\right) - 2M_3x_0'\right]\tau + \cdots,\\
2\psi &= \tau + 0.5\varepsilon^{-2}\left[-0.25C_1A_1^{-1}E^2 + 4z_0'a^{-1} + 3\nu e_1 + E^2a\left(\cos^2\mu - 0.5\right)\right.\\
&\quad \left. + 0.25b\cdot E^2A_1^{-2}\left(\sin^2\mu - 0.5\right) + 0.25E^2\left(0.25bA_1^{-2} - a\right) - 2M_3x_0'\right]\cos^2\mu\tau + \cdots,\\
\phi &= \tau + 0.25\varepsilon^{-2}\left\{2z_0'b^{-1} + 0.25A_1^{-2}E^2 - 1.5\nu e_1 + E^2\left[2a\left(\cos^2\mu - 0.5\right) + 0.5bA_1^{-2}\left(\sin^2\mu - 0.5\right)\right]\right.\\
&\quad \left. - 4M_3x_0' + a\left(1 + B_1\right)E^2\right\}\tau + \cdots.
\end{aligned} \tag{45}$$

Substituting (44) into (42) and (43) and solving the resulted equations, we get p_2^* and γ_2^*. The periodic solutions p_2 and γ_2 are constructed using (28), (32), (41), and (45). Using (5) and (34), we get the first terms of the required solutions as follows:

$$\begin{aligned}
p_1 &= M_1\cos 0.5\tau + M_2\sin 0.5\tau - \varepsilon^{-1}\left(\frac{x_0'}{bB_1} - e_1M_3\cos\tau\right) + \cdots,\\
q_1 &= 0.5A_1^{-1}\left(M_1\sin 0.5\tau - M_2\cos 0.5\tau\right) + \varepsilon^{-1}\left(\frac{y_0'}{aA_1} + e_2A_1^{-1}M_3\sin\tau\right) + \cdots,\\
r_1 &= 1 + 0.25\varepsilon^{-2}\left\{2aM_1^2 - E^2 + 0.5bA_1^{-2}\left(M_2^2 - 0.5E^2\right) + \left(0.25bA_1^{-2} - a\right)\left[\left(M_1^2 - M_2^2\right)\cos\tau + 2M_1M_2\sin\tau\right]\right.\\
&\quad \left. - 4M_3\left[x_0'\left(1 - \cos\tau\right) + y_0'\sin\tau\right]\right\} + \cdots,\\
\gamma_1 &= M_3\cos\tau + \varepsilon^{-1}\nu\left(-M_1\cos\tau + M_1\cos 0.5\tau + M_2\sin 0.5\tau\right) + \cdots,\\
\gamma_1' &= -M_3\sin\tau + \varepsilon^{-1}\left[\nu M_1\sin\tau + 0.5\nu_2\left(-M_1\sin 0.5\tau + M_2\cos 0.5\tau\right)\right] + \cdots,\\
\gamma_1'' &= 1 + \varepsilon^{-1}M_3E\left[a\cos\mu + 0.5\left(b\omega A_1^{-1} - a\right)\cos\left(0.5\tau - \mu\right) - 0.25\left(bA_1^{-1} + 2a\right)\cos\left(1.5\tau - \mu\right)\right]\\
&\quad + \varepsilon^{-2}\left\{M_3\left(1 - a\right)^{-1}x_0' + \frac{0.5M_3^2z_0'\left(a - b\right)}{\left(a + b - 1\right)} + M_3\left(1 - b\right)^{-1}y_0'\sin\tau - M_3\left(1 - a\right)^{-1}x_0'\cos\tau - \frac{0.5M_3^2z_0'\left(a - b\right)\cos 2\tau}{\left(a + b - 1\right)}\right.\\
&\quad + E^2\left[\nu a\left(\cos^2\mu - 0.5\right) - 0.25bA_1^{-1}\nu_2\left(\sin^2\mu - 0.5\right) - 0.125\left(4\nu a + bA_1^{-1}\nu_2\right)\cos 2\left(0.5\tau - \mu\right)\right]\\
&\quad \left. - 0.5E^2\left[\left(a\cos^2\mu - 0.5\right) + 0.25bA_1^{-2}\left(\sin^2\mu - 0.5\right) + 0.125\left(bA_1^{-2} - 4\right)\cos 2\left(0.5\tau - \mu\right)\right]\right\} + \cdots.
\end{aligned} \tag{46}$$

The correction of the period is

$$\alpha\left(\varepsilon\right) = \varepsilon^{-2}\pi n\left\{2M_3x_0' - 2z_0' - 0.125A_1^{-2}E^2 - E^2\left[a\left(\cos^2\mu - 0.5\right) + 0.25bA_1^{-2}\left(\sin^2\mu - 0.5\right)\right] - 0.5aE^2\left(1 + B_1\right)\right\} + \cdots. \tag{47}$$

5. Geometric Interpretation of Motion

In this section, we describe the body motion using Euler's angles $\xi, \zeta,$ and η which come from the obtained solutions (Figure 2). Replacing the time t by $t + t_0$ where t_0 is an arbitrary interval, the periodic solutions remain periodic since the initial system is autonomous [9]. For this case, we obtain from (32),

$$\eta_0 = 0.5\pi + r_0^{-1}t_0 + \cdots, \tag{48}$$

$$\xi_0 = \tan^{-1}M_3, \tag{49}$$

where η_0 are ξ_0 are arbitrary initial angles.

Making use of (46) and (49) when $\tau = r_0^{-1}t$, we find Euler's angles as follows:

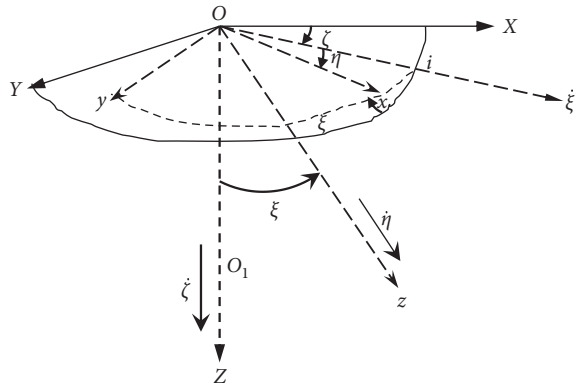

Figure 2: The rotational planes in terms of Euler's angles.

$$\xi = \xi_0 - \varepsilon^{-1} E[\xi_1(t+t_0) - \xi_1(t_0)] - \varepsilon^{-2}[\xi_2(t+t_0) - \xi_2(t_0)] + \cdots,$$
$$\zeta = \zeta_0 + 0.5Mg\ell C^{-1} r_0 \cos^2\xi_0 Q_{10} t + 0.5\varepsilon^{-1}\sec\xi_0[\zeta_1(t+t_0) - \zeta_1(t_0)] + 0.5\varepsilon^{-2}\cos\xi_0[\zeta_2(t+t_0) - \zeta_2(t_0)] + \cdots,$$
$$\eta = \eta_0 + \left(r_0^{-1} - 0.5Mg\ell C^{-1} r_0 \cos^3\xi_0 h_{10}\right)t - 0.5\varepsilon^{-1}\cot\xi_0[\eta_1(t+t_0) - \eta_1(t_0)] - 0.5\varepsilon^{-2}\cos^2\xi_0[\eta_2(t+t_0) - \eta_2(t_0)] + \cdots, \tag{50}$$

where

$$\xi_1(t) = 0.5\left(0.5bA_1^{-1} - a\right)\cos\left(\frac{t}{2r_0} + \mu\right) - 0.5\left(0.5bA_1^{-1} + a\right)\cos\left(\frac{3t}{2r_0} - \mu\right),$$

$$\xi_2(t) = y_0' a^{-1} A_1^{-1} \sin\frac{t}{r_0} + b^{-1}B_1^{-1}x_0'\cos\frac{t}{r_0} - 0.5\tan\xi_0 z_0'\left(\frac{a-b}{a+b-1}\right)\cos 2\frac{t}{r_0}$$
$$- 0.5E^2\cot\xi_0\left[a(\nu - 0.5) + 0.25bA_1^{-1}\left(\nu_2 + 0.5A_1^{-1}\right)\right]\cos\left(\frac{t}{r_0} - 2\mu\right),$$

$$\zeta_1(t) = \eta_1(t) = 0.67\left(1 + 0.5A_1^{-1}\right)\left(M_1\sin\frac{3t}{2r_0} - M_2\cos\frac{3t}{2r_0}\right) + \left(2 - A_1^{-1}\right)\left(M_2\cos\frac{t}{2r_0} + M_1\sin\frac{t}{2r_0}\right),$$

$$\zeta_2(t) = (Q_{11} + Q_{13} + Q_{16})\sin\frac{t}{r_0} - (Q_{11}' + Q_{13}' - Q_{16}')\cos\frac{t}{r_0}$$
$$+ 0.5\left(Q_{12}\sin\frac{2t}{r_0} - Q_{12}'\cos\frac{2t}{r_0}\right) + 2\left(Q_{14}\sin\frac{t}{2r_0} + Q_{14}'\cos\frac{t}{2r_0}\right) + 0.67\left(Q_{15}\sin\frac{3t}{2r_0} - Q_{15}'\cos\frac{3t}{2r_0}\right),$$

$$\eta_2(t) = h_{11}\sin\frac{t}{r_0} - h_{11}'\cos\frac{t}{r_0} + 0.5\left(h_{12}\sin\frac{2t}{r_0} - h_{12}'\cos\frac{2t}{r_0}\right) + \left(h_{13}\sin\frac{t}{r_0} - h_{13}'\cos\frac{t}{r_0}\right) + 2\left(h_{14}\sin\frac{t}{2r_0} + h_{14}'\cos\frac{t}{2r_0}\right)$$
$$+ 0.67\left(h_{15}\sin\frac{3t}{2r_0} - h_{15}'\cos\frac{3t}{2r_0}\right) + \left(h_{16}\sin\frac{t}{r_0} + h_{16}'\cos\frac{t}{r_0}\right) + 0.34\left(h_{17}\sin\frac{3t}{r_0} - h_{17}'\cos\frac{3t}{r_0}\right). \tag{51}$$

Table 1: The analytical solutions p_2, γ_2, and their derivatives.

t	p_2	γ_2	$\dot{p}_2$	$\dot{\gamma}_2$
0	1.5	11.06602	0.8164966	$8.60977E-05$
10	2.018443	8.279188	0.6022027	−7.342405
20	2.361099	1.322297	0.3354627	−10.98657
30	2.498126	−6.300518	0.03950729	−9.096887
40	2.417591	−10.74971	−0.259889	−2.625185
50	2.126507	−9.784271	−0.5366514	5.168785
60	1.650225	−3.890493	−0.7666767	10.35926
70	1.030224	3.962964	−0.9299318	10.33185
80	0.3205004	9.82036	−1.012199	5.10033
90	−0.4171353	10.73134	−1.006313	−2.700216
100	−1.118443	6.237032	−0.9127875	−9.140733
110	−1.722344	−1.398863	−0.7397668	−10.97719
120	−2.176246	−8.330236	−0.5023198	−7.284575
130	−2.440619	−11.06585	−0.2211253	0.07719428
140	−2.492437	−8.227805	0.07932674	7.400064
150	−2.327188	−1.245598	0.3728705	10.9956
160	−1.959263	6.363904	0.6339409	9.052767
170	−1.420706	10.76787	0.839801	2.550172
180	−0.7584189	9.748108	0.9725226	−5.236892
190	−0.0300812	3.818282	1.020547	−10.38613
200	0.7008771	−4.034786	0.9796914	−10.30393
210	1.370795	−9.855532	0.8535145	−5.031701
220	1.921331	−10.71208	0.6530044	2.774997
230	2.304537	−6.172976	0.3956243	9.183975
240	2.48704	1.475497	0.1037893	10.9671
250	2.452946	8.380901	−0.1970856	7.226189
260	2.205224	11.06502	−0.4807954	−0.1544821
270	1.765449	8.175891	−0.7226327	−7.457364
280	1.171921	1.168729	−0.9015357	−11.00408
290	0.4763283	−6.427075	−1.001924	−9.008176
300	−0.2607465	−10.78558	−1.015054	−2.474989

Table 2: The numerical solutions p_2, γ_2, and their derivatives.

t	p_2	γ_2	$\dot{p}_2$	$\dot{\gamma}_2$
0	1.5	11.06602	0.8164966	$8.60977E-05$
10	2.018441	8.279626	0.6022035	−7.341455
20	2.361096	1.324263	0.3354649	−10.9858
30	2.498125	−6.297489	0.03951085	−9.098105
40	2.417592	−10.74771	−0.2598841	−2.629244
50	2.126513	−9.78573	−0.5366458	5.163152
60	1.650237	−3.896276	−0.7666712	10.3552
70	1.030242	3.954753	−0.9299275	10.33263
80	0.3205241	9.813907	−1.012197	5.107155
90	−0.4171081	10.73098	−1.006314	−2.68967
100	−1.118414	6.244486	−0.9127917	−9.131646
110	−1.722318	−1.38609	−0.739775	−10.97505
120	−2.176226	−8.318236	−0.5023316	−7.291935
130	−2.440607	−11.06137	−0.2211403	0.06275124
140	−2.492436	−8.234457	0.07930994	7.385382
150	−2.3272	−1.261325	0.372853	10.9887
160	−1.959289	6.346504	0.6339244	9.058519
170	−1.420744	10.75812	0.8397874	2.567106
180	−0.7584675	9.752295	0.9725135	−5.216549
190	−0.03013661	3.835833	1.020544	−10.37296
200	0.7008187	−4.011765	0.9796954	−10.30583
210	1.37074	−9.83878	0.8535257	−5.049277

Table 2: Continued.

t	p_2	γ_2	$\dot{p}_2$	$\dot{\gamma}_2$
220	1.921283	−10.71119	0.6530228	2.749476
230	2.304503	−6.190003	0.3956484	9.163264
240	2.487025	1.44783	0.1038172	10.96256
250	2.452952	8.356145	−0.1970554	7.24163
260	2.205252	11.05635	−0.4807664	−0.1255394
270	1.765499	8.189053	−0.7226074	−7.429035
280	1.171988	1.198392	−0.9015169	−10.99124
290	0.4764102	−6.395274	−1.001913	−9.018668
300	−0.2606581	−10.76818	−1.015054	−2.504935

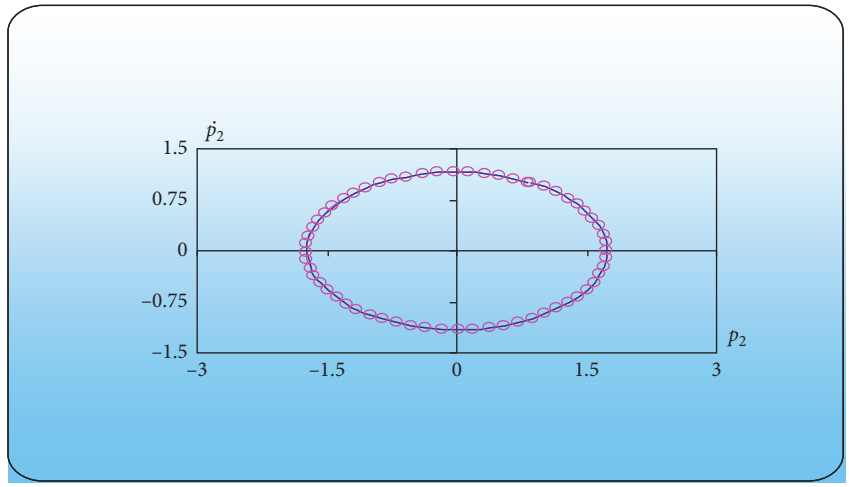

Figure 3: The stability of the analytical and numerical solutions $\dot{p}_2$ and p_2.

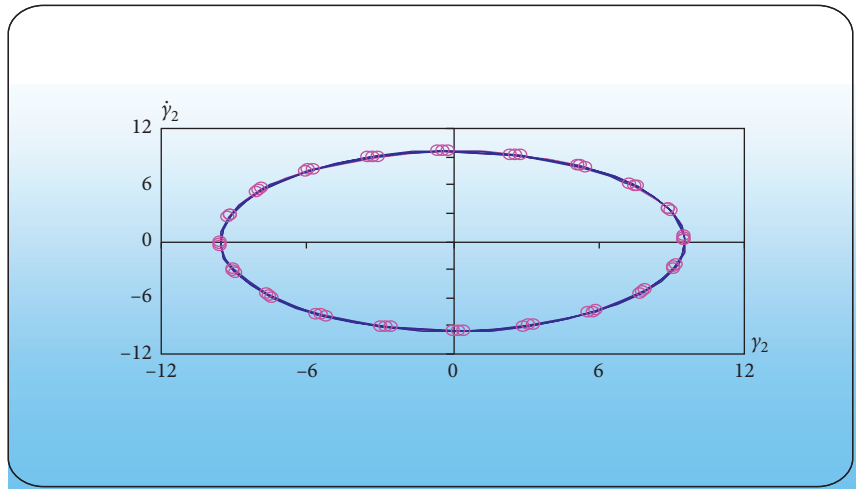

Figure 4: The stability of the analytical and numerical solutions $\dot{\gamma}_2$ and γ_2.

6. The Numerical Solutions

In this section, we assume numerical values data for the parameters of a rigid body, and we achieve a computer program to solve the quasilinear system using the fourth order Runge–Kutta method [7]. We make another program to represent the analytical solutions numerically in a period t between 0 and 300 (Table 1). We use the initial values from Table 1 for obtaining the numerical solutions represented in Table 2. The comparison between the obtained numerical solutions and analytical ones is presented to know the difference between them. The numerical and analytical solutions are in good agreement with others which proves the accuracy of used methods and obtained results.

7. Conclusion

The solutions (46) and the correction of the period (47) are obtained using the large parameter method, which had never been used for solving this kind of problem in the presence of the new assumptions for motion (the weak oscillations of the body about the minor or the major axis of the ellipsoid of inertia instead of the strong oscillations in the previous works). The advantage of this method is that the energy motion of the body is assumed to be sufficiently small instead of sufficiently large with other techniques [10–12]. Also, the obtained solutions treat a singular situation for the natural frequency which was excluded from previous works [13, 14].

Equations (50) and (51) describe the rotation of the body at any time and show that this motion depends on four arbitrary constants $\xi_0, \zeta_0, \eta_0, \text{and} r_0$, such that r_0 is sufficiently small. The obtained solutions give special cases of motions when $(M_1 = M_2 = 0)$ and when $M_1 = 0$, $M_2 \neq 0$, or $M_2 = 0$, $M_1 \neq 0$. Also, the obtained solutions give many gyroscopic motions, which depend on the values of the moments of inertia and the initial position of the body center of gravity. In the end, we obtain the case of regular precession [10] as a special case.

The analytical solutions (46) are represented indefinite intervals of time through computer programs (Table 1). The numerical solutions are obtained using the fourth order Runge–Kutta method in terms of another program (Table 2). Tables 1 and 2 give in detail the obtained results of both the analytical solutions and numerical ones. These results show that the analytical solutions are in full agreement with the numerical ones which proves the accuracy of the considered techniques and results. This case of study is considered as a general case of such ones studied in [5]. The stability phase diagrams of the solutions p_2 and γ_2 are given (Figures 3 and 4). From these diagrams, we note that the stability for both the analytical and the numerical solutions in full agreement. This gives the validity of the obtained solutions and the considered procedures. The considered procedures and results are very useful for the general reader's concern with the new applications dealing with the use of functionally graded materials in such structures based on the recent works [15].

Data Availability

Data sharing is not applicable to this article as no datasets were generated or analyzed during the current study.

Conflicts of Interest

The authors declare that they have no conflicts of interest.

References

[1] F. E. Udwadia and R. E. Kalaba, *Analytical Dynamics: A New Approach*, Cambridge University Press, Cambridge, UK, 2007.

[2] T. S. Amer, A. I. Ismail, and W. S. Amer, "Application of the Krylov-Bogoliubov-Mitropolski technique for a rotating heavy solid under the influence of a gyrostatic moment," *Journal of Aerospace Engineering*, vol. 25, no. 3, pp. 421–430, 2012.

[3] A. I. Ismail, "On the motion of a rigid body in a Newtonian field of force exerted by three attractive centers," *Journal of Aerospace Engineering*, vol. 21, no. 1, pp. 67–77, 2011.

[4] A. H. Nayfeh, *Introduction to Perturbation Technique*, Wiley, Hoboken, NJ, USA, 2011.

[5] A. I. Ismail, "Solving a problem of rotary motion for a heavy solid using the large parameter method," *Advances in Astronomy*, vol. 2020, Article ID 2764867, 7 pages, 2020.

[6] S. V. Ershkov and D. Leshchenko, "On a new type of solving procedure for Euler-Poisson equations (rigid body rotation over the fixed point)," *Acta Mechanica*, vol. 230, no. 3, pp. 871–883, 2019.

[7] C. T. Wu, L. Wang, B. Bonello, L. Ling, N. Ma, and M. A. Schweitzer, "Advanced Mesh-based and particle-based numerical methods for engineering and applied mathematics problems," *Mathematical Problems in Engineering*, vol. 2017, Article ID 1273017, 2 pages, 2017.

[8] A. I. Ismail and T. S. Amer, "A necessary and sufficient condition for solving a rigid body problem," *Technische Mechanik*, vol. 31, no. 1-2, pp. 50–57, 2011.

[9] L. D. Akulenko, Y. S. Zinkevich, T. A. Kozachenko, and D. D. Leshchenko, "The evolution of the motions of a rigid body close to the Lagrange case under the action of an unsteady torque," *Journal of Applied Mathematics and Mechanics*, vol. 81, no. 2, pp. 79–84, 2017.

[10] A. Sanders Jan, V. Ferdinand, and M. James, "Averaging methods in nonlinear dynamical systems," *Applied Mathematical Sciences*, vol. 59, no. 2, p. 434, 2007.

[11] F. L. Chernousko, L. D. Akulenko, and D. D. Leshchenko, *Evolution of Motions of a Rigid Body about Its Center of Mass*, Springer International Publishing, Berlin, Germany, 2017.

[12] A. I. Ismail and F. D. El-Haiby, "Torque free axi-symmetric gyros with changing moments of inertia," *Applied Mathematics*, vol. 7, no. 16, p. 1934, 2016.

[13] T. S. Amer, "On the dynamical motion of a gyro in the presence of external forces," *Advances in Mechanical Engineering*, vol. 9, no. 2, pp. 1–13, 2017.

[14] T. S. Amer and I. M. Abady, "On the motion of a gyro in the presence of a Newtonian force field and applied moments," *Mathematics and Mechanics of Solids*, vol. 23, no. 9, pp. 1263–1273, 2017.

[15] N. Bendenia, M. Zidour, and A. A. Bousahla, "Deflections, stresses and free vibration studies of FG-CNT reinforced sandwich plates resting on Pasternak elastic foundation," *Computers and Concrete*, vol. 26, no. 3, pp. 213–226, 2020.

Hindawi
Advances in Astronomy
Volume 2020, Article ID 8868137, 10 pages
https://doi.org/10.1155/2020/8868137

Research Article

Approximate Analytical Three-Dimensional Multiple Time Scales Solution to a Circular Restricted Three-Body Problem

Fabao Gao and Yongqing Wang

School of Mathematical Science, Yangzhou University, Yangzhou 225002, China

Correspondence should be addressed to Fabao Gao; gaofabao@sina.com

Received 25 August 2020; Revised 11 October 2020; Accepted 29 October 2020; Published 11 November 2020

Academic Editor: Gang Zhang

We illustrate the chaotic nature of the circular restricted three-body problem from the perspective of the bifurcation diagram with respect to the mass ratio parameter. Moreover, it is shown that when the frequency ratio in different directions of the classical problem is irrational, it has the quasiperiodic characteristics. In addition, a three-dimensional approximate solution to this problem under two time scales is proposed by using the multiple time scales method.

1. Introduction

As early as the 19th century, plenty of mathematicians, such as Dirichlet and Weierstrass, et al. [1], expected to obtain a series solution of the three-body problem in the following form:

$$\sum_{j=1}^{\infty}\left[A_j\cos\left(\sum_{i=1}^{k}(j_i\omega_i)\right)t+B_j\sin\left(\sum_{i=1}^{k}(j_i\omega_i)\right)t\right]. \quad (1)$$

The rate of change of the solution with respect to time t in equation (1) appears as a combination of many incommensurable frequencies, $\omega_i i = 1, 2, \ldots, k$, often called quasiperiodic solution.

Almost half a century ago, Farquhar and Kamel [2] proposed an approximation to construct the periodic orbits described above. A few years later, Richardson [3, 4] developed third-order analytic solutions to collinear libration points (CLP) for a class of circular restricted three-body problem (CRTBP) based on a method similar to Lindstedt–Poincaré and successive approximation. The constructed solutions are the basis of determining halo orbits around these points, and they can provide approximate initial values of halo orbits. Furthermore, the solutions can also be developed to investigate spacecraft formation flying. The more accurate the approximate analytical solutions, the less fuel in the system will be consumed. Ruijgrok [5] solved a planar three-body problem for equal mass particles under a particular class of three-body forces. Zagouras and Markellos [6] studied a periodic spatial solution to Hill's problem, which is the limiting case of a restricted three-body problem (R3BP). Papadakis et al. [7] considered the periodic orbits of the three-body problem generated by CLP and provided the second-order approximate analytic expressions of such orbits. Gómez et al. [8] computed quasihalo orbits in CRTBP semianalytically through the Lindstedt–Poincaré technique. Ten years ago, Lu and Zhao [9] proposed an improved and more precise third-order analytic solution than Richardson's classical analytic solution. Gidea and Deppe [10] numerically studied the influence of small perturbations on the dynamics of an infinitesimal third body. They investigated the chaotic orbits in an RTBP, which also indicated the complexity and difficulty of obtaining approximate analytic solutions to the problem.

In recent years, Šuvakov and Dmitrašinovic [11] presented some creative results for the periodic orbits of the three-body problem. Thirteen new, zero-angular-

momentum, distinct equal mass, planar collisionless periodic orbits are displayed in three new categories. When the two primaries are both oblate spheres, Mittal et al. [12] used the predictor-corrector algorithm to construct periodic orbits. They showed the corresponding periodic orbits under different energy constants, mass ratios, and oblateness factors of the two primaries. Based on photogravitational planar RTBP with oblateness, Pathak et al. [13] studied the seventh-, ninth-, and eleventh-order internal resonance periodic orbits of the Sun-Earth system by using Runge–Kutta–Gill method. For a generalized photogravitational RTBP model, the two primaries are oblate spheroid and are under the gravity of an asteroid belt. Abouelmagd et al. [14] found a secular solution that can be reduced to a periodic one near the triangular libration points when the mass ratio is equal to the critical mass value. Similar results can also be found in [15]. Selim et al. [16] analyzed the stable motion solutions of long-period orbits and short-period orbits when the primary is a triaxial rigid body and the Euler angle of rotation satisfies certain conditions. Besides, for two types of the perturbed RTBP, Gao et al. [17, 18] utilized the Lindstedt–Poincaré perturbation method to give an approximate analytical solution to the periodic orbits near the CLP.

Considering that the dynamical equation of the third body in CR3BP is a time-varying high-dimensional nonlinear system in the inertial frame, it can hardly be solved by using analytical approaches. However, this case will be better in the rotating coordinate system, for the aforementioned governing equations are time-independent, and there is an integrable motion. Using the method of multiple time scales, Nayfeh [19, 20] studied the $3:1$ and $2:1$ small-amplitude resonances near the triangular libration points in the plane when the potential function was expanded to the second- and third-order terms of a small parameter, respectively.

Based on the number of terms expanded by the potential function of the problem, the existing time-scale solutions mainly include the three-dimensional single time-scale solution when the potential function expands to the third-order, the three-dimensional (3D) double time-scale solution when the potential function expands to the second-order, and the planar approximate analytic solution. Accordingly, when the third body is also considered to vibrate with a small amplitude in space, the multiple time scales method [21] will be used to construct the approximate 3D CR3BP solution in this paper. The 3D multiple time scales solution has the following form:

$$\mathbf{u} = \sum_{l=1}^{2} \varepsilon^{l} \mathbf{u}_{l}(t, \varepsilon t), \tag{2}$$

where $\mathbf{u} = (x, y, z)$, $\mathbf{u}_l = (x_1, y_1, z_1)$, $l = 1, 2$, and ε is a small, dimensionless parameter.

2. Dynamic Equations of Classical CRTBP

In this section, the dynamic equations of classical CRTBP in three-dimensional space will be described.

In a rotating framework, it is well known that the governing equations of the classical CRTBP can be characterized by the following set of differential equations:

$$\begin{matrix} \ddot{x} - 2\dot{y} = x - U_x, \\ \ddot{y} \end{matrix} + 2\dot{x} = y - U_y, \qquad \ddot{z} = -U_Z, \tag{3}$$

where the potential function

$$\begin{aligned} U(x, y, z) = &- \frac{1-\mu}{\left[(x+\mu)^2 + y^2 + z^2\right]^{(1/2)}} \\ &- \frac{\mu}{\left[(x-1+\mu)^2 + y^2 + z^2\right]^{(1/2)}}. \end{aligned} \tag{4}$$

For more details on the establishment of equation (3), please refer to [22].

It is easy to find that μ in equation (4) is the only parameter in the classical CRTBP. In this paper, we define it as the ratio of the mass of one primary to the mass sum of the two primaries, so it is called the mass ratio parameter, and its value range is between 0 and 1. Under the initial conditions $[-0.001, 0.2, 0.1, -0.3, 0.87, 0.01]$, we divide the range of μ into 1000 equal parts, and then, respectively, return its corresponding coordinates of three different planes (x-y, x-z, y-z) for each value of μ, and the bifurcation diagram with respect to the parameter μ based on ode45 algorithm shows that any small change of μ will lead to the third body's apparent chaotic dynamic behavior (see Figure 1). We find that any value of μ corresponds to an infinite number of points rather than a single point, which means that the probability of obtaining periodic solutions of the three-body problem by numerical simulation is almost zero. Moreover, even if there are some results that are seem to be periodic, part of the existing conclusions based on numerical simulation will no longer hold when the step size continues to shrink. When the iteration accuracy is gradually improved, it is difficult for the orbit of the three-body system with chaotic characteristics to come back after iteration from a particular initial point, and researchers do not even know what will happen when the accuracy is less than 10^{-16}. Therefore, we expect that the periodic solution which is beneficial to the actual mission can be realized by "construction."

Next, we first deal with the complex potential function $U(x, y, z)$ by introducing Legendre polynomials P_n, which satisfies Rodrigues formula:

$$P_n(x) = \frac{1}{2^n n!} \frac{\mathrm{d}^n}{\mathrm{d}x^n}\left(x^2 - 1\right)^n, \quad n = 0, 1, 2, 3, \ldots. \tag{5}$$

Then, we have [22]

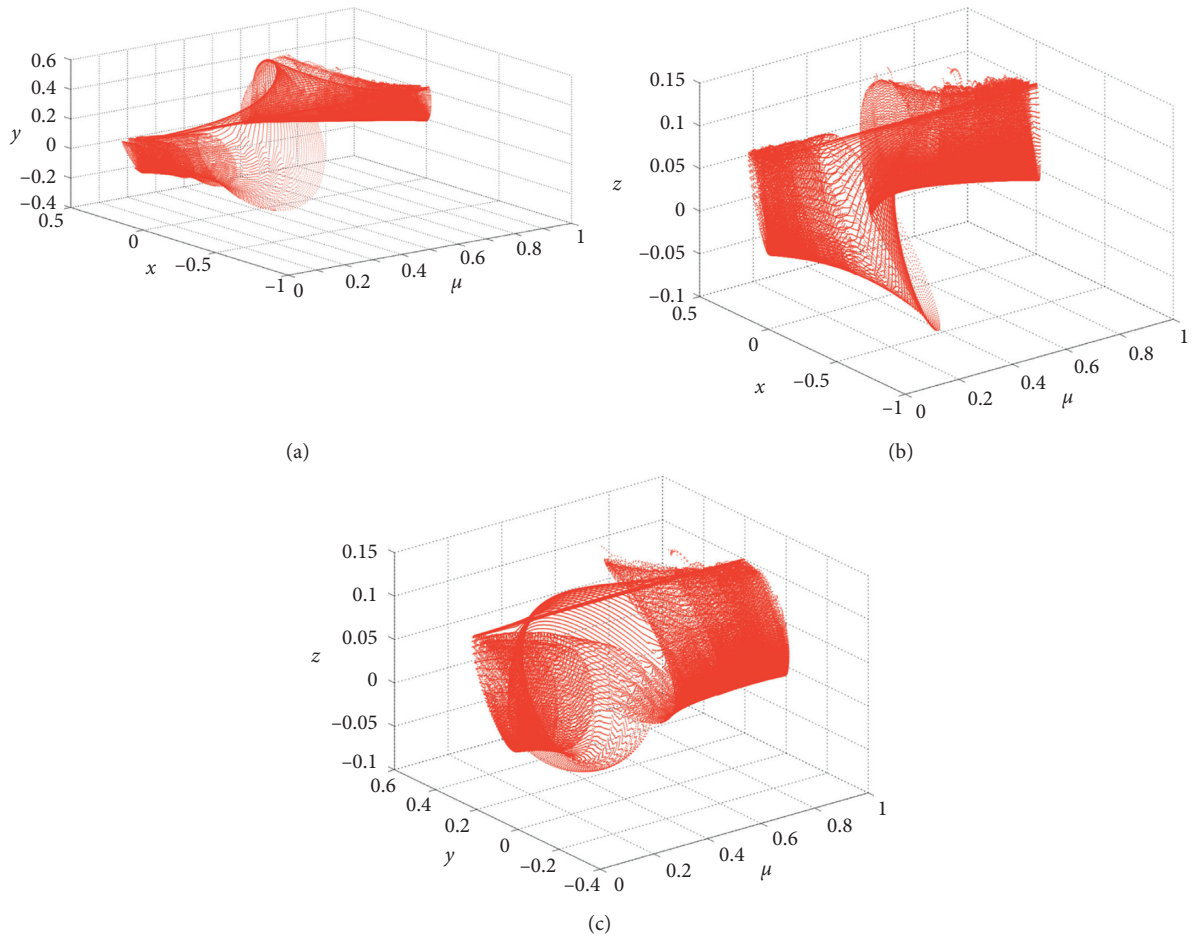

FIGURE 1: (a–c) Bifurcation diagrams of mass ratio parameters in μ-x-y, μ-x-z, and μ-y-z frames, respectively.

$$\frac{1}{\left[(x-A)^2+(y-B)^2+(z-C)^2\right]^{(1/2)}}=\frac{1}{D}\sum_{n=0}^{\infty}\left(\frac{\rho}{D}\right)^n P_n\left(\frac{Ax+By+Cz}{D\rho}\right), \tag{6}$$

where $D^2 = A^2 + B^2 + C^2$ and $\rho = x^2 + y^2 + z^2$.

Substituting equations (4) and (6) into equation (3), it yields

$$\ddot{x}-2\dot{y}-(1+2c_2)x=\frac{\partial}{\partial x}\sum_{n\geq 3}c_n\rho^n P_n\left(\frac{x}{\rho}\right),\quad \ddot{y}+2\dot{x}+(c_2-1)y=\frac{\partial}{\partial y}\sum_{n\geq 3}c_n\rho^n P_n\left(\frac{x}{\rho}\right),\quad \ddot{z}+c_2 z=\frac{\partial}{\partial z}\sum_{n\geq 3}c_n\rho^n P_n\left(\frac{x}{\rho}\right), \tag{7}$$

where $c_n = (1/\gamma_L^3)[(\pm 1)^n\mu + (-1)^n((1-\mu)\gamma_L^{n+1}/(1\mp\gamma_L)^{n+1})]$, for libration points L_1 and L_2 and $c_n = (1/\gamma_L^3)[1-\mu+(\mu\gamma_L^{n+1}/(1+\gamma_L)^{n+1})]$, for libration point L_3, $\gamma_L = n_1^{(2/3)}$, where n_1 represents the angular velocity of relative motion between the two primaries.

Then, equation (7), up to the third approximation, can be written in the following form:

$$\ddot{x} - 2\dot{y} - (1+2c_2)x = \frac{3}{2}c_3\left(2x^2 - y^2 - z^2\right) + 2c_4\left(2x^2 - 3y^2 - 3z^2\right),$$
$$\ddot{y} + 2\dot{x} + (c_2 - 1)y = -3c_3xy - \frac{3}{2}c_4y\left(4x^2 - y^2 - z^2\right),$$
$$\ddot{z} + c_2z = -3c_3xz - \frac{3}{2}c_4z\left(4x^2 - y^2 - z^2\right). \tag{8}$$

3. Construction of Approximate 3D Multiple Time Scales Solution

Consider the small amplitude of nonhomogeneous terms of equation (8). Then,

$$\ddot{x} - 2\dot{y} - (1+2c_2)x = \frac{3}{2}\varepsilon c_3\left(2x^2 - y^2 - z^2\right) + 2\varepsilon c_4\left(2x^2 - 3y^2 - 3z^2\right),$$
$$\ddot{y} + 2\dot{x} + (c_2 - 1)y = -3\varepsilon c_3xy - \frac{3}{2}\varepsilon c_4y\left(4x^2 - y^2 - z^2\right),$$
$$\ddot{z} + c_2z = -3\varepsilon c_3xz - \frac{3}{2}\varepsilon c_4z\left(4x^2 - y^2 - z^2\right). \tag{9}$$

We write the solution of equation (9) as follows:

$$x = \sum_{l=1}^{2}\varepsilon^l x_l(T_0, T_1),$$
$$y = \sum_{l=1}^{2}\varepsilon^l y_l(T_0, T_1), \tag{10}$$
$$z = \sum_{l=1}^{2}\varepsilon^l z_l(T_0, T_1),$$

where $T_0 = t$ and $T_1 = \varepsilon t$.

Then, time derivatives become

$$\frac{\mathrm{d}}{\mathrm{d}t} = \frac{\partial}{\partial T_0}\frac{\mathrm{d}T_0}{\mathrm{d}t} + \frac{\partial}{\partial T_1}\frac{\mathrm{d}T_1}{\mathrm{d}t} + \cdots = D_0 + \varepsilon D_1 + \cdots, \tag{11}$$

$$\frac{\mathrm{d}^2}{\mathrm{d}t^2} = \left(D_0 + \varepsilon D_1 + \cdots\right)^2 = D_0^2 + 2\varepsilon D_0D_1 + \cdots, \tag{12}$$

where $D_k = (\partial/\partial T_k)$, $k = 0, 1, \ldots$.

Substituting equations (10)–(12) into equation (9), we find

$$\left[D_0^2x_1 - 2D_0y_1 - (1+2c_2)x_1\right]\varepsilon + \left[D_0^2x_2 + 2D_0D_1x_1 - 2D_0y_2 - 2D_1y_1 - (1+2c_2)x_2\right]\varepsilon^2 + 2\left(D_0D_1x_2 - D_1y_2\right)\varepsilon^3$$
$$= \frac{3}{2}c_3\left(2x_1^2 - y_1^2 - z_1^2\right)\varepsilon^3 + \left[2c_4\left(2x_1^2 - 3y_1^2 - 3z_1^2\right)x_1 + 3c_3\left(2x_1x_2 - y_1y_2 - z_1z_2\right)\right]\varepsilon^4 + \mathrm{O}\left(\varepsilon^5\right), \tag{13a}$$

$$\left[D_0^2y_1 + 2D_0x_1 + (c_2 - 1)y_1\right]\varepsilon + \left[D_0^2y_2 + 2D_0D_1y_1 + 2D_0x_2 + 2D_1x_1 + (c_2 - 1)y_2\right]\varepsilon^2 + 2\left(D_0D_1y_2 + D_1x_2\right)\varepsilon^3$$
$$= -3c_3x_1y_1\varepsilon^3 - 3\left[c_3\left(x_1y_2 + x_2y_1\right) + \frac{1}{2}c_4\left(4x_1^2 - y_1^2 - z_1^2\right)y_1\right]\varepsilon^4 + \mathrm{O}\left(\varepsilon^5\right), \tag{13b}$$

$$\left(D_0^2z_1 + c_2z_1\right)\varepsilon + \left(D_0^2z_2 + 2D_0D_1z_1 + c_2z_2\right)\varepsilon^2 + 2D_0D_1z_2\varepsilon^3$$
$$= -3c_3x_1z_1\varepsilon^3 - 3\left[c_3\left(x_1z_2 + x_2z_1\right) + \frac{1}{2}c_4\left(4x_1^2 - y_1^2 - z_1^2\right)z_1\right]\varepsilon^4 + \mathrm{O}\left(\varepsilon^5\right). \tag{13c}$$

Now, from equations (13a)–(13c), equating the coefficients of ε, ε^2, and ε^3 to zero, it leads to the following three sets of equations.

Order ε:

$$\begin{aligned} D_0^2 x_1 - 2D_0 y_1 - (1 + 2c_2)x_1 &= 0, \\ D_0^2 y_1 + 2D_0 x_1 + (c_2 - 1)y_1 &= 0, \\ D_0^2 z_1 + c_2 z_1 &= 0. \end{aligned} \tag{14}$$

Order ε^2:

$$\begin{aligned} D_0^2 x_2 + 2D_0 D_1 x_1 - 2D_0 y_2 - 2D_1 y_1 - (1 + 2c_2)x_2 &= 0, \\ D_0^2 y_2 + 2D_0 D_1 y_1 + 2D_0 x_2 + 2D_1 x_1 + (c_2 - 1)y_2 &= 0, \\ D_0^2 z_2 + 2D_0 D_1 z_1 + c_2 z_2 &= 0. \end{aligned} \tag{15}$$

Order ε^3:

$$\begin{aligned} 2D_0 D_1 x_2 - 2D_1 y_2 &= \frac{3}{2} c_3 \left(2x_1^2 - y_1^2 - z_1^2\right), \\ 2D_0 D_1 y_2 + 2D_1 x_2 &= -3c_3 x_1 y_1, \\ 2D_0 D_1 z_2 &= -3c_3 x_1 z_1. \end{aligned} \tag{16}$$

Consider that the last equation of (14) is decoupled from the first two equations of (14). We employ the following transformations:

$$\begin{aligned} x_1 &= \omega_1, \\ \dot{\omega_1} &= \omega_2, \\ y_1 &= \omega_3, \\ \dot{\omega_3} &= \omega_4. \end{aligned} \tag{17}$$

Then, the first two equations of (14) can be represented by the following equivalent form:

$$\begin{aligned} \dot{\omega_1} &= \omega_2, \\ \dot{\omega_2} &= (1 + 2c_2)\omega_1 + 2\omega_4, \\ \dot{\omega_3} &= \omega_4, \\ \dot{\omega_4} &= -2\omega_2 + (1 - c_2)\omega_3. \end{aligned} \tag{18}$$

Thus, the coefficient matrix of equation (18) can be denoted as

$$\begin{bmatrix} 0 & 1 & 0 & 0 \\ 1 + 2c_2 & 0 & 0 & 2 \\ 0 & 0 & 0 & 1 \\ 0 & -2 & 1 - c_2 & 0 \end{bmatrix}. \tag{19}$$

Therefore, the characteristic equation can be obtained as

$$\widehat{\lambda}^4 + (2 - c_2)\widehat{\lambda}^2 + (1 + 2c_2)(1 - c_2) = 0, \tag{20}$$

where

$$\begin{aligned} \widehat{\lambda}_1 &= \frac{1}{2}\left[-4 + 2c_2 + 2\left(9c_2^2 - 8c_2\right)^{(1/2)}\right]^{(1/2)}, \\ \widehat{\lambda}_2 &= -\frac{1}{2}\left[-4 + 2c_2 + 2\left(9c_2^2 - 8c_2\right)^{(1/2)}\right]^{(1/2)}, \\ \widehat{\lambda}_3 &= \frac{1}{2}\left[-4 + 2c_2 - 2\left(9c_2^2 - 8c_2\right)^{(1/2)}\right]^{(1/2)}, \\ \widehat{\lambda}_4 &= -\frac{1}{2}\left[-4 + 2c_2 - 2\left(9c_2^2 - 8c_2\right)^{(1/2)}\right]^{(1/2)}. \end{aligned} \tag{21}$$

It is noticed that $\widehat{\lambda}_1$ and $\widehat{\lambda}_2$ are two equal and opposite real roots, and $\widehat{\lambda}_3$ and $\widehat{\lambda}_4$ are a pair of pure imaginary roots. Hence, the general solution of equation (14) assumes the following form:

$$\begin{aligned} x_1 &= I_1 e^{\widehat{\lambda}_1 t} + I_2 e^{-\widehat{\lambda}_2 t} + I_3 \cos(\lambda t) + I_4 \sin(\lambda t), \\ y_1 &= -k_1 I_1 e^{\widehat{\lambda}_1 t} + k_1 I_2 e^{-\widehat{\lambda}_2 t} - k_2 I_3 \sin(\lambda t) + k_2 I_4 \cos(\lambda t), \\ z_1 &= J_1 \cos(\omega t) + J_2 \sin(\omega t), \end{aligned} \tag{22}$$

where coefficients $I_1, \ldots, I_4, k_1, k_2, J_1$ and J_2 are all constants and λ is the mould of $\widehat{\lambda}_3$ and $\widehat{\lambda}_4$.

Since the motion of the third body may be unbounded due to the influence of exponential terms, appropriate initial conditions are selected such that $I_1 = I_2 = 0$, which implies that

$$\begin{aligned} x_1 &= I_3 \cos(\lambda t) + I_4 \sin(\lambda t), \\ y_1 &= -k_2 I_3 \sin(\lambda t) + k_2 I_4 \cos(\lambda t), \\ z_1 &= J_1 \cos(\omega t) + J_2 \sin(\omega t), \end{aligned} \tag{23}$$

i.e.,

$$\begin{aligned} x_1 &= -A_x \cos(\lambda t + \phi), \\ y_1 &= k_2 A_x \sin(\lambda t + \phi), \\ z_1 &= A_z \sin(\omega t + \psi), \end{aligned} \tag{24}$$

where

$$\begin{aligned} A_x &= \sqrt{I_3^2 + I_4^2}, \\ A_Z &= \sqrt{J_1^2 + J_2^2}, \\ k_2 &= \frac{1 + 2c_2 + \lambda^2}{2\lambda} = \frac{2\lambda}{\lambda^2 - c_2 + 1}, \\ \cos\phi &= -\frac{I_3}{A_x}, \\ \sin\phi &= \frac{I_4}{A_x}, \\ \cos\psi &= -\frac{J_2}{A_Z}, \\ \sin\psi &= \frac{J_1}{A_Z}. \end{aligned} \tag{25}$$

If the value of (λ/ω) in equation (24) is an irrational number, according to the time history diagrams in Figure 2, this linearization motion of the system appears to make the periodic motion in the x and y components, respectively. However, it is not periodic but Lissajous-type quasiperiodic in the x-y plane, and this fact can be verified by the integral curves with respect to x and y (see Figure 3) and its projections in the x-y plane, as well as the portraits in the frame of x-y-z (see Figure 4). The significance of Figures 2–4 is that if the frequency of the third body in all directions is not commensurable, it will exhibit a quasiperiodic motion. Therefore, the value of (λ/ω) is a rational number that performs a critical role in the motion law of the system. In general, if the value of (λ/ω) is an irrational number, the time history diagram can only serve as a reference but a standard to judge if the system makes the periodic motion or not. On the contrary, the motion law of the system can be judged by phase portraits and time history diagrams.

In addition, note that the halo-type periodic orbits play particular importance in the actual mission ACE, ISEE-3/ICE, MAP, SOHO, Genesis, etc., that is, the in-plane and out-of-plane motion makes those characteristic frequencies equal within the sufficiently large motion region. Therefore, without loss of generality, we consider here the case of $\lambda = \omega$. Then, equation (24) can be represented as

$$\begin{aligned} x_1 &= A_1(T_1)e^{i\lambda T_0} + \overline{A}_1(T_1)e^{-i\lambda T_0}, \\ y_1 &= ik_2 A_1(T_1)e^{i\lambda T_0} - ik_2\overline{A}_1(T_1)e^{-i\lambda T_0}, \\ z_1 &= A_2(T_1)e^{i\lambda T_0} + \overline{A}_2(T_1)e^{-i\lambda T_0}. \end{aligned} \tag{26}$$

Substituting equation (26) into equation (15), it yields

$$\begin{aligned} D_0^2 x_2 - 2D_0 y_2 - (1 + 2c_2)x_2 + 2i\lambda D_1 A_1 e^{i\lambda T_0} - 2i\lambda D_1 \overline{A}_1 e^{-i\lambda T_0} - 2ik_2 D_1 A_1 e^{i\lambda T_0} + 2ik_2 D_1 \overline{A}_1 e^{-i\lambda T_0} &= 0, \\ D_0^2 y_2 + 2D_0 x_2 + (c_2 - 1)y_2 - 2\lambda k_2 D_1 A_1 e^{i\lambda T_0} - 2\lambda k_2 D_1 \overline{A}_1 e^{-i\lambda T_0} + 2D_1 A_1 e^{i\lambda T_0} + 2D_1 \overline{A}_1 e^{-i\lambda T_0} &= 0, \\ D_0^2 z_2 + c_2 z_2 + 2i\lambda D_1 A_2 e^{i\lambda T_0} - 2i\lambda D_1 \overline{A}_2 e^{-i\lambda T_0} &= 0. \end{aligned} \tag{27}$$

Let the secular term be equal to zero, and we find that

$$\begin{aligned} D_1 A_1(\lambda - k_2) &= 0, \\ D_1 A_1(k_2 - 1) &= 0, \\ D_1 A_2 &= 0. \end{aligned} \tag{28}$$

Hence,

$$\begin{aligned} A_1 &= \frac{\rho_1}{2}, \\ A_2 &= \frac{\rho_2}{2}, \end{aligned} \tag{29}$$

where ρ_1 and ρ_2 are constants.

Substituting equation (29) into equation (26), and set constant $k_2 = \delta$, we obtain

$$\begin{aligned} x_1 &= \rho_1 \cos(\lambda t), \\ y_1 &= -\delta\rho_1 \sin(\lambda t), \\ z_1 &= \rho_2 \cos(\lambda t). \end{aligned} \tag{30}$$

Then, equation (27) can be expressed as

$$\begin{aligned} D_0^2 x_2 - 2D_0 y_2 - (1 + 2c_2)x_2 &= 0, \\ D_0^2 y_2 + 2D_0 x_2 + (c_2 - 1)y_2 &= 0, \\ D_0^2 z_2 + c_2 z_2 &= 0. \end{aligned} \tag{31}$$

Similarly, solutions to equation (31) can be denoted as

$$\begin{aligned} x_2 &= B_1(T_1)e^{i\lambda T_0} + \overline{B}_1(T_1)e^{-i\lambda T_0}, \\ y_2 &= i\delta B_1(T_1)e^{i\lambda T_0} - i\delta\overline{B}_1(T_1)e^{-i\lambda T_0}, \\ z_2 &= B_2(T_1)e^{i\lambda T_0} + \overline{B}_2(T_1)e^{-i\lambda T_0}. \end{aligned} \tag{32}$$

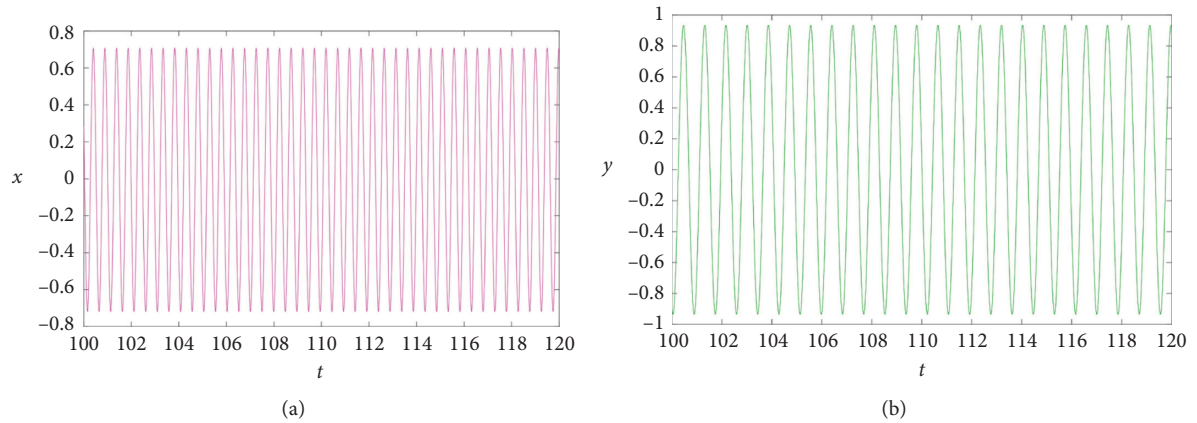

Figure 2: Time history diagrams with respect to (a) x and (b) y, respectively, when $\mu = 0.0123$.

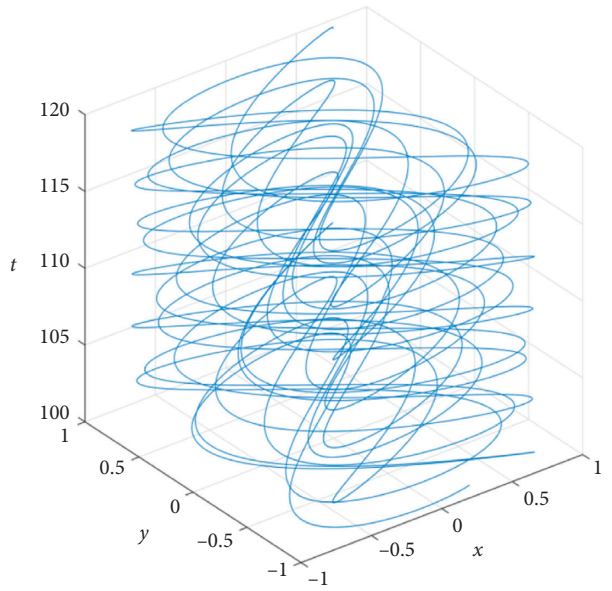

Figure 3: Quasiperiodic orbit of Lissajous type in x-y-t space for $\mu = 0.0123$.

Substituting equations (26) and (32) into equation (16), it yields

$$\begin{aligned}
2i(\lambda-\delta)D_1B_1e^{i\lambda T_0}+2i(\delta-\lambda)D_1\overline{B}_1e^{-i\lambda T_0}&=\frac{3}{4}c_3\left[\left(\left(2+\delta^2\right)\rho_1^2-\rho_2^2\right)\cos\left(2\lambda T_0\right)+\left(2-\delta^2\right)\rho_1^2-\rho_2^2\right],\\
2(1-\lambda\delta)D_1B_1e^{i\lambda T_0}+2(1-\lambda\delta)D_1\overline{B}_1e^{-i\lambda T_0}&=-3c_3i\delta A_1^2e^{i2\lambda T_0}+3c_3i\delta\overline{A}_1^2e^{-i2\lambda T_0},\\
2i\lambda D_1B_2e^{i\lambda T_0}-2i\lambda D_1\overline{B}_2e^{-i\lambda T_0}&=-3c_3A_1A_2e^{i2\lambda T_0}-3c_3\overline{A}_1\overline{A}_2e^{-i2\lambda T_0}-3c_3\left(A_1\overline{A}_2+\overline{A}_1A_2\right).
\end{aligned}\tag{33}$$

We define

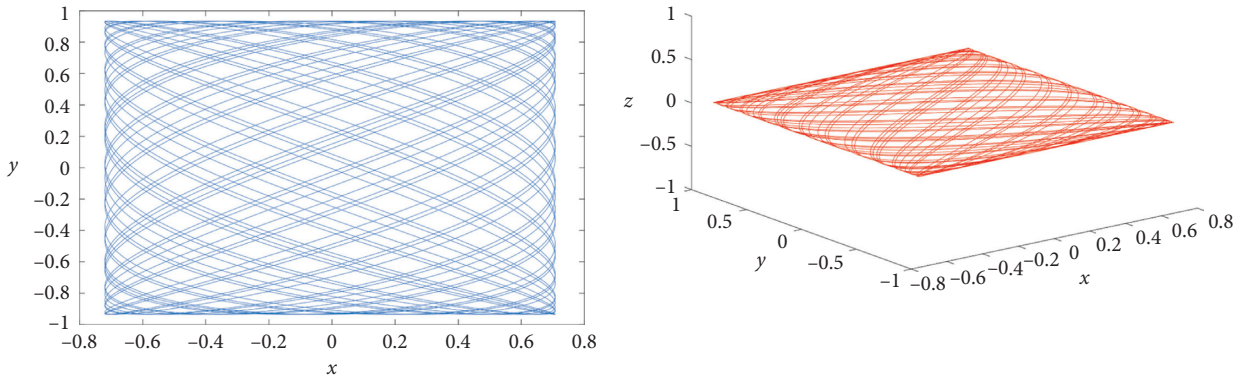

(a) (b)

Figure 4: Quasiperiodic orbit of Lissajous type in the (a) x-y plane and (b) x-y-z space, respectively, when $\mu = 0.0123$.

$$B_1(T_1) = \frac{1}{2}\alpha_1(T_1)e^{i\beta_1(T_1)},$$
$$B_2(T_1) = \frac{1}{2}\alpha_2(T_1)e^{i\beta_2(T_1)}. \tag{34}$$

Thus,

$$\begin{aligned} D_1B_1 &= \frac{1}{2}\alpha_1' e^{i\beta_1} + \frac{1}{2}\alpha_1 e^{i\beta_1}(i\beta_1'),\\ D_1\overline{B}_1 &= \frac{1}{2}\alpha_1' e^{-i\beta_1} + \frac{1}{2}\alpha_1 e^{-i\beta_1}(-i\beta_1'),\\ D_1B_2 &= \frac{1}{2}\alpha_2' e^{i\beta_2} + \frac{1}{2}\alpha_1 e^{i\beta_2}(i\beta_2'),\\ D_1\overline{B}_2 &= \frac{1}{2}\alpha_2' e^{-i\beta_2} + \frac{1}{2}\alpha_2 e^{i\beta_2}(-i\beta_2'). \end{aligned} \tag{35}$$

Substituting equations (35) and (30) into equation (33), we get

$$\begin{aligned} 2(\lambda-\delta)[\alpha_1'\sin(\lambda T_0+\beta_1) + \alpha_1\beta_1'\cos(\lambda T_0+\beta_1)] &= \frac{3}{4}c_3\left[\left(\left(2+\delta^2\right)\rho_1^2 - \rho_2^2\right)\cos(2\lambda T_0) + \left(2-\delta^2\right)\rho_1^2 - \rho_2^2\right],\\ 2(1-\lambda\delta)[\alpha_1'\cos(\lambda T_0+\beta_1) - \alpha_1\beta_1'\sin(\lambda T_0+\beta_1)] &= \frac{3}{2}c_3\delta\rho_1^2\sin(2\lambda T_0),\\ -2\lambda[\alpha_2'\sin(\lambda T_0+\beta_2) + \alpha_2\beta_2'\cos(\lambda T_0+\beta_2)] &= -\frac{3}{2}c_3\delta\rho_1\rho_2[\cos(2\lambda T_0)+1]. \end{aligned} \tag{36}$$

Then, it can be followed from equation (36) that

$$\alpha_1'(T_1) = \frac{3}{8(\delta-\lambda)}c_3\left[\left(\left(2+\delta^2\right)\rho_1^2-\rho_2^2\right)\cos(2\lambda t)+\left(2-\delta^2\right)\rho_1^2-\rho_2^2\right]\sin\left(\lambda t+\beta_1(T_1)\right)+\frac{3}{4(1-\lambda\delta)}c_3\delta\rho_1^2\sin(2\lambda t)\cos\left(\lambda t+\beta_1(T_1)\right),$$

$$\alpha_1\beta_1'(T_1) = \frac{3}{8(\delta-\lambda)}c_3\left[\left(\left(2+\delta^2\right)\rho_1^2-\rho_2^2\right)\cos(2\lambda t)+\left(2-\delta^2\right)\rho_1^2-\rho_2^2\right]\cos\left(\lambda t+\beta_1(T_1)\right)-\frac{3}{4(1-\lambda\delta)}c_3\delta\rho_1^2\sin(2\lambda t)\sin\left(\lambda t+\beta_1(T_1)\right). \tag{37}$$

Substituting equation (34) into equation (32), we arrive at

$$\begin{aligned} x_1 &= \alpha_1(T_1)\cos\left(\lambda t+\beta_1(T_1)\right),\\ y_1 &= -\delta\alpha_1(T_1)\sin\left(\lambda t+\beta_1(T_1)\right),\\ z_1 &= \alpha_2(T_1)\cos\left(\lambda t+\beta_2(T_1)\right). \end{aligned} \tag{38}$$

Combining equations (10), (30), and (38), an approximate 3D multiple time scales solution to equation (9) can be represented as

$$\begin{aligned} x &= \varepsilon\rho_1\cos(\lambda t)+\varepsilon^2\cos\left(\lambda t+\beta_1(\varepsilon t)\right),\\ y &= -\varepsilon\delta\rho_1\sin(\lambda t)-\varepsilon^2\delta\alpha_1(\varepsilon t)\sin\left(\lambda t+\beta_1(\varepsilon t)\right),\\ z &= \varepsilon\rho_2\cos(\lambda t)+\varepsilon^2\alpha_2(\varepsilon t)\cos\left(\lambda t+\beta_2(\varepsilon t)\right). \end{aligned} \tag{39}$$

where α_1 and β_1 satisfy equation (37) and α_2 and β_2 satisfy the third equation of (36).

4. Conclusions

In this paper, we first show the chaotic characteristics of the classical CRTBP through the bifurcation diagram concerning the mass parameter μ, which indicates that it is challenging to find the periodic orbit by adjusting the initial conditions of the problem. The astronomer Poincaré has also shown that the probability of the event is zero. Secondly, we also show that even though sometimes the third body may exhibit corresponding periodic motions in different directions in space, the incommensurability of their frequencies will cause the third body to have quasiperiodic characteristics.

When the third body moves with a small amplitude, we construct a kind of approximate 3D multiscale solution by decomposing the conventional time contained in the solution of the CRTBP into the coupling effect of multiple time scales. The shortcoming of this type of solution is that, like other known approximate solutions (such as those based on the Lindstedt–Poincaré method), the result of error analysis is not satisfactory because of the chaotic nature of the problem. In theory, we need more infinite terms in solution series and time scales to make it approach the exact solution of the problem, but this is worthless, and the analytical calculation under the current technological level is almost impossible to achieve. Therefore, we only need the series approximation of two or three terms, so that the multiple time scales solution can be used as an initial guess or approximation of the low-energy transfer orbital mission (such as Genesis discovery mission), and then generate spacecraft orbit through some differential correction procedures. In addition, the classic ISEE-3 mission actually used a similarly constructed approximate solution as the initial solution for orbit design.

Data Availability

No data were used to support this study.

Conflicts of Interest

The authors declare that they have no conflicts of interest.

Acknowledgments

The authors gratefully acknowledge the support of the National Natural Science Foundation of China (NSFC) through grant no. 11672259 and the China Scholarship Council through grant no. 201908320086.

References

[1] J. L. Zhou and Y. S. Sun, *Celestial Mechanics: A Story From an Apple/10000 Selected Problems in Sciences*, Astronomy Volume, Science Press, Beijing, China, 2010, in Chinese.

[2] R. W. Farquhar and A. A. Kamel, "Quasi-periodic orbits about the translunar libration point," *Celestial Mechanics*, vol. 7, pp. 458–473, 1973.

[3] D. L. Richardson, "Halo orbit formulation for the ISEE-3 mission," *Journal of Guidance and Control*, vol. 3, pp. 543–548, 1980.

[4] D. L. Richardson, "Analytical construction of periodic orbits about the collinear points," *Celestial Mechanics*, vol. 22, pp. 241–253, 1980.

[5] T. W. Ruijgrok, "The exact solution of a three-body problem," *European Journal of Physics*, vol. 5, pp. 21–24, 1984.

[6] C. Zagouras and V. V. Markellos, "Three-dimensional periodic solutions around equilibrium points in hill's problem," *Celestial Mechanics*, vol. 35, pp. 257–267, 1985.

[7] K. Papadakis, E. Perdios, and V. V. Markellos, "Nonlinear approximation of periodic three-body motions around collinear equilibrium configurations," *Astrophysics and Space Science*, vol. 140, pp. 373–383, 1988.

[8] G. Gómez, J. J. Masdemont, and C. Simó, "Quasihalo orbits associated with libration points," *The Journal of the Astronautical Sciences*, vol. 46, pp. 135–176, 1998.

[9] S. T. Lu and Y. S. Zhao, "The improvement of Richardson's three order approximate analytical solution of halo orbit," *Journal of Astronautics*, vol. 30, pp. 863–869, 2009, (in Chinese).

[10] M. Gidea and F. Deppe, "Chaotic orbits in a restricted three-body problem: numerical experiments and heuristics," *Communications in Nonlinear Science and Numerical Simulation*, vol. 11, pp. 161–171, 2006.
[11] M. Suvakov and V. Dmitrasinovic, "Three classes of Newtonian three-body planar periodic orbits," *Physical Review Letters*, vol. 110, Article ID 114301, 2013.
[12] A. Mittal, M. S. Suraj, and R. Aggarwal, "The analysis of periodic orbits generated by lagrangian solutions of the restricted three-body problem with non-spherical primaries," *New Astronomy*, vol. 74, Article ID 101287, 2020.
[13] N. Pathak, E. I. Abouelmagd, and V. O. Thomas, "On higher order resonant periodic orbits in the photo-gravitational planar restricted three-body problem with oblateness," *The Journal of the Astronautical Sciences*, vol. 66, pp. 475–505, 2019.
[14] E. I. Abouelmagd, M. E. Awad, E. M. A. Elzayat, and I. A. Abbas, "Reduction the secular solution to periodic solution in the generalized restricted three-body problem," *Astrophysics and Space Science*, vol. 350, pp. 495–505, 2014.
[15] E. I. Abouelmagd and J. L. G. Guirao, "Periodic and secular solutions in the restricted three-body problem under the effect of zonal harmonic parameters," *Applied Mathematics & Information Sciences*, vol. 9, no. 4, pp. 1659–1669, 2015.
[16] H. H. Selim, J. L. G. Guirao, and E. I. Abouelmagd, "Libration points in the restricted three-body problem: Euler angles, existence and stability," *Discrete and Continuous Dynamical Systems Series S*, vol. 12, no. 5, pp. 703–710, 2019.
[17] F. B. Gao and Y. Q. Wang, "Approximate analytical periodic solutions to the restricted three-body problem with perturbation, oblateness, radiation and varying mass," *Universe*, vol. 6, no. 8, p. 110, 2020.
[18] F. B. Gao and R. F. Wang, "Bifurcation analysis and periodic solutions of the HD 191408 system with triaxial and radiative perturbations," *Universe*, vol. 6, no. 2, p. 35, 2020.
[19] A. H. Nayfeh, "Three-to-one resonances near the equilateral libration points," *AIAA Journal*, vol. 8, pp. 2245–2251, 1970.
[20] A. H. Nayfeh, "Two-to-one resonances near the equilateral libration points," *AIAA Journal*, vol. 9, pp. 23–27, 1971.
[21] A. H. Nayfeh and D. T. Mook, *Nonlinear Oscillations*, Wiley-Vch Verlag GmbH & Co. KGaA, Hoboken, NJ, USA, 2004.
[22] W. S. Koon, M. W. Lo, J. E. Marsden, and S. D. Ross, *Dynamical Systems, the Three-Body Problem and Space Mission Design*, Marsden Books, Wellington, New Zealand, 2011.

Hindawi
Advances in Astronomy
Volume 2020, Article ID 4179590, 12 pages
https://doi.org/10.1155/2020/4179590

Research Article

The Slow Spinning Motion of a Rigid Body in Newtonian Field and External Torque

A. I. Ismail [1,2]

[1]*Department of Mechanics, College of Engineering and Islamic Architecture, Umm Al-Qura University, P.O. Box 5555, Mecca, Saudi Arabia*
[2]*Department of Mathematics, Faculty of Science, Tanta University, P.O. Box 31527, Tanta, Egypt*

Correspondence should be addressed to A. I. Ismail; aiismail@uqu.edu.sa

Received 27 June 2020; Revised 7 August 2020; Accepted 12 August 2020; Published 15 October 2020

Guest Editor: Gang Zhang

In this paper, the problem of the slow spinning motion of a rigid body about a point O, being fixed in space, in the presence of the Newtonian force field and external torque is considered. We achieve the slow spin by giving the body slow rotation with a sufficiently small angular velocity component r_0 about the moving z-axis. We obtain the periodic solutions in a new domain of the angular velocity vector component $r_0 \longrightarrow 0$, define a large parameter proportional to $1/r_0$, and use the technique of the large parameter for solving this problem. Geometric interpretations of motions will be illustrated. Comparison of the results with the previous works is considered. A discussion of obtained solutions and results is presented.

1. Introduction

In [1], the problem of rigid body dynamics is considered. The author in [2] gave important space applications to this problem. In [3], the authors presented valuable and important studies for the evolution of motions of a rigid body about its mass center. In [4], the authors introduced a new procedure for solving Euler–Poisson equations (of a rotatory rigid body over a fixed point). The author in [5] constructed periodic solutions for Euler–Poisson equations utilizing power series expansion containing a small parameter proportional to the inverse of sufficiently high angular velocity component. In [6], the author studied many perturbation techniques for solving the linear and nonlinear systems of ordinary and partial differential equations such as Poincare's method, KBM method, Poincaré–Lindstedt method, and multiple scales method. The authors in [7] studied new types of integrable two-variable systems with quartic second integrals. The study in [8] presented the motion for the rigid body in the presence of a gyrostatic momentum in cases of external effects and without external effects. The author considered the fast spin motion of a rigid body and achieved a small parameter proportional to the inverse of high angular components about the z-axis. The author applies the small parameter of Poincare's method for solving this problem. In [9], the author investigated the motion over the fixed point O of a fast spinning heavy solid in a uniform gravity field (the classical problem). He assumed fast spinning of the body, achieved a small parameter, and used Poincare's method for the solution. In all previous works, the rotary motion for a fast-spinning body with gyro moments was studied. Initially, the authors assumed that the body rotates with a sufficiently large angular velocity component r_o about the moving z-axis which moves with the body. The authors achieved a small parameter proportional to $1/r_0$ and used the small parameter technique to solve the considered problems in the domain $(t, r_o \longrightarrow \infty, \varepsilon \longrightarrow 0)$. The fact of slow motion of that body which must be achieved on a new parameter named the large parameter and must be solved using a new procedure named the large parameter technique was not considered, although this motion saves high energy given at the initial moment of the body and can solve the problem in a new domain $(t, r_o \longrightarrow 0, \varepsilon \longrightarrow \infty)$.

2. Equations of Motion and Change of Variables

Consider a rigid body of mass M [10], with arbitrary ellipsoid of inertia surface, rotating about a fixed point O in the presence of the Newtonian force field O_1 under the influence of the external torque vector about the moving axes $\underline{\ell} = \ell_1 \underline{\hat{i}} + \ell_2 \underline{\hat{j}} + \ell_3 \underline{\hat{k}}$. Let the attracting center O_1 lie on the Z-axis which is fixed in space. Let the element dm lie on the body at the point $p\,(x, y, z)$ and have a position vector $\underline{\rho}$ from O and a position vector $\underline{r}$ from O_1. Equations of motion and their first integrals are achieved and solved with a sufficiently large parameter proportional to $1/r_0$, where r_0 is sufficiently small. We deduce the system of equations of motion and their first integrals of the considered problem and use the large parameter method for solving it.

The differential equations of motion and their first integrals are obtained [10]. Let $\underline{h}_o$ be the angular momentum vector which rotates in space at the same angular velocity $\underline{\omega}$ of the rigid body and $\underline{\hat{k}} = (\gamma, \gamma', \gamma'')$ be the unit vector fixed in space in the direction of the downward Z-axis, so

$$\underline{h}_o = (Ap + \ell_1)\underline{\hat{i}} + (Bq + \ell_2)\underline{\hat{j}} + (Cr + \ell_3)\underline{\hat{k}}, \tag{1}$$

$$\underline{\omega} = p\underline{\hat{i}} + q\underline{\hat{j}} + r\underline{\hat{k}}, \tag{2}$$

where $A, B,$ and C are the body's principal moments of inertia in the moving frame. The six nonlinear equations of motion for this case are obtained in the following form:

$$\begin{aligned}\frac{\mathrm{d}\underline{h}_o}{\mathrm{d}t} &= \left[A\frac{\partial p}{\partial t} + (C-B)qr\right]\underline{\hat{i}} + \left[B\frac{\partial q}{\partial t} + (A-C)pr\right]\underline{\hat{j}} \\ &\quad + \left[C\frac{\partial r}{\partial t} + (B-A)pq\right]\underline{\hat{k}},\end{aligned} \tag{3}$$

$$\frac{\mathrm{d}\underline{\hat{K}}}{\mathrm{d}t} = \frac{\partial \underline{\hat{K}}}{\partial t} + \underline{\omega} \wedge \underline{\hat{K}} = \underline{0}\,. \tag{4}$$

These equations have three first integrals named as follows:

(a) The Jacobi-integral

$$T + V = \text{const}, \tag{5}$$

where T is the kinetic energy of the body and V is the potential one.

(b) The angular momentum integral

$$\underline{h}_o . \underline{\hat{K}} = \text{const}. \tag{6}$$

(c) The geometric integral

$$\underline{\hat{K}} . \underline{\hat{K}} = 1. \tag{7}$$

Equations (3) and (4) are nonlinear differential equations for the motion of a rigid body around a fixed point in the field of Newtonian force with the presence of rotary torque vector $\underline{\ell}(\ell_1, \ell_2, \ell_3)$, around the x-axis, the y-axis, and the z-axis, respectively.

These equations are of first order in unknown variables $p, q, r, \gamma, \gamma', \text{and } \gamma''$. The quantities $A, B, C, \ell_1, \ell_2, \text{and } \ell_3$ are constants. The integration of such equations gives the solutions $p, q, r, \gamma, \gamma', \text{and } \gamma''$ as functions in time t and the rigid body parameters.

The equations of motion for a coherent object around a fixed point in the asymmetric attraction field [5, 9] and their three initial integrals result as special cases from equations (3), (4), (5), (6), and (7).

Let (x_0, y_0, z_0) be the center of mass in the moving coordinate system $(Oxyz)$; R is the distance from the fixed point O to the attracting center O_1; $p_0, q_0, r_0, \gamma_0, \gamma_0', \text{and } \gamma_0''$ are the initial values of the corresponding variables. Initially, let the body rotate about the z-axis with a sufficiently small angular velocity component r_0 such that the z-axis makes an angle $\theta_0 \neq 0.5n\pi\,(n = 0, 1, 2, \ldots)$ with Z-axis being fixed in space.

Without a loss of generality, we choose the positive z-axis, and the x-axis does not make an obtuse angle with Z-axis. According to this restriction, we obtain [9]

$$\gamma_0 \geq 0, 0 < \gamma_0'' < 1. \tag{8}$$

Assume the parameters as follows:

$$\begin{aligned} a &= \frac{A}{C}, \quad (ab), \\ c^2 &= \frac{Mg\ell}{C}, \\ \varepsilon &= \frac{c\sqrt{\gamma_0''}}{r_0}, \\ x_0 &= \ell x_0', (x_o y_o z_o), \\ \ell^2 &= x_0^2 + y_0^2 + z_0^2, \end{aligned} \tag{9}$$

where ε is large since r_0 is small and symbols such as (abc) mean cyclic permutations and indicate equations which are omitted.

Introducing new variables as follows:

$$\begin{aligned} p &= c\sqrt{\gamma_0''}\,p_1, \\ r &= r_0 r_1, \\ \gamma &= \gamma_0''\gamma_1, \quad (pq, \gamma\gamma'\gamma''), \\ k &= \frac{3g}{R}c^{-2}, \\ t &= \frac{\tau}{r_0}. \end{aligned} \tag{10}$$

Substituting equation (10) into equations (3) to (7) when $\ell_1 = \ell_2 = 0$, we obtain

$$\dot{p}_1 + A_1 q_1 r_1 + A^{-1} r_0^{-1} q_1 \ell_3 = \varepsilon^{-1} a^{-1} (y_0' \gamma_1'' - z_0' \gamma_1' + k a A_1 \gamma_1' \gamma_1''), \tag{11}$$

$$\dot{q}_1 + B_1 p_1 r_1 - B^{-1} r_0^{-1} p_1 \ell_3 = \varepsilon^{-1} b^{-1} (z_0' \gamma_1 - x_0' \gamma_1'' + k b B_1 \gamma_1 \gamma_1''), \tag{12}$$

$$\dot{r}_1 = \varepsilon^{-2} (-C_1 p_1 q_1 + x_0' \gamma_1' - y_0' \gamma_1 + k C_1 \gamma_1 \gamma_1'), \tag{13}$$

$$\dot{\gamma}_1 = r_1 \gamma_1' - \varepsilon^{-1} q_1 \gamma_1'', \tag{14}$$

$$\dot{\gamma}_1' = \varepsilon^{-1} p_1 \gamma_1'' - r_1 \gamma_1, \tag{15}$$

$$\dot{\gamma}_1'' = \varepsilon^{-1} (q_1 \gamma_1 - p_1 \gamma_1'), \quad \left(. \equiv \frac{\mathrm{d}}{\mathrm{d}\tau} \right), \tag{16}$$

$$r_1^2 = 1 + \varepsilon^{-2} S_1, \tag{17}$$

$$r_1 \gamma_1'' = 1 + \varepsilon^{-1} S_2, \tag{18}$$

$$\gamma_1^2 + \gamma_1'^2 + \gamma_1''^2 = (\gamma_0'')^{-2}, \tag{19}$$

where

$$\begin{aligned} S_1 &= a\left(p_{10}^2 - p_1^2\right) + b\left(q_{10}^2 - q_1^2\right) \\ &\quad - 2\left[x_0'(\gamma_{10} - \gamma_1) + y_0'(\gamma_{10}' - \gamma_1') + z_0'(1 - \gamma_1'')\right] \\ &\quad + k\left[a\left(\gamma_{10}^2 - \gamma_1^2\right) + b\left(\gamma_{10}'^2 - \gamma_1'^2\right) + \left(1 - \gamma_1''^2\right)\right], \\ S_2 &= a(p_{10}\gamma_{10} - p_1\gamma_1) + b(q_{10}\gamma_{10}' - q_1\gamma_1') + \frac{(1 - \gamma_1'')\ell_3}{\left(Cc\sqrt{\gamma_0''}\right)}. \end{aligned} \tag{20}$$

3. Reduction of the Equations of Motion to a Quasi-Linear Autonomous System

In this section, we reduce the equations of motion to a quasi-linear autonomous system [11]. From equations (17) and (18), we obtain

$$\begin{aligned} r_1 &= 1 + 0.5\varepsilon^{-2}\left[S_1 + 2z_0'(1 - \gamma_1'') - k\left(1 - \gamma_1''^2\right)\right] + \cdots, \\ \gamma_1'' &= 1 + \varepsilon^{-1} S_2 - 0.5\varepsilon^{-2}\left[S_1 + 2z_0'(1 - \gamma_1'') - k\left(1 - \gamma_1''^2\right)\right] + \cdots. \end{aligned} \tag{21}$$

Differentiating equations (11) and (14) and using (21), one obtains

$$\begin{aligned} p_1 + \omega'^2 p_1 &= \varepsilon^{-1}\left\{z_0'\left(a^{-1} - A_1 b^{-1}\right)\gamma_1 + A_1 b^{-1} x_0' + k\left(\omega^2 - A_1\right)\gamma_1 + \left[b^{-1}(x_0' - z_0'\gamma_1) - kB_1\gamma_1\right]A^{-1} r_0^{-1}\ell_3\right\} \\ &\quad + \varepsilon^{-2}\left\{\left[-\omega^2 p_1 S_1 + A_1 b^{-1} x_0' S_2 + A_1 C_1 p_1 q_1^2 - A_1 q_1 x_0'\gamma_1' - y_0'\gamma_1 + a^{-1} y_0'(q_1\gamma_1 - p_1\gamma_1') - a^{-1} z_0' p_1\right]\right. \\ &\quad + A_1 k\left[p_1\left(1 - \gamma_1'^2\right) + q_1(1 - C_1)\gamma_1\gamma_1' - S_2(1 + B_1)\gamma_1\right] + 0.5 r_0^{-1}\ell_3 p_1\left(A^{-1}B_1 - A_1 B^{-1}\right) \\ &\quad \times \left.\left[S_1 + 2z_0'(1 - \gamma_1'') - k\left(1 - \gamma_1''^2\right)\right] + A^{-1} r_0^{-1}\ell_3\left(b^{-1}x_0' - kb_1\gamma_1\right)S_2\right\} \\ &\quad + \varepsilon^{-3}\left\{0.5 z_0'\left(a^{-1} - A_1 b^{-1}\right)\gamma_1\left[S_1 + 2z_0'(1 - \gamma_1'') - k\left(1 - \gamma_1''^2\right)\right]\right. \\ &\quad \left. + 0.5 A^{-1} r_0^{-1}\ell_3\left(kB_1\gamma_1 - b^{-1}x_0'\right)\left[S_1 + 2z_0'(1 - \gamma_1'') - k\left(1 - \gamma_1''^2\right)\right] + p_1 S_2\left(2kA_1 - a^{-1}z_0'\right)\right\} + \cdots, \end{aligned} \tag{22}$$

$$\begin{aligned} \gamma_1 + \gamma_1 &= \varepsilon^{-1}\left[(1 + B_1) - B^{-1} r_0^{-1}\ell_3\right]p_1 \\ &\quad + \varepsilon^{-2}\left[-S_1\gamma_1 + (1 + B_1)p_1 S_2 + (1 - C_1)p_1 q_1\gamma_1' + x_0'\gamma_1'^2 + x_0' b^{-1} - \gamma_1\left(y_0'\gamma_1' + z_0' b^{-1} + q_1^2\right) + k\left(C_1\gamma_1'^2 - B_1\right)\gamma_1'\right] \\ &\quad + \varepsilon^{-3}\left[2b^{-1}x_0' - \gamma_1\left(b^{-1}z_0' + 2kB_1\right)\right]S_2 + \cdots, \end{aligned} \tag{23}$$

where

$$\begin{aligned} \omega^2 &= -A_1 B_1 = \frac{(A - C)(B - C)}{AB} = \frac{(a - 1)(b - 1)}{ab}, \\ \omega'^2 &= \omega^2 - \left(A^{-1}B_1 - A_1 B^{-1}\right) r_0^{-1}\ell_3. \end{aligned} \tag{24}$$

We note that $\omega^2 > 0$ when $A < B < C$ or $A > B > C$ but $\omega'^2 > 0$ when $A < B < C$ only.

In case $A > B > C$, we find that the term $(A^{-1}B_1 - A_1 B^{-1})$ is positive and since r_o is sufficiently small; that is, the term $(A^{-1}B_1 - A_1 B^{-1}) r_0^{-1}\ell_3$ tends to infinity, and ω'^2 is negative.

Solving equation (11) for q_1 and equation (14) for γ_1', we obtain

$$q_1 = A_1^{-1} r_1^{-1}\left(1 - A^{-1}A_1^{-1}r_0^{-1}\ell_3 r_1^{-1} + \cdots\right) \cdot \left[-\dot{p}_1 + \varepsilon^{-1}a^{-1}\left(y_0'\gamma_1'' - z_0'\gamma_1' + kaA_1\gamma_1'\gamma''\right)\right], \tag{25}$$

$$\gamma_1' = r_1^{-1}\left(\dot{\gamma}_1 + +\varepsilon^{-1}q_1\gamma_1''\right). \tag{26}$$

Making use of equations (21) and (26) into equations (22) and (23), we obtain a quasi-linear autonomous system with two degrees of freedom and depend on $p_1, \dot{p}_1, \gamma_1, \dot{\gamma}_1, p_{10}, \dot{p}_{10}, \gamma_{10}$, and $\dot{\gamma}_{10}$.

Introducing the new variables as follows:

$$\begin{aligned} p_2 &= p_1 - \varepsilon^{-1}(\chi + \chi_1\gamma_2), \\ \gamma_2 &= \gamma_1 - \varepsilon^{-1}\nu p_2, \end{aligned} \tag{27}$$

where

$$\begin{aligned} \chi &= x_0'\left(b\omega'^2\right)^{-1}\left(A_1 + A^{-1}r_0^{-1}\ell_3\right), \\ \nu &= \left(1 - \omega'^2\right)^{-1}\left[1 + B_1 - B^{-1}r_0^{-1}\ell_3\right], \\ \chi_1 &= \left(1 - \omega'^2\right)^{-1}\left[-z_0'\left(a^{-1} - A_1b^{-1}\right) + k\left(A_1 - \omega^2\right) + A^{-1}r_0^{-1}\ell_3\left(b^{-1}z_0' + kB_1\right)\right]. \end{aligned} \tag{28}$$

Using equations (27), (21), and (26), we obtain

$$S_i = S_{i1} + 2^{2-i}\varepsilon^{-1}S_{i2} + \cdots, \quad (i = 1, 2), \tag{29}$$

where

$$\begin{aligned} S_{11} &= a\left(p_{20}^2 - p_2^2\right) + b\chi_3^2\left(\dot{p}_{20}^2 - \dot{p}_2^2\right) - 2x_0'(\gamma_{20} - \gamma_2) - 2y_0'\left(\dot{\gamma}_{20} - \dot{\gamma}_2\right) + k\left[a\left(\gamma_{20}^2 - \gamma_2^2\right) + b\left(\dot{\gamma}_{20}^2 - \dot{\gamma}_2^2\right)\right], \\ S_{12} &= a\left[\chi(p_{20} - p_2) + \chi_1(p_{20}\gamma_{20} - p_2\gamma_2)\right] - b\chi_3^2\left[a^{-1}y_0'\left(\dot{p}_{20} - \dot{p}_2\right) - \chi_2\left(\dot{p}_{20}\dot{\gamma}_{20} - \dot{p}_2\dot{\gamma}_2\right)\right] - \nu x_0'(p_{20} - p_2) \\ &\quad - y_0'\nu_1\left(\dot{p}_{20} - \dot{p}_2\right) + (z_0' - k)S_{21} + k\left[\nu a(p_{20}\gamma_{20} - p_2\gamma_2) + \nu_1 b\left(\dot{p}_{20}\dot{\gamma}_{20} - \dot{p}_2\dot{\gamma}_2\right)\right], \\ S_{21} &= a(p_{20}\gamma_{20} - p_2\gamma_2) - b\chi_3\left(\dot{p}_{20}\dot{\gamma}_{20} - \dot{p}_2\dot{\gamma}_2\right), \\ S_{22} &= a\left[\nu\left(p_{20}^2 - p_2^2\right) + \chi(\gamma_{20} - \gamma_2) + \chi_1\left(\gamma_{20}^2 - \gamma_2^2\right)\right] + b\chi_3\left[-\nu_1\left(\dot{p}_{20}^2 - \dot{p}_2^2\right) + a^{-1}y_0'\left(\dot{\gamma}_{20} - \dot{\gamma}_2\right) - \chi_2\left(\dot{\gamma}_{20}^2 - \dot{\gamma}_2^2\right)\right] - \frac{S_{21}\ell_3}{\left(Cc\sqrt{\gamma_0''}\right)}, \end{aligned} \tag{30}$$

where

$$\begin{aligned} \chi_3 &= A_1^{-1}\left(1 - A^{-1}A_1^{-1}r_0^{-1}\ell_3\right), \\ \chi_2 &= \chi_1 + a^{-1}z_0' - kA_1, \\ \nu_1 &= \nu - \chi_3. \end{aligned} \tag{31}$$

Formulas (21) and (29) lead to

$$\begin{aligned} r_1 &= 1 + 0.5\varepsilon^{-2}S_{11} + \varepsilon^{-3}\left(S_{12} - z_0'S_{21} + kS_{21}\right) + \cdots, \\ \gamma_1'' &= 1 + \varepsilon^{-1}S_{21} + \varepsilon^{-2}\left(S_{22} - 0.5S_{11}\right) - \varepsilon^{-3}\left(S_{12} - z_0'S_{21} + kS_{21}\right) + \cdots. \end{aligned} \tag{32}$$

In terms of $p_2 \cdot \gamma_2$, and the rigid body parameters, we find that

$$\begin{aligned} q_1 &= -\chi_3\dot{p}_2 + \varepsilon^{-1}\chi_3\left(a^{-1}y_0' - \chi_2\dot{\gamma}_2\right) + \varepsilon^{-2}\left[\chi_3\nu_1\dot{p}_2\left(kA_1 - a^{-1}z_0'\right) + S_{11}\dot{p}_2\left(\chi_3 - 0.5A_1^{-1}\right) + \chi_3S_{21}\left(kA_1\dot{\gamma}_2 + a^{-1}y_0'\right)\right] + \cdots, \\ \gamma_1' &= \dot{\gamma}_2 + \varepsilon^{-1}\nu_1\dot{p}_2 + \varepsilon^{-2}\left[\chi_3\left(a^{-1}y_0' - \chi_2\dot{\gamma}_2 - S_{21}\dot{p}_2\right) - 0.5S_{11}\dot{\gamma}_2\right] + \cdots. \end{aligned} \tag{33}$$

Substituting equations (27), (29), (30), (32), and (33) into equations (23) and (24), we obtain a quasi-linear autonomous system of two degrees of freedom in the following form:

$$\begin{aligned} \ddot{p}_2 + \omega'^2 p_2 &= \varepsilon^{-2}F\left(p_2, \dot{p}_2, \gamma_2, \dot{\gamma}_2, \varepsilon^{-1}\right), \\ \ddot{\gamma}_2 + \gamma_2 &= \varepsilon^{-2}\phi\left(p_2, \dot{p}_2, \gamma_2, \dot{\gamma}_2, \varepsilon^{-1}\right), \end{aligned} \tag{34}$$

where

$$
\begin{aligned}
&F = F_2 + \varepsilon^{-1}F_3 + \ldots, \phi = \phi_2 + \varepsilon^{-1}\phi_3 + \ldots,\\
&F_2 = f_2 - \nu\chi_1\left(1-\omega'^2\right)p_2, \phi_2 = \varphi_2 + \nu\left(1-\omega'^2\right)(\chi+\chi_1\gamma_2),\\
&F_3 = f_2 - \chi_1\varphi_2 - \nu\chi_1\left(1-\omega'^2\right)(\chi+\chi_1\gamma_2), \phi_3 = \varphi_3 - \nu f_2 + \nu^2\chi_1\left(1-\omega'^2\right)p_2,\\
&f_2 = -\omega^2 S_{11}p_2 + A_1x_0'\left(b^{-1}S_{21} + \chi_3\dot\gamma_2\dot p_2\right) + A_1C_1\chi_3^2p_2\dot p_2^2\\
&\quad - y_0'\chi_3\gamma_2\dot p_2\left(A_1 + a^{-1}\right) - a^{-1}p_2\left(z_0' + y_0'\dot\gamma_2\right) + A_1k\left(1-\dot\gamma_2^2\right)p_2 + (C_1-1)\chi_3\gamma_2\dot\gamma_2\dot p_2\\
&\quad - (1+B_1)S_{21}\gamma_2 + 0.5r_0^{-1}\ell_3\left[2p_2\left(A^{-1}B_1 - A_1B^{-1}\right)S_{11} + A^{-1}\left(b^{-1}x_0' - kB_1\gamma_2\right)S_{21}\right],\\
&f_3 = -2\omega^2p_2S_{12} + (\chi+\chi_1\gamma_2)\left\{-\omega^2S_{11} - a^{-1}\left(z_0' + y_0'\dot\gamma_2\right) + A_1\left[C_1\chi_3^2\dot p_2^2 + k\left(1-\dot\gamma_2^2\right)\right]\right\} + A_1b^{-1}x_0'S_{22}\\
&\quad + A_1\chi_3\dot p_2\left(x_0'\nu_1\dot p_2 - y_0'\nu p_2\right) - p_2\dot p_2\left[a^{-1}y_0'(\nu_1+\nu\chi) + 2A_1k\nu_1\dot\gamma_2\right]\\
&\quad + \chi_3\dot p_2\left(\nu_1\gamma_2\dot p_2 + \nu\dot\gamma_2p_2\right)(C_1-1) - (1-B_1)\left(\nu S_{21}p_2 + S_{22}\gamma_2\right)\\
&\quad + 0.5z_0'\left(a^{-1} - A_1b^{-1}\right)\gamma_2S_{11} + \left(2kA_1 - a^{-1}z_0'\right)p_2S_{21} + \chi_3\left(a^{-1}y_0' - \chi_2\dot\gamma_2\right)\\
&\quad \times\left[-A_1\left(2C_1\chi_3p_2\dot p_2 + x_0'\dot\gamma_2\right) + y_0'\gamma_2\left(A_1 + a^{-1}\right) + \gamma_2\dot\gamma_2^2(1-C_1)\right]\\
&\quad + 0.5r_0^{-1}\ell_3\left\{\left(A^{-1}B_1 - A_1B^{-1}\right)\left[2p_2\left(S_{12} - z_0'S_{21} + kS_{21}\right) + (\chi+\chi_1\gamma_2)S_{11}\right] + \left[2A^{-1}\left[\left(b^{-1}x_0' - kB_1\gamma_2\right)S_{22} - kB_1\nu S_{21}p_2\right]\right.\right.\\
&\quad \left.\left. + A^{-1}\left(kB_1\gamma_2 - b^{-1}x_0'\right)S_{11}\right]\right\},\\
&\varphi_2 = \left[(1+B_1)S_{21} - (1-C_1)\chi_3\dot\gamma_2\dot p_2\right]p_2 + x_0'\left(b^{-1} + \dot\gamma_2^2\right) + \left[k\left(C_1\dot\gamma_2^2 - B_1\right) - y_0'\dot\gamma_2 - z_0'b^{-1} - \chi_3^2\dot p_2^2 - S_{11}\right]\gamma_2,\\
&\varphi_3 = (1+B_1)\left[p_2S_{22} + (\chi+\chi_1\gamma_2)S_{21}\right] + \chi_3(1-C_1)\times\left\{\left(a^{-1}y_0' - \chi_2\dot\gamma_2\right)\dot\gamma_2p_2 - \dot p_0\left[\nu_1p_2\dot p_2 + (\chi+\chi_1\gamma_2)\dot\gamma_2\right]\right\}\\
&\quad - 2\gamma_2S_{12} - \nu p_2S_{11} + 2x_0'\nu_1\dot\gamma_2\dot p_2 - y_0'\left(\nu_1\gamma_2\dot p_2 + \nu\dot\gamma_2p_2\right) - \nu p_2\left(b^{-1}z_0' + \chi_3^2\dot p_2^2\right) + 2\chi_3^2\left(a^{-1}y_0' - \chi_2\dot\gamma_2\right)\times\gamma_2\dot p_2\\
&\quad + k\left[2C_1\nu_1\gamma_2\dot\gamma_2\dot p_2 + \nu\left(C_1\dot\gamma_2^2 - B_1\right)p_2\right] + \left[2b^{-1}x_0' - \left(b^{-1}z_0' + 2kB_1\right)\gamma_2\right]S_{21}.
\end{aligned}
\tag{35}
$$

System (34) has the first integral obtained from equations (17)–(19) as follows:

$$
\gamma_2^2 + \dot\gamma_2^2 + 2\varepsilon^{-1}\left(\nu\gamma_2p_2 + \nu_1\dot\gamma_2\dot p_2 + S_{21}\right) + \varepsilon^{-2}\left[\nu^2p_2^2 + 2\chi_3\dot\gamma_2\left(a^{-1}y_0' - \chi_2\dot\gamma_2 - S_{21}\dot p_2\right) - \left(1+\dot\gamma_2^2\right)S_{11} + 2S_{22}\right] + \cdots = \left(\gamma_0''\right)^{-2} - 1.
\tag{36}
$$

We aim to find the periodic solutions for system (36) under the condition $A<B<C$ (ω'^2 is positive) [12]. In this case, the body rotates about the minor axis of the ellipsoid of inertia surface [13] with initial sufficiently small angular velocity r_0.

4. Formal Construction of the Periodic Solutions

Without a loss of generality, since the system (34) is autonomous, we assume that [14]

$$
\begin{aligned}
p_2(0,0) &= 0,\\
\dot p_2(0,0) &= 0,\\
\dot\gamma_2\left(0,\varepsilon^{-1}\right) &= 0.
\end{aligned}
\tag{37}
$$

The generating system of equation (34) is

$$
\begin{aligned}
\ddot p_2^{(0)} + \omega'^2p_2^{(0)} &= 0,\\
\ddot\gamma_2^{(0)} + \gamma_2^{(0)} &= 0,
\end{aligned}
\tag{38}
$$

which has periodic solutions as follows:

$$p_2^{(0)} = M_1 \cos \omega' \tau + M_2 \sin \omega' \tau,$$
$$\gamma_2^{(0)} = M_3 \cos \tau, \tag{39}$$

with a period $T_0 = 2\pi n$, where $M_i, i = (1, 2, 3)$, are constants to be determined. Consider the required periodic solutions of system (34) in the following form:

$$p_2\left(\tau, \varepsilon^{-1}\right) = (M_1 + \beta_1)\cos \omega' \tau + (M_2 + \beta_2)\sin \omega' \tau + \sum_{k=2}^{\infty} \varepsilon^{-k} G_k(\tau),$$
$$\gamma_2\left(\tau, \varepsilon^{-1}\right) = (M_3 + \beta_3)\cos \tau + \sum_{k=2}^{\infty} \varepsilon^{-k} H_k(\tau), \tag{40}$$

with a period $T(\varepsilon^{-1}) = T_0 + \alpha(\varepsilon^{-1})$. The quantities $\beta_1, \omega'\beta_2$, and β_3 represent the deviations of solutions $p_2, \dot{p}_2$, and γ_2 at any ε from their initial values when $\varepsilon \longrightarrow \infty$. Let the initial condition of system (40) be of the following form:

$$p_2\left(0, \varepsilon^{-1}\right) = M_1 + \beta_1,$$
$$\dot{p}_2\left(0, \varepsilon^{-1}\right) = \omega'(M_2 + \beta_2),$$
$$\gamma_2\left(0, \varepsilon^{-1}\right) = M_3 + \beta_3,$$
$$\dot{\gamma}_2\left(0, \varepsilon^{-1}\right) = 0. \tag{41}$$

Consider the new function as follows:

$$U = u + \frac{\partial u}{\partial M_1}\beta_1 + \frac{\partial u}{\partial M_2}\beta_2 + \frac{\partial u}{\partial M_3}\beta_3 + 0.5\frac{\partial^2 u}{\partial M_1^2}\beta_1^2 + \cdots,$$
$$\begin{pmatrix} U = G_k, H_k \\ u = g_k, h_k \end{pmatrix}, \tag{42}$$

such that

$$g_k(\tau) = \frac{1}{\omega'}\int_0^{\tau} F_k'(t_1)\sin \omega'(\tau - t_1)\mathrm{d}t_1,$$
$$h_k(\tau) = \int_0^{\tau} \phi_k'(t_1)\sin(\tau - t_1)\mathrm{d}t_1 \quad (k = 2, 3), \tag{43}$$

where

$$F_k'(\tau) = \frac{1}{(k-2)!}\left(\frac{\mathrm{d}^{k-2}F}{\mathrm{d}\varepsilon^{2-k}}\right)_{\beta=\varepsilon^{-1}=0},$$
$$\phi_k'(\tau) = \frac{1}{(k-2)!}\left(\frac{\mathrm{d}^{k-2}\phi}{\mathrm{d}\varepsilon^{2-k}}\right)_{\beta=\varepsilon^{-1}=0}. \tag{44}$$

We note that the right-hand sides of (34) begin with terms of order ε^{-2} and so

$$F_k'(\tau) = F_k\left(p_2^{(0)}, \dot{p}_2^{(0)}, \gamma_2^{(0)}, \dot{\gamma}_2^{(0)}\right) \equiv F_k^{(0)},$$
$$\phi_k'(\tau) = \phi_k\left(p_2^{(0)}, \dot{p}_2^{(0)}, \gamma_2^{(0)}, \dot{\gamma}_2^{(0)}\right) \equiv \phi_k^{(0)}, \quad k = 2, 3. \tag{45}$$

Now, we find the expressions of $\phi_k^{(0)}$ and $F_k^{(0)}$. Periodic solutions (39) are reformulated in the following form:

$$p_2^{(0)} = E\cos(\omega'\tau - \eta),$$
$$\gamma_2^{(0)} = M_3 \cos \tau, \tag{46}$$

where $E = \sqrt{M_1^2 + M_2^2}$ and $\eta = \tan^{-1}(M_2/M_1)$.

Using equations (29) and (39), we obtain

$$S_{ij}^{(0)} = S_{ij}^{(0)}\left(p_2^{(0)}, \dot{p}_2^{(0)}, \gamma_2^{(0)}, \dot{\gamma}_2^{(0)}\right) \quad (i, j = 1, 2),$$
$$S_{11}^{(0)} = E^2\left[a\left(\cos^2 \eta - 0.5\right) + b\chi_3^2\omega'^2\left(\sin^2 \eta - 0.5\right) + 0.5\left(b\chi_3^2\omega'^2 - a\right)\cos 2(\omega'\tau - \eta)\right]$$
$$- 2M_3\left[x_0'(1 - \cos \tau) + y_0' \sin \tau\right] - 0.5kM_3^2C_1(1 - \cos 2\tau),$$
$$S_{21}^{(0)} = M_3E\left\{a\cos^2 \eta + 0.5(b\omega'\chi_3 - a)\cos\left[(\omega' - 1)\tau - \eta\right] - 0.5(b\omega'\chi_3 + a)\cos\left[(\omega' + 1)\tau - \eta\right]\right\},$$
$$S_{12}^{(0)} = aE\{\chi_3[\cos \eta - \cos(\omega'\tau - \eta)] + \chi_1 M_3[\cos \eta - \cos \tau \cos(\omega'\tau - \eta)]\} - b\chi_3^2 E[\cos \eta - \cos(\omega'\tau - \eta)]$$
$$+ \chi_2 M_3 \sin \tau \sin(\omega'\tau - \eta)$$
$$- \nu x_0' E[\cos \eta - \cos(\omega'\tau - \eta)] + kEM_3\{\nu a[\cos \eta - \cos \tau \cos(\omega'\tau - \eta)] - \nu_1 b \sin \tau \sin(\omega'\tau - \eta)\} + (z_0' - k)S_{21}^{(0)},$$
$$S_{22}^{(0)} = a\left\{\nu E^2\left[\cos^2 \eta - \cos^2(\omega'\tau - \eta)\right] + \chi M_3(1 - \cos \tau) + \chi_1 M_3^2 \sin^2 \tau\right\}$$
$$+ b\chi_3\left\{a^{-1}y_0' M_3 \sin \tau - \nu_1 E^2\omega'^2\left[\sin^2 \eta - \sin^2(\omega'\tau - \eta)\right] + \chi_2 M_3^2 \sin^2 \tau\right\} - S_{21}^{(0)}\ell_3/\left(Cc\sqrt{\gamma_0''}\right). \tag{47}$$

Substituting equations (46) and (47) into equation (35), we obtain

$$\begin{aligned} F_2^{(0)} &= M_1 L(\omega')\cos\omega'\tau + M_2 L(\omega')\sin\omega'\tau + \cdots, \\ \phi_2^{(0)} &= M_3 N(\omega')\cos\tau + \cdots, \end{aligned} \tag{48}$$

$$\begin{aligned} L(\omega') = {} & \omega^2\left[-\left(aM_1^2 + b\omega'^2\chi_3^2M_2^2\right) + b\omega'^2\chi_3^2\left(M_1^2 + M_2^2\right)\right] \\ & + A_1C_1\omega'^2\chi_3^2\left(M_1^2 + M_2^2\right) + 2M_3x_0'\omega^2 + k\left(A_1 + 0.5M_3^2\omega^2C_1\right) - \left[z_0'a^{-1} + \nu\chi_1\left(1 - \omega'^2\right)\right] \\ & + 0.5r_0^{-1}\ell_3\left(A^{-1}B_1 - A_1B^{-1}\right)\left[aM_1^2 + b\omega'^2\chi_3^2M_2^2 - b\omega'^2\chi_3^2\left(M_1^2 + M_2^2\right) - 2M_3x_0' - 0.5kM_3^2C_1\right], \end{aligned} \tag{49}$$

$$\begin{aligned} N(\omega') = {} & -\left(aM_1^2 + b\omega'^2\chi_3^2M_2^2\right) - \left(M_1^2 + M_2^2\right)\left[aB_1 + \omega'^2\chi_3^2(1-b)\right] \\ & + 2M_3x_0' - \left[z_0'b^{-1} - \nu\chi_1\left(1 - \omega'^2\right)\right] + k\left(M_3^2C_1 - B_1\right). \end{aligned} \tag{50}$$

From equations (33), (49), and (50), we obtain

$$\begin{aligned} & g_2(T_0) = -\pi n(\omega')^{-1}M_2L(\omega'), \dot{g}_2(T_0) = \pi nM_1L(\omega'), \\ & h_2(T_0) = 0, \dot{h}_2(T_0) = \pi nM_3N(\omega'), \end{aligned} \tag{51}$$

where the constants $M_1, \omega' M_2,$ and M_3, the deviations $\beta_1(\varepsilon^{-1}), \omega'\beta_2(\varepsilon^{-1})$, and $\beta_3(\varepsilon^{-1})$, and the correction of the period α are determined from the periodicity conditions and their derivatives:

$$\begin{aligned} \psi_1 &= p_2\left(T_0 + \alpha, \varepsilon^{-1}\right) - p_2\left(0, \varepsilon^{-1}\right) = 0, \\ \psi_2 &= \dot{p}_2\left(T_0 + \alpha, \varepsilon^{-1}\right) - \dot{p}_2\left(0, \varepsilon^{-1}\right) = 0, \\ \psi_3 &= \gamma_2\left(T_0 + \alpha, \varepsilon^{-1}\right) - \gamma_2\left(0, \varepsilon^{-1}\right) = 0, \\ \psi_4 &= \dot{\gamma}_2\left(T_0 + \alpha, \varepsilon^{-1}\right) - \dot{\gamma}_2\left(0, \varepsilon^{-1}\right) = 0. \end{aligned} \tag{52}$$

Due to the existence of first integral (36) for system (34), the condition $\psi_3 = 0$ is not independent [15]; then, integral (36) becomes

$$\begin{aligned} & \gamma_2^2\left(T_0 + \alpha, \varepsilon^{-1}\right) + \dot{\gamma}_2^2\left(T_0 + \alpha, \varepsilon^{-1}\right) + 2\varepsilon^{-1}\left[\nu\gamma_2\left(T_0 + \alpha, \varepsilon^{-1}\right)p_2\left(T_0 + \alpha, \varepsilon^{-1}\right) + \nu_1\dot{\gamma}_2\left(T_0 + \alpha, \varepsilon^{-1}\right) \times \dot{p}_2\left(T_0 + \alpha, \varepsilon^{-1}\right) + S_{21}\left(T_0 + \alpha, \varepsilon^{-1}\right)\right] \\ & \quad + \varepsilon^{-2}\left\{\nu^2p_2^2\left(T_0 + \alpha, \varepsilon^{-1}\right) + 2\chi_3\dot{\gamma}_2\left(T_0 + \alpha, \varepsilon^{-1}\right)\left[a^{-1}y_0' - \chi_2\dot{\gamma}_2\left(T_0 + \alpha, \varepsilon^{-1}\right) - S_{21}\left(T_0 + \alpha, \varepsilon^{-1}\right)\dot{p}_2\left(T_0 + \alpha, \varepsilon^{-1}\right)\right]\right. \\ & \quad \left. - S_{11}\left(T_0 + \alpha, \varepsilon^{-1}\right)\left[1 + \dot{\gamma}_2^2\left(T_0 + \alpha, \varepsilon^{-1}\right)\right]\right\} + 2S_{22}\left(T_0 + \alpha, \varepsilon^{-1}\right)\Big\} + \ldots \\ & = \gamma_2^2\left(0, \varepsilon^{-1}\right) + \dot{\gamma}_2^2\left(0, \varepsilon^{-1}\right) + 2\varepsilon^{-1}\left[\nu\gamma_2\left(0, \varepsilon^{-1}\right)p_2\left(0, \varepsilon^{-1}\right) + \nu_1\dot{\gamma}_2\left(0, \varepsilon^{-1}\right)\dot{p}_2\left(0, \varepsilon^{-1}\right) + S_{21}\left(0, \varepsilon^{-1}\right)\right] \\ & \quad + \varepsilon^{-2}\left\{\nu^2p_2^2\left(0, \varepsilon^{-1}\right) + 2\chi_3\dot{\gamma}_2\left(0, \varepsilon^{-1}\right)\left[a^{-1}y_0' - \chi_2\dot{\gamma}_2\left(0, \varepsilon^{-1}\right) - S_{21}\left(0, \varepsilon^{-1}\right)\dot{p}_2\left(0, \varepsilon^{-1}\right)\right] - S_{11}\left(0, \varepsilon^{-1}\right)\right. \\ & \quad \left. \cdot\left[1 + \dot{\gamma}_2^2\left(0, \varepsilon^{-1}\right)\right] + 2S_{22}\left(0, \varepsilon^{-1}\right)\right\} + \ldots. \end{aligned} \tag{53}$$

Using condition (41) and equation (52), we obtain

$$\psi_3^2 + 2(M_3 + \beta_3)\psi_3 + \varepsilon^{-1}\varphi_1\left(\psi_1, \psi_2, \psi_4, \varepsilon^{-1}\right) = 0, \tag{54}$$

where φ_1 is an entire function in their variables and $\varphi_1(0, 0, 0, \varepsilon^{-1}) = 0$; then if $M_3 \neq 0$, form (54) gives

$$\psi_3 = f_1\left(\psi_1, \psi_2, \psi_4, \varepsilon^{-1}\right), \tag{55}$$

where f_1 is an entire function in all their arguments and $f_1(0, 0, 0, \varepsilon^{-1}) = 0$; then, the condition $\psi_3 = 0$ in (52) is satisfied with the following condition:

$$\psi_1 = \psi_2 = \psi_4 = 0. \tag{56}$$

Substituting initial conditions (41) into equation (56) with $\tau = 0$, we obtain

$$M_3^2 + 2M_3\beta_3 + \beta_3^2 + 2\varepsilon^{-1}\nu M_3(M_1 + \beta_1) + \cdots = \left(\gamma_0''\right)^{-2} - 1. \tag{57}$$

Assume that γ_0'' does not depend on ε; we obtain that

$$\begin{aligned} M_3^2 &= \left(\gamma_0''\right)^{-2} - 1, \\ \beta_3^2 + 2M_3\beta_3 + 2\varepsilon^{-1}\nu M_3(M_1 + \beta_1) + \cdots &= 0. \end{aligned} \tag{58}$$

From (58) and (8), we obtain

$$M_3 = \frac{\sqrt{\left(1-\gamma_0''^2\right)}}{\gamma_0''}, \quad 0 < M_3 < \infty, \qquad (59)$$

$$\beta_3 = -\varepsilon^{-1}\nu(M_1+\beta_1)+\cdots,$$

where γ_0'' is an arbitrary parameter and M_3 is the arbitrary constant.

This means that periodic solutions (40) depend on arbitrary constant M_3 and the function $\beta_3(\varepsilon^{-1})$ which is equal to 0 when $\varepsilon \longrightarrow \infty$. Independent periodic solutions (52) are expanded in a power series of α (neglecting terms of $\varepsilon^{-2}\alpha$); then, we obtain

$$\begin{aligned} p_2\left(T_0,\varepsilon^{-1}\right)+\alpha\dot{p}_2\left(T_0,\varepsilon^{-1}\right)+\ldots &= p_2\left(0,\varepsilon^{-1}\right),\\ \dot{p}_2\left(T_0,\varepsilon^{-1}\right)+\alpha\ddot{p}_2\left(T_0,\varepsilon^{-1}\right)+\ldots &= \dot{p}_2\left(0,\varepsilon^{-1}\right),\\ \dot{\gamma}_2\left(T_0,\varepsilon^{-1}\right)+\alpha\ddot{\gamma}_2\left(T_0,\varepsilon^{-1}\right)+\ldots &= \dot{\gamma}_2\left(0,\varepsilon^{-1}\right). \end{aligned} \qquad (60)$$

Using initial values (41) in the above relations, we put independent periodicity conditions (56) in the following form:

$$\begin{aligned} p_2\left(T_0,\varepsilon^{-1}\right)+\alpha\omega'(M_2+\beta_2) &= (M_1+\beta_1),\\ \dot{p}_2\left(T_0,\varepsilon^{-1}\right)-\omega'(M_2+\beta_2) &= \alpha\omega'(M_1+\beta_1),\\ \dot{\gamma}_2\left(T_0,\varepsilon^{-1}\right) &= \alpha(M_3+\beta_3). \end{aligned} \qquad (61)$$

Using equations (40), (59), and the last equation of (61), we obtain the following function:

$$\alpha\left(\varepsilon^{-1}\right) = \varepsilon^{-2}(M_3+\beta_3)^{-1}\left[\dot{H}_2(T_0)+\varepsilon\dot{H}_3(T_0)+\ldots\right]. \qquad (62)$$

Thus, neglecting the terms of order α^2 and $\varepsilon^{-2}\alpha$ in (61), we find that the terms of the order ε^{-4} are neglected. Using equations (37) and (41), we obtain the periodic solutions with basic amplitudes equal to zero, that is [16],

$$M_1 = M_2 = 0. \qquad (63)$$

Substituting equations (62), (63), and (40) into the first two equations from (61), we obtain the following system for determining β_1 and β_2:

$$\begin{aligned} G_2(T_0)+\varepsilon^{-1}G_3(T_0)+\omega'\beta_2(M_3+\beta_3)^{-1}\left[\dot{H}_2(T_0)+\varepsilon^{-1}\dot{H}_3(T_0)\right]+\varepsilon^{-2}(\ldots) &= 0,\\ \dot{G}_2(T_0)+\varepsilon^{-1}\dot{G}_3(T_0)-\omega'^2\beta_1(M_3+\beta_3)^{-1}\left[\dot{H}_2(T_0)+\varepsilon^{-1}\dot{H}_3(T_0)\right]+\varepsilon^{-2}(\ldots) &= 0. \end{aligned} \qquad (64)$$

Due to (51), the above system becomes

$$\begin{aligned} -\pi n\beta_2(\omega')^{-1}\left[L_1(\omega')-\omega'^2N_1(\omega')\right]+\varepsilon^{-1}\left[G_3(T_0)+\ldots\right] &= 0,\\ \pi n\beta_1\left[L_1(\omega')-\omega'^2N_1(\omega')\right]+\varepsilon^{-1}\left[\dot{G}_3(T_0)+\ldots\right] &= 0, \end{aligned} \qquad (65)$$

where $L_1(\omega')$ and $N_1(\omega')$ are obtained from (50) replacing M_1, M_2, M_3 by β_1, β_2, and $M_3+\beta_3$. Making use of equations (24), (28), (31), and (49), we obtain

$$\begin{aligned} L_1(\omega')-\omega'^2N_1(\omega') = \left(\beta_1^2+\beta_2^2\right)W_1(\omega')+z_0'W_2(\omega')\\ +kW_3(\omega')+W_4(\omega'), \end{aligned} \qquad (66)$$

where

$$\begin{aligned} W_1(\omega') &= d_1+(d_2+d_3)r_0^{-1}\ell_3,\\ W_2(\omega') &= (d_4-d_5d_6d_7)+r_0^{-1}\ell_3\left[d_5d_6(d_8+d_9)+B^{-1}d_7-d_{10}\left(1+a^{-1}d_6d_7\right)\right],\\ W_3(\omega') &= (d_5d_6d_{11}+d_{12})+r_0^{-1}\ell_3\left\{d_5\left[(d_{13}-d_{14})-B^{-1}d_{11}\right]+b^{-1}d_{10}\left(a^{-1}d_6d_{11}+d_{15}\right)\right]\right\}r_0^{-1}\ell_3,\\ W_4(\omega') &= -0.5ad_{10}\left[\beta_1^2+\left(\frac{a-1}{b-1}\right)\beta_2^2\right]r_0^{-1}\ell_3,\\ d_1 &= b^{-1}(a-1)(2a-b-1),\\ d_2 &= b^{-2}[b(a-b)+(a-1)]\left[aA^{-1}(a-1)(1-b)^{-1}+bB^{-1}\right], \end{aligned}$$

$$
\begin{aligned}
d_3 &= 0.5A^{-1}(1-A)\left[ab^{-1}(1-a)(1-b)^{-1}+AB^{-1}\right],\\
d_4 &= a^{-1}\left[1-b^{-2}(a-1)(b-1)\right],\\
d_5 &= (ab)^{-2}[ab+(a-1)(b-1)],\\
d_6 &= b^{-1}(a+b-1),\\
d_7 &= (ab)^{-1}(2b-1)[ab+(a-1)(b-1)],\\
d_8 &= (Ab)^{-1}[ab+(a-1)(b-1)],\\
d_9 &= (ab)^{-1}(2b-1)\left[A^{-1}a(a-1)+B^{-1}b(b-1)\right],\\
d_{10} &= (Ab)^{-1}(a-1)+(aB)^{-1}(b-1),\\
d_{11} &= (ab)^{-1}(1-b)(a+b-1)[ab+(a-1)(b-1)],\\
d_{12} &= \left(ab^2\right)^{-1}(1-b)\left[b^2-(a-1)^2+0.05b(a-1)(b-a)M_3^2\right],\\
d_{13} &= (Ab)^{-1}(a-1)[ab+(a-1)(b-1)],
\end{aligned}
\tag{67}
$$

$$
\begin{aligned}
d_{14} &= (ab)^{-1}(1-b)(a+b-1)\left[aA^{-1}(a-1)+bB^{-1}(b-1)\right],\\
d_{15} &= 0.75b(b-a)M_3^2-(a-1).
\end{aligned}
\tag{68}
$$

Since the z-axis is oriented towards the minor axis of the ellipsoid of inertia for the body, then $W_1(\omega')>0$ for all ω' under consideration. Assume that [17]

$$z_0'W_2(\omega')+kW_3(\omega')\neq 0. \tag{69}$$

Using (65), the expressions for β_1 and β_2 are obtained in the form of power series expansions beginning with terms of order greater than ε^{-2}. So, we obtain the first terms of the required periodic solutions and the correction of the period $\alpha(\varepsilon^{-1})$ in the following forms:

$$p_1=\varepsilon^{-1}\left\{-x_0'(a-1)^{-1}\left[1+bB^{-1}(a-1)^{-1}r_0^{-1}\ell_3\right]+\chi_1M_3\cos\tau\right\}+\cdots, \tag{70}$$

$$q_1=\varepsilon^{-1}a(1-b)^{-1}\left\{y_0'a^{-1}+\chi_2M_3\sin\tau-A^{-1}(1-b)^{-1}r_0^{-1}\ell_3\left[y_0'+(z_0'-kaA_1)M_3\sin\tau+ad_5\left[kb(1-b)d_6-z_0'(2b-1)\right]\right]\right\}+\cdots, \tag{71}$$

$$r_1=1-\varepsilon^{-2}M_3\left[x_0'(1-\cos\tau)+y_0'\sin\tau+0.25M_3C_1(1-\cos2\tau)\right]+\cdots, \tag{72}$$

$$\gamma_1=M_3\cos\tau+\cdots, \tag{73}$$

$$\gamma_1'=-M_3\sin\tau+\cdots, \tag{74}$$

$$
\begin{aligned}
\gamma_1''=1+\varepsilon^{-2}\Big\{&(1-b)^{-1}M_3y_0'\sin\tau+(1-a)^{-1}M_3x_0'(1-\cos\tau)-0.5b^{-1}(1-b)^{-1}d_7M_3^2z_0'(1-\cos2\tau)\\
&+0.25M_3^2k\left(2abd_5d_6+C_1\right)(1-\cos2\tau)\\
&+r_0^{-1}\ell_3\Big[-abA^{-1}(1-B)^{-2}M_3y_0'\sin\tau+abB^{-1}(a-1)^{-2}M_3x_0'(1-\cos\tau)+0.5b^{-1}(1-b)^{-1}\times z_0'M_3^2(1-\cos2\tau)\\
&\cdot\left[A^{-1}a^2bd_5(1-b)^{-1}\left(2b^2-2b+1\right)+d_9\right]\\
&+0.5k(1-b)^{-1}M_3^2(1-\cos)\tau\left[b^{-1}d_{13}-aA^{-1}d_{11}(1-b)^{-1}-(1-b)(2b-1)^{-1}d_6d_9\right]\Big]\Big\}+\cdots,
\end{aligned}
\tag{75}
$$

$$
\begin{aligned}
\alpha\left(\varepsilon^{-1}\right)=\varepsilon^{-2}\pi n\Big\{&M_3x_0'-z_0'b^{-1}+(ab)^{-1}\left(kd_{11}-z_0'd_7\right)d_6+k\left(M_3^2C_1-B_1\right)+(ab)^{-1}r_0^{-1}\ell_3\Big[z_0'\Big[d_6\left(d_8+d_9\right)+d_7B^{-1}\Big]\\
&+k\left[d_6\left(d_{13}-d_{14}\right)-d_{11}B^{-1}\right]\Big]\Big\}+\ldots.
\end{aligned}
\tag{76}
$$

New solutions (70)–(76) are obtained in terms of the large parameter ε and a sufficiently small angular velocity component r_o about the minor axis of the ellipsoid of inertia. The case of the motion of the body with a sufficiently small angular velocity component r_o about the major axis of the ellipsoid of inertia is considered in a separate paper since ω'^2 is negative in this case. The motion considered here is a generalization of many problems studied in a previous work [18]. That is, the obtained solutions give many special cases for gyroscopic problems with new treatment by the large parameter technique [19] which saves high energy given for the body at the initial motion. The correction terms in our solutions in terms of the parameter ε are

$$\begin{aligned}
\triangle p_1 &= \varepsilon^{-1}\left\{x_0' b^{-1}\left[B_1^{-1}\left(1-\omega^2\omega'^{-2}\right)+\omega'^{-2}A^{-1}r_0^{-1}\ell_3\right]+(\chi-\chi_1^*)M_3\cos\tau\right\}+\cdots,\\
\triangle q_1 &= \varepsilon^{-1}\left\{-y_0'\left(aAA_1^2\right)^{-1}r_0^{-1}\ell_3+A_1^{-1}M_3\sin\tau\left[\chi_1-\chi_1^*-\chi_2A^{-1}A_1^{-1}r_0^{-1}\ell_3\right]\right\}+\cdots,\\
\triangle r_1 &= \varepsilon^{-3}[0]+\ldots,\triangle\gamma_1=\varepsilon^{-1}[0]+\ldots,\triangle\gamma_1'=\varepsilon^{-1}[0]+\cdots,\\
\triangle\gamma_1'' &= \varepsilon^{-2}\left\{aM_3(\chi-\chi^*)(1-\cos\tau)-bM_3y_0'\left(aAA_1^2\right)^{-1}r_0^{-1}\ell_3\sin\tau\right.\\
&\quad\left.+0.5M_3^2(1-\cos2\tau)\left[a(1-b)^{-1}(\chi_1-\chi_1^*)-\chi_2b\left(AA_1^2\right)^{-1}r_0^{-1}\ell_3\right]\right\}+\cdots,\\
\Delta\alpha\left(\varepsilon^{-1}\right) &= \varepsilon^{-2}\pi n\left\{(1-B_1)(\chi_1-\chi_1^*)-B^{-1}\chi_1r_0^{-1}\ell_3\right\}+\cdots.
\end{aligned}\tag{77}$$

Also,

$$\begin{aligned}
\Delta p_{11} &= \Delta p_1+\varepsilon^{-1}(\chi_1^*-\chi_1^{**})M_3\cos\tau+\cdots,\\
\Delta q_{11} &= \Delta q_1+\varepsilon^{-1}A_1^{-1}M_3(\chi_1^*-\chi_1^{**}-kA_1)\sin\tau+\cdots,\\
\Delta r_{11} &= -0.25\varepsilon^{-2}M_3^2C_1(1-\cos2\tau)+\cdots,\\
\Delta\gamma_{11} &= \varepsilon^{-1}[0]+\ldots,\Delta\gamma_{11}'\\
\Delta\gamma_{11}'' &= \Delta\gamma_1''+\varepsilon^{-2}\left\{0.25kM_3^2C_1(1-\cos2\tau)+0.5M_3^2(1-\cos\tau)\left[a(1-b)^{-1}(\chi_1^*-\chi_1^{**})-kb\right]\right\}+\cdots,\\
\Delta\alpha_1\left(\varepsilon^{-1}\right) &= \Delta\alpha+\varepsilon^{-2}\pi n\left[z_0'(2-b)^{-1}+k\left(M_3^2C_1-B_1\right)+\chi_1^*(1+B_1)\right]+\cdots,
\end{aligned}\tag{78}$$

where

$$\begin{aligned}
\chi^* &= A_1x_0'\left(b\omega^2\right)^{-1},\\
\chi_1^* &= \left(1-\omega^2\right)^{-1}\left[k\left(A_1-\omega^2\right)-z_0'\left(a^{-1}-A_1b^{-1}\right)\right],\\
\chi_1^{**} &= -z_0'\left(1-\omega^2\right)^{-1}\left(a^{-1}-A_1b^{-1}\right).
\end{aligned}\tag{79}$$

5. Geometric Interpretation of Motion

In this section, we explain the geometric interpretation of motion using Euler's angles θ, ψ, and φ [20] which are determined from the obtained periodic solutions. Since the initial system is autonomous, the periodic solutions remain so, if the time t is replaced by $(t+t_0)$, where t_0 is the arbitrary interval time. So, Euler's angles for this problem are given by

$$\begin{aligned}
\cos\theta &= \gamma'',\\
\frac{d\psi}{dt} &= \frac{(p\gamma+q\gamma')}{\left(1-\gamma''^2\right)},\\
\tan\varphi_0 &= \frac{\gamma_0}{\gamma_0'},\\
\frac{d\varphi}{dt} &= r-\cos\theta\left(\frac{d\psi}{dt}\right).
\end{aligned}\tag{80}$$

Substituting equations (70)–(76) into equation (80) in which t is replaced by $(t+t_0)$ and using the relations (10), the following expressions for Euler's angles θ, ψ, and φ are obtained:

Table 1: The differences between the previous works and the considered work.

Ser.	The previous problems	The considered problem
1	The body rotates fast	The body rotates slow
2	r_o is sufficiently high	r_o is sufficiently small
3	$\varepsilon \longrightarrow 0$	$\varepsilon \longrightarrow \infty$
4	Poincare's method is used for solving the problems	The large parameter method is used for solving the problem
5	High kinetic energy is required for the motions	Low kinetic energy is required for the motion
6	The domain of the solutions $F\,(t, r_o \longrightarrow \infty, \varepsilon \longrightarrow 0)$	The domain of the solutions $F\,(t, r_o \longrightarrow 0, \varepsilon \longrightarrow \infty)$
7	θ, ψ, and φ have the domain $G\,(t, r_o \longrightarrow \infty, \varepsilon \longrightarrow 0)$	θ, ψ, and φ have the domain $G\,(t, r_o \longrightarrow 0, \varepsilon \longrightarrow \infty)$
8	ω'^2 is positive for $A<B<C$ or $A>B>C$	ω'^2 is positive for $A<B<C$ and negative for $A>B>C$

$$
\begin{aligned}
\varphi_0 &= \left(\frac{\pi}{2}\right) + r_0^{-1} t_0 + \cdots,\\
\theta_0 &= \tan^{-1} M_3,\\
\theta &= \theta_0 - \varepsilon^{-2}\left[\theta_1(t+t_0) - \theta_1(t_0)\right],\\
\psi &= \psi_0 + \varepsilon^{-1} c \operatorname{cosec}\theta_0 \sqrt{\cos\theta_0}\left[\psi_1(t+t_0) - \psi_1(t_0)\right],\\
\varphi &= \varphi_0 + r_0^{-1} t - \varepsilon^{-1} c \cot\theta_0 \sqrt{\cos\theta_0}\left[\varphi_1(t+t_0) - \varphi_1(t_0)\right]\\
&\quad - \varepsilon^{-2}\tan\theta_0\left[\varphi_2(t+t_0) - \varphi_2(t_0)\right],
\end{aligned}
\tag{81}
$$

where

$$
\begin{aligned}
\theta_1(t) &= a_1 \sin r_0^{-1} t - a_2 \cos r_0^{-1} t - a_3 \tan\theta_0 \cos 2r_0^{-1} t,\\
\psi_1(t) &= a_4 r_0^{-1} \sin r_0^{-1} t + a_5 r_0^{-1} \cos r_0^{-1} t + 0.5(\chi_1 - a_6)\tan\theta_0\\
&\quad + 0.25 r_0^{-1}(\chi_1 - a_6)\tan\theta_0 \sin 2r_0^{-1} t, \varphi_1(t) = \psi_1(t),\\
a_1 &= (1-b)^{-1} y_0'\left[1 - abA^{-1}(1-b)^{-1} r_0^{-1}\ell_3\right],\\
a_2 &= (1-a)^{-1} x_0'\left[1 + abB^{-1}(1-a)^{-1} r_0^{-1}\ell_3\right],\\
a_3 &= 0.5 z_0' b^{-1}(1-b)^{-1}\left\{r_0^{-1}\ell_3\left[a^2 b d_5 A^{-1}(1-b)^{-1}\left(2b^2 - 2b + 1\right) + d_9\right] - d_7\right\}\\
&\quad + 0.25k\left\{\left(2abd_5 d_6 + C_1\right) + 2(1-b)^{-1} r_0^{-1}\ell_3\left[b^{-1} d_{13} - aA^{-1}(1-b)^{-1} d_{11} + (b-1)(2b-1)^{-1} d_6 d_9\right]\right\},\\
a_4 &= -x_0'(a-1)^{-1}\left[1 + bB^{-1}(a-1)^{-1} r_0^{-1}\ell_3\right],\\
a_5 &= (1-b) y_0' - aA^{-1}(1-b)^{-2} r_0^{-1}\ell_3\left\{y_0' + ad_5\left[kb(1-b)d_6 - z_0'(2b-1)\right]\right\},\\
a_6 &= a(1-b)^{-1}\left[\chi_2 - aA^{-1} r_0^{-1}\ell_3(1-b)^{-1}(\chi_2 - \chi_1)\right],\\
a_7 &= x_0' + 0.25 k C_1 \tan\theta_0.
\end{aligned}
\tag{82}
$$

6. Comparison between the Previous Problems and the Considered Problem

In this section, we make a comparison between the previous works and the considered work through Table 1.

7. Conclusions

From this study, we treat the problem of the slow spinning motion about the minor axis of the ellipsoid of inertia of a rigid body to find the periodic solutions and the correction

of the period of the equations of motion of it in the presence of Newtonian force field and an external torque. This problem is solved in a new domain of the angular velocity component $r_o \longrightarrow 0$.

The well-known Poincare's method [5] cannot solve this problem because we cannot achieve the small parameter which must be proportional to a sufficiently high angular velocity component $r_o \longrightarrow \infty$. So we must search other techniques that come from the sufficiently small assumption of r_o and depend on achieving large parameter instead of a small one. This technique is named the large parameter method. The advantage of this method is as follows: assuming low energy at the initial instant instead of high energy, obtaining a slow periodic motion instead of a fast periodic one, and giving the solutions in a new domain of motion $r_o \longrightarrow 0$ and $\varepsilon \longrightarrow \infty$. The case when $A < B <$ C [21] cannot be solved here since ω'^2 is negative in this case. So we will treat this case separately in the future, in shaa Allah. The correction terms for our solutions are given in terms of r_o and ε. The geometric interpretation of motions is given to describe the orientation of the motion at any instant of time. The cases of gyroscopic motions and regular precession are obtained as special cases from this study when we apply the symmetry conditions. The practical importance of this work is very wide since it is used in many applications of life such as military life and civil one. The case of the gyro motion which is symmetric about the z-axis, i.e., $A = B < C$, is obtained as a special case from our work [22]. There are many interesting space applications of these problems in [2].

Data Availability

The data used to support the findings of this study are available from the corresponding author upon reasonable request.

Conflicts of Interest

The authors declare that they have no conflicts of interest.

References

[1] A. V. Borisov and I. S. Mamaev, *Rigid Body Dynamics*, p. 521, Walter de Gruyter, Berlin, Germany, 2018.

[2] V. S. Aslanov, *Rigid Body Dynamics for Space Applications*, p. 400, Butter-Worth Heinemann, Oxford, UK, 2017.

[3] F. L. Chernousko, L. D. Akulenko, and D. D. Leshchenko, *Evolution of Motions of a Rigid Body About Its Center of Mass*, p. 241, Springer, Cham, Switzerland, 2017.

[4] S. V. Ershkov, "A Riccati-type solution of Euler-Poisson equations of rigid body rotation over the fixed point," *Acta Mechanica*, vol. 228, no. 7, pp. 2719–2723, 2017.

[5] I. A. Arkhangel'skii, "Construction of periodic solutions for the Euler-Poisson equations by means of power series expansion containing a small parameter," *Colloquia Mathematica Societatis Janos Bolyai. Differential Equations*, pp. 27–50, Elsevier, Keszthely, Hungary, 1975.

[6] A. H. Nayfeh, *Introduction to Perturbation Techniques*, p. 532, John Wiley & Sons, New York, NY, USA, 1993.

[7] H. M. Yehia and A. M. Hussein, "New families of integrable two-dimensional systems with quartic second integrals," *Nelineinaya Dinamika*, vol. 16, no. 2, pp. 211–242, 2020.

[8] G. A. Sahli, "The motion of a rigid body in the presence of a gyrostatic momentum in cases of l_3 and $l_3 = 0$," *Arab Journal of Sciences and Research Publishing*, vol. 3, no. 1, p. 22, 2019.

[9] T. S. Amer, A. I. Ismail, and W. S. Amer, "Application of the krylov-bogoliubov-mitropolski technique for a rotating heavy solid under the influence of a gyrostatic moment," *Journal of Aerospace Engineering*, vol. 25, no. 3, pp. 421–430, 2012.

[10] A. I. Ismail and T. S. Amer, "The fast spinning motion of a rigid body in the presence of a gyrostatic momentum l_3," *Acta Mechanica*, vol. 154, no. 1–4, pp. 31–46, 2002.

[11] G. V. Gorr and A. M. Kovalev, *The Motion of a Rigid Body*, Naukova Dumka, Kyiv, Ukraine, 2013.

[12] J. A. Simon, *An Introduction to Lagrangian and Hamiltonian Mechanics*, Heriot-Watt University, Edinburgh, Scotland, 2014.

[13] I. A. Arkhangel'skii, "On the motion about a fixed point of a fast spinning heavy solid," *Journal of Applied Mathematics and Mechanics*, vol. 27, no. 5, pp. 864–877, 1963.

[14] H. M. Yehia, "On the regular precession of an asymmetric rigid body acted upon by uniform gravity and magnetic fields," *Egyptian Journal of Basic and Applied Sciences*, vol. 2, no. 3, pp. 200–205, 2015.

[15] T. S. Amer, "The rotational motion of the electromagnetic symmetric rigid body," *Applied Mathematics & Information Sciences*, vol. 10, no. 4, pp. 1453–1464, 2016.

[16] M. Ehud, *Nonlinear Physics of Ecosystems*, Taylor & Francis, Oxford, UK, 2019.

[17] M. Iñarrea, V. Lanchares, A. I. Pascual, and A. Elipe, "Stability of the permanent rotations of an asymmetric gyrostat in a uniform Newtonian field," *Applied Mathematics and Computation*, vol. 293, pp. 404–415, 2017.

[18] A. A. Elmandouh, "New integrable problems in rigid body dynamics with quartic integrals," *Acta Mechanica*, vol. 226, no. 8, pp. 2461–2472, 2015.

[19] A. A. Elmandouh, "New integrable problems in the dynamics of particle and rigid body," *Acta Mechanica*, vol. 226, no. 11, pp. 3749–3762, 2015.

[20] H. M. Yehia and A. A. Elmandouh, "Integrable 2D time-irreversible systems with a cubic second integral," *Advances in Mathematical Physics*, vol. 2016, Article ID 8958747, 10 pages, 2016.

[21] W. S. Amer, "The necessary and sufficient condition for the stability of a rigid body," *Journal of Advances in Physics*, vol. 13, no. 4, pp. 4999–5003, 2017.

[22] T. S. Amer and I. M. Abady, "On the solutions of the Euler's dynamic equations for the motion of a rigid body," *Journal of Aerospace Engineering*, vol. 30, no. 4, 2017.

Hindawi
Advances in Astronomy
Volume 2020, Article ID 2764867, 7 pages
https://doi.org/10.1155/2020/2764867

Research Article

Solving a Problem of Rotary Motion for a Heavy Solid Using the Large Parameter Method

A. I. Ismail [1,2]

[1]*Department of Mechanics, College of Engineering and Islamic Architecture, Umm Al-Qura University, P.O. Box 5555, Makkah, Saudi Arabia*
[2]*Mathematics Department, Faculty of Science, Tanta University, P.O. Box 31527, Tanta, Egypt*

Correspondence should be addressed to A. I. Ismail; aiismail@uqu.edu.sa

Received 29 May 2020; Revised 17 June 2020; Accepted 26 June 2020; Published 1 September 2020

Guest Editor: Abdullah A. Ansari

The small parameter method was applied for solving many rotational motions of heavy solids, rigid bodies, and gyroscopes for different problems which classify them according to certain initial conditions on moments of inertia and initial angular velocity components. For achieving the small parameter method, the authors have assumed that the initial angular velocity is sufficiently large. In this work, it is assumed that the initial angular velocity is sufficiently small to achieve the large parameter instead of the small one. In this manner, a lot of energy used for making the motion initially is saved. The obtained analytical periodic solutions are represented graphically using a computer program to show the geometric periodicity of the obtained solutions in some interval of time. In the end, the geometric interpretation of the stability of a motion is given.

1. Introduction

Consider a heavy solid of mass M rotating about a fixed point O in presence of a uniform gravity field of force [1]. The fundamental equations of motion and their three first integrals are presented and reduced to a quasilinear autonomous system having one first integral [2]. Consider that the ellipsoid of inertia of the body is arbitrary [3]. The well-known general equations of motion and their first integrals are [4]

$$\begin{gathered}\frac{dp}{dt} + A_1 qr = MgA^{-1}\left(y_0\gamma'' - z_0\gamma'\right),\\ \frac{d\gamma}{dt} = r\gamma' - q\gamma'',\\ \left(pqr, A_1B_1C_1, ABC, \gamma\gamma'\gamma'', x_o y_o z_o\right),\\ Ap^2 + Bq^2 + Cr^2 - 2Mg\left(x_0\gamma + y_0\gamma' + z_0\gamma''\right) = \text{const.},\\ (Ap)\gamma + (Bq)\gamma' + (Cr)\gamma'' = \text{const.},\\ \gamma^2 + \gamma'^2 + \gamma''^2 = 1,\end{gathered} \tag{1}$$

where

$$A_1 = \frac{C-B}{A},$$
$$B_1 = \frac{A-C}{B}, \quad (2)$$
$$C_1 = \frac{B-A}{C}.$$

System (1) of equations of motion represents nonlinear differential equations of the considered problem. These equations are of the first order in unknown angular velocity components p, q, and r and geometric angles γ, γ', and γ''. The quantities A, B, and C represent the moments of inertia of the body and (x_0, y_0, z_0) represent its gravity center. g denotes the gravity acceleration. t denotes the time of the motion. The aim is to find the solution to this system using the large parameter method [5].

Let the initial value of the angular velocity component $r = r_o$ about the moving z axis be sufficiently small. The following variables are introduced:

$$p_1 = pc^{-1}\sqrt{\gamma_0''},$$
$$q_1 = qc^{-1}\sqrt{\gamma_0''},$$
$$r_1 = \frac{r}{r_0},$$
$$\gamma_1 = \frac{\gamma}{\gamma_0''},$$
$$\gamma_1' = \frac{\gamma'}{\gamma_0''},$$
$$\gamma_1'' = \frac{\gamma''}{\gamma_0''},$$
$$\tau = r_o^{-1}t,$$
$$\left(. \equiv \frac{\mathrm{d}}{\mathrm{d}\tau}\right),$$
$$p_2 = p_1 - e\lambda^{-1} - \lambda^{-1}e_1\gamma_2,$$
$$\gamma_2 = \gamma_1 - \lambda^{-1}\upsilon p_2,$$
$$c = \sqrt{\frac{Mg\ell}{C}},$$
$$\lambda = \frac{c\sqrt{\gamma_o''}}{r_0},$$
$$e = \frac{x_o' A_1}{b\omega^2},$$
$$e_1 = \frac{z_o'\left[A_1/b - a^{-1}\right]}{(1-\omega^2)}, \quad (3)$$
$$\upsilon = \frac{(1+B_1)}{(1-\omega^2)},$$
$$\omega^2 = -A_1B_1,$$
$$a = \frac{A}{C},$$
$$b = \frac{B}{C},$$
$$x_o = \ell x_o',$$
$$y_o = \ell y_o',$$
$$z_o = \ell z_o',$$
$$\ell^2 = x_o^2 + y_o^2 + z_o^2,$$

where r_0 and γ_0'' are the initial values of the corresponding quantities.

The nonlinear equations of motions and their first integrals (1) are reduced to a quasilinear autonomous system [6]:

$$\begin{aligned} \ddot{p}_2 + \omega^2 p_2 &= \lambda^{-2}F\left(p_2, \dot{p}_2, \gamma_2, \dot{\gamma}_2, \frac{1}{\lambda}\right), \\ \ddot{\gamma}_2 + \gamma_2 &= \lambda^{-2}\Phi\left(p_2, \dot{p}_2, \gamma_2, \dot{\gamma}_2, \frac{1}{\lambda}\right), \end{aligned} \quad (4)$$

where

$$\begin{aligned} F &= C_1A_1^{-1}p_2\dot{p}_2^2 + x_0'\dot{p}_2\dot{\gamma}_2 - y_0'a^{-1}p_2\dot{\gamma}_2 - y_0'A_1^{-1}\left(A_1 + a^{-1}\right)\gamma_2\dot{p}_2 - z_0'a^{-1}p_2 \\ &\quad - \nu e_1\left(1-\omega^2\right)p_2 - \omega^2 p_2 s_{11} + A_1b^{-1}x_0's_{21} + O\left(\frac{1}{\lambda}\right) + \ldots, \\ \Phi &= -(1-C_1)A_1^{-1}p_2\dot{p}_2\dot{\gamma}_2 + x_0'\dot{\gamma}_2^2 - y_0'\gamma_2\dot{\gamma}_2 - z_0'b^{-1}\gamma_2 + x_0'b^{-1} - A_1^{-2}\gamma_2\dot{p}_2^2 \\ &\quad + \nu\left(1-\omega^2\right)(e + e_1\gamma_2) - \gamma_2 s_{11} + (1+B_1)p_2s_{21} + O\left(\frac{1}{\lambda}\right) + \ldots, \end{aligned} \quad (5)$$

$$s_{11} = \frac{a\left(p_{20}^2 - p_2^2\right) + b\left(\dot{p}_{20}^2 - \dot{p}_2^2\right)}{A_1^2 - 2\left[x_0'(\gamma_{20} - \gamma_2) + y_0'(\dot{\gamma}_{20} - \dot{\gamma}_2)\right]},$$
$$s_{21} = a\left(p_{20}\gamma_{20} - p_2\gamma_2\right) - bA_1^{-1}\left(\dot{p}_{20}\dot{\gamma}_{20} - \dot{p}_2\dot{\gamma}_2\right),$$
$$\upsilon_2 = \upsilon - A_1^{-1},$$

such that p_{20} and γ_{20} are the initial values of the corresponding quantities.

The variables $q_1, r_1, \gamma_1', \text{and } \gamma_1''$ are obtained as follows:

$$\begin{aligned} q_1 &= -A_1^{-1}\dot{p}_2 + \lambda^{-1}A_1^{-1}\left(y_0'a^{-1} - e_2\dot{\gamma}_2\right) + \ldots, \\ r_1 &= 1 + 0.5\lambda^{-2}s_{11} + \ldots, \\ \gamma_1' &= \dot{\gamma}_2 + \lambda^{-1}v_2\dot{p}_2 + \ldots, \\ \gamma_1'' &= 1 + \lambda^{-1}s_{21} + \lambda^{-2}\left(s_{22} - 0.5s_{11}\right) + \ldots, \end{aligned} \tag{6}$$

where

$$\begin{aligned} s_{22} &= a\left[\nu\left(p_{20}^2 - p_2^2\right) + e\left(\gamma_{20} - \gamma_2\right) + e_1\left(\gamma_{20}^2 - \gamma_2^2\right)\right] \\ &\quad + bA_1^{-1}\left[-\nu_2\left(\dot{p}_{20}^2 - \dot{p}_2^2\right) + a^{-1}y_0'\left(\dot{\gamma}_{20} - \dot{\gamma}_2\right) - e_2\left(\dot{\gamma}_{20}^2 - \dot{\gamma}_2^2\right)\right], \cdot \\ e_2 &= e_1 + a^{-1}z_o' \end{aligned} \tag{7}$$

Assuming that the velocity r_o is sufficiently small, the parameter λ is large.

2. Construction of Periodic Solutions, with Zero Basic Amplitudes

In this section, the periodic solutions, with zero basic amplitudes [7], of the autonomous system (4) are achieved and the large parameter method is applied. Without loss of generality of solutions, it is considered that

$$p_2(0,0) = \dot{p}_2(0,0) = \dot{\gamma}_2\left(0, \frac{1}{\lambda}\right) = 0. \tag{8}$$

Consider the generating system $((1/\lambda) = 0)$, that is, $(\lambda \longrightarrow \infty)$, of (4) in the form:

$$\begin{aligned} \ddot{p}_2^{(0)} + \omega^2 p_2^{(0)} &= 0, \\ \ddot{\gamma}_2^{(0)} + \gamma_2^{(0)} &= 0, \end{aligned} \tag{9}$$

with a period $T_0 = 2\pi n$. There are three possibilities of the values of frequency ω which are $1 - \omega = 1$; $2 - \omega = m/n$ where m and n are primes; $3 - \omega$ equals an irrational number.

Consider the case when $\omega = m/n$, then the solution of the generating system (9) becomes

$$\begin{aligned} p_2^{(0)} &= a_0^* \cos\omega\tau, \\ \gamma_2^{(0)} &= b_0^* \cos\tau, \end{aligned} \tag{10}$$

where a_0^* and b_0^* are the constants to be determined. The autonomous system (4) has periodic solutions with a period $T_0 + \alpha$, where α is a function of $1/\lambda$ such that $\alpha(0) = 0$. These solutions are reduced to the generating ones (10) when $(1/\lambda) = 0$ $(\lambda \longrightarrow \infty)$ and written in the form:

$$\begin{aligned} p_2 &= a^* \cos\psi + \sum_{n=1}^{N}\left(\frac{1}{\lambda}\right)^n p_n^*\left(a^*, \psi\right) + O\left(\frac{1}{\lambda}\right)^{N+1}, \\ \gamma_2 &= b^* \cos\phi + \sum_{n=1}^{N}\left(\frac{1}{\lambda}\right)^n \gamma_n^*\left(a^*, \phi\right) + O\left(\frac{1}{\lambda}\right)^{N+1}. \end{aligned} \tag{11}$$

With initial conditions:

$$\begin{aligned} p_2\left(0, \frac{1}{\lambda}\right) &= a^* = a_0^* + a^*\left(\frac{1}{\lambda}\right), \\ \gamma_2\left(0, \frac{1}{\lambda}\right) &= b^* = b_0^* + b^*\left(\frac{1}{\lambda}\right), \\ \dot{\gamma}_2\left(0, \frac{1}{\lambda}\right) &= 0, \end{aligned} \tag{12}$$

where $a^*(1/\lambda) = 0$ and $b^*(1/\lambda) = 0$ when $(1/\lambda) = 0$.

From the first integral (4) and initial conditions (12), one has the following:

$$\begin{aligned} 0 < b_0^* &= \left(1 - \gamma_0''^2\right)^{1/2}\left(\gamma_0''\right)^{-1} < \infty, \\ b^*\left(\frac{1}{\lambda}\right) &= -\left(\frac{1}{\lambda}\right)\nu\left[a_0^* + a^*\left(\frac{1}{\lambda}\right)\right] + \ldots. \end{aligned} \tag{13}$$

Let a^*, ψ, and ϕ change with time according to

$$\dot{a}^* = \sum_{n=1}^{N}\left(\frac{1}{\lambda}\right)^n A_n^*\left(a^*\right) + O\left(\frac{1}{\lambda}\right)^{N+1}, \tag{14}$$

$$\dot{\psi} = \omega + \sum_{n=1}^{N}\left(\frac{1}{\lambda}\right)^n \psi_n\left(a^*\right) + O\left(\frac{1}{\lambda}\right)^{N+1}, \tag{15}$$

$$\dot{\phi} = 1 + \sum_{n=1}^{N}\left(\frac{1}{\lambda}\right)^n \phi_n\left(a^*\right) + O\left(\frac{1}{\lambda}\right)^{N+1}. \tag{16}$$

The following derivatives are obtained:

$$
\begin{aligned}
\dot{p}_2 &= -a^*\omega\sin\psi + O\left(\frac{1}{\lambda}\right),\\
\dot{\gamma}_2 &= -b^*\sin\phi + O\left(\frac{1}{\lambda}\right),\\
\dot{p}_2^{\cdot} &= -a^*\omega^2\cos\psi + \frac{1}{\lambda}\left[\omega^2\frac{\partial^2 p_1^*}{\partial\psi^2} - 2a^*\omega\psi_1\cos\psi - 2\omega A_1^*\sin\psi\right]\\
&\quad + \left(\frac{1}{\lambda}\right)^2\left[2\omega A_1^*\frac{\partial^2 p_1^*}{\partial a^*\partial\psi} - 2\left(\omega A_2^* + A_1^*\psi_1\right)\sin\psi + A_1^*\frac{dA_1^*}{da^*}\cos\psi + \omega^2\frac{\partial^2 p_2^*}{\partial\psi^2}\right.\\
&\quad \left. + 2\omega\psi_1\frac{\partial^2 p_1^*}{\partial\psi^2} - a^*\left(\psi_1^2 + 2\omega\psi_2\right)\cos\psi - a^*A_1^*\sin\psi\frac{d\psi_1}{da^*}\right] + O\left(\frac{1}{\lambda}\right)^3,\\
\ddot{\gamma}_2 &= -b^*\cos\phi + \frac{1}{\lambda}\left[\frac{\partial^2\gamma_1^*}{\partial\phi^2} - 2b^*\phi_1\cos\phi\right] + \left(\frac{1}{\lambda}\right)^2\left[\frac{\partial^2\gamma_2^*}{\partial\phi^2} + 2\phi_1\frac{\partial^2\gamma_1^*}{\partial\phi^2}\right.\\
&\quad \left. - b^*\left(\phi_1^2 + 2\phi_2\right)\cos\phi + 2A_1^*\frac{\partial^2\gamma_1^*}{\partial a^*\partial\phi} - b^*A_1^*\frac{d\phi_1}{da^*}\sin\phi\right] + O\left(\frac{1}{\lambda}\right)^3.
\end{aligned}
\tag{17}
$$

From (5), (7), (11), and (17), it is obtained that

$$
\begin{aligned}
s_{11}^{(0)} &= aa_0^{*2}\left(\cos^2\psi_0 - \cos^2\psi\right) - bA_1^{-2}a_0^{*2}\omega^2\sin^2\psi - 2b_0^*\left[x_0'\left(\cos\phi_0 - \cos\phi\right) + y_0'\sin\phi\right],\\
s_{21}^{(0)} &= a_0^*b_0^*\left[a\left(\cos\psi_0\cos\phi_0 - \cos\psi\cos\phi\right) + bA_1^{-1}\omega\sin\psi\sin\phi\right],\\
s_{22}^{(0)} &= a\left[\nu a_0^{*2}\left(\cos^2\psi_0 - \cos^2\psi\right) + eb_0^*\left(\cos\phi_0 - \cos\phi\right) + e_1b_0^{*2}\left(\cos^2\phi_0 - \cos^2\phi\right)\right]\\
&\quad + bA_1^{-1}\left[\nu_2a_0^{*2}\omega^2\sin^2\psi + a^{-1}y_0'b_0^*\sin\phi + e_2b_0^{*2}\sin^2\phi\right],
\end{aligned}
\tag{18}
$$

where ψ_0 and ϕ_0 are the initial values of the corresponding quantities.

Using (5), (11), and (17), the following is obtained:

$$
\begin{aligned}
F^{(0)} &= C_1A_1^{-1}a_0^{*3}\omega^2\cos\psi\sin^2\psi + \omega a_0^*b_0^*x_0'\sin\psi\sin\phi\\
&\quad + a^{-1}a_0^*b_0^*y_0'\cos\psi\sin\phi + \omega A_1^{-1}\left(A_1 + a^{-1}\right)a_0^*b_0^*y_0'\sin\psi\cos\phi\\
&\quad - z_0'a^{-1}a_0^*\cos\psi - \nu e_1\left(1 - \omega^2\right)a_0^*\cos\psi\\
&\quad - \omega^2a_0^*\cos\psi\left\{aa_0^{*2}\left(\cos^2\psi_0 - \cos^2\psi\right) - bA_1^{-2}a_0^{*2}\omega^2\sin^2\psi\right.\\
&\quad \left. -2b_0^*\left[x_0'\left(\cos\phi_0 - \cos\phi\right) + y_0'\sin\phi\right]\right\}\\
&\quad + A_1b^{-1}x_0'a_0^*b_0^*\left[a\left(\cos\psi_0\cos\phi_0 - \cos\psi\cos\phi\right) + bA_1^{-1}\omega\sin\psi\sin\phi\right],\\
\Phi^{(0)} &= \frac{1}{2}\left(C_1 - 1\right)A_1^{-1}\omega a_0^{*2}b_0^*\sin2\psi\sin\phi + \frac{1}{2}x_0'b_0^{*2}\left(1 - \cos2\phi\right)\\
&\quad + \frac{1}{2}y_0'b_0^{*2}\sin2\phi - z_0'b^{-1}b_0^*\cos\phi + x_0'b^{-1}\\
&\quad - \frac{1}{2}A_1^{-2}\omega^2a_0^{*2}b_0^*\left(1 - \cos2\psi\right)\cos\phi + \nu e\left(1 - \omega^2\right) + \nu e_1\left(1 - \omega^2\right)b_0^*\cos\phi
\end{aligned}
$$

$$
\begin{aligned}
&- aa_0^{*2}b_0^*\cos^2\psi_0\cos\phi + \frac{1}{2}aa_0^{*2}b_0^*\,(1+\cos 2\psi)\cos\phi \\
&+ \frac{1}{2}bA_1^{-2}\omega^2 a_0^{*2}b_0^*\,(1-\cos 2\psi)\cos\phi + 2x_0'b_0^{*2}\cos\phi_0\cos\phi \\
&- x_0'b_0^{*2}(1+\cos 2\phi) + y_0'b_0^{*2}\sin 2\phi + a_0^{*2}b_0^*\,(1+B_1)\left[bA_1^{-1}\omega\sin\psi\sin\phi\right. \\
&\left.+a(\cos\psi_0\cos\phi_0-\cos\psi\cos\phi)\right]\cos\psi.
\end{aligned}
\tag{19}
$$

Substituting (11), (17), and (19) into system (4) and equating coefficients of similar power terms of $1/\lambda$, the following is obtained:

$$
\begin{aligned}
\frac{\partial^2 p_1^*}{\partial\psi^2} + p_1^* &= \frac{2a_0^*}{\omega}\psi_1\cos\psi + \frac{2A_1^*}{\omega}\sin\psi, \\
\frac{\partial^2 \gamma_1^*}{\partial\phi^2} + \gamma_1^* &= 2b_0^*\,\phi_1\cos\phi, \\
\frac{\partial^2 p_2^*}{\partial\psi^2} + p_2^* &= \frac{2A_2^*}{\omega}\sin\psi + \frac{a_0^*}{\omega^2}\left[2\omega\psi_2 + \frac{1}{4}\omega^2 C_1 A_1^{-1}a_0^{*2} + \frac{3}{4}\omega^2 aa_0^{*2} - aa_0^{*2}\right. \\
&\quad \left.-z_0'a^{-1} - \nu e_1\left(1-\omega^2\right) + \frac{1}{4}bA_1^{-2}a_0^{*2}\omega^4 + 2\omega^2 x_0'b_0^*\cos\phi_0\right]\cos\psi \\
&\quad + \frac{1}{4}a_0^{*3}\left(a - C_1A_1^{-1} - \omega^2 bA_1^{-2}\right)\cos 3\psi + \frac{aa_0^*}{\omega^2}x_0'A_1b^{-1}b_0^*\cos\psi_0\cos\phi_0 \\
&\quad + x_0'a_0^*b_0^*\left(\frac{1}{\omega} - \frac{aA_1}{2b\omega^2} - 1\right)\cos(\phi-\psi) - x_0'a_0^*b_0^*\left(1 + \frac{1}{\omega} + \frac{aA_1}{2b\omega^2}\right)\cos(\phi+\psi) \\
&\quad + y_0'a_0^*b_0^*\left(1 + \frac{1}{2a\omega^2} - \frac{A_1 + a^{-1}}{2A_1\omega}\right)\sin(\phi-\psi) + y_0'a_0^*b_0^*\left(1 + \frac{1}{2a\omega^2} + \frac{A_1 + a^{-1}}{2A_1\omega}\right)\sin(\phi+\psi), \\
\frac{\partial^2 \gamma_2^*}{\partial\phi^2} + \gamma_2^* &= \left[2\phi_2 - z_0'b^{-1} + \frac{1}{2}A_1^{-2}\omega^2 a_0^{*2}(b-1) + \nu e_1\left(1-\omega^2\right) - aa_0^{*2}\cos^2\psi_0\right. \\
&\quad \left.-\frac{1}{2}aB_1a_0^{*2} + 2x_0'b_0^*\cos\phi_0\right]b_0^*\cos\phi - \frac{1}{2}x_0'b_0^{*2} + x_0'b^{-1} + \nu e\left(1-\omega^2\right) \\
&\quad + (1+B_1)aa_0^{*2}b_0^*\cos\psi_0\cos\phi_0\cos\psi - \frac{3}{2}x_0'b_0^{*2}\cos 2\phi + \frac{3}{2}y_0'b_0^{*2}\sin 2\phi \\
&\quad + a_0^{*2}\left\{\left[\frac{1}{2}A_1^{-2}\omega^2(1-b) - \frac{1}{2}aB_1 + A_1^{-1}\omega b_0^*\,(b-1)\right]\cos(2\psi-\phi)\right. \\
&\quad \left.+\left[\frac{1}{2}A_1^{-2}\omega^2(1-b) - \frac{1}{2}aB_1 - A_1^{-1}\omega b_0^*\,(b-1)\right]\cos(2\psi+\phi)\right\}.
\end{aligned}
\tag{20}
$$

Canceling the singular terms [8] from (20), one gets

$$\psi_1 = A_1^* = \phi_1 = A_2^* = 0,$$

$$\psi_2 = \frac{1}{2\omega}\left[-\frac{1}{4}\omega^2 C_1 A_1^{-1} a_0^{*2} - \frac{3}{4}\omega^2 a a_0^{*2} + a a_0^{*2} + z_0' a^{-1} + \nu e_1\left(1-\omega^2\right)\right.$$

$$\left.-\frac{1}{4}bA_1^{-2}\omega^4 a_0^{*2} - 2\omega^2 x_0' b_0^* \cos\phi_0\right], \tag{21}$$

$$\phi_2 = \frac{1}{2}\left[z_0' b^{-1} - \frac{1}{2}A_1^{-2}\omega^2 a_0^{*2}(b-1) - \nu e_1\left(1-\omega^2\right) + a a_0^{*2}\left(\frac{1}{2}B_1 + \cos^2\psi_0\right)\right.$$

$$\left.-2x_0' b_0^* \cos\phi_0\right].$$

Substituting (21) into (14), (15), and (16) and integrating, it is obtained that

$$a^* = a_0^* \text{ (arbitrary const.)},$$

$$\psi = \omega\tau + \frac{1}{2}\left(\frac{1}{\lambda}\right)^2\left[-\frac{1}{4}\omega C_1 A_1^{-1} a_0^{*2} - \frac{3}{4}\omega a a_0^{*2} + a a_0^{*2}\omega^{-1} + z_0^1 a^{-1}\omega^{-1}\right.$$

$$\left.+\nu e_1\left(\omega^{-1}-\omega\right) - \frac{1}{4}bA_1^{-2}\omega^3 a_0^{*2} - 2\omega x_0' b_0^* \cos\phi_0\right]\tau, \tag{22}$$

$$\phi = \tau + \frac{1}{2}\left(\frac{1}{\lambda}\right)^2\left[z_0' b^{-1} - \frac{1}{2}A_1^{-2}\omega^2 a_0^{*2}(b-1) - \nu e_1\left(1-\omega^2\right) + a a_0^{*2}\left(1+\frac{1}{2}B_1\right) - 2x_0' b_0^*\right]\tau.$$

From the previous results, the following is obtained:

$$\psi(0) = \psi_0 = 0,$$
$$\phi(0) = \phi_0 = 0. \tag{23}$$

Making use of (21), (22), (11), and (13), the periodic solutions p_2 and γ_2 of the autonomous system are deduced. Using (6), (18), (22), and (23), the following periodic solutions, with zero basic amplitudes, are obtained:

$$p_1 = -\frac{x_0'}{\lambda b B_1} + \frac{1}{\lambda}e_1 b_0^* \cos\tau + \ldots,$$

$$q_1 = \frac{y_0'}{\lambda a A_1} + \frac{1}{\lambda}e_1 A_1^{-1} b_0^* \sin\tau + \ldots,$$

$$r_1 = 1 - \frac{1}{\lambda^2}b_0^*\left[x_0'(1-\cos\tau) + y_0'\sin\tau\right] + \ldots,$$

$$\gamma_1 = b_0^* \cos\tau + \ldots, \tag{24}$$

$$\gamma_1' = -b_0^* \sin\tau + \ldots,$$

$$\gamma_1'' = 1 + \frac{1}{\lambda^2}\left[b_0^*(1-a)^{-1}x_0' + \frac{1}{2}b_0^{*2}z_0'\left(\frac{a-b}{a+b-1}\right) + b_0^*(1-b)^{-1}y_0'\sin\tau\right.$$

$$\left.-b_0^*(1-a)^{-1}x_0'\cos\tau - \frac{1}{2}b_0^{*2}z_0'\left(\frac{a-b}{a+b-1}\right)\cos 2\tau\right] + \ldots,$$

where the correction of the period α becomes

$$\alpha\left(\frac{1}{\lambda}\right) = \frac{2}{\lambda}\pi n\left[b_0^* x_0' - z_0'\right] + \ldots. \tag{25}$$

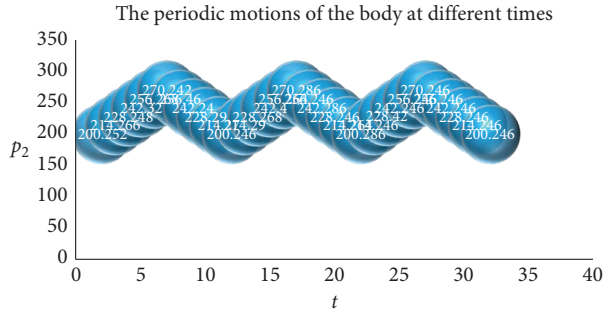

Figure 1: The periodic motion p_2 against the time t.

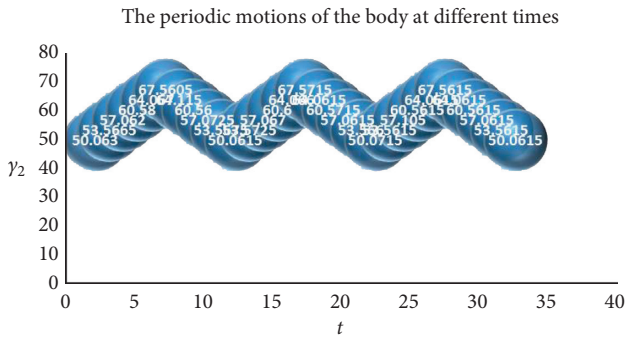

Figure 2: The periodic motion γ_2 against the time t.

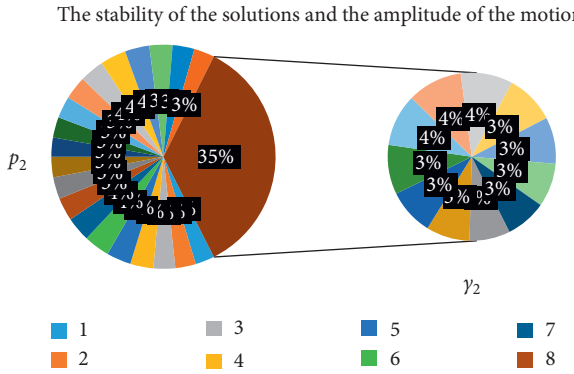

Figure 3: The stability of the solution p_2 against γ_2.

3. Conclusion

It is concluded that the method of the small parameter failed to solve this problem under the studied condition r_0 which is sufficiently small because achieving the solutions by this method depends on assuming sufficiently large angular velocity r_0 to define the small parameter (ε) proportional to $(1/r_o)$. With the sufficiently small assumption, the choosing of the small parameter (ε) is impossible, and so the author had to look for another technique.

The large parameter technique is the only one that solves this problem under the studied condition. The advantage of this method is that you save an enormous amount of energy given to the body at the start of the motion. The presented method proves the ability to solve this problem when the component of the angular velocity about the moving z-axis is sufficiently small. Under this technique, gyroscopic motions are obtained under low energy initially instead of high energy in using the small parameter technique. It is clear about the periodicity of the solutions p_2 and γ_2 from Figures 1 and 2 in a defined interval of time. The simple smooth closed curves with different amplitudes of the solution p_2 against γ_2 show the stability [9] of the motions, see Figure 3.

Data Availability

No datasets were generated or analyzed during the current study.

Conflicts of Interest

The author declares that there are no conflicts of interest.

References

[1] F. L. Chernousko, L. D. Akulenko, and D. D. Leshchenko, *Evolution of Motions of a Rigid Body about its Center of Mass*, p. 1, Springer International Publishing AG, Cham, Switzerland, 2017.

[2] G. M. Scarpello and D. Ritelli, "Motions about a fixed point by hypergeometric functions: new non-complex analytical solutions and integration of the herpolhode," *Celestial Mechanics and Dynamical Astronomy*, vol. 130, no. 42, 2018.

[3] T. S. Amer and W. S. Amer, "Substantial condition for the fourth first integral of the rigid body problem," *Mathematics and Mechanics of Solids*, vol. 23, no. 8, pp. 1237–1246, 2018.

[4] A. V. Borisov and I. S. Mamaev, *Rigid Body Dynamics*, Higher education press and Walter de Gruyter GmbH, Berlin, Germany, 2018.

[5] A. H. Nayfeh, *Introduction to Perturbation Techniques*, pp. 360–364, WILEY-VCH Verlag GmbH & Co. KGaA, Weinheim, Germany, 2011.

[6] A. I. Ismail and T. S. Amer, "The fast spinning motion of a rigid body in the presence of a gyrostatic momentum," *Acta Mechanica*, vol. 154, no. 1–4, pp. 31–46, 2002.

[7] https://courses.lumenlearning.com/physics/chapter/16-10-superposition-and-interference/.

[8] T. D. Lee, *Selected Papers: Field Theory and Symmetry Principles*, Contemporary physicists Gerald Feinberg, Birkhäuser, Basel, Switzerland, 1986.

[9] http://ddebiftool.sourceforge.net/demos/neuron/html/demo1_psol.html.

Hindawi
Advances in Astronomy
Volume 2020, Article ID 7421396, 12 pages
https://doi.org/10.1155/2020/7421396

Research Article

Balanced Low Earth Satellite Orbits

A. Mostafa [1,2] and M. H. El Dewaik [3]

[1] *University of Jeddah, College of Science and Arts at Khulis, Department of Mathematics, Jeddah, Saudi Arabia*
[2] *Ain Shams University, Faculty of Science, Department of Mathematics, Cairo, Egypt*
[3] *Department of Basic Science, Faculty of Engineering, The British University in Egypt, Cairo, Egypt*

Correspondence should be addressed to A. Mostafa; ahmedmostafa@sci.asu.edu.eg

Received 28 May 2020; Accepted 10 July 2020; Published 19 August 2020

Guest Editor: Euaggelos E. Zotos

The present work aims at constructing an atlas of the balanced Earth satellite orbits with respect to the secular and long periodic effects of Earth oblateness with the harmonics of the geopotential retained up to the 4th zonal harmonic. The variations of the elements are averaged over the fast and medium angles, thus retaining only the secular and long periodic terms. The models obtained cover the values of the semi-major axis from 1.1 to 2 Earth's radii, although this is applicable only for 1.1 to 1.3 Earth's radii due to the radiation belts. The atlas obtained is useful for different purposes, with those having the semi-major axis in this range particularly for remote sensing and meteorology.

1. Introduction

The problem of the motion of an artificial satellite of the Earth was not given serious attention until 1957. At this time, little was known about the magnitudes of the coefficients of the tesseral and sectorial harmonics in the Earth's gravitational potential. It was pretty well known at this time (1957–1960) that the contributions of the 3rd, 4th, and 5th zonal harmonics were of order higher than the contribution of the 2nd zonal harmonic, but the values of the coefficients C_{30}, C_{40}, and C_{50} were not very well established. No reliable information was available for the tesseral or the sectorial coefficients except that the observations of orbiting satellites indicated that these coefficients must be small, certainly no more than the first order with respect to C_{20}.

For low Earth orbits within an altitude less than 480 km, if the satellite attitude is stabilized, or at least a mean projected area could be estimated, the perturbative effects of atmospheric drag should be included. Unfortunately, the literature is still void of even a mention of this topic of balancing this kind of very low Earth orbits. The reason may be the present increased interest in space communications and broadcasting, which still make use of the geostationary orbits that lie beyond the effects of atmospheric drag, though they still suffer the effects of drift solar radiation pressure.

With the advance of the space age, it became clear that most space applications require fixing, as strictly as possible, the areas covered by the satellite or the constellation of satellites. In turn, fixing the coverage regions requires fixed nodes and fixed apsidal lines. This in turn leads to the search for orbits satisfying these requirements. The families of orbits satisfying such conditions are called "*frozen orbits*" [1–5]. Clearly, the design of such orbits includes the effects of the perturbing influences that affect the motion of the satellite. As the present work is interested in low Earth orbits, only the effect of Earth oblateness is taken into concern. These have been extensively treated in the literature [6–10].

This paper is aiming at constructing an atlas of the balanced low Earth satellite orbits, which fall in the range from 600 km to 2000 km above sea surface, in the sense that the variations of the elements are averaged over the fast angle to keep only long periodic and secular variations that affect the orbit accumulatively with time. In this paper, a model is given for the averaged effects (over the mean anomaly) of

Earth oblateness. Then, the Lagrange planetary equations for perturbations of the elements are investigated to get sets of orbital values at which the variations of the elements can be cancelled simultaneously.

2. Earth Potential

The actual shape of the Earth is that of an eggplant. The center of mass does not lie on the spin axis, and neither the meridian nor the latitudinal contours are circles. The net result of this irregular shape is to produce a variation in the gravitational acceleration to that predicted using a point mass distribution. This variation reaches its maximum value at latitude 45 deg and approaches zero at latitudes 0 and 90 deg.

The motion of a particle around the Earth can be visualized best by resolving it into individual motions along the meridian and the latitudinal contours. The motion around the meridian can be thought of as consisting of different periodic motions called "zonal harmonics." Similarly, the motion along a latitudinal contour can be visualized as consisting of different periodic motions called "tesseral harmonics." The zonal harmonics describe the deviations of a meridian from a great circle, while the tesseral harmonics describe the deviations of a latitudinal contour from a circle.

At points exterior to the Earth, the mass density is zero, thus, at external points the gravitational potential satisfies

$$\nabla^2 V = 0, \tag{1}$$

where V is a scalar function representing the potential. Also, the gravitational potential of the Earth must vanish as we recede to infinitely great distances. With these conditions on the above equation, the potential V at external points can be represented in the following form [11]:

$$V = \frac{-\mu}{r} \sum_{n\geq 0} \sum_{m=0}^{n} \left(\frac{R}{r}\right)^n P_n^m (\sin\delta)\left(C_{nm}\cos m\alpha + S_{nm}\sin m\alpha\right). \tag{2}$$

This expression of the potential is called "Venti potential," and it was adopted by the IAU (International Astronomical Union) in 1961. The terms arising in the above equation are C_{nm} and S_{nm} are harmonic coefficients (they are bounded as is always the case in physical problems), R is the equatorial radius of the Earth, $\mu = GM$ is the Earth's gravitational constant, G is the universal constant of gravity, M is the mass of the Earth, and (r, α, δ) are the geocentric coordinates of the satellite (Figure 1, [12]) with α measured east of Greenwich, and $P_n^m(\sin\delta)$ represents the associated Legendre polynomials.

The terms with $m = 0$ are called "zonal harmonics."

The terms with $0 < m < n$ are called "tesseral harmonics."

The terms with $m = n$ are called "sectorial harmonics."

The case of axial symmetry is expressed by taking $m = 0$, while if equatorial symmetry is assumed, we consider only even harmonics since $P_{2n+1}(-x) = -P_{2n+1}(x)$. Also, the coefficients C_{21} and S_{21} are vanishingly small. Further if the origin is taken at the center of mass, the coefficients C_{10}, C_{11}, and S_{11} will be equal to zero.

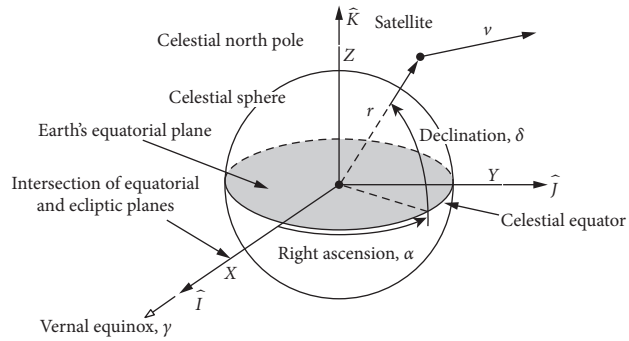

Figure 1: Geocentric coordinates of the satellite.

Considering axial symmetry, with origin at the center of mass, we can write

$$\begin{aligned} V &= \frac{-\mu}{r} \sum_{n\geq 0} \left(\frac{R}{r}\right)^n P_n(\sin\delta) C_{n0} \\ &= \frac{-\mu}{r} + \sum_{n\geq 2} J_n \frac{R^n}{r^{n+1}} P_n(\sin\delta), \end{aligned} \tag{3}$$

where $J_n = -C_{n0}$.

Taking terms up to j_4, we can write V in the following form:

$$V = \sum_{i=1}^{4} V_i, \tag{4}$$

where

$$\begin{aligned} V_0 &= -\frac{\mu}{r}, \\ V_1 &= 0, \\ V_2 &= J_2 \frac{R^2}{r^3} P_2(\sin\delta) = \frac{1}{2} J_2 \frac{R^2}{r^3}\left(3\sin^2\delta - 1\right), \\ V_3 &= J_3 \frac{R^3}{r^4} P_3(\sin\delta) = \frac{1}{2} J_3 \frac{R^3}{r^4}\left(5\sin^3\delta - 3\sin\delta\right), \\ V_4 &= J_4 \frac{R^4}{r^5} P_4(\sin\delta) = \frac{1}{8} J_4 \frac{R^4}{r^5}\left(3 - 30\sin^2\delta + 35\sin^4\delta\right). \end{aligned} \tag{5}$$

It is a purely geometrical transformation to express the potential function $V(r, \delta)$, given by the above equations, as a function of the Keplerian orbital elements a, e, i, Ω, ω, and I in their usual meanings (Figure 2, [12]), where a and e are the semi-major axis and the eccentricity of the orbit, respectively, i is the inclination of the orbit to the Earth's equatorial plane, Ω and ω describes the position of the orbit in space where Ω is the longitude of the ascending node and ω is the argument of perigee, and finally, l is the mean anomaly to describe the position of the satellite with respect to the orbit.

Then, $V(a, e, i, \Omega, \omega, I)$ is in a form suitable to use in Lagrange's planetary equations, and in canonical

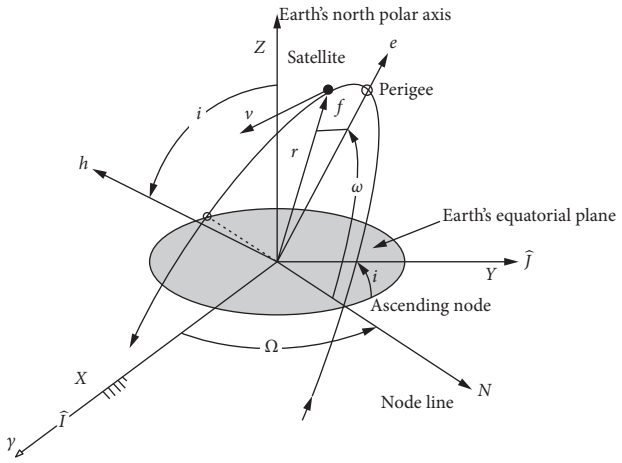

Figure 2: Keplerian orbital elements of the satellite.

perturbations methods through the relation. From the spherical trigonometry of the celestial sphere, we have

$$\sin\delta = Si\sin(f+\omega), \tag{6}$$

where f is the true anomaly, ω is the argument of perigee, and $Si = \sin i$, $Ci = \cos i$.

Substituting for δ, in $P_n(\sin\delta)$, we get

$$\begin{aligned}
P_2(\sin\delta) &= \frac{1}{2}\left\{3Si^2\sin^2(f+g)-1\right\}\\
&= \frac{1}{4}\left\{\left(1-3Ci^2\right)-3Si^2\cos(2g+2f)\right\},\\
P_3(\sin\delta) &= \frac{1}{2}\left\{5Si^3\sin^3(g+f)-3Si\sin(f+g)\right\}\\
&= \frac{1}{8}\left\{\left(15Si^3-12Si\right)\sin(f+g)-5Si^3\sin(3f+3g)\right\},\\
P_4(\sin\delta) &= \frac{1}{8}\left\{3-30Si^2\sin^2(g+f)+35Si^4\sin^4(g+f)\right\}\\
&= \frac{1}{64}\left\{\left(9-90Ci^2+105Ci^4\right)\right.\\
&\quad +\left(-20+160Ci^2-140Ci^4\right)\cos(2f+2g)\\
&\quad \left.+35Si^4\cos(4f+4g)\right\}.
\end{aligned} \tag{7}$$

Thus, we get V_2, V_3, and V_4 as functions of the orbital elements.

We now proceed to evaluate the effects of Earth oblateness, considering the geopotential up to the zonal harmonic J_4.

In the present solution, we consider only the secular and long periodic terms, averaging over the mean anomaly l.

2.1. The Disturbing Function. The disturbing function R is defined as follows:

$$R = -\left(V_2+V_3+V_4\right), \tag{8}$$

where V_2, V_3, and V_4 are the 2nd, 3rd, and 4th terms of the geopotential, namely

$$\begin{aligned}
V_2 &= \frac{\mu j_2 R^2}{4r^3}\left[\left(1-3Ci^2\right)-3Si^2\cos(2f+2\omega)\right],\\
V_3 &= \frac{\mu j_3 R^3}{8r^4}\left[\left(15Si^3-12Si\right)\sin(f+\omega)-5Si^3\sin(3f+3\omega)\right],\\
V_4 &= \frac{\mu j_4 R^4}{64r^5}\left[\left(9-90Ci^2+105Ci^4\right)\right.\\
&\quad +\left(-20+160Ci^2-140Ci^4\right)\cos(2f+2\omega)\\
&\quad \left.+35Si^4\cos(4f+4\omega),\right.
\end{aligned} \tag{9}$$

where $Ci = \cos(i)$, $Si = \sin(i)$, and f is the true anomaly.

Since terms depending only on the fast variable l will not affect the orbit in an accumulating way with time, we average the perturbing function R over the mean anomaly with its period 2π. The average function is defined by

$$\langle F(l)\rangle = \frac{1}{2\pi}\int_0^{2\pi} F(l)\,\mathrm{d}l. \tag{10}$$

As the perturbing function R is a function of the true anomaly f not the mean anomaly l, we use the relation

$$\mathrm{d}l = \frac{1}{\sqrt{1-e^2}}\left(\frac{r}{a}\right)^2\mathrm{d}f, \tag{11}$$

where both angles have the same period and the same end points 0 and 2π, and therefore the average function will be given by

$$\langle F(f)\rangle = \frac{1}{2\pi\sqrt{1-e^2}}\int_0^{2\pi}\left(\frac{r}{a}\right)^2 F(f)\mathrm{d}f. \tag{12}$$

Applying the required integrals, we get the averaged disturbing function $\langle R\rangle$

$$\langle R\rangle = -\left[\langle V_2\rangle_l+\langle V_3\rangle_l+\langle V_4\rangle_l\right], \tag{13}$$

where

$$\begin{aligned}
\langle V_2\rangle_l &= \frac{\mu j_2 R^2}{4a^3}\left(1-e^2\right)^{-(3/2)}\left(1-3Ci^2\right),\\
\langle V_3\rangle_l &= \frac{\mu j_3 R^3}{8a^4}e\left(1-e^2\right)^{-(5/2)}\left(15Si^3-12Si\right)\sin(\omega),\\
\langle V_4\rangle_l &= \frac{\mu j_4 R^4}{64a^5}\left(1-e^2\right)^{-(7/2)}\left(1+\frac{3e^2}{2}\right)\left(9-90Ci^2+105Ci^4\right)\\
&\quad +\frac{3\mu j_4 R^4}{256a^5}e^2\left(1-e^2\right)^{-(7/2)}\left(-20+160Ci^2-140Ci^4\right)\cos(2\omega).
\end{aligned} \tag{14}$$

2.2. Lagrange Equations for the Averaged Variations of the Elements. The Lagrange planetary equations for the variations of the elements for a disturbing potential R are as follows [13]:

$$\dot{a} = \frac{2}{na}\frac{\partial R}{\partial l},$$

$$\dot{e} = \frac{-\sqrt{1-e^2}}{na^2 e}\frac{\partial R}{\partial \omega} + \frac{1-e^2}{na^2 e}\frac{\partial R}{\partial l},$$

$$\dot{i} = \frac{-1}{na^2 Si\sqrt{1-e^2}}\frac{\partial R}{\partial h} + \frac{\cot(i)}{na^2\sqrt{1-e^2}}\frac{\partial R}{\partial \omega},$$

$$\dot{\Omega} = \frac{1}{na^2 Si\sqrt{1-e^2}}\frac{\partial R}{\partial i}, \tag{15}$$

$$\dot{\omega} = \frac{\sqrt{1-e^2}}{na^2 e}\frac{\partial R}{\partial e} - Ci\dot{\Omega},$$

$$\dot{l} = n - \frac{2}{na}\left(\frac{\partial R}{\partial a}\right)_n - \frac{1-e^2}{na^2 e}\frac{\partial R}{\partial e},$$

where n is the mean motion given by $n = \sqrt{\mu/a^3}$.

Substituting for the averaged disturbing function $\langle R\rangle$ due to Earth oblateness, the Lagrange equations become

$$\dot{a} = 0, \tag{16}$$

$$\dot{e} = \frac{-\sqrt{1-e^2}}{na^2 e}\frac{\partial\langle R\rangle}{\partial \omega}, \tag{17}$$

$$\dot{i} = \frac{-1}{na^2 Si\sqrt{1-e^2}}\frac{\partial\langle R\rangle}{\partial \Omega} + \frac{\cot(i)}{na^2\sqrt{1-e^2}}\frac{\partial\langle R\rangle}{\partial \omega}, \tag{18}$$

$$\dot{\Omega} = \frac{1}{na^2 Si\sqrt{1-e^2}}\frac{\partial\langle R\rangle}{\partial i}, \tag{19}$$

$$\dot{\omega} = \frac{\sqrt{1-e^2}}{na^2 e}\frac{\partial\langle R\rangle}{\partial e} - Ci\dot{\Omega}, \tag{20}$$

where the equation for l is neglected because we concentrate on balancing the orbit position not the satellite motion in the orbit.

2.3. Variations of the Elements due to Earth Oblateness. Substituting for the required derivatives in equations (16) to (20) yields

$$\dot{e} = \frac{3\sqrt{\mu}j_3 R^3}{2a^{9/2}}\left(1-e^2\right)^{-2}\left(\frac{5}{4}Si^2 - 1\right)Si\cos(\omega) - \frac{15\sqrt{\mu}j_4 R^4}{32a^{11/2}}e\left(1-e^2\right)^{-3}\left(-1 + 8Ci^2 - 7Ci^4\right)\sin(2\omega). \tag{21}$$

Defining

$$\eta = \left(1-e^2\right),$$

$$c_1 = \frac{3j_3}{2},$$

$$F_{1i} = \left(\frac{5}{4}Si^2 - 1\right)Si, \tag{22}$$

$$c_2 = \frac{15j_4}{32},$$

$$F_{2i} = \left(-1 + 8Ci^2 - 7Ci^4\right),$$

We get

$$\dot{e} = \frac{\sqrt{\mu}R^4}{\eta^3 a^{11/2}}\left(c_1\eta\frac{a}{R}F_{1i}Cos(\omega) - c_2 e F_{2i}\sin(2\omega)\right),$$

$$\dot{i} = \frac{\cot(i)}{n}\left\{\frac{3\mu j_3 R^3}{2a^6}e\left(1-e^2\right)^{-3}\left(\frac{5}{4}Si^2 - 1\right)Si\cos(\omega) - \frac{15\mu j_4 R^4}{16a^7}e^2\left(1-e^2\right)^{-4}\left(-1 + 8Ci^2 - 7Ci^4\right)\sin(2\omega)\right\}, \tag{23}$$

or

$$\dot{i} = -\frac{e\cot(i)}{\eta}\dot{e},$$

$$\dot{\Omega} = \frac{-Ci}{n}\left\{\frac{3\mu j_2 R^2}{2a^5}\left(1-e^2\right)^{-2} + \frac{\mu j_3 R^3}{8a^6}e\left(1-e^2\right)^{-3}\left(45Si - \frac{12}{Si}\right)\sin(\omega) + \frac{15\mu j_4 R^4}{16a^7}\left(1-e^2\right)^{-4}\left[\left(1+\frac{3e^2}{2}\right)\left(3 - 7Ci^2\right) + e^2\left(-4 + 7Ci^2\right)\cos(2\omega)\right]\right\}. \tag{24}$$

Defining

$$c_3 = \frac{3j_2}{2},$$

$$c_4 = \frac{3j_3}{8},$$

$$c_5 = \frac{15j_4}{16}, \tag{25}$$

$$F_{3i} = 15Si - \frac{4}{Si},$$

$$F_{4i} = 3 - 7Ci^2,$$

$$F_{5i} = -4 + 7Ci^2.$$

We get

$$\dot{\Omega} = \frac{-Ci\sqrt{\mu}R^4}{\eta^4 a^{11/2}} \left\{ c_3 \left(\frac{a}{R}\right)^2 \eta^2 + c_4 \frac{a}{R} e\eta F_{3i} \sin(\omega) + c_5 \left[\left(1 + \frac{3e^2}{2}\right) F_{4i} + e^2 F_{5i} \cos(2\omega) \right] \right\}, \tag{26}$$

$$\dot{\omega} = -Ci\dot{\Omega} - \frac{3\mu j_2 R^2}{4na^5}\left(1-e^2\right)^{-2}\left(1-3Ci^2\right) - \frac{3\mu j_3 R^3}{2na^6 e}\left(1+4e^2\right)\left(1-e^2\right)^{-3}\left(\frac{5}{4}Si^2 - 1\right)Si\sin(\omega) - \frac{15\mu j_4 R^4}{32na^7}\left(1-e^2\right)^{-4}\left[\left(1+\frac{3e^2}{4}\right)\left(3-30Ci^2+35Ci^4\right) + \left(1+\frac{5}{2}e^2\right)\left(-1+8Ci^2-7Ci^4\right)\cos(2\omega)\right]. \tag{27}$$

Defining as in equation (28), we get equation (29):

$$c_6 = \frac{3j_2}{4}, \qquad F_{6i} = \left(1-3Ci^2\right), \qquad F_{7i} = 3 - 30Ci^2 + 35Ci^4, \tag{28}$$

$$\dot{\omega} = -\frac{\sqrt{\mu}R^4}{\eta^4 a^{11/2}}\left[c_6\left(\frac{a}{R}\right)^2 \eta^2 F_{6i} + c_1 \frac{a}{R}\left(1+4e^2\right)\frac{\eta}{e}F_{1i}\sin(\omega) + c_2\left(\left(1+\frac{3e^2}{4}\right)F_{7i} + \left(1+\frac{5}{2}e^2\right)F_{2i}\cos(2\omega)\right)\right] - Ci\dot{\Omega}. \tag{29}$$

Equations (22)–(29) give the average effects of Earth oblateness including the zonal harmonics of the geopotential up to J_4 on the Keplerian elements of the satellite orbit.

3. Balanced Low Earth Satellite Orbits

In what follows, we try to find orbits that are balanced in the sense that the averaged (over the fast variable l) variations of the orbit elements are set equal to zero. In equation (23), we put it equal to zero and get a relation between the argument of perigee ω and the inclination i, while treating the eccentricity e and the semi-major axis a as parameters. This will give a range of values for ω and i at different values of e and a, which are all give balanced orbits with respect to both the eccentricity e and the inclination i. The same is done with equations (26) and (29), while putting $\dot{\Omega} = 0$ and $\dot{\omega} = 0$.

The applicable ranges for this model of the semi-major axis a are $1.1R \le a \le 1.3R$, where the range $1.4R$–$2R$ is avoided due to the predominance of the radiation belts at these levels, to avoid the damages of the equipment that it may produce, besides its fatal effects on human life (for inhabited spacecrafts). The values for the eccentricity e are taken between 0.01 (almost circular orbit) and 0.5.

3.1. Orbits with Fixed Eccentricity and Inclination. By equating the variation of e by zero, we get

$$\dot{e} = \frac{\sqrt{\mu}R^4}{\eta^3 a^{11/2}}\left(c_1 \frac{a}{R}\eta F_{1i}\cos(\omega) + c_2 e F_{2i}\sin(2\omega)\right) = 0. \tag{30}$$

This implies

$$c_1 \frac{a}{R}\eta F_{1i}\cos(\omega) + c_2 e F_{2i}\sin(2\omega) = 0. \tag{31}$$

So either $\cos(\omega) = 0$ or

$$\sin(\omega) = \frac{a\left(1-e^2\right)}{eR}C_1 F(i), \tag{32}$$

where

$$C_1 = \frac{8J_3}{5J_4}, \qquad F(i) = \frac{\left(1-(5/4)\sin^2(i)\right)\sin(i)}{1-8\cos^2(i)+7\cos^4(i)}. \tag{33}$$

Equations (32) and (33) give the family of low orbits that have both the eccentricity and the inclination fixed.

The condition for the existence of such orbits is clearly that

$$-1 \le \sin(\omega) \le 1, \tag{34}$$

which is guaranteed by

$$-1 \le \frac{a\left(1-e^2\right)}{eR}C_1 F(i) \le 1. \tag{35}$$

We put it as a condition on the eccentricity i only when

$$\frac{-eR}{C_1 a\left(1-e^2\right)} \le F(i) \le \frac{eR}{C_1 a\left(1-e^2\right)}. \tag{36}$$

3.2. Orbits with Fixed Node. The families of orbits for which $d\Omega/dt = 0$ (i.e with fixed nodes) are obtained from

$$\frac{-Ci\sqrt{\mu}R^4}{\eta^4 a^{11/2}}\left\{c_3\left(\frac{a}{R}\right)^2\eta^2 + c_4\frac{a}{R}e\eta F_{3i}\sin(\omega) + c_5\left[\left(1+\frac{3e^2}{2}\right)F_{4i} + e^2 F_{5i}\cos(2\omega)\right]\right\} = 0. \tag{37}$$

This implies

$$c_3\left(\frac{a}{R}\right)^2\eta^2 + c_4\frac{a}{R}e\eta F_{3i}\sin(\omega) + c_5\left[\left(1+\frac{3e^2}{2}\right)F_{4i} + e^2 F_{5i}\left(1-2\sin^2(\omega)\right)\right] = 0. \tag{38}$$

Table 1: Real values of i (in degree) corresponding to the given values of $F(i)$.

$F(i)$	i_1	$180 - i_1$	i_2	$-180 - i_2$
0.01	63.63	116.37	−63.22	−116.78
0.05	64.27	115.73	−62.11	−117.89
0.10	64.84	115.16	−59.76	−120.24
0.15	65.25	114.75	−55.14	−124.86
0.20	65.56	114.44	−47.16	−132.84

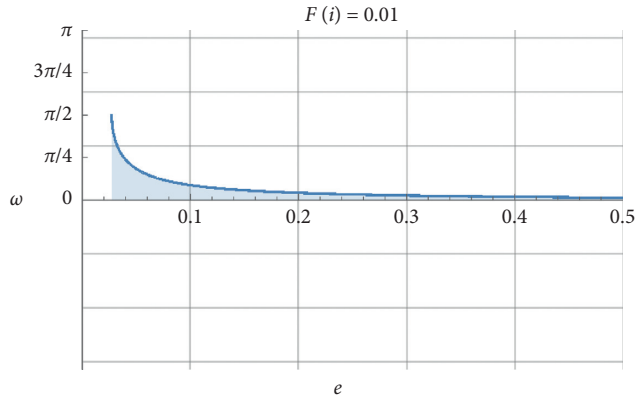

Figure 3: The curve $\omega(e)$ at which $\dot{e} = \dot{i} = 0$ for $F(i) = 0.01$.

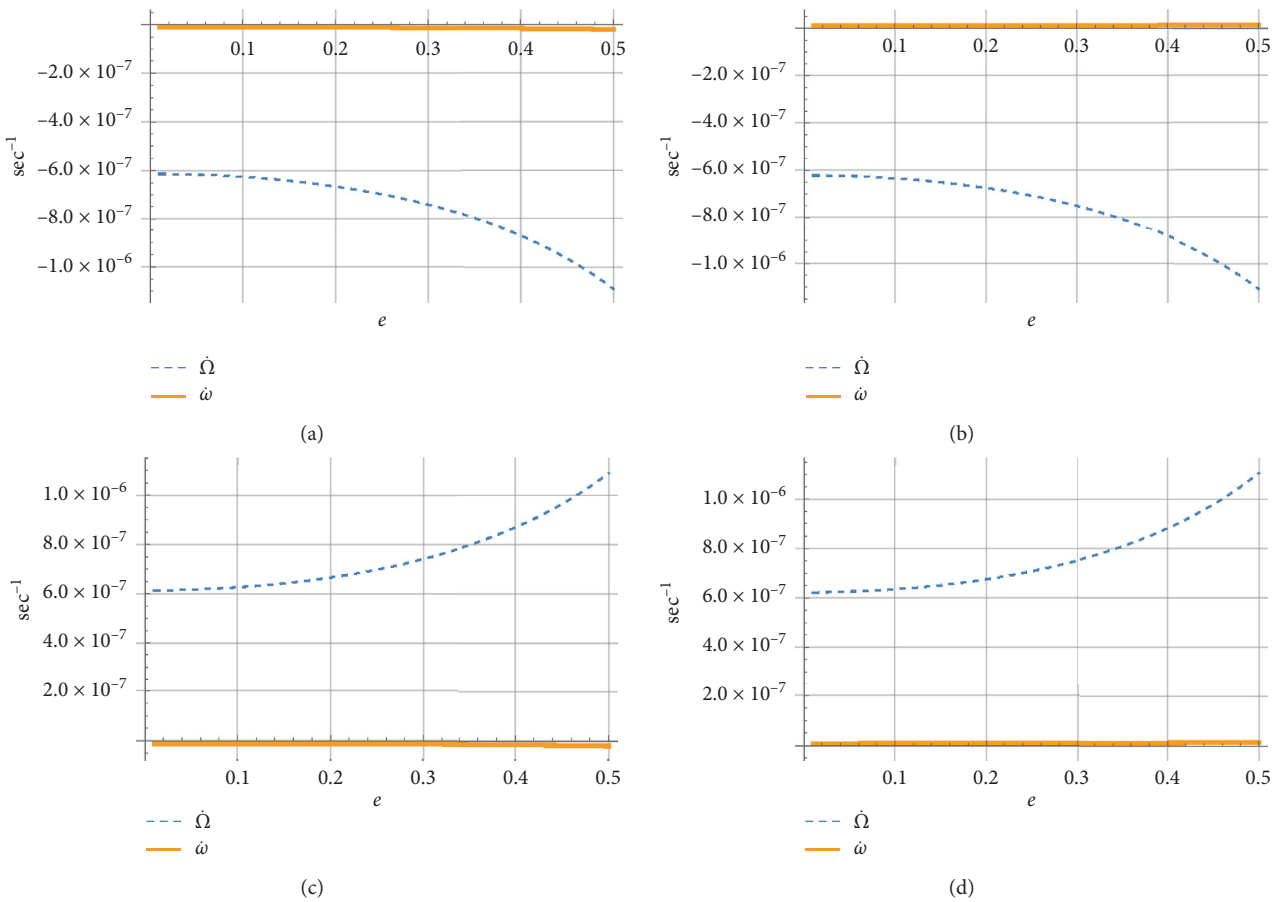

Figure 4: Curves of $\dot{\Omega}$ and $\dot{\omega}$ with e for the 4 cases corresponding to $F(i) = 0.01$. (a) $i = 63.63$, (b) $i = -63.22$, (c) $i = 116.37$, and (d) $i = 116.78$.

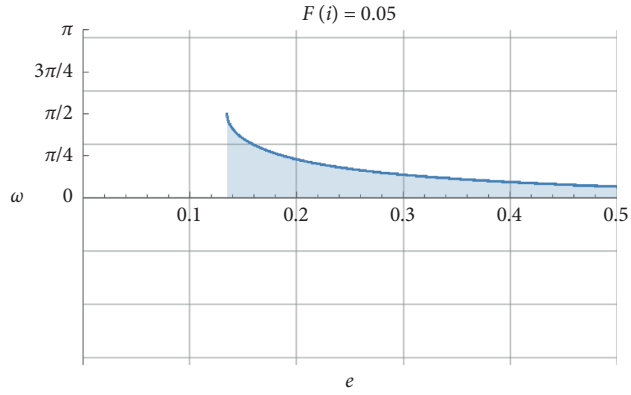

Figure 5: The curve $\omega(e)$ at which $\dot{e} = \dot{i} = 0$ for $F(i) = 0.05$.

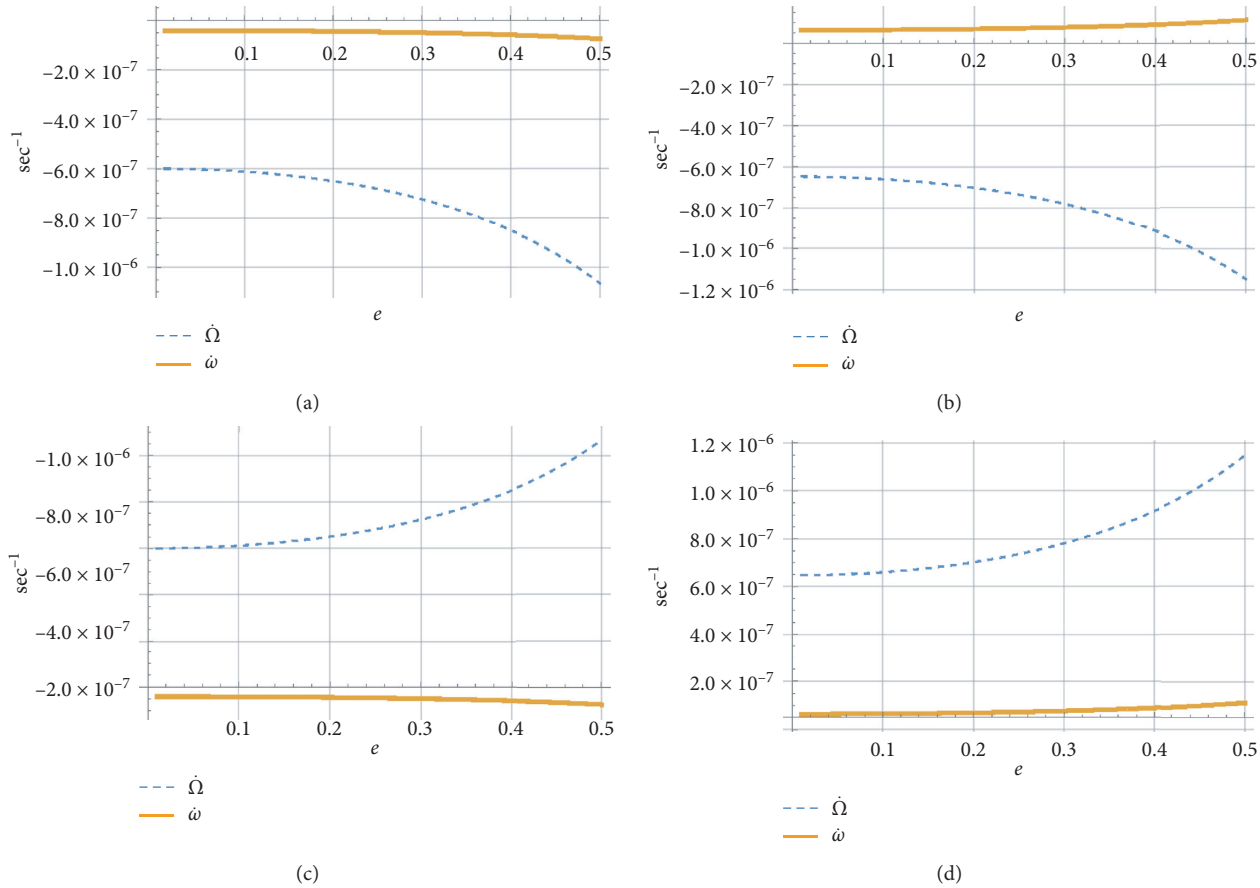

Figure 6: Curves of $\dot{\Omega}$ and $\dot{\omega}$ with e for the 4 cases corresponding to $F(i) = 0.05$. (a) $i = 64.27$, (b) $i = -62.11$, (c) $i = 115.73$, and (d) $i = -117.89$.

This can be arranged as a second order equation for $\sin(\omega)$, giving a family of orbits with fixed argument of perigee for different values of ω as a function of the inclination i, the semi-major axis a, and the eccentricity e.

$$-2c_5e^2F_{5i}\sin^2(\omega) + c_4\frac{a}{R}e\eta F_{3i}\sin(\omega) + c_3\left(\frac{a}{R}\right)^2\eta^2 + c_5\left[\left(1+\frac{3e^2}{2}\right)F_{4i} + e^2F_{5i}\right] = 0. \tag{39}$$

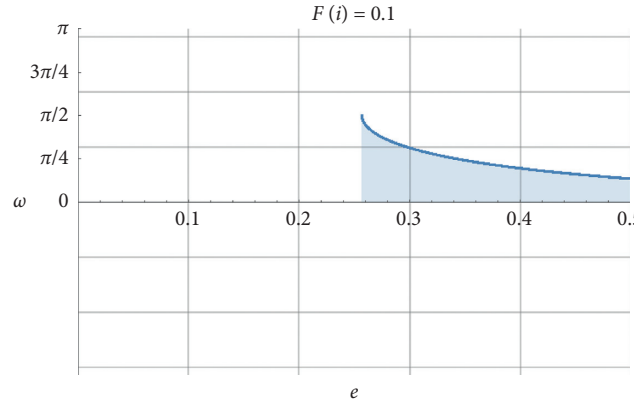

Figure 7: The curve $\omega(e)$ at which $\dot{e} = \dot{i} = 0$ for $F(i) = 0.01$.

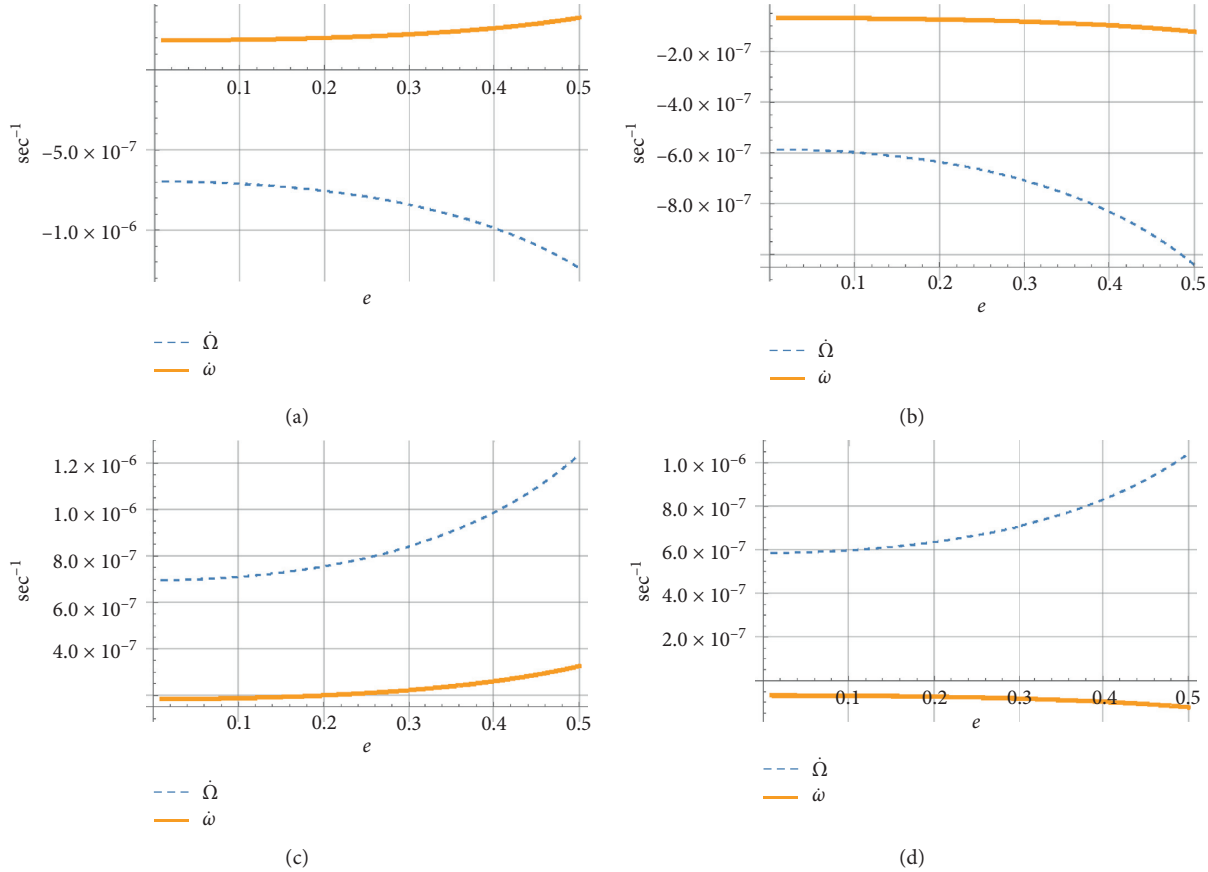

Figure 8: Curves of $\dot{\Omega}$ and $\dot{\omega}$ with e for the 4 cases corresponding to $F(i) = 0.1$. (a) $i = -59.76$, (b) $i = 64.84$, (c) $i = -120.24$, and (d) $i = 115.16$.

When solving for $\sin(\omega)$, we get the family of orbits for which the longitude of the node is balanced,

$$\sin(\omega) = \frac{2c_4 z F_{3i} \pm \sqrt{4c_4^2 z^2 F_{3i}^2 + 16c_5 F_{5i}\left(2c_3 z^2 + c_5 F_{4i}\left(2 + 3e^2\right) + 2c_5 e^2 F_{5i}\right.}}{8c_5 e F_{5i}}, \tag{40}$$

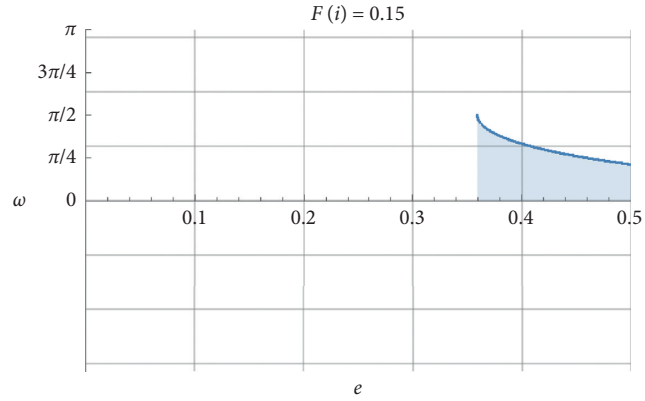

Figure 9: The curve $\omega(e)$ at which $\dot{e} = \dot{i} = 0$ for $F(i) = 0.15$.

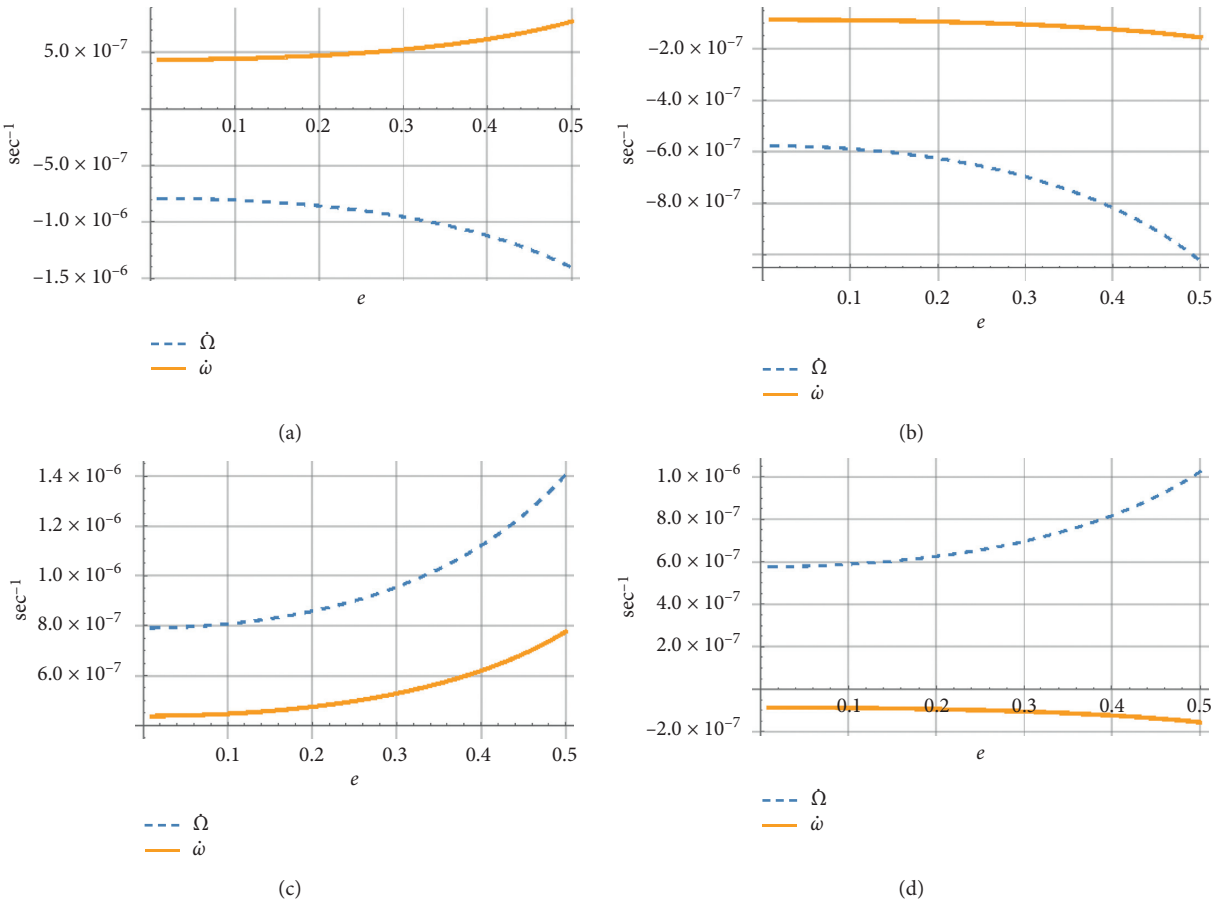

Figure 10: Curves of $\dot{\Omega}$ and $\dot{\omega}$ with e for the 4 cases corresponding to $F(i) = 0.15$. (a) $i = -55.14$, (b) $i = 65.25$, (c) $i = -124.86$, and (d) $i = 114.75$.

where

$$z = \frac{a}{R}\eta. \tag{41}$$

The condition for having the orbit if real solution exists is again that $-1 \le \sin(\omega) \le 1$, which gives

$$-1 \le \frac{2c_3 z^2 + (2 + 3e^2)c_5 F_{4i} + 2e^2(c_5 - 1)F_{5i}}{c_4 e z F_{3i}} \le 1, \quad F_{5i}, F_{3i} \neq 0. \tag{42}$$

3.3. Orbits with Fixed Perigee. For the argument of perigee to balance, we solve $\dot{\omega} = 0$.We substitute from equation (26) into equation (29) then expand $\cos(2\omega)$ and collect terms with respect to $\sin(\omega)$. We get

$$\dot{\omega} = A\sin^2(\omega) + B\sin(\omega) + C. \tag{43}$$

Thus for $\dot{\omega} = 0$, we get

$$\sin(\omega) = \frac{-B \pm \sqrt{B^2 - 4AC}}{2A}, \tag{44}$$

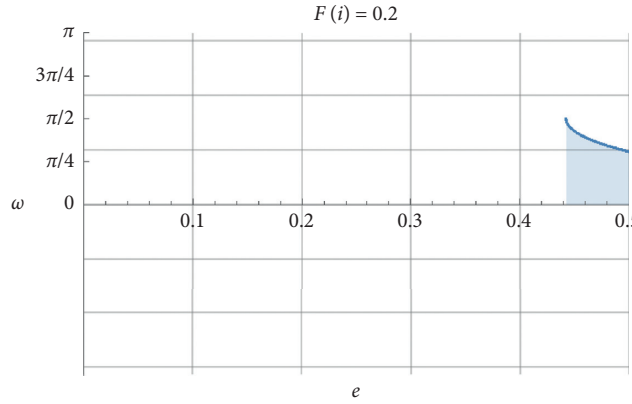

Figure 11: The curve $\omega(e)$ at which $\dot{e} = \dot{i} = 0$ for $F(i) = 0.2$.

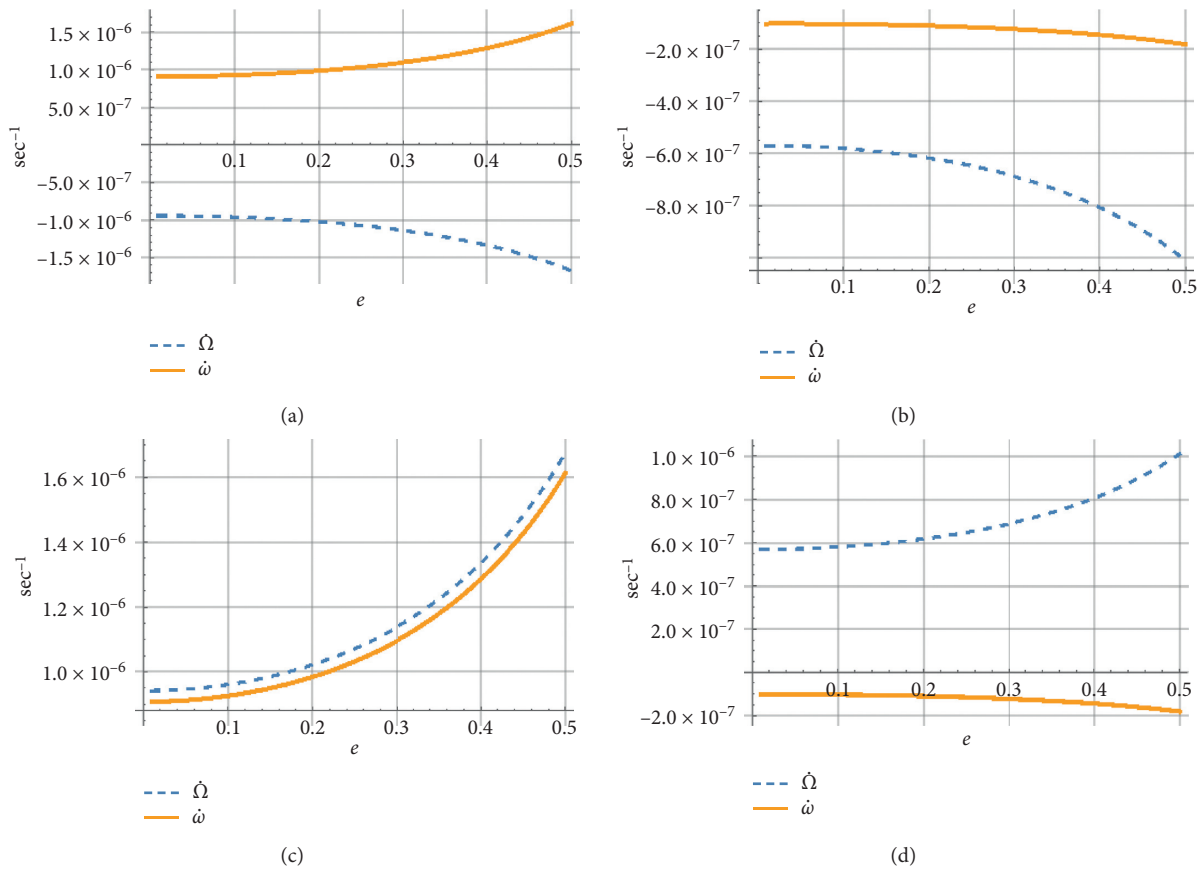

Figure 12: Curves of $\dot{\Omega}$ and $\dot{\omega}$ with e for the 4 cases corresponding to $F(i) = 0.2$. (a) $i = -47.16$, (b) $i = 65.56$, (c) $i = -132.84$, and (d) $i = 114.44$.

where

$$A = -2c_5e^2F_5\cos^2(i) + 2c_2\left(1 + \frac{5}{2}e^2\right)F_2, \tag{45}$$

$$B = c_4ezF_3\cos^2(i) - c_1z\left(4e + \frac{1}{e}\right)F_1, \tag{46}$$

$$C = \cos^2(i)\left(c_3z^2 + c_5\left(e^2F_5 + \left(1 + \frac{3e^2}{2}\right)F_4\right)\right) - c_6z^2F_6 - c_2\left(\left(1 + \frac{3e^2}{4}\right)F_7 + \left(\left(1 + \frac{5e^2}{2}\right)\right)F_2\right). \tag{47}$$

Equations (44)–(47) give the relation between $\sin(\omega)$ and the inclination i, the semi-major axis a, and the eccentricity e, which gives the family of orbits that balance the argument of perigee ω, subject of course to the restriction that $\sin(\omega)$ is a real value between -1 and 1.

4. Numerical Results

In this section, numerical results and graphs are obtained for the case of seasat $a = 7100$ km by putting ω as a function of e and i from equations (32) and (33). The curves are plotted within the possible range given by condition (36) to give curves of balanced e and i. The curves are against the eccentricity e in the range [0.01, 0.5]. The numerical values involved are $J_2 = 0.001082645$, $J_3 = -0.000002546$, $J_4 = -0.000001649$, $R = 6378.165$ km, $\alpha = 7100$ m, and $\mu = 398600.5\ \text{km}^3\text{sec}^{-2}$.

The condition (36) gives the upper and lower bounds of the function $F(i)$ as a function of e, and since the function $eR/(C_1 a(1-e^2))$ is increasing with e and has no critical points in the interval [0.01, 0.5], then the minimum value occurs at $e = 0.01$ and the maximum at $e = 0.5$, which gives $-0.24 \le F(i) \le 0.24$. The graphs are plotted for different values of $F(i)$, which corresponds to specific values of i found by solving the equation resulting from setting $F(i)$ equal to the required values. After that we plot $\dot{\Omega} = 0$ and $\dot{\omega} = 0$ simultaneously for the same values of $F(i)$ at each specific i-value, to find the orbit values at which we have nearest values for $\dot{\Omega} = 0$ and $\dot{\omega} = 0$. In the graphs of $\dot{\Omega}$ and $\dot{\omega}$, the relation (32) was kept to ensure that e and i are already balanced.

Five selected values of $F(i)$ are chosen: $F(i) = 0.01$, 0.5, 0.10, 0.15, and 0.20. Negative values will give the same results with negative sign since $F(i)$ is odd with respect to i. Also for each value, the solution of $F(i) = x$, with x equals one of the above values we get four real values of i on the form: i_1, $180 - i_1$, i_2, and $-180 - i_2$, where i_1 and i_2 are near the critical inclination one of them is positive and the other is negative. Table 1 gives the values of i corresponding to the selected values of $F(i)$.

We note that as $F(i)$ increases, i gets away from the critical inclination, and the curve gets shorter indicating less stability of ω as expected.

The graphs are plotted for each value of $F(i)$ first for the balanced values of e and i, then for the corresponding four values of i, four graphs are plotted for $\dot{\Omega}$ and $\dot{\omega}$ to find the nearest values of zero variation for both elements.

Figures 3–12 show the possibility of balancing ω with e and i, while Ω will have a variation of order 10^{-6}/sec or it must be balanced alone at $i = 90$ deg (as shown in equation (26)), according to the orbit kind. Figures 3, 5, 7, 9, and 11 show the possible values of $\omega(e)$ that balance e and i, while Figures 4, 6, 8, 10, and 12 show the curves of $\dot{\Omega}$ and $\dot{\omega}$ at the values of i at which $\dot{e} = \dot{i} = 0$.

5. Conclusion

Let balanced orbits be defined as those for which the orbital elements are set equal to zero under the effect of secular and long periodic perturbations. In this work, the effect of Earth oblateness is the considered perturbing force because of dealing with low Earth orbits. The above analysis then shows that such an orbit will be balanced within a reliable tolerance only for few weeks since we are forced to accept the motion of either the node or the perigee by about 10^{-6} deg/sec. The reason is that under the influence of the Earth oblateness, $\dot{\Omega} = 0$ (exactly) for $i \cong (\pi/2)$, while $\dot{\omega} = 0$ only near the critical inclination $i_c \cong 63.4$ deg. Hence, the best procedure is to design a satellite constellation for which the nodal shifts due to the perturbative effects and Earth rotation are modeled to yield continuous coverage. The perigees are either fixed or arranged to realize that the perigee (or the apogee) be overhead the coverage region (regions) in due times. This may require near commensurability with the admitted nodal periods.

Data Availability

No data were used to support this study.

Conflicts of Interest

The authors declare that they have no conflicts of interest.

Acknowledgments

This work was funded by the University of Jeddah, Saudi Arabia, under grant no. UJ-26-18-DR. Thus, the author therefore acknowledges with thanks the university technical and financial support.

References

[1] N. Delsate, P. Robutel, A. Lemaître, and T. Carletti, "Frozen orbits at high eccentricity and inclination: application to mercury orbiter," *Celestial Mechanics and Dynamical Astronomy*, vol. 108, no. 3, pp. 275–300, 2010.

[2] E. Condoleo, M. Cinelli, E. Ortore, and C. Circi, "Stable orbits for lunar landing assistance," *Advances in Space Research*, vol. 60, no. 7, pp. 1404–1412, 2017.

[3] A. Elipe and M. Lara, "Frozen orbits about the moon," *Journal of Guidance, Control, and Dynamics*, vol. 26, no. 2, pp. 238–243, 2003.

[4] C. Circi, E. Condoleo, and E. Ortore, "A vectorial approach to determine frozen orbital conditions," *Celestial Mechanics and Dynamical Astronomy*, vol. 128, no. 2-3, pp. 361–382, 2017.

[5] E. Condoleo, M. Cinelli, E. Ortore, and C. Circi, "Frozen orbits with equatorial perturbing bodies: the case of Ganymede, Callisto, and Titan," *Journal of Guidance, Control, and Dynamics*, vol. 39, no. 10, pp. 2264–2272, 2016.

[6] V. Kudielka, "Balanced earth satellite orbits," *Celestial Mechanics & Dynamical Astronomy*, vol. 60, no. 4, pp. 455–470, 1994.

[7] S. L. Coffey, A. Deprit, and E. Deprit, "Frozen orbits for satellites close to an earth-like planet," *Celestial Mechanics & Dynamical Astronomy*, vol. 59, no. 1, pp. 37–72, 1994.

[8] M. Lara, A. Deprit, and A. Elipe, "Numerical continuation of families of frozen orbits in the zonal problem of artificial satellite theory," *Celestial Mechanics & Dynamical Astronomy*, vol. 62, no. 2, pp. 167–181, 1995.

[9] D. Brouwer, "Solution of the problem of artificial satellite theory without drag," *The Astronomical Journal*, vol. 64, p. 378, 1959.

[10] Y. Kozai, "The motion of a close earth satellite," *The Astronomical Journal*, vol. 64, p. 367, 1959.
[11] P. M. Fitzpatrick, *Principles of Celestial Mechanics*, Academic Press, Cambridge, MA, USA, 1970.
[12] H. D. Curtis, *Orbital Mechanics for Engineering Students*, Elsevier, Amsterdam, Netherlands, 2005.
[13] D. Brower and G. M. Clemence, *Methods of Celestial Mechanics*, Academic Press, Cambridge, MA, USA, 1961.

Hindawi
Advances in Astronomy
Volume 2020, Article ID 5263750, 18 pages
https://doi.org/10.1155/2020/5263750

Research Article

Central Configurations and Action Minimizing Orbits in Kite Four-Body Problem

B. Benhammouda,[1] **A. Mansur**,[1] **M. Shoaib**,[1] **I. Szücs-Csillik**,[2] **and D. Offin**[3]

[1]*Higher Colleges of Technology, Abu Dhabi, UAE*
[2]*Romanian Academy, Astronomical Institute, Cluj-Napoca, Romania*
[3]*Queen's University, Mathematics and Statistics Department, Kingston, ON, Canada*

Correspondence should be addressed to D. Offin; offind@queensu.ca

Received 19 February 2020; Accepted 22 April 2020; Published 1 August 2020

Guest Editor: Elbaz I. Abouelmagd

In the current article, we study the kite four-body problems with the goal of identifying global regions in the mass parameter space which admits a corresponding central configuration of the four masses. We consider two different types of symmetrical configurations. In each of the two cases, the existence of a continuous family of central configurations for positive masses is shown. We address the dynamical aspect of periodic solutions in the settings considered and show that the minimizers of the classical action functional restricted to the homographic solutions are the Keplerian elliptical solutions. Finally, we provide numerical explorations via Poincaré cross-sections, to show the existence of periodic and quasiperiodic solutions within the broader dynamical context of the four-body problem.

1. Introduction

To understand the dynamics presented by a total collision of the masses or the equilibrium state of a rotating system, we are led to the concept of central configurations. A configuration of n bodies is central if the acceleration of each body is a scalar multiple of its position [1–4]. Let $r_i \in \mathbb{R}^2$ and m_i, $i = 1, \ldots, n$, denote the position and the mass of the ith body, respectively. Also, let $r_{ij} = \|r_i - r_j\|$ represent the distance between the ith and jth bodies. An n-body system forms a planar noncollinear central configuration [5, 6] if

$$f_{ij} = \sum_{k=0, k\neq i,j}^{n-1} m_k \left(R_{ik} - R_{jk}\right)\Delta_{ijk} = 0, \tag{1}$$

where $R_{ij} = r_{ij}^{-3}$ and $\Delta_{ijk} = (\mathbf{r}_i - \mathbf{r}_j)\wedge(\mathbf{r}_i - \mathbf{r}_k)$ represent the area of the triangle determined by the sides $\|\mathbf{r}_i - \mathbf{r}_j\|$ and $\|\mathbf{r}_i - \mathbf{r}_k\|$.

The four-body problem can be considered from two different perspectives. The perturbative approach where we study the dynamical aspects as a perturbation of the three-body dynamics and assume that one of the masses is vanishingly small, or the global approach where we allow the masses to vary independently and stay positive. In this paper, we take the global approach and will study analytically the problem of central configurations and their dynamical aspects.

The computation of central configurations is a difficult problem for $n \geq 4$. To overcome this difficulty, symmetries or other restriction methods are used to reduce the number of variables and obtain partial answers; see, for example, Cors and Roberts [7]; Albouy et al. [8]; Shoaib et al. [9]; Érdi and Czirják [10]. In this paper, we consider a four-body problem with one axis of symmetry so that the four different masses make a convex or concave kite.

Since the classification of central configurations as one of the problems for the 21st century by Smale [11], it has attracted a lot of attention in recent years and has helped in the understanding of the n-body problem [12–23]. Ji et al. [24] and Waldvogel [25] study a rhomboidal four-body problem with two pairs of masses and use Poincaré sections to find regions of stability for the rhomboidal four-body problem. In addition,

Waldvogel [25] also takes advantage of the simplicity of the equations and study its collisions and escape manifolds. Yan [26] considers the same problem for four equal masses and studies the linear stability of its periodic orbits. One of our results will consider the same model but with only one pair of masses. We will analytically derive regions of central configurations and will also investigate the existence of periodic orbits. Mello and Fernandez [27] prove the existence of kite central configurations for four- and five-body problems on a circle. In one special case, our rhomboidal model is similar to their model for which we also identify a number of periodic orbits and discuss its action minimizing orbits. Gordon [28] has proved that the elliptic Keplerian orbit minimizes the Lagrangian action of the two-body problem with periodic boundary conditions. It is also known that the Eulerian and Lagrangian elliptical solutions for the planar three-body problem are the variational minimizers of the Lagrangian action functional [29, 30]. In the study by Mansur and Offin [31]; Mansur et al. [32]; Mansur et al. [33], the authors have extended these ideas to prove that the homographic solutions to the constrained parallelogram four-body problem are the variational minimizers of the Lagrangian action functional. In this paper, we prove that the minimizers for the action functional restricted to the homographic solutions are the Keplerian elliptical solutions for the four-body problem with three equal and unequal masses. Perez-Chavela and Santoprete [13] show the existence of kite central configurations for a pair of symmetric masses and show that such a configuration must always possess a symmetry. Similarly, Celli [34] proves the existence of planar diamond and trapezoidal central configurations for two pairs of equal masses. Corbera and Llibre [35] give a complete classification of the same problem and show that this setup has exactly 34 different classes of central configurations.

More recently, Deng et al. [36] and Corbera et al. [37] prove that any four-body setup with perpendicular diagonals must be a kite [35, 38]. Santoprete [39] studies a four-body problem with a pair of equal masses and a pair of parallel opposite sides and show that if the opposite masses are equal, then the four-body arrangement must have a line of symmetry and will be a kite.

The paper is organized as follows: Section 2 discusses the equations of motion for the four-body problem. Section 3 discusses the existence of central configurations and the action minimizing orbits for the four-body problem where three masses are equal and arranged at vertices of an isosceles triangle and the fourth mass is on the axis of symmetry. In Section 4, we discuss the variational techniques where the action functional corresponding to these family of solutions is shown to be a minimizer. Section 5 discusses the existence of central configurations and the action minimizing orbits for the four-body problem where two symmetric masses are equal on the horizontal axis and two nonequal masses are on the vertical axis.

2. Equations of Motion

Consider four positive point masses m_0, m_1, m_2, and m_3 having position vectors $\mathbf{r}_i$ and interbody distances r_{ij}. For a general four-body setup, equation (1) gives the following six central configuration equations when $n = 4$:

$$\begin{aligned}
f_{01} &= m_2(R_{02} - R_{12})\Delta_{012} + m_3(R_{03} - R_{13})\Delta_{013} = 0,\\
f_{02} &= m_1(R_{01} - R_{21})\Delta_{021} + m_3(R_{03} - R_{23})\Delta_{023} = 0,\\
f_{03} &= m_1(R_{01} - R_{31})\Delta_{031} + m_2(R_{02} - R_{32})\Delta_{032} = 0,\\
f_{12} &= m_0(R_{10} - R_{20})\Delta_{120} + m_3(R_{13} - R_{23})\Delta_{123} = 0,\\
f_{13} &= m_0(R_{10} - R_{30})\Delta_{130} + m_2(R_{12} - R_{32})\Delta_{132} = 0,\\
f_{23} &= m_0(R_{20} - R_{30})\Delta_{230} + m_1(R_{21} - R_{31})\Delta_{231} = 0.
\end{aligned} \tag{2}$$

Lemma 1. *Consider a four-body problem with masses m_0, m_1, m_2, and m_3 and position vectors $\mathbf{r}_0 = (0, c)$, $\mathbf{r}_1 = (-1, -a)$, $\mathbf{r}_2 = (0, b)$, and $\mathbf{r}_3 = (1, -a)$, where $a > 0$ and $b > c$, then*

(a) The symmetric masses m_1 and m_3 are equal.

(b) The central configuration equations are

$$\begin{aligned}
f_{01} &= m_1(R_{03} - R_{13})\Delta_{013} + m_2(R_{02} - R_{12})\Delta_{012},\\
f_{12} &= m_0(R_{10} - R_{20})\Delta_{120} + m_1(R_{13} - R_{23})\Delta_{123}.
\end{aligned} \tag{3}$$

Proof. Consider four positive masses m_0, m_1, m_2, and m_3 with position vectors $\mathbf{r}_0 = (0, c)$, $\mathbf{r}_1 = (-1, -a)$, $\mathbf{r}_2 = (0, b)$, and $\mathbf{r}_3 = (1, -a)$, where $a > 0$ and $b > c$. Using the definitions of R_{ij}, Δ_{ijk}, and $\mathbf{r}_i\,(i = 0, 1, 2, 3, 4)$, we obtain

$$\begin{aligned}
R_{01} = R_{03} = R_{30} &= \frac{1}{\left((a+c)^2 + 1\right)^{3/2}},\\
R_{13} &= \frac{1}{8},\\
R_{02} &= \frac{1}{(b-c)^3},\\
R_{12} = R_{21} = R_{32} &= \frac{1}{\left((a+b)^2 + 1\right)^{3/2}},
\end{aligned} \tag{4}$$

with

$$\begin{aligned}
&\Delta_{ijk} = -\Delta_{jik} = -\Delta_{ikj} = -\Delta_{kji},\\
&\Delta_{ijk} = \Delta_{jki} = \Delta_{kij},\\
&\Delta_{ijk} = 0, \quad \text{if } i = j \text{ or } i = k \text{ or } j = k,\\
&\Delta_{012} = \Delta_{023} = c - b,\\
&\Delta_{013} = 2(a + c),\\
&\Delta_{123} = -2(a + b).
\end{aligned} \tag{5}$$

Using the symmetry of the problem and the relations (4) and (5), it is trivial to see that

$$f_{02} = (m_1 - m_3)(R_{01} - R_{21})\Delta_{021} = 0. \tag{6}$$

Since $\Delta_{021} \neq 0$ and $R_{21} \neq R_{01}$, therefore $m_3 = m_1$. This completes the proof of Lemma 1 (a).

From the geometry of the problem, $\Delta m_1 m_0 m_3$ and $\Delta m_1 m_2 m_3$ are both isosceles, and therefore $R_{01} = R_{03}$, $R_{12} = R_{32}$, and $\Delta_{032} = \Delta_{012}$ and hence $f_{03} = f_{01}$. This also implies that $f_{13} \equiv 0$. By a similar argument, it can be shown that $f_{23} = f_{12}$. This leaves two independent equations f_{01} and f_{12} from the set of equations given in (2). This completes the proof of Lemma 1.

3. Three Equal Masses at the Vertices of a Triangle and a Fourth Mass on the Axis of Symmetry

In this section, we consider a four-body problem where three equal masses ($m_1 = m_2 = m_3$) are arranged at the vertices of an isosceles triangle and a fourth mass m_0 is on the axis of symmetry as shown in Figure 1. We start by showing the existence of central configuration for a concave kite four-body problem and then explicitly find regions where such a configuration exists for positive masses. We also discuss the action minimizing orbits for this particular problem.

3.1. Central Configurations

Theorem 1. *Consider four point masses m_0 and $m_1 = m_2 = m_3$ having position vectors $\mathbf{r}_0 = (0,0)$, $\mathbf{r}_1 = (-1,-a)$, $\mathbf{r}_2 = (0,b)$, and $\mathbf{r}_3 = (1,-a)$, where $a>0$ and $b>0$. Then, there exists a unique mass ratio $\mu_0(a,b)$:*

$$\mu_0 = \frac{m_0}{m_1} = \frac{\left(\left((a+b)^2+1\right)^{3/2} - 8\right)(a+b)b^2\left(a^2+1\right)^{3/2}}{4\left(\left(a^2+1\right)^{3/2} - b^3\right)\left((a+b)^2+1\right)^{3/2}}, \tag{7}$$

such that $\mathbf{r} = (\mathbf{r}_0, \mathbf{r}_1, \mathbf{r}_2, \mathbf{r}_3)$ is a central configuration for $\mu_0 > 0$ in $R_{\mu_0}(a,b)$ subject to the constraint $g(a,b) = 0$. The region $R_{\mu_0}(a,b)$ and the constraint $g(a,b)$ are given below:

$$R_{\mu_0}(a,b) = \left\{(a,b) \mid \left(\frac{2}{\sqrt{3}} < b < \sqrt{3} \wedge \left(0 < a < \sqrt{3} - b \vee a > \sqrt{b^2-1}\right)\right) \vee \left(b \geq \sqrt{3} \wedge a > \sqrt{b^2-1}\right)\right\},$$
$$g(a,b) = -b\left(\frac{1}{b^3} - \frac{1}{\alpha}\right) + 2a\left(-\frac{1}{8} + \frac{1}{\beta}\right) = 0, \tag{8}$$

where $\alpha = \left((a+b)^2+1\right)^{3/2}$ and $\beta = \left(a^2+1\right)^{3/2}$.

Before we attempt to prove Theorem 1, we will need help from the following lemmas.

Lemma 2. *The function g defined by (8) is negative for all $0 < a < \sqrt{3}$ and $0 < b \leq B = (2/\sqrt{3})((3/7) + (2\sqrt{3}/7))^{1/4} \simeq 1.13$.*

Proof. Let $0 < a < \sqrt{3}$ and $0 < b \leq B$, then we have

$$\frac{g(a,b)}{b} = \frac{1}{\alpha} + \frac{2a}{b}\left(\frac{1}{\beta}\right) - \frac{4+ab^2}{4b^3}. \tag{9}$$

Consider the equation of the straight line segment that lies in the first quadrant:

$$x + \frac{2a}{b}y - \frac{4+ab^2}{4b^3} = 0. \tag{10}$$

For positive x and y,

$$x + \frac{2a}{b}y - \frac{4+ab^2}{4b^3} < 0, \tag{11}$$

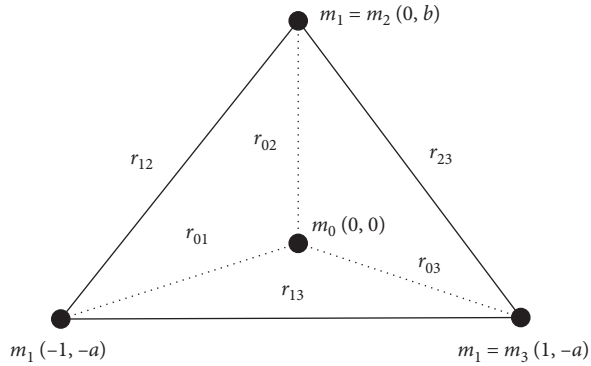

Figure 1: Concave kite four-body configurations with three equal masses $m_1 = m_2 = m_3$.

is equivalent to

$$x < \frac{4+ab^2}{4b^3}, \qquad y < \frac{4+ab^2}{8ab^2}. \tag{12}$$

To prove that $g(a,b)b^{-1} < 0$, we need to show that

$$\frac{1}{\alpha} < \frac{4+ab^2}{4b^3}, \qquad \frac{1}{\beta} < \frac{4+ab^2}{8ab^2}. \tag{13}$$

For $(1/\alpha) < (4 + ab^2/4b^3)$, it is trivial to see that

$$\frac{1}{\alpha} = \frac{1}{\left(1+(a+b)^2\right)^{3/2}} < \frac{1}{b^3} < \frac{4+ab^2}{4b^3}. \tag{14}$$

Similarly, to show that $(1/\beta) < (4 + ab^2/8ab^2)$, we need

$$\beta > \frac{8ab^2}{4+ab^2}, \tag{15}$$

$$\text{or } \left(1+a^2\right)^3 > \left(\frac{8ab^2}{4+ab^2}\right)^2. \tag{16}$$

Inequality (16) is equivalent to

$$\left(1+a^2\right)^3\left(4+ab^2\right)^2 - 64a^2b^4 > 0. \tag{17}$$

Expanding the left-hand side of (17), we obtain the following:

$$\begin{aligned} p(a,b) &= b^4a^8 + 8b^2a^7 + \left(16+3b^4\right)a^6 + 24b^2a^5 \\ &\quad + \left(48+3b^4\right)a^4 + 24b^2a^3 + \left(48-63b^4\right)a^2 + 8b^2a + 16. \end{aligned} \tag{18}$$

For positive a and b,

$$\begin{aligned} p(a,b) &> 48a^4 + \left(48-63b^4\right)a^2 + 16, \\ &\geq 48a^4 + \left(48-63B^4\right)a^2 + 16, \\ &= 48\left(a^2 - \frac{1}{\sqrt{3}}\right)^2 \geq 0. \end{aligned} \tag{19}$$

Consequently, $g(a,b) < 0$ for $0 < a < \sqrt{3}$ and $0 < b \leq B$. This completes the proof of Lemma 2.

Lemma 3. *The partial derivative of g defined by (3) satisfies $g_b(a,b) > (3/\alpha^2)$, for all $a > 0$ and $b > 0$.*

Proof. For positive a and b, we have

$$\begin{aligned} g_b(a,b) &= \frac{2}{b^3} + \frac{\alpha - b\alpha_b}{\alpha^2}, \\ &= \frac{2}{b^3} + \frac{\alpha - 3b(a+b)\gamma}{\alpha^2}, \end{aligned} \tag{20}$$

where $\gamma = (1 + (a+b)^2)^{1/2}$ and α_b is the derivative of α w.r.t. b.

Since $b^3 < \alpha$ for all $a > 0$ and $b > 0$, then

$$g_b(a,b) > \frac{2}{\alpha} + \frac{\alpha - 3b(a+b)\gamma}{\alpha^2}. \tag{21}$$

Using the fact that $\alpha = \gamma^3$ and $\gamma^2 = 1 + (a+b)^2$, we get

$$g_b(a,b) > \frac{3\sqrt{1+(a+b)^2}\left(1+a^2+ab\right)}{\gamma^6}. \tag{22}$$

Since a and b are positive, therefore

$$g_b(a,b) > \frac{3}{\alpha^2}. \tag{23}$$

This completes the proof of Lemma 3.

Remark 1. Numerically, it is easy to show that $g(a,2) = 0$ when $a = 0.14$ and $a = 1.32$. For $a \in I = (0.14, 1.32)$, $g(a,1) < 0$ and $g(a,2) > 0$, when $a \in I$, see Figure 2.

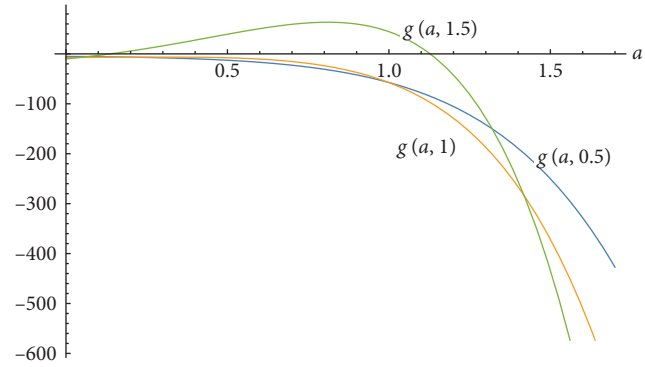

Figure 2: Graph of $g(a,b)$ for values of $b = 0.5, 1$, and 1.5.

Therefore, by intermediate value theorem $g(a,b)$ has at least one root $b \in (1,2)$ when $a \in I$.

Lemma 4. *Consider the function g defined by (3). Then, for any $a_0 \in I = (0.14, 1.32)$ there exists an interval $U \subset I$ containing a_0 and an interval $V \subset (1,2)$ containing b_0 such that there is a unique continuously differentiable function $b = \psi(a)$ defined on U with $b \in V$ that satisfies $g(a,b) = 0$.*

Proof. Let a_0 be any number in the interval $I = (0.14, 1.32)$; then, using Lemma 3, we have $g(a_0, 1) < 0$. Then, numerically, one can check that $g(a_0, 2) > 0$ for $a_0 \in I$. Thus, by the mean value theorem, there exists at least one $b_0 \in (1,2)$, solution of $g(a_0, b) = 0$. By Lemma 3, $g_b(a_0, b) > 0$ for all $b > 0$, hence the solution b_0 is unique. Since g has continuous partial derivatives and $g(a_0, b_0) = 0$, with $g_b(a_0, b_0) \neq 0$, then by the implicit function theorem, there exists an open interval $U \subset I$ containing a_0 and an interval $V \subset (1,2)$ containing b_0 such that there is a unique continuously differentiable function $b = \psi(a)$ defined on U with $b \in V$ that satisfies $g(a,b) = 0$. This completes the proof of Lemma 4.

Proof of Theorem 1. Let $m_1 = m_2 = m_3$ and $c = 0$, and then from Lemma 1, we obtain the following central configuration equations:

$$\begin{aligned} f_{01} &= (R_{01} - R_{13})\Delta_{013} + (R_{02} - R_{12})\Delta_{012} = 0, \\ f_{12} &= m_0(R_{01} - R_{02})\Delta_{012} + m_1(R_{13} - R_{12})\Delta_{123} = 0. \end{aligned} \tag{24}$$

Solving the above equations, we obtain

$$\mu_0(a,b) = \frac{m_0}{m_1} = \frac{\phi_1(a,b)(a+b)b^2\left(a^2+1\right)^{3/2}}{4\phi_2(a,b)\left((a+b)^2+1\right)^{3/2}}, \tag{25}$$

such that constraint (3) holds, where $\phi_1(a,b) = ((a+b)^2+1)^{3/2} - 8$ and $\phi_2(a,b) = (a^2+1)^{3/2} - b^3$. It is proved in Lemmas 2, 3, and 4 that constraint (8) is satisfied by showing the existence of a smooth curve:

$$\psi(a) = \{(a,b) \mid g(a,b) = 0, 0 < a < \sqrt{3}, 1 < b < \sqrt{2}\}. \tag{26}$$

To find the region where $\mu_0 > 0$, we solve the following inequality for a and b:

$$\frac{\phi_1(a,b)}{\phi_2(a,b)} > 0. \tag{27}$$

The functions $\phi_1(a,b)$ and $\phi_2(a,b)$ are positive in R_{ϕ_1} and R_{ϕ_2}, respectively, where

$$R_{\phi_1} = \{(a,b) \mid (0 < b \le \sqrt{3} \wedge a > \sqrt{3} - b) \vee (b > \sqrt{3} \wedge a > 0)\},$$
$$R_{\phi_2} = \left\{(a,b) \mid (0 < b \le 1 \wedge a > 0) \vee \left(b > 1 \wedge a > \sqrt{b^2 - 1}\right)\right\}. \tag{28}$$

Therefore, the configuration $\mathbf{r} = (\mathbf{r}_0, \mathbf{r}_1, \mathbf{r}_2, \mathbf{r}_3)$ shown in Figure 1 forms a central configuration in $R_{\mu_0} = (R_{\phi_1} \cap R_{\phi_2}) \cup (R^c_{\phi_1} \cap R^c_{\phi_2})$, where

$$\begin{aligned} R_{\mu_0} &= \left(R_{\phi_1} \cap R_{\phi_2}\right) \cup \left(R^c_{\phi_1} \cap R^c_{\phi_2}\right) \\ &= \left\{(a,b) \mid (0 < b \le 1 \wedge a > \sqrt{3} - b) \vee \left(1 < b < \frac{2}{\sqrt{3}} \wedge \left(0 < a < \sqrt{b^2 - 1} \vee (a > \sqrt{3} - b)\right)\right)\right. \\ &\quad \left. \vee \left(b = \frac{2}{\sqrt{3}} \wedge \left(0 < a < \frac{1}{\sqrt{3}} \vee \left(a > \frac{1}{\sqrt{3}}\right)\right)\right)\right) \vee \left(\frac{2}{\sqrt{3}} < b < \sqrt{3} \wedge \left(0 < a < \sqrt{3} - b \vee a > \sqrt{b^2 - 1}\right)\right) \vee \left(b \ge \sqrt{3} \wedge a > \sqrt{b^2 - 1}\right)\right\}, \end{aligned} \tag{29}$$

such that (8) holds. Since $g(a,b) = 0$ has an absolute minimum at $(a_0, b_0) = (0.53, 1.15)$ and is monotonically decreasing for $0 < a < 0.53$ and increasing for $a > 0.53$. Therefore, $g(a,b) \neq 0$ for $b < 1.15$. Hence, the region R_{μ_0} simplifies to

$$R_{\mu_0} = \left\{(a,b) \mid \left(\frac{2}{\sqrt{3}} < b < \sqrt{3} \wedge \left(0 < a < \sqrt{3} - b \vee a > \sqrt{b^2 - 1}\right)\right) \vee \left(b \ge \sqrt{3} \wedge a > \sqrt{b^2 - 1}\right)\right\}. \tag{30}$$

The region R_{μ_0} is shown in Figure 3. This completes the proof of Theorem 1.

To be able to comment on the values of μ_0 in the central configuration region, we use interpolation techniques and write the solution of $g(a,b) = 0$ as $b = \psi(a)$, where

$$\begin{aligned} \psi(a) = &-99.4142a^{11} + 713.882a^{10} - 2296.59a^9 \\ &+ 4371.32a^8 - 5475.35a^7 + 4748.21a^6 \\ &- 2919.84a^5 + 1282.71a^4 - 400.891a^3 \\ &+ 88.7673a^2 - 13.8585a + 2.4259. \end{aligned} \tag{31}$$

The function $\psi(a)$ accurately approximates the solution of $g(a,b) = 0$ in the central configuration region where μ_0 is positive. The approximation error is between 10^{-10} and 10^{-6}. This gives μ_0 as a function of a as follows:

$$\mu_0(a) = \frac{\left(\left((a + \psi(a))^2 + 1\right)\right)^{3/2} - 8\Big)(a + \psi(a))\psi^2(a)(a^2 + 1)^{3/2}}{4\left((a^2 + 1)^{3/2} - \psi(a)^3\right)\left((a + \psi(a))^2 + 1\right)^{3/2}}. \tag{32}$$

The function $\mu_0(a)$ is a bounded, well-defined continuous function of a except when $q(a) = a^2 + 1 - \psi(a)^2 = 0$. To identify the values of a where $q(a) = 0$, we write it as

$$\begin{aligned} q(a) = &-9883.18a^{22} + 141940.a^{21} - 966255.a^{20} \\ &+ 4.14813 \times 10^6 a^{19} - 1.26042 \times 10^7 a^{18} \\ &+ 2.88398 \times 10^7 a^{17} - 5.16176 \times 10^7 a^{16} \\ &+ 7.41023 \times 10^7 a^{15} - 8.68138 \times 10^7 a^{14} \\ &+ 8.40051 \times 10^7 a^{13} - 6.77049 \times 10^7 a^{12} \\ &+ 4.57074 \times 10^7 a^{11} - 2.59398 \times 10^7 a^{10} \\ &+ 1.2402 \times 10^7 a^9 - 5.00236 \times 10^6 a^8 \\ &+ 1.705 \times 10^6 a^7 - 492405.a^6 + 120891.a^5 \\ &- 25214.6a^4 + 4405.41a^3 - 621.741a^2 \\ &+ 67.2389a - 4.88501 = 0. \end{aligned} \tag{33}$$

The numerical solution of $q(a) = 0$ shows that it has three real roots $a = 1.14605$, $a = 1.2471$, and $a = 1.44556$. However, a careful observation of the region of existence of central configuration for the four-body problem in Figure 1 shows that $a = 1.14605$ defines a boundary between the region of existence and nonexistence and $a = 1.2471$ and $a = 1.44556$ are outside the domain of interest. Hence, $\mu_0(a)$ uniquely defines the positive values of the mass ratio m_0/m_3 for the four-body problem as described in Theorem 1. The region of existence of central configuration for the four-body problem with three equal masses is given in Figure 3. Taking

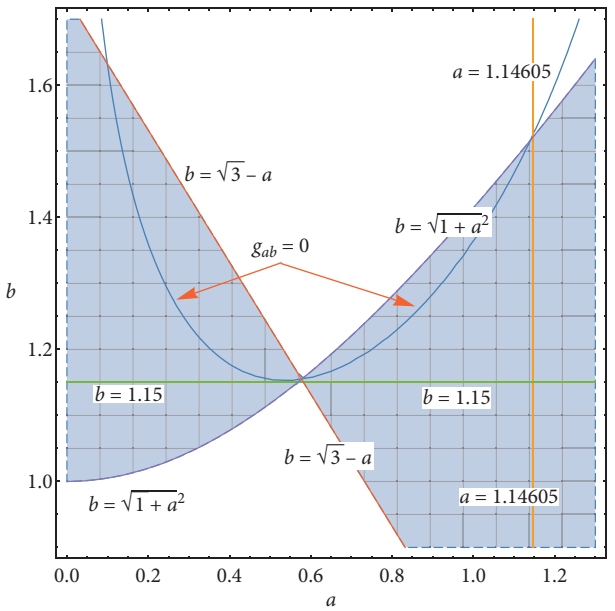

Figure 3: Region of existence of central configuration for the concave kite four-body problem with $(m_1 = m_2 = m_3, m_0)$.

advantage of the interpolated expression $b = \psi(a)$, $\mu_0(a)$ is given for $b \in (0.1, 1.14)$ in Figure 4 which shows $\mu_0(a)$ to be an increasing function of a with the minimum and maximum at the end points of the domain.

3.2. Action Minimizing Orbits in the Triangular Four-Body Problem. In this section, we introduce the analytical description of a family of periodic solutions in the four-body problem using variational techniques.

Theorem 2. *For the four-body problem considered in Theorem 1, the minimizers for $A(q)$ restricted to the homographic solutions $q_i(t) = \phi(t)q_{i,0}$ are precisely the Keplerian elliptical solutions and the minimum of the action is equal to $(3/2)(2\pi)^{2/3}T^{1/3}(\xi(a,b)/\eta(a,b))^{2/3}$.*

Define the Lagrangian action as

$$A(q) = \int_0^T L(q(t), \dot{q}(t))\mathrm{d}t, \tag{34}$$

where the Lagrangian L is defined by

$$L(q,\dot{q}) = \sum_{i=1}^{4} \frac{m_i}{2}\|\dot{q}\|^2 - U(q),$$
$$U(q) = \sum_{i<j} \frac{m_i m_j}{\|q_i - q_j\|}. \tag{35}$$

Let us call Ω_{cm} the y-coordinate of the center of mass in the configuration described earlier in Section 2, then

$$\Omega_{cm} = \frac{(b-2a)m_1}{3m_1 + m_0}, \tag{36}$$

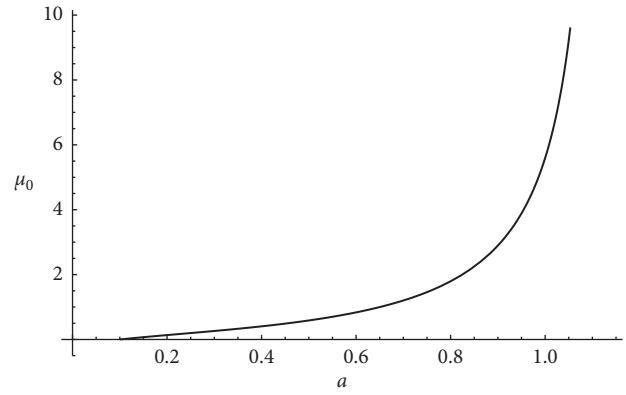

Figure 4: Values of $\mu_0(a)$ in the region of central configuration.

and the center of mass is

$$\mathrm{COM} = (0, \Omega_{cm}). \tag{37}$$

In this case, we have the following Cartesian coordinates for the points $q_{0,0}, q_{1,0}, q_{2,0}, q_{3,0}$:

$$\begin{aligned} q_{0,0} &= (0, \Omega_{cm}),\\ q_{1,0} &= (-1, -a - \Omega_{cm}),\\ q_{2,0} &= (0, b - \Omega_{cm}),\\ q_{3,0} &= (1, -a - \Omega_{cm}). \end{aligned} \tag{38}$$

Observe that

$$\begin{aligned} r_0 &= |q_{0,0}| = \Omega_{cm},\\ r_1 &= r_3 = \sqrt{1 + (a + \Omega_{cm})^2},\\ r_2 &= b - \Omega_{cm}. \end{aligned} \tag{39}$$

We focus on solutions of the form $q_i(t) = \phi(t)q_{i,0}$. These solutions are called homographic solutions. We will restrict the action functional to solutions of this type.

Proof of Theorem 2. The kinetic energy term K is equal to

$$K = \frac{1}{2}\sum_{i=0}^{3} m_i|\dot{q}_i(t)|^2 = |\dot{\phi}(t)|^2 r_1^2\left(m_1 + \frac{1}{2}\left(m_0\left(\frac{r_0}{r_1}\right)^2 + m_1\left(\frac{r_2}{r_1}\right)^2\right)\right)$$
$$= |\dot{q}_i(t)|^2\left(m_1 + \frac{1}{2}\left(m_0\left(\frac{r_0}{r_1}\right)^2 + m_1\left(\frac{r_2}{r_1}\right)^2\right)\right), \tag{40}$$

where we have used $|\dot{q}_1(t)|^2 = |\dot{\phi}(t)|^2 r_1^2$. The potential energy is given by

$$U = \sum_{0 \le i < j \le 3} \frac{m_i m_j}{|q_i - q_j|}, \tag{41}$$

and using $|q_i - q_j| = |\phi(t)||q_{i,0} - q_{j,0}|$, we get

$$U = \frac{m_0 m_1}{|\phi(t)|}\left(\frac{2}{\sqrt{a^2+1}} + \frac{1}{b}\right) + \frac{m_1^2}{|\phi(t)|}\left(\frac{2}{\sqrt{(a+b)^2+1}} + \frac{1}{2}\right). \tag{42}$$

Multiplying and dividing by r_1, we obtain

$$U = \frac{1}{|q_1|}\left(m_0 m_1 r_1\left(\frac{2}{\sqrt{a^2+1}} + \frac{1}{b}\right) + m_1^2 r_1\left(\frac{2}{\sqrt{(a+b)^2+1}} + \frac{1}{2}\right)\right). \tag{43}$$

As defined previously, we use $(m_0/m_1) = \mu_0$, and by letting $m_1 = 1$, we have

$$U = \frac{1}{|q_1|}\left(\mu_0 r_1\left(\frac{2}{\sqrt{a^2+1}} + \frac{1}{b}\right) + r_1\left(\frac{2}{\sqrt{(a+b)^2+1}} + \frac{1}{2}\right)\right). \tag{44}$$

Now, we are ready to compute the action restricted to this class of homographic solutions. We have

$$\begin{aligned} A &= \int_0^T \left(1 + \frac{1}{2}\left(m_0\left(\frac{r_0}{r_1}\right)^2 + \left(\frac{r_2}{r_1}\right)^2\right)\right)\frac{|\dot{q}_1|^2}{2}\,dt \\ &\quad + \int_0^T \left(\mu_0 r_1\left(\frac{2}{\sqrt{a^2+1}} + \frac{1}{b}\right) + r_1\left(\frac{2}{\sqrt{(a+b)^2+1}} + \frac{1}{2}\right)\right)\frac{1}{|q_1|}\,dt \\ &= \left(2 + \left(m_0\left(\frac{r_0}{r_1}\right)^2 + \left(\frac{r_2}{r_1}\right)^2\right)\right)\int_0^T \frac{|\dot{q}_1|^2}{2}\,dt \\ &\quad + \left(\mu_0 r_1\left(\frac{2}{\sqrt{a^2+1}} + \frac{1}{b}\right) + r_1\left(\frac{2}{\sqrt{(a+b)^2+1}} + \frac{1}{2}\right)\right)\int_0^T \frac{1}{|q_1|}\,dt. \end{aligned} \tag{45}$$

Let

$$\begin{aligned} \eta(a,b) &= 2 + \left(m_0\left(\frac{r_0}{r_1}\right)^2 + \left(\frac{r_2}{r_1}\right)^2\right), \\ \xi(a,b) &= \mu_0 r_1\left(\frac{2}{\sqrt{a^2+1}} + \frac{1}{b}\right) + r_1\left(\frac{2}{\sqrt{(a+b)^2+1}} + \frac{1}{2}\right). \end{aligned} \tag{46}$$

Then,

$$A(q) = \eta\int_0^T \frac{|\dot{q}_1|^2}{2}\,dt + \xi\int_0^T \frac{1}{|q_1|}\,dt. \tag{47}$$

The infimum of $A(q)$ is

$$\begin{aligned} \inf_q A(q) &= \inf_{a>0,b>0}\inf_{q_1}\left\{\eta\int_0^T \frac{|\dot{q}_1|^2}{2}\,dt + \xi\int_0^T \frac{1}{|q_1|}\,dt\right\} \\ &= \inf_{a>0,b>0}\left\{\eta\inf_{q_1}\left(\int_0^T \frac{|\dot{q}_1|^2}{2}\,dt + \frac{\xi}{\eta}\int_0^T \frac{1}{|q_1|}\,dt\right)\right\}. \end{aligned} \tag{48}$$

By Gordon's result, we have

$$\inf_{q_1}\left(\int_0^T \frac{|\dot{q}_1|^2}{2}\,dt + \frac{\xi}{\eta}\int_0^T \frac{1}{|q_1|}\,dt\right) = \frac{3}{2}(2\pi)^{2/3}T^{1/3}\left(\frac{\xi(a,b)}{\eta(a,b)}\right)^{2/3}. \tag{49}$$

Then,

$$\begin{aligned} \inf_q A(q) &= \inf_{a>0,b>0}\left\{\eta(a,b)\frac{3}{2}(2\pi)^{2/3}T^{1/3}\left(\frac{\xi(b,c)}{\eta(b,c)}\right)^{2/3}\right\} \\ &= \inf_{a>0,b>0}\left\{\frac{3}{2}(2\pi)^{2/3}T^{1/3}\eta(a,b)^{1/3}(\xi(a,b))^{2/3}\right\}. \end{aligned} \tag{50}$$

Let $\phi(a,b) = (3/2)(2\pi)^{2/3}T^{1/3}\eta(a,b)^{1/3}(\xi(a,b))^{2/3}$, then $\phi(a,b)$ attains its infimum at (a_0,b_0) if and only if $\eta(a,b)(\xi(a,b))^2$ attains its infimum at (a_0,b_0). It is challenging to see that for positive values of a_0 and b_0, the function $\phi(a,b)$ is convex and coercive. However, we have proved that b can be written as $b = \psi(a)$ and used interpolation to find $\psi(a)$ as given in equation (31). Hence, we can now write $\eta(a,b)$, $\xi(a,b)$, and $\phi(a,b)$ as functions of one variable. For convexity, we use the second derivative test and show that $(\partial^2\phi(a)/\partial a^2) > 0$ when $a \in (0.1, 1.14)$ Hence, $\phi(a)$ is convex when $a \in (0.1, 1.14)$. For coercivity, we see that $\phi(a)$ is continuous for all positive values of a, $\phi(a) \longrightarrow \infty$ as $a \longrightarrow 0$, and when $a \longrightarrow \infty$, $\phi(a) \longrightarrow \infty$, which implies $\phi(a)$ is coercive. Hence, $\phi(a)$ attains $\inf_{a>0}\{\phi(a)\}$ at unique $a_0 > 0$ and satisfies $\phi(a_0) = 0$.

4. Three Unequal Masses $m_3 = m_1 \neq m_2 \neq m_0$

In this section, we discuss a four-body problem which has two symmetric equal masses $(m_3 = m_1)$ on the horizontal axis and two nonequal masses m_0 and m_2 on the vertical axis. The position vectors of the four masses m_0, m_1, m_2, and m_3 are $\mathbf{r}_0 = (0,c)$, $\mathbf{r}_1 = (-1,0)$, $\mathbf{r}_2 = (0,b)$, and $\mathbf{r}_3 = (1,0)$, respectively. For $c > 0$, the four masses make an isosceles triangle with m_0 inside the triangle (Figure 5), and for $c < 0$, the convex kite configuration is obtained (Figure 6).

4.1. Central Configurations

Theorem 3. *Consider four point masses m_0, $m_1 = m_3 \neq m_2$ having position vectors $\mathbf{r}_0 = (0,c)$, $\mathbf{r}_1 = (-1,0)$, $\mathbf{r}_2 = (0,b)$, and $\mathbf{r}_3 = (1,0)$, where $b > 0$ and $b > c$ such that $\mathbf{r} = (\mathbf{r}_0, \mathbf{r}_1, \mathbf{r}_2, \mathbf{r}_3)$ is a central configuration.*

(a) Then, there exist unique mass ratios:

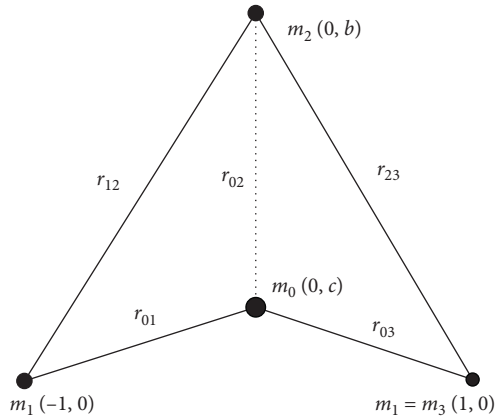

Figure 5: Concave four-body configurations with a pair of equal masses $(m_1 = m_3)$.

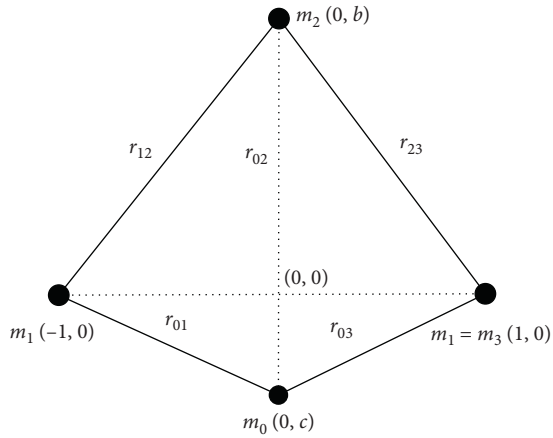

Figure 6: Convex four-body kite configurations with two equal masses $(m_1 = m_3)$.

$$\mu_0 = \frac{m_0}{m_1} = \frac{b\left(8 - \left(b^2+1\right)^{3/2}\right)(b-c)^2\left(c^2+1\right)^{3/2}}{4\left((b-c)^3 - \left(c^2+1\right)^{3/2}\right)\left(b^2+1\right)^{3/2}},$$
$$\mu_2 = \frac{m_2}{m_1} = \frac{c\left(8 - \left(c^2+1\right)^{3/2}\right)(c-b)^2\left(b^2+1\right)^{3/2}}{4\left(\left(b^2+1\right)^{3/2} - (b-c)^3\right)\left(c^2+1\right)^{3/2}}. \tag{51}$$

(b) The region of existence of central configuration where the four positive masses are arranged in a concave kite configuration is given by

$$R_t = \left\{(b,c) \mid \left(0 < c < \frac{1}{\sqrt{3}} \wedge c + \sqrt{c^2+1} < b < \sqrt{3}\right) \vee \left(\frac{1}{\sqrt{3}} < c < \sqrt{3} \wedge \sqrt{3} < b < c + \sqrt{c^2+1}\right)\right\}. \tag{52}$$

(c) The region of existence of central configuration where the four positive masses are arranged in a convex kite configuration is given by

$$R_r = \left\{(b,c) \mid \left(-\sqrt{3} < c \le -\frac{1}{\sqrt{3}} \wedge c + \sqrt{c^2+1} < b < \sqrt{3}\right) \vee \left(-\frac{1}{\sqrt{3}} < c < -2 + \sqrt{3} \wedge \frac{c^2-1}{2c} < b < \sqrt{3}\right)\right\}. \tag{53}$$

Proof of Theorem 3. Consider four point masses with position vectors $(\mathbf{r}_0, \mathbf{r}_1, \mathbf{r}_2, \mathbf{r}_3)$ and masses m_0, m_1, m_2, and m_3, where $m_3 = m_1$. The solution of $f_{01} = 0$ and $f_{12} = 0$ gives

$$\mu_0 = \frac{m_0}{m_1} = \frac{(R_{12} - R_{13})\Delta_{123}}{(R_{01} - R_{02})\Delta_{012}} = \frac{\beta\gamma b(\alpha - 8)}{4\alpha(b-c)(\beta - \gamma)},$$
$$\mu_2 = \frac{m_2}{m_1} = \frac{(R_{01} - R_{13})\Delta_{013}}{(R_{12} - R_{02})\Delta_{012}} = \frac{\alpha\gamma c(8 - \beta)}{4\beta(b-c)(\alpha - \gamma)}, \tag{54}$$

where $\alpha = (1+b^2)^{3/2}$, $\beta = (1+c^2)^{3/2}$, and $\gamma = (b-c)^3$. The mass ratios μ_0 and μ_2 are well-defined functions of b and c except at $b = c$ and $b = c \pm \sqrt{1+c^2}$.

To find central configuration regions where $\mu_0 > 0$, it is sufficient to show that $\alpha - 8$ and $\beta - \gamma$ have the same sign. It is trivial to see that $R\alpha - 8 = 0$ when $b = \sqrt{3}$. Similarly, $\beta - \gamma = 0$ when $b = c + \sqrt{c^2+1}$. Hence, $\beta - \gamma$ is positive in

$$R_a = \left\{(a,b) \mid b > 0 \wedge c < b \wedge b < c + \sqrt{c^2+1}\right\}. \tag{55}$$

The complement of R_a, where $\beta - \gamma < 0$, is given by

$$R_a^c = \left\{(a,b) \mid b > 0 \wedge c < \left(b^2 - 1\right)(2b)^{-1}\right\}. \tag{56}$$

It is to be noted that the sign of c will be determined according to whether the four-body configuration is concave $(c > 0)$ or convex $(c < 0)$. After some simplifications, the central configuration region for $\mu_0 > 0, c > 0$ is given by

$$R_{t_1} = \left\{(b,c) \mid \left(0 < c < \frac{1}{\sqrt{3}} \wedge \sqrt{c^2+1} + c < b < \sqrt{3}\right) \vee \left(\frac{1}{\sqrt{3}} < c \le \sqrt{3} \wedge \sqrt{3} < b < \sqrt{c^2+1} + c\right) \vee \left(c > \sqrt{3} \wedge c < b < \sqrt{c^2+1} + c\right)\right\}. \tag{57}$$

Similarly, the central configuration region for $\mu_0 > 0, c < 0$ is given by

$$R_{r_1} = \left\{(b,c) \mid c < 0, c + \sqrt{c^2+1} < b < \sqrt{3}\right\}. \tag{58}$$

Consider the mass ratio μ_2. Let $c > 0$. Since $b > c$, therefore for $\mu_2 > 0$, $(\beta - 8)(\alpha - \gamma)^{-1}$ must have the same sign. It is trivial to see that $8 - \beta > 0$ when $c \in (0, \sqrt{3})$ and $\alpha - \gamma > 0$ for all $b > 0$ and $c > 0$. Therefore, $\mu_2 > 0$ in

$$R_{t_2} = \left\{(b,c) \mid (0 < b \le \sqrt{3} \wedge 0 < c < b) \vee (b > \sqrt{3} \wedge 0 < c < \sqrt{3})\right\}. \tag{59}$$

Similarly, when $c < 0$ (rhomboidal configuration), the central configuration region where $\mu_2 > 0$ is given by

$$R_{r_2} = \{(b,c) \mid (0 < b \le \sqrt{3} \wedge 0 < c < b) \vee (b > \sqrt{3} \wedge 0 < c < \sqrt{3})\}. \tag{60}$$

Hence, the region of existence of central configuration for the concave kite four-body problem where all the masses m_0, $m_1 = m_3$, and m_2 are positive is given by $R_t = R_{t_1} \cap R_{t_2}$ and the corresponding convex kite central configuration region is given by $R_r = R_{r_1} \cap R_{r_2}$, where

$$\begin{aligned} R_t &= \left\{(b,c) \mid \left(0 < c < (\sqrt{3})^{-1} \wedge c + \sqrt{c^2+1} < b < \sqrt{3}\right) \vee \left((\sqrt{3})^{-1} < c < \sqrt{3} \wedge \sqrt{3} < b < c + \sqrt{c^2+1}\right)\right\}, \\ R_r &= \left\{(b,c) \mid \left(-\sqrt{3} < c \le -(\sqrt{3})^{-1} \wedge c + \sqrt{c^2+1} < b < \sqrt{3}\right) \vee \left(-(\sqrt{3})^{-1} < c < \sqrt{3} - 2 \wedge \left(c^2-1\right)(2c)^{-1} < b < \sqrt{3}\right)\right\}. \end{aligned} \tag{61}$$

The regions R_t and R_r are shown in Figures 7 and 8, respectively.

4.2. Action Minimizing Orbits in the Convex Kite Four-Body Problem. In this section, we discuss the minimization property of a four-body problem which has two equal masses ($m_1 = m_3$) on the horizontal axis and two positive masses m_2 and m_0 on the vertical axis, which is also the axis of symmetry.

Theorem 4. *For the four-body problem considered in Theorem 1, the minimizers for $A(q)$ restricted to the homographic solutions $q_i(t) = \phi(t) q_{i,0}$ are precisely the Keplerian elliptical solutions, and the minimum of the action is equal to $(3/2)(2\pi)^{2/3} T^{1/3} (\xi(b,c)/\eta(b,c))^{2/3}$.*

Let us call Ω_{cm} the y-coordinate of the center of mass in the configuration described earlier in Section 3.1, then

$$\Omega_{cm} = \frac{m_0 c + m_2 b}{m_0 + 2m_1 + m_2}, \tag{62}$$

and the center of mass is COM $= (0, \Omega_{cm})$. Observe that

$$\begin{aligned} r_0 &= |q_{0,0}| = |c - \Omega_{cm}|, \\ r_1 &= r_3 = \sqrt{1 + \Omega_{cm}^2}, \\ r_2 &= |b - \Omega_{cm}|. \end{aligned} \tag{63}$$

Proof of Theorem 4. The kinetic energy term K is equal to

$$\begin{aligned} K &= \frac{1}{2} \sum_{i=0}^{3} m_i |\dot{q}_i(t)|^2 = |\dot{\phi}(t)|^2 \left(m_1 r_1^2 + \frac{m_2}{2} r_2^2 + \frac{m_0}{2} r_0^2\right) \\ &= |\dot{\phi}(t)|^2 r_1^2 \left(m_1 + \frac{1}{2}\left(\frac{m_2 r_2^2 + m_0 r_0^2}{r_1^2}\right)\right) \\ &= |\dot{q}_1(t)|^2 \left(m_1 + \frac{1}{2}\left(\frac{m_2 r_2^2 + m_0 r_0^2}{r_1^2}\right)\right), \end{aligned} \tag{64}$$

where we have used the fact that $|\dot{q}_1(t)|^2 = |\dot{\phi}(t)|^2 r_1^2$.

On the other hand, the potential energy is given by

$$U = \sum_{0 \le i < j \le 3} \frac{m_i m_j}{|q_i - q_j|}, \tag{65}$$

and using $|q_i - q_j| = |\phi(t)||q_{i,0} - q_{j,0}|$, we get

$$U = \frac{1}{|\phi(t)|} \left(\frac{m_1^2}{2} + \frac{2m_1 m_2}{\sqrt{1+b^2}} + \frac{2m_1 m_0}{\sqrt{1+c^2}} + \frac{m_2 m_0}{|c-b|}\right). \tag{66}$$

Multiplying and dividing by r_1, we obtain

$$U = \frac{1}{|q_1|} \left(\frac{m_1^2 r_1}{2} + \frac{2m_1 m_2 r_1}{\sqrt{1+b^2}} + \frac{2m_1 m_0 r_1}{\sqrt{1+c^2}} + \frac{m_2 m_0 r_1}{|c-b|}\right). \tag{67}$$

Defining $\mu_0 = m_0/m_1$, $\mu_2 = m_2/m_1$, and $m_1 = 1$,

$$U = \frac{1}{|q_1|} \left(\frac{r_1}{2} + \frac{2\mu_2 r_1}{\sqrt{1+b^2}} + \frac{2\mu_0 r_1}{\sqrt{1+c^2}} + \frac{\mu_2 \mu_0 r_1}{|c-b|}\right). \tag{68}$$

Now, we are ready to compute the action restricted to this class of homographic solutions:

$$\begin{aligned} A &= \int_0^T \left(1 + \frac{1}{2}\left(\frac{\mu_2 r_2^2 + \mu_0 r_0^2}{r_1^2}\right)\right) \frac{|\dot{q}_1|^2}{2} \, dt \\ &\quad + \int_0^T \left(\frac{r_1}{2} + \frac{2\mu_2 r_1}{\sqrt{1+b^2}} + \frac{2\mu_0 r_1}{\sqrt{1+c^2}} + \frac{\mu_2 \mu_0 r_1}{|c-b|}\right) \frac{1}{|q_1|} \, dt \\ &= 2 + \left(\frac{\mu_2 r_2^2 + \mu_0 r_0^2}{r_1^2}\right) \int_0^T \frac{|\dot{q}_1|^2}{2} \, dt \\ &\quad + \left(\frac{r_1}{2} + \frac{2\mu_2 r_1}{\sqrt{1+b^2}} + \frac{2\mu_0 r_1}{\sqrt{1+c^2}} + \frac{\mu_2 \mu_0 r_1}{|c-b|}\right) \int_0^T \frac{1}{|q_1|} \, dt. \end{aligned} \tag{69}$$

Let

$$\begin{aligned} \eta(b,c) &= 1 + \frac{1}{2}\left(\frac{\mu_2 r_2^2 + \mu_0 r_0^2}{r_1^2}\right), \\ \xi(b,c) &= \frac{r_1}{2} + \frac{2\mu_2 r_1}{\sqrt{1+b^2}} + \frac{2\mu_0 r_1}{\sqrt{1+c^2}} + \frac{\mu_2 \mu_0 r_1}{|c-b|}. \end{aligned} \tag{70}$$

Therefore,

$$A(q) = \eta \int_0^T \frac{|\dot{q}_1|^2}{2} \, dt + \xi \int_0^T \frac{1}{|q_1|} \, dt. \tag{71}$$

The infimum of $A(q)$ is

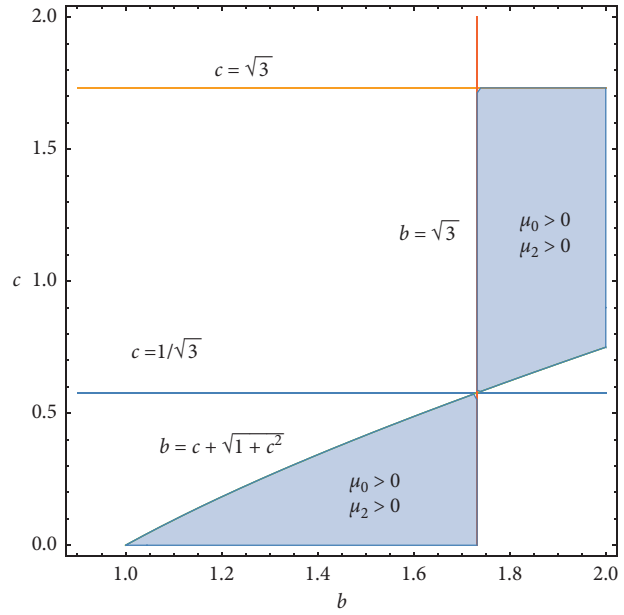

Figure 7: Region of existence of central configuration for the concave kite four-body configuration where $m_1 = m_3 = m \neq m_0 \neq m_2$.

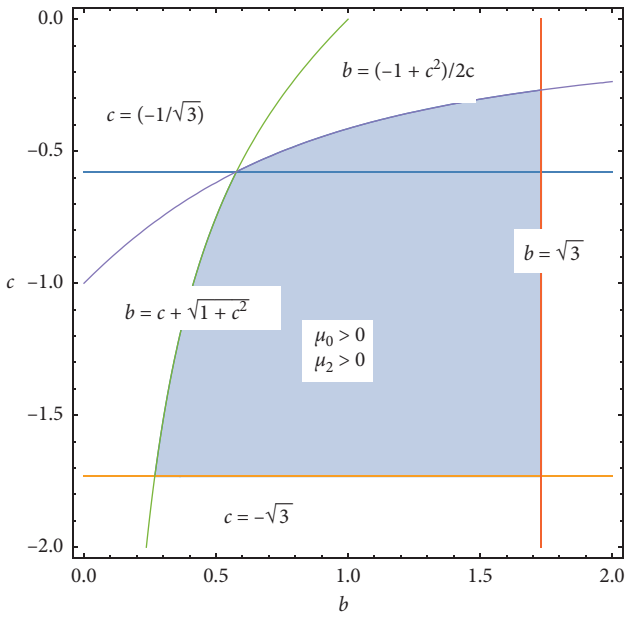

Figure 8: Region of existence of central configuration for the convex kite four-body configuration where $m_1 = m_3 = m \neq m_0 \neq m_2$.

$$\inf_q A(q) = \inf_{b>0,c>0} \inf_{q_1} \left\{ \eta \int_0^T \frac{|\dot{q}_1|^2}{2} dt + \xi \int_0^T \frac{1}{|q_1|} dt \right\}$$
$$= \inf_{b>0,c>0} \left\{ \eta \inf_{q_1} \left(\int_0^T \frac{|\dot{q}_1|^2}{2} dt + \frac{\xi}{\eta} \int_0^T \frac{1}{|q_1|} dt \right) \right\}. \quad (72)$$

By Gordon's result, we have

$$\inf_{q_1} \left(\int_0^T \frac{|\dot{q}_1|^2}{2} dt + \frac{\xi}{\eta} \int_0^T \frac{1}{|q_1|} dt \right)$$
$$= \frac{3}{2} (2\pi)^{2/3} T^{1/3} \left(\frac{\xi(b,c)}{\eta(b,c)} \right)^{2/3}. \quad (73)$$

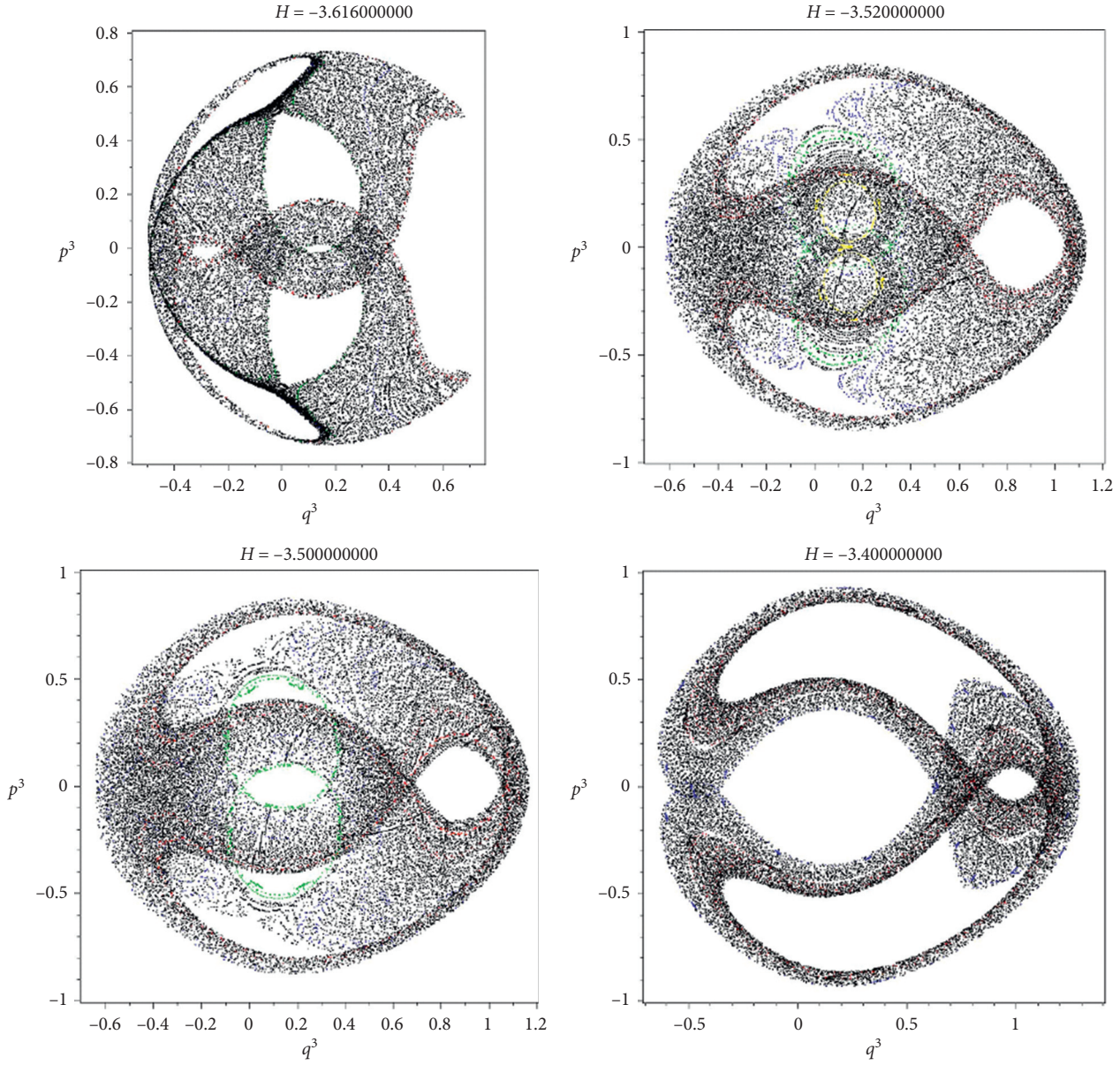

FIGURE 9: The progressive evolution of a Poincaré surface of sections for different energy levels in the unequal masses case ($m_0 = 1.28155$, $m_2 = 0.31$, $m_3 = m_1 = 1$, $b = 1.1$, and $c = 0.1$).

Then,

$$\inf_q A(q) = \inf_{b>0,c>0} \left\{ \eta(b,c) \frac{3}{2} (2\pi)^{2/3} T^{1/3} \left(\frac{\xi(b,c)}{\eta(b,c)} \right)^{2/3} \right\}$$

$$= \inf_{b>0,c>0} \left\{ \frac{3}{2} (2\pi)^{2/3} T^{1/3} \eta(b,c)^{1/3} (\xi(b,c))^{2/3} \right\}. \quad (74)$$

Let $\phi(b,c) = (3/2)(2\pi)^{2/3} T^{1/3} \eta(b,c)^{1/3} (\xi(b,c))^{2/3}$, and then $\phi(b,c)$ attains its infimum at (b_0, c_0) if and only if $\eta(b,c)(\xi(b,c))^2$ attains its infimum at (b_0, c_0). Similar to the concave case, we need to show that for positive values of b_0 and c_0, the function $\phi(b,c)$ is convex and coercive. For convexity, we compute the Hessian matrix for $\phi(b,c)$ and numerically show that $H(b,c)$ is positive semidefinite in the region R_r.

That concludes that the function $\phi(b,c)$ is convex. For coercivity, we see that $\phi(b,c)$ is continuous for all positive values of b and c, $\phi(b,c) \longrightarrow \infty$ as $(b,c) \longrightarrow (0,0)$, and when $b \longrightarrow \infty$ and $c \longrightarrow \infty$, $\phi(b,c)$ tends to ∞, which implies $\phi(b,c)$ is coercive. Hence, $\phi(b,c)$ attains $\inf_{b>0,c>0} \{\phi(b,c)\}$ at unique (b_0, c_0), $b_0 > 0$, $c_0 > 0$, and satisfies$\phi(b_0, c_0) = 0$.

5. Hamiltonian Formulation of the Problem: Some Numerical Examples

It is well known that the study of the trajectories of celestial bodies under their mutual gravitational attractions is important for understanding their movement and

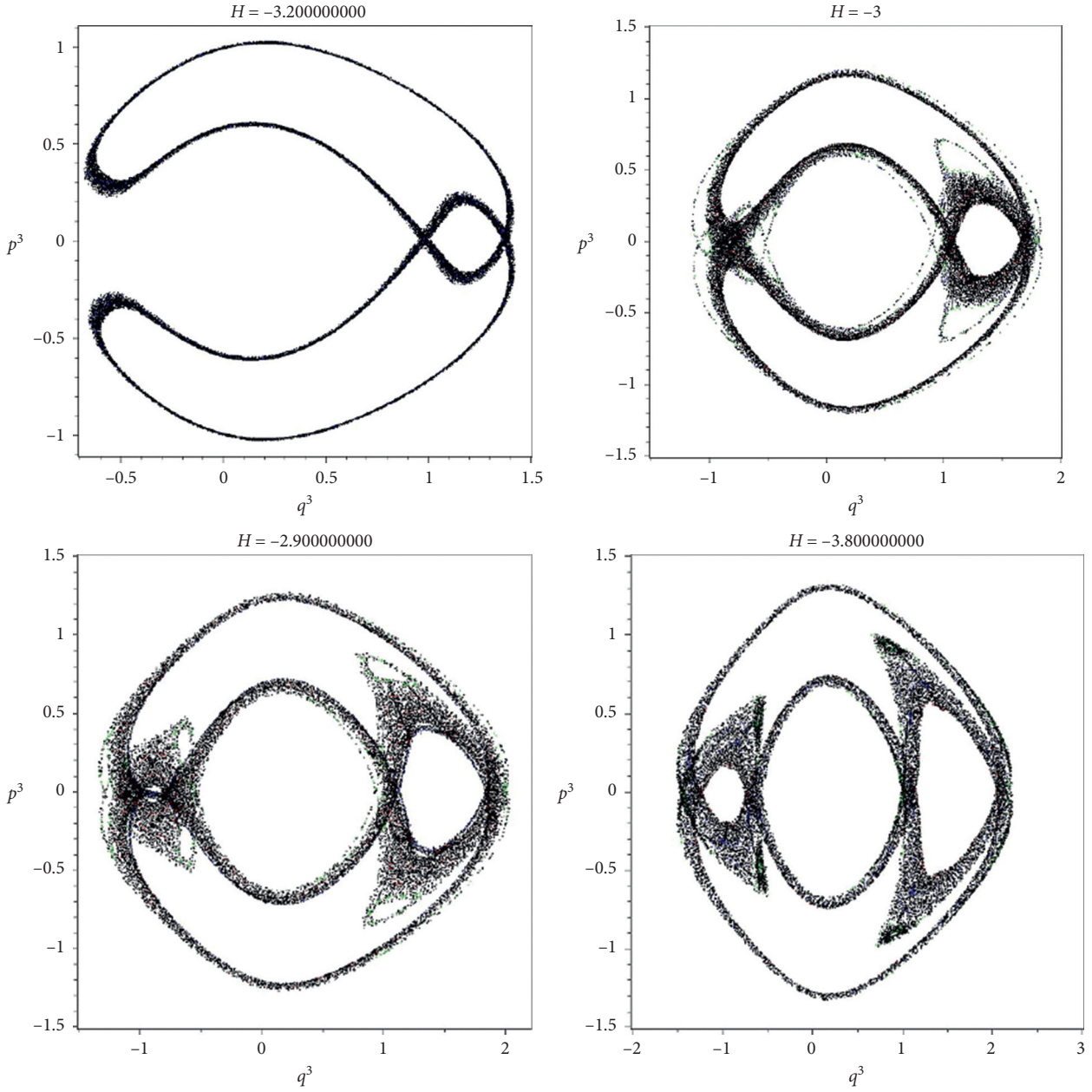

Figure 10: The progressive evolution of a Poincaré surface of sections for different energy levels in the unequal masses case ($m_0 = 1.28155$, $m_2 = 0.31$, $m_3 = m_1 = 1$, $b = 1.1$, and $c = 0.1$).

navigation. In that sense, a special type of the four-body problem with analytical and numerical investigation can contribute to the understanding of the dynamical behavior of quadruple stellar systems (e.g., the HD 98800 quadruple system with two pairs of stars orbiting each other). Several authors studied the stability and dynamical evolution of symmetric quadruple systems for stars and exoplanetary systems of two planets [40, 41]. In this section, we will study the periodic behavior of the kite four-body problem.

Consider the four-body problem introduced in Lemma 1, which has a pair of equal masses and one axis of symmetry. Using the symmetries and position coordinates from Lemma 1, we obtain the following reduced Hamiltonian in the case of unequal masses:

$$H = \sum_{i=0}^{3} \frac{p_i^2}{2m_i} - \frac{m_0 m_1}{r_{01}} - \frac{m_0 m_2}{r_{02}} - \frac{m_0 m_3}{r_{03}} - \frac{m_1 m_2}{r_{12}} - \frac{m_1 m_3}{r_{13}} - \frac{m_2 m_3}{r_{23}}, \tag{75}$$

where

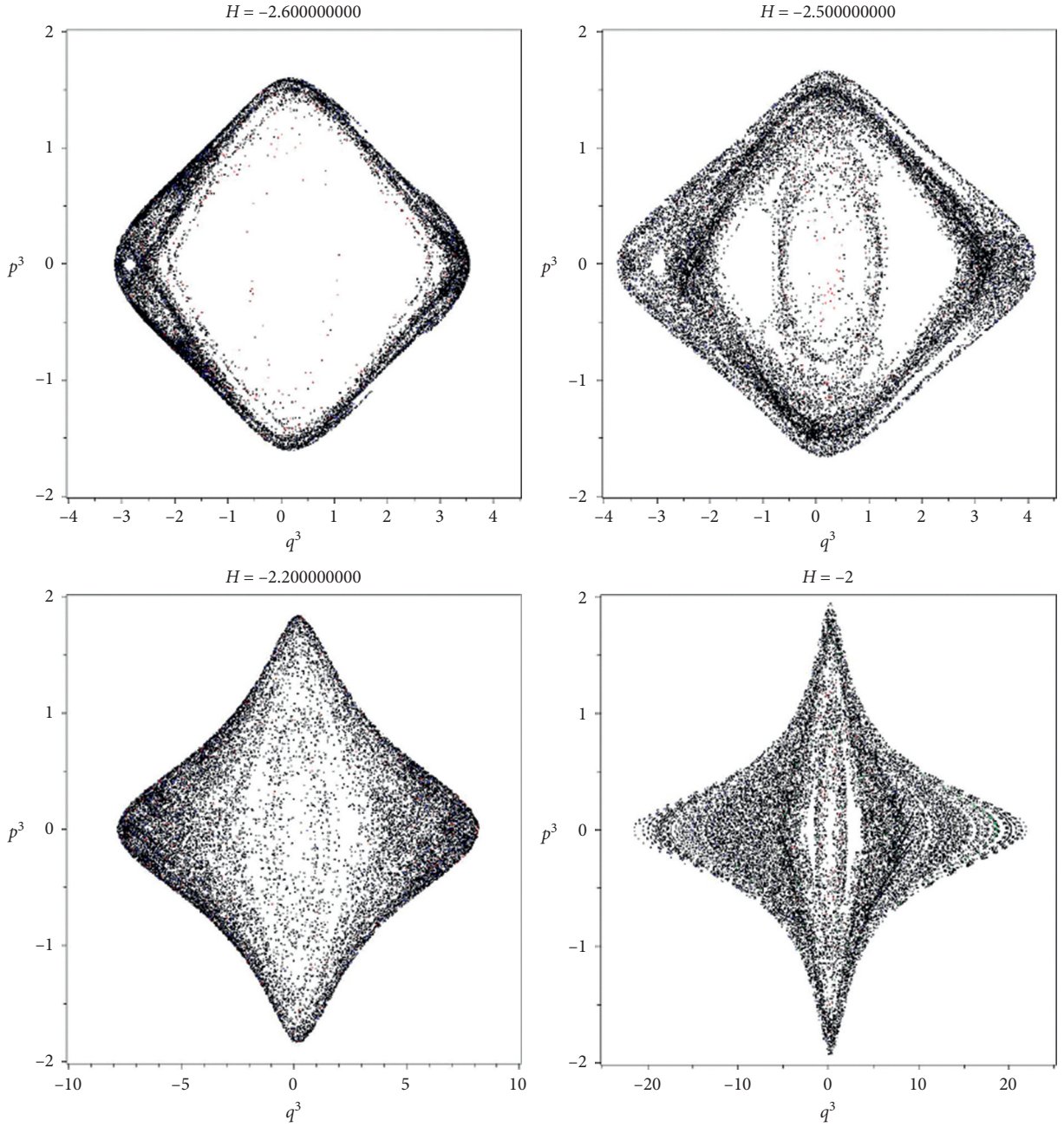

Figure 11: The progressive evolution of a Poincaré surface of sections for different energy levels in the unequal masses case ($m_0 = 1.28155$, $m_2 = 0.31$, $m_3 = m_1 = 1$, $b = 1.1$, and $c = 0.1$).

$$
\begin{aligned}
r_{01}^2 &= 1 + (q_1 - c)^2, \\
r_{02}^2 &= (b - c)^2, \\
r_{03}^2 &= 1 + (q_3 - c)^2, \\
r_{12}^2 &= 1 + (q_1 - b)^2, \\
r_{13}^2 &= 4 + (q_1 - q_3)^2, \\
r_{23}^2 &= 1 + (b - q_3)^2, \\
b &> c,
\end{aligned}
\tag{76}
$$

and q_i and p_i, $i = \overline{0,3}$, are the generalized coordinates and momenta (we assume for simplicity that the gravitational constant is equal to 1).

For the investigation of the reduced Hamiltonian equations of motion (75), we have selected examples from concave and convex kite four-body problems introduced in Section 2. We have used classical numerical methods and found periodic orbits for a given vector field. The stability of a periodic orbit for an autonomous vector field can be calculated by Poincaré maps, which replaces the flow of the n-dimensional continuous vector field with an

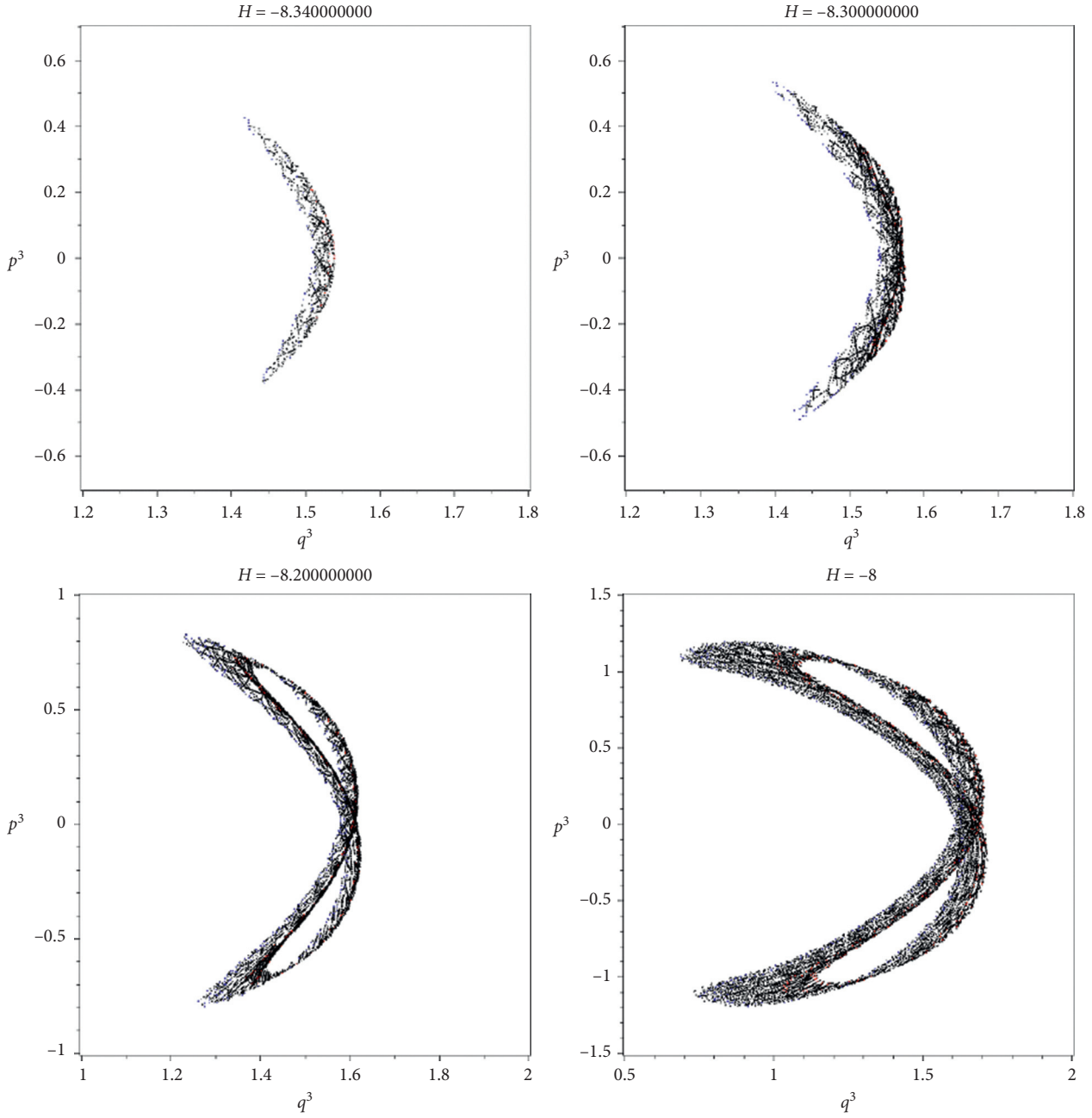

FIGURE 12: The progressive changing of a Poincaré surface of sections for different energy levels in the unequal masses case ($m_0 = 2.658$, $m_2 = 1.03$, $m_3 = m_1 = 1$, $b = 1.9$, and $c = 0.7$).

$(n-1)$-dimensional map [42]. In this article, the analysis of periodic and quasiperiodic orbits is performed using the Poincaré surface of the section technique by picking the phase element $p_1 = 0$. In the n-dimensional case, the Poincaré surface of the section has dimensionality $2n-2$. The intersection points of the solution curves with the corresponding (p_i, q_i), $i = \overline{0, n-1}$, plane still lie on a smooth curve [43].

In order to construct the Poincaré surface of the section and to find the corresponding periodic orbits, we plot the motion from the 4D phase space (q_1, q_3, p_1, p_3) in a "cut plane" $p_1(t) = 0, q_1 t > 0$. Since H is conserved, any point on this surface of the section will uniquely define the orbit. Our Poincaré surface of sections (Figures 9–11) describe the concave four-body problem in the unequal mass case with energy values $E \in \{-3.52, \ldots, -2\}$, plotting $q_3(t)$ versus $p_3(t)$, and $m_0 = 1.28155$, $m_2 = 0.31$, $m_3 = m_1 = 1$, $b = 1.1$, and $c = 0.1$. The initial conditions considered here satisfy the central configuration equations introduced in Section 2. We wish to note that in case of the energy level −3.52, we can see many little islands of quasiperiodic orbits. It should be emphasized that increasing the energy levels increase the Poincaré surface of sections in size, as a blowing up effect (see Figures 9–11).

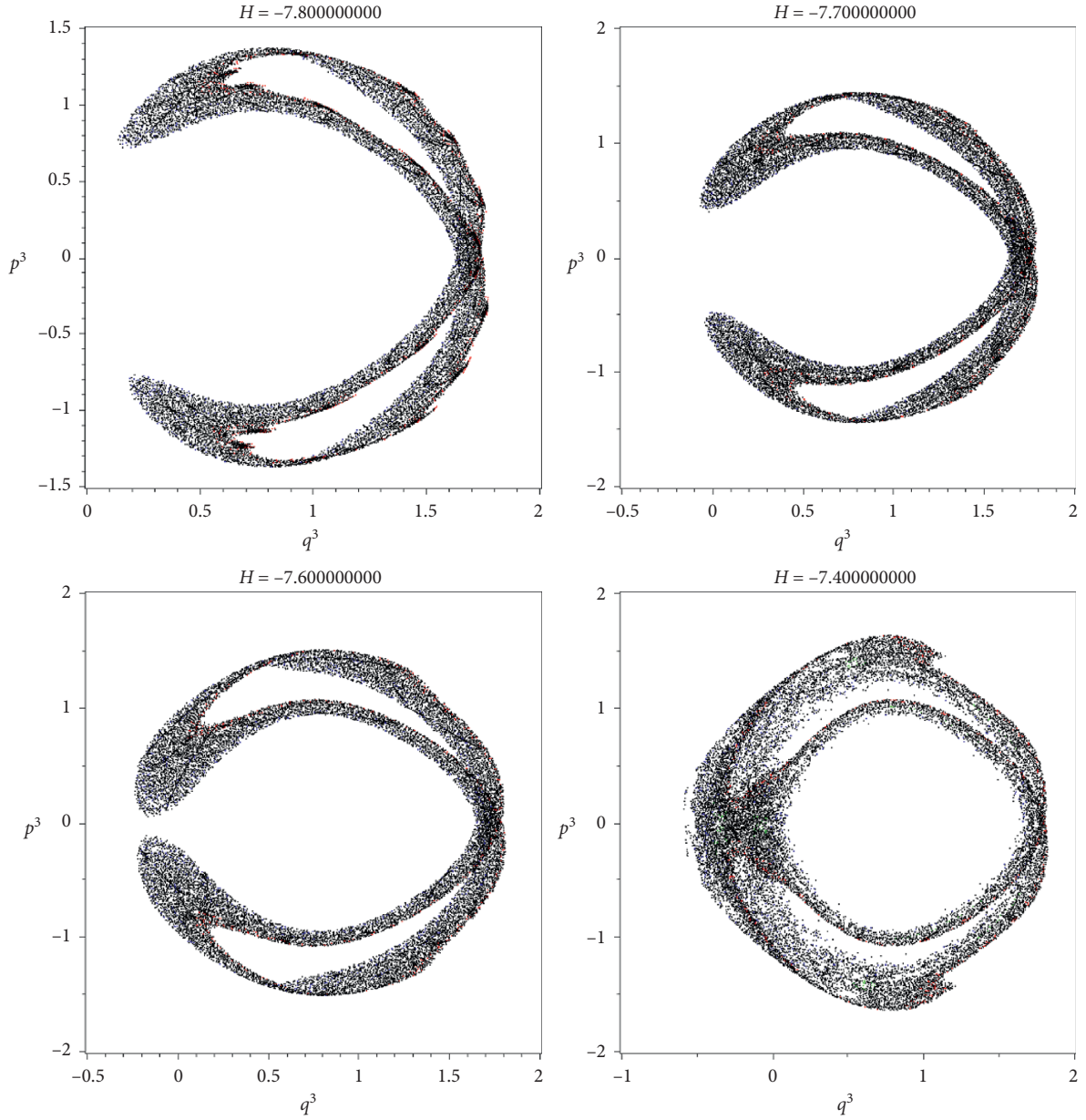

Figure 13: The progressive changing of a Poincaré surface of sections for different energy levels in the unequal masses case ($m_0 = 2.658$, $m_2 = 1.03$, $m_3 = m_1 = 1$, $b = 1.9$, and $c = 0.7$).

Another interesting unequal mass case is for increased masses $m_0 = 2.658$, $m_2 = 1.03$, and $m_3 = m_1 = 1$ compared to the previous case. Similarly, using different energy levels, in this case for energy values $E \in \{-8.34, \ldots, -7.3\}$, the variation of the "horseshoe with open side to the left" as the letter D shape to the "horseshoe with open side to the right" as the letter C shape can be observed (Figures 12–14). As earlier, in this particular case, we observe quasiperiodic orbits and the increasing size of the Poincaré surface of sections.

In the equal mass case, we have chosen the following particular case: $m_4 = 5.17662$, $m = 1$, $b = 1.9$, and $c = 0.7$. In this situation, we detected an interesting transformation of the Poincaré surface of sections through the energy levels $E \in \{-13.6, \ldots, -11\}$. In the case of lower energy levels, the outside part of the orbit indicates chaotic behavior. Moreover, by increasing the energy levels, the inside part of the orbit disintegrates, but the size of the Poincaré surface of sections has just a minor variation (Figure 15).

Consequently, we developed the surface of sections with around 300 points, which presents the progressive disintegration of the surfaces of solution curves of regular motion (KAM surface) generated with the increase in H from −3.615 to −2 in our first example (Figures 9–11), from −8.34 to −7 in our second example (Figures 12–14),

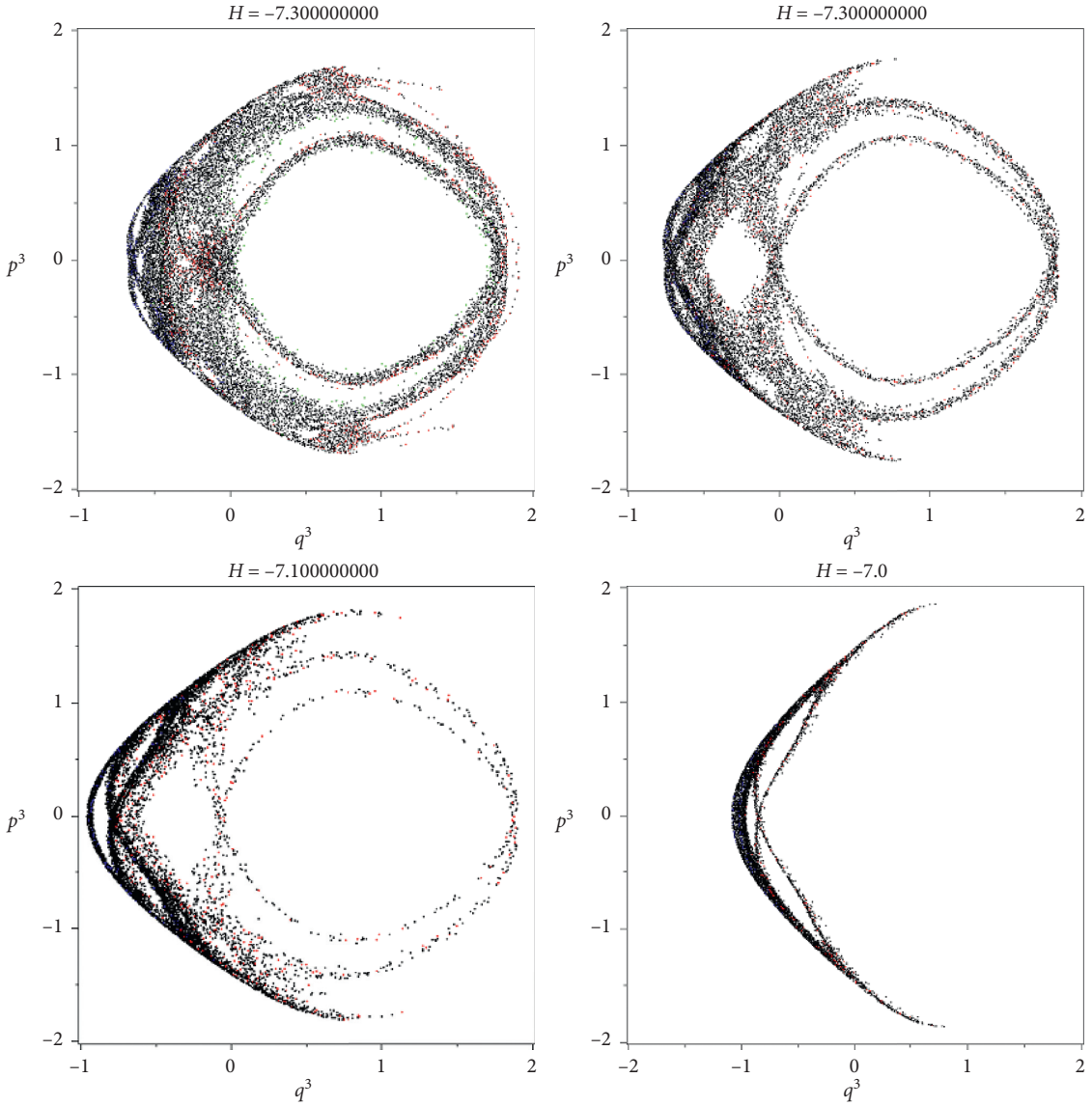

Figure 14: The progressive changing of a Poincaré surface of sections for different energy levels in the unequal masses case ($m_0 = 2.658$, $m_2 = 1.03$, $m_3 = m_1 = 1$, $b = 1.9$, and $c = 0.7$).

and from −13.6 to −11 in our third example (Figure 15). It seems that there exist invariant curves (for example, in the plots for H equal to −3.5) near resonances. These invariant curves could form "island sequences" (small groups in a row) and "islands cycles" (small islands inside of islands). One can observe that transitions between levels fuse at progressive integration, and the KAM surfaces progressively disappear.

In both cases (nonequal and equal masses), the surfaces show unique types of orbits, including quasiperiodic and island orbits. Let us mention that comparing both cases, when the values of m_0 are increased, then there is a noticeable effect influence on the stability and the existence of quasiperiodic orbits in concave and convex kite four-body problems. In other words, we conjecture that the increasing central mass plays a stabilizing role.

The described Poincaré surface of sections allows to study the local stability of the kite four-body problem, the transition from ordered to stochastic motion. They contribute significantly in numerical studies and in verification of the concordance between analytical and numerical results.

6. Conclusions

In this paper, we investigated the central configurations of convex and concave kite four-body problems, deriving

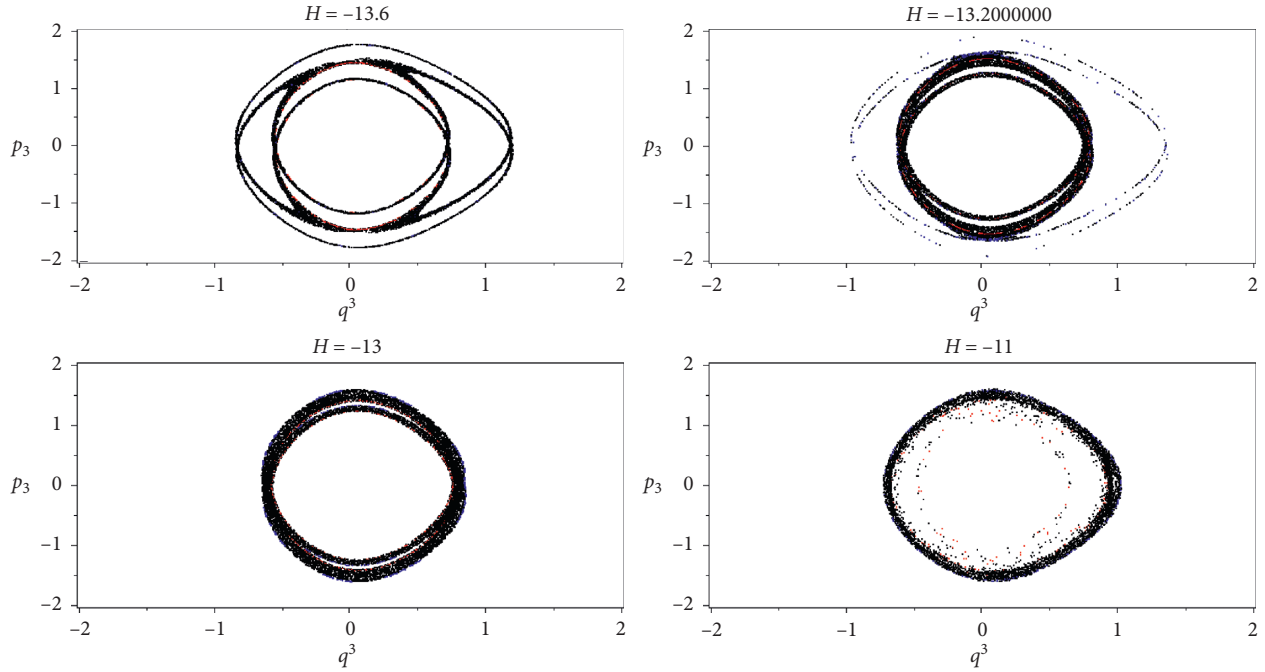

Figure 15: The progressive transformation of a Poincaré surface of sections for different energy levels in the equal masses case (m_0 = 5.17662, m = 1, b = 1.9, and c = 0.7).

regions of central configuration. Three four-body arrangements are discussed which include two concave four-body configurations and one convex four-body configuration. In one of the concave configurations, three of the masses on the vertices of the triangle are equal and the mass on the axis of symmetry can take various positive values. In the second case of concave configuration and the case of the convex configuration, there is only a pair of equal masses and the two masses on the axis of symmetry are nonequal. In each of the three cases, regions of central configuration are derived for positive masses. In the first concave case, we can write the mass ratios as a function of one variable and show its optimum values give values of the parameter. In the other two cases, the mass ratios are written as functions of two variables. The action minimizing orbits for both the concave and convex configurations is analyzed, and it is shown that the minimizers of the action functional restricted to the homographic solutions are the Keplerian elliptical solutions. Using the Hamiltonian formalism, we have identified regions with periodic and quasiperiodic orbits. Moreover, we studied the chaotic behavior in the phase space utilizing the Poincaré surface of sections. It was shown that increasing the value of the central mass m_0 plays a stabilizing role in the case of both convex and concave four-body problems.

Data Availability

No data were used to support this study.

Conflicts of Interest

The authors declare that they have no conflicts of interest.

Acknowledgments

I. Szücs-Csillik was partially supported by a grant of the Romanian Ministry of National Education and Scientific Research, RDI Programme for Space Technology and Advanced Research—SAFE SPACE, project number 236/04.04.2018. II. Daniel Offin was partially supported by a Discovery Grant from NSERC of Canada.

References

[1] C. Deng and S. Zhang, "Planar symmetric concave central configurations in Newtonian four-body problems," *Journal of Geometry and Physics*, vol. 83, pp. 43–52, 2014.

[2] W. D. MacMillan and W. Bartky, "Permanent configurations in the problem of four bodies," *Transactions of the American Mathematical Society*, vol. 34, no. 4, p. 838, 1932.

[3] M. Shoaib, A. R. Kashif, and A. Sivasankaran, "Planar Central Configurations of symmetric five-body problems with two pairs of equal masses," *Advances in Astronomy*, vol. 2016, Article ID 9897681, 11 pages, 2016.

[4] C. Simó, "Relative equilibrium solutions in the four body problem," *Celestial Mechanics*, vol. 18, pp. 165–184, 1978.

[5] J. Llibre, "A note on the Dziobek central configurations," *Proceedings of the American Mathematical Society*, vol. 143, no. 8, pp. 3587–3591, 2015.

[6] J. Llibre, R. Moeckel, and C. Simó, *Central Configurations*, Springer, Basel, Switzerland, 2015.

[7] J. M. Cors and G. E. Roberts, "Four-body co-circular central configurations," *Nonlinearity*, vol. 25, no. 2, pp. 343–370, 2012.

[8] A. Albouy, Y. Fu, and S. Sun, "Symmetry of planar four-body convex central configurations," *Proceedings of the Royal Society of London A: Mathematical, Physical and Engineering Sciences*, vol. 464, no. 2093, pp. 1355–1365, 2008.

[9] M. Shoaib, A. R. Kashif, and I. Szücs-Csillik, "On the planar central configurations of rhomboidal and triangular four- and five-body problems," *Astrophysics and Space Science*, vol. 362, no. 10, p. 182, 2017.

[10] B. Érdi and Z. Czirják, "Central configurations of four bodies with an axis of symmetry," *Celestial Mechanics and Dynamical Astronomy*, vol. 125, no. 1, pp. 33–70, 2016.

[11] S. Smale, "Mathematical problems for the next century," *The Mathematical Intelligencer*, vol. 20, no. 2, pp. 7–15, 1998.

[12] V. Barutello and S. Terracini, "Action minimizing orbits in then-body problem with simple choreography constraint," *Nonlinearity*, vol. 17, no. 6, pp. 2015–2039, 2004.

[13] E. Perez-Chavela and M. Santoprete, "Convex four-body central configurations with some equal masses," *Archive for Rational Mechanics and Analysis*, vol. 185, no. 3, pp. 481–494, 2007.

[14] K.-C. Chen, "Action-minimizing orbits in the parallelogram four-body problem with equal masses," *Archive for Rational Mechanics and Analysis*, vol. 158, no. 4, pp. 293–318, 2001.

[15] K.-C. Chen, "Variational methods on periodic and quasi-periodic solutions for the N-body problem," *Ergodic Theory and Dynamical Systems*, vol. 23, no. 6, pp. 1691–1715, 2003.

[16] L. Bakker and S. Simmons, "Stability of the rhomboidal symmetric-mass orbit," *Discrete & Continuous Dynamical Systems—A*, vol. 35, no. 1, pp. 1–23, 2015.

[17] J. Simmons and E. Perez-Chavela, "The rhomboidal four-body problem," *Global Flow on the Total Collision manifold, The Geometry of Hamiltonian Systems:*, Springer, New York, NY, USA, 1991.

[18] M. Gidea and J. Llibre, "Symmetric planar central configurations of five bodies: euler plus two," *Celestial Mechanics and Dynamical Astronomy*, vol. 106, no. 1, pp. 89–107, 2010.

[19] E. A. Lacomba and E. Pérez-Chavela, "A compact model for the planar rhomboidal 4-body problem," *Celestial Mechanics and Dynamical Astronomy*, vol. 54, no. 4, pp. 343–355, 1992.

[20] E. Piña and P. Lonngi, "Central configurations for the planar Newtonian four-body problem," *Celestial Mechanics and Dynamical Astronomy*, vol. 108, no. 1, pp. 73–93, 2010.

[21] M. Shoaib, B. A. Steves, and A. Széll, "Stability analysis of quintuple stellar and planetary systems using a symmetric five-body model," *New Astronomy*, vol. 13, no. 8, pp. 639–645, 2008.

[22] M. Shoaib, "Central configurations in the trapezoidal four-body problems," *Applied Mathematical Sciences*, vol. 9, no. 40, pp. 1971–1979, 2015.

[23] A. Sivasankaran, B. A. Steves, and W. L. Sweatman, "A global regularisation for integrating the Caledonian symmetric four-body problem," *Celestial Mechanics and Dynamical Astronomy*, vol. 107, no. 1-2, pp. 157–168, 2010.

[24] J.-h. Ji, X.-h. Liao, and L. Liu, "The phase space structure of the rhomboidal four-body problem," *Chinese Astronomy and Astrophysics*, vol. 24, no. 3, pp. 381–386, 2000.

[25] J. Waldvogel, "The rhomboidal symmetric four-body problem," *Celestial Mechanics and Dynamical Astronomy*, vol. 113, no. 1, pp. 113–123, 2012.

[26] D. Yan, "Existence and linear stability of the rhomboidal periodic orbit in the planar equal mass four-body problem," *Journal of Mathematical Analysis and Applications*, vol. 388, no. 2, pp. 942–951, 2012.

[27] L. F. Mello and A. C. Fernandes, "New classes of spatial central configurations for the -body problem," *Nonlinear Analysis: Real World Applications*, vol. 12, no. 1, pp. 723–730, 2011.

[28] W. B. Gordon, "A minimizing property of Keplerian orbits," *American Journal of Mathematics*, vol. 99, no. 5, pp. 961–971, 1977.

[29] S. Q. Zhang and Q. Zhou, "A minimizing property of Lagrangian solution," *Acta Mathematica Sinica, English Series*, vol. 17, no. 3, pp. 497–500, 2001.

[30] S. Zhang and Q. Zhou, "A minimizing property of Eulerian solutions," *Celestial Mechanics and Dynamical Astronomy*, vol. 90, no. 3-4, pp. 239–243, 2004.

[31] A. M. Mansur and D. C. Offin, "A minimizing property of homographic solutions," *Acta Mathematica Sinica, English Series*, vol. 30, no. 2, pp. 353–360, 2014.

[32] A. Mansur, D. Offin, and M. Lewis, "Instability for a family of homographic periodic solutions in the parallelogram four body problem," *Qualitative Theory of Dynamical Systems*, vol. 16, no. 3, pp. 671–688, 2017.

[33] A. Mansur, D. Offin, and A. Arsie, "Extensions to chen's minimizing equal mass parallelogram solutions," *Taiwanese Journal of Mathematics*, vol. 21, no. 6, pp. 1437–1453, 2017.

[34] M. Celli, "The central configurations of four masses x, $-x$, y, $-y$," *Journal of Differential Equations*, vol. 235, no. 2, pp. 668–682, 2007.

[35] M. Corbera and J. Llibre, "Central configurations of the 4-body problem with masses $m_1 = m_2 > m_3 = m_4 = m > 0$ and smmall," *Applied Mathematics and Computation*, vol. 246, pp. 121–147, 2014.

[36] Y. Deng, B. Li, and S. Zhang, "Some notes on four-body co-circular central configurations," *Journal of Mathematical Analysis and Applications*, vol. 453, no. 1, pp. 398–409, 2017.

[37] M. Corbera, J. M. Cors, and G. E. Roberts, "A four-body convex central configuration with perpendicular diagonals is necessarily a kite," *Qualitative Theory of Dynamical Systems*, vol. 17, no. 2, pp. 367–374, 2018.

[38] M. Corbera, J. M. Cors, J. Llibre, and E. Pérez-Chavela, "Trapezoid central configurations," *Applied Mathematics and Computation*, vol. 346, pp. 127–142, 2019.

[39] M. Santoprete, "Four-body central configurations with one pair of opposite sides parallel," *Journal of Mathematical Analysis and Applications*, vol. 464, no. 1, pp. 421–434, 2018.

[40] B. A. Steves and A. E. Roy, "Some special restricted four-body problems-I. Modelling the Caledonian problem," *Planetary and Space Science*, vol. 46, no. 11-12, pp. 1465–1474, 1998.

[41] A. E. Roy and B. A. Steves, "The caledonian symmetrical double binary four-body problem I: surfaces of zero-velocity using the energy integral," *New Developments in the Dynamics of Planetary Systems*, vol. 78, pp. 299–318, 2001.

[42] I. Szücs-Csillik, "The lie integrator and the hénon-heiles system," *Romanian Astronomical Journal*, vol. 20, no. 1, pp. 49–66, 2010.

[43] E. S. Cheb-Terrab and H. P. Oliveira, "Poincaré sections of Hamiltonian systems," *Computer Physics Communications*, vol. 95, no. 2-3, pp. 171–189, 1996.